GENOMICS AND EPIGENOMICS OF CANCER IMMUNOTHERAPY: CHALLENGES AND CLINICAL IMPLICATIONS,
2nd Edition

EDITED BY: Xiao-Jie Lu, Malak Abedalthagafi and Xiaochen Wang
PUBLISHED IN: Frontiers in Oncology and Frontiers in Genetics

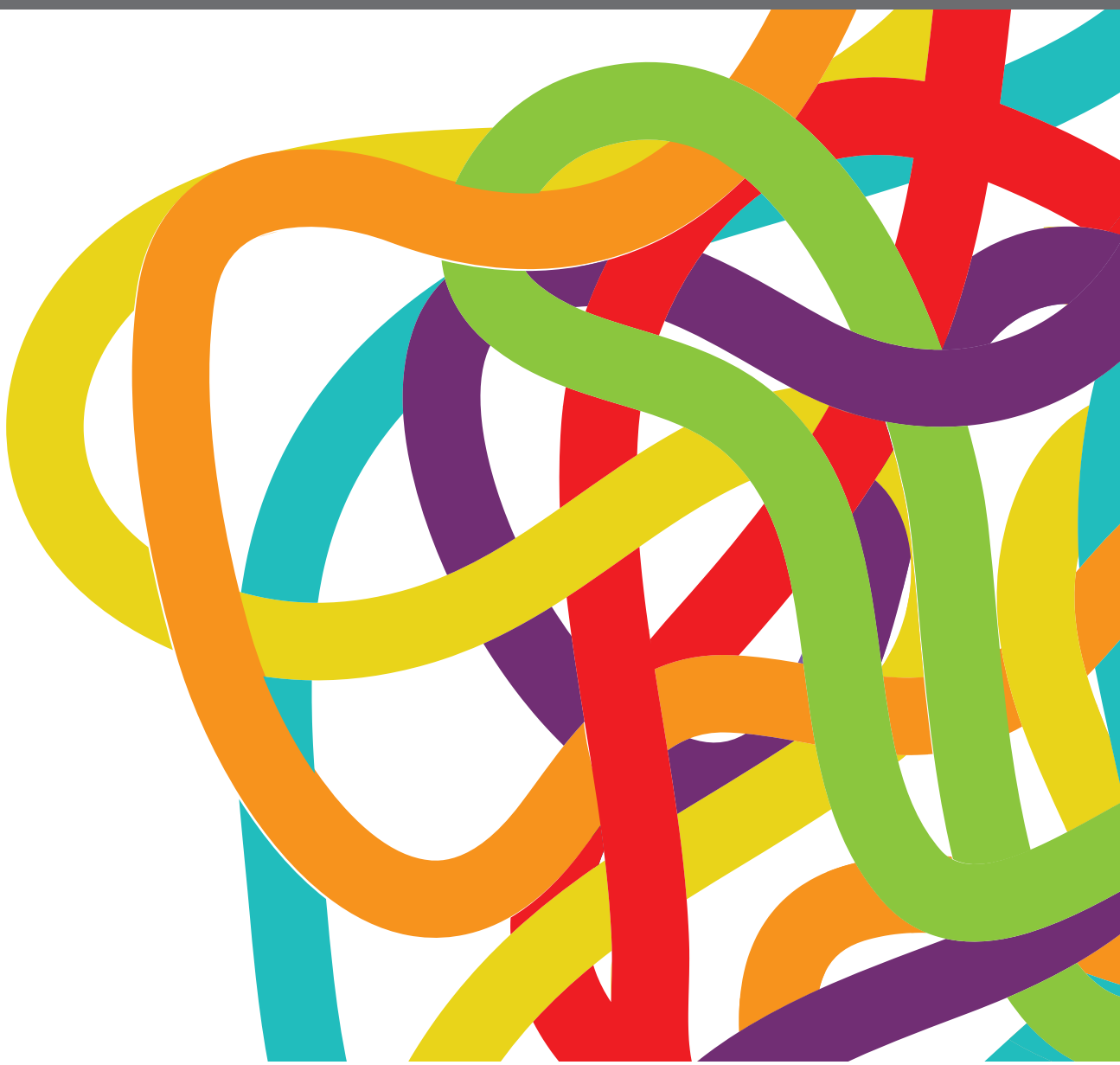

frontiers Research Topics

ISSN 1664-8714
ISBN 978-2-8325-5311-4
DOI 10.3389/978-2-8325-5311-4

About Frontiers

Frontiers is more than just an open-access publisher of scholarly articles: it is a pioneering approach to the world of academia, radically improving the way scholarly research is managed. The grand vision of Frontiers is a world where all people have an equal opportunity to seek, share and generate knowledge. Frontiers provides immediate and permanent online open access to all its publications, but this alone is not enough to realize our grand goals.

Frontiers Journal Series

The Frontiers Journal Series is a multi-tier and interdisciplinary set of open-access, online journals, promising a paradigm shift from the current review, selection and dissemination processes in academic publishing. All Frontiers journals are driven by researchers for researchers; therefore, they constitute a service to the scholarly community. At the same time, the Frontiers Journal Series operates on a revolutionary invention, the tiered publishing system, initially addressing specific communities of scholars, and gradually climbing up to broader public understanding, thus serving the interests of the lay society, too.

Dedication to Quality

Each Frontiers article is a landmark of the highest quality, thanks to genuinely collaborative interactions between authors and review editors, who include some of the world's best academicians. Research must be certified by peers before entering a stream of knowledge that may eventually reach the public - and shape society; therefore, Frontiers only applies the most rigorous and unbiased reviews.
Frontiers revolutionizes research publishing by freely delivering the most outstanding research, evaluated with no bias from both the academic and social point of view. By applying the most advanced information technologies, Frontiers is catapulting scholarly publishing into a new generation.

What are Frontiers Research Topics?

Frontiers Research Topics are very popular trademarks of the Frontiers Journals Series: they are collections of at least ten articles, all centered on a particular subject. With their unique mix of varied contributions from Original Research to Review Articles, Frontiers Research Topics unify the most influential researchers, the latest key findings and historical advances in a hot research area! Find out more on how to host your own Frontiers Research Topic or contribute to one as an author by contacting the Frontiers Editorial Office: frontiersin.org/about/contact

GENOMICS AND EPIGENOMICS OF CANCER IMMUNOTHERAPY: CHALLENGES AND CLINICAL IMPLICATIONS, 2nd Edition

Topic Editors:
Xiao-Jie Lu, Nanjing Medical University, China
Malak Abedalthagafi, King Abdulaziz City for Science and Technology, Saudi Arabia
Xiaochen Wang, University of Texas Southwestern Medical Center, United States

Publisher's note: This is a 2nd edition due to an article retraction.

Citation: Lu, X.-J., Abedalthagafi, M., Wang, X., eds. (2024). Genomics and Epigenomics of Cancer Immunotherapy: Challenges and Clinical Implications, 2nd Edition. Lausanne: Frontiers Media SA. doi: 10.3389/978-2-8325-5311-4

Table of Contents

frontiers in Oncology

EDITORIAL
published: 22 July 2021
doi: 10.3389/fonc.2021.704397

Editorial: Genomics and Epigenomics of Cancer Immunotherapy: Challenges and Clinical Implications

Malak Abedalthagafi *

King Fahd Medical City, Saudi Genome Project, King Abdulaziz City for Science and Technology, Riyadh, Saudi Arabia

Keywords: genomic, epigenomic, cancer, immunotherapy, oncology

Editorial on the Research Topic

Genomics and Epigenomics of Cancer Immunotherapy: Challenges and Clinical Implications

Aberrant gene function and altered gene expression are hallmarks of cancer. While the success of cancer immunotherapy has provided a qualitative leap in cancer management, not all patients have not benefited from immunotherapies available today as they fail to achieve complete responses, suffer frequent relapses, or develop life-threatening drug related toxicities. It is now well understood that genetics, epigenetics as well as the immune system plays a vital role in the invasiveness, migration and progression of cancer. Genomic and epigenetic signatures in immune and cancer cells may provide accurate prediction of patients treated with immunotherapeutics. Tumor-associated macrophages are polarized into phenotypes M1 and M2 (1), where the M1 polarized macrophages secrete pro-inflammatory cytokines to eliminate tumor cells, while M2 polarized macrophages secrete anti-inflammatory cytokines and have implications on tumor angiogenesis, metastasis and growth and may result in a worse prognosis (2). Successful cancer immunotherapy will be aided by modulating M2-type macrophage function that predominates human cancers to produce growth-promoting molecules thereby stimulating tumor growth into M1-type, which have the ability to retard cancer growth. This interplay between pro- and anti-inflammatory mechanisms is known to regulate tumor progression and predict cancer susceptibility. The fact that macrophages and thereby, the innate immunity, can be modulated to play a central role in combating cancer is a breakthrough that is imperative for the realization of success in the use of immunotherapy against cancer (3). During cancer progression, neoplastic cells undergo reversible transitions in multiple phenotypic states. Of these, the extremes are defined as the epithelial and mesenchymal phenotypes. Epithelial-to-mesenchymal transition (EMT) remains fundamental to the metastatic process and is associated with changes in the expression of multiple genes, characterized by the downregulation of epithelial markers, and upregulation of mesenchymal markers. Understanding these functional interactions between such EMT-inducing factors and chromatin modulators will provide insights into the mechanisms underlying cancer progression. Furthermore, these studies can enable development of new diagnostic and therapeutic modalities for treating high-grade malignancies (4). Interestingly, EMT is not only controlled at a genetic level, but also at a post-transcriptional level by miRNAs and long noncoding RNAs (lncRNAs). lncRNAs are transcripts >200 nucleotides in length lacking any protein coding potential and are uniquely expressed in differentiated tissues or specific cancer types. Their roles in the modulation of cellular signaling pathways, including those associated with the immune system are only starting to be unraveled. Interestingly, lncRNAs are

OPEN ACCESS

Edited and reviewed by:
Heather Cunliffe,
University of Otago,
New Zealand

***Correspondence:**
Malak Abedalthagafi
malthagafi@kfmc.med.sa

Specialty section:
This article was submitted to Cancer Genetics, a section of the journal Frontiers in Oncology

Received: *02 May 2021*
Accepted: *26 May 2021*
Published: *22 July 2021*

Citation:
Abedalthagafi M (2021) Editorial: Genomics and Epigenomics of Cancer Immunotherapy: Challenges and Clinical Implications. Front. Oncol. 11:704397. doi: 10.3389/fonc.2021.704397

highly regulated and are restricted more stringently to specific cell types than mRNA (5). lncRNAs are also evolutionarily conserved with regards to the function, secondary structure, and regions of micro homology, despite minimum sequence similarity (6, 7) and have remained oblivious to a rule-based framework for understanding the impact of sequence on function. LncRNAs modulate gene expression, including chromatin modification as well as transcriptional and posttranscriptional processing (8) and have recently gained attention as they can function as a competing endogenous RNA (ceRNA), which can hinder the function of miRNAs in tumors (9), adding another layer of complexity to the mechanisms involved in tumor progression. Several lncRNAs are reported to participate in macrophage polarization while the function of others remains to be unraveled.

Of the 18 manuscripts in this collection, 9 address the role of lcnRNAs in cancers and the interplay between the regulation of lncRNAs, miRNAs, and cellular signaling pathways involving cell migration, proliferation and invasiveness across different cancer subtypes. Wang J et al. explore the role of lncGNAT1-1 in suppression of liver cancer progression by modulating EMT and another manuscript elucidates the role of lncCCAT-1 in promoting EMT, cellular migration and invasion in lung adenocarcinoma by suppressing mir 219-1 (Wang W et al.). Functional and cellular mechanisms involved in migration and invasion of different tumors have been studied for specific lncRNAs in 7 manuscripts (Du et al.; Tu et al.; Ai et al.; Ma et al.; Li et al.; Sun et al.; Jia et al.). The role of lncRNAs derived from macrophage exosomes and their impact on inhibiting the progression of oral squamous cell carcinoma *via* miR-182-5p/FOXO3 pathway has specifically been addressed by Ai et al. and the influence of M2 Polarized Macrophages in Cholangiocarcinoma through modulation of miR-326 and RhoA-ROCK Signaling Pathway has been studied by Tu et al. Immunological infiltration of tumors is the starting point for a successful cancer immunotherapy. 3 manuscripts in this collection address the prognostic value of specific biomarkers by correlating tumor mutational burden and immunological infiltration (Dai et al.; Zhou et al.; Feng et al.). The modulation of tumor microenvironment by BCL9 has been addressed by 2 manuscripts (Wei et al.; Zhu et al.) where the role of BCL 9 in the regulation of the endothelial cell function and fibroblast function has been investigated in the context of tumor microenvironment. Liu et al. explore the role of CD47 expression levels in the progression of endometrial cancer and Zhao et al. explore the role of 22 subsets of tumor-infiltrating immune cells and identify nuclear factors of activated T cells-4 (NFAT4) as the key immune-function related gene associated with poor prognosis in AML mediated *via* recruitment of T regulatory cells (Tregs). Lu et al. explore the role of LINC00675 as a competing endogenous RNA (ceRNA) in HCC cells and its function in restraining metastasis in hepatocellular carcinoma by sponging miR-942-5p. Lastly, the role of TGFβ1 as a prognostic factor in the assessment of tumor immune microenvironment in colon cancer is explored in the study by Wang et al.

The Research Topic of 18 manuscripts covers emerging themes in the field of cancer immunotherapy and we envisage that this collection contributes to the interdisciplinary work involving cellular signaling, miRNAs, genomic and epigenetic characterizations and the implications of lncRNAs across the spectrum of cancer subtypes. These studies on the genomics and epigenetic mechanisms are imperative to the development of novel biomarkers and advance our understanding in elucidating mechanisms involved in immune escape and eventually, help develop improved immunotherapeutic treatment modalities against cancer.

AUTHOR CONTRIBUTIONS

The author confirms being the sole contributor of this work and has approved it for publication.

REFERENCES

1. Mills CD. Anatomy of a Discovery: M1 and M2 Macrophages. *Front Immunol* (2015) 6:212. doi: 10.3389/fimmu.2015.00212
2. Chanmee T, Ontong P, Konno K, Itano N. Tumor-Associated Macrophages as Major Players in the Tumor Microenvironment. *Cancers (Basel)* (2014) 6 (3):1670–90. doi: 10.3390/cancers6031670
3. Mills CD, Lenz LL, Harris RA. A Breakthrough: Macrophage-Directed Cancer Immunotherapy. *Cancer Res* (2016) 76(3):513–6. doi: 10.1158/0008-5472.CAN-15-1737
4. Tam WL, Weinberg RA. The Epigenetics of Epithelial-Mesenchymal Plasticity in Cancer. *Nat Med* (2013) 19(11):1438–49. doi: 10.1038/nm.3336
5. Diederichs S. The Four Dimensions of Noncoding RNA Conservation. *Trends Genet* (2014) 30(4):121–3. doi: 10.1016/j.tig.2014.01.004
6. Quinn JJ, Zhang QC, Georgiev P, Ilik IA, Akhtar A, Chang HY, et al. Rapid Evolutionary Turnover Underlies Conserved lncRNA-Genome Interactions. *Genes Dev* (2016) 30(2):191–207. doi: 10.1101/gad.272187.115
7. Hezroni H, Zhang QC, Georgiev P, Ilik IA, Akhtar A, Chang HY. Principles of Long Noncoding RNA Evolution Derived From Direct Comparison of Transcriptomes in 17 Species. *Cell Rep* (2015) 11(7):1110–22. doi: 10.1016/j.celrep.2015.04.023
8. Sun Q, Hao Q, Prasanth KV. Nuclear Long Noncoding RNAs: Key Regulators of Gene Expression. *Trends Genet* (2018) 34(2):142–57. doi: 10.1016/j.tig.2017.11.005
9. Long J, Xiong J, Bai Y, Mao J, Lin J, Xu W, et al. Construction and Investigation of a lncRNA-Associated ceRNA Regulatory Network in Cholangiocarcinoma. *Front Oncol* (2019) 9:649. doi: 10.3389/fonc.2019.00649

Conflict of Interest: The author declares that the research was conducted in the absence of any commercial or financial relationships that could be construed as a potential conflict of interest.

frontiers in Oncology

ORIGINAL RESEARCH
published: 26 August 2020
doi: 10.3389/fonc.2020.01525

CD47 Enhances Cell Viability and Migration Ability but Inhibits Apoptosis in Endometrial Carcinoma Cells via the PI3K/Akt/mTOR Signaling Pathway

Yun Liu[*†], *Yue Chang*[†], *Xinhong He, Yixuan Cai, Hao Jiang, Ru Jia and Jiyan Leng*

Department of Obstetrics and Gynecology, Beijing Friendship Hospital Affiliated to Capital Medical University, Beijing, China

Purposes: To measure expression levels of CD47 during endometrial carcinoma development, and to determine specific modulatory effects.

Methods: CD47 expression levels in endometrial carcinoma tissues and adjacent tissues were analyzed using qRT-PCR. CD47-overexpressed or downregulated cell models were established using CD47 plasmid or CD47 shRNA. The effects of CD47 on HEC-1A and Ishikawa cell growth were evaluated using CCK-8 assays. Migration ability of transfected HEC-1A and Ishikawa cells were examined using wound healing assays. Flow cytometry was used to measure the effects of CD47 on apoptosis and the cell cycle in HEC-1A and Ishikawa cells. Western blot was used to analyze the correlation between CD47 expression level and PI3K/Akt/mTOR signaling pathway.

Results: Highly expressed CD47 was observed in endometrial carcinoma tissues, with higher levels in more advanced tissues than in early tissues. Upregulation of CD47 enhanced cell viability and migration ability in HEC-1A and Ishikawa cells, while silencing CD47 caused the opposite results. CD47 overexpression suppressed apoptosis and inhibited cell cycle arrest in HEC-1A and Ishikawa cells. CD47 upregulation contributes to the activation of PI3K/Akt/mTOR signaling pathway in endometrial carcinoma cells.

Conclusion: CD47 exerts oncogenic functions in endometrial carcinoma by activating PI3K/Akt/mTOR signaling, suggesting it may be a novel immunotherapeutic target for therapeutic interventions.

Keywords: CD47, endometrial carcinoma, cell viability, migration, apoptosis

OPEN ACCESS

Edited by:
Xiaochen Wang,
University of Texas Southwestern Medical Center, United States

Reviewed by:
Sainan Li,
Massachusetts General Hospital and Harvard Medical School, United States
Donghua Xu,
Weifang Medical University, China

***Correspondence:**
Yun Liu
liuyun.bjfh@ccmu.edu.cn

[†]*These authors share first authorship*

Specialty section:
This article was submitted to Cancer Genetics, a section of the journal Frontiers in Oncology

Received: *18 May 2020*
Accepted: *16 July 2020*
Published: *26 August 2020*

Citation:
Liu Y, Chang Y, He X, Cai Y, Jiang H, Jia R and Leng J (2020) CD47 Enhances Cell Viability and Migration Ability but Inhibits Apoptosis in Endometrial Carcinoma Cells via the PI3K/Akt/mTOR Signaling Pathway. Front. Oncol. 10:1525. doi: 10.3389/fonc.2020.01525

INTRODUCTION

Endometrial carcinoma accounts for ∼85% of endometrial cancer; it is one of the commonly diagnosed gynecologic malignancies (1, 2). Despite the fact that many patients with endometrial carcinoma achieve good outcomes, mortality in advanced disease remains high (3). In recent years, treatments have not increased survival. For these reasons, clinically effective targets are needed.

Recently, immunotherapy has attracted increasing attention. Several studies demonstrated the ability of immunotherapy to improve the prognosis of various cancers via regulation of checkpoint

inhibitors; it may also be effective in endometrial carcinoma (4). Piulats et al. reported two endometrial carcinoma patients in poor condition who were successfully treated with nivolumab, an anti-PD-1 monoclonal antibody (5). The patients were found to harbor mutations that may confer sensitivity to immune checkpoint inhibitors (5). Di et al. identified several regulatory targets of immunotherapy in endometrial carcinoma, suggesting new options for treatment (6). These findings suggest that immunotherapy is a promising therapeutic strategy to improve the prognosis of endometrial carcinoma patients.

CD47, the "don't eat me" signal, is an important immune checkpoint inhibitor that contributes to the progression of cancer (7). Normally, CD47 and its specific receptor, signal regulatory protein-α (SIRPα), are expressed in all cell types; however, they are upregulated in cancerous tissues and cell lines. Several studies have found that upregulation of CD47 promotes the progression of various tumors by blockading immune reactions (8, 9). For example, CD47 overexpression promoted the development of ovarian cancer by reducing the activity of macrophage phagocytosis (8). CD47 was upregulated in the membranes of human small-cell lung cancer cells, and Weiskopf et al. found that CD47 knockdown significantly suppressed tumor proliferation (10). CD47 also plays an oncogenic role in the progression of breast cancer (11). By synergistic action with inflammatory mediators, CD47 enhanced the migration capacity of colon tumor cells and promoted colon cancer development (12). Nevertheless, studies of CD47 in endometrial carcinoma are limited (13).

In recent years, the oncogenic effects of phosphatidylinositol 3-kinase (PI3K)/Akt/mammalian target of rapamycin (mTOR) signaling in cancer, including in endometrial carcinoma, have received increasing recognition (14, 15). Philip et al. reported that inhibition of PI3K/Akt/mTOR signaling increased the sensitivity of endometrial carcinoma cells to some targeted therapies (16). Cao et al. observed that claudin-6 (CLDN6) knockdown suppressed the proliferation and migration of endometrial carcinoma cell by regulating the PI3K/Akt/mTOR signaling pathway (17). A correlation between CD47 and the PI3K/Akt/mTOR pathway has also been identified. Liu et al. found that increased CD47 promoted human glioblastoma progression by modulating the PI3K/Akt signaling pathway (18). Nevertheless, there remain no studies of CD47-PI3K/Akt/mTOR signaling and endometrial carcinoma.

In the present study, we explored the relationship between CD47 expression and the development of endometrial carcinoma. We measured expression levels of CD47 in 22 paired carcinoma-normal endometrial tissues. CD47 overexpression- or knockdown-cell lines of endometrial carcinoma were established by transfection with plasmid or shRNA. Subsequently, functional experiments were performed to evaluate the effects of CD47 on endometrial carcinoma.

MATERIALS AND METHODS

Tissue Collection

A total of 22 paired cancer-normal samples of endometrial carcinoma patients were collected from the Beijing Friendship Hospital Affiliated to Capital Medical University. These patients had not yet received chemoradiotherapy prior to sample collection. The pathological stages of endometrial cancer patients were classed according to the International Federation of Gynecology and Obstetrics (FIGO) criteria of endometrial cancer, including 10 stage III–IV and 12 stage I–II tumors. All samples were obtained during surgery and were stored for subsequent RNA analysis (Genstar, Beijing, China) at −20°C. Before tissue collection, written informed consent was obtained from the patients or their families. This study was approved by Ethics Review Board of Beijing Friendship Hospital Affiliated to Capital Medical University.

Cell Culture

Human endometrial carcinoma cell lines, Ishikawa and HEC-1A, were obtained from Nanjing Keygen Biotech (Nanjing, China). Both cell types were maintained in Dulbecco's modified Eagle's medium (DMEM) (HyClone, Victoria, Australia), containing 1% penicillin/streptomycin and 10% fetal bovine serum

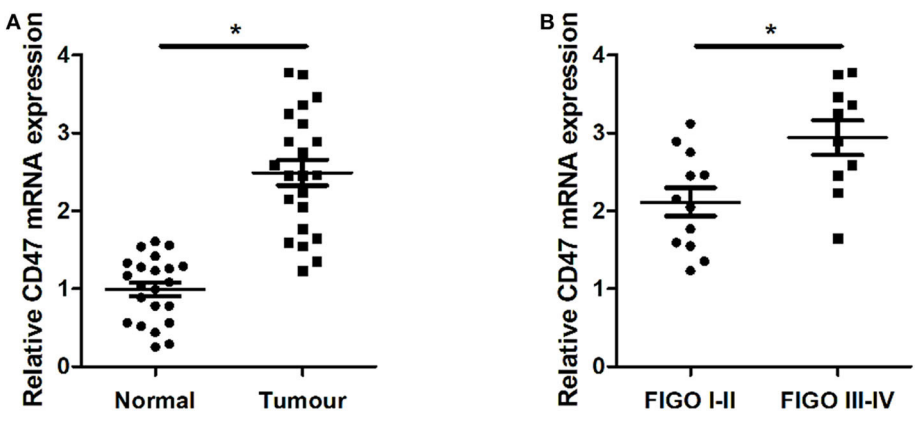

FIGURE 1 | Up-regulation of CD47 mRNA expression levels measured in endometrial carcinoma tissues, and compared with adjacent tissues. **(A)** Expression levels of CD47 mRNA were relatively higher in endometrial carcinoma tissues. **(B)** Higher CD47 mRNA levels measured in endometrial carcinoma patients at advanced stages. $^{*}p < 0.05$.

(FBS) (Gibco, Gaithersburg, MD, USA). The two endometrial carcinoma cell lines were cultured in an incubator with a humidified atmosphere at 37°C and 5% CO_2.

Plasmid Construction and Transfection

Before transfection, HEC-1A and Ishikawa cells were seeded into 6-well plates at 1×10^5 cells per well and cultured for 24 h. Subsequently, a total of 1 μg plasmid or shRNA was added to each well-plates to increase or reduce CD47 expression levels. pIRES2-ZsGreen1-CD47 (Hanbio, Shanghai, China) was used to up-regulate CD47 expression levels in HEC-1A and Ishikawa cells, while the empty plasmid was used as the control. The shRNA (5′-CCGGGCACAATTACTTGGACTAG TTCTCGAGAACTAGTCCAAGTAATTGTGCTTTTT-3′) that inhibits the expression of CD47, was purchased from GeneChem Biotech Company (Shanghai, China).

qRT-PCR

Endometrial carcinoma tissues and the adjacent tissues were homogenized using a TissueLyser to isolate RNA. TRIzol regent (Invitrogen, Carlsbad, CA, USA) was used to extracted RNA from target tissues according to manufacturer's instructions. cDNA was synthesized using a reverse transcription kit (Takara, Dalian, China), and was then used to measure expression levels of CD47 using SYBR II Premix Taq (Takara, Dalian, China). The fold-changes of CD47 expression were calculated using the 2-ΔΔCT method, with GAPDH as the reference. The primers purchased from Sangon Biotech (Shanghai, China) were as follows:

CD47: Forward primer: 5′-AGAAGGTGAAACGATCAT CGAGC-3′; Reverse primer: 5′-CTCATCCATACCACCGG ATCT-3′.

GAPDH: Forward primer: 5′-ACCACAGTCCATGCCATCA C-3′; Reverse primer: 5′- TCCACCACCCTGTTGCTGTA-3′.

Cell Viability Assay

HEC-1A and Ishikawa endometrial carcinoma cells were seeded into 96-well plates at 1×10^3 cells per well, and were then transfected with CD47 plasmid or CD47 shRNA after incubation for 24 h. Subsequently, these cells were cultured at 37°C and 5% CO^2 for 1 week to construct CD47 up-regulated or down-regulated cell lines. The viability of transfected cells was measured using a spectrophotometer after adding 10 μl CCK-8 (Dojindo, Kumamoto, Japan) into each well for 1 h. Absorbance (OD) at 450 nm was measured at 4 and 48 h after transfection, and the values at 4 h after transfection were used as the control level.

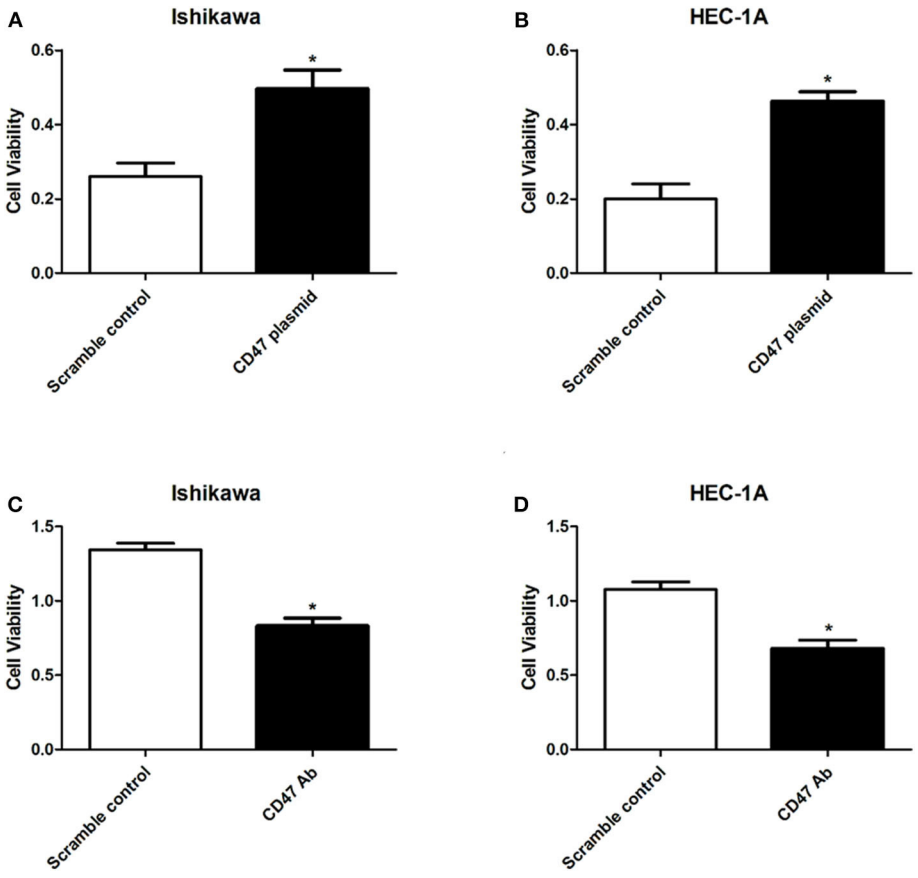

FIGURE 2 | CD47 overexpression enhanced cell viability in HEC-1A and Ishikawa cells. **(A,B)** Overexpressed CD47 promoted cell proliferation in HEC-1A and Ishikawa cell lines. **(C,D)** CD47 knockdown inhibited cell proliferation in HEC-1A and Ishikawa cell lines. *$p < 0.05$.

Wound Healing Assay

To measure the effects of CD47 on endometrial carcinoma cell migration, a wound healing assay was performed. Briefly, 5×10^6 target cells were transferred into 6-well plates and incubated at 37°C until 90% confluence. A 20 μl tip was used to scrape a straight wound in HEC-1A and Ishikawa endometrial carcinoma cell monolayers. After washing the cells with PBS, the plates were incubated for 24 h. Wound distance was measured under light microscopy.

Flow Cytometry

After CD47 overexpressed or knockdown cell lines were established, apoptosis of targeted cells was measured by flow cytometry using an Annexin V-FITC/PI kit (GenStar, Beijing, China) according to the manufacturer's instructions. The cell cycle of transfected HEC-1A and Ishikawa cells were analyzed using the Cell Cycle and Apoptosis Analysis Kit (Beyotime Biotechnology, Shanghai, China), according to the manufacturer's protocol.

Western Blot

Total protein was extracted from cells using radio immunoprecipitation assay lysis buffer (KeyGen BioTech, Nanjing, China) according to the manufacturer's instructions. Proteins were separated by gel electrophoresis with 12% sodium dodecyl sulfate polyacrylamide and transferred onto a polyvinylidene fluoride membrane (PVDF) (Millipore, Billerica, MA, USA). The membranes were then blocked in skimmed milk for 1 h at 20°C and then incubated with primary antibodies overnight at 4°C. Primary antibodies against PI3K (1:2000),

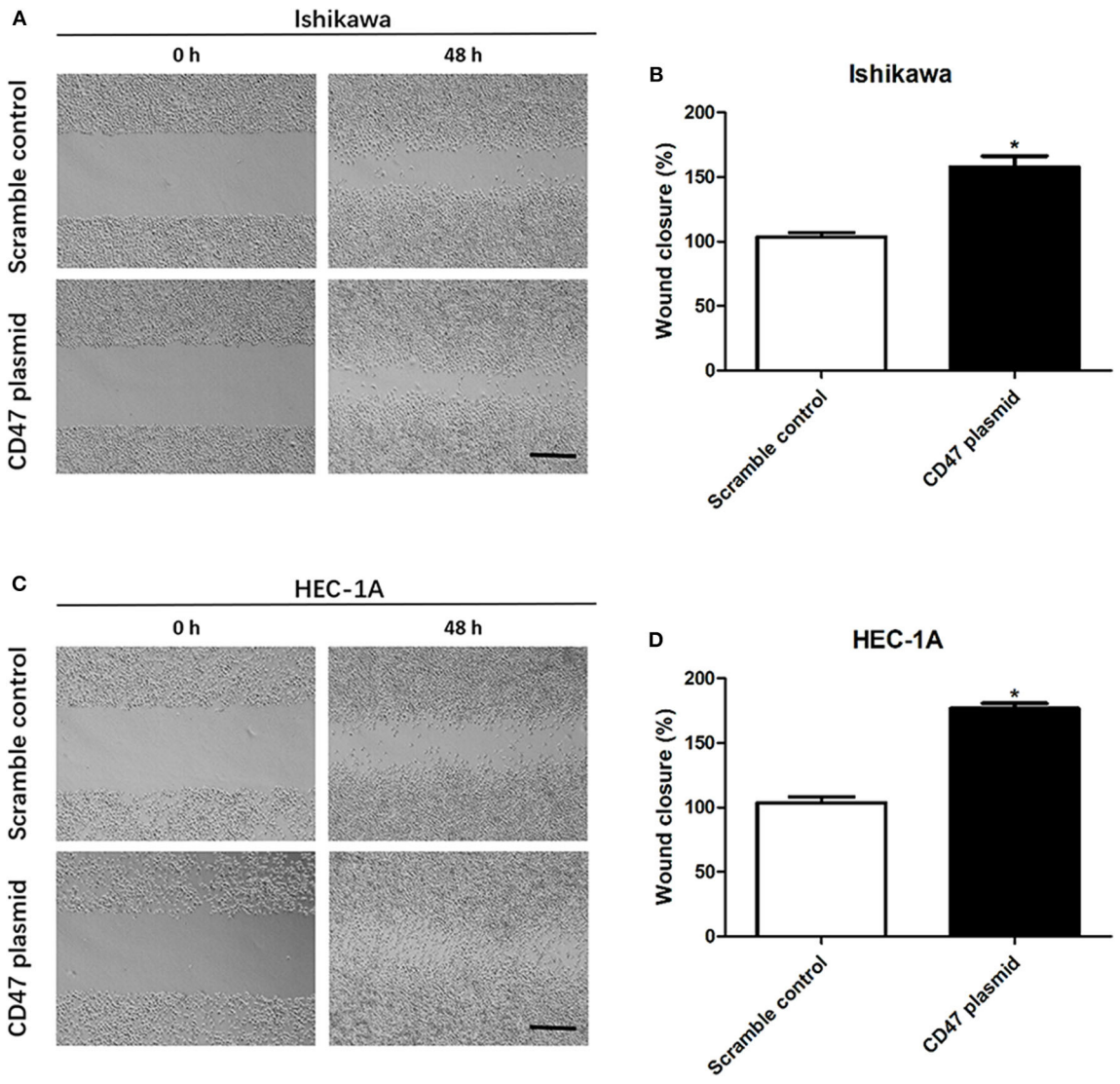

FIGURE 3 | CD47 up-regulation promoted migration in HEC-1A and Ishikawa cells. **(A,B)** CD47 overexpression accelerated the rate of wound closure in Ishikawa cells. **(C,D)** CD47 overexpression accelerated the rate of wound closure in HEC-1A cells. Scale bar = 200 um. *$p < 0.05$.

Akt (1:2000), mTOR (1:2000), and glyceraldehyde-3-phosphate dehydrogenase (GAPDH) (1:500) were purchased from Cell Signaling Technology (Danvers, MA, USA). Membranes were cultured with secondary antibodies (Santa Cruz Biotechnology, Santa Cruz, CA, USA) the following day for 1 h at 20°C. The immunocomplexes were detected using an enhanced chemiluminescence detection kit (Thermo Fisher Scientific, Waltham, MA, USA).

Statistical Analysis

Data were analyzed using SPSS version 19.0 software (IBM, Chicago, IL, USA) and $p < 0.05$ indicated statistical significance. All data were obtained by experiments at least in triplicate and were expressed as mean ± SD. The paired Student's *t*-test was used to determine significant differences between groups.

RESULTS

CD47 Was Up-Regulated in Endometrial Carcinoma Tissues and Was Negatively Related to Pathological Stage

We analyzed expression levels of CD47 mRNA in two paired carcinoma tissues and adjacent normal tissues using qRT-PCR. We found that CD47 expression was upregulated in carcinoma tissues (**Figure 1A**). We classified pathological stages of endometrial cancer patients according to FIGO criteria and found CD47 mRNA expression levels were higher in the stage III-IV groups (**Figure 1B**), further suggesting a correlation between CD47 mRNA expression levels and endometrial carcinoma progression.

CD47 Enhances the Cell Viability of HEC-1A and Ishikawa Endometrial Carcinoma Cells

To determine the regulatory effects of CD47 on endometrial carcinoma cell phenotypes, we selected endometrial carcinoma HEC-1A and Ishikawa cells for subsequent assays. CD47 plasmid, CD47 shRNA or the control were injected into HEC-1A and Ishikawa cells to construct CD47 up- or down-regulation cell models. Subsequently, the effects of CD47 on cell viability were measured using a CCK-8 assay. The results showed that up-regulation of CD47 promoted the proliferation of endometrial carcinoma cells (**Figures 2A,B**), while down-regulation of CD47 suppressed its growth (**Figures 2C,D**). Both results suggested that CD47 enhances cell viability in HEC-1A and Ishikawa cells.

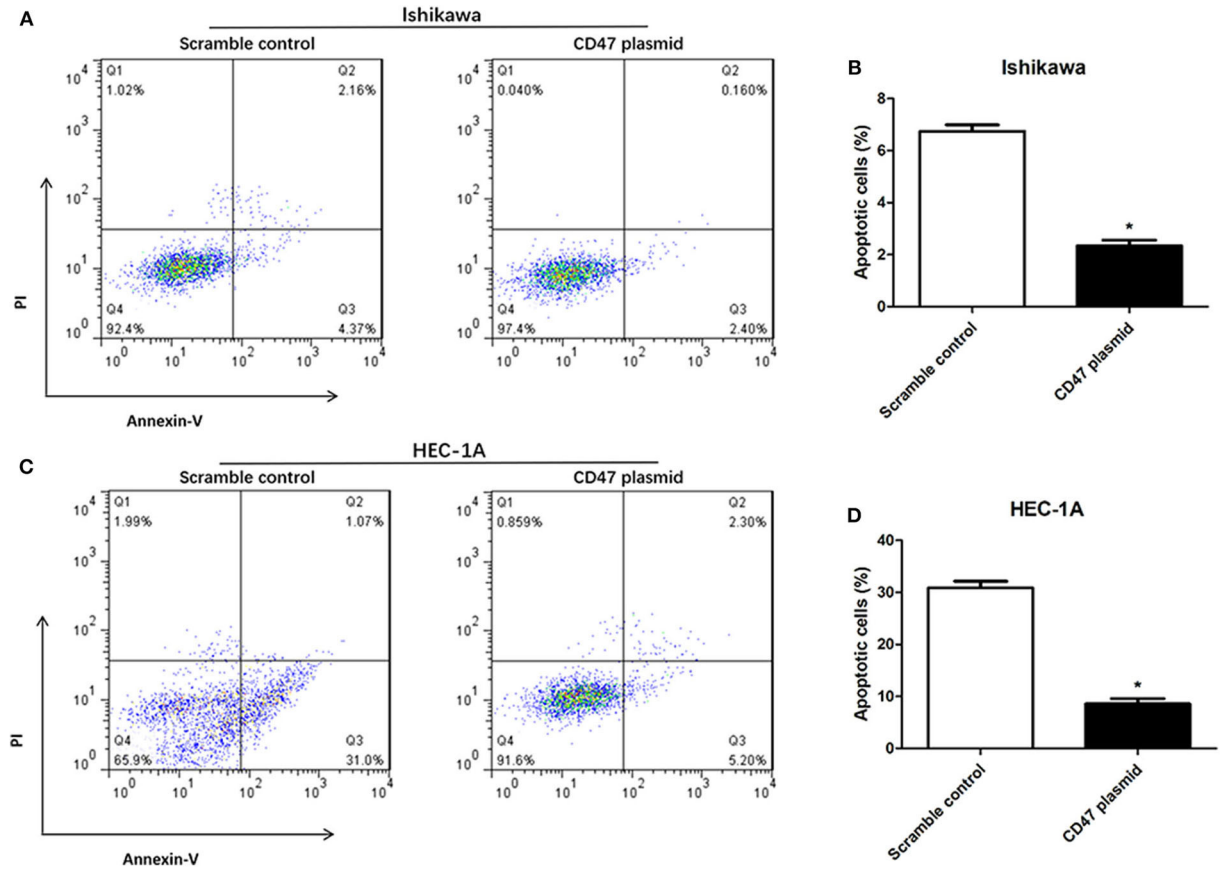

FIGURE 4 | CD47 up-regulation inhibited apoptosis in HEC-1A and Ishikawa cells. **(A,B)** Up-regulation of CD47 inhibited cell apoptosis in Ishikawa cell line. **(C,D)** CD47 overexpression inhibited cell apoptosis in HEC-1A cell line. *$p < 0.05$.

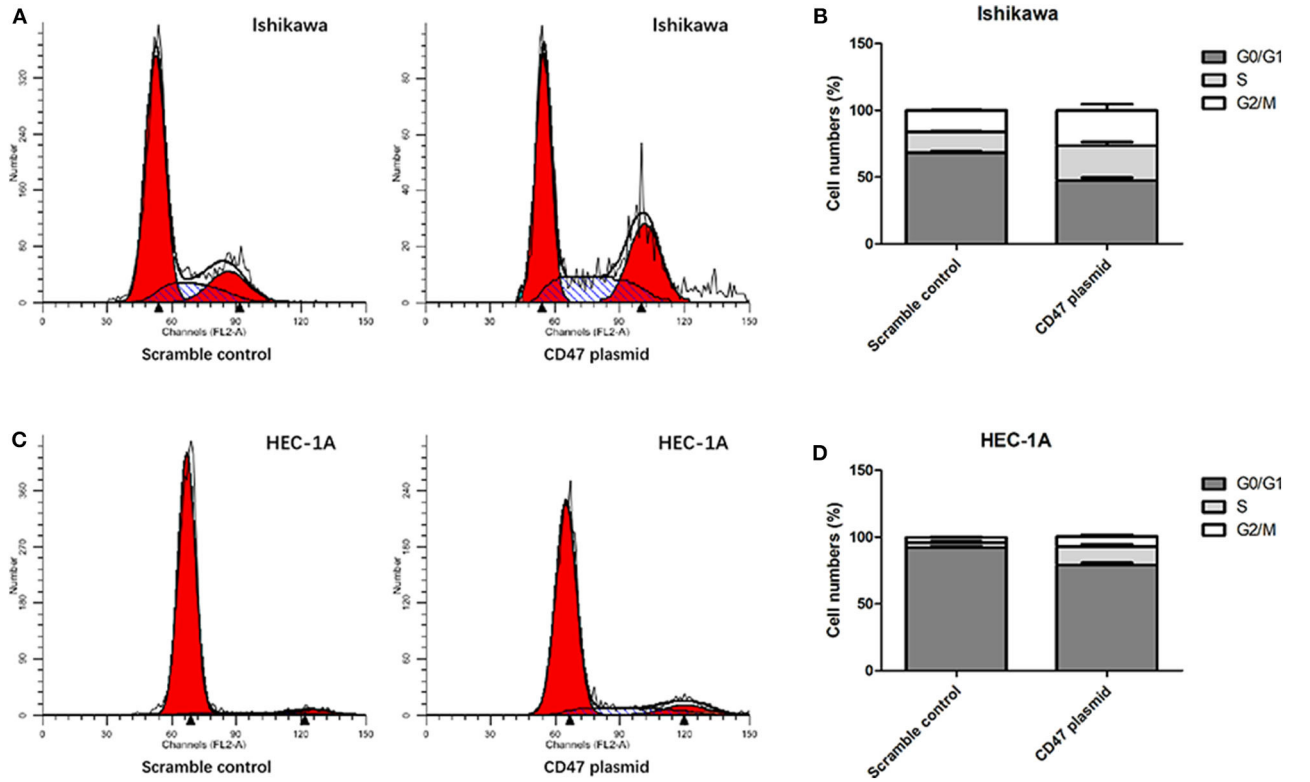

FIGURE 5 | Up-regulation of CD47 promoted cell cycle arrested in HEC-1A and Ishikawa cells. **(A,B)** Upregulation of CD47 reduced the rate of S and G2.M stage cells in Ishikawa cell line. **(C,D)** Upregulation of CD47 reduced the rate of S and G2.M stage cells in HEC-1A cell line.

CD47 Promotes Cell Migration in HEC-1A and Ishikawa Endometrial Carcinoma Cells

To further determine the effects of CD47 on endometrial carcinoma progression, wound healing assays were performed to analyze the role of CD47 in endometrial carcinoma cell migration. The wound area was smaller in the CD47 overexpression group (**Figures 3A–D**), suggesting that increasing expression levels of CD47 contributed to migratory ability of HEC-1A and Ishikawa cells.

Up-Regulation of CD47 Suppresses the Apoptosis and Cell Cycle Arrest of Endometrial Carcinoma Cells

Flow cytometry assays were carried out to analyze the modulatory effects of CD47 on endometrial carcinoma cell cycle and apoptosis. The results showed that upregulating CD47 expression inhibited apoptosis in HEC-1A and Ishikawa cells (**Figures 4A–D**). We also detected a negative correlation between CD47 expression and the ratio of S and G2/M stage cells in HEC-1A and Ishikawa cells (**Figures 5A–D**), suggesting that up-regulation of CD47 inhibited apoptosis in endometrial carcinoma cells by modulating the cell cycle.

CD47 Overexpression Activates PI3K/Akt/mTOR Signaling Pathway in Endometrial Carcinoma Cell Lines

To investigate the mechanisms underlying the effects of CD47 on endometrial carcinoma, western blot was performed to measure PI3K/Akt/mTOR signaling pathway protein levels after injection of CD47 plasmid into endometrial carcinoma cells. Expression levels of PI3K, Akt and mTOR were measured in CD47 plasmid injected Ishikawa and HEC-1A cells. We found that CD47 up-regulation increased PI3K, Akt and mTOR expression in endometrial carcinoma cells (**Figures 6A–C**), suggesting that CD47 exerted oncogenic effects in endometrial carcinoma via up-regulating the PI3K/Akt/mTOR signaling pathway. Besides, CD47 down-regulation reduced PI3K, Akt, and mTOR expression in endometrial carcinoma cells (**Figures 6D–G**) further confirmed this.

DISCUSSION

The incidence of endometrial cancer is only less than that of cervical cancer and ovarian cancer among gynecologic malignancies and is rapidly increasing (19). Though the prognosis of many endometrial carcinomas is good, there are frequent relapses and metastases in advanced patients, giving rise

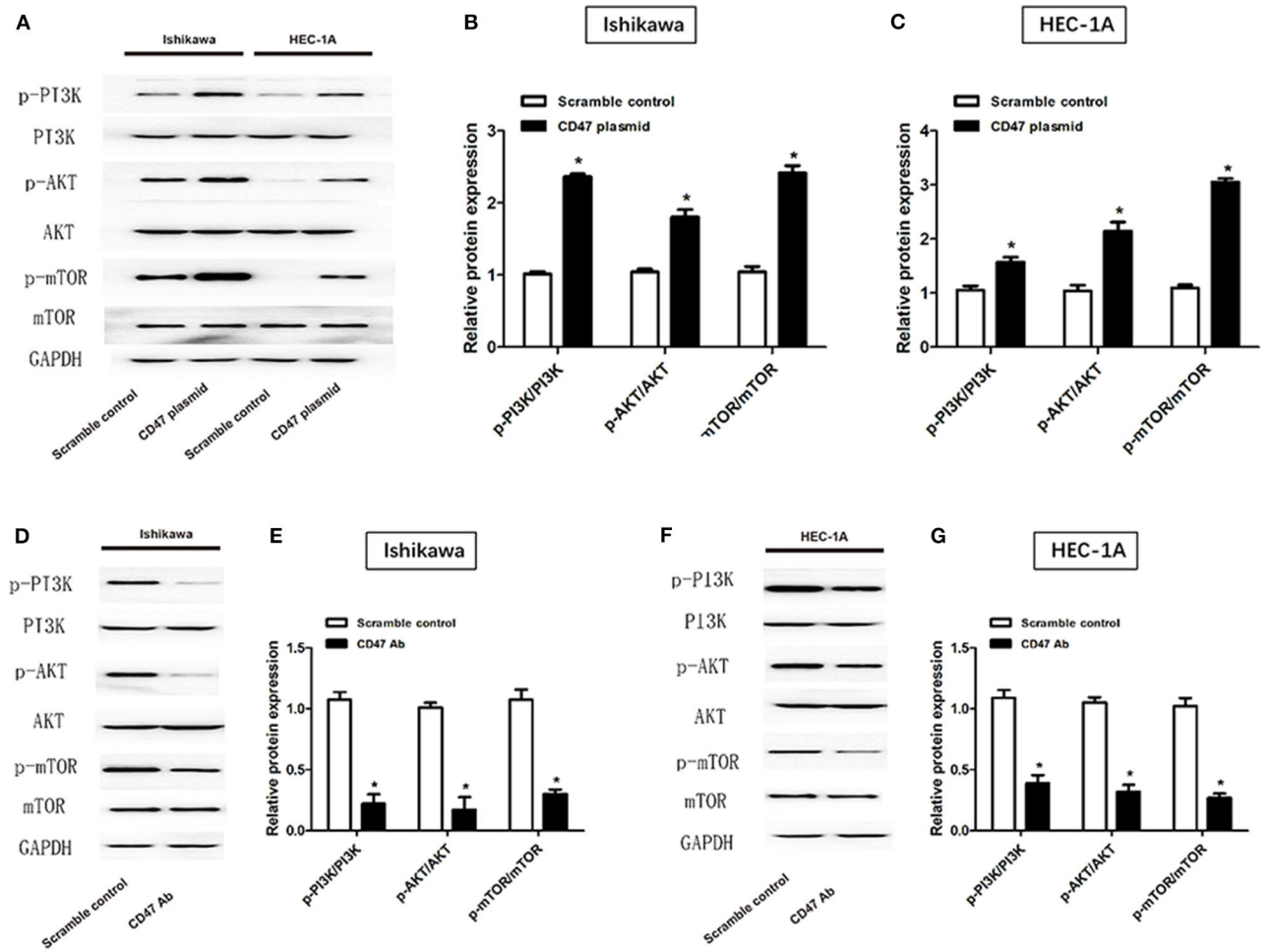

FIGURE 6 | CD47 up-regulation activated PI3K/Akt/mTOR signaling pathway in HEC-1A and Ishikawa cell lines. **(A–C)** CD47 overexpression increased expression levels of PI3K, Akt, and mTOR proteins. **(D–G)** CD47 down-regulation decreased expression levels of PI3K, Akt, and mTOR proteins. *$p < 0.05$.

to low survival rates (20). In recent decades, surgical treatment has not improved the survival of advanced endometrial cancer patients, suggesting that new approaches are needed.

In this present study, we measured expression levels and regulatory effects of CD47 in endometrial carcinoma. CD47 was upregulated in endometrial carcinoma tissues compared with normal endometrial tissue, and higher CD47 expression was observed in endometrial carcinoma patients with later pathological stage, compared with the early stage. Both CD47 expression assays revealed that CD47 was positively associated with endometrial carcinoma development. After transfected cells were established, functional experiments were performed to analyze the modulatory effects of CD47 on endometrial carcinoma cells. We found that up-regulation of CD47 promoted the proliferation and migration of HEC-1A and Ishikawa endometrial carcinoma cells, and inhibited apoptosis. CD47 down-regulation was a significant suppressive factor of endometrial carcinoma cell viability. All these results reconfirmed that CD47 is an important oncogenic factor in endometrial carcinoma.

Recently, several studies found that immunotherapy may be an effective strategy in the treatment of endometrial carcinoma (21). Generally, the microenvironment of tumor contributes to the immune evasion of cancerous cells by expressing proteins such as programmed cell death-1 (PD-1) and B7-H4 (22, 23). It may be the case that expression of these proteins may change the activity of immune system in cancer cells. For example, Sobecki et al. reported that anti-PD-1 immunotherapy may be an appropriate treatment for endometrial cancer patients with mismatch repair-deficiencies (24). There also are other checkpoint inhibitors that can act as immunotherapeutic targets in endometrial carcinoma (25). The CD47/SIRPα axis was also identified as an immune checkpoint inhibitor in cancer therapy (9, 26). A previous study observed that CD47 suppresses the progression of endometrial cancer cells by enhancing the sensitivity of M2 Polarized Macrophages on tumor cells (13). In this study, CD47 overexpression was also found a protective mechanism in endometrial carcinoma development and down-regulation of CD47 inhibited the proliferation and

migration of endometrial carcinoma cells. Blocking CD47 may be an immunotherapeutic pathway for the treatment of endometrial carcinoma.

After binding with the growth factor ligand, membranous receptor tyrosine kinases and G protein-coupled receptors are activated, thereby stimulating the production of phosphatidylinositol- 3,4,5-trisphosphate (PIP3), originated from PI3K (27). Subsequently, PIP3 interacts with Akt, thereby increasing expression levels of mTOR (28–30). Up-regulation of the PI3K/Akt/mTOR signaling cascade causes disturbance of cell survival and growth, ultimately resulting in a competitive proliferation advantage, angiogenesis, metastatic competence, and therapeutic resistance. In this manner, the signaling pathway is a potential target for the treatment of various cancers (31, 32). We observed overactivity of the PI3K/Akt/mTOR signaling pathway in CD47 overexpressing Ishikawa and HEC-1A cell lines. These results suggest that CD47 promotes endometrial carcinoma progression via regulating the PI3K/Akt/mTOR signaling pathway.

CONCLUSION

We found that CD47 expression was higher in endometrial carcinoma tissues, compared with the adjacent tissues. Upregulation of CD47 promoted progression of endometrial carcinoma by activating PI3K/Akt/mTOR signaling pathway. These findings suggest a novel immunotherapeutic pathway for investigating interventions to treat endometrial carcinoma.

DATA AVAILABILITY STATEMENT

The original contributions presented in the study are included in the article/supplementary files, further inquiries can be directed to the corresponding author/s.

ETHICS STATEMENT

The studies involving human participants were reviewed and approved by Beijing Friendship Hospital Affiliated to Capital Medical University. The patients/participants provided their written informed consent to participate in this study.

AUTHOR CONTRIBUTIONS

YL designed the study, wrote the paper, and had overall responsibility for the research. YL, YCh, XH, HJ, RJ, JL, and YCa carried out the experiments. YCh and YCa contributed to data analysis. YL, XH, HJ, RJ, and JL revised the first-manuscript and submitted revised-manuscript. All authors approved the final manuscript version. All authors contributed to the article and approved the submitted version.

FUNDING

This work was supported by the Beijing Natural Science Foundation (7184211), National Natural Science Foundation of China (81801402), Beijing Natural Science Foundation Program and Scientific Research Key Program of Beijing Municipal Commission of Education (KM201610025023), and the Beijing Key Clinical Specialty Project.

REFERENCES

1. Llobet D, Pallares J, Yeramian A, Santacana M, Eritja N, Velasco A, et al. Molecular pathology of endometrial carcinoma: practical aspects from the diagnostic and therapeutic viewpoints. *J Clin Pathol.* (2009) 62:777–85. doi: 10.1136/jcp.2008.056101
2. Siegel RL, Miller KD, Jemal A. Cancer statistics, 2017. *CA Cancer J Clin.* (2017) 67:7–30. doi: 10.3322/caac.21387
3. Ferlay J, Soerjomataram I, Dikshit R, Eser S, Mathers C, Rebelo M, et al. Cancer incidence and mortality worldwide: sources, methods and major patterns in GLOBOCAN 2012. *Int J Cancer.* (2015) 136:E359–86. doi: 10.1002/ijc.29210
4. Velcheti V, Schalper K. Basic overview of current immunotherapy approaches in cancer. *Am Soc Clin Oncol Educ Book.* (2016) 35:298–308. doi: 10.14694/EDBK_156572
5. Piulats JM, Matias-Guiu X. Immunotherapy in endometrial cancer: in the nick of time. *Clin Cancer Res.* (2016) 22:5623–5. doi: 10.1158/1078-0432.CCR-16-1820
6. Di Tucci C, Capone C, Galati G, Iacobelli V, Schiavi MC, Di Donato V, et al. Immunotherapy in endometrial cancer: new scenarios on the horizon. *J Gynecol Oncol.* (2019) 30:e46. doi: 10.3802/jgo.2019.30.e46
7. Matlung HL, Szilagyi K, Barclay NA, van den Berg TK. The CD47-SIRPalpha signaling axis as an innate immune checkpoint in cancer. *Immunol Rev.* (2017) 276:145-64. doi: 10.1111/imr.12527
8. Liu R, Wei H, Gao P, Yu H, Wang K, Fu Z, et al. CD47 promotes ovarian cancer progression by inhibiting macrophage phagocytosis. *Oncotarget.* (2017) 8:39021–32. doi: 10.18632/oncotarget.16547
9. Tong B, Wang M. CD47 is a novel potent immunotherapy target in human malignancies: current studies and future promises. *Future Oncol.* (2018) 14:2179–88. doi: 10.2217/fon-2018-0035
10. Weiskopf K, Jahchan NS, Schnorr PJ, Cristea S, Ring AM, Maute RL, et al. CD47-blocking immunotherapies stimulate macrophage-mediated destruction of small-cell lung cancer. *J Clin Invest.* (2016) 126:2610–20. doi: 10.1172/JCI81603
11. Betancur PA, Abraham BJ, Yiu YY, Willingham SB, Khameneh F, Zarnegar M, et al. A CD47-associated super-enhancer links pro-inflammatory signalling to CD47 upregulation in breast cancer. *Nat Commun.* (2017) 8:14802. doi: 10.1038/ncomms14802
12. Zhang Y, Sime W, Juhas M, Sjolander A. Crosstalk between colon cancer cells and macrophages via inflammatory mediators and CD47 promotes tumour cell migration. *Eur J Cancer.* (2013) 49:3320–34. doi: 10.1016/j.ejca.2013.06.005
13. Gu S, Ni T, Wang J, Liu Y, Fan Q, Wang Y, et al. CD47 blockade inhibits tumor progression through promoting phagocytosis of tumor cells by M2 polarized macrophages in endometrial cancer. *J Immunol Res.* (2018) 2018:6156757. doi: 10.1155/2018/6156757
14. Porta C, Paglino C, Mosca A. Targeting PI3K/Akt/mTOR signaling in cancer. *Front Oncol.* (2014) 4:64. doi: 10.3389/fonc.2014.00064
15. Barra F, Evangelisti G, Ferro Desideri L, Di Domenico S, Ferraioli D, Vellone VG, et al. Investigational PI3K/AKT/mTOR inhibitors in development for endometrial cancer. *Expert Opin Investig Drugs.* (2019) 28:131–42. doi: 10.1080/13543784.2018.1558202
16. Philip CA, Laskov I, Beauchamp MC, Marques M, Amin O, Bitharas J, et al. Inhibition of PI3K-AKT-mTOR pathway sensitizes endometrial

cancer cell lines to PARP inhibitors. *BMC Cancer.* (2017) 17:638. doi: 10.1186/s12885-017-3639-0
17. Cao X, He GZ. Knockdown of CLDN6 inhibits cell proliferation and migration via PI3K/AKT/mTOR signaling pathway in endometrial carcinoma cell line HEC-1-B. *Onco Targets Ther.* (2018) 11:6351–60. doi: 10.2147/OTT.S174618
18. Liu X, Wu X, Wang Y, Li Y, Chen X, Yang W, et al. CD47 promotes human glioblastoma invasion through activation of the PI3K/Akt pathway. *Oncol Res.* (2019) 27:415–22. doi: 10.3727/096504018X15155538502359
19. Yeramian A, Moreno-Bueno G, Dolcet X, Catasus L, Abal M, Colas E, et al. Endometrial carcinoma: molecular alterations involved in tumor development and progression. *Oncogene.* (2013) 32:403–13. doi: 10.1038/onc.2012.76
20. McAlpine JN, Temkin SM, Mackay HJ. Endometrial cancer: not your grandmother's cancer. *Cancer.* (2016) 122:2787–98. doi: 10.1002/cncr.30094
21. Ventriglia J, Paciolla I, Pisano C, Cecere SC, Di Napoli M, Tambaro R, et al. Immunotherapy in ovarian, endometrial and cervical cancer: state of the art and future perspectives. *Cancer Treat Rev.* (2017) 59:109–16. doi: 10.1016/j.ctrv.2017.07.008
22. Vanderstraeten A, Luyten C, Verbist G, Tuyaerts S, Amant F. Mapping the immunosuppressive environment in uterine tumors: implications for immunotherapy. *Cancer Immunol Immunother.* (2014) 63:545–57. doi: 10.1007/s00262-014-1537-8
23. He C, Qiao H, Jiang H, Sun X. The inhibitory role of b7-h4 in antitumor immunity: association with cancer progression and survival. *Clin Dev Immunol.* (2011) 2011:695834. doi: 10.1155/2011/695834
24. Sobecki-Rausch J, Barroilhet L. Anti-programmed death-1 immunotherapy for endometrial cancer with microsatellite instability-high tumors. *Curr Treat Options Oncol.* (2019) 20:83. doi: 10.1007/s11864-019-0679-5
25. Liu J, Liu Y, Wang W, Wang C, Che Y. Expression of immune checkpoint molecules in endometrial carcinoma. *Exp Ther Med.* (2015) 10:1947-52. doi: 10.3892/etm.2015.2714
26. Weiskopf K. Cancer immunotherapy targeting the CD47/SIRPalpha axis. *Eur J Cancer.* (2017) 76:100–9. doi: 10.1016/j.ejca.2017.02.013
27. Engelman JA, Luo J, Cantley LC. The evolution of phosphatidylinositol 3-kinases as regulators of growth and metabolism. *Nat Rev Genet.* (2006) 7:606–19. doi: 10.1038/nrg1879
28. Slomovitz BM, Coleman RL. The PI3K/AKT/mTOR pathway as a therapeutic target in endometrial cancer. *Clin Cancer Res.* (2012) 18:5856–64. doi: 10.1158/1078-0432.CCR-12-0662
29. Sarbassov DD, Guertin DA, Ali SM, Sabatini DM. Phosphorylation and regulation of Akt/PKB by the rictor-mTOR complex. *Science.* (2005) 307:1098–101. doi: 10.1126/science.1106148
30. DiNitto JP, Cronin TC, Lambright DG. Membrane recognition and targeting by lipid-binding domains. *Sci STKE.* (2003) 2003:re16. doi: 10.1126/stke.2132003re16
31. Chen YL, Law PY, Loh HH. Inhibition of PI3K/Akt signaling: an emerging paradigm for targeted cancer therapy. *Curr Med Chem Anticancer Agents.* (2005) 5:575–89. doi: 10.2174/156801105774574649
32. Hennessy BT, Smith DL, Ram PT, Lu Y, Mills GB. Exploiting the PI3K/AKT pathway for cancer drug discovery. *Nat Rev Drug Discov.* (2005) 4:988–1004. doi: 10.1038/nrd1902

Conflict of Interest: The authors declare that the research was conducted in the absence of any commercial or financial relationships that could be construed as a potential conflict of interest.

frontiers in Genetics

ORIGINAL RESEARCH
published: 24 September 2020
doi: 10.3389/fgene.2020.01029

Long Non-coding RNA lnc-GNAT1-1 Suppresses Liver Cancer Progression via Modulation of Epithelial–Mesenchymal Transition

Jianchu Wang[1]†, Wei Wang[1]†, Qianli Tang[1,2]†, Libai Lu[1], Zongjiang Luo[1], Wenchuan Li[1], Yuan Lu[1] and Jian Pu[1]*

[1] Department of Hepatobiliary Surgery, Affiliated Hospital of Youjiang Medical University for Nationalities, Baise, China, [2] Clinic Medicine Research Center of Hepatobiliary Diseases, Affiliated Hospital of Youjiang Medical University for Nationalities, Baise, China

Recent studies have investigated the modulatory roles of long non-coding RNAs in the onset and progression of liver cancer. The present study aimed to elucidate the role of lnc-GNAT1-1 in liver cancer development and to explore the underlying mechanisms. Quantitative real-time polymerase chain reaction was performed to measure the expression levels of lnc-GNAT1-1 in cancerous tissues from patients with liver cancer and in liver cancer cell lines. The proliferative ability and apoptotic rates of liver cancer cells were measured using the counting kit-8 (CCK-8), colony formation, and flow cytometry assays. The abilities to invade and migrate were measured using Transwell assays. Epithelial–mesenchymal transition (EMT)-related proteins, E-cadherin, N-cadherin, and vimentin, were measured using western blotting. A nude mouse model was injected with xenografts to evaluate tumor growth *in vivo*. Downregulation of lnc-GNAT1-1 was observed in cancerous tissues from patients with liver cancer and in liver cancer cell lines, and low expression levels of lnc-GNAT1-1 were related to advanced TNM stage. Lnc-GNAT1-1 knockdown promoted invasion, migration, and proliferation of liver cancer cells and inhibited apoptosis, while lnc-GNAT1-1 upregulation exerted the opposite effects. The expression levels of lnc-GNAT1-1 negatively correlated with *in vivo* tumor growth in a xenograft nude mouse model. Mechanistic experiments revealed that lnc-GNAT1-1 exerted anti-tumor effects in liver cancer cells by inhibiting EMT. In conclusion, this study suggests that lnc-GNAT1-1 suppresses liver cancer progression by modulating EMT.

Keywords: long non-coding RNA, liver cancer, lnc-GNAT1-1, anti-tumour, EMT

OPEN ACCESS

Edited by:
Xiaochen Wang,
University of Texas Southwestern Medical Center, United States

Reviewed by:
Arsheed A. Ganaie,
University of Minnesota Twin Cities, United States
Xiaoling Weng,
Fudan University, China

***Correspondence:**
Jianchu Wang
wjianchu@sina.com

†*These authors share first authorship*

Specialty section:
This article was submitted to Cancer Genetics, a section of the journal Frontiers in Genetics

Received: *11 May 2020*
Accepted: *11 August 2020*
Published: *24 September 2020*

Citation:
Wang J, Wang W, Tang Q, Lu L, Luo Z, Li W, Lu Y and Pu J (2020) Long Non-coding RNA lnc-GNAT1-1 Suppresses Liver Cancer Progression via Modulation of Epithelial–Mesenchymal Transition. Front. Genet. 11:1029. doi: 10.3389/fgene.2020.01029

INTRODUCTION

Liver cancer was the fourth leading cause of cancer death in 2018 (Bray et al., 2018). It was also one of the five leading causes of death in China (Zhou et al., 2019). In recent years, tremendous advances have been made in liver cancer treatment, including liver resection, radiofrequency and microwave ablation, liver transplantation, and chemotherapy. The early detection rate of human cancer has increased, and this has improved survival (Couri and Pillai, 2019). Nevertheless, liver cancer detected at advanced stages remains difficult to treat and survival rates remain low. It is therefore essential to explore the molecular mechanisms underlying liver cancer initiation and progression to offer novel insights for treatment.

Long non-coding RNAs (lncRNAs), that is, those containing more than 200 nucleotides, are a type of non-coding RNA that regulate the initiation and development of various cancers (Cho et al., 2018; Kim et al., 2018; Tang et al., 2019). Several studies have reported that numerous functional lncRNAs play vital roles in the development of various cancers. For example, increasing the expression of lncRNA-PVT1 was reported to decrease the sensitivity of radiotherapy in lung cancer by targeting miR-195 (Wu et al., 2017). Increased lnc-ROR was detected in breast cancer tissues and overexpressed lnc-ROR promoted epithelial–mesenchymal transition (EMT) and tamoxifen resistance by acting as a molecular sponge for miR-205 and increasing the expression of ZEB1 and ZEB2, given the binding sites between miR-205 and ZEB2 (Zhang et al., 2017). Additionally, lnc-ROR also promoted estrogen independence and tamoxifen resistance by activating the MAPK/ERK signaling pathway (Peng et al., 2017). LncRNA-MALAT1 increased levels of β-catenin in nuclear and activated the Wnt/β-catenin signaling pathway to exert oncogenic effects in colorectal cancer (Ji et al., 2013). The important functions of lncRNAs in liver cancer progression were also reported by several studies. For example, Mo et al. (2019) reported that lncRNA-FAM99B affected the prognosis of hepatocellular carcinoma (HCC) and proposed that the molecule may serve as a novel therapeutic target for HCC. Increasing the expression level of lncRNA-PDPK2P promoted invasion, migration, and proliferation of HCC cells by modulating the PDK1/Akt/caspase 3 cascade (Pan et al., 2019). By activating the BMP pathway, lncRNA-HAND2-AS1 enhanced liver cancer stem cell self-renewal and initiated liver cancer progression (Wang et al., 2019).

Previous studies have indicated that lnc-GNAT1-1 plays an anti-tumor role in malignancies of the digestive tract, including colorectal (Ye et al., 2016) and gastric cancers (Liu et al., 2018). Nevertheless, there are no studies of lnc-GNAT1-1 in liver cancer. Therefore, in the present study, we measured the expression levels and explored the potential functions of lnc-GNAT1-1 in liver cancer. We found downregulation of lnc-GNAT1-1 in both liver cancer tissues and cell lines. Cancerous tissues with advanced TNM stage showed lower lnc-GNAT1-1 expression levels. Functional assays showed that lnc-GNAT1-1 suppressed liver cancer cell proliferation, invasion, and migration and promoted apoptosis. *In vivo* studies showed that increasing the expression levels of lnc-GNAT1-1 inhibited the growth of xenograft tumors and that lnc-GNAT1-1 knockdown contributed to cancer development. We also found that lnc-GNAT1-1 exerted anti-tumor effects and may be a new effective therapeutic target for liver cancer.

MATERIALS AND METHODS

Clinical Sample Collection and Processing

A total of 42 paired normal–cancer liver tissues were obtained during surgery from the same patients. The target specimens were washed in DPEC water, cut using special scissors, and immediately stored in liquid nitrogen until RNA extraction. The diagnosis of liver cancer was confirmed through postoperative pathology and all patients were staged on the basis of the World Health Organization criteria for the classification of liver cancer. Before collecting these specimens, no patient had received anti-tumor therapy. Consent was obtained from all patients. We received approval from the ethics committee of the Affiliated Hospital of Youjiang Medical University for Nationalities, Baise, Guangxi Zhuang Autonomous Region, China.

Cell Culture and Mice

The normal human liver cell line LO2 and cancerous cell lines QGY-7703, SMMC-7721, Huh7, Hep3B, and GSG7701 were purchased from the Shanghai Cell Bank. Cells were grown in Dulbecco's modified essential medium containing 10% fetal bovine serum (FBS) and 100 μg/ml penicillin/streptomycin. We used a special incubator containing 5% CO_2 and cultured target cells at 37°C. Female BALB/C nude mice (28–35 days old) were provided by the Animal Core Facility (Shanghai, China) and housed at 25°C under pathogen-free conditions.

RNA Extraction and Quantitative Real-Time Polymerase Chain Reaction (qRT-PCR)

Total RNA was extracted from cancerous tissues of patients with liver cancer and from liver cancer cell lines using TRIzol reagent (Invitrogen, United States), following the manufacturer's protocol. qRT-PCR was performed using SYBR II Premix Taq (Takara, Japan) according to the manufacturer's protocol. GAPDH mRNA was used as the internal reference. All experiments were carried out in triplicate. The PCR primers used were designed as follows: lnc-GNAT1-1 forward: 5′-ATGTGTCCCCAGGTTCCTGTT-3′; lnc-GNAT1-1 reverse: 5′-CCCCTGAGGACTTGAGTAGC-3′; GAPDH forward: 5′-CTGGGCTACACTGAGCACC-3′; GAPDH reverse: 5′-AAGTGGTCGTTGAGGGCAATG-3′.

Plasmid Construction and Transfection

The lnc-GNAT1-1 expression vector LV-lnc-GNAT1-1 was provided by Genepharm (Hangzhou, China). The sh-RNA used to silence lnc-GNAT1-1 in liver cancer cell lines and corresponding sh-NC were also purchased from Genepharm. The transfection was carried out using Lipofectamine 2000 (Invitrogen, United States) according to the manufacturer's protocol. The QGY-7703 cell line was transfected with LV-lnc-GNAT1-1 to construct cell lines overexpressing lnc-GNAT1-1 and was screened with 2.0 μg/ml puromycin for 14 days. Sh-RNA was transfected into the SMMC-7721 cell line to construct cell lines silencing lnc-GNAT1-1 and these cells were also screened with puromycin (2.0 μg/ml) for 14 days. Fluorescence was measured after 48 h.

Counting Kit-8 (CCK-8) Assay

After transfection, SMMC-7721 and QGY-7703 cells were seeded into 96-well plates containing approximately 1,000 cells per well.

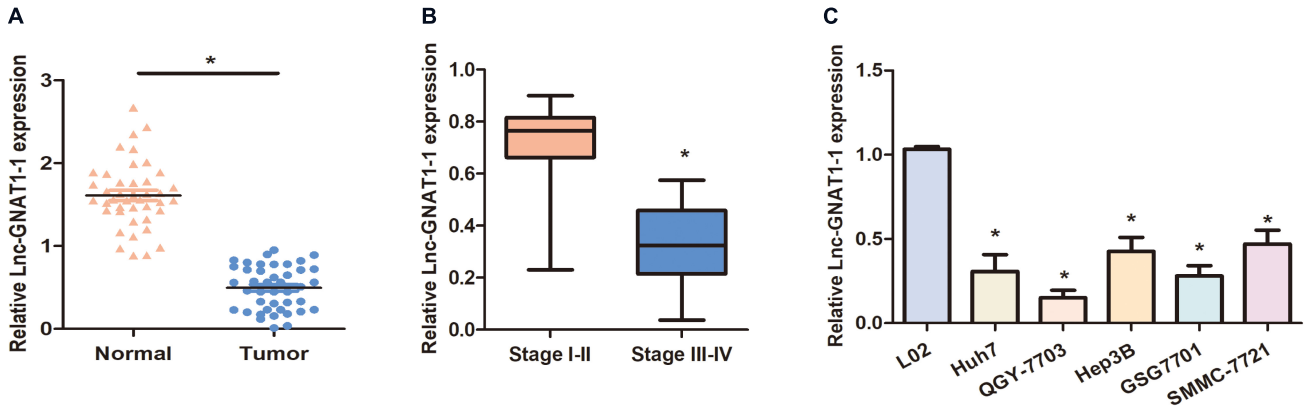

FIGURE 1 | Downregulation of lnc-GNAT1-1 was observed in liver cancer tissues and cell lines. **(A)** Expression levels of lnc-GNAT1-1 in paired normal–cancer liver tissues. **(B)** Expression levels of lnc-GNAT1-1 in liver cancer tissues with various TNM stages. **(C)** Relative lnc-GNAT1-1 expression in liver cancer cell lines. *Significant differences compared with control groups are shown at $P < 0.05$. Each experiment was carried out in triplicate.

Then, we added 10 μl CCK-8 reagent to each well and used a microplate reader (Tecan, Mechelen, Belgium) to measure the optical density at 0, 24, 48, 72, and 96 h. This experiment was carried out three times.

Colony Formation Assay

The transfected SMMC-7721 and QGY-7703 cells were seeded into six-well plates at 500 cells per well and were cultured for 7 days. After visible colonies were formed, 2 ml of 4% paraformaldehyde was added to each well for 15 min. After washing with phosphate-buffered saline (PBS), the wells were stained with a Giemsa stain kit for 30 min. The colonies were counted using an ordinary optical microscope.

Flow Cytometry

The apoptotic rates of target cells were measured using an FITC/Annexin V Apoptosis Detection Kit (BD Biosciences, Franklin Lakes, NJ, United States) on the basis of the manufacturer's protocol. SMMC-7721 cells transfected with sh-lnc-GNAT1-1 or LV-lnc-GNAT1-1 were seeded into six-well plates with 4×10^5 cells per well for 24 h and then harvested and washed twice with PBS. Subsequently, the cells were suspended in 400 μl binding buffer and we added 5 μl propidium iodide and Annexin V-FITC into the cell suspension. Cells were incubated in the dark for 15 min at 37°C. Then, flow cytometry was used to measure the apoptotic rates of these transfected cells.

Cell Migration and Invasion Assays

The invasion and migration assays of SMMC-7721 cells transfected with sh-lnc-GNAT1-1 and QGY-7703 cells transfected with LV-lnc-GNAT1-1 were performed using Transwell chambers with 8 μmol/l pore size (Corning, NY, United States). The target cells were seeded into the upper chamber at 1×10^5 cells per well and cultured with serum-free medium to carry out the invasion (with Matrigel; Beijing, China) and migration assays. Medium containing 20% FBS was added into the lower chamber to serve as a chemoattractant. Using cotton swabs, we removed the non-invading cells and stained invasive or migrated cells with hematoxylin–eosin in the membranes after 24 h incubation.

Subcutaneous Metastasis Model in Nude Mice

Twenty-four mice were randomly divided into four groups. Sh-NC- or sh-lnc-GNAT-1-transfected SMMC-7721 cells and LV-NC- or LV-lnc-GNAT1-1-transfected QGY-7703 cells were seeded into the subcutaneous area of the necks of the nude mice. The tumors were dissected from the mice and the tumor volumes were measured from 12 to 30 days at 3 day intervals. Tumor volume was calculated as (width × length × height)/2. Approval for all animal experiments was obtained from the Institutional Committee for Animal Research.

Western Blotting

Cell suspension was added into 60 mm dishes at 1×10^6 cells per well. Cells were collected and washed with PBS three times. Using RIPA lysis buffer (KeyGen BioTech, Nanjing, China), total protein was extracted from target cells according to the manufacturer's protocol, and the protein concentration was measured using a bicinchoninic acid protein assay kit (KeyGen BioTech). Subsequently, 30 μg of protein was separated using 12% sodium dodecyl sulfate–polyacrylamide gel electrophoresis at 120 V for 1.5 h. Then, the proteins were transferred onto polyvinylidene difluoride membranes (Millipore, Billerica, MA, United States) at 300 mA for 1 h. After blocking the membranes with 5% non-fat skimmed milk for 1.5 h at 20°C, the membranes were incubated with the primary antibodies for 12 h at 4°C. Primary antibodies against GAPDH, N-cadherin, vimentin, and E-cadherin were purchased from Cell Signaling Technology (Denver, CO, United States). The next day, the membranes were further incubated with anti-mouse or anti-rabbit secondary antibodies for 1 h at 20°C. Following three washes with TBS-T (10 min per time), expression levels of these proteins were measured

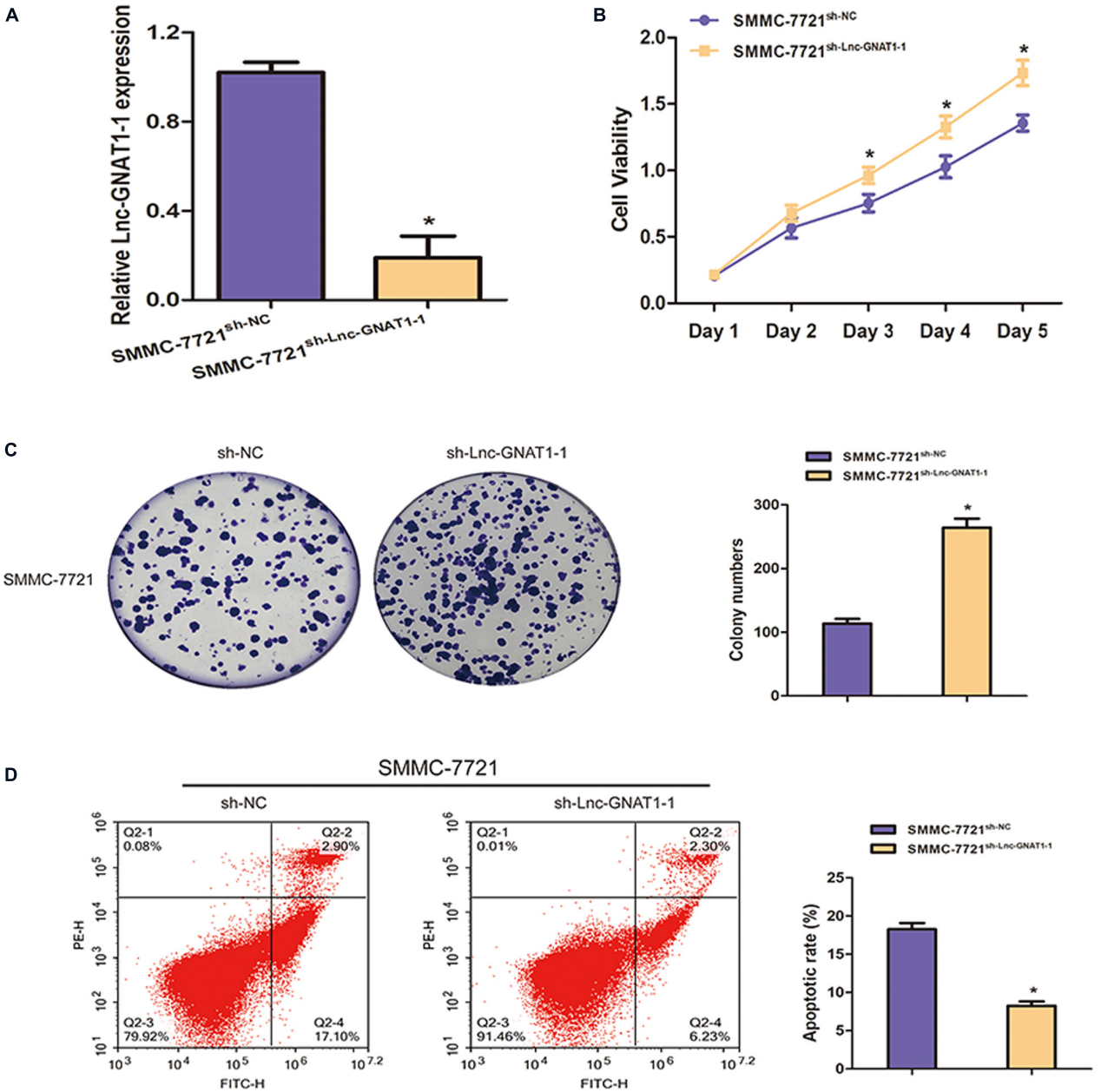

FIGURE 2 | Lnc-GNAT1-1 knockdown enhanced cell proliferative ability and inhibited apoptosis in SMMC-7721 liver cancer cells. **(A)** The expression levels of lnc-GNAT1-1 in SMMC-7721 cells after transfection with sh-lnc-GNAT1-1 or sh-NC. **(B,C)** Cell proliferative ability of SMMC-7721 cells after sh-lnc-GNAT1-1 or sh-NC transfection was examined by CCK-8 assay **(B)** and colony formation assay **(C)**. **(D)** Cell apoptosis was evaluated by flow cytometry. *Significant differences are shown as $P < 0.05$. Each experiment was carried out in triplicate.

using an enhanced chemiluminescence detection kit (Thermo Fisher, United States).

Statistical Analysis

All data were analyzed using SPSS 19.0 software (IBM, Chicago, IL, United States) and are expressed as means ± standard deviation. The paired Student's *t*-test was used to analyze significant differences between groups. Significant differences are shown as $P < 0.05$.

RESULTS

Downregulation of lnc-GNAT1-1 Was Detected in Liver Cancer Tissues and Cell Lines

We carried out qRT-PCR to measure the expression levels of lnc-GNAT1-1 in 42 paired normal–cancer liver tissues. Significant downregulation of lnc-GNAT1-1

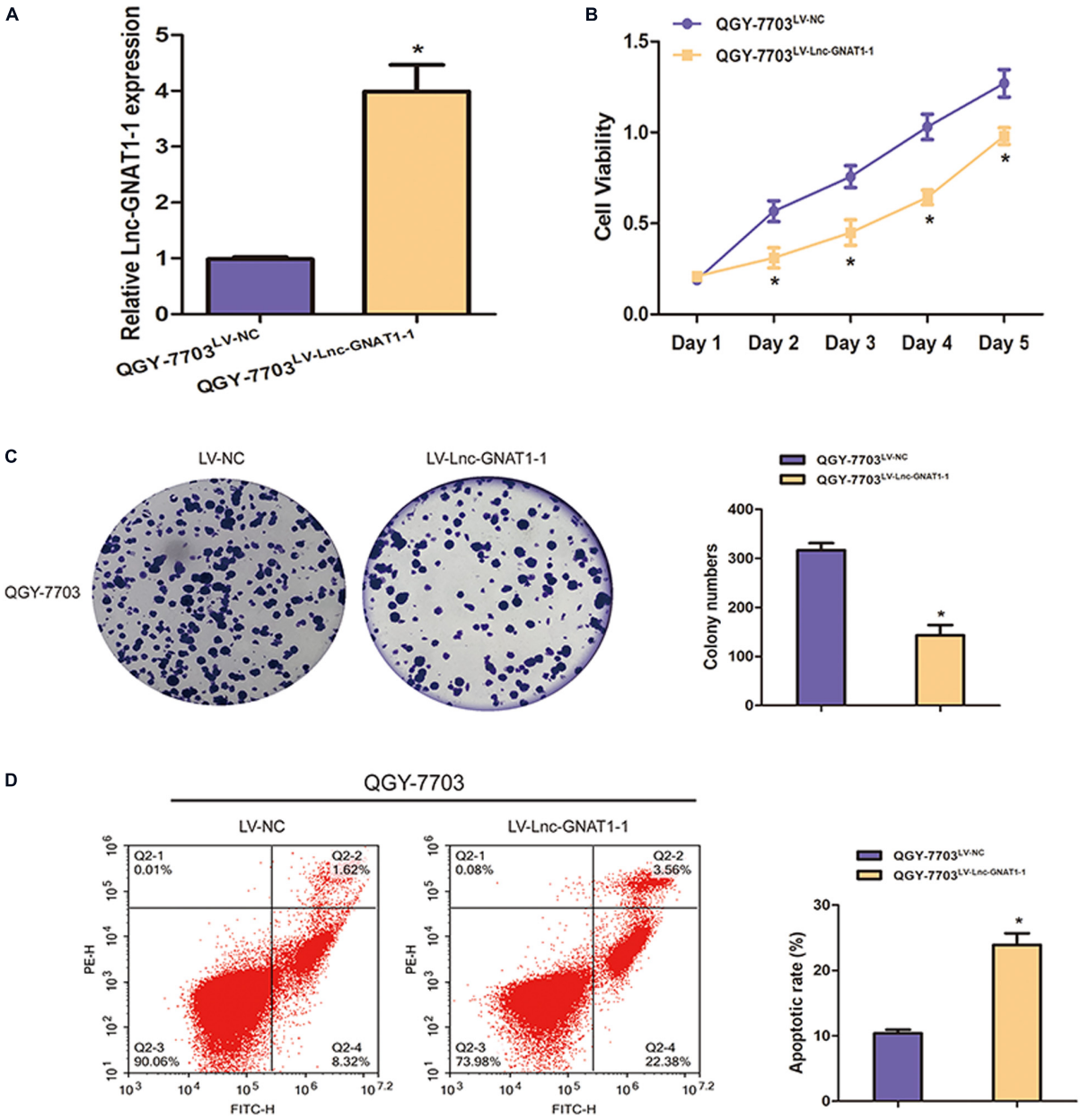

FIGURE 3 | Lnc-GNAT1-1 silencing promoted the invasion and migration of SMMC-7721 liver cancer cells, while lnc-GNAT1-1 overexpression exerted an opposite effect in QGY-7703 cells. **(A,B)** Transwell assays were carried out to evaluate the ability to invade and migrate of SMMC-7721 cells after sh-lnc-GNAT1-1 or sh-NC transfection. **(C,D)** Transwell assays were carried out to evaluate the ability to invade and migrate of QGY-7703 cells after LV-lnc-GNAT1-1 or LV-NC transfection. *Significant differences are shown as $P < 0.05$. Each experiment was carried out in triplicate.

was observed in liver cancer tissues (**Figure 1A**). Low lnc-GNAT1-1 levels in liver cancer tissues negatively correlated with advanced TNM stage (**Figure 1B**). Downregulation of lnc-GNAT1-1 was also observed in the liver cancer cell lines (Huh7, QGY-7703, Hep3B, GSG7701, SMMC-7721) when compared with the normal liver cell line (LO2; **Figure 1C**). These findings suggest that lnc-GNAT1-1 correlated with the progression of liver cancer.

Silencing lnc-GNAT1-1 Promoted Proliferation, Invasion, and Migration and Inhibited Apoptosis of the SMMC-7721 Liver Cancer Cell Line

We constructed an lnc-GNAT1-1-silencing vector (sh-lnc-GNAT1-1) and used an empty vector for comparison. Expression levels of lnc-GNAT1-1 in the control group were approximately fivefold higher than those in the silencing group (**Figure 2A**).

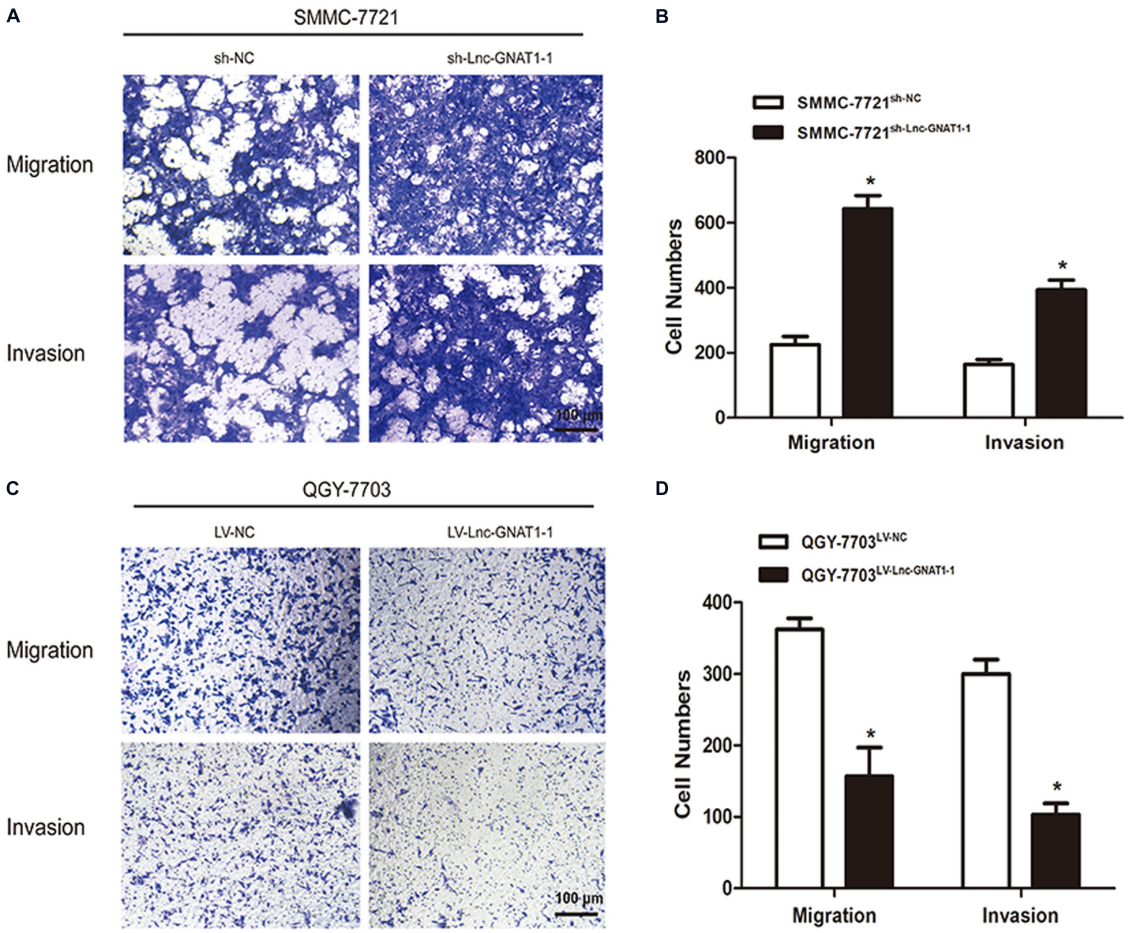

FIGURE 4 | Lnc-GNAT1-1 overexpression suppressed cell proliferation and promoted apoptosis in QGY-7703 liver cancer cells. **(A)** Quantitative real-time polymerase chain reaction analysis of lnc-GNAT1-1 expression levels in QGY-7703 cells after transfection with LV-lnc-GNAT1-1 or LV-NC. **(B,C)** Cell proliferative ability of QGY-7703 cells after LV-lnc-GNAT1-1 or LV-NC transfection was detected by CCK-8 assay **(B)** and colony formation assay **(C)**. **(D)** Apoptosis was evaluated by flow cytometry. *Significant differences are shown as $P < 0.05$. Each experiment was carried out in triplicate.

The CCK-8 assay indicated that the proliferative ability of SMMC-7721 cells transfected with sh-lnc-GNAT1-1 was greater than that of cells in the sh-NC group, and this result was consistent with that of the colony formation assay (**Figures 2B,C**). Cell invasion and migration assays revealed that the ability to invade and migrate was significantly enhanced in the sh-lnc-GNAT1-1 group (**Figures 3A,B**). Apoptosis was suppressed after sh-lnc-GNAT1-1 transfection in SMMC-7721 cells (**Figure 2D**).

Upregulation of lnc-GNAT1-1-Inhibited Liver Cancer Cell Proliferation, Invasion, and Migration and Increased Apoptosis Rates

LV-lnc-GNAT1-1 was transfected into the QGY-7703 liver cancer cell line to upregulate the expression of lnc-GNAT1-1 (**Figure 4A**). The proliferation, invasion, and migration of QGY-7703 cells were significantly inhibited by overexpression of lnc-GNAT1-1 compared with values from the control group (**Figures 3C,D**, **4B,C**). Apoptosis was markedly induced after LV-lnc-GNAT1-1 transfection (**Figure 4D**).

Lnc-GNAT1-1 Suppressed *in vivo* Liver Cancer Growth of Xenograft Tumors

SMMC-7721 cells transfected with sh-lnc-GNAT1-1 or sh-NC and QGY-7703 cells transfected with LV-lnc-GNAT1-1 or LV-NC were injected into the subcutaneous area of the necks of nude mice. After dissection, tumor volume was measured, and a greater tumor volume was observed in the sh-lnc-GNAT1-1 group than in the control group (**Figures 5A,B**). Similarly, reduced tumor volume was found in QGY-7703 cells that had been transfected with LV-lnc-GNAT1-1 (**Figures 5C,D**).

Lnc-GNAT1-1 Exerts Regulatory Effects in Liver Cancer Progression by Modulating EMT

The expression levels of EMT-related proteins in SMMC-7721 cells were measured using western blotting assays.

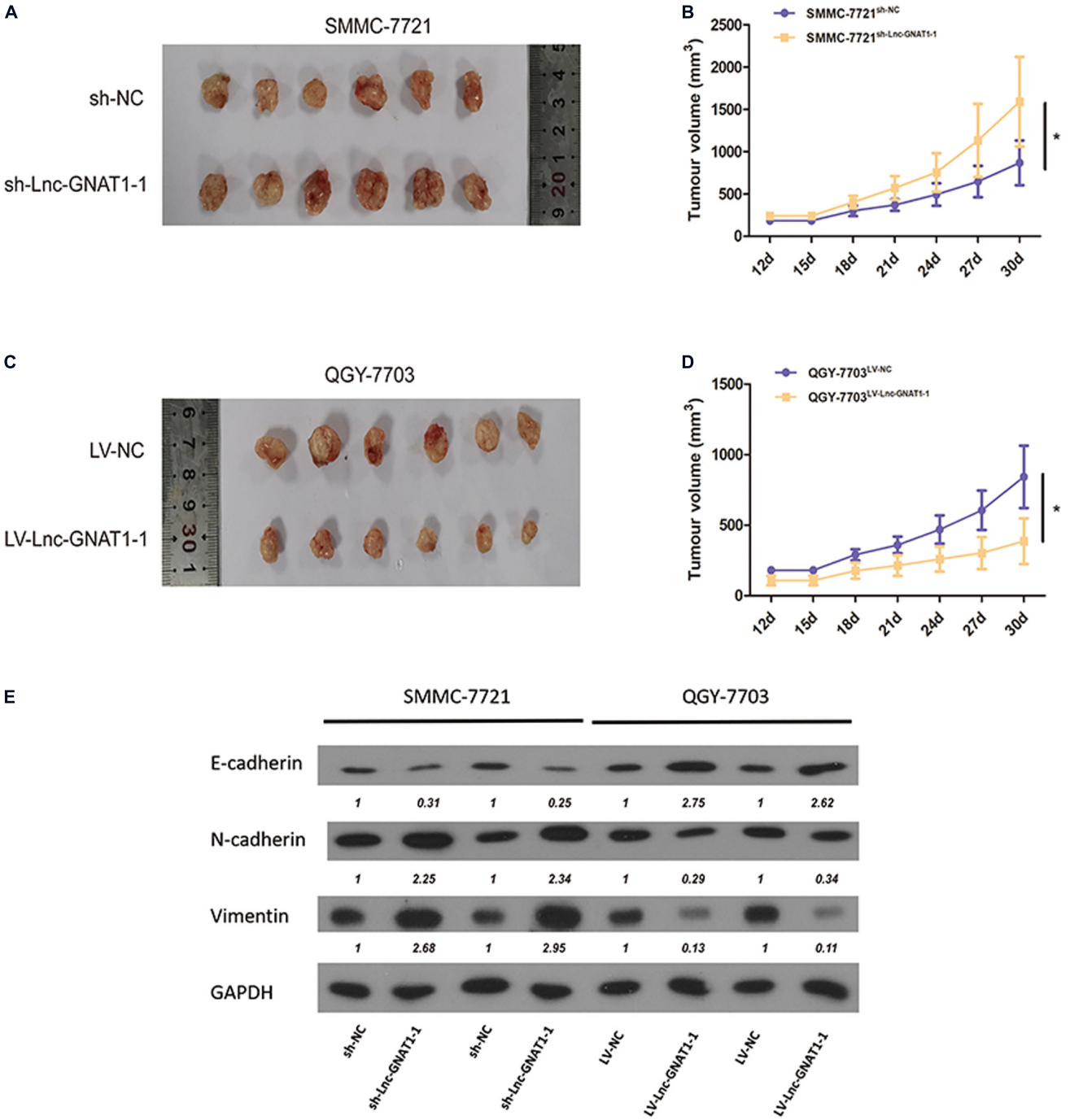

FIGURE 5 | Knockdown of lnc-GNAT1-1 promoted *in vivo* tumor growth of the xenograft model in nude mice, while lnc-GNAT1-1 overexpression exerted the opposite effect. The underlying mechanism may be that lnc-GNAT1-1 downregulated EMT. **(A,B)** Tumor volume changed in mice injected with SMMC-7721 cells after sh-lnc-GNAT1-1 or sh-NC transfection. **(C,D)** Tumor volume changed in mice injected with QGY-7703 cells after LV-lnc-GNAT1-1 or LV-NC transfection. **(E)** The expression levels of E-cadherin, N-cadherin, and vimentin in QGY-7703 cells transfected with LV-lnc-GNAT1-1 or LV-NC and SMMC-7721 cells transfected with sh-lnc-GNAT1-1 or sh-NC. *Significant differences are shown as $P < 0.05$.

Downregulated expression levels of E-cadherin and upregulated expression levels of vimentin and N-cadherin were found in the sh-lnc-GNAT1-1 group (**Figure 5E**). Upregulated expression levels of E-cadherin and downregulated expression levels of N-cadherin and vimentin were found in QGY-7703 cells with LV-lnc-GNAT1-1 transfection (**Figure 5E**). These results suggest that lnc-GNAT1-1 inhibited liver cancer progression by downregulating EMT.

DISCUSSION

In recent years, lncRNAs have attracted increasing attention because of their important regulatory roles in gene expression (Canzio et al., 2019; Lin et al., 2019; Mumbach et al., 2019); an immense amount of investigation has revealed that lncRNAs are involved in cancer onset and development (Esposito et al., 2019; Hu et al., 2019). For example, lncRNA-PVT1 regulates the development of a variety of cancers by interacting with the c-*Myc* gene, acting as a molecular sponge of various microRNAs (miRNAs) and modulating gene transcription and protein expression (Li et al., 2019). LncRNAs can be utilized as diagnostic biomarkers, prognostic biomarkers, and therapeutic targets to improve survival rates (Li et al., 2019). LncRNA-ATB and many other lncRNAs are defined as indispensable cancer-related lncRNAs (Gao and Lian, 2016; Li et al., 2016, 2017); however, the mechanisms and functions of lncRNAs in malignancies remain elusive.

Among these lncRNAs, lnc-GNAT1-1 attracted our attention because of its important effects in the progression of digestive system cancers. Ye et al. (2016) reported that lnc-GNAT1-1 silencing promoted the malignant phenotypes, especially the invasion and migration of colorectal cancer cells, and upregulation of lnc-GNAT1-1 showed the opposite effect. The authors also found that lnc-GNAT1-1 was related to the occurrence of liver metastasis in colorectal cancer, which is rarely reported. The underlying mechanism is thought to be related to the regulation of the RKIP-NF-κB-Snail circuit (Ye et al., 2016). Downregulation of lnc-GNAT1-1 was observed in patients with gastric cancer and lower levels of *Helicobacter pylori* infection and increased expression levels of lnc-GNAT1-1 suppressed gastric cancer growth by inactivating the Wnt/β-catenin pathway (Liu et al., 2018). Against this background, we explored the roles of lnc-GNAT1-1 in liver cancer development and the mechanisms used by lnc-GNAT1-1 to exert modulatory effects on liver cancer progression.

In this present study, we observed obvious downregulation of lnc-GNAT1-1 in liver cancer tissues as well as in cell lines (SMMC-7721, QGY-7703, Huh7, Hep3B, and GSG7701). Among these cell lines, lnc-GNAT1-1 showed higher expression levels in SMMC-7721 and lower levels in QGY-7703. We carried out lnc-GNAT1-1 knockdown in SMMC-7721 cells and overexpressed lnc-GNAT1-1 in QGY-7703 cells. Functional assays showed that downregulation of lnc-GNAT1-1 promoted proliferation, invasion, migration, and *in vivo* growth and reduced cell apoptosis rates in liver cancer cells, while lnc-GNAT1-1 overexpression had the opposite effects.

EMT is crucial for metastasis and invasion of various cancer cells, and upregulation of EMT has been observed in many types of cancer, including liver cancer (Thiery et al., 2009). E-cadherin, N-cadherin, and vimentin are three vital proteins that are normally regarded as EMT markers. E-cadherin inhibits EMT, and vimentin and N-cadherin induce it. The excessive activation of EMT induces loss of cell–cell contacts because of the absence of E-cadherin (Gheldof and Berx, 2013; Wong et al., 2018; Loh et al., 2019). Overexpression of vimentin and N-cadherin contributes to increased cell motility; as a result, these cells easily spread to distant or surrounding tissues (Liu et al., 2015; Loh et al., 2019; Rai and Ahmed, 2019). In liver cancer, studies have found that EMT activation induces liver fibrogenesis and carcinogenesis (Pinzani, 2011) and also promotes the invasion and migration of liver cancer cells (Peng et al., 2018; Zhang et al., 2018). In the present study, the investigation of underlying mechanisms revealed that lnc-GNAT1-1 exerted regulatory effects by modulating the EMT process in liver cancer cells. Our data revealed that lnc-GNAT1-1 silencing increased the expression levels of N-cadherin and vimentin, and reduced E-cadherin expression, while upregulation of lnc-GNAT1-1 showed the opposite result. These findings suggest that upregulation of lnc-GNAT1-1 enhances invasion and migration in liver cancer via the activation of EMT. Normally, lncRNAs exert biological effects in physiological and pathological processes through binding to miRNAs and reducing their levels (Salmena et al., 2011; Sumazin et al., 2011). However, we have not identified relevant miRNAs targeted by lnc-GNAT1-1 to exert anti-tumor effects in liver cancer; this requires further exploration. The associated miRNAs and other potential target genes may be elucidated in our future studies.

CONCLUSION

Lnc-GNAT1-1 plays an anti-tumor role in digestive tract cancer development and exerts tumor inhibitory activity to suppress cell proliferation, invasion, and migration and to induce apoptosis in liver cancer cells. We found that lnc-GNAT1-1 inhibited liver cancer progression by regulating EMT. Lnc-GNAT1-1 constitutes a new potential target for improving the quality of life of patients with liver cancer.

DATA AVAILABILITY STATEMENT

The raw data supporting the conclusions of this article will be made available by the authors, without undue reservation.

ETHICS STATEMENT

The studies involving human participants were reviewed and approved by Affiliated Hospital of Youjiang Medical University for Nationalities. The patients/participants provided their written informed consent to participate in this study. The animal study was reviewed and approved by Affiliated Hospital of Youjiang Medical University for Nationalities.

AUTHOR CONTRIBUTIONS

JW and JP designed the study and wrote the manuscript. WW, QT, and LL carried out the experiments. ZL, WL, and YL

contributed to data analysis. JP had overall responsibility for the research. All authors approved the final manuscript version.

FUNDING

This work was supported by the Guangxi Clinic Medicine Research Center of Hepatobiliary Diseases (AD17129025), the Guangxi Medical High-level Leading Talents Training "139" Project, Special Funding for Guangxi Special Experts, and The First Batch of High-level Talent Scientific Research Projects of the Affiliated Hospital of Youjiang Medical University for Nationalities in 2019, contract no. R20196302.

SUPPLEMENTARY MATERIAL

The Supplementary Material for this article can be found online at: https://www.frontiersin.org/articles/10.3389/fgene.2020.01029/full#supplementary-material

REFERENCES

Bray, F., Ferlay, J., Soerjomataram, I., Siegel, R. L., Torre, L. A., and Jemal, A. (2018). Global cancer statistics 2018: GLOBOCAN estimates of incidence and mortality worldwide for 36 cancers in 185 countries. *CA Cancer J. Clin.* 68, 394–424. doi: 10.3322/caac.21492

Canzio, D., Nwakeze, C. L., Horta, A., Rajkumar, S. M., Coffey, E. L., Duffy, E. E., et al. (2019). Antisense lncRNA Transcription Mediates DNA Demethylation to Drive Stochastic Protocadherin alpha Promoter Choice. *Cell* 177, 639–53e15. doi: 10.1016/j.cell.2019.03.008

Cho, S. W., Xu, J., Sun, R., Mumbach, M. R., Carter, A. C., Chen, Y. G., et al. (2018). Promoter of lncRNA Gene PVT1 Is a Tumor-Suppressor DNA Boundary Element. *Cell* 173, 1398–412e22. doi: 10.1016/j.cell.2018.03.068

Couri, T., and Pillai, A. (2019). Goals and targets for personalized therapy for HCC. *Hepatol. Int.* 13, 125–137. doi: 10.1007/s12072-018-9919-1

Esposito, R., Bosch, N., Lanzos, A., Polidori, T., Pulido-Quetglas, C., and Johnson, R. (2019). Hacking the Cancer Genome: Profiling Therapeutically Actionable Long Non-coding RNAs Using CRISPR-Cas9 Screening. *Cancer Cell* 35, 545–557. doi: 10.1016/j.ccell.2019.01.019

Gao, K. T., and Lian, D. (2016). Long non-coding RNA MALAT1 is an independent prognostic factor of osteosarcoma. *Eur. Rev. Med. Pharmacol. Sci.* 20, 3561–3565.

Gheldof, A., and Berx, G. (2013). Cadherins and epithelial-to-mesenchymal transition. *Prog. Mol. Biol. Transl. Sci.* 116, 317–336. doi: 10.1016/B978-0-12-394311-8.00014-5

Hu, Q., Ye, Y., Chan, L. C., Li, Y., Liang, K., Lin, A., et al. (2019). Oncogenic lncRNA downregulates cancer cell antigen presentation and intrinsic tumor suppression. *Nat. Immunol.* 20, 835–851. doi: 10.1038/s41590-019-0400-7

Ji, Q., Liu, X., Fu, X., Zhang, L., Sui, H., Zhou, L., et al. (2013). Resveratrol inhibits invasion and metastasis of colorectal cancer cells via MALAT1 mediated Wnt/beta-catenin signal pathway. *PLoS One* 8:e78700. doi: 10.1371/journal.pone.0078700

Kim, J., Piao, H. L., Kim, B. J., Yao, F., Han, Z., Wang, Y., et al. (2018). Long noncoding RNA MALAT1 suppresses breast cancer metastasis. *Nat. Genet.* 50, 1705–1715. doi: 10.1038/s41588-018-0252-3

Li, J., Li, Z., Zheng, W., Li, X., Wang, Z., Cui, Y., et al. (2017). LncRNA-ATB: An indispensable cancer-related long noncoding RNA. *Cell Prolif.* 50:e12381. doi: 10.1111/cpr.12381

Li, L., Gu, M., You, B., Shi, S., Shan, Y., Bao, L., et al. (2016). Long non-coding RNA ROR promotes proliferation, migration and chemoresistance of nasopharyngeal carcinoma. *Cancer Sci.* 107, 1215–1222. doi: 10.1111/cas.12989

Li, M. Y., Tang, X. H., Fu, Y., Wang, T. J., and Zhu, J. M. (2019). Regulatory Mechanisms and Clinical Applications of the Long Non-coding RNA PVT1 in Cancer Treatment. *Front. Oncol.* 9:787. doi: 10.3389/fonc.2019.00787

Lin, H., Jiang, M., Liu, L., Yang, Z., Ma, Z., Liu, S., et al. (2019). The long noncoding RNA Lnczc3h7a promotes a TRIM25-mediated RIG-I antiviral innate immune response. *Nat. Immunol.* 20, 812–823. doi: 10.1038/s41590-019-0379-0

Liu, C. Y., Lin, H. H., Tang, M. J., and Wang, Y. K. (2015). Vimentin contributes to epithelial-mesenchymal transition cancer cell mechanics by mediating cytoskeletal organization and focal adhesion maturation. *Oncotarget* 6, 15966–15983. doi: 10.18632/oncotarget.3862

Liu, L., Shuai, T., Li, B., Zhu, L., and Li, X. (2018). Long noncoding RNA lncGNAT11 inhibits gastric cancer cell proliferation and invasion through the Wnt/betacatenin pathway in *Helicobacter* pylori infection. *Mol. Med. Rep.* 18, 4009–4015. doi: 10.3892/mmr.2018.9405

Loh, C. Y., Chai, J. Y., Tang, T. F., Wong, W. F., Sethi, G., Shanmugam, M. K., et al. (2019). The E-Cadherin and N-Cadherin Switch in Epithelial-to-Mesenchymal Transition: Signaling, Therapeutic Implications, and Challenges. *Cells* 8:1118. doi: 10.3390/cells8101118

Mo, M., Liu, S., Ma, X., Tan, C., Wei, L., Sheng, Y., et al. (2019). A liver-specific lncRNA, FAM99B, suppresses hepatocellular carcinoma progression through inhibition of cell proliferation, migration, and invasion. *J. Cancer Res. Clin. Oncol.* 145, 2027–2038. doi: 10.1007/s00432-019-02954-8

Mumbach, M. R., Granja, J. M., Flynn, R. A., Roake, C. M., Satpathy, A. T., Rubin, A. J., et al. (2019). HiChIRP reveals RNA-associated chromosome conformation. *Nat. Methods* 16, 489–492. doi: 10.1038/s41592-019-0407-x

Pan, W., Li, W., Zhao, J., Huang, Z., Zhao, J., Chen, S., et al. (2019). lncRNA-PDPK2P promotes hepatocellular carcinoma progression through the PDK1/AKT/Caspase 3 pathway. *Mol. Oncol.* 13, 2246–2258. doi: 10.1002/1878-0261.12553

Peng, J. M., Bera, R., Chiou, C. Y., Yu, M. C., Chen, T. C., Chen, C. W., et al. (2018). Actin cytoskeleton remodeling drives epithelial-mesenchymal transition for hepatoma invasion and metastasis in mice. *Hepatology* 67, 2226–2243. doi: 10.1002/hep.29678

Peng, W. X., Huang, J. G., Yang, L., Gong, A. H., and Mo, Y. Y. (2017). Linc-RoR promotes MAPK/ERK signaling and confers estrogen-independent growth of breast cancer. *Mol. Cancer* 16:161. doi: 10.1186/s12943-017-0727-3

Pinzani, M. (2011). Epithelial-mesenchymal transition in chronic liver disease: fibrogenesis or escape from death? *J. Hepatol.* 55, 459–465. doi: 10.1016/j.jhep.2011.02.001

Rai, K. H., and Ahmed, J. (2019). A Correlative Study of N-Cadherin Expression with Different Grades of Oral Squamous Cell Carcinoma Projecting as a Marker of Epithelial to Mesenchymal Transition in Tumor Progression. *Asian Pac. J. Cancer Prev.* 20, 2327–2332. doi: 10.31557/APJCP.2019.20.8.2327

Salmena, L., Poliseno, L., Tay, Y., Kats, L., and Pandolfi, P. P. (2011). A ceRNA hypothesis: the Rosetta Stone of a hidden RNA language? *Cell* 146, 353–358. doi: 10.1016/j.cell.2011.07.014

Sumazin, P., Yang, X., Chiu, H. S., Chung, W. J., Iyer, A., Llobet-Navas, D., et al. (2011). An extensive microRNA-mediated network of RNA-RNA interactions regulates established oncogenic pathways in glioblastoma. *Cell* 147, 370–381. doi: 10.1016/j.cell.2011.09.041

Tang, X., Qiao, X., Chen, C., Liu, Y., Zhu, J., and Liu, J. (2019). Regulation Mechanism of Long Noncoding RNAs in Colon Cancer Development and Progression. *Yonsei Med. J.* 60, 319–325. doi: 10.3349/ymj.2019.60.4.319

Thiery, J. P., Acloque, H., Huang, R. Y., and Nieto, M. A. (2009). Epithelial-mesenchymal transitions in development and disease. *Cell* 139, 871–890. doi: 10.1016/j.cell.2009.11.007

Wang, Y., Zhu, P., Luo, J., Wang, J., Liu, Z., Wu, W., et al. (2019). LncRNA HAND2-AS1 promotes liver cancer stem cell self-renewal via BMP signaling. *EMBO J.* 38:e101110. doi: 10.15252/embj.2018101110

Wong, S. H. M., Fang, C. M., Chuah, L. H., Leong, C. O., and Ngai, S. C. (2018). E-cadherin: Its dysregulation in carcinogenesis and clinical implications. *Crit. Rev. Oncol. Hematol.* 121, 11–22. doi: 10.1016/j.critrevonc.2017.11.010

Wu, D., Li, Y., Zhang, H., and Hu, X. (2017). Knockdown of Lncrna PVT1 Enhances Radiosensitivity in Non-Small Cell Lung Cancer by

Sponging Mir-195. *Cell Physiol. Biochem.* 42, 2453–2466. doi: 10.1159/000480209

Ye, C., Shen, Z., Wang, B., Li, Y., Li, T., Yang, Y., et al. (2016). A novel long non-coding RNA lnc-GNAT1-1 is low expressed in colorectal cancer and acts as a tumor suppressor through regulating RKIP-NF-kappaB-Snail circuit. *J. Exp. Clin. Cancer Res.* 35:187. doi: 10.1186/s13046-016-0467-z

Zhang, H. Y., Liang, F., Zhang, J. W., Wang, F., Wang, L., and Kang, X. G. (2017). Effects of long noncoding RNA-ROR on tamoxifen resistance of breast cancer cells by regulating microRNA-205. *Cancer Chemother. Pharmacol.* 79, 327–337. doi: 10.1007/s00280-016-3208-2

Zhang, Y. Y., Kong, L. Q., Zhu, X. D., Cai, H., Wang, C. H., Shi, W. K., et al. (2018). CD31 regulates metastasis by inducing epithelial-mesenchymal transition in hepatocellular carcinoma via the ITGB1-FAK-Akt signaling pathway. *Cancer Lett.* 429, 29–40. doi: 10.1016/j.canlet.2018.05.004

Zhou, M., Wang, H., Zeng, X., Yin, P., Zhu, J., Chen, W., et al. (2019). Mortality, morbidity, and risk factors in China and its provinces, 1990–2017: a systematic analysis for the Global Burden of Disease Study 2017. *Lancet* 394, 1145–1158. doi: 10.1016/S0140-6736(19)30427-1

Conflict of Interest: The authors declare that the research was conducted in the absence of any commercial or financial relationships that could be construed as a potential conflict of interest.

frontiers in Genetics

ORIGINAL RESEARCH
published: 16 October 2020
doi: 10.3389/fgene.2020.00929

Long Non-coding RNA Colon Cancer-Associated Transcript-1 Promotes Migration, Invasion, and Epithelial Mesenchymal Transition of Lung Adenocarcinoma by Suppressing miR-219-1

Wenbo Wang[1], Zhiliang Hou[1], Chengcai Wen[2], Liyue Ge[3] and Lili Ge[4]**

[1]Department of Thoracic Surgery, Henan Provincial Chest Hospital, Zhengzhou, China, [2]Huai'an Second People's Hospital and The Affiliated Huai'an Hospital of Xuzhou Medical University, Huai'an, China, [3]Department of Oncology, Huai'an Second People's Hospital and The Affiliated Huai'an Hospital of Xuzhou Medical University, Huai'an, China, [4]Department of Clinical Laboratory, Huai'an Second People's Hospital and The Affiliated Huai'an Hospital of Xuzhou Medical University, Huai'an, China

OPEN ACCESS

Edited by:
Xiao-Jie Lu,
Nanjing Medical University, China

Reviewed by:
Qingchun Lu,
Northwestern Medicine, United States
Xiaoling Weng,
Fudan University, China

***Correspondence:**
Liyue Ge
gly671129@163.com
Lili Ge
gelili13861587076@126.com

Specialty section:
This article was submitted to Cancer Genetics, a section of the journal Frontiers in Genetics

Received: *01 June 2020*
Accepted: *27 July 2020*
Published: *16 October 2020*

Citation:
Wang W, Hou Z, Wen C, Ge L and Ge L (2020) Long Non-coding RNA Colon Cancer-Associated Transcript-1 Promotes Migration, Invasion, and Epithelial Mesenchymal Transition of Lung Adenocarcinoma by Suppressing miR-219-1. Front. Genet. 11:929. doi: 10.3389/fgene.2020.00929

Previous evidence suggests that long non-coding colon cancer-associated transcript-1(CCAT1) plays a pivotal role in the progression of a variety of tumors. However, little is known about its role in lung adenocarcinoma (LAD). In this study, we found LAD tissue samples had a higher expression of CCAT1 but a lower expression of miR-219-1 compared to their adjacent non-tumor tissues. CCAT1 negatively regulated the expression of miR-219-1. miR-219-1 suppressed the proliferation of A549 and H1299 cells. Knockdown of CCAT1 inhibited the proliferation, migration, and invasion of A549 and H1299 cells, which were reversed by the miR-219-1 inhibitor. CCAT1 knockdown increased the expression of E-cadherin but decreased the expressions of N-cadherin and vimentin, which were restored by the miR-219-1 inhibitor. *In vivo*, knockdown of CCAT1 suppressed the tumor growth of LAD xenografts, which were rescued by the inhibition of miR-219-1. In summary, our findings suggested that CCAT1 promotes the progression of LAD *via* sponging miR-219-1, providing a potential therapeutic target for LAD.

Keywords: lung adenocarcinoma, colon cancer-associated transcript-1, miR-219-1, epithelial-mesenchymal transition, invasion

INTRODUCTION

Lung cancer is the leading cause of cancer-related death in China and worldwide (Bray et al., 2018). Of note, lung adenocarcinoma (LAD) is the most common subtype of non-small-cell lung cancer with high rates of mortality and metastasis (Travis et al., 2015). Despite the advances in therapeutic strategies in the last few decades, the prognosis of LAD patients is still unsatisfying (Miller et al., 2016). LAD can spread to lymph nodes, contralateral lung, and distant organs because of early invasion and metastasis (Guan et al., 2019). Efforts in uncovering the molecular

mechanisms of LAD's aggressiveness would facilitate the development of novel and effective therapeutic targets or prognostic biomarkers.

Long non-coding RNAs (lncRNAs) are a class of non-protein-coding transcripts longer than 200 nucleotides in length. Dysregulation of some lncRNAs promotes cellular processes related to cancer, including proliferation, invasion, metastasis, apoptosis, and drug resistance (Lu et al., 2017; Guan et al., 2019; Hu et al., 2019; Wang et al., 2019). Therefore, lncRNAs are considered a group of promising markers for predicting cancer prognosis and developing new therapeutic strategies. LncRNA colon cancer-associated transcript-1(CCAT1) was significantly upregulated in colon cancer tissue and cells (Nissan et al., 2012). Recently, CCAT1 has been studied in various cancers (Guo and Hua, 2017; Shi et al., 2017; Han et al., 2019; Hu et al., 2019; Li G. et al., 2019). CCAT1 plays a role in promoting the proliferation and invasion of cervical cancer by regulating the miR-181a-5p/MMP14 axis (Shen et al., 2019) and promotes endometrial carcinoma progression by miR-181a-5p (Yu et al., 2019). CCAT1 was also found to be an oncogene in nasopharyngeal carcinoma (Dong et al., 2018).

Silencing CCAT1 suppressed the proliferation, migration, and invasion and epithelial-mesenchymal transition (EMT) in NSCLC (Dong et al., 2018). However, the roles of CCAT1 in the pathogenesis of LAD remained mostly unknown. In this study, we observed significant upregulation of CCAT1 in LAD tissues compared to adjacent non-tumor tissues. The expression of CCAT1 was negatively associated with the expression of miR-219-1. CCAT1 promoted the growth of LAD xenografts *via* regulating miR-219-1. This study unveiled a potential therapeutic target for treating LAD.

MATERIALS AND METHODS

Patient Samples

Twenty pairs of tumor and adjacent non-tumor tissues were collected from patients who received surgery for LAD at the Henan Provincial Chest Hospital between June 2016 and June 2018. Immediately after surgery, these tissues were snap-frozen using liquid nitrogen and were subsequently stored at a temperature of −80°C for future RNA extraction. No patients received radiotherapy or chemotherapy before surgery in this study. We obtained informed consent from all patients. The study was approved by the Ethics Committee of the Henan Provincial Chest Hospital.

Cell Culture and Transfection

Two human LAD cell lines (A549 and H1299) were cultured in RPMI1640 medium supplemented with 10% fetal bovine serum (10099141, Invitrogen), 100 U/ml penicillin, and 100 μg/ml streptomycin (Invitrogen). A549 and H1299 are widely used as models of LAD. The condition was set as 5% CO_2 at 37°C in a humidified incubator. The short hairpin RNAs against CCAT1 (CCAT1 shRNA and CCAT1 shRNA-2), control (shRNA NC), miR-219-1 mimic, and miR-219-1 inhibitor were designed by the Genepharma Co., Ltd. (Shanghai, China). Cell transfection was carried out using Lipofectamine 3000 (Invitrogen, CA, United States) in line with the manufacturer's instructions. Quantitative real-time PCR (qRT-PCR) was used to confirm the efficiency of transfection. The cells were harvested for analysis 48 h after transfection.

Luciferase Reporter Assays

The mutant (miR-219-1-MUT) and wild (miR-219-1-WT) types of miR-219-1 were cloned into the plasmid pGL3 (Promega). The CCAT1 luciferase vector was co-transfected with miR-219-1, miR-219-1-MUT, or miR-219-1-WT into HEK-239 T cells. After 48 h of transfection, the luciferase reporter assay was analyzed using the GloMax Multi Plus (Promega).

RNA Extraction and Quantitative Real-Time PCR

Total RNA was extracted from the LAD tissues or cultured cell lines using the TRIzol reagent (15596018, Invitrogen, Thermo Fisher Scientific, United States). Total RNA was reverse transcribed to cDNA using the M-MLV reverse transcriptase (M1705, Promega, Madison, WI, United States). Real-time PCR analyses were performed with the SYBR Green system (Q221, Vazyme Biotech Co, Nanjing, China). The relative expression was calculated using the comparative threshold cycle method. Results were normalized to the expression of GAPDH for CCAT1 or U6 for miR-219-1, E-cadherin, N-cadherin, and vimentin.

Cell Proliferation

We used the cell counting kit-8 (CCK-8; CK04, Dojindo, Kumamoto, Japan) to assess cell viability. Briefly, LAD cells transfected with shRNA NC, CCAT1 shRNA, or the miR-219-1 inhibitor were seeded in 96-well plates (1×10^4 cells/well). Incubation lasted 1 h at 37°C in 5% CO_2. Changes in cell viability were measured at 0, 1, 2, 3, 4, and 5 days. The absorbance at 450 nm was performed with a microplate reader Model 680 (Bio-Rad, CA, United States). All experiments were performed in triplicate.

Wound-Healing Assay

Following transfection, we seeded cells in six-well plates (4×10^5 cells/well) and cultured them until they reached approximately 90% confluence. Cell monolayers were scratched using a 200 μl pipette tip and were then cultured for 48 h. The scratched areas were photographed with the help of an inverted microscope and digital imaging system (Olympus, Japan) at 0 and 24 h.

Cell Invasion Assay

The capacity of cell invasion was determined using 24-well Transwell chambers (3374, Corning, United States). Forty-eight hours post-transfection, we seeded the cells at a density of 5×10^4 into the upper chamber of an insert coated with Matrigel (BD biosciences, United States) and filled the wells with 500 μl RPMI1640 containing 10% FBS. After incubation at 37°C for 48 h, we removed the cells on the upper side of the membrane with clean cotton swabs, fixed the cells on the

underside with 1% formaldehyde solution for 15 min, and stained them with 0.1% of crystal violet for 15 min. Ten fields randomly selected were viewed under an inverted microscope. Experiments were conducted in triplicate.

Xenograft Model

Male nude mice (8 weeks old) were purchased from the Model Animal Research Center of Nanjing University. The mice were housed under standard conditions with free access to food and water. The nude mice were randomly divided into six groups (six per group): A549 + shRNA NC, A549 + CCAT1 shRNA, A549 + CCAT1 shRNA + miR-219-1 inhibitor, H1299 + shRNA NC, H1299 + CCAT1 shRNA, and H1299 + CCAT1 shRNA + miR-219-1 inhibitor. An amount of 1×10^7 cells were subcutaneously injected into the right rear limb of each mouse. The mice were weighed and the xenografts were measured every 3 days. The tumor volume was calculated as follows: tumor volume = (length × width^2)/2. After 13 days, the mice were sacrificed, and the xenografts were harvested for further experiments. All procedures were approved by the Animal Care and Use Committee of the Huai'an Second People's Hospital.

Western Blot Analysis

The proteins of LAD tissues and cell lines were extracted with RIPA lysis buffer (KGP702, KeyGene Biotech, Nanjing, China). The protein concentration was measured using the Pierce™ BCA Protein Assay Kit (23227, Thermo Scientific™, United States). We separated equal amounts of protein (60ug) by 10% SDS-PAGE and transferred them to PVDF membranes. Firstly, we blocked the membranes using 5% non-fat milk in TBS Tween 20 (TBST). Then we incubated the membranes with primary antibodies in 5% bovine at 4°C overnight. The primary antibodies included E-cadherin (4A2C7, Invitrogen), N-cadherin (3B9, Invitrogen), and vimentin (V9, Invitrogen). The GAPDH antibody was used as a control. The membranes were washed three times with TBST and were incubated with horseradish peroxidase-conjugated secondary antibodies. The bands were measured using the Enhanced Chemiluminescence Kit (GE Healthcare, Chicago, IL, United States).

Statistical Analysis

Statistical analysis was performed using SPSS version 22.0 (SPSS, IBM, United States). Differences between groups were compared by two-tailed Student's *t*-test. Correlation between CCAT1 and miR-219-1 was calculated with Spearman correlation analysis. Data are shown as means and standard deviations (SD). Differences were considered statistically significant if $p < 0.05$. $^*p < 0.05$; $^{**}p < 0.01$.

RESULTS

CCAT1 Is Upregulated in LAD Tissues

qRT-PCR was conducted to examine the relative expression of CCAT1 and miR-219-1 in 20 pairs of cancer and corresponding adjacent non-tumor tissues from patients with LAD. We found that lncRNA CCAT1 was significantly upregulated in LAD tissues compared to adjacent non-tumor tissues (**Figure 1A**). At the same time, the expression of miR-219-1 was significantly lower in LAD tissues compared to adjacent non-tumor tissues (**Figure 1B**). We also found that CCAT1 was negatively correlated with miR-219-1 (**Figure 1C**, Pearson's $r = -0.22$, $p < 0.05$). To determine the relationship between CCAT1 and miR-219-1, bioinformatics analysis identified a potential miR-219-1 binding site in CCAT1 (**Figure 1D**).

Next, we used the luciferase reporter assay to validate the binding capability of miR-219-1 to CCAT1. We observed that the luciferase activity was reduced in cells transfected with miR-219-1-WT (**Figure 1E**). After transfection with CCAT1 shRNA and CCAT1 shRNA-2, the expression of miR-219-1 was significantly increased in both A549 and H1299 cells (**Figures 1F,G**). Moreover, knockdown of CCAT1 markedly suppressed the proliferation of A549 and H1299 cells (**Figures 1H,I**). These results suggested that CCAT1 promoted the proliferation of A549 and H1299 cells and negatively regulated miR-219-1.

Then we examined the effects of miR-219-1 in A549 and H1299 cells using the miR-219-1 mimic and inhibitor. We confirmed that the expressions of miR-219-1 in A549 and H1299 were successfully upregulated by the miR-219-1 mimic (**Figure 1J**). The cell viability of A549 and H1299 was significantly suppressed by the overexpression of miR-219-1 (**Figures 1K,L**). Additionally, the expressions of miR-219-1 in A549 and H1299 were inhibited by the miR-219-1 inhibitor (**Figure 1M**). The inhibition of miR-219-1 significantly increased the cell viability of A549 and H1299 (**Figures 1N,O**). These results suggested that miR-219-1 suppressed the proliferation of A549 and H1299 cells.

Knockdown of CCAT1 Inhibits LAD Cell Proliferation *via* miR-219-1

CCAT1 shRNA was used in subsequent experiments. The transfection efficiency was validated by qRT-PCR. Following transfection with CCAT1 shRNA, the CCAT1 expression was significantly decreased while the expression of miR-219-1 was increased in A549 and H1299 cells (**Figures 2A–D**). Co-transfection with CCAT1 shRNA and the miR-219-1 inhibitor did not affect the expression of CCAT1 and removed the inhibition effect of CCAT1 shRNA on the expression of miR-219-1 (**Figures 2A–D**). Downregulation of CCAT1 continuously suppressed the proliferation of A549 and H1299 cells, which could be rescued by the miR-219-1 inhibitor (**Figures 2E,F**). These results indicated that CCAT1 modulated the proliferation of LAD cells by targeting miR-219-1.

CCAT1 Knockdown Inhibits LAD Cell Migration and Invasion *via* miR-219-1

To further delineate the roles of CCAT1 and miR-219-1 in the migration and invasion of LAD cells, we used

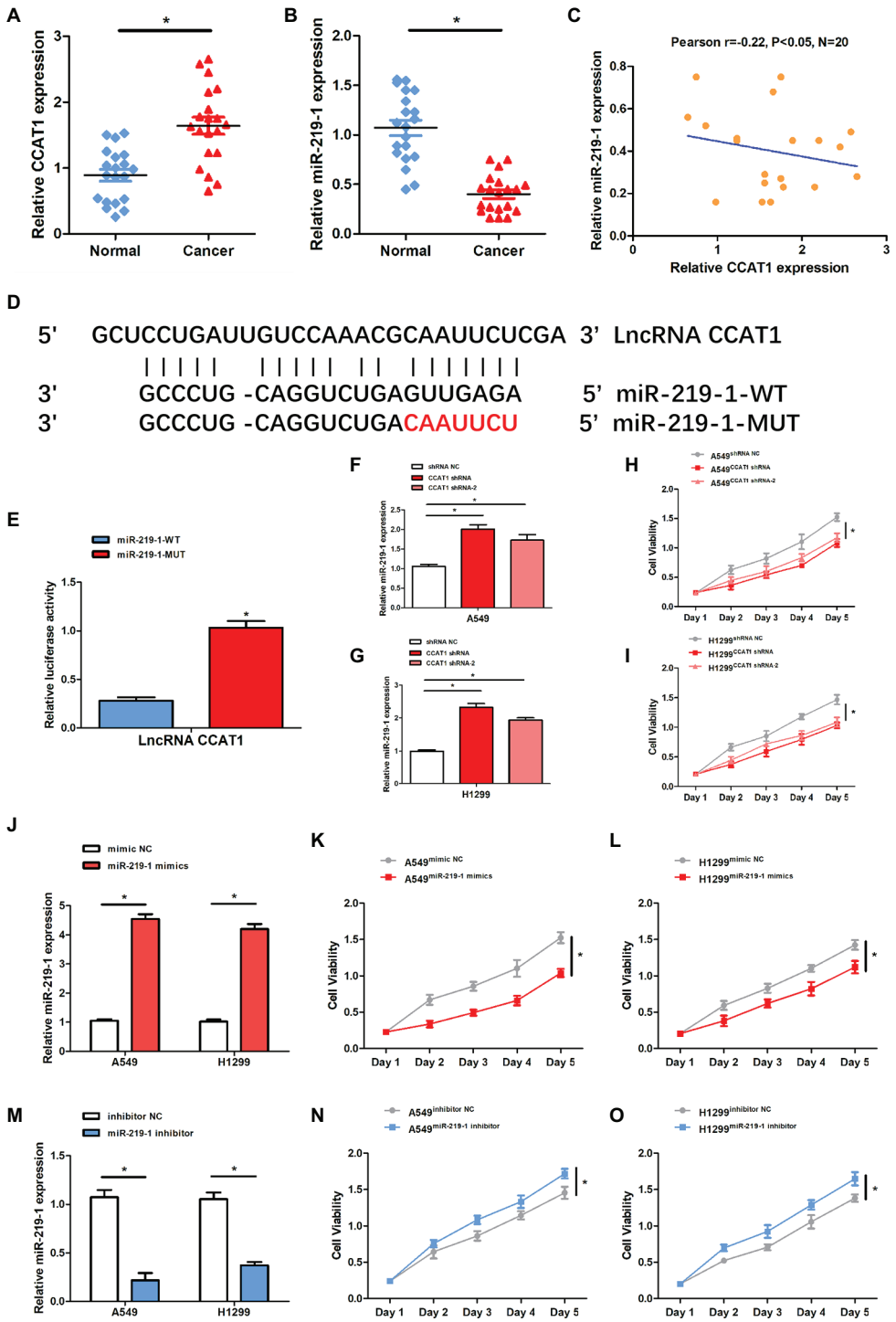

FIGURE 1 | The expression of colon cancer-associated transcript-1(CCAT1) was negatively related to the miR-219-1 expression. **(A)** Relative CCAT1 expression in human lung adenocarcinoma (LAD) and adjacent non-tumor tissues. **(B)** Relative miR-219-1 expression in human LAD and adjacent normal tissues. **(C)** An inverse correlation between CCAT1 and miR-219-1 expressions in LAD tissue samples. **(D)** Bioinformatics analysis was performed to identify miR-219-1 binding sites in CCAT1. **(E)** A luciferase reporter assay was used to examine the relationship between CCAT1 and miR-219-1. **(F,G)** Relative miR-219-1 expression in A549 and H1299 cells transfected with CCAT1 shRNA and CCAT1 shRNA-2. **(H,I)** Cell viability of A549 and H1299 transfected with CCAT1 shRNA and CCAT1 shRNA-2. **(J)** Relative miR-219-1 expression in A549 and H1299 transfected with the miR-219-1 mimic and NC. **(K,L)** Cell viability of A549 and H1299 transfected with the miR-219-1 mimic and NC. **(M)** Relative miR-219-1 expression in A549 and H1299 transfected with the miR-219-1 inhibitor and NC. **(N,O)** Cell viability of A549 and H1299 transfected with the miR-219-1 inhibitor and NC. Data are shown as means ± SD. $^{*}p < 0.05$.

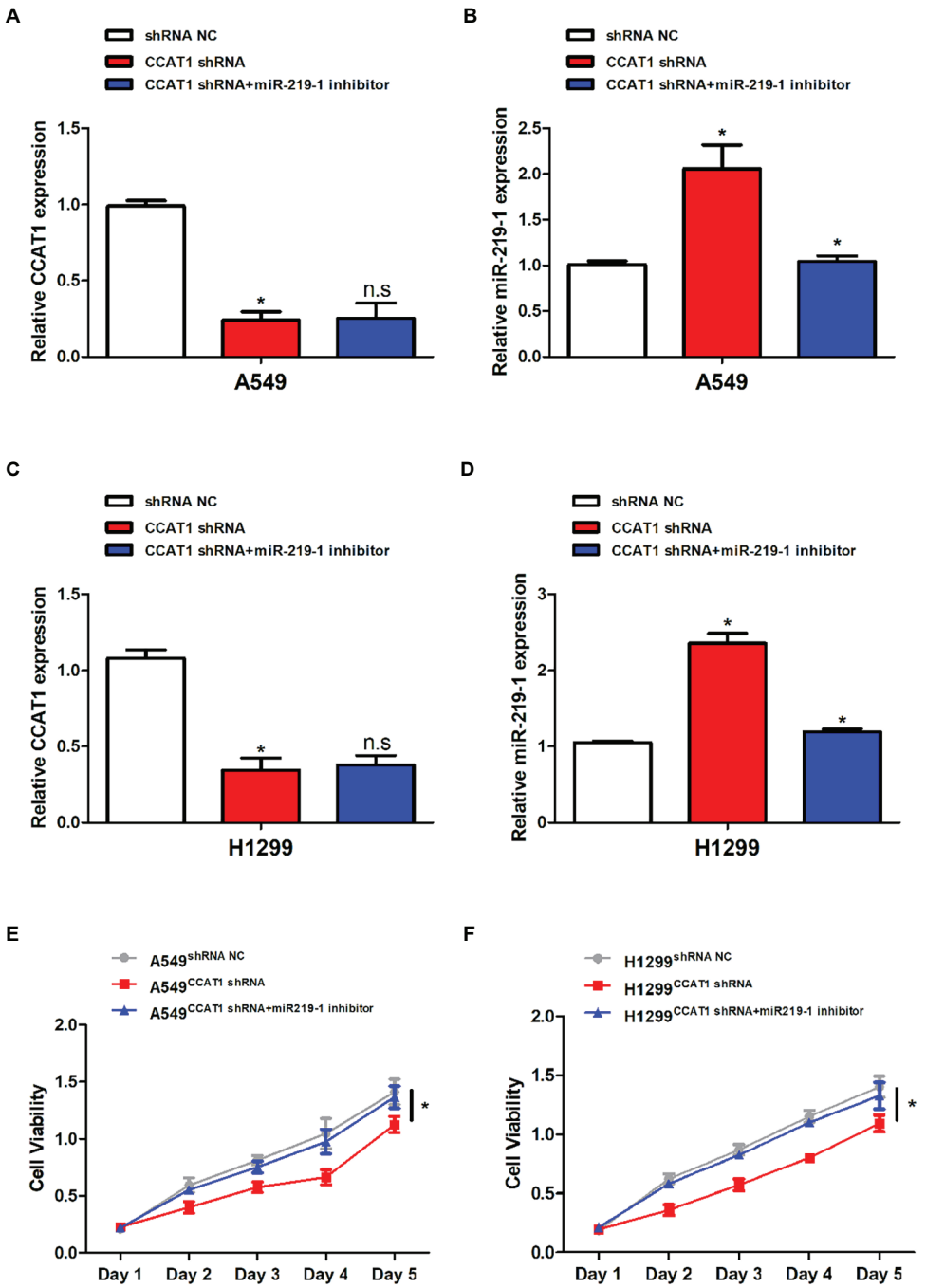

FIGURE 2 | CCAT1 promoted cell proliferation by targeting miR-219-1. **(A,C)** The relative expression of CCAT1 in A549 and H1299 cells transfected with shRNA NC, CCAT1 shRNA, and CCAT1 shRNA+ by the miR-219-1 inhibitor by quantitative real-time PCR (qRT-PCR). **(B,D)** The relative expression of miR-219-1 in A549 and H1299 cells transfected with shRNA NC, CCAT1 shRNA, and CCAT1 shRNA+ by the miR-219-1 inhibitor. **(E,F)** The effects of CCAT1 knockdown on cell proliferation analyzed by CCK-8 assay. Data are shown as means ± SD. NS, not significant, $^{*}p < 0.05$.

wound-healing and cell invasion experiments. We observed that the migration of A549 and H1299 cells was significantly decreased in the CCAT1 shRNA group compared to the shRNA NC group (**Figures 3A,C**). Similarly, knockdown of CCAT1 suppressed the invasive capacity of A549 and H1299 cells (**Figures 3B,D**). Co-transfection with the miR-219-1 inhibitor rescued the effects of CCAT1 on the migration and invasion of A549 and H1299 cells (**Figures 3A–D**). Taken together, these results suggested that CCAT1 promoted the migration and invasion of LAD cells *via* miR-219-1.

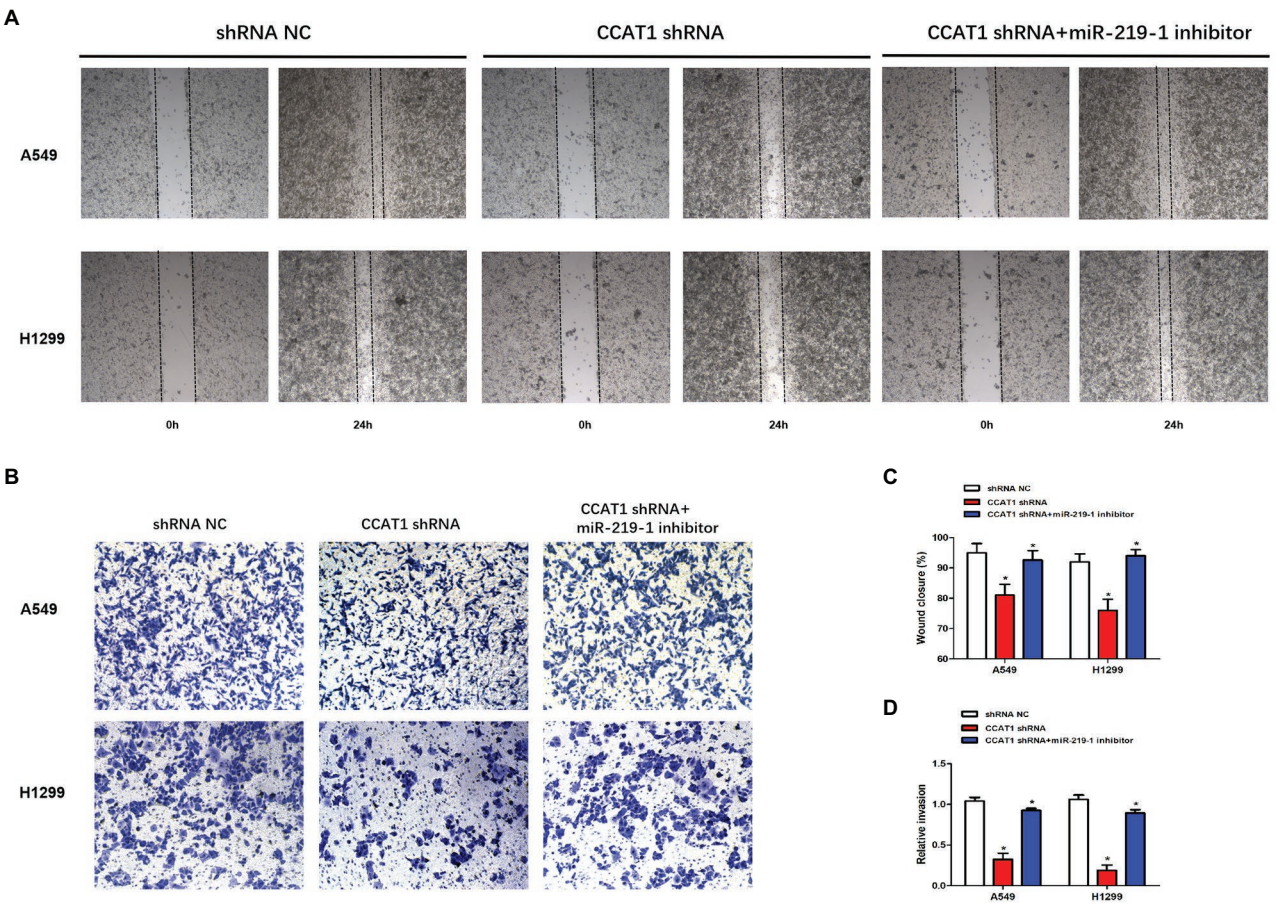

FIGURE 3 | CCAT1 knockdown suppresses the migration and invasion of LAD cells. **(A,C)** The effect of CCAT1 knockdown on cell migration determined by the wound-healing experiment. Pictures were taken at 0 and 24 h. **(B,D)** The effect of CCAT1 knockdown on cell invasion determined by the Transwell invasion assay. $^*p < 0.05$.

CCAT1 Knockdown Inhibits Epithelial-Mesenchymal Transition *via* miR-219-1

To further explore the effects of CCAT1 and miR-219-1 on EMT, we measured the expression of E-cadherin, N-cadherin, and vimentin by qRT-PCR and western blot. We found that CCAT1 knockdown increased the mRNA expression of E-cadherin but decreased the expression of N-cadherin and vimentin in A549 and H1299 cells, which were reversed by the miR-219-1 inhibitor (**Figures 4A,B**). Western blot revealed similar changes in the patterns of protein expressions of E-cadherin, N-cadherin, and vimentin (**Figures 4C–E**). These data suggested that CCAT1 knockdown inhibited the EMT of LAD cells *via* miR-219-1.

CCAT1 Knockdown Inhibits the Growth of Tumor Xenografts in Nude Mice *via* miR-219-1

To determine the effect of CCAT1 on tumor growth *in vivo*, we established a nude mice xenograft model by implanting A549 or H1129 cells with the vector CCAT1 shRNA and the CCAT1 shRNA + miR-219-1 inhibitor. We found that knockdown of CCAT1 drastically suppressed the tumor growth of A549 and H1129 cells, which was partially restored by the miR-219-1 inhibitor (**Figures 5A,B**). Likewise, tumor weights were significantly decreased by CCAT1 knockdown, which was rescued by the inhibition of miR-219-1 (**Figures 5C,D**). Using qRT-PCR, we observed that the expression of CCAT1 in A549 xenografts was effectively suppressed by the CCAT1 shRNA but was not affected by the miR-219-1 inhibitor (**Figure 5E**). The expression of miR-219-1 was significantly increased by the CCAT1 shRNA, which was rescued by the miR-219-1 inhibitor (**Figure 5F**). The same trends were found for H1299 xenografts (**Figures 5G,H**). Besides, western blot analysis showed that CCAT1 knockdown increased the mRNA expression of E-cadherin but decreased the expression of N-cadherin and vimentin, which were reversed by the miR-219-1 inhibitor (**Figures 5I–K**). These results indicated that CCAT1 knockdown inhibited the growth and EMT of LAD tumor xenografts by regulating miR-219-1.

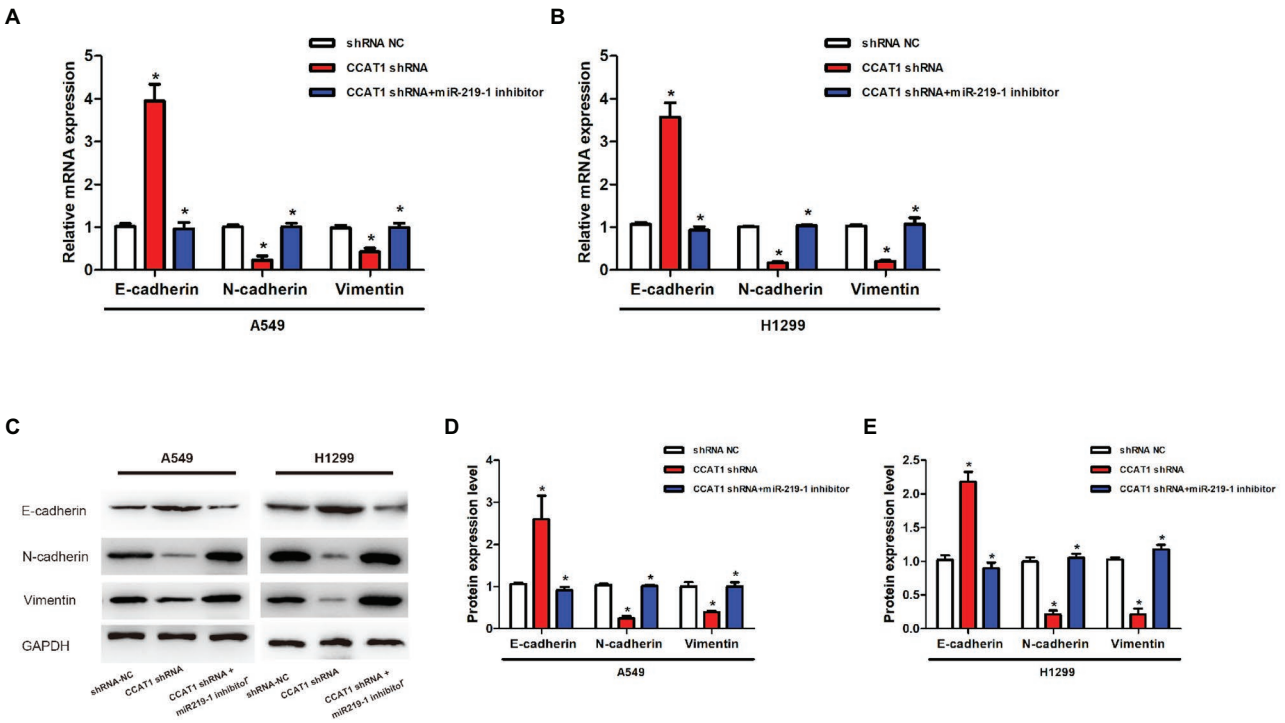

FIGURE 4 | Effects of CCAT1 and miR-219-1 on the expression of protein in LAD cells. **(A,B)** The relative expressions of mRNA of E-cadherin, N-cadherin, and vimentin in A549 and H1299 cells transfected with shRNA NC, CCAT1 shRNA, and CCAT1 shRNA+ by the miR-219-1 inhibitor. **(C–E)** Expression of E-cadherin, N-cadherin, and vimentin determined by western blot. $^*p < 0.05$.

DISCUSSION

It is now well established that lncRNAs are important regulators of human diseases. Previous studies have shown that lncRNA CCAT1 is upregulated in a series of cancers, including colorectal cancer (Nissan et al., 2012), non-small cell lung cancer (Luo et al., 2014), breast cancer (Han et al., 2019), hepatocellular carcinoma (Guo et al., 2019), gastric cancer (Li Y. et al., 2019), gallbladder cancer (Ma et al., 2015), acute myeloid leukemia (Chen et al., 2016), endometrial carcinoma (Yu et al., 2019), nasopharyngeal carcinoma (Dong et al., 2018), and cervical cancer (Shen et al., 2019). In this study, we found that the expression of CCAT1 was significantly increased in LAD tissues than that of adjacent non-tumor tissues. The knockdown of CCAT1 reduced the proliferation, migration, and invasion of LAD cells, which is consistent with a previous study (Luo et al., 2014). Moreover, our *in vivo* experiments showed that knockdown of CCAT1 suppressed the growth of LAD tumor xenografts. These findings indicate that CCAT1 may play a part in the development of LAD.

Accumulating evidence suggests that lncRNAs exert their oncogenic capacities in promoting cell proliferation, migration, and invasion through interacting with miRNAs (Guo and Hua, 2017). The ceRNA hypothesis has proposed that RNA transcripts, such as mRNAs, lnRNAs, and circRNAs, regulate the expression of each other by competitively binding the miRNAs, thus constructing a regulatory network (Salmena et al., 2011). HOXA-AS3 has a significant role in the growth and cell cycle regulation of A549 cells (Zhang et al., 2018). CCAT1 promotes the proliferation and invasion of cervical cancer cells *via* the miR-181a-5p/MMP14 axis (Shen et al., 2019) and promotes endometrial carcinoma *via* miR-181a-5p (Yu et al., 2019). CCAT1 promotes the progression of triple-negative breast cancer by suppressing miR-218/ZFX signaling (Han et al., 2019). CCAT1 boosts gallbladder cancer development *via* sponging miRNA-218-5p (Ma et al., 2015). In acute myeloid leukemia, CCAT1 could upregulate c-Myc through its competing effects on miR-155 (Chen et al., 2016). CCAT1 accelerates the proliferation, migration, and invasion of oral squamous cell carcinoma *via* inhibiting miR-181a (Li G. et al., 2019). In our study, bioinformatics analysis identified miR-219-1 as a binding partner for CCAT1. miR-219-1 was negatively regulated by CCAT1 in LAD cells. Besides, miR-219-1 counteracted the effects of CCAT1 on cell proliferation, migration, invasion, and tumor growth. Together, these results illustrate the importance of miR-219-1 in the CCAT1-mediated growth and metastasis of LAD.

EMT is a process by which a cell transforms from a polarized epithelial phenotype into a mesenchymal phenotype. EMT is featured by the loss of E-cadherin and enhanced expression of N-cadherin, fibronectin, and vimentin. In light of the current evidence, EMT programs are integral components of the malignant progression of all types of carcinoma,

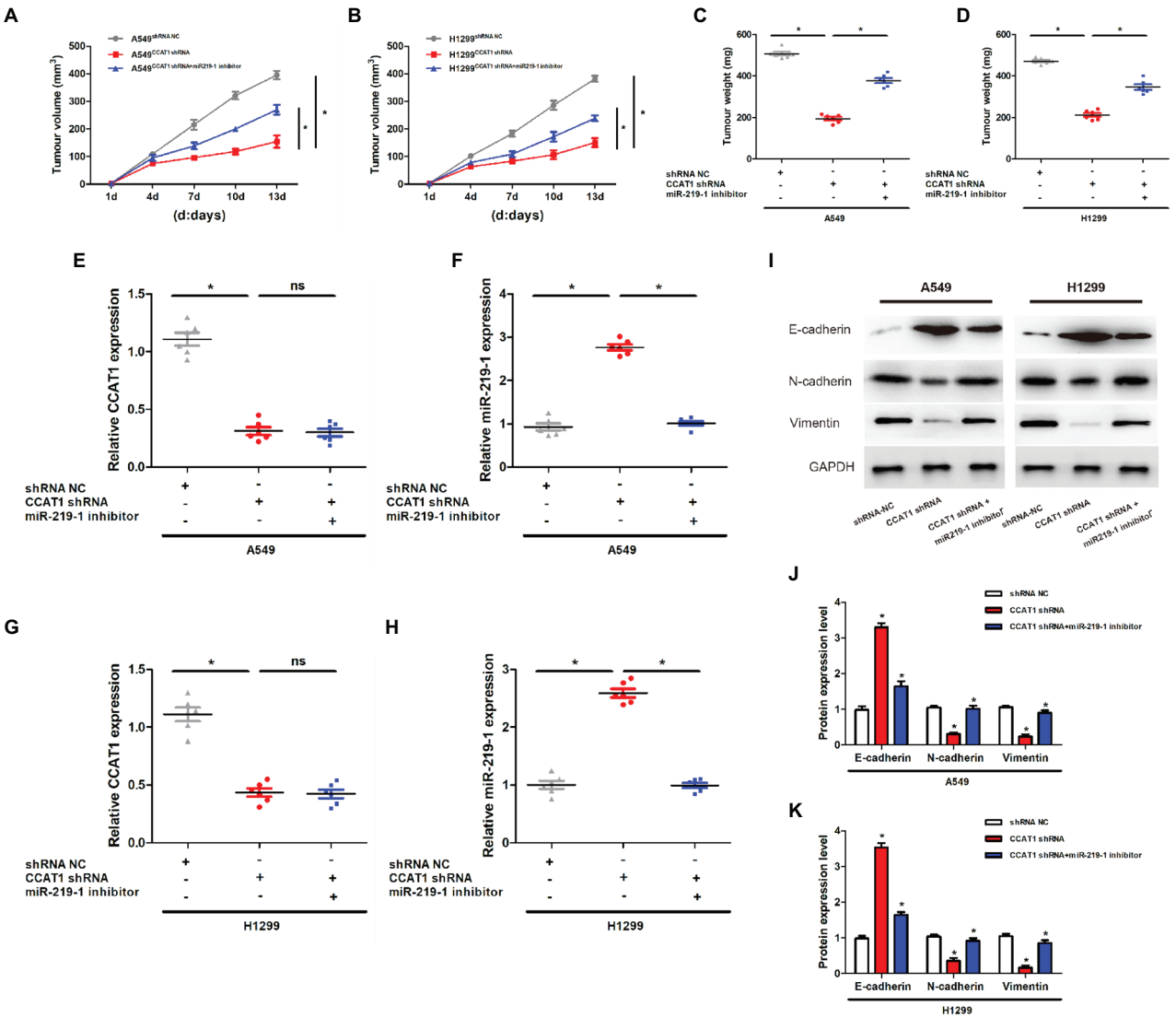

FIGURE 5 | CCAT1 knockdown inhibits the growth of tumor xenografts in nude mice *via* miR-219-1. **(A,B)** Tumor volumes of the xenografts in nude mice. **(C,D)** Tumor weights of the xenografts in nude mice. **(E,G)** The expression of CCAT1 in mice with shRNA NC, CCAT1 shRNA, and CCAT1 shRNA+ by the miR-219-1 inhibitor. **(F,H)** The expression of miR-219-1 in mice with shRNA NC, CCAT1 shRNA, and CCAT1 shRNA+ by the miR-219-1 inhibitor. **(I–K)** Expression of E-cadherin, N-cadherin, and vimentin. *$p < 0.05$; ns: not significant.

including breast, pancreatic, lung, colorectal, hepatocellular, and bladder (Dongre and Weinberg, 2019). The knockdown of lncRNA TTN-AS1 could lead to a significantly higher expression of E-cadherin and lower expressions of N-cadherin, Twist, Snail, and ZEB1 in LAD cell lines (Jia et al., 2019). LncRNA FAM83A-AS1 is found to promote LAD cell proliferation, migration, invasion, and EMT *via* targeting miR-150-5p (Xiao et al., 2019). In non-small cell lung cancer, lncRNA linc00673 could regulate the expression of ZEB1, a key regulator in EMT (Lu et al., 2017). A previous study observed that knockdown of CCAT1 induced a marked reduction in fibronectin and vimentin but upregulated E-cadherin, thereby restoring the epithelial phenotype of H1975 cells, which failed to consider the underlying mechanism of the effects of CCAT1 on EMT (Luo et al., 2014). miR-219 is increasingly recognized as a tumor suppressor in gastric cancer (Li Y. et al., 2019), hepatocellular carcinoma (Gong et al., 2019), and ovarian cancer (Xing et al., 2018). The role of miR-219-1 in LAD was unclear. Our *in vitro* and *in vivo* experiments confirmed that CCAT1 knockdown enhanced the expression of E-cadherin and decreased the expression of N-cadherin and vimentin, which can be rescued by the miR-219-1 inhibitor. Our findings fill the missing link between CCAT1 and EMT by introducing miR-219-1. Moreover, LAD patients with higher CCAT1 expression had a markedly lower overall survival time (Luo et al., 2014). Future epidemiological

studies are warranted to assess the value of CCAT1 in predicting the prognosis of LAD patients.

CONCLUSION

This study has provided an insight into the roles of CCAT1 and miR-219-1 in LAD progression. CCAT1 promotes the proliferation, migration, invasion, and EMT of LAD cells by sponging miR-219-1. Knockdown of CCAT1 inhibited the growth of tumors *in vivo*. Targeting the CCAT1/miR-219-1 pathway may be a strategy for developing novel LAD treatments. Future work is required to understand the implications of CCAT1 in LAD.

DATA AVAILABILITY STATEMENT

All datasets presented in this study are included in the article/supplementary material.

ETHICS STATEMENT

The studies involving human participants were reviewed and approved by the Ethics Committee of Henan Provincial Chest Hospital. The patients/participants provided their written informed consent to participate in this study. The animal study was reviewed and approved by the Animal Care and Use Committee of the Huai'an Second People's Hospital.

AUTHOR CONTRIBUTIONS

WW, LyG, and LlG designed the study. WW, ZH, and CW collected the samples and performed the experiment. WW and ZH analyzed the data. WW, LlG, and LlG drafted and revised this manuscript. All authors contributed to the article and approved the submitted version.

REFERENCES

Bray, F., Ferlay, J., Soerjomataram, I., Siegel, R. L., Torre, L. A., and Jemal, A. (2018). Global cancer statistics 2018: GLOBOCAN estimates of incidence and mortality worldwide for 36 cancers in 185 countries. *CA Cancer J. Clin.* 68, 394–424. doi: 10.3322/caac.21492

Chen, L., Wang, W., Cao, L., Li, Z., and Wang, X. (2016). Long non-coding RNA CCAT1 acts as a competing endogenous RNA to regulate cell growth and differentiation in acute myeloid leukemia. *Mol. Cell* 39, 330–336. doi: 10.14348/molcells.2016.2308

Dong, Y., Yuan, H., and Jin, G. (2018). Identification of long non-coding RNA CCAT1 as an oncogene in nasopharyngeal carcinoma. *Oncol. Lett.* 16, 2750–2756. doi: 10.3892/ol.2018.8969

Dongre, A., and Weinberg, R. A. (2019). New insights into the mechanisms of epithelial-mesenchymal transition and implications for cancer. *Nat. Rev. Mol. Cell Biol.* 20, 69–84. doi: 10.1038/s41580-018-0080-4

Gong, T., Ning, X., Deng, Z., Liu, M., Zhou, B., Chen, X., et al. (2019). Propofol-induced miR-219-5p inhibits growth and invasion of hepatocellular carcinoma through suppression of GPC3-mediated Wnt/beta-catenin signalling activation. *J. Cell. Biochem.* 120, 16934–16945. doi: 10.1002/jcb.28952

Guan, H., Zhu, T., Wu, S., Liu, S., Liu, B., Wu, J., et al. (2019). Long noncoding RNA LINC00673-v4 promotes aggressiveness of lung adenocarcinoma via activating WNT/β-catenin signaling. *Proc. Natl. Acad. Sci. U. S. A.* 116, 14019–14028. doi: 10.1073/pnas.1900997116

Guo, X., and Hua, Y. (2017). CCAT1: an oncogenic long noncoding RNA in human cancers. *J. Cancer Res. Clin. Oncol.* 143, 555–562. doi: 10.1007/s00432-016-2268-3

Guo, J., Ma, Y., Peng, X., Jin, H., and Liu, J. (2019). LncRNA CCAT1 promotes autophagy via regulating ATG7 by sponging miR-181 in hepatocellular carcinoma. *J. Cell. Biochem.* 120, 17975–17983. doi: 10.1002/jcb.29064

Han, C., Li, X., Fan, Q., Liu, G., and Yin, J. (2019). CCAT1 promotes triple-negative breast cancer progression by suppressing miR-218/ZFX signaling. *Aging* 11, 4858–4875. doi: 10.18632/aging.102080

Hu, M., Zhang, Q., Tian, X. H., Wang, J. L., Niu, Y. X., and Li, G. (2019). lncRNA CCAT1 is a biomarker for the proliferation and drug resistance of esophageal cancer via the miR-143/PLK1/BUBR1 axis. *Mol. Carcinog.* 58, 2207–2217. doi: 10.1002/mc.23109

Jia, Y., Duan, Y., Liu, T., Wang, X., Lv, W., Wang, M., et al. (2019). LncRNA TTN-AS1 promotes migration, invasion, and epithelial mesenchymal transition of lung adenocarcinoma via sponging miR-142-5p to regulate CDK5. *Cell Death Dis.* 10:573. doi: 10.1038/s41419-019-1811-y

Li, G., Ma, Z., and Wang, X. (2019). Long non-coding RNA CCAT1 is a prognostic biomarker for the progression of oral squamous cell carcinoma via miR-181a-mediated Wnt/β-catenin signaling pathway. *Cell Cycle* 18, 2902–2913. doi: 10.1080/15384101.2019.1662257

Li, Y., Zhu, G., Ma, Y., and Qu, H. (2019). lncRNA CCAT1 contributes to the growth and invasion of gastric cancer via targeting miR-219-1. *J. Cell. Biochem.* 120, 19457–19468. doi: 10.1002/jcb.29239

Lu, W., Zhang, H., Niu, Y., Wu, Y., Sun, W., Li, H., et al. (2017). Long non-coding RNA linc00673 regulated non-small cell lung cancer proliferation, migration, invasion and epithelial mesenchymal transition by sponging miR-150-5p. *Mol. Cancer* 16:118. doi: 10.1186/s12943-017-0685-9

Luo, J., Tang, L., Zhang, J., Ni, J., Zhang, H., Zhang, L., et al. (2014). Long non-coding RNA CARLo-5 is a negative prognostic factor and exhibits tumor pro-oncogenic activity in non-small cell lung cancer. *Tumor Biol.* 35, 11541–11549. doi: 10.1007/s13277-014-2442-7

Ma, M. Z., Chu, B. F., Zhang, Y., Weng, M. Z., Qin, Y. Y., Gong, W., et al. (2015). Long non-coding RNA CCAT1 promotes gallbladder cancer development via negative modulation of miRNA-218-5p. *Cell Death Dis.* 6:e1583. doi: 10.1038/cddis.2014.541

Miller, K. D., Siegel, R. L., Lin, C. C., Mariotto, A. B., Kramer, J. L., Rowland, J. H., et al. (2016). Cancer treatment and survivorship statistics, 2016. *CA Cancer J. Clin.* 66, 271–289. doi: 10.3322/caac.21349

Nissan, A., Stojadinovic, A., Mitrani-Rosenbaum, S., Halle, D., Grinbaum, R., Roistacher, M., et al. (2012). Colon cancer associated transcript-1: a novel RNA expressed in malignant and pre-malignant human tissues. *Int. J. Cancer* 130, 1598–1606. doi: 10.1002/ijc.26170

Salmena, L., Poliseno, L., Tay, Y., Kats, L., and Pandolfi, P. P. (2011). A ceRNA hypothesis: the Rosetta stone of a hidden RNA language? *Cell* 146, 353–358. doi: 10.1016/j.cell.2011.07.014

Shen, H., Wang, L., Xiong, J., Ren, C., Gao, C., Ding, W., et al. (2019). Long non-coding RNA CCAT1 promotes cervical cancer cell proliferation and invasion by regulating the miR-181a-5p/MMP14 axis. *Cell Cycle* 18, 1110–1121. doi: 10.1080/15384101.2019.1609829

Shi, D., Wu, F., Gao, F., Qing, X., and Shao, Z. (2017). Prognostic value of long non-coding RNA CCAT1 expression in patients with cancer: a meta-analysis. *PLoS One* 12:e179346. doi: 10.1371/journal.pone.0179346

Travis, W. D., Brambilla, E., Nicholson, A. G., Yatabe, Y., Austin, J., Beasley, M. B., et al. (2015). The 2015 World Health Organization classification of lung tumors: impact of genetic, clinical and radiologic advances since the 2004 classification. *J. Thorac. Oncol.* 10, 1243–1260. doi: 10.1097/JTO.0000000000000630

Wang, G., Zhang, Z., Jian, W., Liu, P., Xue, W., Wang, T., et al. (2019). Novel long noncoding RNA OTUD6B-AS1 indicates poor prognosis and inhibits clear cell renal cell carcinoma proliferation via the Wnt/β-catenin signaling pathway. *Mol. Cancer* 18:15. doi: 10.1186/s12943-019-0942-1

Xiao, G., Wang, P., Zheng, X., Liu, D., and Sun, X. (2019). FAM83A-AS1 promotes lung adenocarcinoma cell migration and invasion by targeting

miR-150-5p and modifying MMP14. *Cell Cycle* 18, 2972–2985. doi: 10.1080/15384101.2019.1664225

Xing, F., Song, Z., and He, Y. (2018). MiR-219-5p inhibits growth and metastasis of ovarian cancer cells by targeting HMGA2. *Biol. Res.* 51:50. doi: 10.1186/s40659-018-0199-y

Yu, J., Jiang, L., Gao, Y., Sun, Q., Liu, B., Hu, Y., et al. (2019). LncRNA CCAT1 negatively regulates miR-181a-5p to promote endometrial carcinoma cell proliferation and migration. *Exp. Ther. Med.* 17, 4259–4266. doi: 10.3892/etm.2019.7422

Zhang, H., Liu, Y., Yan, L., Zhang, M., Yu, X., Du, W., et al. (2018). Increased levels of the long noncoding RNA, HOXA-AS3, promote proliferation of A549 cells. *Cell Death Dis.* 9:707. doi: 10.1038/s41419-018-0725-4

Conflict of Interest: The authors declare that the research was conducted in the absence of any commercial or financial relationships that could be construed as a potential conflict of interest.

frontiers in Genetics

ORIGINAL RESEARCH
published: 27 November 2020
doi: 10.3389/fgene.2020.573124

Increased NFATC4 Correlates With Poor Prognosis of AML Through Recruiting Regulatory T Cells

*Chong Zhao[1], Shaoxin Yang[2], Wei Lu[2], Jiali Liu[1], Yanyu Wei[2], Hezhou Guo[2], Yanjie Zhang[2] and Jun Shi[2]**

[1] Department of Hematology, Shanghai Jiao Tong University Affiliated Sixth People's Hospital, Shanghai, China, [2] Department of Hematology, Shanghai Ninth People's Hospital, Shanghai Jiao Tong University School of Medicine, Shanghai, China

Despite that immune responses play important roles in acute myeloid leukemia (AML), immunotherapy is still not widely used in AML due to lack of an ideal target. Therefore, we identified key immune genes and cellular components in AML by an integrated bioinformatics analysis, trying to find potential targets for AML. Eighty-six differentially expressed immune genes (DEIGs) were identified from 751 differentially expressed genes (DEGs) between AML patients with fair prognosis and poor prognosis from the TCGA database. Among them, nine prognostic immune genes, including NCR2, NPDC1, KIR2DL4, KLC3, TWIST1, SNORD3B-1, NFATC4, XCR1, and LEFTY1, were identified by univariate Cox regression analysis. A multivariable prediction model was established based on prognostic immune genes. Kaplan–Meier survival curve analysis indicated that patients in the high-risk group had a shorter survival rate and higher mortality than those in the low-risk group ($P < 0.001$), indicating good effectiveness of the model. Furthermore, nuclear factors of activated T cells-4 (NFATC4) was recognized as the key immune gene identified by co-expression of differentially expressed transcription factors (DETFs) and prognostic immune genes. ATP-binding cassette transporters (ABC transporters) were the downstream KEGG pathway of NFATC4, identified by gene set variation analysis (GSVA) and gene set enrichment analysis (GSEA). To explore the immune responses NFATC4 was involved in, an immune gene set of T cell co-stimulation was identified by single-cell GSEA (ssGSEA) and Pearson correlation analysis, positively associated with NFATC4 in AML ($R = 0.323$, $P < 0.001$, positive). In order to find out the immune cell types affected by NFATC4, the CIBERSORT algorithm and Pearson correlation analysis were applied, and it was revealed that regulatory T cells (Tregs) have the highest correlation with NFATC4 ($R = 0.526$, $P < 0.001$, positive) in AML from 22 subsets of tumor-infiltrating immune cells. The results of this study were supported by multi-omics database validation. In all, our study indicated that NFATC4 was the key immune gene in AML poor prognosis through recruiting Tregs, suggesting that NFATC4 might serve as a new therapy target for AML.

Keywords: acute myeloid leukemia, NFATc4, regulatory T cells, immune response, prognosis

OPEN ACCESS

Edited by:
Xiao-Jie Lu,
Nanjing Medical University, China

Reviewed by:
Chandramani Pathak,
Amity University, India
Vladimir Lazarevic,
Skåne University Hospital, Sweden

***Correspondence:**
Jun Shi
junshi@sjtu.edu.cn

Specialty section:
This article was submitted to Cancer Genetics, a section of the journal Frontiers in Genetics

Received: *16 June 2020*
Accepted: *27 October 2020*
Published: *27 November 2020*

Citation:
Zhao C, Yang S, Lu W, Liu J, Wei Y, Guo H, Zhang Y and Shi J (2020) Increased NFATC4 Correlates With Poor Prognosis of AML Through Recruiting Regulatory T Cells. Front. Genet. 11:573124. doi: 10.3389/fgene.2020.573124

INTRODUCTION

Acute myeloid leukemia (AML) is the most common type of acute leukemia in adults, which often confronts high recurrence risk and low 5-years survival after diagnosis (Li et al., 2020). Over the past decades, therapies targeting mutated or critical proteins in leukemia have come to the market with some promising impact on prognosis (Pollyea, 2018; Cerrano and Itzykson, 2019). However, immune therapy which has gained significant clinical impact on other neoplastic diseases still faces great challenges in AML. This indicates us to pay more attention to immune regulation in AML.

The progression of AML is closely associated with immune imbalance. As important participants in immune responses, changes in the type and proportion of immune cells are involved in cancer progression. The percentage of regulatory T cells (Tregs) in bone marrow is higher in AML patients than in healthy donors (Niedzwiecki et al., 2019; Williams et al., 2019). Increased Treg phenotype may promote disease progression and lead to poor prognosis in AML through contributing to immune evasion (Govindaraj et al., 2014; Arandi et al., 2018). However, how immune cells involved in immune imbalance are regulated in AML remains unclear.

Immune genes in tumor cells may promote the secretion of inflammatory cytokines by activating the downstream signaling pathway and recruit Tregs, thus avoiding immune damage (Yue et al., 2020). Therefore, we screened immune genes from ImmPort to study how immune genes in leukemia cells regulate immune responses in AML. Limiting the target to immune genes might help us identify immune factors associated with AML prognosis more accurately. In this study, we identified key immune genes correlated with AML prognosis and explored the associated immune gene set and immune cells by ssGSEA and CIBERSORT algorithm with the expression profiles from the TCGA database, trying to find novel targets for immunotherapy.

MATERIALS AND METHODS

Data Preparation and Analysis of Differentially Expressed Genes (DEGs)

RNA-seq profiles and clinical information of AML samples with different risk stratifications were downloaded from The Cancer Genome Atlas (TCGA) database (https://tcgadata.nci.nih.gov/tcga/). Primary AML samples with complete clinical information and not M3 subtype were selected for our following analysis. Data of 2,498 immune-related genes were retrieved from the ImmPort database (https://www.import.org/) (Bhattacharya et al., 2018). Data of 318 cancer-related transcription factors (TFs) were obtained from the Cistrome Cancer database (http://cistrome.org/) (Mei et al., 2017). HTseq-count and fragments per kilobase of exon per million reads mapped (FPKM) profiles of AML samples, divided into two groups with fair prognosis (risk stratification: favorable/intermediate) and poor prognosis (risk stratification: poor), were assembled. To identify significantly DEGs, the edgeR method was used (Robinson et al., 2010) while $P < 0.05$ and the log (fold change) > 1 or < -1 were set as the cutoffs. The heatmap showed the DEGs with each row normalized by z-score. The volcano plot was generated to highlight DEGs. Gene Ontology (GO) and Kyoto Encyclopedia of Genes and Genomes (KEGG) enrichment analysis of DEGs were performed to reveal the potential mechanism.

The Identification of Prognostic Immune Genes

DEIGs were extracted from the previously identified DEG list and immune-related genes. Heatmap and volcano plot were applied to show the DEIGs. Then, the univariate Cox regression analysis was performed to identify prognostic immune genes based on DEIGs and clinical information.

Construction of Prognostic Prediction Model Based on the Prognostic Immune Genes

To assess the significance of each prognostic immune gene with the β-value, the multivariate Cox regression analysis was carried out. Based on the model, the risk score of each sample was calculated to evaluate prognostic risk according to the following formula:

$$\text{Risk score} = \sum_{i=1}^{n} \beta\text{i} \times xi$$

In the formula, "n" represents the number of integrated genes in the model. "β" represents the regression coefficient of each integrated gene. "χ" represents the expression level of each integrated gene. Then, based on the median risk score, samples were medially divided into high- and low-risk groups. The area under the ROC curve (AUC) was applied to evaluate the accuracy of the model. Kaplan–Meier survival analysis was performed to compare the survival between the two groups. Next, based on the risk score, individuals were reordered. The risk curve, survival state-related scatterplot, and heatmap of prognostic immune genes were plotted.

Then, to assess the independent prognostic value of the risk score, age, gender, morphology code (FAB subtype), and risk category, the univariate and multivariate Cox regression analyses modified by baseline information were performed.

The Identification of the Key Immune Gene

Differentially expressed transcription factors (DETFs) were obtained by intersecting DEGs and all the cancer-related TFs, shown by the heatmap and volcano plot. Then, Pearson correlation analysis was conducted to uncover the regulation and association between DETFs and prognostic immune genes.

Abbreviations: AML, Acute myeloid leukemia; ABC transporters, ATP binding cassette transporters; AUC, Area Under the Curve; DEGs, Differentially expressed genes; GSEA, Gene set enrichment analysis; GSVA, Gene set variation analysis; GO, Go Ontology; KEGG, Kyoto Encyclopedia of Genes and Genomes; KIR2DL4, Killer cell immunoglobulin-like receptor 2DL4; KLC3, Kinesin light chain 3; NFATC4, Nuclear factor activated T cells-4; NCR2, Natural cytotoxicity triggering receptor 2; NPDC1, Neural proliferation, differentiation and control 1; RAG1, Recombination activating gene-1; Tregs, Regulatory T cells; ssGSEA, Single sample gene set enrichment analysis.

The regulation pair with the highest coefficient and $P < 0.05$ was selected as the significant regulation pair. The immune gene in the significant regulation was recognized as the key immune gene. The expression of the key immune gene in different AML risk stratifications was shown in the box plot.

Identification of Potential Downstream KEGG Pathways, Immune Gene Sets, and Immune Cells

To explore the downstream KEGG pathways of key immune gene related to AML prognosis, gene set variation analysis (GSVA) was performed. ssGSEA was applied to identify the immune gene sets related to AML prognosis from those overexpressed in the tumor microenvironment (Barbie et al., 2009; Charoentong et al., 2017). CIBERSORT was used to quantify the proportions of immune cells related to AML prognosis (Newman et al., 2015). Pearson correlation analysis was performed to clarify the correlation relationship between key immune gene and KEGG pathways, immune gene sets, and immune cells, shown by the co-expression heatmap. The correlation scores were fitted by linear regression. Meanwhile, GSEA was also performed to find out the critical KEGG pathway. The overlap of GSVA and GSEA was shown by the Venn plot. The KEGG pathways identified by both GSVA and GSEA were recognized as the key signaling pathway.

Multidimensional Validation and Construction of the Protein–Protein Interaction Network

With the aim of decreasing the bias based on different platforms, multidimensional validation was utilized. Moreover, genes that represented the KEGG pathway were available from Pathway Card (https://pathcards.genecards.org/). The databases of Gene Expression Profiling Interactive Analysis (GEPIA) (Tang et al., 2017), Oncomine (Rhodes et al., 2004), PROGgeneV2 (Goswami and Nakshatri, 2014), UALCAN (Chandrashekar et al., 2017), Linkedomics (Vasaikar et al., 2018), cBioportal (Cerami et al., 2012), Genotype-Tissue Expression (GTEx) (Consortium, 2015), UCSC xena (Goldman et al., 2015), Cancer Cell Line Encyclopedia (CCLE) (Ghandi et al., 2019), Expression atlas (Papatheodorou et al., 2018), The Human Protein Altas (Uhlen et al., 2015), and String (Snel et al., 2000) were applied to validate the scientific hypothesis.

To better reveal the mechanism related to AML prognostic status, a protein–protein interaction (PPI) network was built to illustrate the interaction among prognostic TF, immune genes, KEGG pathways, immune gene sets, and immune cells by Cytoscape 3.7.1 (Shannon et al., 2003). Accordingly, a signaling diagram was displayed to show the AML prognostic related hypothesis based on the bioinformatics.

Statistical Analysis

R version 3.5.1 (Institute for Statistics and Mathematics, Vienna, Austria; https://www.r-project.org) was used for all the statistical analyses. For descriptive statistics, mean ± standard deviation (*SD*) was used to express the continuous variables in normal distribution while the median (range) was used in abnormal distribution. Classified variables were expressed by counts and percentages. Only two-tailed $P < 0.05$ was considered statistically significant.

TABLE 1 | Baseline information of 134 patients with AML from the TCGA database.

Variables	Total patients (*N* = 134)
Age, Years	
Mean ± *SD*	55 ± 33
Gender	
Female	60 (44.8%)
Male	74 (55.2%)
Risk Stratification	
Favorable/intermediate	105 (78.4%)
Poor	29 (21.6%)
Morphology Code	
M0	15 (11.2%)
M1	34 (25.4%)
M2	38 (28.3%)
M4	28 (20.9%)
M5	15 (11.2%)
M6	2 (1.5%)
Other	2 (1.5%)

SD, Standard deviation.

RESULTS

Nine Prognostic Immune Genes Were Identified in AML

The analysis procedure is shown in **Supplementary Figure 1**. There were 134 AML patients meeting the inclusion criteria that consisted of 105 with fair prognosis and 29 with poor prognosis. The baseline information is presented in **Table 1**. DEGs between the two groups, including 630 up- and 121 down- genes, were shown by the heatmap and volcano plot (**Figures 1A,B**). Then, GO and KEGG analyses were performed to reveal the underlying mechanism. As shown in **Figures 1C,D**, immune-related pathways such as "MAPK signaling pathway" and "ABC transporters" were included in the top 10 enrichment items.

DEIGs (75 up- and 11 down- genes) were shown by the heatmap and volcano plot in **Figures 2A,B**. To find out prognostic immune genes, the DEIGs and prognosis data were sent for univariate Cox regression analysis. Nine prognostic immune genes, including NCR2, NPDC1, KIR2DL4, KLC3, TWIST1, SNORD3B-1, NFATC4, XCR1, and LEFTY1, were identified (**Figure 2C**).

To make our results more convincing, we also divided AML patients in three groups including favorable, intermediate, and poor prognosis for nonparametric tests. As shown in **Supplementary Figure 2**, most of the prognostic immune genes did differ among the three groups ($P < 0.05$).

Then, the prognostic immune genes and clinical information were integrated into a multivariate Cox regression analysis to establish the prognostic prediction model. The Lasso regression

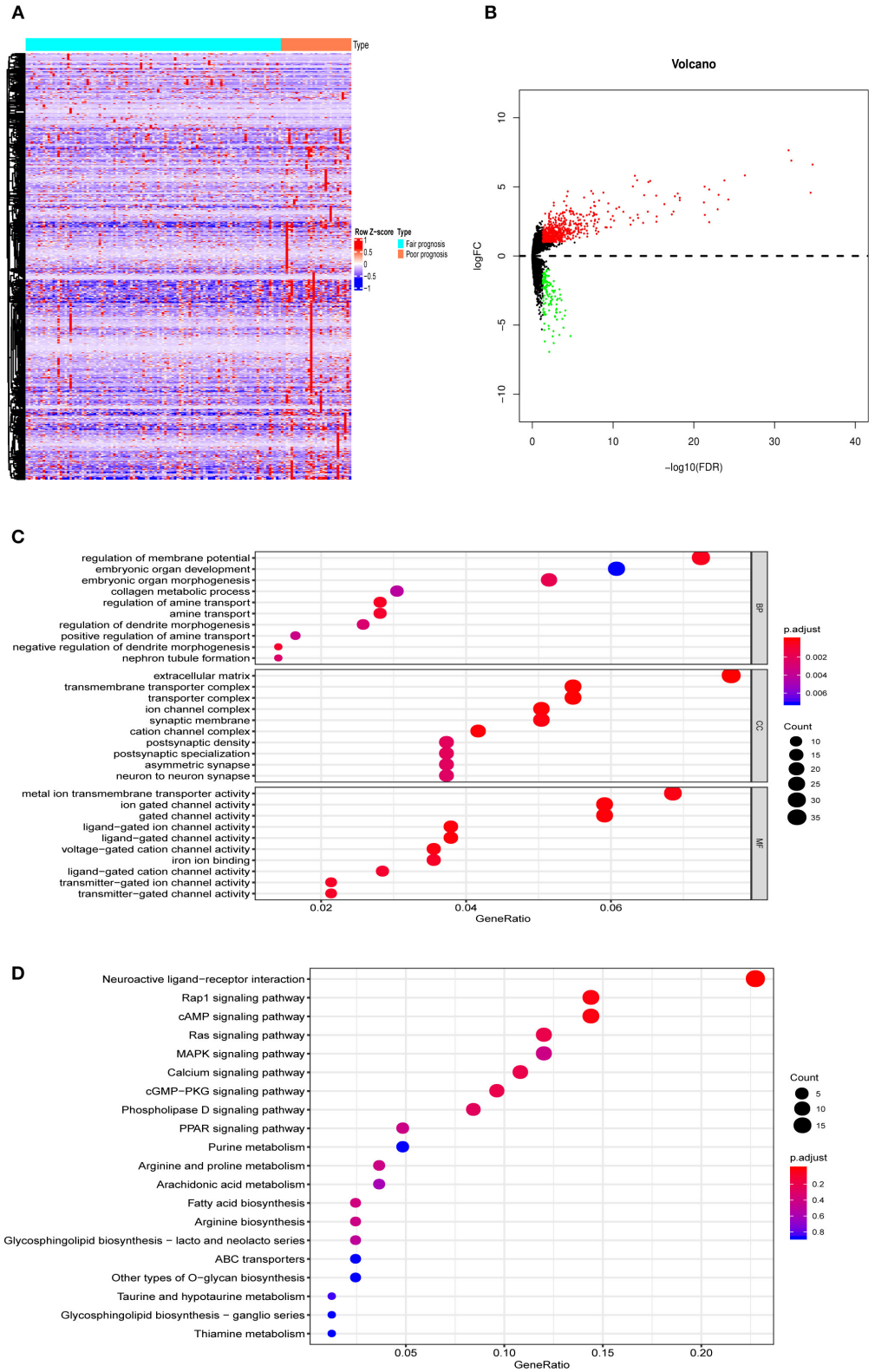

FIGURE 1 | The DEGs between AML with fair and poor prognosis. **(A)** The heatmap and **(B)** volcano plot of 751 DEGs between 105 AML with fair prognosis and 29 AML with poor prognosis. **(C)** The GO and **(D)** KEGG analysis of 751 DEGs. Note: Fair prognosis, risk stratification: favorable/intermediate; poor prognosis, risk stratification: poor. AML, acute myeloid leukemia; DEGs, differentially expressed genes; GO, Go Ontology; KEGG, Kyoto Encyclopedia of Genes and Genomes.

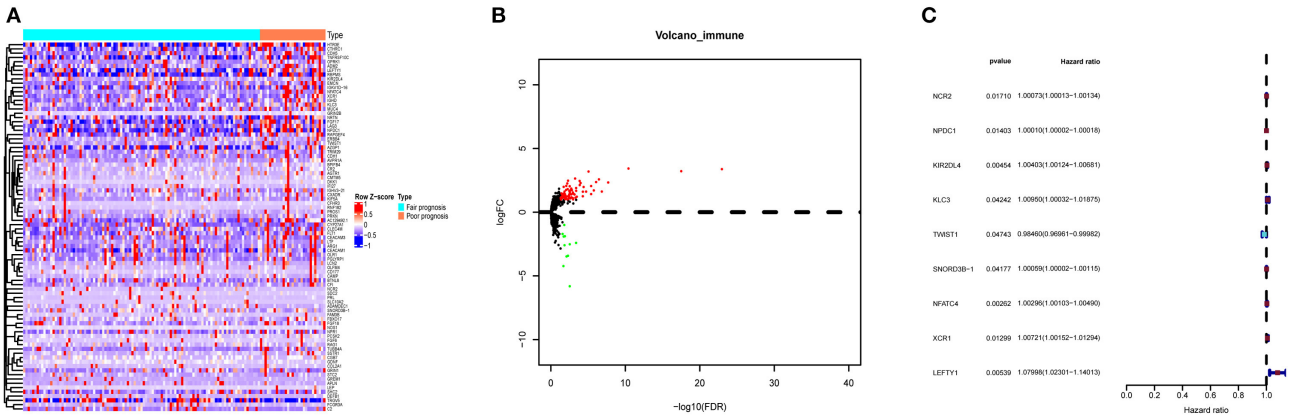

FIGURE 2 | The DEIGs between AML with fair and poor prognosis. **(A)** The heatmap and **(B)** volcano plot of 86 DEIGs; **(C)** forest plot to show the nine prognostic immune genes. Red: high-risk gene; blue: low-risk gene. DEIGs, differentially expressed immune genes.

was performed to avoid overfitting of the model. The AUC was 0.970 in the ROC curve, indicating that all these nine genes were essential for modeling (**Figure 3A**). The risk score of each sample was calculated accordingly. Individuals were divided into two groups with high and low risk with the median value of 1.000. The Kaplan–Meier curve showed that the survival probability of samples in the high-risk group was significantly lower than in the low-risk group ($P < 0.001$), suggesting good effectiveness of the prediction model (**Figure 3B**).

Then, the risk curve and scatterplot were generated to show the risk score and survival status of each individual with AML. Patients in the high-risk group showed higher mortality than those in the low-risk group, as shown in **Figure 3C**. The expression of prognostic immune genes screened by Lasso regression were displayed by the heatmap in **Figure 3D**.

To assess the independent prognostic value of risk score, we sent age, gender, morphology code, risk category, and risk score to the univariate and multivariate Cox regression analysis. As shown in **Figures 3E,F**, both the univariate (HR = 1.169, 95% CI (1.111–1.230), $P < 0.001$) and multivariate (HR = 1.151, 95% CI (1.091–1.215), $P < 0.001$) Cox regression analyses indicated that the risk score was an independent prognostic factor in AML.

NFATC4 Was the Key Immune Gene Associated With Poor Prognosis of AML

To further find out the critical immune gene related to poor prognosis of AML, the co-expression analysis of DETFs and prognostic immune genes was performed. Two up-DETFs between AML patients with fair prognosis and poor prognosis were displayed with the heatmap and volcano plot in **Figures 4A,B**. Then, Pearson correlation analysis between DETFs and prognostic immune genes was carried out. As shown in **Table 2**, only the pair of recombination activating gene-1 (RAG1) and nuclear factors of activated T cells-4 (NFATC4) was significant ($R = 0.248$, $P < 0.01$, positive), suggesting that RAG1 upregulated NFATC4 in AML. NFATC4 was recognized as the key immune gene. The expression of NFATC4 in different AML prognostic statuses is shown in **Figure 4C**. Patients with poor prognosis showed higher expression of NFATC4.

NFATC4 Was Co-expressed With ATP-Binding Cassette (ABC) Transporter Signaling Pathway in AML Poor Prognosis

To explore the potential mechanism of NFATC4 regulating AML prognosis, GSVA was performed and a total of 21 KEGG signaling pathways related to AML poor prognosis were identified. Then, Pearson correlation analysis was carried out to construct the correlation relationship between NFATC4 and prognosis-related KEGG pathways (**Figure 5A**). Meanwhile, to identify the key KEGG pathway mostly correlated with AML prognosis, GSEA was also conducted. The pathways identified by GSVA and GSEA were intersected. The overlap in GSVA and GSEA was shown by the Venn plot. As shown in **Figure 5B**, there was only one pathway significant in both GSEA and GSVA. The GSEA analysis of the ABC transporter pathway is shown in **Figure 5C** ($P < 0.001$). The correlation relationship between the NFATC4 and ABC transporter pathway was displayed by linear regression in **Figure 5D** ($R = 0.309$, $P < 0.001$, positive), suggesting that NFATC4 might positively regulate ABC transporters in AML.

NFATC4 Was Co-expressed With Immune Gene Set of T Cell Co-stimulation, Tregs in AML

Immune genes are involved in immune responses via affecting immune cells; thus, we identified AML prognosis-related immune gene sets and immune cells by ssGSEA and CIBERSORT algorithm. As shown in **Figures 6A,B**, the correlation relationship between NFATC4 and AML prognosis-related immune gene sets and immune cells was presented by the heatmap. **Figures 6C–E** show the top three immune gene sets correlated with NFATC4. Among them, the correlation relationship between immune gene sets of T cell co-stimulation and NFATC4 was the most significant ($R = 0.323$, $P < 0.001$,

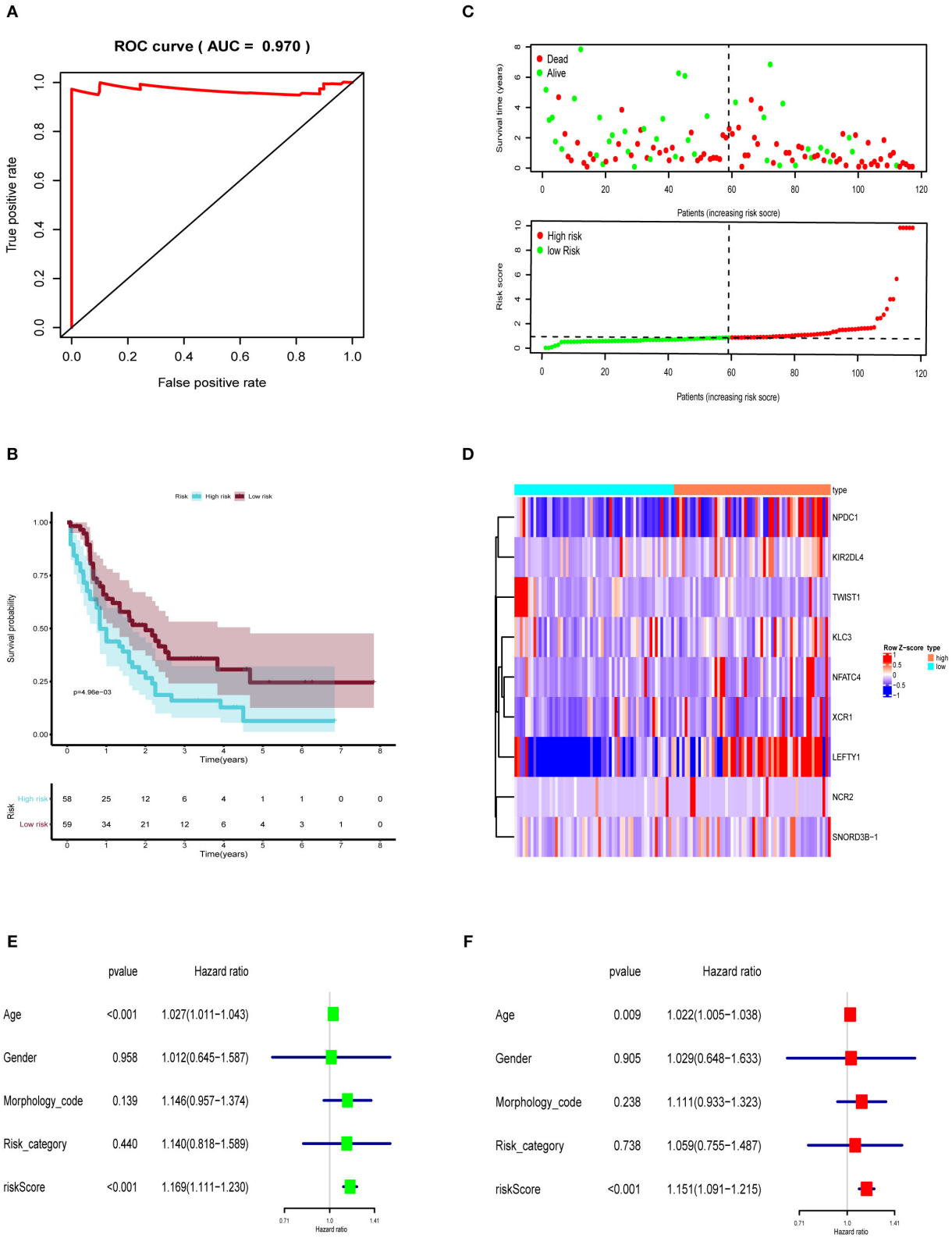

FIGURE 3 | The prognostic prediction model based on prognostic immune genes. **(A)** ROC curve for (AUC = 0.970) prognostic immune genes. **(B)** The Kaplan–Meier curve to identify the efficacy of risk score in OS. **(C)** The high and low risk score group in scatterplot and risk plot. **(D)** The heatmap to illustrate each prognostic immune genes screened by Lasso regression. The forest plot of univariate **(E)** and multivariate **(F)** Cox regression analysis. OS, overall survival; AUC, area under the curve.

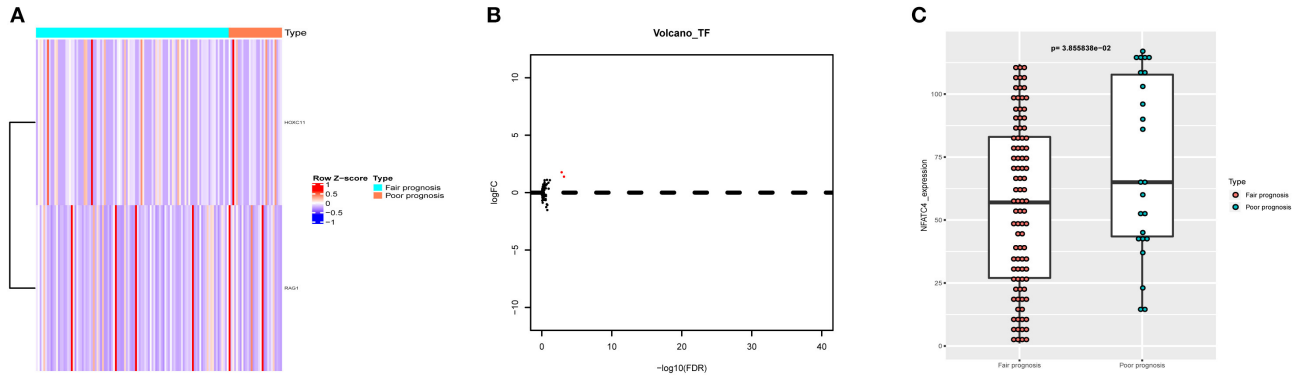

FIGURE 4 | The DETFs between AML with fair prognosis and poor prognosis. **(A)** The heatmap and **(B)** volcano plot of 2 DETFs. **(C)** The box plot to show the expression of NFATC4 in AML with different prognostic statuses. DETFs, differentially expressed transcription factors; RAG1, recombination activating gene-1; NFATC4, nuclear factor of activated T cells-4.

TABLE 2 | The correlation analysis results of DETFs and prognostic immune genes.

TF	Immune gene	Correlation	*P*-value	Regulation
RAG1	NFATC4	0.247618294	0.007108929	Positive

TF, transcription factor; RAG1, recombination activating gene-1; NFATC4, nuclear factors of activated T cells-4.

positive), suggesting that NFATC4 might affect T cell co-stimulation in AML. The top three immune cells correlated with NFATC4 were Tregs ($R = 0.526$, $P < 0.001$, positive), $CD8^+$ T cells ($R = 0.339$, $P < 0.001$, positive), and plasma cells ($R = 0.263$, $P < 0.01$, positive) (**Figures 6F–H**). Of them, the correlation relationship between NFATC4 and Tregs was most significant, as shown in **Figure 6F**, indicating that NFATC4 might modulate the cellular communication between leukemia cells and Tregs in the progression of AML.

Multidimensional Validation Further Confirmed Association Between Key Biomarkers in Our Analysis With AML Prognosis

Multidimensional validation based on GEPIA (**Supplementary Figure 3**), Oncomine (**Supplementary Figure 4**), PROGgeneV2 (**Supplementary Figure 5**), UALCAN (**Supplementary Figure 6**), Linkedomics (**Supplementary Figure 7**), cBioportal (**Supplementary Figure 8**), GTEx (**Supplementary Figure 9**), UCSC xena (**Supplementary Figure 10**), CCLE (**Supplementary Figure 11**), Expression atlas, The Human Protein Altas (**Supplementary Figure 12**), and String (**Supplementary Figure 13**) was utilized.

The top five genes that represented the critical KEGG pathway were NSR, INS, PDX1, RBFOX2, and HNF1A. The genes' interaction relationship from the cBioportal database is shown in **Supplementary Table 1**. The differential expression of genes is summarized in **Supplementary Table 2**. RAG1 (**Supplementary Figures 4B, 8B, 10A**), NFATC4 (**Supplementary Figure 8A**), RBFOX2 (**Supplementary Figure 8**) and HNF1A (**Supplementary Figures 8E, 10A**), and INSR (**Supplementary Figures 3C, 4C, 6C, 8C, 10A, 11B**) were highly expressed in AML. PDX1 (**Supplementary Figures 4C, 10A, 11C**) was lowly expressed in AML. The validation of association between these genes and prognosis is summarized in **Supplementary Table 3**. The integrated genes ($P < 0.05$, PROGgeneV2, **Supplementary Figure 5K**), ISNR ($P < 0.05$, PROGgeneV2, **Supplementary Figure 5J**; $P < 0.001$, Linkedomics, **Supplementary Figure 7C**), and RBFOX2 ($P < 0.05$, GEPIA, **Supplementary Figure 3**) were significantly related to overall survival, and INSR ($P < 0.05$, cBioportal, **Supplementary Figure 8C**) was also significantly related to disease/progression-free survival.

To better show our findings, we constructed a schematic diagram of this scientific hypothesis (**Supplementary Figure 14C**). The crucial TF, immune gene, downstream pathway, and associated immune gene set and immune cells were RAG1, NFATC4, ABC transporter signaling pathway and T cell co-stimulation and Tregs, respectively.

DISCUSSION

Immune imbalance plays important roles in the progression of AML. However, the crosstalk between leukemia cells and immune cells, the critical participant of immune responses, remains elusive. Previous studies of immune responses have a limited view to a specific subset of immune cells to explore how they were regulated by leukemia cells. This may be misleading and are not comprehensive as various immune cells surrounding cancer cells are important. In the current study, we focused on expression of immune genes in leukemia cells and applied the CIBERSORT tool to explore the communication between leukemia cells and immune cells. Finally, NFATC4 was the key immune gene in poor prognosis of AML through recruiting Tregs.

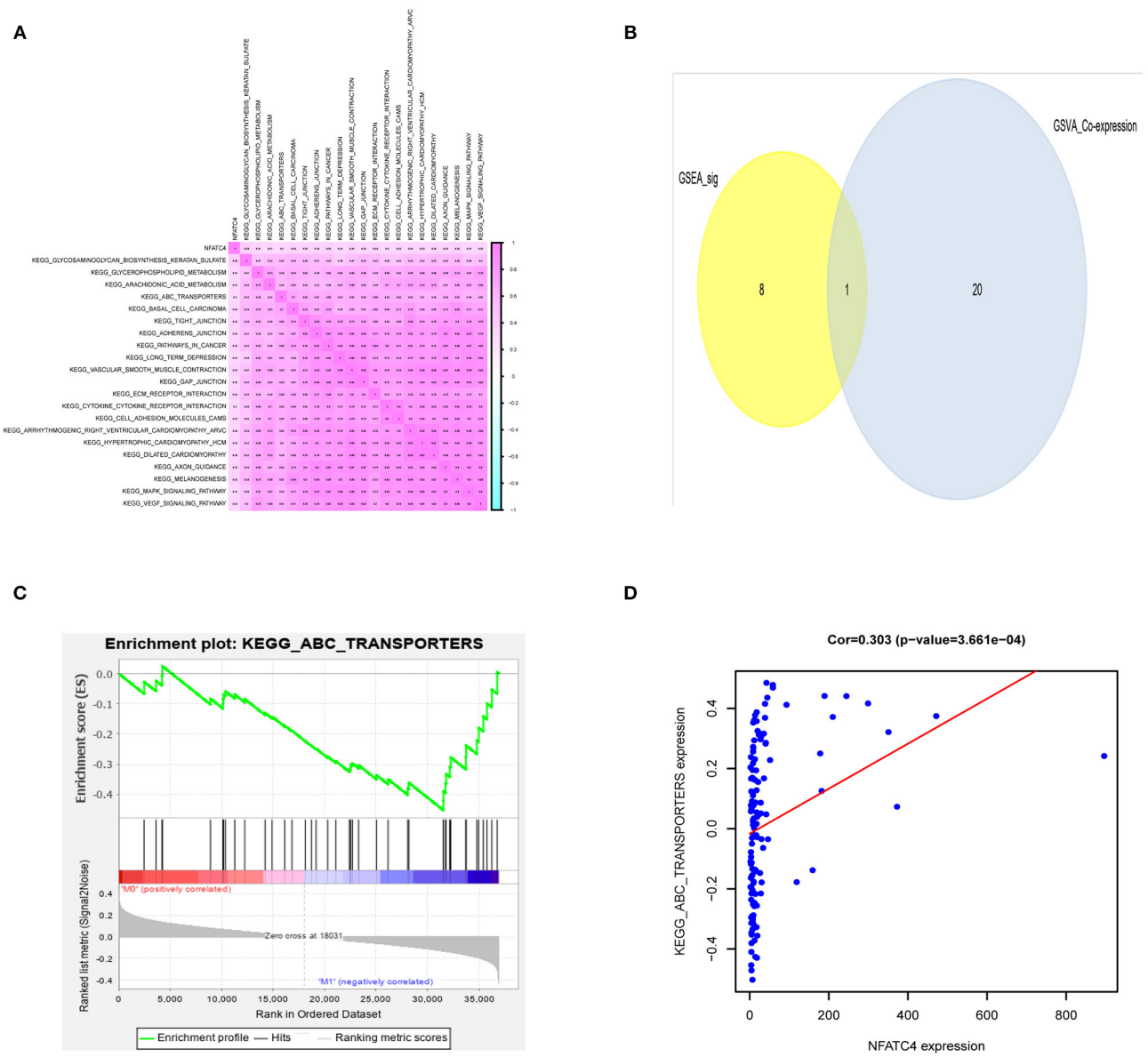

FIGURE 5 | The downstream KEGG pathways of NFATC4 related to AML prognosis. **(A)** The co-expression heatmap of NFATC4 with KEGG pathways selected by GSVA. **(B)** The Venn plot to show overlap KEGG pathways in both GSVA and GSEA. **(C)** The GSEA analysis of ABC transporter pathway. **(D)** The linear regression to show the correlation between NFATC4 and ABC transporters pathway. GSVA, gene set variation analysis; GSEA, gene set enrichment analysis; ABC transporters, ATP-binding cassette transporters.

In this study, RAG1 was found to be positively correlated with NFATC4 in the process of searching for key immune genes through co-expression analysis. Thus, we concluded that RAG1 transcriptionally regulated the expression of NFATC4. RAG1 is a key component of the RAG complex which is the main driving factor of oncogenic genome deletion and translocation (Han et al., 2019). High expression of RAG1 was associated with high proliferation markers in adult ALL and poor prognosis in gastric cancer (Han et al., 2019; Kang et al., 2019), which revealed the role of RAG1 in cancer progression. The transcriptional function of RAG1 for NFATC4 has not been described previously. However, the list of cancer-related TFs in our analysis was from Cistrome Cancer, a comprehensive resource for predicted TF targets in cancer. The prediction was based on TCGA expression profiles and public Chip-seq profiles. Therefore, we speculated that RAG1 was a transcription factor of NFATC4 in AML, while its transcriptional regulatory function needs further experimental verification.

The NFAT proteins were widely concerned in the immune system, while recent studies indicated that they are functionally active in several nonimmune cells and participate in tumor progression (Baksh et al., 2002; Graef et al., 2003; Neal and

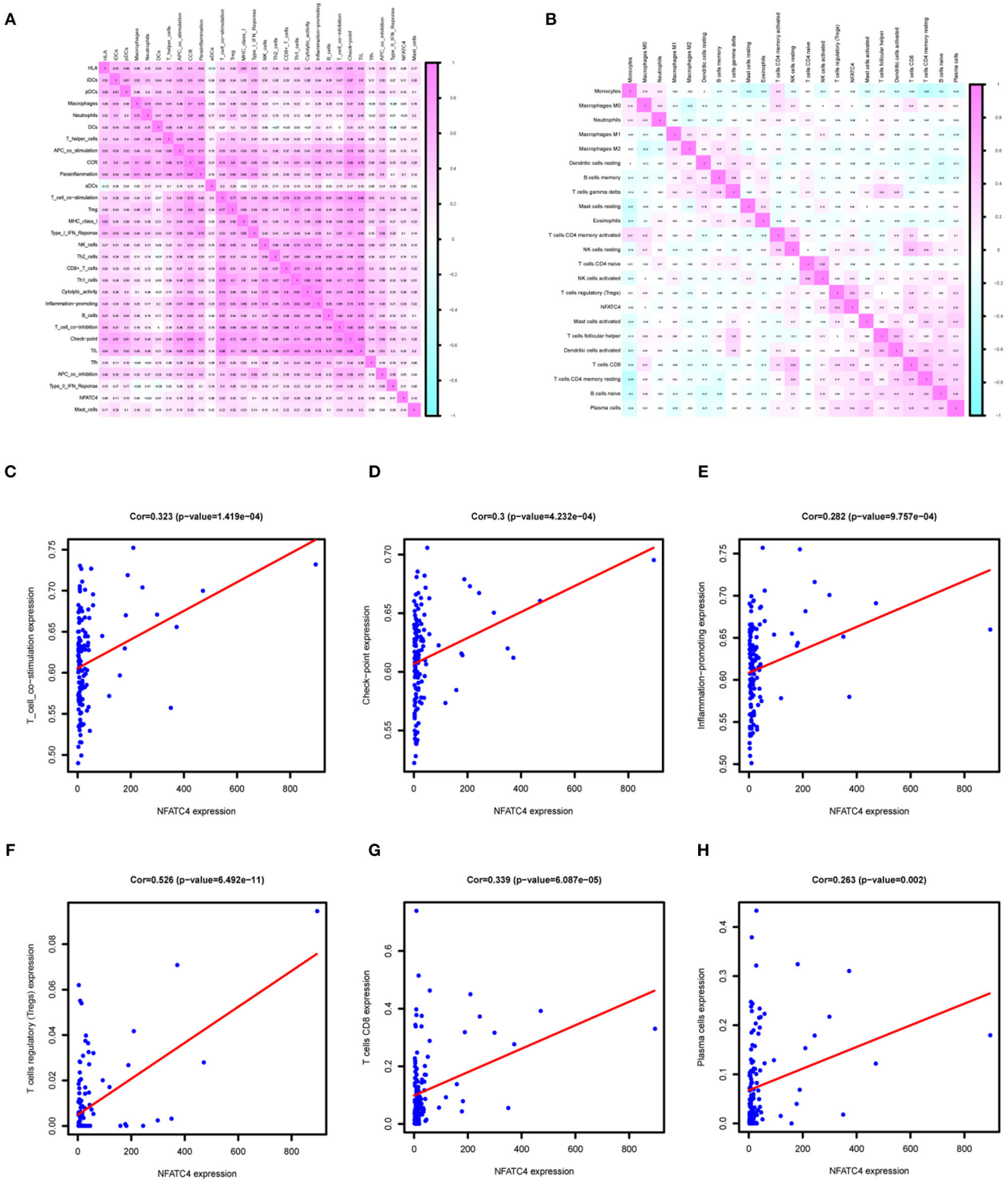

FIGURE 6 | The immune gene sets and immune cells related to NFATC4 in AML. The co-expression heatmap of NFATC4 with **(A)** immune gene sets and **(B)** immune cells. The linear regression to show the correlation between NFATC4 and **(C)** T cell co-stimulation, **(D)** check-point, and **(E)** inflammation promoting. The linear regression to show the correlation between NFATC4 and **(F)** Tregs, **(G)** $CD8^+$ T cells, and **(H)** plasma cells. Tregs, Regulatory T cells.

Clipstone, 2003). Our study discovered that high expression of NFATC4 was associated with poor prognosis of AML, which was consistent with reports in pancreatic cancer and ovarian cancer (Hessmann et al., 2016; Cole et al., 2020). In these tumors, NFATC4 participates in cancer progression through promoting tumor cell proliferation or chemotherapy resistance, while we inferred that it regulates immune responses in the progression of AML. Another isotype of NFATs, NFAT1, increases neutrophil infiltration through promoting the transcriptional induction of IL8 in breast cancer (Kaunisto et al., 2015). This indicates the role of NFAT family to regulate immune cells in cancer development. Besides, NFATC4 is reported to induce TNF-α expression in lung cells apart from involving in transcription of TNF-α in immune cells (Ke et al., 2006; Falvo et al., 2008). The repressed NFATC4 transcription activity in adipocytes also inhibited the secretion of inflammatory factors (Kim et al., 2010). Moreover, it is worth noting that NFATC4 signaling mediates the expression of chemokines CCL2 and CXCL10 in rat fibroblasts (Kuwata et al., 2018). Also, CCL2 was reported to recruit Tregs in the progression of esophageal squamous cell carcinoma (Yue et al., 2020). In this study, we found that Tregs were positively associated with NFATC4 in AML by CIBERSORT and Pearson correlation analysis, indicating that NFATC4 might involve in the progression of AML through recruiting Tregs.

As a nuclear factor, NFATC4 needs to activate downstream pathways to mediate the crosstalk between leukemia cells and Tregs. Pearson correlation analysis showed that NFATC4 was positively associated with ABC transporters, identified by GSVA and GSEA. In a previous study, NFATC2 promoted the downregulation of ABCA1 in an innate immunity signaling process, proving that NFATs could regulate ABC transporters (Maitra et al., 2009). Thus, we inferred that NFATC4 could enhance the expression of ABC transporters in AML. ABC transporters represent one of the largest transmembrane protein families, consisting of seven gene subfamilies (Begicevic and Falasca, 2017). Some ABC transporters participate in metabolite transportation, drug efflux, antigen processing, and immunity (Fukuda et al., 2015; Liu, 2019). So they may mediate the excretion of inflammatory factors to assist leukemia cells in recruiting Tregs. Furthermore, we found that the immune gene set of T cell co-stimulation was positively associated with NFATC4 in AML by ssGSEA and Pearson correlation analysis. One member in this immune gene set, TNFSF14, was known as a costimulatory factor for the activation of lymphoid cells and stimulation of the proliferation of T cells. The expression of TNFSF14 in melanoma cells contributes to regulate T-cell responses to tumor cells (Mortarini et al., 2005). Thus, we speculated that NFATC4 might affect the activation of Tregs through modulating the immune gene set of T cell co-stimulation.

To be honest, there are some limitations in our study. Firstly, the expression profiles and clinical information of samples in public database are limited. Besides, all the data for our speculation was from public databases, which lacked validation experiments. However, our study is a correlation analysis, aiming to provide reliable guidance for fundamental research of AML. Moreover, we also performed multidimensional online validation to support our results. All in all, our study indicated that increased NFATC4 might recruit Tregs in the progression of AML through affecting ABC transporters and T cell co-stimulation (**Supplementary Figure 13**). Further experiments will be carried out to verify our hypothesis.

CONCLUSIONS

Our study, firstly, inferred that NFATC4 was key immune gene associated with poor prognosis of AML through recruiting Tregs. Our findings further uncover the mechanism of AML progression and might provide guidance for its treatment.

DATA AVAILABILITY STATEMENT

The original contributions presented in the study are included in the article/**Supplementary Materials**, further inquiries can be directed to the corresponding author/s.

AUTHOR CONTRIBUTIONS

CZ, SY, WL, JL, YW, HG, YZ, and JS: conception/design and final approval of manuscript. CZ and SY: collection and/or assembly of data. CZ: data analysis and interpretation. CZ, SY, and JS: manuscript writing. All authors contributed to the article and approved the submitted version.

FUNDING

This study was supported by the National Natural Science Foundation of China (No. 81870132).

ACKNOWLEDGMENTS

We thank the TCGA team of the National Cancer Institute for using their data.

SUPPLEMENTARY MATERIAL

The Supplementary Material for this article can be found online at: https://www.frontiersin.org/articles/10.3389/fgene.2020.573124/full#supplementary-material

REFERENCES

Arandi, N., Ramzi, M., Safaei, F., and Monabati, A. (2018). Overexpression of indoleamine 2,3-dioxygenase correlates with regulatory T cell phenotype in acute myeloid leukemia patients with normal karyotype. *Blood Res.* 53, 294–298. doi: 10.5045/br.2018.53.4.294

Baksh, S., Widlund, H. R., Frazer-Abel, A. A., Du, J., Fosmire, S., Fisher, D. E., et al. (2002). NFATc2-mediated repression of cyclin-dependent kinase 4 expression. *Mol. Cell* 10, 1071–1081. doi: 10.1016/S1097-2765(02)00701-3

Barbie, D. A., Tamayo, P., Boehm, J. S., Kim, S. Y., Moody, S. E., Dunn, I. F., et al. (2009). Systematic RNA interference reveals that oncogenic KRAS-driven cancers require TBK1. *Nature* 462, 108–112. doi: 10.1038/nature08460

Begicevic, R. R., and Falasca, M. (2017). ABC transporters in cancer stem cells: beyond chemoresistance. *Int. J. Mol. Sci.* 18:112362. doi: 10.3390/ijms18112362

Bhattacharya, S., Dunn, P., Thomas, C. G., Smith, B., Schaefer, H., Chen, J., et al. (2018). ImmPort, toward repurposing of open access immunological assay data for translational and clinical research. *Sci. Data* 5:180015. doi: 10.1038/sdata.2018.15

Cerami, E., Gao, J., Dogrusoz, U., Gross, B. E., Sumer, S. O., Aksoy, B. A., et al. (2012). The cBio cancer genomics portal: an open platform for exploring multidimensional cancer genomics data. *Cancer Discov.* 2, 401–404. doi: 10.1158/2159-8290.CD-12-0095

Cerrano, M., and Itzykson, R. (2019). New treatment options for acute myeloid leukemia in 2019. *Curr. Oncol. Rep.* 21:16. doi: 10.1007/s11912-019-0764-8

Chandrashekar, D. S., Bashel, B., Balasubramanya, S. A. H., Creighton, C. J., Ponce-Rodriguez, I., Chakravarthi, B., et al. (2017). UALCAN: a portal for facilitating tumor subgroup gene expression and survival analyses. *Neoplasia* 19, 649–658. doi: 10.1016/j.neo.2017.05.002

Charoentong, P., Finotello, F., Angelova, M., Mayer, C., Efremova, M., Rieder, D., et al. (2017). Pan-cancer immunogenomic analyses reveal genotype-immunophenotype relationships and predictors of response to checkpoint blockade. *Cell Rep.* 18, 248–262. doi: 10.1016/j.celrep.2016.12.019

Cole, A. J., Iyengar, M., Panesso-Gomez, S., O'Hayer, P., Chan, D., Delgoffe, G. M., et al. (2020). NFATC4 promotes quiescence and chemotherapy resistance in ovarian cancer. *JCI Insight* 5:131486. doi: 10.1172/jci.insight.131486

Consortium, G. (2015). Human genomics. The Genotype-Tissue Expression (GTEx) pilot analysis: multitissue gene regulation in humans. *Science* 348, 648–660. doi: 10.1126/science.1262110

Falvo, J. V., Lin, C. H., Tsytsykova, A. V., Hwang, P. K., Thanos, D., Goldfeld, A. E., et al. (2008). A dimer-specific function of the transcription factor NFATp. *Proc. Natl. Acad. Sci. U. S. A.* 105, 19637–19642. doi: 10.1073/pnas.0810648105

Fukuda, Y., Lian, S., and Schuetz, J. D. (2015). Leukemia and ABC transporters. *Adv. Cancer Res.* 125, 171–196. doi: 10.1016/bs.acr.2014.10.006

Ghandi, M., Huang, F. W., Jane-Valbuena, J., Kryukov, G. V., Lo, C. C., McDonald, E. R. 3rd, Barretina, J., et al. (2019). Next-generation characterization of the cancer cell line encyclopedia. *Nature* 569, 503–508. doi: 10.1038/s41586-019-1186-3

Goldman, M., Craft, B., Swatloski, T., Cline, M., Morozova, O., Diekhans, M., et al. (2015). The UCSC cancer genomics browser: update 2015. *Nucl. Acids Res.* 43, D812–D817. doi: 10.1093/nar/gku1073

Goswami, C. P., and Nakshatri, H. (2014). PROGgeneV2: enhancements on the existing database. *BMC Cancer* 14:970. doi: 10.1186/1471-2407-14-970

Govindaraj, C., Madondo, M., Kong, Y. Y., Tan, P., Wei, A., and Plebanski, M. (2014). Lenalidomide-based maintenance therapy reduces TNF receptor 2 on CD4 T cells and enhances immune effector function in acute myeloid leukemia patients. *Am. J. Hematol.* 89, 795–802. doi: 10.1002/ajh.23746

Graef, I. A., Wang, F., Charron, F., Chen, L., Neilson, J., Tessier-Lavigne, M., et al. (2003). Neurotrophins and netrins require calcineurin/NFAT signaling to stimulate outgrowth of embryonic axons. *Cell* 113, 657–670. doi: 10.1016/S0092-8674(03)00390-8

Han, Q., Ma, J., Gu, Y., Song, H., Kapadia, M., Kawasawa, Y. I., et al. (2019). RAG1 high expression associated with IKZF1 dysfunction in adult B-cell acute lymphoblastic leukemia. *J. Cancer* 10, 3842–3850. doi: 10.7150/jca.33989

Hessmann, E., Zhang, J. S., Chen, N. M., Hasselluhn, M., Liou, G. Y., Storz, P., et al. (2016). NFATc4 regulates Sox9 gene expression in acinar cell plasticity and pancreatic cancer initiation. *Stem Cells Int.* 2016:5272498. doi: 10.1155/2016/5272498

Kang, T., Ge, M., Wang, R., Tan, Z., Zhang, X., Zhu, C., et al. (2019). Arsenic sulfide induces RAG1-dependent DNA damage for cell killing by inhibiting NFATc3 in gastric cancer cells. *J. Exp. Clin. Cancer Res.* 38:487. doi: 10.1186/s13046-019-1471-x

Kaunisto, A., Henry, W. S., Montaser-Kouhsari, L., Jaminet, S. C., Oh, E. Y., Zhao, L., et al. (2015). NFAT1 promotes intratumoral neutrophil infiltration by regulating IL8 expression in breast cancer. *Mol. Oncol.* 9, 1140–1154. doi: 10.1016/j.molonc.2015.02.004

Ke, Q., Li, J., Ding, J., Ding, M., Wang, L., Liu, B., et al. (2006). Essential role of ROS-mediated NFAT activation in TNF-alpha induction by crystalline silica exposure. *Am. J. Physiol. Lung Cell Mol. Physiol.* 291, L257–L264. doi: 10.1152/ajplung.00007.2006

Kim, H. B., Kumar, A., Wang, L., Liu, G. H., Keller, S. R., Lawrence, J. C. Jr., et al. (2010). Lipin 1 represses NFATc4 transcriptional activity in adipocytes to inhibit secretion of inflammatory factors. *Mol. Cell Biol.* 30, 3126–3139. doi: 10.1128/MCB.01671-09

Kuwata, H., Yuzurihara, C., Kinoshita, N., Taki, Y., Ikegami, Y., Washio, S., et al. (2018). The group VIA calcium-independent phospholipase A2 and NFATc4 pathway mediates IL-1β-induced expression of chemokines CCL2 and CXCL10 in rat fibroblasts. *FEBS J.* 285, 2056–2070. doi: 10.1111/febs.14462

Li, Z., Philip, M., and Ferrell, P. B. (2020). Alterations of T-cell-mediated immunity in acute myeloid leukemia. *Oncogene* 39, 3611–3619. doi: 10.1038/s41388-020-1239-y

Liu, X. (2019). ABC family transporters. *Adv. Exp. Med. Biol.* 1141, 13–100. doi: 10.1007/978-981-13-7647-4_2

Maitra, U., Parks, J. S., and Li, L. (2009). An innate immunity signaling process suppresses macrophage ABCA1 expression through IRAK-1-mediated downregulation of retinoic acid receptor α and NFATc2. *Mol. Cell Biol.* 29, 5989–5997. doi: 10.1128/MCB.00541-09

Mei, S., Qin, Q., Wu, Q., Sun, H., Zheng, R., Zang, C., et al. (2017). Cistrome Data Browser: a data portal for ChIP-Seq and chromatin accessibility data in human and mouse. *Nucl. Acids Res.* 45, D658–D662. doi: 10.1093/nar/gkw983

Mortarini, R., Scarito, A., Nonaka, D., Zanon, M., Bersani, I., Montaldi, E., et al. (2005). Constitutive expression and costimulatory function of LIGHT/TNFSF14 on human melanoma cells and melanoma-derived microvesicles. *Cancer Res.* 65, 3428–3436. doi: 10.1158/0008-5472.CAN-04-3239

Neal, J. W., and Clipstone, N. A. (2003). A constitutively active NFATc1 mutant induces a transformed phenotype in 3T3-L1 fibroblasts. *J. Biol. Chem.* 278, 17246–17254. doi: 10.1074/jbc.M300528200

Newman, A. M., Liu, C. L., Green, M. R., Gentles, A. J., Feng, W., Xu, Y., et al. (2015). Robust enumeration of cell subsets from tissue expression profiles. *Nat. Methods* 12, 453–457. doi: 10.1038/nmeth.3337

Niedzwiecki, M., Budzilo, O., Adamkiewicz-Drozynska, E., Pawlik-Gwozdecka, D., Zielinski, M., Maciejka-Kemblowska, L., et al. (2019). CD4(+)CD25(high)CD127(low/-)FoxP3 (+) regulatory T-cell population in acute leukemias: a review of the literature. *J. Immunol. Res.* 2019:2816498. doi: 10.1155/2019/2816498

Papatheodorou, I., Fonseca, N. A., Keays, M., Tang, Y. A., Barrera, E., Bazant, W., et al. (2018). Expression Atlas: gene and protein expression across multiple studies and organisms. *Nucl. Acids Res.* 46, D246–D251. doi: 10.1093/nar/gkx1158

Pollyea, D. A. (2018). New drugs for acute myeloid leukemia inspired by genomics and when to use them. *Hematol. Am. Soc. Hematol. Educ. Program* 2018, 45–50. doi: 10.1182/asheducation-2018.1.45

Rhodes, D. R., Yu, J., Shanker, K., Deshpande, N., Varambally, R., Ghosh, D., et al. (2004). ONCOMINE: a cancer microarray database and integrated data-mining platform. *Neoplasia* 6, 1–6. doi: 10.1016/S1476-5586(04)80047-2

Robinson, M. D., McCarthy, D. J., and Smyth, G. K. (2010). edgeR: a Bioconductor package for differential expression analysis of digital gene expression data. *Bioinformatics* 26, 139–140. doi: 10.1093/bioinformatics/btp616

Shannon, P., Markiel, A., Ozier, O., Baliga, N. S., Wang, J. T., Ramage, D., et al. (2003). Cytoscape: a software environment for integrated models of biomolecular interaction networks. *Genome Res.* 13, 2498–2504. doi: 10.1101/gr.1239303

Snel, B., Lehmann, G., Bork, P., and Huynen, M. A. (2000). STRING: a web-server to retrieve and display the repeatedly occurring neighbourhood of a gene. *Nucl. Acids Res.* 28, 3442–3444. doi: 10.1093/nar/28.18.3442

Tang, Z., Li, C., Kang, B., Gao, G., Li, C., and Zhang, Z. (2017). GEPIA: a web server for cancer and normal gene expression profiling and interactive analyses. *Nucl. Acids Res.* 45, W98–W102. doi: 10.1093/nar/gkx247

Uhlen, M., Fagerberg, L., Hallstrom, B. M., Lindskog, C., Oksvold, P., Mardinoglu, A., et al. (2015). Proteomics. Tissue-based map of the human proteome. *Science* 347:1260419. doi: 10.1126/science.1260419

Vasaikar, S. V., Straub, P., Wang, J., and Zhang, B. (2018). LinkedOmics: analyzing multi-omics data within and across 32 cancer types. *Nucl. Acids Res.* 46, D956–D963. doi: 10.1093/nar/gkx1090

Williams, P., Basu, S., Garcia-Manero, G., Hourigan, C. S., Oetjen, K. A., Cortes, J. E., et al. (2019). The distribution of T-cell subsets and the expression of immune checkpoint receptors and ligands in patients with newly diagnosed and relapsed acute myeloid leukemia. *Cancer* 125, 1470–1481. doi: 10.1002/cncr.31896

Yue, Y., Lian, J., Wang, T., Luo, C., Yuan, Y., Qin, G., et al. (2020). Interleukin-33-nuclear factor-kappaB-CCL2 signaling pathway promotes progression of esophageal squamous cell carcinoma by directing regulatory T cells. *Cancer Sci.* 111, 795–806. doi: 10.1111/cas.14293

Conflict of Interest: The authors declare that the research was conducted in the absence of any commercial or financial relationships that could be construed as a potential conflict of interest.

frontiers in Oncology

ORIGINAL RESEARCH
published: 08 January 2021
doi: 10.3389/fonc.2020.607593

GFI1-Mediated Upregulation of LINC00675 as a ceRNA Restrains Hepatocellular Carcinoma Metastasis by Sponging miR-942-5p

Libai Lu[1†], Shubo Li[2†], Ying Zhang[3†], Zongjiang Luo[1], Yichen Chen[1], Jiasheng Ma[1], Pengyu Chen[1], Wei Wang[1], Jian Pu[1] and Jianchu Wang[1]*

[1] Department of Hepatobiliary Surgery, Affiliated Hospital of Youjiang Medical University for Nationalities, Baise, China,
[2] Department of Biochemistry and Molecular Biology, Youjiang Medical University for Nationalities, Baise, China,
[3] Library of Youjiang Medical University for Nationalities, Baise, China

OPEN ACCESS

Edited by:
Xiaochen Wang,
University of Texas Southwestern Medical Center, United States

Reviewed by:
Zhenna Xiao,
University of Texas MD Anderson Cancer Center, United States
Donghua Xu,
Weifang Medical University, China
Tuoye Xu,
Massachusetts General Hospital, United States

***Correspondence:**
Jianchu Wang
wjianchu@sina.com

[†]These authors have contributed equally to this work

Specialty section:
This article was submitted to Cancer Genetics, a section of the journal Frontiers in Oncology

Received: 17 September 2020
Accepted: 11 November 2020
Published: 08 January 2021

Citation:
Lu L, Li S, Zhang Y, Luo Z, Chen Y, Ma J, Chen P, Wang W, Pu J and Wang J (2021) GFI1-Mediated Upregulation of LINC00675 as a ceRNA Restrains Hepatocellular Carcinoma Metastasis by Sponging miR-942-5p. Front. Oncol. 10:607593. doi: 10.3389/fonc.2020.607593

Hepatocellular carcinoma (HCC) is a common malignant liver tumor worldwide. Tumor recurrence and metastasis contribute to the bad clinical outcome of HCC patients. Substantial studies have displayed lncRNAs modulate various tumorigenic processes of many cancers. Our current work was aimed to investigate the function of LINC00675 in HCC and to recognize the potential interactions between lncRNAs and microRNAs. GFI1 can exhibit a significant role in the progression of human malignant tumors. Firstly, GFI1 was identified using real-time PCR in HCC tissues and cells. In this work, we indicated GFI1 was remarkably reduced in HCC tissues and cells. Meanwhile, GFI1 specifically interacted with the promoter of LINC00675. Up-regulation of LINC00675 obviously repressed the migration and invasion capacity of SMCC-7721 and QGY-7703 cells *in vitro*. Moreover, decrease of LINC00675 competitively bound to miR-942-5p that contributed to the miRNA-mediated degradation of GFI1, thus facilitated HCC metastasis. The ceRNA function of LINC00675 in HCC cells was assessed and confirmed using RNA immunoprecipitation assay and RNA pull-down assays in our work. Additionally, we proved overexpression of miR-942-5p promoted HCC progression, which was reversed by the up-regulation of GFI1. In summary, LINC00675 might act as a prognostic marker for HCC, which can inhibit HCC development *via* regulating miR-942-5p and GFI1.

Keywords: growth factor independent 1 transcriptional repressor, lncRNA, HCC, hepatocellular carcinoma, LINC00675

INTRODUCTION

Hepatocellular carcinoma (HCC) is a frequent malignant tumor and it is the third common cause of cancer-related death across the world (1, 2). In spite of the therapeutic treatment for HCC, its survival rate is still poor because of the recurrence after surgery (3, 4). Hence, novel insights into the mechanism of HCC are in need to recognize the prognostic molecular markers to improve HCC patient survival (5).

Growth factor independent 1 transcriptional repressor (GFI1) is located in chromosome 1p22 in the human genome (6). GFI1 can act as a transcriptional repressor by interacting with other cofactors (7). It has been reported that GFI1 exhibits an important role in hematopoietic stem cells. GFI1 inhibits proliferation and preserves functional integrity in regulating self-renewal of hematopoietic stem cells (8). However, the functional role of GFI1 in HCC carcinogenesis has not been fully investigated.

LncRNAs are non-coding RNAs are longer than 200 nts, and they play few or no capacity of protein-coding (9–11). In addition, lncRNAs are dys-regulated in specific tumor types. Studies have indicated that lncRNAs can promote cancer phenotypes through interacting with DNA, RNA, and protein (12–14). Besides, it has been reported that lncRNA exhibits significant roles in HCC progression (15, 16). For example, MCM3AP-AS1 can induce the growth of HCC through regulating miR-194-5p and FOXA1 (17). LncRNA MALAT1 can contribute to HCC development through up-regulating SRSF1 and the activation of mTOR (18).

LINC00675 is also known as TMEM238L, and it has been reported to be dys-regulated in many cancers. For instance, in gastric cancer, LINC00675 is able to enhance phosphorylation of vimentin on Ser83 (19). LINC00675 represses colorectal cancer progression through sponging miR-942 and regulating Wnt/β-catenin signaling (20). Additionally, LINC00675 indicates short survival in patients of pancreatic ductal adenocarcinoma (21). The detailed value of LINC00675 in HCC remains unknown.

In our current study, we reported that LINC00675 repressed HCC metastasis *via* functioning as a ceRNA to reduce miR-942-5p expression level and activated the expression of GFI1. In addition, GFI1 can interact with the promoter of LINC00675 in HCC.

MATERIALS AND METHODS

Clinical Tissues

Fifty pairs of primary human HCC cancerous tissues and corresponding adjacent liver tissues were acquired at Affiliated Hospital of Youjiang Medical University for Nationalities from 2012 to 2016. The patients given chemotherapy or radiotherapy were excluded in our work. Study approaches were approved by the Ethics Committee of Affiliated Hospital of Youjiang Medical University for Nationalities, and the informed consents were provided according to the committee regulations. Tissues were kept in liquid nitrogen upon hepatectomy immediately for future study.

Cell Culture

Human HCC cell lines (Hep-3B, QGY-7703, SMMCC-7721, and MHCC-97L) and hepatocyte QSG-7701 cells were obtained from the Type Culture Collection of the Chinese Academy of Sciences. DMEM medium was added with 10% FBS, 100 U/ml penicillin, and 100 μg/ml streptomycin. A humidified chamber with 5% CO_2 at 37°C was used to maintain the cells.

Cell Transfection

The GFI siRNA and miR-942-5p mimics and inhibitors were obtained from GenePharma (Shanghai, China). Overexpression of GFI1 and LINC00675 was performed by transfection with the recombinant GFI1 and LINC00675 pcDNA3.1(+) plasmid. Lentiviral vectors for LINC00675 shRNA were constructed by Bio-Link Gene (Shanghai, China). HCC cells were transfected using lipofectamine 3000 under the official instructions.

CCK-8 Assay

Cell viability was tested by CCK-8 kit (Dojindo, Shanghai, China). After transfection, cells were grown into 96-well plates. Then, 10 μl CCK-8 was added at various days. After 2 h, the absorbance was determined at 450 nm on a microplate reader.

EdU Staining Assay

EdU assay was carried out using Click iT^{TM} EdU cell proliferation assay kit (Invitrogen, Carlsbad, CA, USA). Cells were stained using 50 μM EdU for 2 h. Then, the cells were washed using PBS and fixed. Cell nuclei were stained by DAPI for 10 min. A florescence microscope was used to examine the results of cell staining.

Flow Cytometry

Apoptosis of HCC cells was analyzed by PI and FITC Annexin V Apoptosis Detection Kit I (BD Biosciences, San Jose, CA, USA). After transfection, HCC cells were re-suspended in 1× binding buffer. Afterwards, cells were stained using 5 μl Annexin V-FITC for 15 min and 5 μl PI for 10 min. Subsequently, the apoptosis was assessed using a FACSCanto II flow cytometer.

Cell Cycle Determination

Cells were prepared for cell suspension and washed using pre-cooled PBS. Then, cells were suspended in the mixture with 0.1 ml of pre-cooled PBS and 1 ml of pre-cooled 75% ethanol. Subsequently, cells were incubated with PI and RNase A at a final dose of 50 ng/ml. Cell cycle was determined by flow cytometry analysis.

Cell Migration and Invasion Assay

To perform transwell migration assay, cells were seeded in the top chamber of each insert with a non-coated membrane. Then, to perform invasion assay, cells were placed in the upper chamber of each Matrigel-coated insert. Cells that migrated or invaded were fixed and stained using dye solution containing 0.1% crystal violet and 20% methanol. Afterwards, an IX71 inverted microscope (Olympus Corp, Tokyo, Japan) was used to count the cells.

Western Blotting Analysis

HCC cells were lysed using RIPA buffer. Protein concentration was assessed using BCA protein assay kit. 30 μg protein was separated by 10% SDS-PAGE gel electrophoresis and then transferred onto a nitrocellulose membrane. Afterwards, the membranes were incubated with primary antibodies against GFI1 and GAPDH (1:1,000; Abcam, Cambridge, MA, USA). The bands were blocked with goat anti-rabbit IgG-HRP secondary antibody (1:5,000; Abcam, Cambridge, MA, USA) and were exposed by chemiluminescence substance (Pierce Biotechnology Inc., Thermo Fisher Scientific, Rockford, IL, USA).

RT-PCR

RNA was extracted using TRIzol reagent and RNeasy Plus Micro Kit (QIAGEN, Germantown, MD, USA). Reverse transcription was carried out to synthesize the Bestar qPCR RT Kit (DBI Bioscience, Shanghai, China). Real time-PCR was carried out in Applied Biosystems 7500 Real Time PCR System (Applied Biosystems, Foster City, CA, USA) using SYBR® Green PCR Master Mix (Invitrogen, Thermo Fisher Scientific). Gene expression level was normalized to U6 RNA and GAPDH expression. Relative gene expression was evaluated using $2^{-\Delta\Delta ct}$. Primers were exhibited in **Table 1**.

In Vivo Assay for Metastasis

A total of 20 female BALB/c nude mice (5–6 wk old) were obtained from Beijing Wei-tong Li-hua Laboratory Animals and Technology (Beijing, China). To carry out *in vivo* metastasis assays, 3×10^6 QGY-7703 cells overexpressed LINC00675 or empty vector were suspended in 300 μl serum-free DMEM per female BALB/c mice and injected through the tail vein (10 mice per group). After six weeks, mice were sacrificed and the lungs were dissected. The tissues were fixed using phosphate-buffered neutral formalin. The wax containing xenograft tissues was sliced and the xylene was utilized to do dewaxing and hydrating. The slices were stained using with H&E. Then, the slices were observed using an ECLIPSE Ti2 microscope (Ti2-U, Nikon, Tokyo, Japan). Mice were housed based on the protocols approved by the Medical Experimental Animal Care Commission of Affiliated Hospital of Youjiang Medical University for Nationalities.

Luciferase Reporter Assay

To assess luciferase activity, Dual-Glo Luciferase Assay System (Promega, Madison, WI, USA) was performed. Lipofectamine® 3000 was used to transfect cloned LINC00675/GFI1 wild-type 3′ UTR or mutant 3′UTR purchased from Shanghai GeneChem (Shanghai, China) with miR-942-5p mimics, inhibitors or negative controls. 48 h later, luciferase activity was tested using the dual-luciferase reporter assay system.

Pull Down of Biotin-Coupled miRNA

Biotin was attached to the 3′-end of miR-942-5p. Cells were transfected with miR-942-5p mimics or inhibitors using Lipofectamine 3000. Cell pellets were re-suspended in 0.7 ml lysis buffer, 0.3% NP-40, 50 U of RNase OUT, complete protease inhibitor cocktail. Then, cell lysate was isolated by centrifugation at 10,000 g. Finally, the level of LINC00675 or in the pull down of biotin-miR-942-5p was quantified using real-time PCR.

Statistical Analysis

The data was analyzed using GraphPad Prism 6.0 and SPSS 22.0. Student's t-test was employed to compare two groups and differences among more than two groups were compared by one-way ANOVA. A value of $p < 0.05$ was considered to be statistically significantly.

RESULTS

GFI1 Is Down-Regulated in HCC Patients and Tissues

Firstly, we investigated the expression of GFI1 in HCC tissue samples and adjacent tissues. It was shown that GFI1 was obviously reduced in HCC tissues as displayed in **Figure 1A**. In **Figure 1B**, it was indicated that GFI1 was decreased in advanced HCC tissues (stages T3–T4) compared to T1–T2 stages. In addition, in **Figure 1C**, we found that GFI1 LINC00675 was greatly decreased in HCC tissues with lymphatic metastasis compared. Next, we confirmed that GFI1 was also decreased in HCC cells (Hep3B, QGY-7703, SMCC-7721 and MHCC-97L) compared with the QSG-7701 cells in **Figure 1D**.

LINC00675 Is Modulated by the Transcription Factor GFI1

In order to study the mechanism of LINC00675 down-regulation in HCC, bioinformatical software program JASPAR (http://jaspar.genereg.net/cgi-bin/jaspar_db.pl) was carried out to analyze the promoter regions of LINC00675, and three potential sites of GFI1 binding were predicted. In **Figure 2A**, the DNA motif of GFI1 in UBE4B promoter was demonstrated. QGY-7703 and SMCC-7721 cells were transfected with GFI1 siRNA. LINC00675 expression was significantly decreased after GFI1 was reduced in HCC cells (**Figures 2B, C**). The LINC00675 promoter region including three binding sites of GFI1 was inserted into a PGL3 vector as displayed in **Figure 2D**. As shown in **Figures 2E, F**, GFI1 significantly enhanced the luciferase activity in HCC cells.

Up-Regulation of LINC00675 Represses HCC Cell Proliferation, Migration, and Invasion

Moreover, to study the effect of LINC00675 on HCC cell proliferation, QGY-7703 and SMCC-7721 cells were transfected with LINC00675 overexpression plasmid. EdU assay indicated that overexpression of LINC00675 significantly

TABLE 1 | Primers for real-time PCR.

Genes	Forward (5′–3′)	Reverse (5′–3′)
GAPDH	GGAGATTGTTGCCATCAACG	TTGGTGGTGCAGGATGCATT
LINC00675	GCCTACTGCTCTGGATCATCTGGTA	ACCTGCGTCTCTTCTCCTCTTCC
GFI1	CCGACTCTCAGCTTACCGAG	CTGTGTGGATGAAGGTGTGTTT
miR-942-5p	CUUCUCUGUUUUGGCCAUGUG	CTCTACAGCTATATTGCCAGCCAC
U6	GCTTCGGCAGCACATATACT	AACGCTTCACGAATTTGCGT

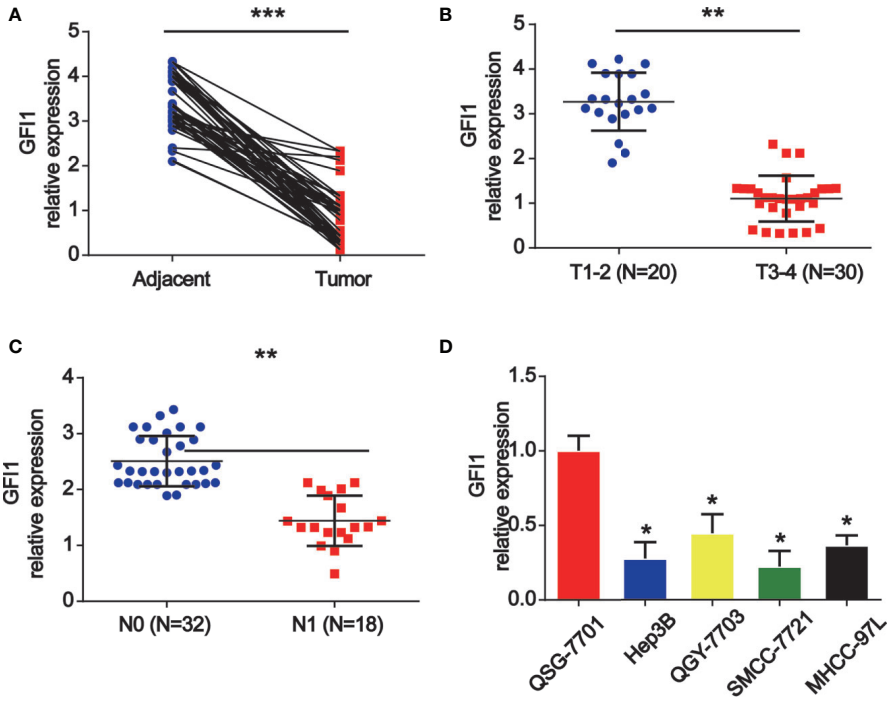

FIGURE 1 | GFI1 was increased in HCC tissues and HCC cells. **(A)** The expression of GFI1 was detected by real-time PCR in in 50 pairs of HCC carcinoma and normal adjacent tissues. **(B)** Expression of GFI1 in HCC tissues at different stages. **(C)** Expression of GFI1 in HCC tissues with metastasis and without metastasis. **(D)** Expression of GFI1 in HCC cells (Hep-3B, QGY-7703, SMCC-7721 and MHCC-97L) and QSG-7701 cells. *P < 0.05; **P < 0.01; ***P < 0.001.

inhibited QGY-7703, SMCC-7721 cell proliferation compared with the control groups in **Figures 3A, B**. As shown in **Figure 3C**, QGY-7703 and SMCC-7721 cell apoptosis was obviously triggered by the overexpressed LINC00675. In addition, in **Figure 3D**, HCC cell cycle distribution was blocked in G1 phase significantly by LINC00675. Transwell migration and invasion assay implied that the migrated and invaded cells in LINC00675 overexpression groups were notably less than the

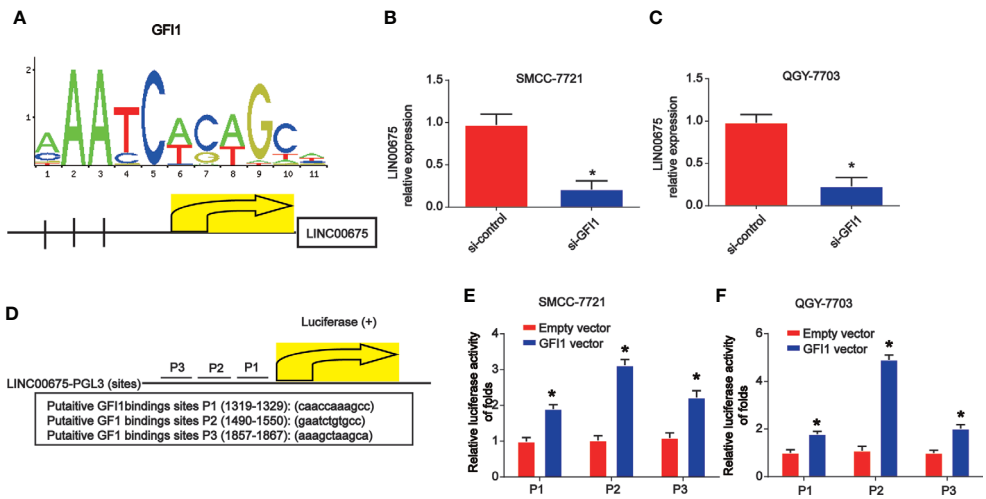

FIGURE 2 | GFI1 acted as a transcription inducer of LINC00675. **(A)** DNA motif of GFI1 in the promoter of LINC00675. **(B, C)** Expression of GFI1 in QGY-7703 and SMCC-7721 cells transfected with siRNA of GFI1 for 48 h. **(D)** The predicted three binding sites of GFI1 in LINC00675 promoter. **(E, F)** Luciferase activity analysis of the binding sites in HCC cells transfected with GFI1 oligonucleotides. *P < 0.05.

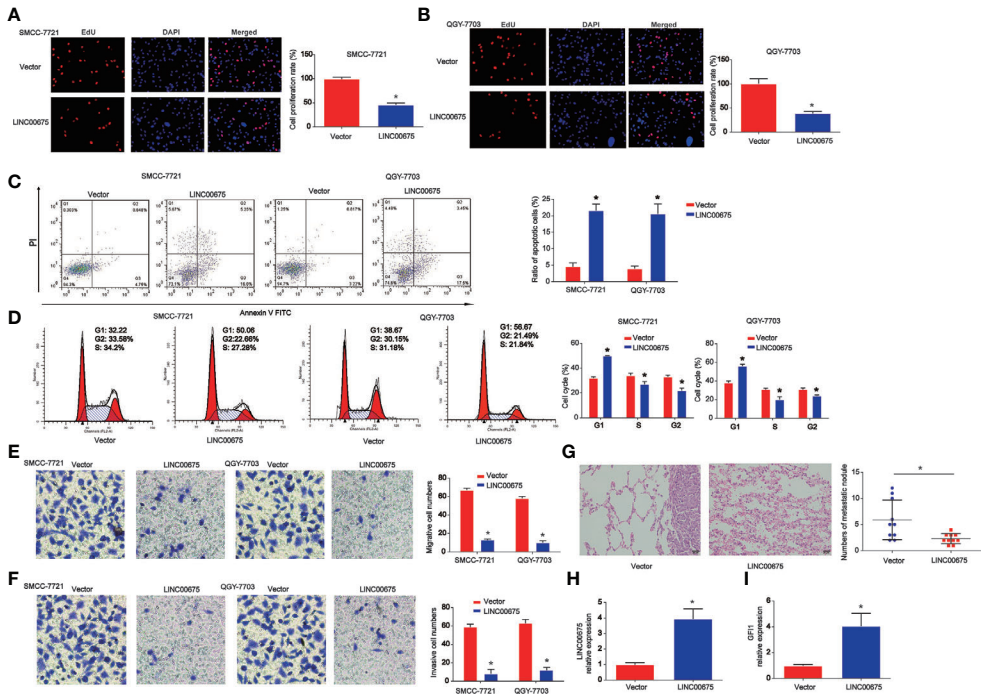

FIGURE 3 | Effects of LINC00675 on HCC cell proliferation, migration, and invasion. **(A, B)** EdU assay was carried to test cell viability. QGY-7703 and SMMC-7721 cells transfected with LINC00675 overexpression vector. **(C, D)** Effects of LINC00675 on HCC cell apoptosis and cell cycle. **(E, F)** Effects of LINC00675 on HCC cell migration and invasion. Transwell migration and invasion assay was carried out to evaluate cell migration and invasion capacity. **(G)** Gross morphology of representative lungs and characteristic H&E staining of metastatic nodules in the lung of nude mice. **(H, I)** LINC00675 and GFI1 expression in lung tissues. n = 10 mice per group. *P < 0.05.

cells in the LV-NC group in **Figures 3E, F**. Then, we implanted either control or QGY-7703 cells with stable overexpressed LINC00675. In **Figure 3G**, it was shown that LINC00675 overexpression significantly depressed the number of metastatic lung nodules. Subsequently, we confirmed that LINC00675 and GFI1 expression was greatly increased in mice lung tissues (**Figures 3H, I**).

LINC00675 Abundantly Sponges miR-942-5p

Then, by using bioinformatics analysis, the binding sites between LINC00675 and miR-942-5p was exhibited in **Figure 4A**. Luciferase reporter plasmids of WT-LINC00675 and MUT-LINC00675 binding sites were displayed in **Figure 4A**. In addition, a negative correlation between LINC00675 and miR-942-5p was shown in HCC tissues (**Figure 4B**). Co-transfection of the WT-LINC00675 with miR-924-5p inhibitors induced the reporter activity while the mimics reduced the reporter activity (**Figure 4C**). In **Figure 4D**, LINC00675 was most abundantly pulled down by miR-942-5p in QGY-7703 and SMCC-7721 cells.

Loss of miR-942-5p Restrains HCC Cell Growth, Migration, and Invasion Induced by Loss of LINC00675

In **Figures 5A, E**, SMCC-7721 and QGY-7703 cells were transfected with LINC00675 shRNA. LINC00675-01 exhibited a better knockdown effect, and it was chosen for the following assays. In addition, GFI1 protein expression was significantly reduced by loss of LINC00675 shRNA in **Figures 5B, F**. Then, SMCC-7721 and QGY-7703 were transfected with miR-942-5p inhibitors after loss of LINC00675. As shown in **Figures 5C, G**, LINC00675 was greatly reduced by LINC00675 shRNA and inhibitors of miR-942-5p induced LINC00675 expression. For another, we observed that miR-942-5p was increased after LINC00675 was increased in QGY-7703 and SMCC-7721 cells, which was successfully decreased by the inhibitors (**Figures 5D, H**). Furthermore, HCC cell proliferation, migration and invasion capacity was obviously enhanced by loss of LINC 00675, which was repressed by miR-942-5p inhibitors (**Figures 5I–L**).

GFI1 Is a Downstream Target of miR-942-5p

Moreover, by using bioinformatics analysis, the binding sites between GFI1 and miR-942-5p was displayed in **Figure 6A**. Luciferase reporter plasmids of WT-GFI1 and MUT-GFI1 binding sites were demonstrated in **Figure 6A**. Co-transfection of the WT-GFI1 with miR-924-5p inhibitors enhanced the reporter activity while the mimics of miR-924-5p inhibited the reporter activity (**Figure 6B**). In addition, miR-924-5p mimics reduced GFI1 mRNA, and protein expression significantly in QGY-7703 and SMCC-7721 cells (**Figures 6C, D**).

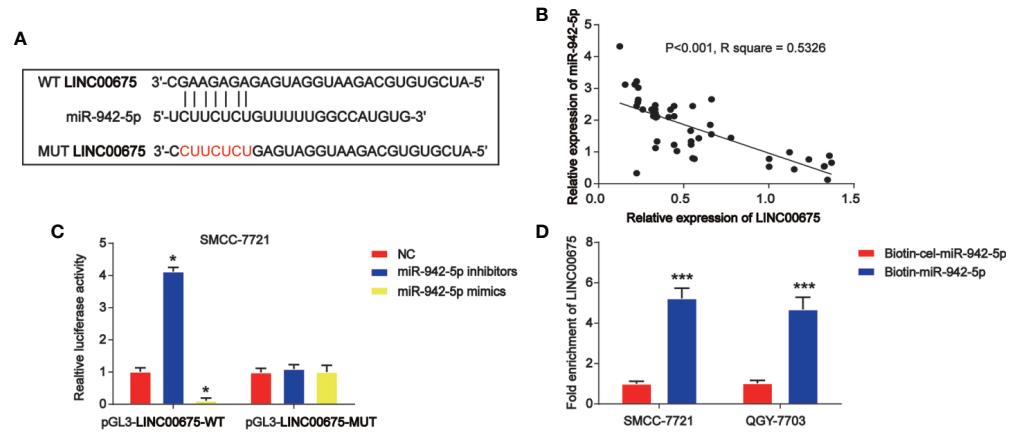

FIGURE 4 | LINC00675 sponged miR-942-5p in HCC cells. **(A)** The putative binding sites between miR-942-5p and LINC00675 and the mutant sites in LINC00675-MUT reporter were displayed. **(B)** Correlation between miR-942-5p and LINC00675 in 50 pairs of HCC tissues. **(C)** Luciferase activity was evaluated in SMCC-7721 cells co-transfected with WT-LINC00675 or MUT-LINC00675 reporter and miR-942-5p inhibitors or mimics. **(D)** LINC00675 was pulled down by biotinylated wild-type miR-942-5p. *P < 0.05, ***P < 0.001.

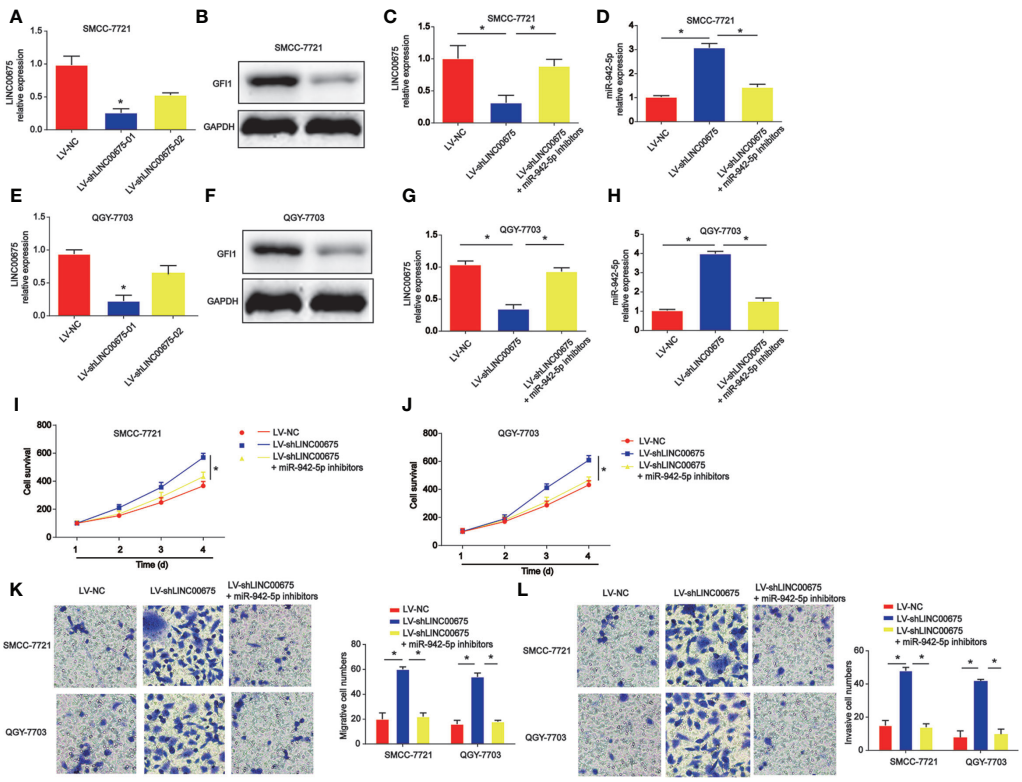

FIGURE 5 | Effects of miR-942-5p on HCC cell proliferation, migration, and invasion. **(A)** Expression of LINC00675 in SMMC-7721 cells transfected with LINC00675 shRNA. **(B)** Expression of GFI1 protein in SMMC-7721 cells transfected with LINC00675 shRNA. **(C)** Expression of LINC00675 in SMMC-7721 cells transfected with LV-shLINC00675 and miR-942-5p inhibitors. **(D)** Expression of miR-942-5p in SMMC-7721 cells transfected with LV-shLINC00675 and miR-942-5p inhibitors. **(E)** Expression of LINC00675 in QGY-7703 cells transfected with LINC00675 shRNA. **(F)** Expression of GFI1 protein in QGY-7703 cells transfected with LINC00675 shRNA. **(G)** Expression of LINC00675 in QGY-7703 cells transfected with LV-shLINC00675 and miR-942-5p inhibitors. **(H)** Expression of miR-942-5p in QGY-7703 cells transfected with LV-shLINC00675 and miR-942-5p inhibitors. **(I, J)** Effects of miR-942-5p on HCC cell proliferation. **(K, L)** Effects of miR-942-5p on HCC cell migration and invasion. *P < 0.05.

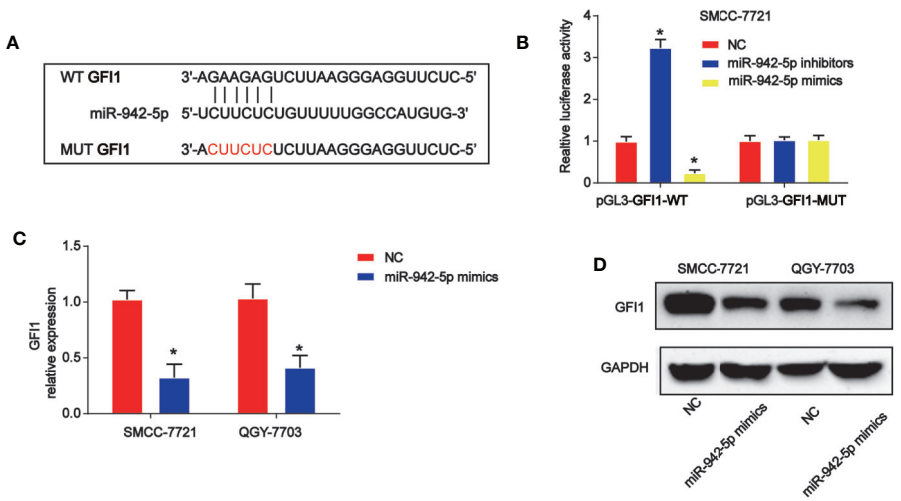

FIGURE 6 | miR-942-5p targeted GFI1 in HCC cells. **(A)** The putative binding sites between miR-942-5p and GFI1 and the mutant sites in GFI1-MUT reporter were displayed. **(B)** Luciferase activity was evaluated in SMCC-7721 cells co-transfected with WT-GFI1 or MUT-GFI1 reporter and miR-942-5p inhibitors or mimics. **(C, D)** GFI1 mRNA and protein expression in SMCC-7721 cells transfected with miR-942-5p mimics. Error bars stand for the mean ± SD of at least triplicate assays. *P < 0.05.

Overexpression of GFI1 Depresses HCC Cell Progression Triggered by miR-924-5p Mimics

Subsequently, QGY-7703 and SMCC-7721 cells were transfected with GFI1 overexpression plasmid after miR-942-5p mimics were transfected into the cells. CCK-8 indicated that HCC cell survival was increased by miR-942-5p overexpression, which was reversed by GFI1 overexpression as shown in **Figures 7A, B**. In **Figure 7C**, we found that HCC cell apoptosis was increased by the up-regulation of GFI1. Additionally, QGY-7703 and SMCC-7721 cell migration and invasion were increased by the mimics of miR-942-5p, which was decreased by increased GFI1 as manifested in **Figures 7D, E**.

DISCUSSION

In our present work, we identified LINC00675 was aberrantly expressed in human HCC tissues and cells. As known, lncRNAs with differential expression in malignant tumors can indicate the prognosis (22–24). A growing number of biomarkers are reported in patients with HCC (25). For example, lncRNA-D16366 has been identified as a potential biomarker for HCC (26). Down-regulation of lncRNA ZNF385D-AS2 expression exhibits a crucial prognostic significance in HCC (27).

The data of our present study displayed that GFI1/LINC00675/miR-942-5p as a prognostic factor in HCC development. GFI1 was frequently reduced in HCC tissues and HCC cell lines. Then, we focused on the potential mechanism responsible for LINC00675 down-regulation in HCC cells. GFI1 could interact with the LINC00675 promoter through the three binding sites. Our current results confirmed the regions on the LINC00675 promoter. miR-942-5p was predicted as a downstream target of LINC00675. Loss of LINC00675 induced HCC cell growth, which was reversed by down-regulation of miR-942-5p. Additionally, GFI1 acted as a direct target for miR-942-5p.

LINC00675 is a kind of intergenic lncRNA, and increasing studies demonstrates LINC00675 is dys-regulated in various cancers. For instance, LINC00675 can regulate cervical cancer cell growth through affecting Wnt/β-catenin signaling (28). LINC00675 can repress tumorigenesis and EMT of esophageal squamous cell carcinoma *via* repressing Wnt/β-catenin pathway (29). In addition, LINC00675 is a significant prognostic factor of glioma, which can regulate cell proliferation, migration and invasion (30). These findings support the potential tumor inhibitory role of LINC00675 in cancers. Here, we observed that LINC00675 was decreased in HCC and up-regulation of LINC00675 significantly repressed HCC cell proliferation, migration and invasion. Then, the detailed mechanism of LINC00675 in regulating HCC progression was investigated.

Transcription factors exhibit crucial roles in determining cell fate and behavior. GFI1 is a kind of DNA binding zinc finger protein and it can mediate transcriptional repression through recruiting histone-modifying enzymes to its targets (31). Down-regulation of GFI1 can promote inflammation-linked metastasis of colorectal cancer, and it is a tumor suppressor gene (32, 33).Currently, we proved that GFI1 was down-regulated in HCC tissues and cells. Meanwhile, GFI1 interacted with the LINC00675 promoter *via* the three binding sites. The binding sites on the LINC00675 promoter contained regulatory elements for the transcription of LINC00675 were exhibited. Additionally, whether GFI1 could serve as a downstream target of LINC00675 was explored.

As well known, lncRNAs can act their roles *via* sponging microRNAs to modulate the target gene expression (34).

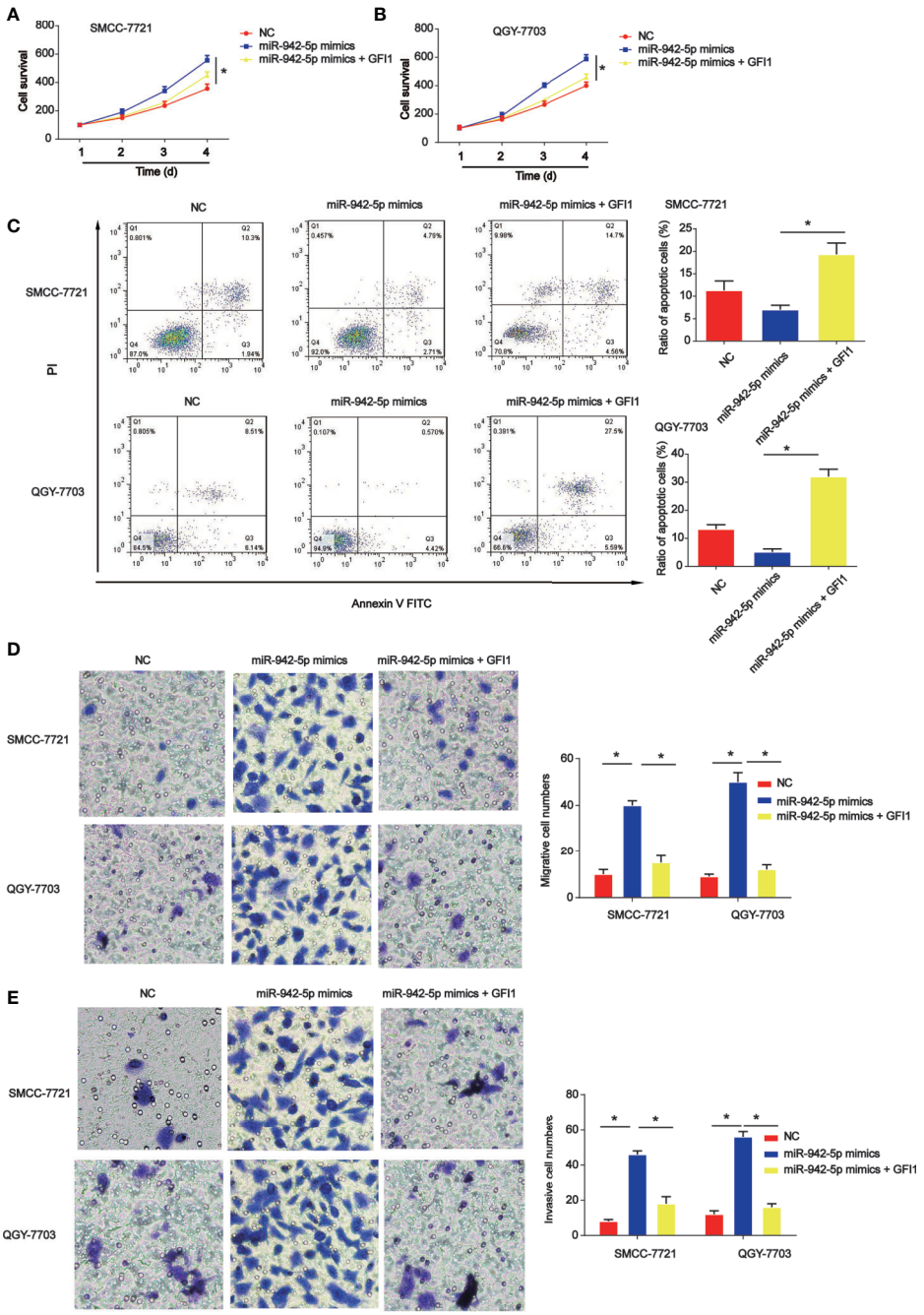

FIGURE 7 | Effects of GFI1 on HCC cell progression was reversed by miR-942-5p mimics. **(A, B)** HCC cell survival was tested using EdU assay. HCC cells were transfected with miR-942-5p mimics and GFI overexpression plasmid. **(C)** Effects of GFI1 on HCC cell apoptosis. **(D, E)** Effects of GFI1 on HCC cell migration and invasion. *P < 0.05.

microRNAs are small non-coding RNAs to repress gene expression through binding to the 3′-UTR of target mRNAs (35). For another, miR-942-5p was predicted as the target for LINC00675. Previously, it has been shown that lncRNA LIFR-AS1 can inhibit invasion and metastasis of lung cancer *via* regulating miR-942-5p and ZNF471 (36). Additionally, miR-942-5p is sequestered by circRNA-AKT1 to induce AKT1 and contributes to cervical cancer progression (37). In the present study, we proved miR-942-5p can interact with LINC00675, and GFI1 acted as a downstream target for miR-942-5p. Thus, LINC00675 could regulate GFI1 expression indirectly *via* sponging miR-942-5p.

In summary, we reported GFI1 was decreased in HCC and it can modulate LINC00675 expression positively. Loss of

LINC00675 might serve as a tumor inhibitor in HCC cell growth and progression *via* sponging miR-942-5p.

DATA AVAILABILITY STATEMENT

The original contributions presented in the study are included in the article/supplementary material. Further inquiries can be directed to the corresponding author.

ETHICS STATEMENT

The studies involving human participants were reviewed and approved by Affiliated Hospital of Youjiang Medical University for Nationalities. The patients/participants provided their written informed consent to participate in this study. The animal study was reviewed and approved by Affiliated Hospital of Youjiang Medical University for Nationalities.

AUTHOR CONTRIBUTIONS

JW designed the research and revised the manuscript. LL, SL and YZ performed the experiments. ZL and YC collected the data. JM and PC did the analysis. WW and JP supported the study. LL drafted the manuscript. All authors contributed to the article and approved the submitted version.

FUNDING

This work was supported by the Grants from Science and Technique Research Projects of Guangxi, No. 2019JJA140524.

REFERENCES

1. Chen W, Zheng R, Baade PD, Zhang S, Zeng H, Bray F, et al. Cancer statistics in China, 2015. *CA: Cancer J Clin* (2016) 66:115–32. doi: 10.3322/caac.21338
2. Siegel RL, Miller KD, Jemal A. Cancer statistics, 2016. *CA: Cancer J Clin* (2016) 66:7–30. doi: 10.3322/caac.21332
3. Forner A, Llovet JM, Bruix J. Hepatocellular carcinoma. *Lancet* (2012) 379:1245–55. doi: 10.1016/S0140-6736(11)61347-0
4. Portolani N, Coniglio A, Ghidoni S, Giovanelli M, Benetti A, Tiberio GA, et al. Early and late recurrence after liver resection for hepatocellular carcinoma: prognostic and therapeutic implications. *Ann Surg* (2006) 243:229–35. doi: 10.1097/01.sla.0000197706.21803.a1
5. Bruix J, Boix L, Sala M, Llovet JM. Focus on hepatocellular carcinoma. *Cancer Cell* (2004) 5:215–9. doi: 10.1016/S1535-6108(04)00058-3
6. Roberts T, Cowell JK. Cloning of the human Gfi-1 gene and its mapping to chromosome region 1p22. *Oncogene* (1997) 14:1003–5. doi: 10.1038/sj.onc.1200910
7. Schmidt T, Karsunky H, Gau E, Zevnik B, Elsasser HP, Moroy T. Zinc finger protein GFI-1 has low oncogenic potential but cooperates strongly with pim and myc genes in T-cell lymphomagenesis. *Oncogene* (1998) 17:2661–7. doi: 10.1038/sj.onc.1202191
8. Hock H, Hamblen MJ, Rooke HM, Schindler JW, Saleque S, Fujiwara Y, et al. Gfi-1 restricts proliferation and preserves functional integrity of haematopoietic stem cells. *Nature* (2004) 431:1002–7. doi: 10.1038/nature02994
9. Jarroux J, Morillon A, Pinskaya M. History, Discovery, and Classification of lncRNAs. *Adv Exp Med Biol* (2017) 1008:1–46. doi: 10.1007/978-981-10-5203-3_1
10. Kopp F, Mendell JT. Functional Classification and Experimental Dissection of Long Noncoding RNAs. *Cell* (2018) 172:393–407. doi: 10.1016/j.cell.2018.01.011
11. Quinn JJ, Chang HY. Unique features of long non-coding RNA biogenesis and function. *Nat Rev Genet* (2016) 17:47–62. doi: 10.1038/nrg.2015.10
12. Wang KC, Chang HY. Molecular mechanisms of long noncoding RNAs. *Mol Cell* (2011) 43:904–14. doi: 10.1016/j.molcel.2011.08.018
13. Guttman M, Rinn JL. Modular regulatory principles of large non-coding RNAs. *Nature* (2012) 482:339–46. doi: 10.1038/nature10887
14. Krol J, Krol I, Alvarez CP, Fiscella M, Hierlemann A, Roska B, et al. A network comprising short and long noncoding RNAs and RNA helicase controls mouse retina architecture. *Nat Commun* (2015) 6:7305. doi: 10.1038/ncomms8305
15. Li G, Zhang H, Wan X, Yang X, Zhu C, Wang A, et al. Long noncoding RNA plays a key role in metastasis and prognosis of hepatocellular carcinoma. *BioMed Res Int* (2014) 2014:780521. doi: 10.1155/2014/780521
16. Liu YR, Tang RX, Huang WT, Ren FH, He RQ, Yang LH, et al. Long noncoding RNAs in hepatocellular carcinoma: Novel insights into their mechanism. *World J Hepatol* (2015) 7:2781–91. doi: 10.4254/wjh.v7.i28.2781
17. Wang Y, Yang L, Chen T, Liu X, Guo Y, Zhu Q, et al. A novel lncRNA MCM3AP-AS1 promotes the growth of hepatocellular carcinoma by targeting miR-194-5p/FOXA1 axis. *Mol Cancer* (2019) 18:28. doi: 10.1186/s12943-019-0957-7
18. Malakar P, Shilo A, Mogilevsky A, Stein I, Pikarsky E, Nevo Y, et al. Long Noncoding RNA MALAT1 Promotes Hepatocellular Carcinoma Development by SRSF1 Upregulation and mTOR Activation. *Cancer Res* (2017) 77:1155–67. doi: 10.1158/0008-5472.CAN-16-1508
19. Zeng S, Xie X, Xiao YF, Tang B, Hu CJ, Wang SM, et al. Long noncoding RNA LINC00675 enhances phosphorylation of vimentin on Ser83 to suppress gastric cancer progression. *Cancer Lett* (2018) 412:179–87. doi: 10.1016/j.canlet.2017.10.026
20. Shan Z, An N, Qin J, Yang J, Sun H, Yang W. Long non-coding RNA Linc00675 suppresses cell proliferation and metastasis in colorectal cancer via acting on miR-942 and Wnt/beta-catenin signaling. *Biomed Pharmacother* (2018) 101:769–76. doi: 10.1016/j.biopha.2018.02.123
21. Li DD, Fu ZQ, Lin Q, Zhou Y, Zhou QB, Li ZH, et al. Linc00675 is a novel marker of short survival and recurrence in patients with pancreatic ductal adenocarcinoma. *World J Gastroenterol* (2015) 21:9348–57. doi: 10.3748/wjg.v21.i31.9348
22. Yarmishyn AA, Kurochkin IV. Long noncoding RNAs: a potential novel class of cancer biomarkers. *Front Genet* (2015) 6:145. doi: 10.3389/fgene.2015.00145
23. Chandra Gupta S, Nandan Tripathi Y. Potential of long non-coding RNAs in cancer patients: From biomarkers to therapeutic targets. *Int J Cancer* (2017) 140:1955–67. doi: 10.1002/ijc.30546
24. Matsui M, Corey DR. Non-coding RNAs as drug targets. *Nat Rev Drug Discover* (2017) 16:167–79. doi: 10.1038/nrd.2016.117
25. Li G, Shi H, Wang X, Wang B, Qu Q, Geng H, et al. Identification of diagnostic long noncoding RNA biomarkers in patients with hepatocellular carcinoma. *Mol Med Rep* (2019) 20:1121–30. doi: 10.3892/mmr.2019.10307
26. Chao Y, Zhou D. lncRNA-D16366 Is a Potential Biomarker for Diagnosis and Prognosis of Hepatocellular Carcinoma. *Med Sci Monit Int Med J Exp Clin Res* (2019) 25:6581–6. doi: 10.12659/MSM.915100
27. Zhang Z, Wang S, Liu Y, Meng Z, Chen F. Low lncRNA ZNF385DAS2 expression and its prognostic significance in liver cancer. *Oncol Rep* (2019) 42:1110–24. doi: 10.3892/or.2019.7238
28. Ma S, Deng X, Yang Y, Zhang Q, Zhou T, Liu Z. The lncRNA LINC00675 regulates cell proliferation, migration, and invasion by affecting Wnt/beta-catenin signaling in cervical cancer. *Biomed Pharmacother = Biomed Pharmacother* (2018) 108:1686–93. doi: 10.1016/j.biopha.2018.10.011
29. Zhong YB, Shan AJ, Lv W, Wang J, Xu JZ. Long non-coding RNA LINC00675 inhibits tumorigenesis and EMT via repressing Wnt/beta-catenin signaling in

esophageal squamous cell carcinoma. *Eur Rev Med Pharmacol Sci* (2018) 22 (23):8288–97. doi: 10.26355/eurrev_201812_16526
30. Li Z, Li Y, Wang Q. LINC00675 is a prognostic factor and regulates cell proliferation, migration and invasion in glioma. *Biosci Rep* (2018) 38(5): BSR20181039. doi: 10.1042/BSR20181039
31. Moroy T, Khandanpour C. Role of GFI1 in Epigenetic Regulation of MDS and AML Pathogenesis: Mechanisms and Therapeutic Implications. *Front Oncol* (2019) 9:824. doi: 10.3389/fonc.2019.00824
32. Xing W, Xiao Y, Lu X, Zhu H, He X, Huang W, et al. GFI1 downregulation promotes inflammation-linked metastasis of colorectal cancer. *Cell Death Differentiation* (2017) 24:929–43. doi: 10.1038/cdd.2017.50
33. Chen MS, Lo YH, Chen X, Williams CS, Donnelly JM, Criss ZK 2nd, et al. Growth Factor-Independent 1 Is a Tumor Suppressor Gene in Colorectal Cancer. *Mol Cancer Res MCR* (2019) 17:697–708. doi: 10.1158/1541-7786.MCR-18-0666
34. Ballantyne MD, McDonald RA, Baker AH. lncRNA/MicroRNA interactions in the vasculature. *Clin Pharmacol Ther* (2016) 99:494–501. doi: 10.1002/cpt.355
35. Mohr AM, Mott JL. Overview of microRNA biology. *Semin Liver Disease* (2015) 35:3–11. doi: 10.1055/s-0034-1397344
36. Wang Q, Wu J, Huang H, Jiang Y, Huang Y, Fang H, et al. lncRNA LIFR-AS1 suppresses invasion and metastasis of non-small cell lung cancer via the miR-942-5p/ZNF471 axis. *Cancer Cell Int* (2020) 20:180. doi: 10.1186/s12935-020-01228-5
37. Ou R, Mo L, Tang H, Leng S, Zhu H, Zhao L, et al. circRNA-AKT1 Sequesters miR-942-5p to Upregulate AKT1 and Promote Cervical Cancer Progression. *Mol Ther Nucleic Acids* (2020) 20:308–22. doi: 10.1016/j.omtn.2020.01.003

Conflict of Interest: The authors declare that the research was conducted in the absence of any commercial or financial relationships that could be construed as a potential conflict of interest.

frontiers in Genetics

ORIGINAL RESEARCH
published: 15 January 2021
doi: 10.3389/fgene.2020.607636

Long Non-coding RNA SNHG17 Upregulates RFX1 by Sponging miR-3180-3p and Promotes Cellular Function in Hepatocellular Carcinoma

Tao Ma[1†], Xujun Zhou[2†], Hailiang Wei[3], Shuguang Yan[4], Yi Hui[4], Yonggang Liu[5], Hui Guo[3], Qian Li[6], Jingtao Li[5], Zhanjie Chang[5] and Xiao-Xin Mu[7,8]*

[1] Department of Clinical Laboratory, Hospital of Chengdu University of Traditional Chinese Medicine, Chengdu, China, [2] Department of Gastroenterology, Wuhan Eighth Hospital, Wuhan, China, [3] Department of General Surgery, The Hospital Affiliated to Shaanxi University of Chinese Medicine, Xianyang, China, [4] College of Basic Medicine, The Shaanxi University of Chinese Medicine, Xianyang, China, [5] Department of Liver Diseases, The Hospital Affiliated to Shaanxi University of Chinese Medicine, Xianyang, China, [6] Medical Experiment Center, The Shaanxi University of Chinese Medicine, Xianyang, China, [7] Key Laboratory of Liver Transplantation, Chinese Academy of Medical Sciences, Nanjing, China, [8] National Health Council (NHC) Key Laboratory of Living Donor Liver Transplantation, Hepatobiliary Center, The First Affiliated Hospital of Nanjing Medical University, Nanjing, China

OPEN ACCESS

Edited by:
Xiaochen Wang,
University of Texas Southwestern Medical Center, United States

Reviewed by:
Jiansong Ji,
Lishui Central Hospital, China
Guohao Wang,
National Institutes of Health (NIH), United States

***Correspondence:**
Xiao-Xin Mu
mux@njmu.edu.cn

[†]These authors have contributed equally to this work

Specialty section:
This article was submitted to Cancer Genetics, a section of the journal Frontiers in Genetics

Received: *17 September 2020*
Accepted: *30 November 2020*
Published: *15 January 2021*

Citation:
Ma T, Zhou X, Wei H, Yan S, Hui Y, Liu Y, Guo H, Li Q, Li J, Chang Z and Mu X-X (2021) Long Non-coding RNA SNHG17 Upregulates RFX1 by Sponging miR-3180-3p and Promotes Cellular Function in Hepatocellular Carcinoma. Front. Genet. 11:607636. doi: 10.3389/fgene.2020.607636

Background: Hepatocellular carcinoma (HCC) is one of the most common types of cancer that is associated with poor quality of life in patients and a global health burden. The mechanisms involved in the development and progression of HCC remain poorly understood.

Methods: Hepatocellular carcinoma human samples and cell lines were subjected to qRT-PCR for expression assessment. CCK-8 assay, Transwell migration and invasion assay, were applied for cell function detection. Animal experiment was used to measure the function of SNHG17 on cell growth *in vivo*. Western blot was conducted to evaluate the level of EMT in cells. RIP, RNA pull-down and luciferase reporter assays were performed to assess the correlation between SNHG17, miR-3180-3p and RFX1.

Results: Our study demonstrated that SNHG17 was upregulated in HCC human samples and involved cell proliferation, migration, invasion progress. SNHG17 promoted HCC cell growth and metastasis *in vivo*. Furthermore, we investigated the downstream factor of SNHG17, SNHG17 acted as a molecular sponge for miR-3180-3p, and SNHG17 regulated RFX1 expression via miR-3180-3p. SNHG17 promotes tumor-like behavior in HCC cells via miR-3180-3p/RFX1.

Conclusion: We determined RFX1 as the target of miR-3810-3p; SNHG17 enhanced the progression of HCC via the miR-3180-3p/RFX1 axis. Taken together, our findings may provide insight into the molecular mechanism involved in the progression of HCC and develop SNHG17 as a novel therapeutic target against HCC.

Keywords: lncRNA, SNHG17, miR-3180-3p, RFX1, hepatocellular carcinoma

INTRODUCTION

Hepatocellular carcinoma (HCC) is the most common subtype of liver cancer (Mcglynn et al., 2015) and is the third cause for cancer-related mortality worldwide (Bray et al., 2018). Reportedly, half of the total global incidences of HCC can be found in China (Lafaro et al., 2015). The widespread risk factors for HCC include hepatitis C virus infection, alcohol consumption, obesity, and metabolic disorders and result in a high rate of morbidity. Owing to the rapidly progressing and metastasizing nature of HCC, majority of patients are diagnosed at later stages. Moreover, high rates of postsurgical recurrence leads to poor outcomes in patients with HCC (Margini and Dufour, 2016). Moreover, the limited treatment available for HCC has resulted in a poor quality of life for patients and a global health burden. Thus, it is imperative to identify novel therapeutic targets for HCC. However, the underlying mechanisms involved in the development and progression of HCC remain to be fully understood.

Long non-coding RNAs (lncRNAs) are > 200 nucleotide-long transcripts that do not encode proteins (Mercer et al., 2009; Liz and Esteller, 2016). LncRNAs have different expression profiles and biological functions in various diseases, especially cancers (Wang et al., 2010; Jarroux et al., 2017; Mathy and Chen, 2017), suggesting the crucial role of lncRNAs in cancer progression. Moreover, lncRNAs induce differential lncRNA-miRNA-mRNA network signatures (Zhang et al., 2016; Fan et al., 2018; Zhang Y. et al., 2018). LncRNAs have recently been implicated in the progression of HCC. Liu et al. showed that lncRNA NEAT-1 promotes the proliferation of HCC cells (Liu et al., 2018). Huang et al. demonstrated that lncRNA PTTG3P regulates HCC progression (Huang J.L. et al., 2018). Yang et al. reported that the lncRNA HOTAIR stimulates HCC progression (Yang et al., 2019). Thus, lncRNAs may be pivotal in the development and progression of HCC.

The lncRNA small nucleolar RNA host gene 17 (SNHG17), located on chromosome 20q11.23, was detected in patients with colorectal cancer. SNHG17 binds to EZH2 and suppresses p57 to stimulate the development of colorectal cancer (Ma et al., 2017). SNHG17 is also involved in the progression of gastric carcinoma (Chen et al., 2019), non-small cell lung cancer (Xu et al., 2019), type 2 diabetes mellitus (Mohamadi et al., 2019), and melanoma (Gao et al., 2019). However, the role of SNHG17 in HCC progression remains unclear.

Based on the literature, we hypothesized that SNHG17 plays a role in HCC progression and exerts its functions via a lncRNA-microRNA-mRNA regulatory network. We performed *in vitro* and *in vivo* experiments to show that SNHG17 was dysregulated in HCC tissues. Bioinformatic analyses, RNA immunoprecipitation (RIP) assays, RNA pull-down assays, and luciferase reporter assays showed that SNHG17 promoted tumor-like behavior in HCC cells via the miRNA-mRNA pathway. Taken together, our findings might help develop SNHG17 as a novel therapeutic target for HCC.

MATERIALS AND METHODS

Clinical Samples

HCC tumor tissues and paired normal tissues were harvested from patients who were diagnosed with HCC based on pathological evaluation; patients underwent curative surgery at The Hospital Affiliated to Shaanxi University of Chinese Medicine between 2015 and 2018 (**Table 1**). None of the patients were administered with therapy targeting HCC before surgery. All the specimens were stored at −80°C until further use. This study was approved by the Ethical Review Committees at The Hospital Affiliated to Shanxi University of Chinese Medicine, and all the patients provided written informed consent. Tumor size and Edmonson-Steiner grade were confirmed by histopathology.

Cell Culture and Transfection

All HCC cell lines and human non-cancerous hepatic cell line L02 were obtained from the American Type Culture Collection (Manassas, United States) and cultured in minimum essential medium (Logan, United States) with 10% fetal bovine serum (Logan, United States) at 37°C in 5% CO_2 and 95% air environment. SNHG17 shRNA and siRNA, miR-3180-3p inhibitor and mimic, and control and RFX1 siRNAs were synthesized by GeneChem (Shanghai, China) and transfected into cells using Lipofectamine 2000 (Invitrogen, MA) following the prescribed protocol.

Quantitative Reverse Transcription-Polymerase Chain Reaction (qRT-PCR)

Total RNA was extracted from cells using TRIzol (Invitrogen, Carlsbad, CA, United States) and reverse transcribed using the RevertAid First Strand cDNA Synthesis kit (Thermo Fisher Scientific, United States). Real-time PCR Master Mix (SYBR Green; TOYOBO, Japan) was used to perform qRT-PCR. GAPDH served as the internal control. Relative expression (fold change) of the target genes were calculated by the $2^{-\Delta\Delta Ct}$ method. **Table 2** lists the primers used for qRT-PCR.

Cell Counting Kit 8 (CCK-8)

Cell proliferation was analyzed using CCK-8 (Dojindo, Japan) as per the kit instructions. Collectively, about 1×10^3 cells were seeded and cultured in a 96-well plates for 24, 48, 72, 96, and 120 h. Subsequently, cells were treated with 10 μl of CCK-8 assay solution for 2 h, and the proliferative capacity of treated cells were measured at 450 nm by an enzyme immunoassay analyzer (Thermo Fisher Scientific, United States).

Transwell Migration Assay

Cell migration was measured using 24-well culture plates with 8 mm pore-containing membrane inserts. Serum-free cell-containing medium (Logan, United States) was added to the upper chamber and the lower chamber contained Dulbecco's modified Eagle medium supplemented with 15%

TABLE 1 | Characteristics of hepatocellular cancer patients.

Characteristics		Cases
Age	<60	10
	≥60	13
Gender	Male	18
	Female	5
Size(cm)	<5	13
	≥5	10
Edmonson-Steiner grade	I–II	9
	III–IV	14
Vascular invasion	Yes	10
	No	13
AFP (ng/ml)	<200	9
	≥200	14
Histologic grade	Low	3
	Middle	12
	High	8

fetal bovine serum (Gibco, Grand Island, NY, United States). This was incubated at 37°C for 3 days. Cells in the lower chamber (below the membrane) were stained with 0.4% trypan blue (Invitrogen) and counted under a light microscope (×20 magnification). Each experiment was performed at least in triplicates.

Western Blotting

Protein extraction reagent (Beyotime) was used to isolate tumor proteins and RIPA lysis buffer (Invitrogen) was used for cellular proteins. The proteins were separated by sodium dodecyl sulfate-polyacrylamide gel electrophoresis followed by transferring onto a polyvinylidene fluoride membrane (Invitrogen). The membrane was blocked at room temperature for 2 h with shaking following which it was incubated overnight with the primary antibody at 4°C followed by the secondary antibody (1:2,000 dilution) for 2 h. The bands corresponding to the proteins were detected and imaged using (Bio-Rad, United States). The antibodies we used in the study as following: E-cadherin (CST, 14472s), Vimentin (CST, 5741s), RFX1 (Abcam, ab244484), GAPDH (CST, 5174s).

Tumor Xenograft

Five-weeks-old male/female nude BALB/7 mice ($n = 30$) were procured from Beijing Vital River Laboratory Animal Technology (Beijing, China). The mice were housed at 25°C with free access to food and water. All animal procedures were approved by The Hospital Affiliated to Shaanxi University of Chinese Medicine. The mice were randomly divided to the experimental and control groups: the experimental group was injected with treated Huh7 and HepG2 cells and control mice were injected with control cells via tail vein following which the mice were sacrificed. All the subcutaneous tumors and lungs were excised to measure tumor growth, size, weight, and metastasis.

Immunohistochemistry

Sections (5 μm) were treated with formalin for immunohistochemical analysis. Tissue sections were incubated overnight with antibodies against E-cadherin (CST, 14472s) and vimentin (CST, 5741s) at 4°C. Scale bar represents 50 μm. The protocols for immunohistochemistry were performed as described previously (Zhang X.P. et al., 2018).

Hematoxylin and Eosin Staining

The paraffin sections were pretreated by dewaxing according to conventional methods followed by hydrating and soaking with xylene as per the instructions of the Hematoxylin-Eosin staining kit (GeneChem, China).

RNA-Binding Protein Immunoprecipitation Assay

The Magna RIP RNA-Binding Protein Immunoprecipitation Kit (Millipore, Massachusetts, United States) was used to perform RIP. Cells were lysed using the RIP lysis buffer (Invitrogen). Magnetic beads (Millipore) conjugated with AGO2 or control IgG antibody were incubated with the cell lysates along with Proteinase K (Millipore). The immunoprecipitated RNA was used for PCR analysis.

Dual-Luciferase Reporter Assay

pmirGLO dual-luciferase reporter plasmids containing the wild-type (wt) or mutant (mt) forms of the 3' untranslated region of SNHG17 or RFX1 were synthesized by GeneChem (Shanghai, China). These constructs and control plasmids were transfected into 293T cells. Luciferase activity was measured using the Dual-Luciferase Reporter Assay System (Promega) according to the kit instructions.

RNA Pull-Down Assay

Biotinylated SNHG17 or miR-3180-3p probes and its controls were synthesized by GeneChem (Shanghai, China) and transfected into 293T cells for 48 h. Cell lysates were incubated with Dynabeads M-280 Streptavidin (Invitrogen, United States) at 4°C for 3 h. Ice-cold lysis buffer was used to wash the beads

TABLE 2 | Primers applied in study.

Primers	Forward (5′∼3′)	Reverse (5′∼3′)
LncSNHG17	TTTTCCCACGCTGTCTGTCA	CAGTTTCCCCCGATGGTGAG
miR-3180-3p	CGTCTAGAAAAAATCTAT GTTGGTTCGATAC	CGGCGGCCGCTAAATTCAGGAC GCGATCGAAG
RFX1	GATCCAAGGCGGCTACAT	CAGCCGTCTCATAGTTGTCC
GAPDH	ATGGGGAAGGTGAAGGTCG	GGGGTCATTGATGGCAACAATA

three times following the kit instructions. Subsequently, PCR was used to analyze the bound RNAs.

Statistical Analysis

GraphPad Prism 6.0 was used for data analysis. Data are represented as mean ± standard deviation. Student's *t*-test to compare data from different groups. The differences represented by *, **, and *** had *p*-values of 0.05, 0.01, and 0.001, respectively.

RESULTS

SNHG17 Levels in HCC Tissues

We measured SNHG17 levels in HCC tumor and matched normal tissues. SNHG17 was significantly overexpressed in tumor tissues compared to that in the matched healthy tissues (**Figure 1A**). We then determined the expression of SNHG17 in HCC tumors of different sizes and Edmonson-Steiner grades. We observed high expression of SNHG17 with increasing tumor size and Edmonson-Steiner grade (**Figures 1B,C**). Based on these results, we speculated that SNHG17 is involved in the progression of HCC. Thus, we determined the expression of SNHG17 in HCC cell lines: SNHG17 was overexpressed in HepG2 cells and downregulated in Huh7 cells (**Figure 1D**). Thus, for our subsequent experiments, we depleted HepG2 cells of SNHG17 and overexpressed SNHG17 in Huh7 cells (**Figure 1E**).

SNHG17 Promotes HCC Cellular Function

To investigate the role of SNHG17 in the progression of HCC, we generated SNHG17 overexpressing and depleted cells and rat models. SNHG17 overexpression promoted cell proliferation (**Figure 2A**) and enhanced cell migration and invasion (**Figures 2B,C**). Epithelial–mesenchymal transition (EMT) is crucial in metastasis (Lo and Zhang, 2018; Pastushenko and Blanpain, 2019). Overexpression of SNHG17 stimulated EMT in HCC (**Figure 2D**). Immunohistochemistry revealed increased staining for E-cadherin and vimentin in rat tumor tissues as compared to that in the matched normal tissues, suggesting that upregulation of SNHG17 stimulated EMT in HCC (**Figure 2E**).

Next, we isolated the subcutaneous tumors from mice and measured the volume and weight. SNHG17 overexpression resulted in increased tumor growth *in vivo* (**Figures 3A–C**). Hematoxylin and eosin staining of lung tissues from mice with HCC revealed overexpression of SNHG17 promoted tumor metastasis (**Figure 3D**).

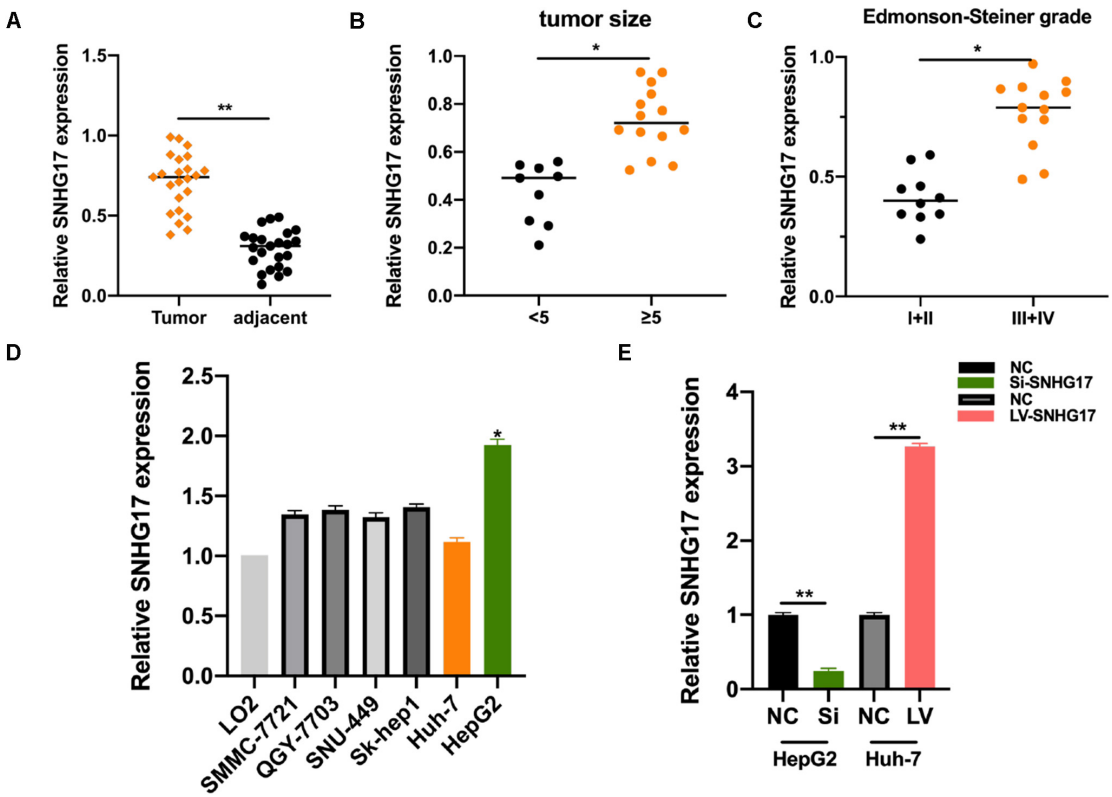

FIGURE 1 | SNHG17 expression in HCC tissues. **(A)** Polymerase chain reaction (PCR) analysis for the expression of SNHG17 in HCC tumor and matched normal tissues. **(B)** SNHG17 levels in HCC tumors with varying size. **(C)** SNHG17 levels in HCC tumors with varying Edmonson-Steiner grades. **(D)** SNHG17 expression in different HCC cell lines. **(E)** Relative expression of SNHG17 in HepG2 cells transfected with si-SNHG17 and its controls and Huh7 cells transfected with LV-SNHG17 and its control plasmids. Error bars represent mean ± SD from at least three experiments. *$p < 0.05$, **$p < 0.01$.

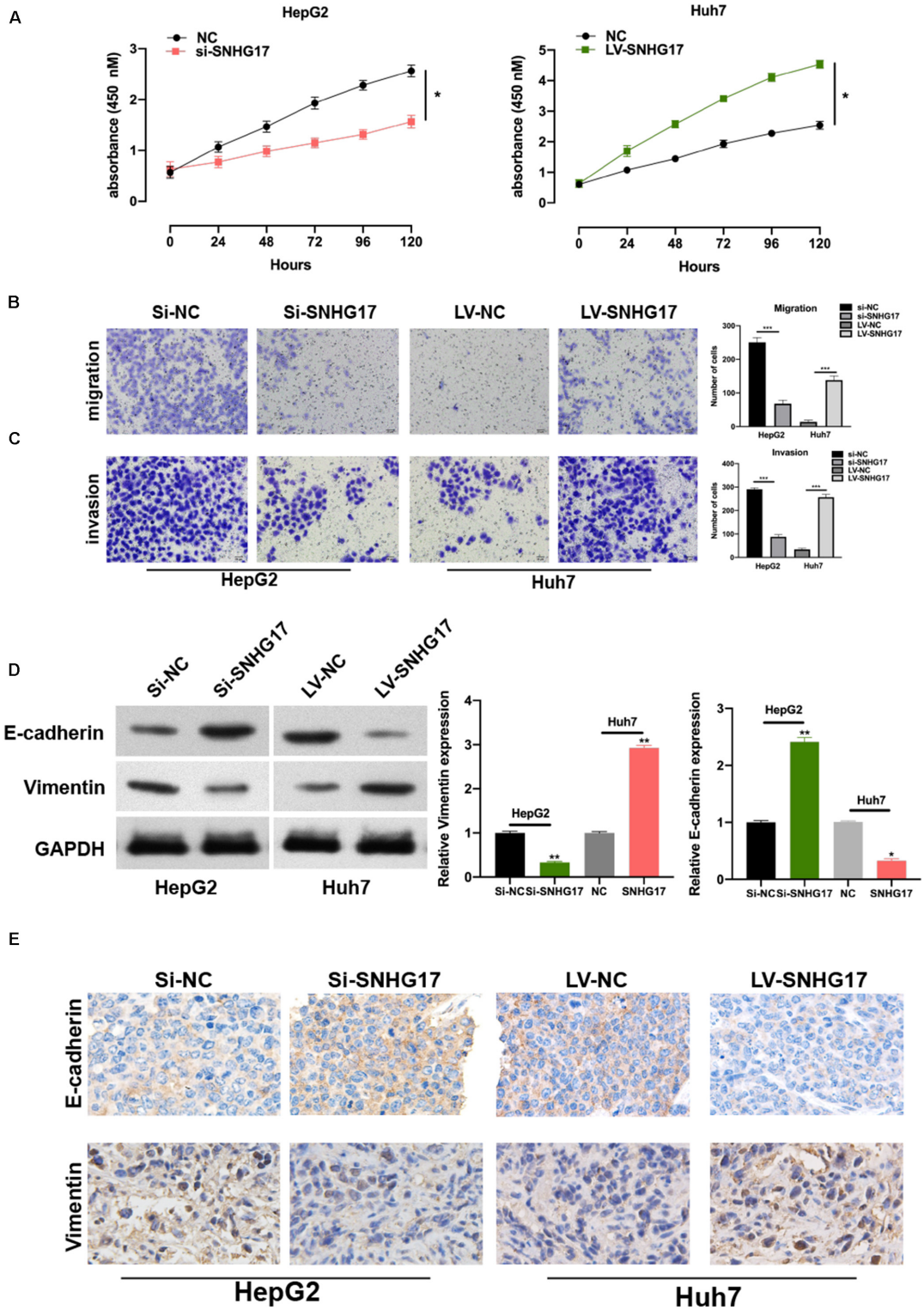

FIGURE 2 | SNHG17 promotes HCC cell functions. **(A)** Proliferation of si-SNHG17-transfected HepG2 cells and LV-SNHG17-transfected Huh7 cells using the cell counting kit-8 (CCK-8). **(B)** Transwell migration assay was used to evaluate the migration of si-SNHG17-transfected HepG2 cells and LV-SNHG17-transfected Huh7 cells. **(C)** Potential for invasion by si-SNHG17-transfected HepG2 cells and LV-SNHG17-transfected Huh7 cells as assayed by the Transwell migration assay. **(D)** PCR and Western blotting for the expression of E-cadherin and vimentin in treated cells. **(E)** Representative images for the immunohistochemical analysis of the expression of E-cadherin and vimentin in human HCC tumor tissues, Scale bar: 20 μm. Error bars represent the mean ± SD from at least three experiments. $^{*}p < 0.05$, $^{**}p < 0.01$, and $^{***}p < 0.001$.

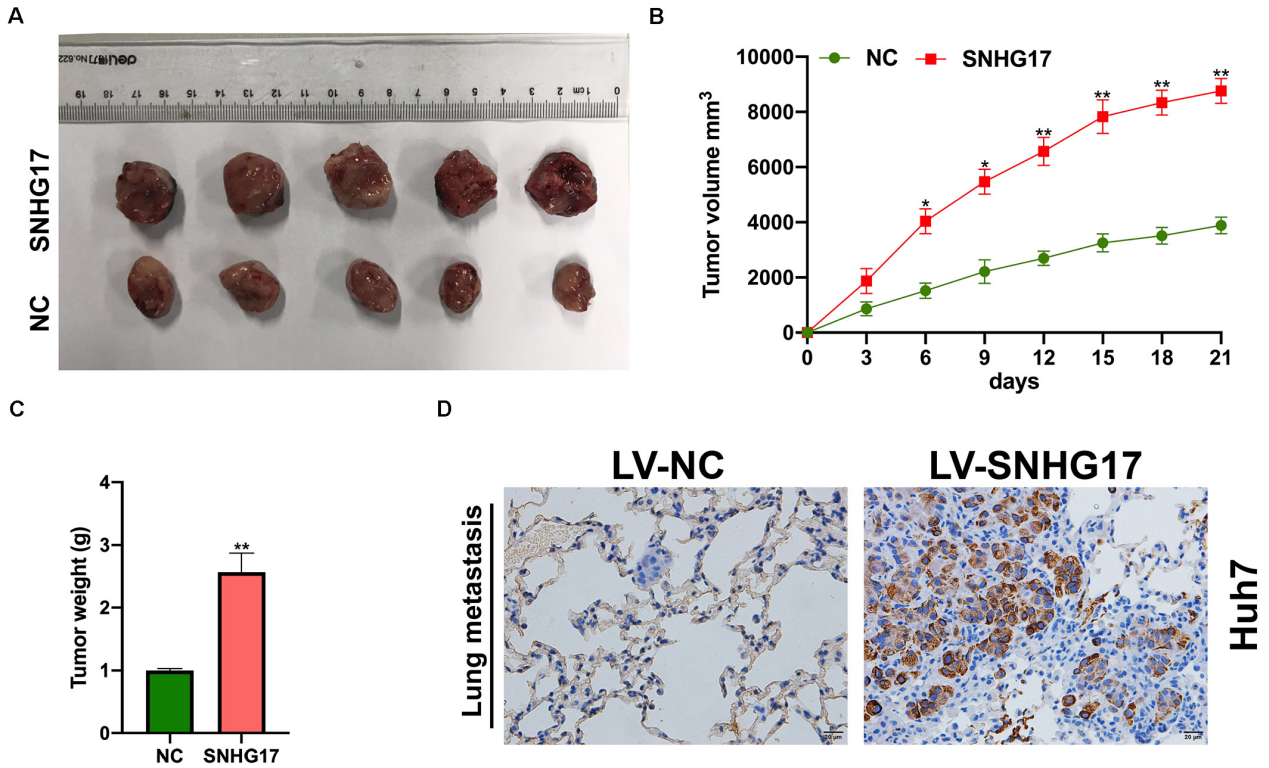

FIGURE 3 | Effect of SNHG17 on tumor volume and weight. **(A)** Representative images of the subcutaneous tumors isolated from mice. Scale bar: 1 cm. **(B)** Subcutaneous tumor volume was measured every 3 days after inoculation. **(C)** Subcutaneous tumor weight was measured on day 21 after inoculation. **(D)** Hematoxylin and eosin staining of lung metastases, Scale bar: 20 μm. Error bars represent mean ± SD from at least three experiments. $^{*}p < 0.05$, $^{**}p < 0.01$.

SNHG17 Sponges miR-3180-3p

LncRNAs bind to and sponge miRNAs to regulate their function. Thus, we used bioinformatic analysis to identify the top 10 miRNAs for further analysis. We performed RNA pull-down to show the extensive enrichment of miR-3180-3p in SNHG17 immunoprecipitated samples (**Figure 4A**). Next, we performed RIP using AGO2 as the bait in Huh7 and HepG2 cells. As shown in **Figures 4B,C**, SNHG17 and miR-3180-3p (not GAPDH) were enriched in the AGO2 immunoprecipitated samples. Subsequently, we analyzed the binding sites between SNHG17 and miR-3180-3p (**Figure 4D**). Luciferase reporter assays showed that overexpressing miR-3180 decreased luciferase activity in cells with wt SNHG17, but increased luciferase activity in cells containing the mt form of SNHG17 (**Figure 4E**). RNA pull-down assays demonstrated the enrichment of SNHG17 in cells transfected with biotinylated miR-3180-3p mimics (**Figure 4F**), suggesting that SNHG17 sponges miR-3180-3p. Furthermore, overexpression of SNHG17 inhibited miR-3180-3p expression in HCC cells (**Figure 4G**).

miR-3180-3p Reverses the Oncogenic Function of SNHG17

We wanted to determine the role of miR-3180-3p in the development and progression of HCC. Firstly, we assessed the effects of miR-3180-3p on HCC cellular progression. As shown in **Supplementary Figure S1**, it was found that miR-3180-3p inhibited HCC cell proliferation, migration, and invasion. Subsequently, we used CCK-8 and Transwell migration assays to analyze proliferation, migration, and invasion of Huh7 cells transfected with SNHG17 and SNHG17+miR-3180-3p mimics. miR-3180-3p mimics reversed the enhanced proliferation, migration, and invasion phenotype of HCC cells observed with SNHG17 overexpression (**Figures 5A,B**). SNHG17 and miR-3180-3p mimic co-transfected Huh7 cells showed reduced EMT as compared to that observed in SNHG17-transfected Huh7 cells (**Figures 5C,D**).

SNHG17 Promotes Tumor-Like Behavior in HCC Cells via miR-3180-3p/RFX1

We used bioinformatic tools to further understand the underlying molecular mechanisms employed by miR-3180-3p in the progression of HCC progression. RFX1 is involved in the progression of various diseases (Wang et al., 2018; Du et al., 2019) and a potential target of miR-3180-3p. Thus, we generated plasmids for the wt and mt versions of RFX1 and miR-3180-3p mimic (**Figure 6A**). Luciferase assays showed a drastic reduction in luciferase activity in 293T cells containing miR-3180-3p and wt RFX1, but not in cells containing mt RFX1 (**Figure 6B**). Next, we measured RFX1 levels in Huh7 and HepG2 cells transfected

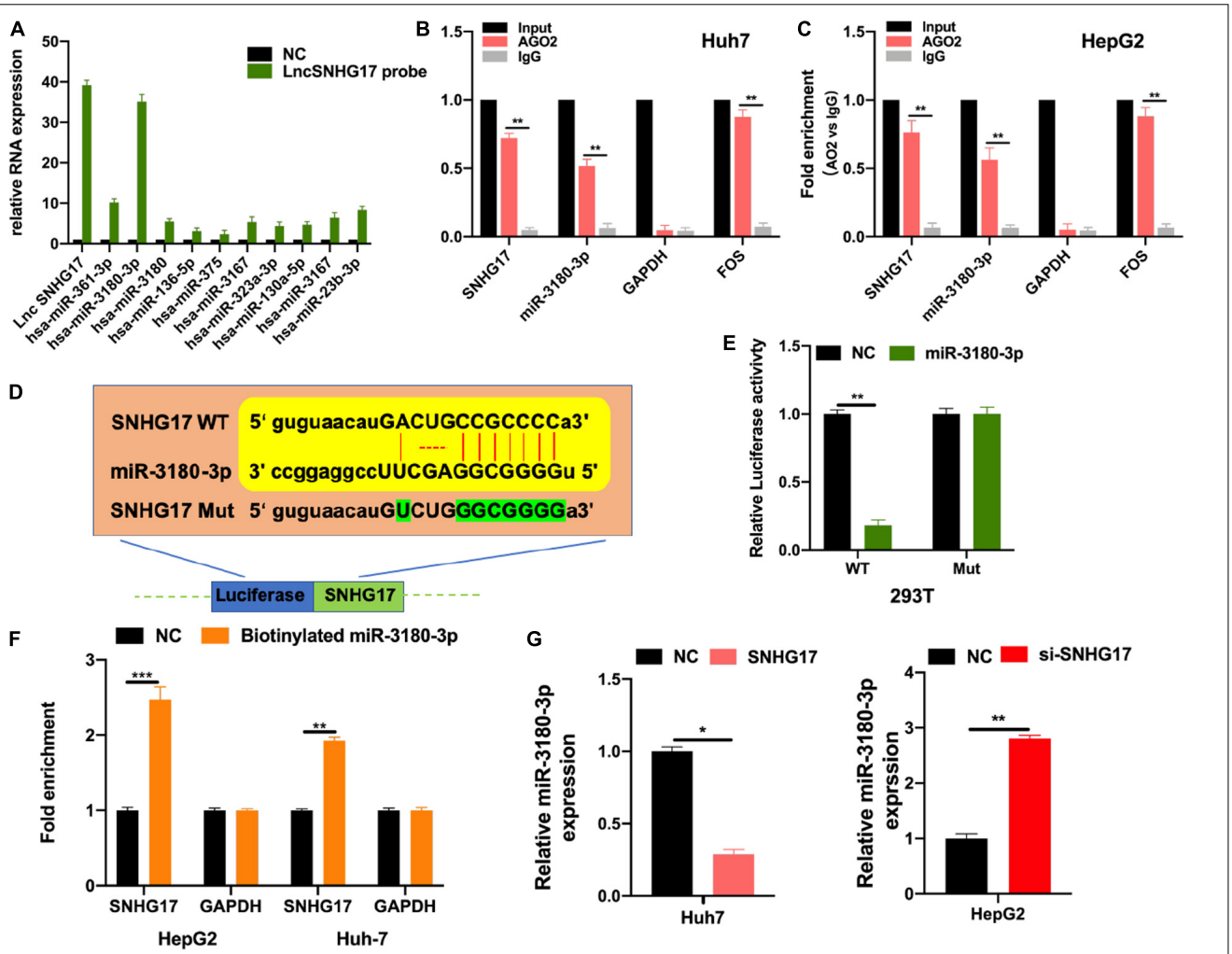

FIGURE 4 | SNHG17 sponges miR-3180-3p. Bioinformatic analysis were conducted to predicted putative targets for SNHG17 (ENCORI database: http://starbase.sysu.edu.cn/index.php; and CLIP Data with high stringency ≥ 3). **(A)** HepG2 cell lysates were used for biotinylated RNA pull-down. Purified RNA was analyzed by PCR using specific miRNA primers. **(B,C)** RIP using antibodies against AGO2, IgG, GAPDH (negative control), and FOS (positive control). **(D)** Binding site for SNHG17 on miR-3180-3p as predicted by bioinformatics (ENCORI, LncBase predicted V2). **(E)** Luciferase activity of transfected 293T cells. **(F)** Biotinylated miR–3180–3p was transfected into cells with SNHG17 overexpression. SNHG17 expression was detected by quantitative real–time PCR, after streptavidin capture. **(G)** Relative expression of miR-3180-3p in si-SNHG17-transfected HepG2 cells and LV-SNHG17-transfected Huh7 cells. Error bars represent mean ± SD from at least three experiments. *$p < 0.05$, **$p < 0.01$, ***$p < 0.001$.

with miR-3180-30 inhibitor, mimic, and controls. miR-3180-3p inhibited RFX1 expression and downregulation of miR-3180-3p promoted RFX1 expression in HCC cells (**Figures 6C,D**). Similarly, RFX1 was upregulated in HCC tumor tissues as compared to that in the normal tissues (**Figures 6E,F**); these high levels of RFX1 correlated with increasing tumor size and grade (**Figures 6G,H**).

Finally, we investigated the role of the SNHG17-miR-3180-3p-RFX1 axis in the progression of HCC using control, SNHG17, SNHG17+si-RFX1, and SNHG17+si-RFX1+miR-3180-3p inhibitor transfected Huh7 cells. SNHG17 promoted HCC cell proliferation (**Figure 7A**), migration (**Figure 7B**), invasion (**Figure 7C**), and EMT (**Figures 7D,E**) by sponging miR-3180-3p and upregulating RFX1.

DISCUSSION

LncRNAs have been implicated in the progression of various diseases, including HCC (Mehra and Chauhan, 2017; Lim et al., 2019). The role and molecular mechanisms employed by the lncRNA SNHG17 have been studied in detail; however, excluding its function in HCC. In this study, we hypothesized that SNHG17 is involved in the progression of HCC. SNHG17 was upregulated in HCC tumor tissues as compared to that in parameter-matched normal tissues. Moreover, high expression of SNHG17 correlated with larger tumor size and higher Edmonson-Steiner grades, suggesting that SNHG17 participates in the progression of HCC.

SNHG17 promotes cell proliferation in colorectal cancer (Ma et al., 2017), regulates cell invasion and migration in breast cancer

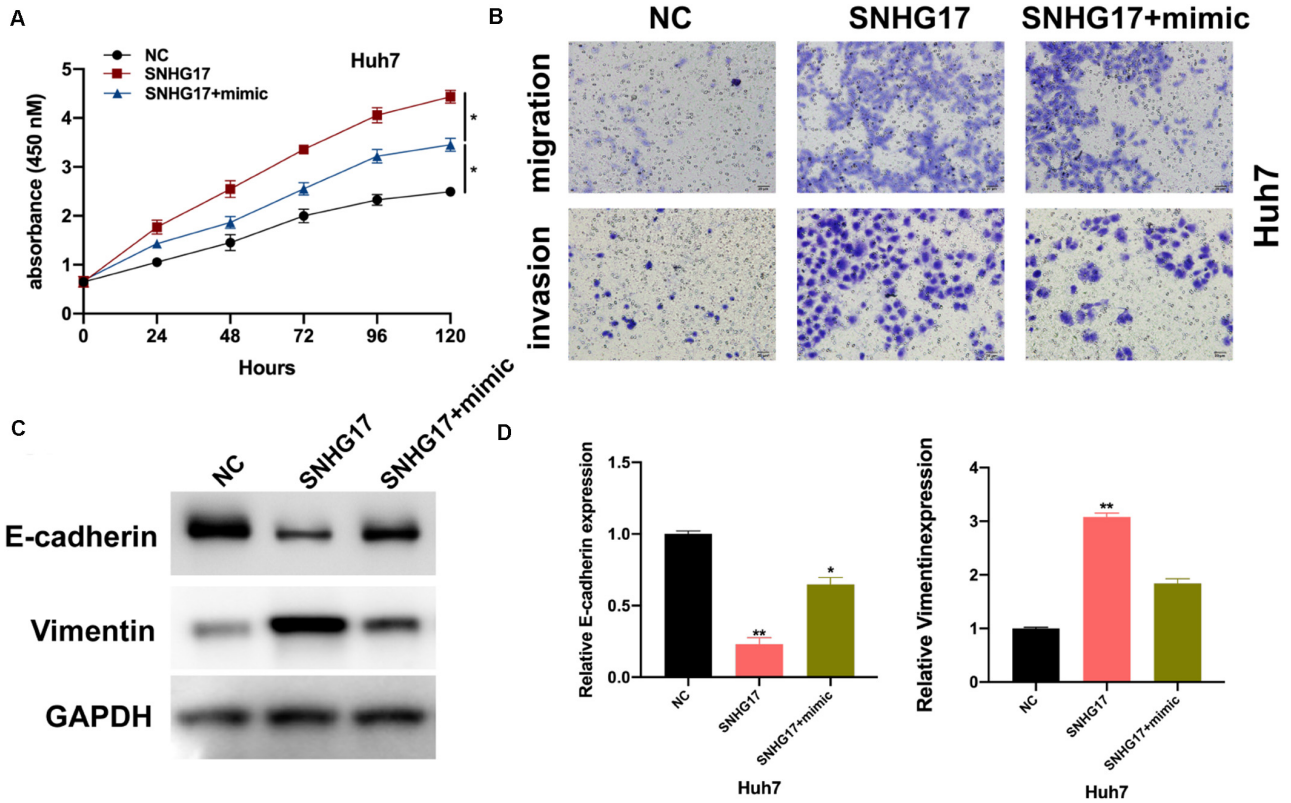

FIGURE 5 | miR-3180-3p reverses the oncogenic effect of SNHG17. Determination of the target of miR-3180-3p was performed using miRmap: https://mirmap.ezlab.org/. **(A)** Proliferation of Huh7 cells transfected with SNHG17 and SNHG17+miR-3180-3p mimic using CCK-8. **(B)** Transwell migration assay for the migration and invasion of Huh7 cells transfected with SNHG17 and SNHG17+miR-3180-3p mimic. **(C,D)** Western blotting and PCR analysis for the expression of EMT biomarkers E-cadherin and vimentin in treated cells. Error bars represent mean ± SD from at least three experiments. $^{*}p < 0.05$, $^{**}p < 0.01$.

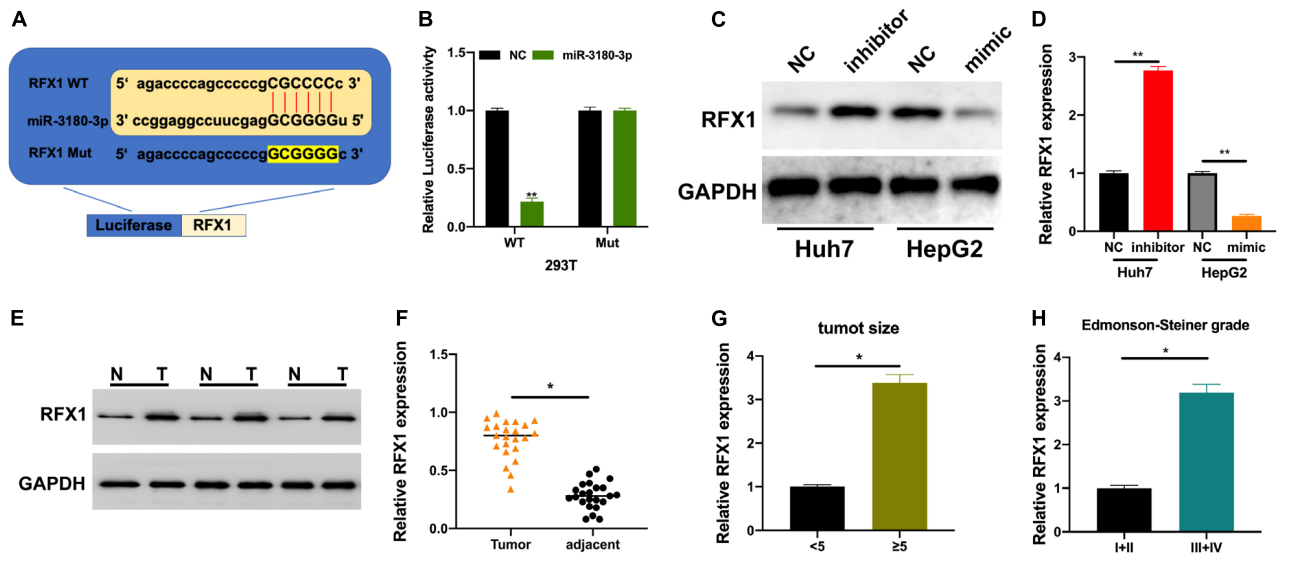

FIGURE 6 | RFX1 overexpression promotes the progression of HCC. **(A)** Binding site for miR-3180-3p on RFX1. **(B)** Luciferase activity for the effect of miR-3180-3p on RFX1. **(C,D)** Western blotting and PCR for the relative expression of RFX1 in Huh7 and HepG2 cells transfected with miR-3180-30 control, inhibitor, and mimic. **(E)** Western blotting for the expression of RFX1 in HCC tumor and matched normal tissues. **(F)** RFX1 expression in HCC tumor and matched normal tissues. **(G)** RFX1 expression in HCC tumor tissues of varying size. **(H)** RFX1 expression in HCC tumor tissues of varying Edmonson-Steiner grade. Error bars represent mean ± SD from at least three experiments. $^{*}p < 0.05$, $^{**}p < 0.01$.

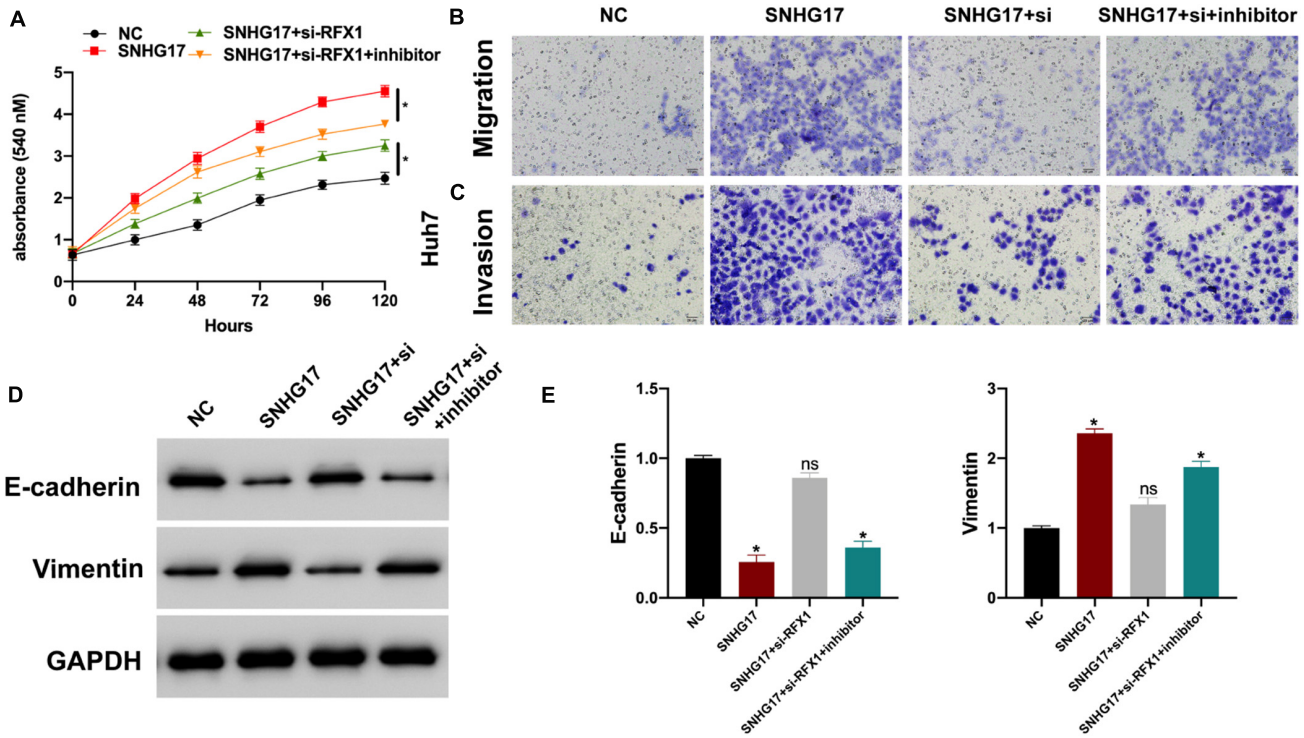

FIGURE 7 | (A) Proliferation of Huh7 cells transfected with SNHG17, SNHG17+si-RFX1, and SNHG17+si-RFX1+inhibitor using CCK-8. **(B)** Transwell migration assay for the migration and invasion of Huh7 cells transfected with SNHG17, SNHG17+si-RFX1, SNHG17+si-RFX1+inhibitor. **(C,D)** Western blotting and PCR analyses for the expression of EMT biomarkers E-cadherin and vimentin in treated cells. **(E)** The SNHG17-miR-3180-3p-RFX1 axis in the progression of HCC. Error bars represent mean ± SD from at least three experiments. *$p < 0.05$.

(Du et al., 2020), and affects cell cycle in gastric cancer (Zhang et al., 2019). Thus, SNHG17 may be involved in the lifecycle of HCC cells. Here, we generated SNHG17 overexpressing and depleted cell and mouse models. Overexpression of SNHG17 promoted cell proliferation, invasion, and migration *in vitro*. Similarly, overexpressing SNHG17 promoted tumor growth and metastasis *in vivo*. Moreover, upregulating SNHG17 promoted EMT in the *in vitro* and *in vivo* models of HCC. The above findings suggest the promotive effect of SNHG17 in HCC progression.

LncRNA-miRNA-mRNA molecular signatures are important in various biological processes (Paraskevopoulou and Hatzigeorgiou, 2016; Huang Y.A. et al., 2018; Zhang G. et al., 2018). SNHG17 regulates cell functions by acting as a molecular sponge for miRNAs in breast cancer (Du et al., 2020), tongue squamous cell carcinoma (Liu et al., 2020), and glioma (Li et al., 2020). Using bioinformatic analyses, AGO2-RIP, luciferase reporter assays, and RNA pull-down assays, we demonstrated that SNHG17 sponges miR-3180-3p and inhibits its expression. The role of miR-3180-3p on HCC progression has not been investigated, our results showed that miR-3180-3p overexpression inhibited HCC cell proliferation, migration, and invasion. Subsequently, we found that miR-3180-3p reversed the oncogenic role of SNHG17. Subsequently, we observed that miR-3180-3p targeted and negatively regulated RFX1 functions in HCC cells. Moreover, the expression of RFX1 in HCC tumor tissues correlated with tumor size and Edmonson-Steiner grade. Using CCK-8 and Transwell assays, we showed that the oncogenic role of SNHG17 in HCC was partially exerted via the miR-3180-3p/RFX1 axis.

In conclusion, SNHG17 was upregulated in HCC tumor tissues. Overexpression of SNHG17 promoted HCC cell proliferation, invasion, and migration *in vitro* and *in vivo*. SNHG17 sponged miR-3180-3p, thereby regulating its functions and upregulating RFX1 in the progression of HCC. Taken together, our findings may provide new insights into the molecular mechanisms involved in HCC and use of the SNHG17/miR-3180-3p/RFX1 axis as a promising therapeutic target for HCC.

DATA AVAILABILITY STATEMENT

The original contributions presented in the study are included in the article/**Supplementary Material**, further inquiries can be directed to the corresponding author/s.

ETHICS STATEMENT

The studies involving human participants were reviewed and approved by the Hospital Affiliated to Shaanxi University of Chinese Medicine. The patients/participants provided their

written informed consent to participate in this study. The animal study was reviewed and approved by The Hospital Affiliated to Shaanxi University of Chinese Medicine.

AUTHOR CONTRIBUTIONS

X-XM, JL, and ZC designed the study. TM, XZ, HW, and SY performed the experiments. TM, XZ, YH, YL, HG, and QL participated in the data analysis. HW wrote the manuscript. JL revised the manuscript. All authors approved the final proof.

SUPPLEMENTARY MATERIAL

The Supplementary Material for this article can be found online at: https://www.frontiersin.org/articles/10.3389/fgene.2020.607636/full#supplementary-material

REFERENCES

Bray, F., Ferlay, J., Soerjomataram, I., Siegel, R. L., Torre, L. A., and Jemal, A. (2018). Global cancer statistics 2018: GLOBOCAN estimates of incidence and mortality worldwide for 36 cancers in 185 countries. *CA Cancer J. Clin.* 68, 394–424. doi: 10.3322/caac.21492

Chen, L. L., He, J., Qiu, X. T., Yu, J., and Wang, Z. M. (2019). The prognostic roles of long non-coding RNA SNHG17 in the patients with gastric cancer. *Eur. Rev. Med. Pharmacol. Sci.* 23, 1063–1068.

Du, P., Gao, K., Cao, Y., Yang, S., Wang, Y., Guo, R., et al. (2019). RFX1 downregulation contributes to TLR4 overexpression in CD14(+) monocytes via epigenetic mechanisms in coronary artery disease. *Clin. Epigenet.* 11:44. doi: 10.1186/s13148-019-0646-9

Du, Y., Wei, N., Hong, J., and Pan, W. (2020). Long non-coding RNASNHG17 promotes the progression of breast cancer by sponging miR-124-3p. *Cancer Cell Int.* 20:40. doi: 10.1186/s12935-020-1129-y

Fan, C. N., Ma, L., and Liu, N. (2018). Systematic analysis of lncRNA-miRNA-mRNA competing endogenous RNA network identifies four-lncRNA signature as a prognostic biomarker for breast cancer. *J. Transl. Med.* 16:264. doi: 10.1186/s12967-018-1640-2

Gao, H., Liu, R., and Sun, X. (2019). STAT3-induced upregulation of lncRNA SNHG17 predicts a poor prognosis of melanoma and promotes cell proliferation and metastasis through regulating PI3K-AKT pathway. *Eur. Rev. Med. Pharmacol. Sci.* 23, 8000–8010.

Huang, J. L., Cao, S. W., Ou, Q. S., Yang, B., Zheng, S. H., Tang, J., et al. (2018). The long non-coding RNA PTTG3P promotes cell growth and metastasis via up-regulating PTTG1 and activating PI3K/AKT signaling in hepatocellular carcinoma. *Mol. Cancer* 17:93. doi: 10.1186/s12943-018-0841-x

Huang, Y. A., Chan, K. C. C., and You, Z. H. (2018). Constructing prediction models from expression profiles for large scale lncRNA-miRNA interaction profiling. *Bioinformatics* 34, 812–819. doi: 10.1093/bioinformatics/btx672

Jarroux, J., Morillon, A., and Pinskaya, M. (2017). History, discovery, and classification of lncRNAs. *Adv. Exp. Med. Biol.* 1008, 1–46. doi: 10.1007/978-981-10-5203-3_1

Lafaro, K. J., Demirjian, A. N., and Pawlik, T. M. (2015). Epidemiology of hepatocellular carcinoma. *Surg. Oncol. Clin. N. Am.* 24, 1–17. doi: 10.1007/978-1-60327-522-4_1

Li, H., Li, T., Huang, D., and Zhang, P. (2020). Long noncoding RNA SNHG17 induced by YY1 facilitates the glioma progression through targeting miR-506-3p/CTNNB1 axis to activate Wnt/beta-catenin signaling pathway. *Cancer Cell Int.* 20:29. doi: 10.1186/s12935-019-1088-3

Lim, L. J., Wong, S. Y. S., Huang, F., Lim, S., Chong, S. S., Ooi, L. L., et al. (2019). Roles and regulation of long noncoding RNAs in hepatocellular carcinoma. *Cancer Res.* 79, 5131–5139. doi: 10.1158/0008-5472.CAN-19-0255

Liu, X., Liang, Y., Song, R., Yang, G., Han, J., Lan, Y., et al. (2018). Long non-coding RNA NEAT1-modulated abnormal lipolysis via ATGL drives hepatocellular carcinoma proliferation. *Mol. Cancer* 17:90. doi: 10.1186/s12943-018-0838-5

Liu, X., Zhang, B., Jia, Y., and Fu, M. (2020). SNHG17 enhances the malignant characteristics of tongue squamous cell carcinoma by acting as a competing endogenous RNA on microRNA-876 and thereby increasing specificity protein 1 expression. *Cell Cycle* 19, 711–725. doi: 10.1080/15384101.2020.1727399

Liz, J., and Esteller, M. (2016). lncRNAs and microRNAs with a role in cancer development. *Biochim. Biophys. Acta* 1859, 169–176. doi: 10.1016/j.bbagrm.2015.06.015

Lo, H. C., and Zhang, X. H. (2018). EMT in metastasis: finding the right balance. *Dev. Cell* 45, 663–665. doi: 10.1016/j.devcel.2018.05.033

Ma, Z., Gu, S., Song, M., Yan, C., Hui, B., Ji, H., et al. (2017). Long non-coding RNA SNHG17 is an unfavourable prognostic factor and promotes cell proliferation by epigenetically silencing P57 in colorectal cancer. *Mol, Biosyst.* 13, 2350–2361. doi: 10.1039/c7mb00280g

Margini, C., and Dufour, J. F. (2016). The story of HCC in NAFLD: from epidemiology, across pathogenesis, to prevention and treatment. *Liver Int.* 36, 317–324. doi: 10.1111/liv.13031

Mathy, N. W., and Chen, X. M. (2017). Long non-coding RNAs (lncRNAs) and their transcriptional control of inflammatory responses. *J. Biol. Chem.* 292, 12375–12382. doi: 10.1074/jbc.r116.760884

Mcglynn, K. A., Petrick, J. L., and London, W. T. (2015). Global epidemiology of hepatocellular carcinoma: an emphasis on demographic and regional variability. *Clin. Liver Dis,* 19, 223–238. doi: 10.1016/j.cld.2015.01.001

Mehra, M., and Chauhan, R. (2017). Long Noncoding RNAs as a Key Player in hepatocellular carcinoma. *Biomark Cancer* 9:1179299X17737301.

Mercer, T. R., Dinger, M. E., and Mattick, J. S. (2009). Long non-coding RNAs: insights into functions. *Nat. Rev. Genet.* 10, 155–159. doi: 10.1038/nrg2521

Mohamadi, M., Ghaedi, H., Kazerouni, F., Erfanian Omidvar, M., Kalbasi, S., Shanaki, M., et al. (2019). Deregulation of long noncoding RNA SNHG17 and TTC28-AS1 is associated with type 2 diabetes mellitus. *Scand. J. Clin. Lab Invest.* 79, 519–523. doi: 10.1080/00365513.2019.1664760

Paraskevopoulou, M. D., and Hatzigeorgiou, A. G. (2016). Analyzing MiRNA-LncRNA Interactions. *Methods Mol. Biol.* 1402, 271–286. doi: 10.1007/978-1-4939-3378-5_21

Pastushenko, I., and Blanpain, C. (2019). EMT transition states during tumor progression and metastasis. *Trends Cell Biol.* 29, 212–226. doi: 10.1016/j.tcb.2018.12.001

Wang, J., Jia, J., Chen, R., Ding, S., Xu, Q., Zhang, T., et al. (2018). RFX1 participates in doxorubicin-induced hepatitis B virus reactivation. *Cancer Med.* 7, 2021–2033. doi: 10.1002/cam4.1468

Wang, J., Liu, X., Wu, H., Ni, P., Gu, Z., Qiao, Y., et al. (2010). CREB up-regulates long non-coding RNA, HULC expression through interaction with microRNA-372 in liver cancer. *Nucleic Acids Res.* 38, 5366–5383. doi: 10.1093/nar/gkq285

Xu, T., Yan, S., Jiang, L., Yu, S., Lei, T., Yang, D., et al. (2019). Gene amplification-driven long noncoding RNA SNHG17 regulates cell proliferation and migration in human non-small-cell lung cancer. *Mol. Ther. Nucleic Acids* 17, 405–413. doi: 10.1016/j.omtn.2019.06.008

Yang, L., Peng, X., Li, Y., Zhang, X., Ma, Y., Wu, C., et al. (2019). Long non-coding RNA HOTAIR promotes exosome secretion by regulating RAB35 and SNAP23 in hepatocellular carcinoma. *Mol. Cancer* 18:78. doi: 10.1186/s12943-019-0990-6

Zhang, G., Pian, C., Chen, Z., Zhang, J., Xu, M., Zhang, L., et al. (2018). Identification of cancer-related miRNA-lncRNA biomarkers using a basic miRNA-lncRNA network. *PLoS One* 13:e0196681. doi: 10.1371/journal.pone.0196681

Zhang, X. P., Jiang, Y. B., Zhong, C. Q., Ma, N., Zhang, E. B., Zhang, F., et al. (2018). PRMT1 promoted HCC growth and metastasis in vitro and in vivo via activating the stat3 signalling pathway. *Cell Physiol. Biochem.* 47, 1643–1654. doi: 10.1159/000490983

Zhang, Y., Tao, Y., and Liao, Q. (2018). Long noncoding RNA: a crosslink in biological regulatory network. *Brief Bioinform.* 19, 930–945. doi: 10.1093/bib/bbx042

Zhang, G., Xu, Y., Wang, S., Gong, Z., Zou, C., Zhang, H., et al. (2019). LncRNA SNHG17 promotes gastric cancer progression by epigenetically silencing of p15 and p57. *J. Cell Physiol.* 234, 5163–5174. doi: 10.1002/jcp.27320

Zhang, Y., Xu, Y., Feng, L., Li, F., Sun, Z., Wu, T., et al. (2016). Comprehensive characterization of lncRNA-mRNA related ceRNA network across 12 major cancers. *Oncotarget* 7, 64148–64167. doi: 10.18632/oncotarget.11637

Conflict of Interest: The authors declare that the research was conducted in the absence of any commercial or financial relationships that could be construed as a potential conflict of interest.

frontiers in Oncology

ORIGINAL RESEARCH
published: 19 January 2021
doi: 10.3389/fonc.2020.603702

Bcl9 Depletion Modulates Endothelial Cell in Tumor Immune Microenvironment in Colorectal Cancer Tumor

Zhuang Wei[1,2], *Mei Feng*[1], *Zhongen Wu*[1], *Shuru Shen*[1] *and Di Zhu*[1,3,4,5,6*]

[1] *Department of Pharmacology, School of Pharmacy, Fudan University, Shanghai, China,* [2] *Key Laboratory of Systems Biology, Innovation Center for Cell Signaling Network, CAS Center for Excellence in Molecular Cell Science, Institute of Biochemistry and Cell Biology, Shanghai Institutes for Biological Sciences, Chinese Academy of Sciences, Shanghai, China,* [3] *Department of Pharmacology, Shanghai Pudong Hospital, Fudan University Pudong Medical Center, Shanghai, China,* [4] *Key Laboratory of Smart Drug Delivery, Ministry of Education, & State Key Laboratory of Molecular Engineering of Polymers, School of Pharmacy, Fudan University, Shanghai, China,* [5] *Shanghai Engineering Research Center of ImmunoTherapeutics, Fudan University, Shanghai, China,* [6] *Yangtze Delta Drug Advanced Research Institute, Nantong, China*

Tumor endothelial cells are an important part of the tumor microenvironment, and angiogenesis inhibitory therapy has shown potential in tumor treatment. However, which subtypes of tumor endothelial cells are distributed in tumors, what are the differences between tumor endothelial cells and normal endothelial cells, and what is the mechanism of angiogenesis inhibitory therapy at the histological level, are all need to be resolved urgently. Using single-cell mRNA sequencing, we analyzed 12 CT26 colon cancer samples from mice, and found that knockdown of the downstream factor BCL9 in the Wnt signaling pathway or inhibitor-mediated functional inhibition can modulate tumor endothelial cells at a relatively primitive stage, inhibiting their differentiation into further extracellular matrix construction and angiogenesis functions. Furthermore, we propose a BCL9-endo-Score based on the differential expression of cells related to different states of BCL9 functions. Using published data sets with normal endothelial cells, we found that this score can characterize endothelial cells at different stages of differentiation. Finally, in the The Cancer Genome Atlas (TCGA) pan-cancer database, we found that BCL9-endo-Score can well predict the prognosis of diseases including colon cancer, kidney cancer and breast cancer, and identified the markers of these tumor subtypes, provide a basis for the prognosis prediction of patients with such types of tumor. Our data also contributed knowledge for tumor precision treatment with angiogenesis inhibitory therapy by targeting the Wnt signaling pathway.

Keywords: tumor immune microenvironment, colorectal cancer, endothelial cell, BCL9, Wnt pathway

OPEN ACCESS

Edited by:
Xiao-Jie Lu,
Nanjing Medical University, China

Reviewed by:
Jiheng Xu,
New York University, United States
Gianluca Santamaria,
Technical University of Munich, Germany

****Correspondence:***
Di Zhu
zhudi@fudan.edu.cn

Specialty section:
This article was submitted to Cancer Genetics, a section of the journal Frontiers in Oncology

Received: *07 September 2020*
Accepted: *18 November 2020*
Published: *19 January 2021*

Citation:
Wei Z, Feng M, Wu Z, Shen S and Zhu D (2021) Bcl9 Depletion Modulates Endothelial Cell in Tumor Immune Microenvironment in Colorectal Cancer Tumor. Front. Oncol. 10:603702. doi: 10.3389/fonc.2020.603702

INTRODUCTION

Endothelial cells and fibroblasts are a type of tumor-related cells that are widespread in tumors. More and more experimental evidence shows that tumor fibroblasts and endothelial cells play a role in promoting the occurrence and development of tumors (1, 2). But for a long time, how the endothelial cells and fibroblasts of tumors play a role in the occurrence and development of tumors has been stuck in the metaphysical imagination, lacking a comprehensive analysis to distinguish between connotation and extension. As we all know, endothelial cells and fibroblasts are a type of cells with the same origin and the potential to differentiate. Fibroblasts are considered as progenitor cells of endothelial cells (3), but the functions of endothelial cells are obviously different from fibroblasts. And endothelial cells also have different groups and stages of differentiation inside. Therefore, which types of cells in the endothelial cell and fibroblast population play an important role in tumors, and what are the similarities and differences in the roles of these cells in different types of tumors have become an urgent question to be answered.

The Wnt gene is synonymous with Wingless gene in Drosophila and Int gene in mice, identified for its proto-oncogene function in breast tumors firstly in 1982 (4). The Wnt ligands family includes 19 secreted cysteine-rich glycoproteins and participate in many biological processes of cell fate determination, such as cell division, proliferation, and migration (5). The Wnt pathway is a highly conserved pathway that plays an important role in embryonic development and tissue homeostasis, and involved in the development of many disease, including malignant tumor (4, 6).

The Wnt signaling pathway is historically divided into canonical and noncanonical pathways. The canonical pathway is β-catenin-dependent pathway, the noncanonical pathway including Wnt/Ca2+ pathway and Wnt/polarity pathway (7). β-catenin is the most critical and core signal transduction factor in canonical Wnt signaling pathway, and is distributed in both cytoplasm and cell membrane (8). The Wnt/β-catenin signaling pathway is a process with multiple steps that include multiple proteins relocalization, phosphorylation, and degradation, further influences the transcription of target genes (8). Briefly, Without Wnt signaling extracellular, β-catenin in the cytoplasm is phosphorylated by a "destruction complex" composed of axis inhibitor (Axin), glycogen synthase kinase-3 β (GSK3β), casein kinase 1 (CK1), adenomatous polyposis coli (APC), and protein phosphatase 2 A (8). Therefore, β-catenin is recognized and ubiquitinated by E3 ubiquitin ligase β-Trcp, which binds β-catenin for proteosomal degradation (8). On the contrary, when the Wnt signaling is activated, Wnt ligands bind to Frizzled (Fzd) and LRP receptor complexes. LRP receptors are then phosphorylated by CK1α and GSK3β, thereby the Dishevelled (Dvl) proteins is recruited to the plasma membrane, which disturbs the stability of "destruction complex" and prevents the phosphorylation degradation of β-catenin (8, 9). This progress lead to the stabilization and accumulation of β-catenin in the cytoplasm, which translocate into the nucleus and contracts with LEF/TCF (lymphoid enhancer factor/T-cell factor). Moreover, β-catenin recruits co-activators (such as CBP/p300, BRG1, BCL9, and Pygo) and forms a "activation complex", which leads to the transcription of target genes (such as CD44, VEGF, c-Myc andcyclinD1 et al.) (8, 10). This progress is tightly correlated with embryogenesis and oncogenesis.

Nuclear β-catenin, which plays a key role in the Wnt pathway, acts as a transcription factor for genes that regulate cell proliferation, migration, and survival (8). Nuclear β-catenin binds to B-cell lymphoma 9 (BCL9) and to its homologue B-cell lymphoma 9-like (BCL9L) (8, 11). BCL9 is a co-activator of the Wnt signaling pathway and regulates the recruitment of Pygopus to the nuclear β-catenin-TCF complex (8, 11). BCL9 enhances β-catenin-mediated transcriptional activity regardless of the mutational status of Wnt signaling components (12). It also promotes cell proliferation, invasion, and migration (12). BCL9 expression is very low in the normal cellular tissues from which tumors originate (12). High expression of BCL9 is often observed in many malignant tumors, including colorectal cancer, liver cancer, and breast cancer and it contributes to tumor progression, recurrence, and metastasis (12–14).

It is estimated that up to 92% CRC patients have at least one mutation in Wnt regulators reported by The Cancer Genome Atlas (TCGA) consortium in 2012 (15). Over 94% of CRC cases process at least one known protein mutation of Wnt/β-catenin pathway (15). In the majority of CRC cases, the Wnt signaling pathway mutations occur in APC gene, which is the main pathogenesis of familial adenomatous polyposis (FAP) syndrome (16, 17). Upon APC is deficient or dysregulated, the β-catenin "destruction complex" fails to be established. β-catenin accumulates and translocates to the nucleus, leading to the transcription of target genes related to CRC development (18). The APC function restoration can in turn recover crypt homeostasis and normal Wnt signaling levels in CRC murine models, regardless of the mutation of Tp53 and KRAS (19). Additionally, it is reported that about 1% of CRC cases display activating mutations of β-catenin (20, 21). The overexpression of β-catenin in the nucleus contribute to a poor outcome in CRC patients (22).

Remarkably, nearly all Wnt/β-catenin pathway mutations in CRC cause β-catenin accumulation in the nucleus eventually. Thus, targeting β-catenin/TCF interactions or inhibitors of transcriptional co-activators provide potential treatment options. B cell lymphoma 9 and its homolog B cell lymphoma 9–like (BCL9/9l) is transcriptional coactivator of β-catenin, forming part of Wnt signal enhanceosome (23). It is reported that peptides targeting BCL9/9l prevent tumor development and inhibit Wnt/β-catenin pathway activity in multiple CRC models (24). Moreover, loss of BCL9/9l suppresses CRC development driven by Wnt pathway effectively in murine models that resembling human cancer (25).

Tumor endothelial cells (TECs) are one cluster of components in tumor microenvironment. Specific tumor endothelial markers and abnormal cytogenetic expression indicate that TECs differ significantly from normal endothelial cells (NECs) (26). TECs play an important role in tumor

progression and metastasis, showing both angiogenic and non-angiogenic function. Tumor angiogenesis is caused by angiogenic factors, such as vascular endothelial growth factor and basic fibroblast growth factor, which are released by tumor cells and stimulate resting endothelial cells (EC) to migrate, proliferate, differentiate, and finally form new blood vessels. Tumor blood vessels help to supply nutrients and O2 to the tumor, and meanwhile, withdraw the waste and CO2. Different from normal blood vessels, tumor vessels are unstable and loosely attached (27), which makes tumor cells easier to permeate into vessels and metastasize. In addition to forming blood vessels, TECs show a non-angiogenic function. TECs are capable to secret angiocrine factors, such as VEGF, bFGF, IL-6, IL-8 and so on, to promote tumor progression (28). TECs can also express some specific molecules, such as FasL (29), PD-L1 (30) and so on, to inhibit immune function. A study revealed the distinction between HM-TEC from highly metastatic and LM-TEC from low metastatic tumors (31) which suggests that TECs themselves take a part in tumor metastasis. Besides, circulating TECs are found to protect tumor cells from anoikis in circulation (32).

A study demonstrated that BCL9 knockdown reduced angiogenesis through down-regulation of vascular endothelial growth factor expressed by tumor cells (12). However, the potential effect of BCL9 on TECs is still unclear.

The role of extracellular substations (ECMs) in tumor micro-environments is not limited to resistance to tumor invasion. An ECM is a repository of cell binding proteins and growth factors that affect tumor cell behavior (33). It is also modified by proteases produced by tumor cells and substation cells (33). In ECMs, Wnt proteins can undergo self-secretion and side secretion of signaling proteins: Wnt ligands form gradients and act as morphological signs to determine the spatial homogeneity of target cells and affect their behavior, such as gene expression, in a concentration-dependent manner (34). Extracellular hardness and Wnt/beta-catenin signal transdivation in physiology and disease transdivine Wnt/beta-catenin signal transdivation paths play a fundamental role in development, stem cell differentiation, and steady state in the body (35), and abnormal activation may lead to disease.

In order to answer these questions, we use RNAi genetic deprivation or small molecule inhibitors to influence the BCL9 and the Wnt signaling pathway in the CT26 colon cancer mice model. Through single-cell mRNA sequencing, cluster analysis, re-clustering analysis, differential expression analysis, and biological process enrichment analysis, we found that one certain type of endothelial cells and fibroblast populations in mouse colon cancer samples were perturbed by the loss of BCL9 function. The perturbed endothelial cells tend to lose normal endothelial cell functions, and exhibit high proliferation and high cell metabolism. To quantify this impact, by using of mathematical methods, we proposed a BCL9-endo-Score endothelial cell function score based on the differential expression gene set obtained from affected and unaffected cells. We verified BCL9-endo-Score score in published endothelial cell related databases, and found this score can distinguish different stages of Endothelial cell differentiation. Finally, in the TCGA database, at the pan-cancer scale, we found that BCL9-endo-Score can predict the prognosis of one type of special marker tumors well. Our data provides a supplement to the function of endothelial cells and fibroblasts in tumors, and provides a basis for further treatment.

MATERIALS AND METHODS

Chemicals and shRNAs

hsBCL9CT-24 was produced by AnaSpec, CA, according to previous protocols. Synthesis and purification of peptides were evaluated by analytical high-performance liquid chromatography (HPLC) and mass spectrometry (MS). hsBCL9CT-24 was dissolved as a 10 mmol/L solution; both were diluted prior to assay. pGIPZ- and/or pTRIPZ (inducible with doxycycline)-based lentiviral shRNAs for human BCL9 shRNA#3 (V3LHS_351822), mouse BCL9 shRNA#5 (V3LMM_429161), human BCL9L shRNA#4 (V2LHS_268755), mouse BCL9L shRNA#1 (V2LMM_69221), human CTNNB1 shRNA#2 (V2LHS_151023), mouse CTNNB1 shRNA#2 (V2LMM_1090), and non-targeting shRNA were obtained from Open Biosystems/GE Dharmacon. The non-targeting (NT) lentiviral shRNA construct expresses an shRNA sequence with no substantial homology to any mammalian transcript, providing a negative control.

Tumor Specimens

Six to 8-week-old BALB/c female mice were purchased from Charles River. For BCL9-shRNA and NT-shRNA group, CT26 BCL9-shRNA and NT-shRNA cancer cells were respectively subcutaneously (s.c.) inoculated (4×10^5 cells in PBS) in the right flank region of three mice. For Vehicle and $hsBCL9_{CT}$-24 group, CT26 wild type cancer cells were s.c. as above in six mice. Vehicle and hsBCL9CT-24 (25 mg/kg) were intraperitoneal (i.p.) injected once every two days, respectively in three mice. For each tumor, at least four regions were sampled. Totally, 12 samples from 12 mice were collected. details information was summarized (**Table 1**). All the procedures were performed according to protocols approved by the University's animal care committee, along with the guidelines of The Association for Assessment and Accreditation of Laboratory Animal Care International.

Specimen Processing

Fresh tumors were collected in MACS Tissues storage solution (130-100-008, Miltenyi Biotec) in the operation room after surgical resection and immediately transferred to the laboratory for processing. Tissues were minced into $<1mm^3$ on ice, transferred to a C tube (130-093-237, Miltenyi Biotec) and enzymatically digested with MACS Tumor Dissociation Kit (130-095-929, Mitenyi Biotec) according to corresponding programs. The resulting suspension was filtered through a 40 μm cell strainer (Falcon) and washed by RPMI 1640 (C11875500BT, Gibco). Erythrocytes were removed by adding

TABLE 1 | Sample information.

ID	Age	Sex	Location	Treatment	Size(mm)	Cell Number
5	10w	Female	s.c.	Vehicle	13*10*5	6,324
8	10w	Female	s.c	Vehicle	12.2*9*4.5	7,889
10	10w	Female	s.c	Vehicle	13.4*8.6*4.3	5,073
4	10w	Female	s.c	$hsBCL9_{CT-24}$	14.3*4.4*2.2	5,873
12	10w	Female	s.c	$hsBCL9_{CT-24}$	11.1*4.6*2.3	6,491
16	10w	Female	s.c	$hsBCL9_{CT-24}$	13.03*6.4*3.2	7,444
18	10w	Female	s.c	NT-shRNA	16.5*8.4*4.2	13,602
19	10w	Female	s.c	NT-shRNA	12.3*10*5	13,873
22	10w	Female	s.c	NT-shRNA	11*10*5	11,470
24	10w	Female	s.c	Bcl9-shRNA	10*7.2*3.6	12,377
25	10w	Female	s.c	Bcl9-shRNA	9*7.4*3.7	16,898
29	10w	Female	s.c	Bcl9-shRNA	8.4*7.6*3.8	13,230

2 ml Red Cell Lysis Buffer (555899, BD bioscieces). A Dead Cell Removal Kit (130-090-101, Miltenyi Biotec) was subsequently used to enrich live cells. After re-suspended in RPMI 1640 (C11875500BT, Gibco), single-cell suspension was obtained. Trypan blue (15250061, Gibco) was next used to check whether cell viability was >90% to be qualified enough for library construction.

10X Library Preparation and Sequencing

Cell concentration was adjusted to 700–1,200 cells/μl to run on a Chromium Single-Cell Platform (10x Genomics ChromiumTM). 10x library was generated according to the manufacturer's protocol of 10X genomics Single Cell 3' Reagent Kits v2. The clustering was performed on a cBot Cluster Generation System with TruSeq PE Cluster Kit v3. Qubit was used for library quantification. The final library was sequenced on an Illumina HiSeq3000 instrument using 150-base-pair paired-end reads.

Single cell analysis: Raw data were normalized by using CellRanger (version 4.0). The percentage of reads with the correct barcode is above 85%, and the percentage of bases with a quality score greater than or equal to 30 in the barcode sequence is above 95%; the number of high-quality cells were lisetd in **Table 1**. The total number of Unique Molecular Identifiers (UMIs) per cell was calculated for the number of UMI sequences in the sample with standardizing the data and for identification of highly variable features. The median UMI is 7,000. Then, data was rescaled according to cell cycle related genes and remove batch effects by using Seurat function FindIntegrationAnchors and IntegrateData (36). Then use principal component analysis (PCA) to reduce the dimension. Next, Find the neighbors of each cell by embedded K-nearest neighbor (KNN) graph, and then use the Louvain algorithm to cluster the cells, and then project the results of the clustering on the dimension reduction results from embedded tSNE (t-Distributed Stochastic Neighbor Embedding) and Umap (Uniform Manifold Approximation and Projection) (36, 37). Mark each cell population with known markers, and then extract the endothelial cells and fibroblasts subpopulations (Cluster 7 and 8) for further Re-clustering analysis.

Pseudotime analysis was done using Monocle2 package Built-in Reversed graph embedding method (38–40). Differential gene analysis along Pseudotime was done by using the Branched expression analysis modeling (BEAM) function.

BCL9-Endo-Score

Use formula (1) to calculate the BCL9-endo-Score of each cell or each patient.

$$\mathrm{BCL9}-endo-Score = \frac{GSVA\ (BCL9\ \ \text{Turge gene list})}{GSVA\ (\text{BCL9}\ \ \text{False gene list}) + \ 0.0000000001} \quad (1)$$

In the formula (1), *GSVA*() is the function of Gene Set Variation Analysis; BCL9 Ture gene list and BCL9 False gene list respectively represent genes enriched in tumor endothelial cells that have been interfered with or not interfered with BCL9. BCL9 Ture gene list: IGFBP7, SPARC, RARRES2, BGN, LOXL1, COL5A2, FSTL1, COL6A2, DCN, MFAP5, SERPING1, AEBP1, GPX3, THY1, MMP2, BMP1, FBN1, ADAMTS2, COL1A1, COL6A3, RCN3, FBLN2, PLPP3, LOXL2, CD248, COL6A1, PDSSTN, RNASE4, COL3A1, COL1A2, COL5A3, C1QTNF6, MGST1, SERPINF1, SOD3, EBF1, EFEMP2, CYGB, SULF1, FXYD1, VCAN, NBL1, FN1, TGFBR2, SERPINA3, SELENOM, MMP14, RCN1, GPX7, BICC1; BCL9 False gene list: TCP1, RPL12, RPL3, RPL4, TMPO, RPL7, PRKG2, RRM2, LARS2, FCER1G, RAD21, EZR, MTAP, CD9, RPS6, TOP2A, HSP90AB1, HSPA9, MT-CYB, HBEGF, AMIGO2, ACTN4, ACTB, CAVIN2, PLA2G7, CENPF, ATP5F1B, HSPA8, EEF2, TUBA1C, RPS18, ANLN, RAN, WDR31, NOLC1, CPE, TM4SF1, HSPD1, SPP1, PHGDH, TUBA1B, S100A4, CD74, UBE2C, LGALS7, HMGB2, CAV2, ESM1, CCND1, HMGA1.

Gene Prognostic Performance in The Cancer Genome Atlas Samples

The TCGA datasets were downloaded from Xena Functional Genomics Explorer (https://xenabrowser.net/). The samples

were divided into high and low expression groups based on Maxstat (maximally selected rank statistics) algorithm. A Kaplan-Meier curve was constructed to compare the overall and disease-free survival in two groups. Log-Rank P value and HR were also calculated.

Gene Set Variation Analysis, Gene Set Enrichment Analysis, and Metascape Analysis

GSVA analysis adopts the corresponding gene list of different sample combinations from single cell data or TCGA data to complete with R software.

GSEA analysis uses the grouping information obtained by single-cell cluster analysis, and uses the C5 signal pathway in the Molecular Signatures Database v7.1 to annotate (41, 42).

The Metascape analysis is done with reference to the reported method (43).

RESULTS

Clustering Analysis of 12 Samples

In order to study the effect of BCL9 dysfunction on tumor single cell at mRNA levels, we grouped and integrated the BCL9 Genetic deprivation and inhibitor-treated single-cell mRNA sequencing data to remove the batch effect. The further standardized data are clustered using UMAP algorithm and adjacent algorithm, displayed in two dimensions of UMAP graph, and marked with sample identifications or processing groups, as shown in **Figure 1A**. The results show that most of the cells from different samples were evenly distributed among different clusters, which indicated that the effect of batch effect processing and the data quality had reached the level at which they could be combined and analyzed. The results of the cluster analysis of the adjacency algorithm are further displayed on the UMAP graph, **Figure 1C**. We performed the data comparison in

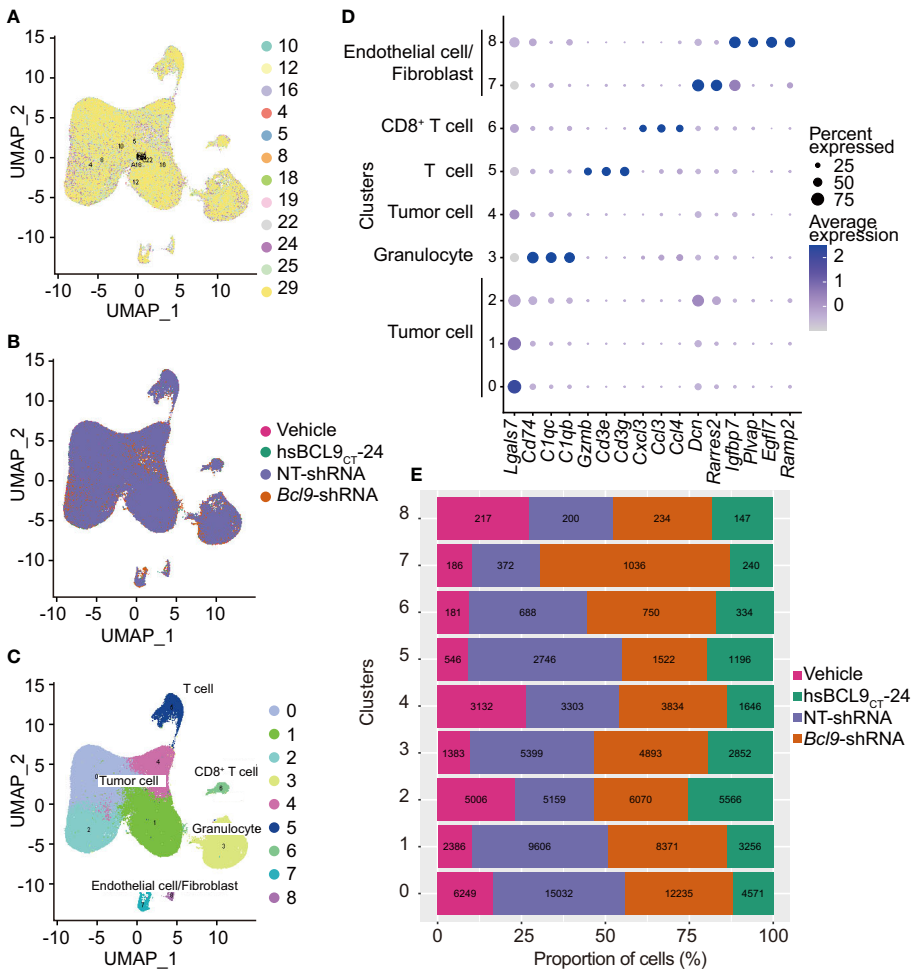

FIGURE 1 | UMAP and cell cluster analysis. **(A)** UMAP of the samples profiled, and UMAP of the associated cell type. Color coded by their associated samples. **(B)** UMAP analysis of sample types of origin (vehicle, hsBCL9CT-24, NT, BCL9-shRNA). **(C)** UMAP of all cells profiled, and UMAP of the associated cell type and clusters. Color coded by their associated clusters. **(D)** Bubble chart of the eight clusters. **(E)** The fraction bar plot of eight clusters originating from vehicle, hsBCL9CT-24, NT, BCL9-shRNA (Numbers show real cell numbers).

the cell annotation database and the differential expression analysis between different clusters in **Figure 1C** to label the cell types. Results showed that all of the samples could be classified as tumor cells, T cells, CD8 T cells, granulocytes, and endothelial/fibroblast cell types are shown in **Figures 1D, E** and **S1**.

To study the perturbation effects of different treatments (BCL9 KD, RNAi control; BCL9 inhibitor or control) on different clusters of cells, we marked the processing group information on the UMAP diagram (**Figure 1B** and **Figure S2A**, **B**). The results showed that most cell clusters did not differ significantly across different treatment groups, but in 7–8 clusters, that is, endothelial/fibroblast clusters, different groups showed different distributions. The four groups are not well merged together, but dispersed (**Figure S2B**), indicating that the two clusters of cells have high heterogeneity. which suggests these two clusters of cells are affected by different treatments.

Re-Clustering and Transcription Analysis of Endothelial Cell

In order to further determine whether the endothelial/fibroblast clusters show different treatment-dependent clustering effects, we performed re-clustering analysis on cell clusters 7–8 using the tSNE algorithm. The results are shown in **Figures 2A–C** and **S2**. The re-clustered clusters 2 and 3 of endothelial/fibroblasts are visibly distinct from those of the main population, **Figures 2A–C**. The cells treated with BCL9 KD and BCL9 inhibitors were

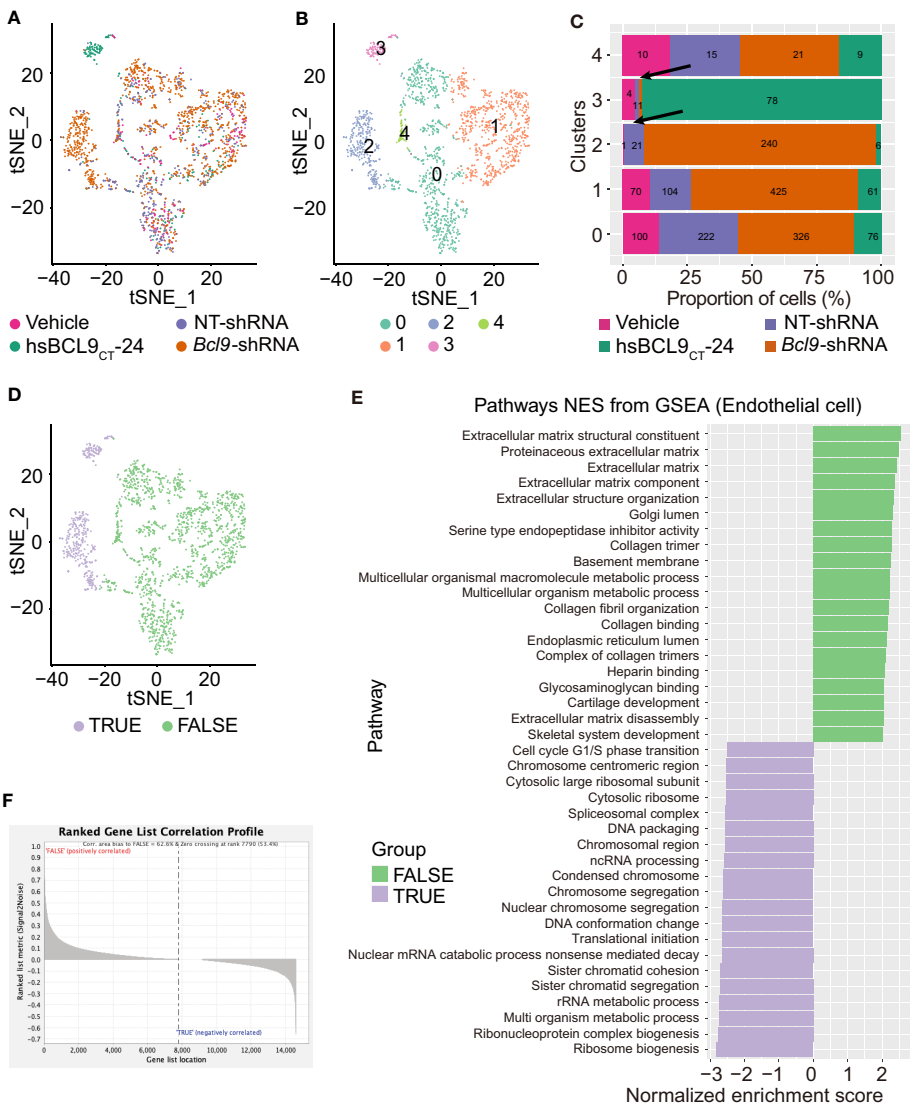

FIGURE 2 | UMAP and GESA analysis of endothelial cell. **(A)** UMAP plot, Sample type of origin (vehicle, hsBCL9CT-24, NT, BCL9-shRNA). **(B)** Four different clusters by UMAP analysis. **(C)** The fraction bar plot of four clusters originating from vehicle, hsBCL9CT-24, NT, BCL9-shRNA (Numbers show real cell numbers). **(D)** UMAP plot of FLASE and TRUE groups. **(E)** GSEA analysis on FLASE and TRUE groups. **(F)** Rank gene correlationship profile of FLASE and TRUE groups.

significantly enriched in clusters 2 and 3. This indicates that treatment with BCL9 KD and BCL9 inhibitors has significantly changed the expression profiles of 2 and 3 clusters of endothelial/fibroblasts.

In order to further study the specific biological processes by which BCL9 KD and BCL9 inhibitor treatment change the expression profiles of clusters 2 and 3 of endothelial/fibroblasts, we performed gene set enrichment analysis (GSEA) on cells belonging to these two clusters of endothelial/fibroblast clusters (True) and those not belonging to these clusters (False). As shown in **Figures 2D, E**, the results show that they do not belong to clusters 2 and 3. The list of genes related to such endothelial cell functions as the establishment of extracellular mechanisms was enriched in the cells, while the cells belonging to clusters 2 and 3 did not show this enrichment effect. Rather, they showed some background differences such as ribosomal changes and metabolic changes. These results indicate that treatment with BCL9 KD and BCL9 inhibitors changes the function or differentiation status of endothelial/fibroblasts. From the results of GSEA, we selected the top 50 genes with high enrichment scores in the True and False clusters and named them the BCL9 True gene list and the BCL9 False gene list, as shown in **Figure 2F**.

Pseudo-Time Analysis of Endothelial Cells

We performed a simulation analysis of endothelial cells/fibroblasts to further study the effect of BCL9 KD and BCL9 inhibitor treatment on the function and differentiation of endothelial cells/fibroblasts. As shown in **Figures 3A–C**, endothelial cells/fibroblasts can be divided into three branches; those belonging to two clusters 2 and 3 endothelial cells/fibroblast clusters (True) are mainly distributed on the right and upstream of the second node, as shown in **Figure 3C**. We show the gene set variation analysis (GSVA) rankings of the BCL9 True gene list and the BCL9 False gene list on the graph of the pseudotime analysis. As shown in **Figures 3D–F**, the cells gradually differentiated from node 1 along two opposite paths. At nodes 2 and 3, the GSVA score of the BCL9 True gene list was higher near node 2, and the GSVA score of the BCL9 False was higher near node 3. The GSVA score of the angiogenic gene list near 3 nodes was also relatively high. This shows that the effect of BCL9 KD and BCL9 inhibitor treatment on endothelial cells may involve angiogenesis. The heat map constructed by the BEAM function shows the changing trend of key genes along pseudotime (**Figure S3** and **S4**).

In order to further study the effect of BCL9 KD and BCL9 inhibitor treatment on endothelial cells at specific stages of endothelial cell differentiation, we reanalyzed the published mouse liver database (GSM3714747) (44). Liver endothelial cells undergo all of the stages of endothelial cell differentiation, including three stages of relatively primitive cell types (1), well-differentiated sinusoidal endothelium (2) and cells similar to astrocytes (fibroblasts) (3). The entire process of endothelial differentiation can be shown. The gene lists BCL9 True and BCL9 False found in the treatment of BCL9 KD and BCL9 inhibitors were used in mouse liver endothelial data for GSVA analysis, and the GSVA scores are shown in terms of the results of the pseudo-time reanalysis (**Figures 3G–I**). The results showed that the BCL9 False gene list was mainly enriched in astrocyte-like cell clusters (3), while the BCL9 True gene list was mainly enriched in the relatively primitive cell clusters (1).On both sides, we also observed weak enrichment of the BCL9 True gene list, but the enrichment trend is obviously biased to the side of cell clusters (2). This shows that the treatment of BCL9 KD and BCL9 inhibitors can block endothelial cells transition from cell clusters (1) to both ends. The angiogenesis genes are enriched in well-differentiated sinusoidal endothelium cell clusters (2) and cell clusters (3). Based on these results, we can conclude that treatment with BCL9 KD and BCL9 inhibitors can differentiate endothelial cells into the branch of astrocyte-like fibroblasts or highly differentiated endothelial cells.

BCL9 Endothelial Function Score (BCL9-Endo-Score) and Clinical Significance

In order to further study the clinical significance of BCL9 KD and BCL9 inhibitor treatment on endothelial/fibroblasts, we propose a BCL9 endothelial function Score (BCL9-endo-Score). BCL9-endo-Score is defined as GSVA (BCL9 True gene list)/GSVA (BCL9 False gene list + 0.0000000001), plotted in **Figures 3J, K**. We can see that the cells with high BCL9-endo-Score are some types of cells between the more primitive cells and differentiated cells, which are more inclined to the angiogenic side. This reflects the essential connotation of BCL9-endo-Score, which is the potential of cells to focus on angiogenesis but not on the secretion of extracellular matrix.

In this project, we also will use the BCL9-endo-Score to score all of the cancer samples in the TCGA database. We performed survival analysis for each cancer type according to the BCL9-endo-Score. These results show that, in most cancer types, patients with high BCL9-endo-Scores have significantly poor prognosis, **Figures 4A–D**. This shows that the effects of BCL9 KD and BCL9 inhibitor treatment on the function and differentiation of endothelial cells/fibroblasts can affect the prognosis of tumor patients, and this may also lay an experimental foundation for clinical medication.

In order to further study the clinical significance of BCL9-endo-Score, we performed Louvain algorithm cluster analysis and UMAP reduction of dimensions for all TCGA tumor patients based on their mRNA expression similarity. The results of the cluster analysis are displayed on the UMAP graph, **Figures 5A–C**. It can be seen that the entire TCGA patients are divided into 40 clusters. These clusters are basically attributable to the site of cancer, but there are also some tumors from different sites that are clustered together, or some subgroups are produced. In order to further clarify the marker gene of each cluster. We have performed differential gene analysis on TCGA cluster, and the results are shown in the figure.

Then we use each cluster as a group, use BCL9-endo-Score to score each patient, and then use BCL9-endo-Score to group the patients in the cluster and use the Maxstat (maximally selected rank statistics) algorithm for survival analysis, **Figures 5D, E**. The results showed that both cluster 21 and 29 showed a strong

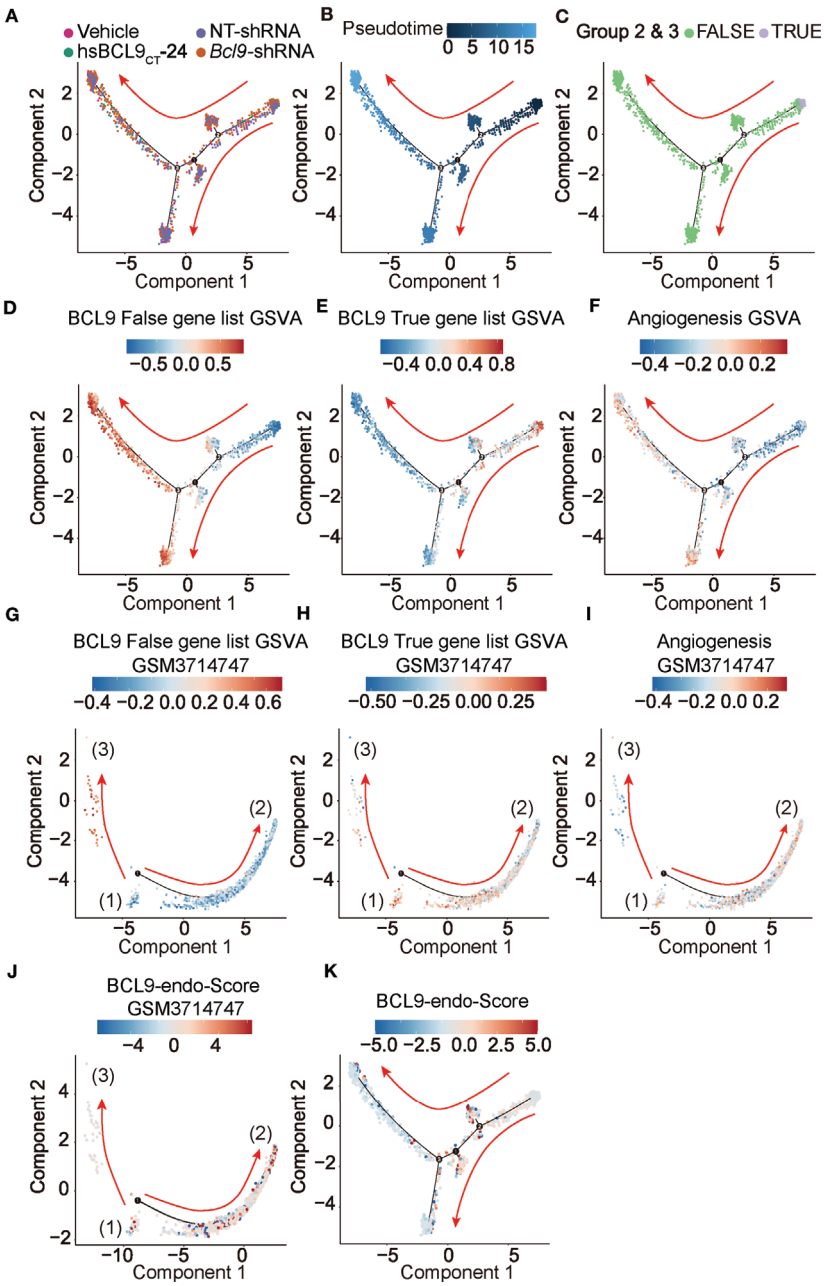

FIGURE 3 | Pseudotime analysis of endothelial cell. **(A–F, K)** Development trajectory of other types of endothelial cells and fibroblast populations along pseudo-time in two-dimensional space in vehicle, hsBCL9CT-24, NT, BCL9-shRNA. **(G–J)** Development trajectory of other types of endothelial cell population from published dataset (GSM3714747). Each point corresponds to a single cell and is color-coded by cell subgroup and differentiation score. Arrows indicate the direction of differentiation.

and significantly high-risk ratio HR. Among them, cluster 29 is composed of part of BRCA (103) and NHSC (7), and cluster 21 is composed of part of KIRC (90), KIRP (37), KICH (25), and SARC (1). Through the differential genes, we can see that the markers of cluster 29 and cluster 21 are SCGB2A2, ADIPOQ gene and UMOD and AQP2 gene, respectively, **Figure 5C**. The above results indicate that in the above-mentioned tumors BCL9-endo-Score can well judge the clinical prognosis.

DISCUSSION

Classification of Tumor Endothelial Cells

Endothelial cells are a type of cells derived from the mesoderm. On the histological level, endothelial cells form the inner walls of various capillaries and large blood vessels in the tissue (45). There is no doubt that endothelial cells play an important role in physiology and pathology. Many important diseases are related

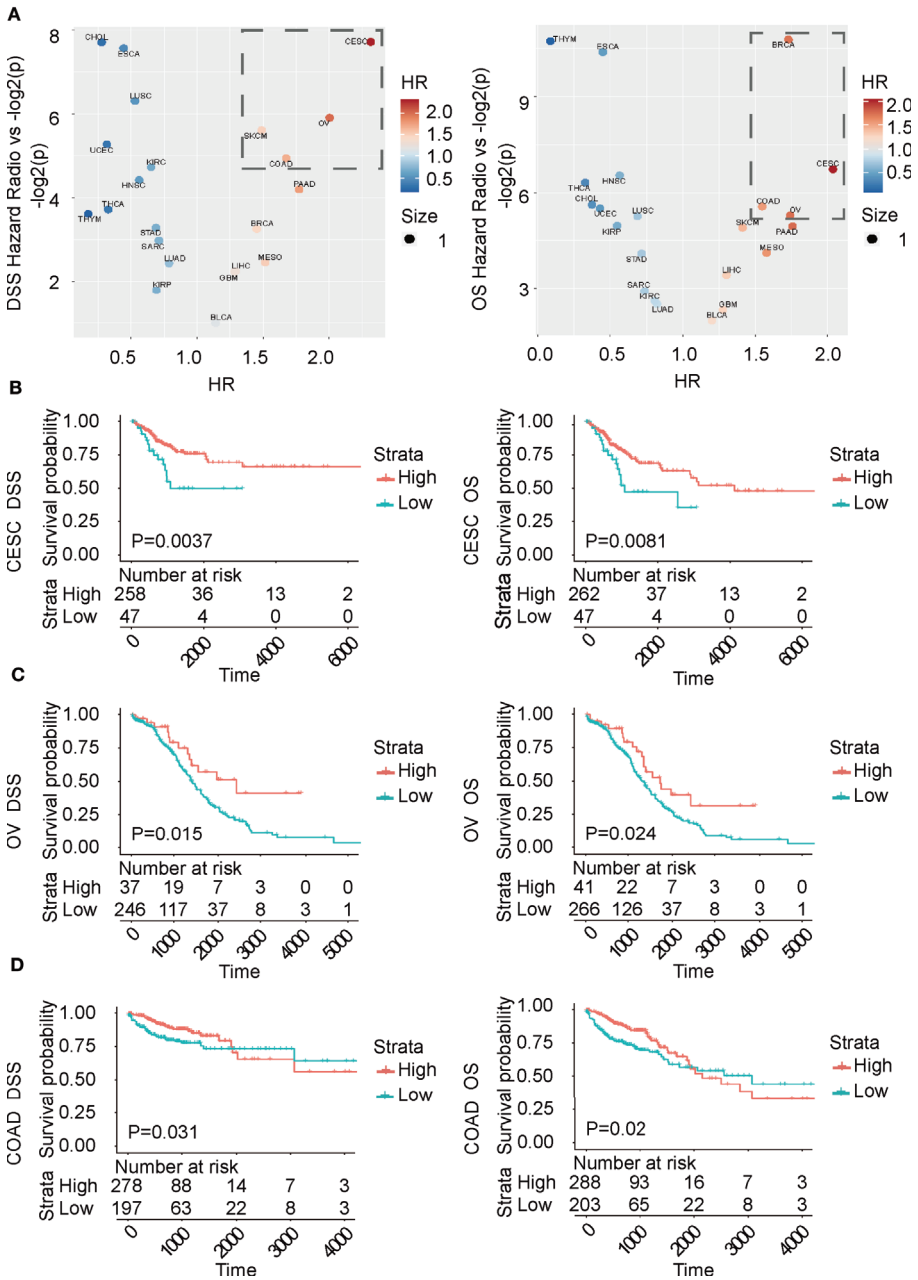

FIGURE 4 | BCL9-endo-Score can predict the prognosis of TCGA tumor patients according to the traditional classification. **(A)** Volcano chart of hazard ratio (HR) of different types of cancer. **(B–D)** Survival analysis chart of TCGA patients according to traditional classification. OS and DSS respectively represent overall survival and disease-specific survival rate.

to disorders of the structure and function of endothelial cells, such as heart disease, diabetes, high blood pressure, liver cirrhosis, pulmonary fibrosis, and so on (45). In tumors, endothelial cells are generally considered to be involved in the formation of blood vessels and are responsible for the communication of material information inside the tumor and outside the tumor (46). Endothelial cells generally develop from mesenchymal stem cells and have a general marker of fibroblasts and mesenchymal stem cells. We grouped single cells of mouse colon cancer cells treated with BCL9 KD and BCL9 inhibitors according to the similarity of their mRNA expression, and found that the two groups 7 and 8 have markers related to endothelial cells and fibroblasts. Among them, many markers are shared by endothelial cells and fibroblasts. For example, the highly expressed marker Ccl4 in the 7 population has been reported to play an important role in the differentiation of endothelial

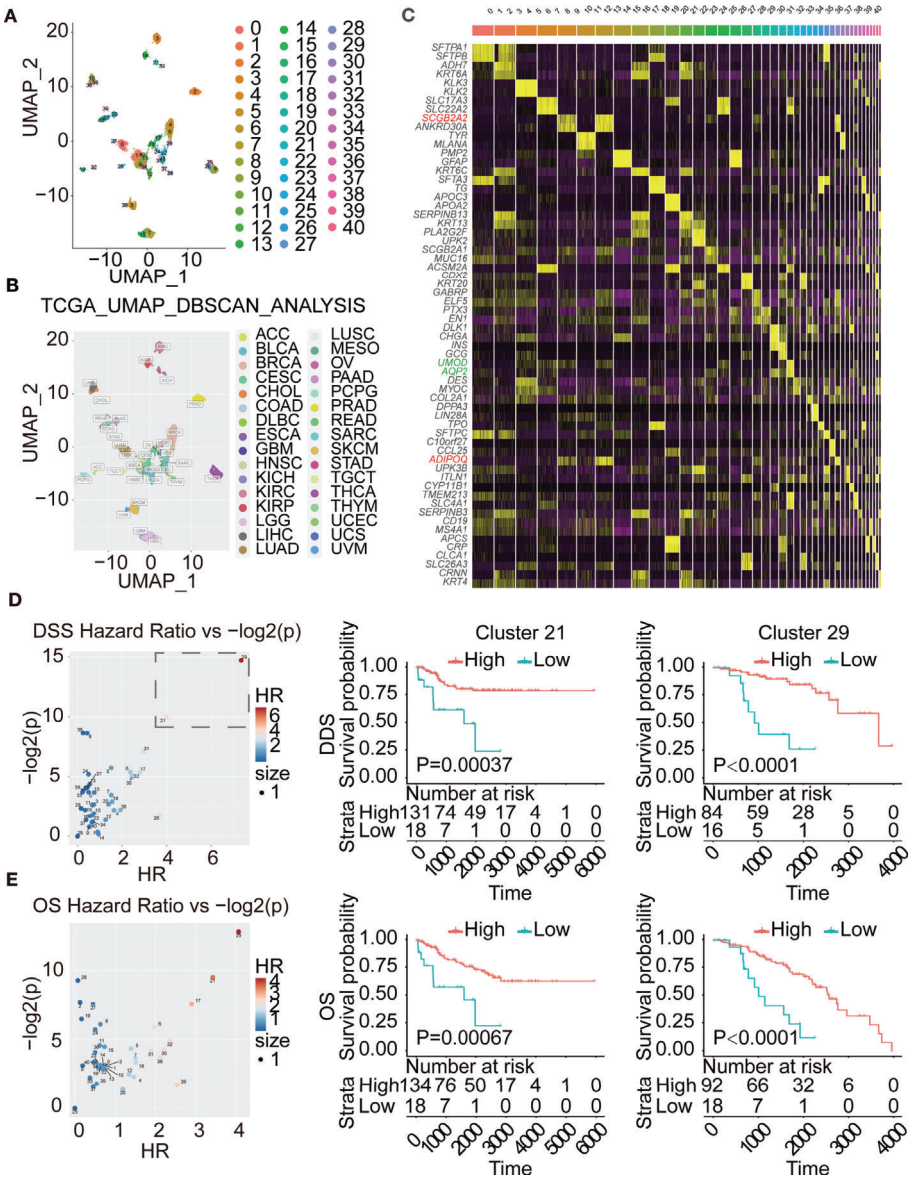

FIGURE 5 | BCL9-endo-Score can predict the prognosis of TCGA tumor patients clustered by gene expression. **(A)** Cluster analysis of TCGA patients according to gene expression patterns. **(B)**. to label with traditional classification **(C)**. Differential gene analysis of patients in different clusters. **(D, E)**. Survival analysis of TCGA patients in different clusters. On the left is the Volcano chart of hazard ratio (HR) of different patient clusters. The survival analysis is on the right.

cells, and collagen Col1a1 is considered to be the marker of endothelial cells (47). Gpihbp1 (48), Egfl7 (49), and Plvap (50) in the eight groups are also considered to be important markers of endothelial cells. Among them, Plvap is considered to form the membrane of glomerular endothelial cells, and belongs to the marker of endothelial differentiation (50). At the same time, Col3a1 (51) in group 7 and Pi16 (52) in group 8 were reported to be fibroblast markers. Therefore, in summary, endothelial cells and fibroblasts share the characteristics of a common marker. In other words, it is difficult to distinguish and define which cells are endothelial cells and which cells are fibroblasts. This result is consistent with previous reports. Fibroblasts and endothelial cells are not only the same in source, but may have the properties of mutual differentiation and transformation. In the UMAP cluster analysis graph of our result, we can observe that the 7 and 8 groups have a connected topological relationship, which also proves the above point.

Functional Differences Between Different Tumor Endothelial Cells

The function of endothelial cells in tumors has been explored for a long time. Even inhibiting the growth of tumor endothelial cells is a very potential target in tumor therapy. On the one hand, the massive growth of endothelial cells promotes the blood supply

inside the tumor (27), so that the internal nutrition of the tumor is sufficient, the tumor grows faster, and the tumor mass is larger, oppressing the surrounding organs and crowding out normal cells; on the other hand, a large number of endothelial cells make the internal oxygen supply of the tumor sufficient, avoiding some EMT transition or metastasis caused by hypoxia (53). Therefore, endothelial cells have dual functions in tumors, and may have completely opposite functions in tumors of different nature. Our research results found that the loss of BCL9 function can make the tumor endothelial cell and fibroblast population clearly grouped. In this type of tumor endothelial cells and fibroblasts derived from BCL9 functional loss samples, the biological processes related to the formation of extracellular matrix have undergone significant changes. In the endothelial cell population with relatively normal BCL9 function, the significantly enriched genes are concentrated in the establishment of extracellular matrix, Golgi lumen function, collagen fibrous tissue, ER lumen function, connective tissue development and bone system development. Blood vessels have always been regarded as an important type of connective tissue in histology. The construction of the special tubular structure of blood vessels is highly dependent on the construction of extracellular matrix (54); the blood vessel walls are arranged with highly organized collagen fibers (27) to maintain the elasticity of blood vessels. At the same time, the extracellular matrix constitutes the basement membrane of the capillaries (54). As we all know, extracellular matrix proteins are a type of typical secreted proteins, which are processed by the endoplasmic reticulum and Golgi apparatus, and finally reach the caveolae and other vesicle systems and are finally secreted outside the cell (55). In summary, the biological function of BCL9 relatively normal endothelial cell population is highly overlapped with the formation of extracellular matrix. However, in the endothelial cells and fibroblast populations whose BCL9 function is affected, that is to say, the endothelial cells and fibroblasts enriched in the samples treated with BCL9 KD and BCL9 inhibitors are not enriched with the formation of extracellular matrix. Instead, it is the enrichment of some related biological processes such as ribosomes, metabolism and cell chromosome formation. Instead, some ribosomes, metabolism, and cell chromosome formation are closely related to the cell cycle. Although the entire analysis process has been corrected for mitochondrial genes and cell cycle, these differences still exist in BCL9 KD and BCL9 cells and their corresponding control cells, which may imply that the mechanism of BCL9's effect on endothelial cell function may be related to the cell cycle. Our further enrichment analysis of these genes with Metascape also shows that cell cycle-related signaling pathways R-HSA-69278 from Reactome are among the best (43, 56), **Figure S5**.

Normal Endothelial Cells Two Kinds, Tumor Endothelial Cells One Kind

Summarizing the mathematical significance of our proposed BCL9-endo-Score (BCL9-endo-Score), it can be explained as the biggest difference in gene expression between loss-of-function endothelial cells and normal endothelial cells, but this difference does not only consider high expression and low expression

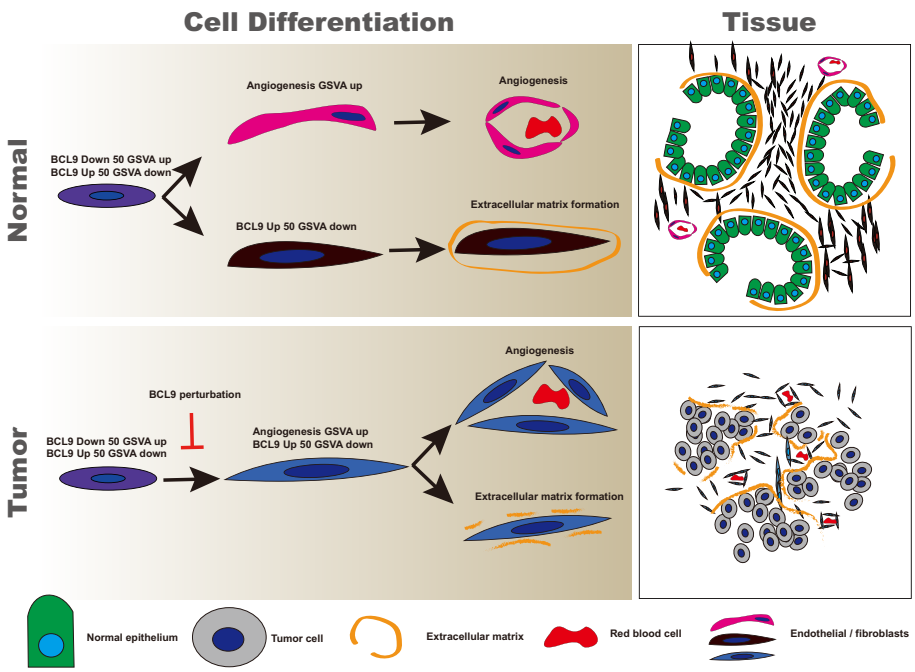

FIGURE 6 | Diagram of the development pattern of endothelium in normal and tumor tissues. It can be seen that fibroblasts and endothelial cells of normal endothelial cells differentiate along two different paths, and ultimately perform different functions. Supplementary File 1 Data of TCGA patients grouped by BCL9-endo-Score (traditional classification).

(**Figure 6**). And we further use the GSVA algorithm to introduce the generation of gene expression changes to cover the possibility of the opposite gene expression situation due to the complementation of functions in the occurrence of real signal pathways. In the virtual time analysis of the endothelial cell population, it can be seen that BCL9-endo-Score and the traditional signal pathway "angiogenesis" have a certain overlap in the development of tumor endothelial cells. However, in the normal endothelial cell population, BCL9-endo-Score is present in the endothelial cell population with an intermediate degree of differentiation, which is similar to the cell population between astrocytes and the most differentiated sinusoidal endothelial cells in the liver. With high scores, these cells also show high "angiogenesis" ability. In other words, most of the endothelial cells that function normally in tumors are endothelial cells similar to astrocytes in the liver. These endothelial cells may not have the ability to form normal blood vessels. This means that the cells with a higher BCL9-endo-Score may be the most primitive cells in the entire endothelial cell population. In normal tissues, they differentiate into cells capable of "angiogenesis" and incapable of vascularization. In tumors, cells differentiated from BCL9-endo-Score high-scoring cells all have the ability to angiogenesis. In other words, the enrichment of BCL9-endo-Score cells in the tumor may mean that the tumor's angiogenesis is hindered.

Relationship Between Clinical Output and Pathological Characteristics

In the TCGA database, we found that the high BCL9-endo-Score indicates a good prognosis in three cancers: COAD, CESC and OV. Angiogenesis inhibitory therapies have been extensively reported and reviewed in the treatment of COAD, CESC and OV, suggesting that tumorigenesis and development depend on angiogenesis. But because the HR we calculated is about 2, it is a medium level. The reason may be that the classification method that depends on the tumor site may not reflect the nature of the tumor cells. Therefore, this classification method based on the tumor site may be less helpful in predicting the prognosis of the tumor.

In the results of our cluster analysis based on TCGA, and then survival analysis based on different categories. We observed HRs with OS exceeding 3 and HRs with DSS exceeding 4, showing a high-risk ratio. In terms of tissue type, the 21 groups with the second highest HR, most of which are composed of three types of kidney cancer. Renal cell carcinoma (KICH, KIRC, KIRP), due to the large distribution of blood vessels in renal cell carcinoma, the important role of angiogenesis in renal cell carcinoma is not difficult to understand. However, the 29 groups with the highest HR consist of some of the BRCA and NHSC that are positive for the SCGB2A2, ADIPOQ gene. Among them, the SCGB2A2 gene is a milk-specific immunoglobulin, and ADIPOQ is the gene of adiponectin. Adiponectin in adults is negatively correlated with fat reserves. In other words, it may be correlated with thin body shape. Because BRCA belongs to the cancer of the glands in the connective tissue inside the skin, and the breast may require a large amount of material exchange when synthesizing and secreting milk, so that it is given to breast the potential of cells to regulate angiogenesis. While NHSC occurs in the skin, it is likely that a small part of it has some similarities with breast development, so it is classified into one category. These results need to be verified by histopathological methods in subsequent studies.

DATA AVAILABILITY STATEMENT

The datasets for this study can be found in the NCBI (Accession: PRJNA675146) and Figshare (https://figshare.com/s/edbc79f329291b06e976). The code involved is published on Github (https://github.com/weizhuang128/bcl9_endo).

AUTHOR CONTRIBUTIONS

ZWe analyzed the data, prepared the figures, and wrote the manuscript. WC prepared the figures and edited the manuscript. MF and SS prepared the samples. DZ conceptualized and wrote the manuscript. All authors contributed to the article and approved the submitted version.

FUNDING

The current study was supported by the Science and Technology Commission of Shanghai (18ZR1403900) (DZ), the National Natural Science Foundation of China (81872895) (DZ), and the project on joint translational research in Shanghai Institute of Materia Medica and Fudan University (FU-SIMM20181010) (DZ). Fudan School of Pharmacy and Pudong hospital Joint Research Fund (RHJJ2018-03 to TY and DZ), Shanghai Science and Technology Commission (18JC1413800 to BZ and DZ).

SUPPLEMENTARY MATERIAL

The Supplementary Material for this article can be found online at: https://www.frontiersin.org/articles/10.3389/fonc.2020.603702/full#supplementary-material

SUPPLEMENTARY FIGURE 1 | Heatmap of the eight clusters. Columns, individual cells; rows, genes (Top20).

SUPPLEMENTARY FIGURE 2 | The analysis process of re-clustering. **(A)** The UMAP plot of all cells shows the expression of marker gene in the endothelial cells and fibroblast populations; **(B)** the enlarged display of the local populations, the arrow shows the areas that are not merged; the re-clustering analysis of the endothelial cells and fibroblast populations, **(C) (D)** show UMAP and tSNE plots, sample type of origin (vehicle, hsBCL9CT-24, NT, BCL9-shRNA), **(E) (F)** shows the UMAP and tSNE plots of re-clustering analysis results of six different clusters. The dotted lines select clusters with similar topological relationships.

SUPPLEMENTARY FIGURE 3 | The trend of the gene expression generated by the BEAM function along pseudotime of endothelial cells and fibroblast populations.

SUPPLEMENTARY FIGURE 4 | The trend of the gene expression generated by the BEAM function along pseudotime of endothelial cell population from published dataset (GSM3714747).

SUPPLEMENTARY FIGURE 5 | Signal pathway enrichment analysis based on Metascape.

REFERENCES

1. Kalluri R, Zeisberg M. Fibroblasts in cancer. *Nat Rev Cancer* (2006) 6:392–401. doi: 10.1038/nrc1877
2. Maishi N, Hida K. Tumor endothelial cells accelerate tumor metastasis. *Cancer Sci* (2017) 108:1921–26. doi: 10.1111/cas.13336
3. Zhang L, Jambusaria A, Hong Z, Marsboom G, Toth PT, Herbert B-S, et al. SOX17 Regulates Conversion of Human Fibroblasts Into Endothelial Cells and Erythroblasts by Dedifferentiation Into CD34(+) Progenitor Cells. *Circulation* (2017) 135:2505–23. doi: 10.1161/CIRCULATIONAHA.116.025722
4. Reya T, Clevers H. Wnt signalling in stem cells and cancer. *Nature* (2005) 434:843–50. doi: 10.1038/nature03319
5. McCartney BM, Nathke IS. Cell regulation by the Apc protein Apc as master regulator of epithelia. *Curr Opin Cell Biol* (2008) 20:186–93. doi: 10.1016/j.ceb.2008.02.001
6. Komiya Y, Habas R. Wnt signal transduction pathways. *Organogenesis* (2008) 4:68–75. doi: 10.4161/org.4.2.5851
7. Holstein TW. The evolution of the Wnt pathway. *Cold Spring Harb Perspect Biol* (2012) 4:a007922. doi: 10.1101/cshperspect.a007922
8. MacDonald BT, Tamai K, He X. Wnt/beta-catenin signaling: components, mechanisms, and diseases. *Dev Cell* (2009) 17:9–26. doi: 10.1016/j.devcel.2009.06.016
9. Zeng X, Tamai K, Doble B, Li S, Huang H, Habas R, et al. A dual-kinase mechanism for Wnt co-receptor phosphorylation and activation. *Nature* (2005) 438:873–7. doi: 10.1038/nature04185
10. Clevers H. Wnt/beta-catenin signaling in development and disease. *Cell* (2006) 127:469–80. doi: 10.1016/j.cell.2006.10.018
11. Willert K, Jones KA. Wnt signaling: is the party in the nucleus? *Genes Dev* (2006) 20:1394–404. doi: 10.1101/gad.1424006
12. Mani M, Carrasco DE, Zhang Y, Takada K, Gatt ME, Dutta-Simmons J, et al. BCL9 promotes tumor progression by conferring enhanced proliferative, metastatic, and angiogenic properties to cancer cells. *Cancer Res* (2009) 69:7577–86. doi: 10.1158/0008-5472.CAN-09-0773
13. Hyeon J, Ahn S, Lee JJ, Song DH, Park C-K. Prognostic Significance of BCL9 Expression in Hepatocellular Carcinoma. *Korean J Pathol* (2013) 47:130–6. doi: 10.4132/KoreanJPathol.2013.47.2.130
14. Elsarraj HS, Hong Y, Valdez KE, Michaels W, Hook M, Smith WP, et al. Expression profiling of in vivo ductal carcinoma in situ progression models identified B cell lymphoma-9 as a molecular driver of breast cancer invasion. *Breast Cancer Res BCR* (2015) 17:128. doi: 10.1186/s13058-015-0630-z
15. Cancer Genome Atlas N. Comprehensive molecular characterization of human colon and rectal cancer. *Nature* (2012) 487:330–7. doi: 10.1038/nature11252
16. Kitaeva MN, Grogan L, Williams JP, Dimond E, Nakahara K, Hausner P, et al. Mutations in beta-catenin are uncommon in colorectal cancer occurring in occasional replication error-positive tumors. *Cancer Res* (1997) 57:4478–81.
17. Suraweera N, Robinson J, Volikos E, Guenther T, Talbot I, Tomlinson I, et al. Mutations within Wnt pathway genes in sporadic colorectal cancers and cell lines. *Int J Cancer* (2006) 119:1837–42. doi: 10.1002/ijc.22046
18. Markowitz SD, Bertagnolli MM. Molecular origins of cancer: Molecular basis of colorectal cancer. *N Engl J Med* (2009) 361:2449–60. doi: 10.1056/NEJMra0804588
19. Dow LE, O'Rourke KP, Simon J, Tschaharganeh DF, van Es JH, Clevers H, et al. Apc Restoration Promotes Cellular Differentiation and Reestablishes Crypt Homeostasis in Colorectal Cancer. *Cell* (2015) 161:1539–52. doi: 10.1016/j.cell.2015.05.033
20. Polakis P. The oncogenic activation of beta-catenin. *Curr Opin Genet Dev* (1999) 9:15–21. doi: 10.1016/S0959-437X(99)80003-3
21. Polakis P, Hart M, Rubinfeld B. Defects in the regulation of beta-catenin in colorectal cancer. *Adv Exp Med Biol* (1999) 470:23–32. doi: 10.1007/978-1-4615-4149-3_3
22. Baldus SE, Monig SP, Huxel S, Landsberg S, Hanisch FG, Engelmann K, et al. MUC1 and nuclear beta-catenin are coexpressed at the invasion front of colorectal carcinomas and are both correlated with tumor prognosis. *Clin Cancer Res* (2004) 10:2790–6. doi: 10.1158/1078-0432.CCR-03-0163
23. Sampietro J, Dahlberg CL, Cho US, Hinds TR, Kimelman D, Xu W. Crystal structure of a beta-catenin/BCL9/Tcf4 complex. *Mol Cell* (2006) 24:293–300. doi: 10.1016/j.molcel.2006.09.001
24. Feng M, Jin JQ, Xia L, Xiao T, Mei S, Wang X, et al. Pharmacological inhibition of ¦Â-catenin/BCL9 interaction overcomes resistance to immune checkpoint blockades by modulating T(reg) cells. *Sci Adv* (2019) 5:eaau5240. doi: 10.1126/sciadv.aau5240
25. Gay DM, Ridgway RA, Muller M, Hodder MC, Hedley A, Clark W, et al. Loss of BCL9/9l suppresses Wnt driven tumourigenesis in models that recapitulate human cancer. *Nat Commun* (2019) 10:723. doi: 10.1038/s41467-019-08586-3
26. Hida K, Hida Y, Amin DN, Flint AF, Panigrahy D, Morton CC, et al. Tumor-associated endothelial cells with cytogenetic abnormalities. *Cancer Res* (2004) 64:8249–55. doi: 10.1158/0008-5472.CAN-04-1567
27. Dudley AC. Tumor endothelial cells. *Cold Spring Harb Perspect Med* (2012) 2:a006536. doi: 10.1101/cshperspect.a006536
28. Pasquier J, Ghiabi P, Chouchane L, Razzouk K, Rafii S, Rafii A. Angiocrine endothelium: from physiology to cancer. *J Trans Med* (2020) 18:52. doi: 10.1186/s12967-020-02244-9
29. Schaaf MB, Garg AD, Agostinis P. Defining the role of the tumor vasculature in antitumor immunity and immunotherapy. *Cell Death Dis* (2018) 9:115. doi: 10.1038/s41419-017-0061-0
30. Taguchi K, Onoe T, Yoshida T, Yamashita Y, Tanaka Y, Ohdan H. Tumor Endothelial Cell-Mediated Antigen-Specific T-cell Suppression via the PD-1/PD-L1 Pathway. *Mol Cancer Res* (2020) 18:1427–40. doi: 10.1158/1541-7786.MCR-19-0897
31. Hida K, Ohga N, Akiyama K, Maishi N, Hida Y. Heterogeneity of tumor endothelial cells. *Cancer Sci* (2013) 104:1391–5. doi: 10.1111/cas.12251
32. Yadav A, Kumar B, Yu J-G, Old M, Teknos TN, Kumar P. Tumor-Associated Endothelial Cells Promote Tumor Metastasis by Chaperoning Circulating Tumor Cells and Protecting Them from Anoikis. *PLoS One* (2015) 10:e0141602–e02. doi: 10.1371/journal.pone.0141602
33. DeClerck YA, Mercurio AM, Stack MS, Chapman HA, Zutter MM, Muschel RJ, et al. Proteases, extracellular matrix, and cancer: a workshop of the path B study section. *Am J Pathol* (2004) 164:1131–39. doi: 10.1016/S0002-9440(10)63200-2
34. Routledge D, Scholpp S. Mechanisms of intercellular Wnt transport. *Dev (Cambridge England)* (2019) 146:1–12. doi: 10.1242/dev.176073
35. Steinhart Z, Angers S. Wnt signaling in development and tissue homeostasis. *Dev (Cambridge England)* (2018) 145:1–8. doi: 10.1242/dev.146589
36. Butler A, Hoffman P, Smibert P, Papalexi E, Satija R. Integrating single-cell transcriptomic data across different conditions, technologies, and species. *Nat Biotechnol* (2018) 36:411–20. doi: 10.1038/nbt.4096
37. Stuart T, Butler A, Hoffman P, Hafemeister C, Papalexi E, Mauck WMR, et al. Comprehensive Integration of Single-Cell Data. *Cell* (2019) 177:1888–902.e21. doi: 10.1016/j.cell.2019.05.031
38. Trapnell C, Cacchiarelli D, Grimsby J, Pokharel P, Li S, Morse M, et al. The dynamics and regulators of cell fate decisions are revealed by pseudotemporal ordering of single cells. *Nat Biotechnol* (2014) 32:381–86. doi: 10.1038/nbt.2859
39. Qiu X, Hill A, Packer J, Lin D, Ma Y-A, Trapnell C. Single-cell mRNA quantification and differential analysis with Census. *Nat Methods* (2017) 14:309–15. doi: 10.1038/nmeth.4150
40. Qiu X, Mao Q, Tang Y, Wang L, Chawla R, Pliner HA, et al. Reversed graph embedding resolves complex single-cell trajectories. *Nat Methods* (2017) 14:979–82. doi: 10.1038/nmeth.4402
41. Mootha VK, Lindgren CM, Eriksson K-F, Subramanian A, Sihag S, Lehar J, et al. PGC-1alpha-responsive genes involved in oxidative phosphorylation are coordinately downregulated in human diabetes. *Nat Genet* (2003) 34:267–73. doi: 10.1038/ng1180
42. Subramanian A, Tamayo P, Mootha VK, Mukherjee S, Ebert BL, Gillette MA, et al. Gene set enrichment analysis: a knowledge-based approach for interpreting genome-wide expression profiles. *Proc Natl Acad Sci U S A* (2005) 102:15545–50. doi: 10.1073/pnas.0506580102
43. Zhou YY, Zhou B, Pache L, Chang M, Khodabakhshi AH, Tanaseichuk O, et al. Metascape provides a biologist-oriented resource for the analysis of systems-level datasets. *Nat Commun* (2019) 10:1–13. doi: 10.1038/s41467-019-09234-6. doi: ARTN 1523.
44. Xiong X, Kuang H, Ansari S, Liu T, Gong J, Wang S, et al. Landscape of Intercellular Crosstalk in Healthy and NASH Liver Revealed by Single-Cell Secretome Gene Analysis. *Mol Cell* (2019) 75:644–60.e5. doi: 10.1016/j.molcel.2019.07.028

45. Sturtzel C. Endothelial Cells. *Adv Exp Med Biol* (2017) 1003:71–91. doi: 10.1007/978-3-319-57613-8_4
46. Hida K, Maishi N, Annan DA, Hida Y. Contribution of Tumor Endothelial Cells in Cancer Progression. *Int J Mol Sci* (2018) 19:1–12. doi: 10.3390/ijms19051272
47. Kendal AR, Layton T, Al-Mossawi H, Appleton L, Dakin S, Brown R, et al. Multi-omic single cell analysis resolves novel stromal cell populations in healthy and diseased human tendon. *Sci Rep* (2020) 10:13939. doi: 10.1038/s41598-020-70786-5
48. Davies BSJ, Goulbourne CN, Barnes RHN, Turlo KA, Gin P, Vaughan S, et al. Assessing mechanisms of GPIHBP1 and lipoprotein lipase movement across endothelial cells. *J Lipid Res* (2012) 53:2690–7. doi: 10.1194/jlr.M031559
49. Fitch MJ, Campagnolo L, Kuhnert F, Stuhlmann H. Egfl7, a novel epidermal growth factor-domain gene expressed in endothelial cells. *Dev Dynamics an Off Publ Am Assoc Anatomists* (2004) 230:316–24. doi: 10.1002/dvdy.20063
50. Guo L, Zhang H, Hou Y, Wei T, Liu J. Plasmalemma vesicle-associated protein: A crucial component of vascular homeostasis. *Exp Ther Medicine* (2016) 12:1639–44. doi: 10.3892/etm.2016.3557
51. Xie T, Wang Y, Deng N, Huang G, Taghavifar F, Geng Y, et al. Single-Cell Deconvolution of Fibroblast Heterogeneity in Mouse Pulmonary Fibrosis. *Cell Rep* (2018) 22:3625–40. doi: 10.1016/j.celrep.2018.03.010
52. Regn M, Laggerbauer B, Jentzsch C, Ramanujam D, Ahles A, Sichler S, et al. Peptidase inhibitor 16 is a membrane-tethered regulator of chemerin processing in the myocardium. *J Mol Cell Cardiol* (2016) 99:57–64. doi: 10.1016/j.yjmcc.2016.08.010
53. Kao S-H, Wu K-J, Lee W-H. Hypoxia, Epithelial-Mesenchymal Transition, and TET-Mediated Epigenetic Changes. *J Clin Medicine* (2016) 5:24. doi: 10.3390/jcm5020024
54. Eble JA, Niland S. The extracellular matrix of blood vessels. *Curr Pharm Design* (2009) 15:1385–400. doi: 10.2174/138161209787846757
55. Mouw JK, Ou G, Weaver VM. Extracellular matrix assembly: a multiscale deconstruction. *Nat Rev Mol Cell Biol* (2014) 15:771–85. doi: 10.1038/nrm3902
56. Fabregat A, Sidiropoulos K, Viteri G, Forner O, Marin-Garcia P, Arnau V, et al. Reactome pathway analysis: a high-performance in-memory approach. *BMC Bioinf* (2017) 18:1–9. doi: 10.1186/s12859-017-1559-2. doi: ARTN 142.

Conflict of Interest: The authors declare that the research was conducted in the absence of any commercial or financial relationships that could be construed as a potential conflict of interest.

frontiers in Oncology

ORIGINAL RESEARCH
published: 21 January 2021
doi: 10.3389/fonc.2020.605877

Long Non-Coding RNA PCAT6 Induces M2 Polarization of Macrophages in Cholangiocarcinoma *via* Modulating miR-326 and RhoA-ROCK Signaling Pathway

Jianfei Tu[1,2†], *Fazong Wu*[1,2†], *Li Chen*[1,2], *Liyun Zheng*[1,2], *Yang Yang*[1,2], *Xihui Ying*[1,2], *Jingjing Song*[1,2], *Chunmiao Chen*[1], *Xianghua Hu*[1], *Zhongwei Zhao*[1,2*] *and Jiansong Ji*[1,2*]

[1] *Key Laboratory of Imaging Diagnosis and Minimally Invasive Intervention Research, the Fifth Affiliated Hospital of Wenzhou Medical University/Affiliated Lishui Hospital of Zhejiang University/Clinical College of The Affiliated Central Hospital of Lishui University, Lishui, China,* [2] *Department of Interventional Diagnosis and Treatment, The Central Hospital of Zhejiang Lishui, Lishui, China*

OPEN ACCESS

Edited by:
Xiaochen Wang, University of Texas Southwestern Medical Center, United States

Reviewed by:
Pan Jiang, Fudan University, China
Shushan Yan, Weifang Medical University, China

***Correspondence:**
Jiansong Ji
jijiansong@zju.edu.cn
Zhongwei Zhao
zhaozw79@163.com

[†]*These authors have contributed equally to this work*

Specialty section:
This article was submitted to Cancer Genetics, a section of the journal Frontiers in Oncology

Received: *13 September 2020*
Accepted: *30 November 2020*
Published: *21 January 2021*

Citation:
Tu J, Wu F, Chen L, Zheng L, Yang Y, Ying X, Song J, Chen C, Hu X, Zhao Z and Ji J (2021) Long Non-Coding RNA PCAT6 Induces M2 Polarization of Macrophages in Cholangiocarcinoma via Modulating miR-326 and RhoA-ROCK Signaling Pathway. Front. Oncol. 10:605877. doi: 10.3389/fonc.2020.605877

LncRNAs can act crucial roles in multiple tumors including cholangiocarcinoma (CCA). M2 polarization of macrophages is crucial for their biological roles in immunologic tolerance, which is able to induce tumorigenesis. Given that increasing evidence have suggested that lncRNAs could participate in modulating immune cell differentiation and function. Our current study was aimed to identify the underlying mechanism of lncRNA prostate cancer-associated transcript 6 (PCAT6) in CCA progression *via* regulating M2 macrophage polarization. PCAT6 has been reported as an oncogene in many cancers. In our work, we observed increased expression of PCAT6 in CCA patients. PCAT6 expression in various types of immune cells derived from CCA patients was tested by quantitative real-time PCR (qRT-PCR). It was revealed that PCAT6 was highly expressed in macrophages, which indicated that PCAT6 might regulate the function of macrophages to promote CCA progression. Then, *via* establishing CCA xenograft mouse model, we found loss of PCAT6 obviously triggered the immune response and reduced the *in vivo* tumor growth. In addition, overexpression of PCAT6 led to the M2 polarization of THP-1-differentiated macrophages. Moreover, miR-326 was predicted and proved as a target for PCAT6. In addition, down-regulation of PCAT6 repressed M2 polarization of macrophages, which was reversed by miR-326 inhibitors. The increase of PCAT6 induced the accumulation of ROS, mitochondrial and metabolic dysfunction in macrophages and mimics of miR-326 exhibited an opposite process. RohA has been recognized as a significant regulator of immune cell function. In our current work, we observed that RohA function as a downstream target for miR-326. In conclusion, our study highlighted a significant role of PCAT6/miR-326/RohA in immune response of macrophages in CCA and indicated PCAT6 as a potential target of immunotherapy in CCA.

Keywords: cholangiocarcinoma, PCAT6, miR-326, RhoA, macrophages, immune response

INTRODUCTION

Cholangiocarcinoma (CCA) is a frequent tumor of extrahepatic bile duct, which can extend from hilar area to bile duct (1). The etiology of CCA is related with cholelithiasis, sclerosing cholangitis and some other diseases (2). Although surgery, radiotherapy and chemotherapy have been widely be employed, the prognosis of CCA still remains poor (3, 4). Therefore, it is significant to explore effective therapies for diagnosis and treatment of CCA.

Tumor-associated macrophages are important immune cells within tumor micro-environment. They are closely associated with tumor angiogenesis and contributes to the worse prognosis (5). Tumor-associated macrophages are polarized into two phenotypes including M1 and M2 (6, 7). M1 polarized macrophages can secrete pro-inflammatory cytokines to remove tumor cells, while M2 polarized macrophages secrete anti-inflammation cytokines (8). Moreover, tumor-associated macrophages are considered to be the polarized M2 phenotype to trigger tumor progression (9).

LncRNAs are transcripts with over 200 bps with a limited protein-coding capacity (10). Increasing studies report lncRNAs are involved in various biological processes (11, 12). LncRNAs have recently drawn increasing attention because they can function as a ceRNA to hinder miRNA functions in tumors, including CCA (13). Furthermore, dozens of lncRNAs have been reported to participate in regulating macrophage polarization. For instance, lncRNA RPPH1 can induce colorectal cancer progression by interacting with TUBB3 to induce macrophage M2 polarization (14). XIST contributes to M2 polarization of macrophages in lung cancer (15). LncRNA PCAT6 has been reported to enhance CCA development by modulating miR-330-5p (16). However, the effect of PCAT6 on macrophage M2 polarization in CCA progression remains poorly known.

In our current work, we found that PCAT6 was increased in CCA patients and in macrophages derived from CCA patients. *Via* using orthotopic CCA mouse model, it was shown loss of PCAT6 repressed the immune response. This indicated PCAT6 may be involved in the immune tolerance of CCA. Subsequently, these data motivated us to investigate the function of PCAT6 in CCA *via* modulating macrophages.

METHODS AND MATERIALS

Clinical Samples

Fresh CCA specimens and para-tumor tissues were collected from patients undergoing surgery in Affiliated Lishui Hospital of Zhejiang University. The histopathologic diagnosis was carried out by the pathologists based on WHO criteria. Peripheral whole blood of CCA patients were maintained in EDTA tubes before surgery. Our study was approved by the Institutional Ethics Committee of Affiliated Lishui Hospital of Zhejiang University. All the participants signed the written informed consent.

Cell Culture

HuCCT1 and THP-1 cells were purchased from the Institute of Biochemistry and Cell Biology, Chinese Academy of Sciences (Shanghai, China). DMEM medium (HyClone Laboratories, Logan, UT, USA) with 10% FBS, 100 U/ml penicillin, and 100 μg/ml streptomycin was used to culture the cells. Cells were maintained at 37°C in a humidified incubator with 5% CO_2. THP-1 cells were seeded and exposed to 320 nM PMA for 48 h to obtain macrophage-like differentiated THP-1 cells. Cells were cultured with 100 ng/ml IFN-γ for 48 h to generate M1 macrophages, while 20 ng/ml IL-4 was used to induce M2 macrophages. Peripheral blood mononuclear cells (PBMCs) were isolated from fresh blood samples of CCA patients by centrifugation over a Ficoll-Triyosom layer (Lymphoprep, Nycomed Pharma, Oslo, Norway), washed twice with saline and resuspended using complete medium (RPMI 1640 supplemented with 10% FBS, 100 U/ml penicillin, and 100 μg/ml streptomycin.

Plasmid Construction and Lentivirus Infection

To over-express PCAT6, the ORF sequence of PCAT6 was cloned into pTracer-CMV2 vector (Jingmai BioTech, Chengdu, China). Then, cells were transfected using 2 μg PCAT6-OE or empty control vector using Lipofectamine 3000. To knockdown PCAT6, small hairpin sequence was cloned into pLKO.1 plasmid. PSPAX2-PMD2G system was used to package the lentivirus.

Western Blotting Analysis

Cells were lysed using the RIPA buffer and protein concentration was tested using BCA protein assay kit. The proteins were separated by 10% sodium dodecyl sulfate polyacrylamide gel electrophoresis (SDS-PAGE) gel electrophoresis and then transferred onto a nitrocellulose membrane (Milipore, Billerica, MA, USA). After blocked using BSA, the membranes were incubated with primary antibodies against RohA, ROCK1, ROCK2, and GAPDH (Cambridge, MA, USA). The bands were indicated with goat anti-rabbit IgG-HRP secondary antibody (1:2,000; Abcam Cambridge, MA, USA) and were exposed using chemiluminescence substance (Thermo Fisher Scientific, Waltham, MA, USA).

ELISA Assay

ELISA kits for the detection of IL-10, IL-6, IL-1β, IL-12, CD163, and Arg-1 levels were obtained from R&D systems (Minneapolis, MN, USA). The assay was carried out with all samples, standards, and controls assayed in duplicate. Subsequently, the absorbance was recorded using BioTek ELx800 (Thermo Fisher Scientific, Waltham, MA, USA).

Immunofluorescence

Briefly, cells were seeded on the slides and fixed in 4% paraformaldehyde. Cells were permeabilized with PBS containing 0.1% Triton X-100. To block the samples, PBS containing 3% BSA was applied for 1 h. Then, the slides were incubated with prehybridization buffer at 40°C for 4 h and hybridized with digoxin-labeled probe for a whole night. Afterward, the slides were indicated with biotin conjugated

anti-digoxin antibody. The samples were photographed using Zeiss Axio Imager Z1 fluorescence microscope.

Immunochemistry

Tissue samples from the mice were fixed in 4% paraformaldehyde for a whole night. After dehydration and embedding, the samples were sliced into 5–8 μm thickness. The slices were stained with Ki-67 antibody overnight and with biotinylated secondary antibody. The sections were applied with DAB substrate and observed using microscopy (Zeiss, German).

Flow Cytometry

To assess ROS levels in cells, 10μM DHE was added to the cells to carry out flow cytometry analysis. In order to test the uptake ability of glucose, 500μM 2-NBDG was added for 4 h. To evaluate the frequencies of IFN-γ+ in CD4+ or CD8+ T cells, the suspension tumor cells were stained using IFN-γ antibody (Abcam, followed by staining with fluorophore-conjugated secondary antibodies), and CD4 or CD8 antibody (eBioscience, San Diego, CA, USA). To assess the polarization of macrophages, 3×10^5 cells were stained using CD11c, F4/80, CD11b, or CD206 antibodies (eBioscience, San Diego, CA, USA).

Luciferase Reporter Assay

The sequence of WT of RohA and PCAT6 mRNA 3′-UTR and sequence of MUT after site-directed mutation of WT target site were synthesized. pGL3-RB-REPORT™ plasmid (RiboBio, Guangzhou, China) was digested by restriction endonuclease. Then the synthetic target gene fragments WT and MUT were inserted into pGL3-RB-REPORT™ vector. The vectors of MUT and WT were co-transferred to the cells with mimic-NC or miR-326 mimic. Luciferase Detection Kit (Beyotime, Shanghai, China) was used to determine the relative lights units.

RNA Immunoprecipitation Assay

RIP was conducted using a Magna RIP RNA-Binding Protein Immunoprecipitation Kit (Millipore, Bedford, MA). Briefly, cell lysates were indicated with magnetic beads conjugated with negative control normal mouse IgG or human anti-Ago2 antibody (Millipore, Bedford, MA). Then, the immunoprecipitated RNAs were extracted and detected by qRT-PCR to confirm the enrichment of binding targets.

Tumor Xenografts

Naïve CD8 + T cells from peripheral blood mononuclear cells (PBMCs) were isolated and then were purified. CCA-specific CD8 + T cells were stimulated using 1 mg/mL CD3 mAb, 5 mg/ml CD28 mAb, 20 ng/mL human rIL-2, 50 U/mL penicillin and 50 mg/Ml streptomycin. These naïve CD8 + T cells were then infected with shRNA of PCAT6 or LV-NC. Dendritic cells were differentiated from adherent monocytes in RPMI 1640 medium with IL-4 and GM-CSF. The obtained DCs were incubated using heat-shocked HuCCT1 cells to get antigen-loaded DCs (APCs). To obtain tumor antigen-specific CD8 + T cells, these treated naïve T cells were incubated with APCs for 3 days. 12 female BALB/c nude mice aged 4-6 weeks were obtained from the Animal research center of Chinese Academy of Sciences (Shanghai, China). Mice were then housed in specific pathogen-free units. 5×10^6 HuCCT1 cells were mixed with Matrigel and subcutaneously injected in the right groin of the mice. To reconstitute human immune system, APC-stimulated naïve CD8 + T cells (pretreated with LV-shPCAT6 or LV-NC) were injected into the caudalmvein. One week later, the tumor weight of tumor blocks was measured using a vernier caliper and measurement was conducted every 3 days. All mice were sacrificed 22d after the surgery by cervical dislocation and the transplantation tumor was collected. All animal experiments were based on the Guide for the Care and Use of Laboratory Animals of the National Institutes of Health.

qRT-PCR

RNA was extracted from CCA cells and tumor samples by TRIzol reagent (Thermo Fisher Scientific, Waltham, MA, USA) and RNeasy Plus Micro Kit (QIAGEN, Germantown, MD, USA). Reverse transcription was carried out to synthesize the Bestar qPCR RT Kit (DBI Bioscience, Shanghai, China). Quantitative RT-PCR was carried out in Applied Biosystems 7900 Real Time PCR System (Applied Biosystems, Foster City, CA, USA). Twenty nanograms of template in 25-μl reaction volume with

TABLE 1 | Primers for real-time PCR.

Genes	Forward (5'-3')	Reverse (5'-3')
GAPDH	AGAAGGCTGGGGCTCATTTG	AGGGGCCATCCACAGTCTTC
PCAT6	CCCCTCCTTACTCTTGGACAAC	GACCGAATGAGGATGGAGACAC
miR-326	CATCTGTCTGTTGGGCTGGA	AGGAAGGGCCCAGAGGCG
RohA	GAGCCGGTGAAACCTGAAGA	TTCCCACGTCTAGCTTGCAG
U6	CTCGCTTCGGCAGCACA	AACGCTTCACGAATTTGCGT
ROCK1	AAAAATGGACAACCTGCTGC	GGCAGGAAAATCCAAATCAT
ROCK2	CGCTGATCCGAGACCCT	TTGTTTTTCCTCAAAGCAGGA
GLUT1	CAATGCTGATGATGAACCTG	GGGATGAAGATGATGCTCA
GLUT3	ATGGGGACACAGAAGGTCACC	AGCCACCAGTGACAGCCAAC
IL-6	GACTGATGTTGTTGACAGCCACTGC	AGCCACTCCTTCTGTGACTCTAACT
IL-1β	TCATGGGATGATGATGATAACCTGCT	CCCATACTTTAGGAAGACAGGGATTT
IL-12	CCACTCACATCTGCTGCTCAACAAG	ACTTCTCATAGTCCCTTTGGTCCAG
CD163	AGCAGACTACTCCAACATCC	TGGCACAGTTGTCTCTATCC
IL-10	GCCACCCTGATGTCTCAGTT	GTGGAGCAGGTGAAGAATGC
Arg-1	TGGA CAGACTAGGAATTGGCA	CCAGTCCGTCAACATCAAAACT

2×Power SYBR® Green PCR Master Mix (Thermo Fisher Scientific, Waltham, MA, USA). The gene expression level for miR-326 was normalized to U6 RNA and mRNA expression was normalized to GAPDH expression using the comparative Ct method. Related primer sequences were provided in **Table 1**.

Assessment of ATP Concentration and Oxygen Uptake Rates

Cellular ATP concentration was tested using the ATP detection kit (Beyotime, Shanghai, China). To measure oxygen uptake rates, MitoXpress Intra Kit (Luxcel Biosciences) was carried out.

Statistical Analysis

Data was analyzed with Prism 6.0. Experiments were carried out in triplicates and the data was expressed as the means ± SD. One-way analysis of variance with multiple comparisons using Dunnett's test was carried out for multiple comparison. p less than 0.05 was considered to be statistically significant.

RESULTS

Expression of PCAT6 Was Significantly Increased in Cholangiocarcinoma Patients

Firstly, to study the relationship between PCAT6 expression and the development of CCA, relative PCAT6 expression levels were obtained compared with non-tumor tissues (**Figure 1A**, n = 20 pairs). We observed that PCAT6 expression was highly increased in CCA tissues compared to the non-tumorous tissues. Further, we explored whether the high expression of PCAT6 participated in the immune response. It was shown that PCAT6 expression level was obviously expressed in the patient-derived in T cells, B cell, macrophages, dendritic cells, neutrophils (**Figure 1B**). The expression of PCAT6 was relatively higher in macrophages. Then, to confirm the expression of PCAT6 in tumor-associated immune cells, immunofluorescence analysis was carried out and we found that PCAT6 expression in CD11b+ cells within tumor tissues was greatly higher (**Figure 1C**). These findings suggested PCAT6 was relatively associated with tumor-associated macrophages in CCA.

Loss of PCAT6 Inhibited the Progression of Cholangiocarcinoma via Activating T Cell Response *In Vivo*

Next, to further explore the role of PCAT6 in immune cells in the tumorigenesis of CCA, HuCCT1 cells were subcutaneously injected in the right groin of the nude mice. LV-shPCAT6 or LV-NC infected naïve CD8 + T cells, which were incubated with CCA antigen-loaded DCs were transferred into these CCA tumor-bearing nude mice. The efficiency of PCAT6 shRNA was confirmed as displayed in **Figure 2A**. Then, the mice were injected by the cells subcutaneously. In **Figures 2B–D**, it was indicated that the growth of the tumors in PCAT6-shRNA group was inhibited than the control mice. Then, mice were sacrificed to study the phenotypes within tumor microenvironment. As shown in **Figure 2E**, the data displayed CD3+ cells in PCAT6-down-regulated mice tissues were significantly larger than the control mice. For another, it was implied that the percentage of IFN-γ-producing CD4+ and CD8+ cells in the tumors of

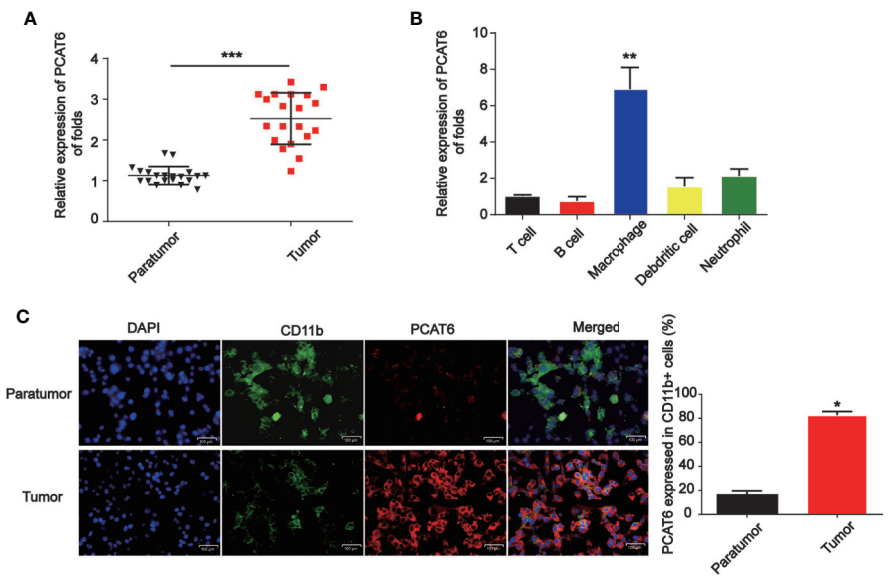

FIGURE 1 | PCAT6 was elevated in cholangiocarcinoma (CCA) patients. **(A)** mRNA expression of PCAT6 in the tumor tissues of CCA patients (n=20) and the healthy tissues (n=20) were compared. **(B)** The expression of PCAT6 in patient-derived immune cells was assessed using qRT-PCR analysis. **(C)** The tissue sections of the paratumors and tumors from CCA patients were analyzed by IFSH. Scale bar, 100 μm. *P < 0.05; **P < 0.01; ***P < 0.001. Compared with the control group.

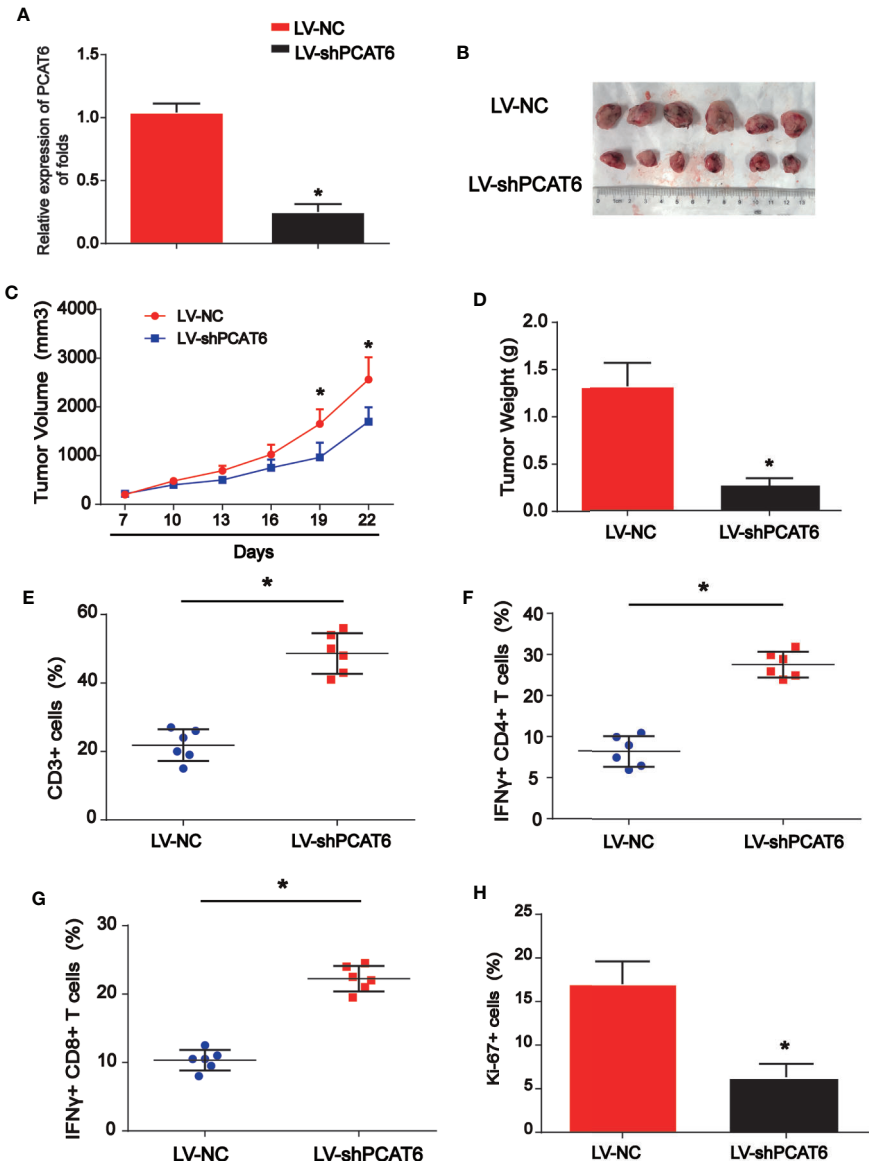

FIGURE 2 | The down-regulation of PCAT6s activated the immune response *in vivo*. **(A)** The efficiency PCAT6 short hairpin RNA (shRNA) was confirmed using qRT-PCR analysis. **(B)** Nude mice with or without PCAT6 shRNA infected naïve CD8 + T cells incubated with CCA antigen-loaded DCs were injected with HuCCT1 cells. **(C)** Tumor growth curve. **(D)** Tumor weight. **(E)** Tumor sections were analyzed by IHC using CD3 antibody. **(F, G)** The frequencies of IFN-γ-producing CD4+ or CD8 + T cells in tumors of both groups were determined by flow cytometry analysis. **(H)** The tumor sections were analyzed by immunohistochemistry. *P < 0.05. Compared with the control group.

PCAT6-down-regulated mice were significantly increased than the control mice (**Figures 2F, G**). In addition, immunochemistry analysis indicated that Ki-67+ cells in PCAT6 shRNA mice were significantly inhibited than the control mice (**Figure 2H**). These manifested the decrease of PCAT6 could enhance the T cell response *in vivo*.**Increase** in **PCAT6 Led to M2 Polarization of Macrophages**

To figure out the potential role of PCAT6, M1, and M2 macrophages were induced in THP-1-diferentiated macrophages. As indicated by the qRT-PCR data in **Figure 3A**, M1 and M2 polarized macrophages were triggered *in vitro* successfully. Next, we tested the mRNA expression level of PCAT6 in M1 and M2 cells. In **Figure 3B**, PCAT6 expression in M2 macrophages was obviously up-regulated than that of M1 macrophages. Then, THP-1-diferentiated macrophages were transfected with PCAT6-OE or the vector. In **Figure 3C**, PCAT6 was successfully induced by PCAT6-OE. Then, we observed that the expression of CD206 (M2 marker) in

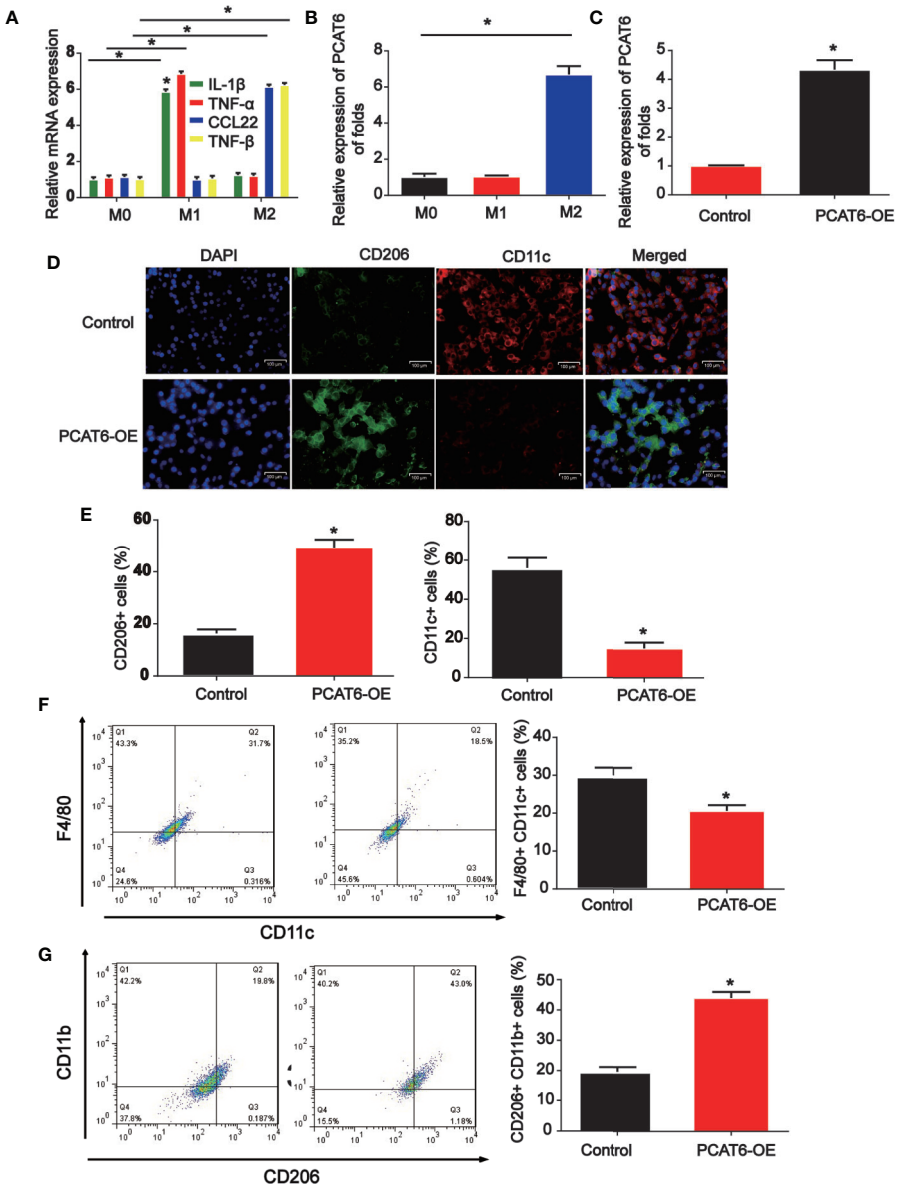

FIGURE 3 | The effect of PCAT short hairpin RNA (shRNA) on M2-like polarization of macrophages. **(A)** Levels of M1 and M2-associated makers were determined in THP-1-diferentiated macrophages. **(B)** RNA was extracted from M1 and M2 and levels of lncRNA PCAT6 was determined using RT-qPCR in THP-1-diferentiated macrophages. **(C)** The efficiency PCAT6-OE was confirmed using qRT-PCR analysis. **(D, E)** Control and PCAT6-overexpressed macrophages were analyzed by immunofluorescence with CD206 and CD11c antibodies. Scale bar, 100 μm. **(F)** The control and PCAT6-overexpressed macrophages were analyzed by flow cytometry with M1 markers (CD11c and F4/80). **(G)** The control and PCAT6-overexpressed macrophages were analyzed with M2 markers (CD206 and CD11b). *$P < 0.05$. Compared with the control group.

PCAT6-OE THP-1-differentiated macrophages. Cells were significantly up-regulated, whereas the expression of CD11c (M1 maker) was down-regulated (**Figures 3D, E**). It was presented that the ratio of F4/80+/CD11c cells were lower in the PCAT6-OE-transfected THP-1-differentiated macrophages in **Figure 3F**. The ratio of CD11b+/CD206+ cells in the PCAT6-OE-transfected THP-1-diferentiated macrophages was significantly induced as shown in **Figure 3G**.

The Interaction Between PCAT6 and miR-326 in Macrophages

Online bioinformatics analysis STARBASE 2.0 (http://starbase.sysu.edu.cn/) was used and we predicted the miR-326 acted as a potential miRNA interacting with PCAT6 (**Figure 4A**). In addition, luciferase reporter vectors containing PCAT6-WT or PCAT6-MUT were constructed and co-transfected with miR-326 mimics or miR-NC into THP-1-differentiated macrophages.

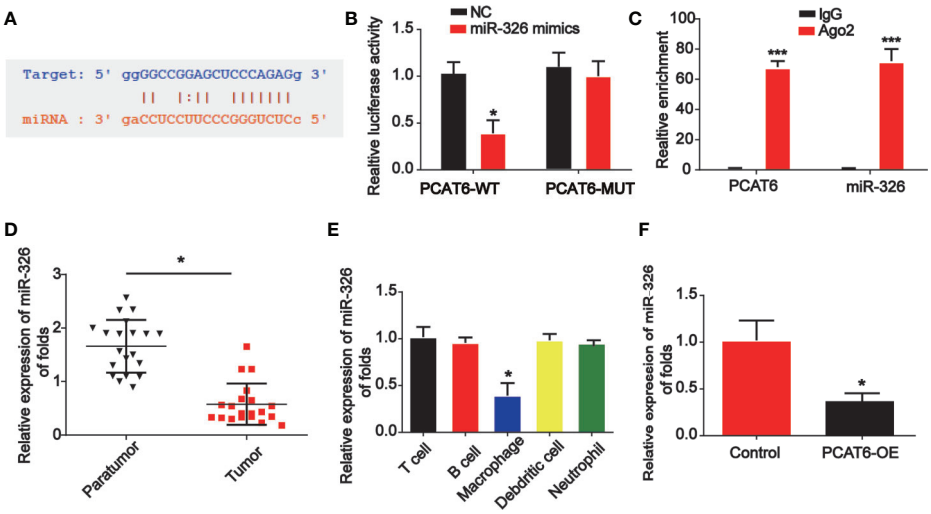

FIGURE 4 | PCAT6 sponged miR-326. **(A)** The putative binding sites between PCAT6 and miR-326. **(B)** Luciferase activity was evaluated in macrophages co-transfected with PCAT6-WT or PCAT6-MUT reporter and miR-326 mimics in THP-1-differentiated macrophages. **(C)** RIP assays were performed using anti-Ago2 and IgG antibodies with extractions from THP-1-differentiated macrophages. **(D)** The expression of miR-326 in the tumor tissues of cholangiocarcinoma (CCA) patients. **(E)** The expression of miR-326 in different types of patient-derived immune cells was assessed using qRT-PCR analysis. **(F)** The expression of miR-326 in macrophages transfected with PCAT6 overexpression plasmid. *P < 0.05. Compared with the control group.

In **Figure 4B**, miR-326 repressed the luciferase activity of PCAT6-WT. In addition, RIP assays were applied in THP-1-differentiated macrophages. PCAT6 and miR-326 were obviously enriched by the anti-Ago2 antibody compared with the IgG antibody (**Figure 4C**). miR-326 expression level was reduced in CCA tissues (**Figure 4D**). Additionally, we found that PCAT6 expression level was obviously decreased in macrophages as indicated in **Figure 4E**. Overexpression of PCAT6 was able to reduce miR-326 expression *in vitro* significantly (**Figure 4F**).

Loss of miR-326 Resulted in M2 Polarization of Macrophages

Then, THP-1-diferentiated macrophages were infected with PCAT6 shRNA and miR-326 inhibitors to assess the effect of

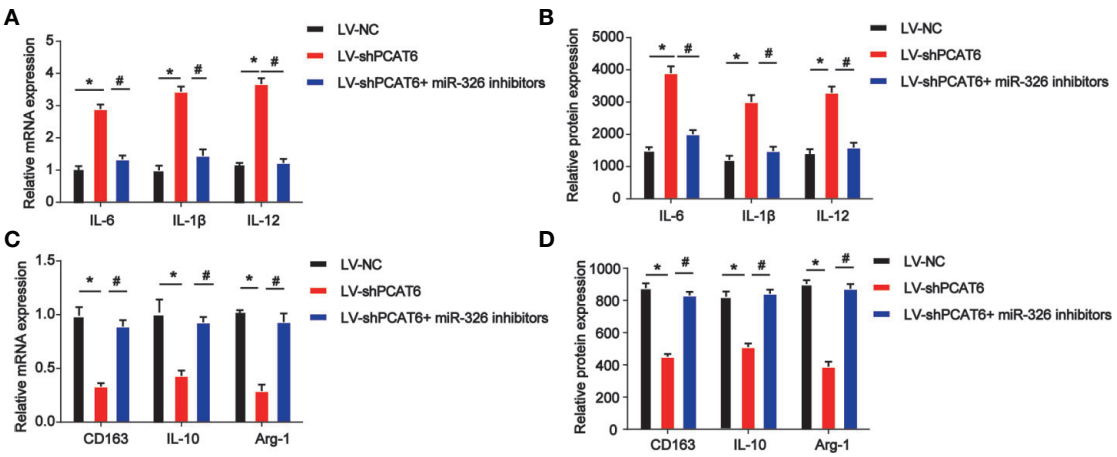

FIGURE 5 | Effects of miR-326 on M2-like polarization of macrophages. THP-1-diferentiated macrophages were infected with PCAT6 short hairpin RNA (shRNA) and miR-326 inhibitors. **(A)** The messenger RNA (mRNA) expression levels of IL-6, IL-1β, and IL-12 were determined by qRT-PCR in THP-1-differentiated macrophages. **(B)** The protein expression levels of IL-6, IL-1β, and IL-12 were determined by ELISA assay in THP-1-differentiated macrophages. **(C)** The mRNA expression levels of IL-10, CD163 and Arg-1 were determined by qRT-PCR in macrophages. **(D)** The protein expression levels of IL-10, CD163, and Arg-1 in THP-1-diferentiated macrophages. *P < 0.05. Compared with the control group. #P < 0.05. Compared with the LV-shPCAT6 group.

miR-326 on M2 polarization of macrophages. In **Figures 5A, B**, the expression of three M1 macrophages specific marker genes, IL-6, IL-1β, and IL-12 were detected. mRNA and protein expression of IL-6, IL-1β, and IL-12 were increased by loss of PCAT6, which was reversed by the inhibitors of miR-326 (**Figures 5A, B**). Further, mRNA and protein expression levels of M2 marker, CD163, IL-10, and Arg-1 were found to be reduced by PCAT6 shRNA and miR-326 inhibitors enhanced their expression *in vitro* (**Figures 5C, D**).

The Increase of PCAT6 Promoted Cellular Reactive Oxygen Species Production, Mitochondrial and Metabolic Dysfunction in Macrophages

Moreover, to determine the role of PCAT6 and miR-326 in the ROS production in macrophages, the PCAT6-upregulated THP-1-diferentiated macrophages was constructed and we examined ROS levels with DCF-DA and mitoSOX probes. PCAT6-upregulated THP-1-diferentiated macrophages exhibited a higher ability of probe combination when compared with the

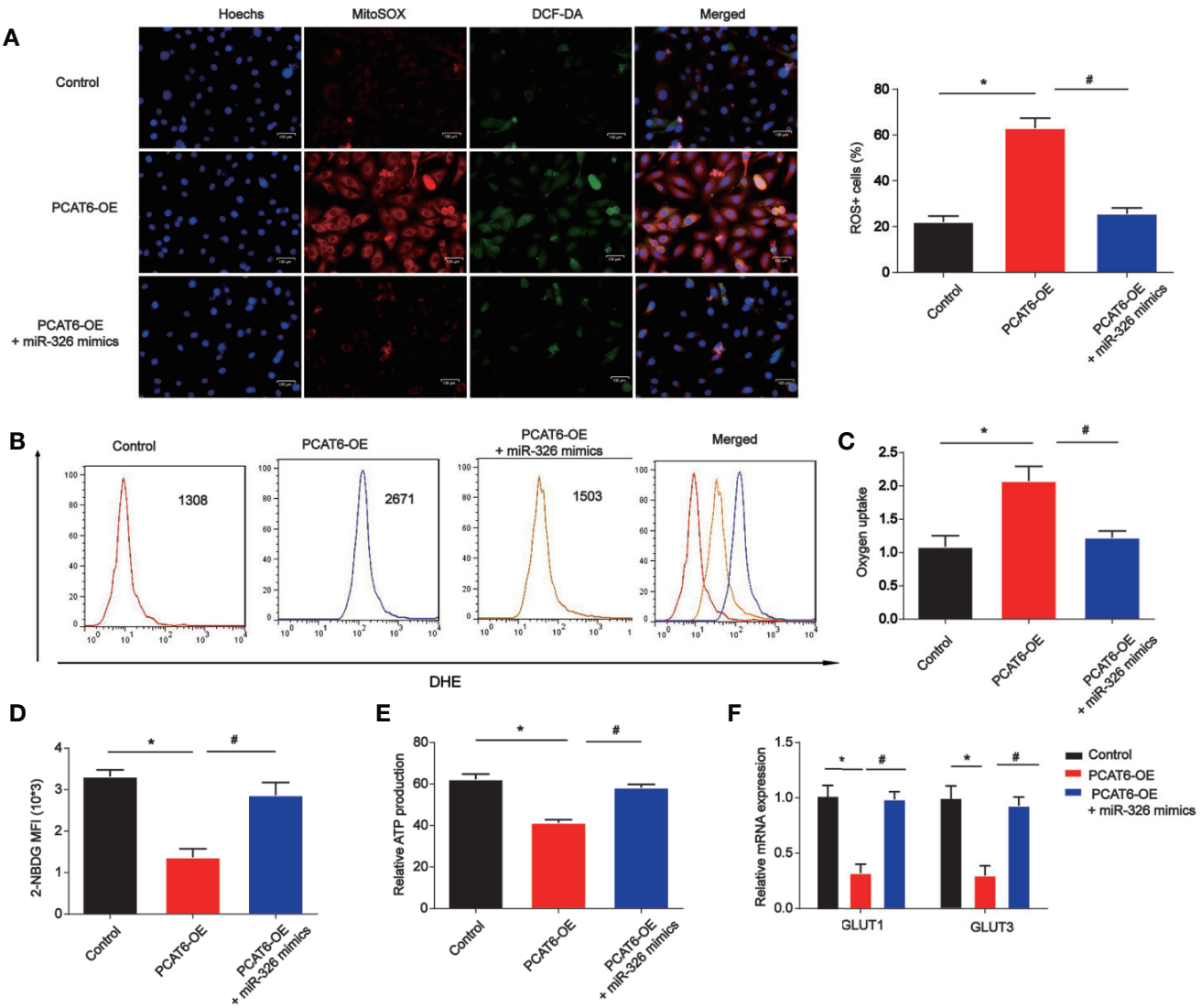

FIGURE 6 | The overexpression of PCAT6 contributed to the accumulation of ROS, mitochondrial and metabolic dysfunction in macrophages. THP-1-diferentiated macrophages were infected with PCAT6 overexpression plasmid and miR-326 mimics. **(A)** Immunofluorescence with DCF-DA and MitoSOX staining were used to detect the levels of cytoplasmic and mitochondrial ROS. ROS+ cells were observed under microscopy. Scale bar, 100 μm. **(B)** The levels of DHE in macrophages were analyzed using flow cytometry. **(C)** Oxygen uptake rate in macrophages. **(D)** The levels of 2-NBDG were analyzed using flow cytometry in macrophages. **(E)** Relative ATP levels of the THP-1-diferentiated macrophages. **(F)** The messenger RNA (mRNA) levels of Glut1 and Glut3 were tested by qRT-PCR. *$P < 0.05$. Compared with the control group. #$P < 0.05$. Compared with the PCAT6 OE group.

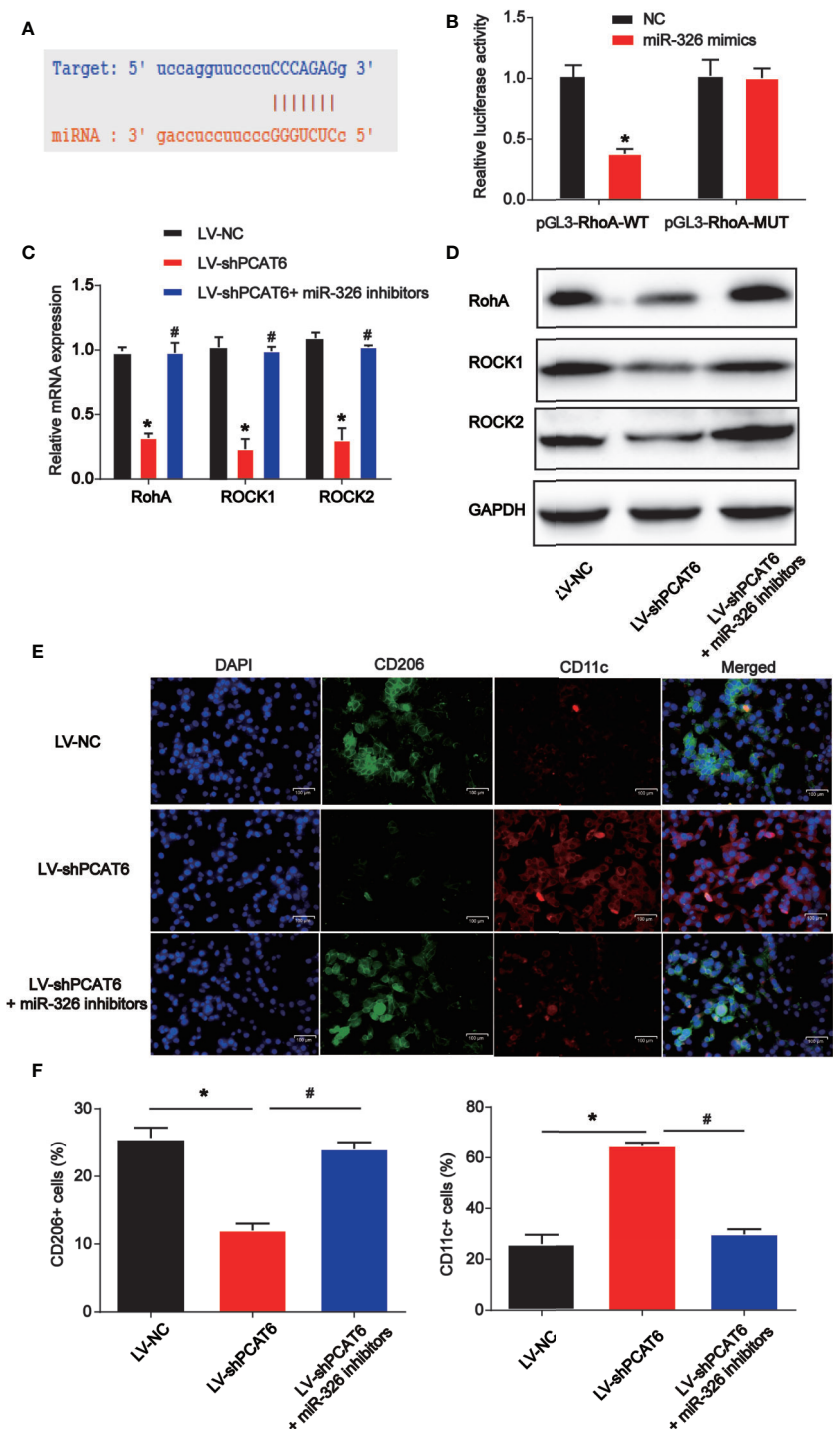

FIGURE 7 | RhoA was a direct target of miR-326. **(A)** The putative binding sites between RhoA and miR-326. **(B)** Luciferase activity was evaluated in THP-1-differentiated macrophages co-transfected with RhoA-WT or RhoA-MUT reporter and miR-326 mimics. **(C, D)** RhoA, ROCK1, and ROCK2 expression in THP-1-differentiated macrophages transfected with PCAT6 short hairpin RNA (shRNA) and miR-326 inhibitors. **(E, F)** Immunofluorescence with M2 marker (CD206) and M1 marker (CD11b) was carried out. Scale bar, 100 μm. *P < 0.05. Compared with the control group. #P < 0.05. Compared with LV-shPCAT6 group.

control THP-1-diferentiated macrophages s, which was reversed by miR-326 mimics (**Figure 6A**). Furthermore, the DHE was used to detect the ROS levels *in vitro*. As shown, the DHE staining intensity of PCAT6-upregulated THP-1-diferentiated macrophages was significantly induced than the control THP-1-differentiated macrophages (**Figure 6B**). The oxygen uptake was

increased by overexpression of PCAT6 while miR-326 mimics decreased that as exhibited in **Figure 6C**. We utilized 2-NBDG to assess the ability of cellular glucose uptake and proved that the incorporation of 2-NBDG in PCAT6-overexpressed THP-1-diferentiated macrophages was reduced and miR-326 overexpression increased 2-NBDG incorporation (**Figure 6D**). ATP production in PCAT6-overexpressed THP-1-diferentiated macrophages was lower (**Figure 6E**). The mRNA level of Glut1 and Glut3 was repressed by PCAT6 overexpression compared with the control cells as manifested in **Figure 6F**.

RhoA Was a Direct Target of miR-326

Next, we explored the downstream mechanism of miR-326 in modulating the immune responses of macrophages. RhoA was predicted as the target of miR-326 and the putative binding sites between then were indicated in **Figure 7A** *via* consulting STARBASE 2.0 (http://starbase.sysu.edu.cn/). Luciferase activity was evaluated in macrophages co-transfected with RhoA-WT or RhoA-MUT reporter and miR-326 mimics. In **Figure 7B**, overexpression of miR-326 obviously repressed the luciferase activity of RhoA-WT. Then, macrophages were infected with PCAT6 shRNA and miR-326 inhibitors. As exhibited in **Figures 7C, D**, loss of PCAT6 greatly reduced RhoA, ROCK1 and ROCK2 mRNA and protein expression in macrophages while miR-326 inhibitors reversed their expression levels. Then, in **Figures 7E, F**, immunofluorescence with M2 marker (CD206) and M1 marker (CD11b) was carried out. Down-regulation of PCAT6 reduced CD206+ cell ratio while induced CD11b+ cell ratio *via* modulating miR-326 in macrophages as shown in **Figures 7E, F**.

DISCUSSION

It has been well reported that lncRNA PCAT6 can act as an oncogene, which can drive the tumor progression in human cancers. For instance, PCAT6 can promote the development of gastric cancer *via* endogenously competing with miR-30 (17). PCAT6 can promote ovarian cancer occurrence and progression by inhibiting PTEN (18). In addition, PCAT6 can repress colon cancer cell apoptosis through regulating ARC expression *via* EZH2 (19). In this work, we observed PCAT6 was increased in CCA tissues and tumor-associated macrophages. Loss of PCAT6 reduced *in vivo* tumor growth *via* activating immune responses. In addition, overexpression of PCAT6 promoted M2 polarization of macrophages. Increase of PCAT6 promoted cellular ROS production, mitochondrial and metabolic dysfunction in macrophages *via* sponging miR-326 and regulating RohA/ROCK signaling.

Macrophages are highly plastic and they can exhibit different phenotypes such as proinflammatory M1 to anti-inflammatory M2 based on the environment (20). Tumor associated macrophages are present in high density in solid tumors sharing many characteristics with M2 macrophages. They have been identified to promote tumor development (21). Many lncRNAs are involved in M2 polarization of macrophages in cancers. For instance, loss of lncRNA SBF2-AS1in M2 macrophage-derived exosomes can elevate miR-122-5p to reduce XIAP and repress pancreatic cancer (22). GNAS-AS1 can induce ER+ breast cancer cell progression through inducing M2 macrophage polarization through modulating miR-433-3p and GATA3 (23). Here, we found that overexpression of PCAT6 induced M2 macrophage polarization in THP-1-differentiated macrophages. We proved that the ratio of M1 macrophages (F4/80+/CD11c cells) was significantly lower in the PCAT6-OE THP-1-differentiated macrophages while the ratio of M2 macrophages (CD11b +/CD206+ cells) in the PCAT6-OE THP-1-differentiated macrophages.

Then, we evaluated the potential mechanism of PCAT6 in regulating M2 macrophage polarization. miR-326 was predicted as a target for PCAT6. The previously identified miR-326 can participate in various cancers (24). For example, miR-326 can regulates endometrial cancer EMT and metastasis through targeting TWIST1 (25). miR-326 can act a tumor inhibitor in breast cancer through regulating ErbB/PI3K (26). The function of miR-326 in CCA progression remains poorly known. In our work, miR-326 was decreased in CCA tissues and overexpression of PCAT6 reduced miR-326 expression. In addition, miR-326 reversed the effect of PCAT6 on cellular ROS production, mitochondrial and metabolic dysfunction in THP-1-differentiated macrophages.

RhoA has been recognized as a member of small GTPase protein of Rho family (27). RhoA/ROCK is proved to be a crucial signaling pathway in tumor progression (28). RhoA can exhibit a crucial role in cancers and ROCK is an effector protein of RhoA. In addition, recent work has implicated aberrant RhoA/ROCK activation is involved in the pathogenesis of autoimmune disorders (29, 30). Targeting RhoA-ROCK pathway reverses T-cell dysfunction in SLE (31). SPON2 can enhance M1-like macrophage recruitment to repress hepatocellular carcinoma by regulating RhoA pathways (32). In addition, RhoA/ROCK has been linked with the progression of different cancers (33). RhoA was a downstream target of miR-326. Down-regulation of PCAT6 repressed RhoA/ROCK signaling *via* inducing miR-326 in macrophages. Many other mRNA targets of miR-326 were also predicted. In our future study, we would like to explore whether they are also involved in M2 polarization of macrophages in CCA.

In this study, PCAT6 was significantly increased in CCA patients and meanwhile, PCAT6 was highly expressed in macrophages. It was proved that PCAT6 participated in the immune response of CCA by modulating macrophages including ROS production, mitochondrial stress response, and M2 polarization through sponging miR-326 and activating RohA signaling. We highlighted PCAT6 might act as a potential target of immunotherapy for CCA treatment.

DATA AVAILABILITY STATEMENT

The raw data supporting the conclusions of this article will be made available by the authors, without undue reservation.

ETHICS STATEMENT

The studies involving human participants were reviewed and approved by the Affiliated Lishui Hospital of Zhejiang University. The patients/participants provided their written informed consent to participate in this study. The animal study was reviewed and approved by the Affiliated Lishui Hospital of Zhejiang University.

AUTHOR CONTRIBUTIONS

JJ and ZZ contributed to the conceptualization and design of the study. JT and FW developed the methodology. LC, LZ, and YY contributed to the acquisition of data. XY and JS contributed to the analysis and interpretation of data. JT and FW contributed to the draft writing. JJ revised the manuscript. CC and XH provided administrative, technical, or material support. All authors contributed to the article and approved the submitted version.

FUNDING

This study was supported by the Provincial and ministerial joint construction of key projects (grant No. WKJ-ZJ-1932), the Public welfare projects of Zhejiang Province (grant Nos. LGF19H180010, LGD19H160002, and LGF19H180009), and the Medical and Health Research Project of Zhejiang Province (grant Nos. 2018KY933).

REFERENCES

1. Rizvi S, Khan SA, Hallemeier CL, Kelley RK, Gores GJ. Cholangiocarcinoma - evolving concepts and therapeutic strategies. *Nat Rev Clin Oncol* (2018) 15:95–111. doi: 10.1038/nrclinonc.2017.157
2. Sha M, Jeong S, Xia Q. Antiviral therapy improves survival in patients with HBV infection and intrahepatic cholangiocarcinoma undergoing liver resection: Novel concerns. *J Hepatol* (2018) 68:1315–6. doi: 10.1016/j.jhep.2018.01.039
3. Laurent S, Verhelst X, Geerts A, Geboes K, De Man M, Troisi R, et al. Update on liver transplantation for cholangiocarcinoma : a review of the recent literature. *Acta Gastroenterol Belg* (2019) 82(3):417–20.
4. Blechacz B. Cholangiocarcinoma: Current Knowledge and New Developments. *Gut Liver* (2017) 11:13–26. doi: 10.5009/gnl15568
5. Chanmee T, Ontong P, Konno K, Itano N. Tumor-associated macrophages as major players in the tumor microenvironment. *Cancers (Basel)* (2014) 6:1670–90. doi: 10.3390/cancers6031670
6. Mills CD. Anatomy of a discovery: m1 and m2 macrophages. *Front Immunol* (2015) 6:212. doi: 10.3389/fimmu.2015.00212
7. Martinez FO, Gordon S. The M1 and M2 paradigm of macrophage activation: time for reassessment. *F1000Prime Rep* (2014) 6:13. doi: 10.12703/P6-13
8. Atri C, Guerfali FZ, Laouini D. Role of Human Macrophage Polarization in Inflammation during Infectious Diseases. *Int J Mol Sci* (2018) 19(6):1801. doi: 10.3390/ijms19061801
9. Rhee I. Diverse macrophages polarization in tumor microenvironment. *Arch Pharm Res* (2016) 39:1588–96. doi: 10.1007/s12272-016-0820-y
10. St Laurent G, Wahlestedt C, Kapranov P. The Landscape of long noncoding RNA classification. *Trends Genet* (2015) 31:239–51. doi: 10.1016/j.tig.2015.03.007
11. Batista PJ, Chang HY. Long noncoding RNAs: cellular address codes in development and disease. *Cell* (2013) 152:1298–307. doi: 10.1016/j.cell.2013.02.012
12. Huang Q, Yan J, Agami R. Long non-coding RNAs in metastasis. *Cancer Metastasis Rev* (2018) 37:75–81. doi: 10.1007/s10555-017-9713-x
13. Long J, Xiong J, Bai Y, Mao J, Lin J, Xu W, et al. Construction and Investigation of a lncRNA-Associated ceRNA Regulatory Network in Cholangiocarcinoma. *Front Oncol* (2019) 9:649. doi: 10.3389/fonc.2019.00649
14. Liang ZX, Liu HS, Wang FW, Xiong L, Zhou C, Hu T, et al. LncRNA RPPH1 promotes colorectal cancer metastasis by interacting with TUBB3 and by promoting exosomes-mediated macrophage M2 polarization. *Cell Death Dis* (2019) 10:829. doi: 10.1038/s41419-019-2077-0
15. Sun Y, Xu J. TCF-4 Regulated lncRNA-XIST Promotes M2 Polarization Of Macrophages And Is Associated With Lung Cancer. *Onco Targets Ther* (2019) 12:8055–62. doi: 10.2147/OTT.S210952
16. Xin Y, He X, Zhao W, Zhan M, Li Y, Xiao J, et al. LncRNA PCAT6 increased cholangiocarcinoma cell proliferation and invasion via modulating miR-330-5p. *Am J Transl Res* (2019) 11(9):6185–95.
17. Xu Y, Sun JY, Jin YF, Yu H. PCAT6 participates in the development of gastric cancer through endogenously competition with microRNA-30. *Eur Rev Med Pharmacol Sci* (2018) 22(16):5206–13. doi: 10.26355/eurrev_201808_15718
18. Kong FR, Lv YH, Yao HM, Zhang HY, Zhou Y, Liu SE. LncRNA PCAT6 promotes occurrence and development of ovarian cancer by inhibiting PTEN. *Eur Rev Med Pharmacol Sci* (2019) 23(19):8230–8. doi: 10.26355/eurrev_201910_19132
19. Huang W, Su G, Huang X, Zou A, Wu J, Yang Y, et al. Long noncoding RNA PCAT6 inhibits colon cancer cell apoptosis by regulating anti-apoptotic protein ARC expression via EZH2. *Cell Cycle* (2019) 18(19):69–83. doi: 10.1080/15384101.2018.1558872
20. Lumeng CN, Bodzin JL, Saltiel AR. Obesity induces a phenotypic switch in adipose tissue macrophage polarization. *J Clin Invest* (2007) 117:175–84. doi: 10.1172/JCI29881
21. Cheng H, Wang Z, Fu L, Xu T. Macrophage Polarization in the Development and Progression of Ovarian Cancers: An Overview. *Front Oncol* (2019) 9:421. doi: 10.3389/fonc.2019.00421
22. Yin Z, Zhou Y, Ma T, Chen S, Shi N, Zou Y, et al. Down-regulated lncRNA SBF2-AS1 in M2 macrophage-derived exosomes elevates miR-122-5p to restrict XIAP, thereby limiting pancreatic cancer development. *J Cell Mol Med* (2020) 24:5028–38. doi: 10.1111/jcmm.15125
23. Liu SQ, Zhou ZY, Dong X, Guo L, Zhang KJ. LncRNA GNAS-AS1 facilitates ER+ breast cancer cells progression by promoting M2 macrophage polarization via regulating miR-433-3p/GATA3 axis. *Biosci Rep* (2020) 40 (7):BSR20200626. doi: 10.1042/BSR20200626
24. Pan YJ, Wan J, Wang CB. MiR-326: Promising Biomarker for Cancer. *Cancer Manag Res* (2019) 11:10411–8. doi: 10.2147/CMAR.S223875
25. Liu W, Zhang B, Xu N, Wang MJ, Liu Q. miR-326 regulates EMT and metastasis of endometrial cancer through targeting TWIST1. *Eur Rev Med Pharmacol Sci* (2017) 21(17):3787–93.
26. Ghaemi Z, Soltani BM, Mowla SJ. MicroRNA-326 Functions as a Tumor Suppressor in Breast Cancer by Targeting ErbB/PI3K Signaling Pathway. *Front Oncol* (2019) 9:653. doi: 10.3389/fonc.2019.00653
27. Yu G, Wang Z, Zeng S, Liu S, Zhu C, Xu R, et al. Paeoniflorin Inhibits Hepatocyte Growth Factor- (HGF-) Induced Migration and Invasion and Actin Rearrangement via Suppression of c-Met-Mediated RhoA/ROCK Signaling in Glioblastoma. *BioMed Res Int* (2019) 2019:9053295. doi: 10.1155/2019/9053295
28. Yuan J, Chen L, Xiao J, Qi XK, Zhang J, Li X, et al. SHROOM2 inhibits tumor metastasis through RhoA-ROCK pathway-dependent and -independent mechanisms in nasopharyngeal carcinoma. *Cell Death Dis* (2019) 10:58. doi: 10.1038/s41419-019-1325-7
29. Pernis AB, Ricker E, Weng CH, Rozo C, Yi W. Rho Kinases in Autoimmune Diseases. *Annu Rev Med* (2016) 67:355–74. doi: 10.1146/annurev-med-051914-022120
30. Ricker E, Chowdhury L, Yi W, Pernis AB. The RhoA-ROCK pathway in the regulation of T and B cell responses. *F1000Res* (2016) 5:F1000 Faculty Rev-2295. doi: 10.12688/f1000research.7522.1

31. Rozo C, Chinenov Y, Maharaj RK, Gupta S, Leuenberger L, Kirou KA, et al. Targeting the RhoA-ROCK pathway to reverse T-cell dysfunction in SLE. *Ann Rheum Dis* (2017) 76:740–7. doi: 10.1136/annrheumdis-2016-209850
32. Zhang YL, Li Q, Yang XM, Fang F, Li J, Wang YH, et al. SPON2 Promotes M1-like Macrophage Recruitment and Inhibits Hepatocellular Carcinoma Metastasis by Distinct Integrin-Rho GTPase-Hippo Pathways. *Cancer Res* (2018) 78:2305–17. doi: 10.1158/0008-5472.CAN-17-2867
33. Yadav S, Kashaninejad N, Nguyen NT. RhoA and Rac1 in Liver Cancer Cells: Induction of Overexpression Using Mechanical Stimulation. *Micromachines (Basel)* (2020) 11(8):729. doi: 10.3390/mi11080729

Conflict of Interest: The authors declare that the research was conducted in the absence of any commercial or financial relationships that could be construed as a potential conflict of interest.

frontiers in Genetics

ORIGINAL RESEARCH
published: 01 February 2021
doi: 10.3389/fgene.2021.620705

Identification of Tumor Microenvironment-Related Prognostic Genes in Sarcoma

Dongjun Dai[1†], Lanyu Xie[2†], Yongjie Shui[1], Jinfan Li[3] and Qichun Wei[1]*

[1] Department of Radiation Oncology, The Second Affiliated Hospital, Zhejiang University School of Medicine, Hangzhou, China, [2] Department of Clinical Medicine, Fuzhou Medical College of Nanchang University, Jiangxi, China, [3] Department of Pathology, The Second Affiliated Hospital, Zhejiang University School of Medicine, Hangzhou, China

Aim: Immune cells that infiltrate the tumor microenvironment (TME) are associated with cancer prognosis. The aim of the current study was to identify TME related gene signatures related to the prognosis of sarcoma (SARC) by using the data from The Cancer Genome Atlas (TCGA).

Methods: Immune and stromal scores were calculated by estimation of stromal and immune cells in malignant tumor tissues using expression data algorithms. The least absolute shrinkage and selection operator (lasso) based cox model was then used to select hub survival genes. A risk score model and nomogram were used to predict the overall survival of patients with SARC.

Results: We selected 255 patients with SARC for our analysis. The Kaplan–Meier method found that higher immune ($p = 0.0018$) or stromal scores ($p = 0.0022$) were associated with better prognosis of SARC. The estimated levels of CD4+ ($p = 0.0012$) and CD8+ T cells ($p = 0.017$) via the tumor immune estimation resource were higher in patients with SARC with better overall survival. We identified 393 upregulated genes and 108 downregulated genes ($p < 0.05$, fold change >4) intersecting between the immune and stromal scores based on differentially expressed gene (DEG) analysis. The univariate Cox analysis of each intersecting DEG and subsequent lasso-based Cox model identified 11 hub survival genes (*MYOC*, *NNAT*, *MEDAG*, *TNFSF14*, *MYH11*, *NRXN1*, *P2RY13*, *CXCR3*, *IGLV3-25*, *IGHV1-46*, and *IGLV2-8*). Then, a hub survival gene-based risk score gene signature was constructed; higher risk scores predicted worse SARC prognosis ($p < 0.0001$). A nomogram including the risk scores, immune/stromal scores and clinical factors showed a good prediction value for SARC overall survival (C-index = 0.716). Finally, connectivity mapping analysis identified that the histone deacetylase inhibitors trichostatin A and vorinostat might have the potential to reverse the harmful TME for patients with SARC.

Conclusion: The current study provided new indications for the association between the TME and SARC. Lists of TME related survival genes and potential therapeutic drugs were identified for SARC.

Keywords: sarcoma, tumor microenvironment, TCGA, ESTIMATE algorithms, nomogram, HDAC inhibitors

OPEN ACCESS

Edited by:
Xiao-Jie Lu,
Nanjing Medical University, China

Reviewed by:
Pranjal Sarma,
University of Cincinnati, United States
Xueqiu Lin,
Stanford University, United States

****Correspondence:***
Qichun Wei
qichun_wei@zju.edu.cn

[†] These authors have contributed equally to this work

Specialty section:
This article was submitted to Cancer Genetics, a section of the journal Frontiers in Genetics

Received: *23 October 2020*
Accepted: *06 January 2021*
Published: *01 February 2021*

Citation:
Dai D, Xie L, Shui Y, Li J and Wei Q (2021) Identification of Tumor Microenvironment-Related Prognostic Genes in Sarcoma. Front. Genet. 12:620705. doi: 10.3389/fgene.2021.620705

INTRODUCTION

Sarcoma (SARC) is a term used for a heterogeneous group of cancers that originate from somatic mesenchymal tissues. SARC is a rare neoplasm that accounts for less than 1% of newly diagnosed adult cancers (Hui, 2016). The most common therapy for localized SARC to date is surgery in combination with radiation therapy and chemotherapy (Raj et al., 2018). However, a high recurrence rate of nearly 50% has been reported in patients with SARC, and the chemotherapy used for metastatic SARC does not significantly improve the survival of patients. The median overall survival time of metastatic SARC is between 8 and 12 months (Raj et al., 2018). Hence, new therapies are required for the treatment of SARC.

Immunotherapy is an attractive alternative treatment option for SARC. Recently, therapies using immune checkpoint inhibitors, such as anti-cytotoxic T lymphocyte-associated antigen 4 (anti-CTLA-4), and the anti-programmed cell death protein 1 pathway (anti-PD-1/PD-L1) have performed well in the treatment of cancers. However, the efficiency of immune checkpoint inhibitor treatment has been limited in the treatment of SARC (Maki et al., 2013; D'Angelo et al., 2017; Tawbi et al., 2017; Toulmonde et al., 2018).

The immunotherapy response is dependent on complex interactions between the tumor and immune cells within the tumor microenvironment (TME). Various processes within the TME suppress the interactions between tumors and immune effector cells, thus, tumor cells can escape from the attacking immune cells. Therefore, a better understanding of the TME of SARCs is important for improving response to immunotherapy, and will enable the development of more effective therapies (Raj et al., 2018).

The TME comprises various cell types, such as immune, stromal, endothelial, inflammatory, and mesenchymal cells (Hanahan and Coussens, 2012). Among these, immune and stromal cells are two major non-cancer cell types found in the TME that are associated with the prognosis of cancers (Garcia-Gomez et al., 2018). Recently, with the development of sequencing technology and the establishment of large molecular databases such as The Cancer Genome Atlas (TCGA), many algorithms were developed to exploit the TME (Carter et al., 2012; Yoshihara et al., 2013). For example, the estimation of stromal and immune cells in malignant tumor tissues using expression data (ESTIMATE) algorithm uses gene expression signatures to infer the infiltration level of stromal and immune cells in tumor samples by calculating stromal and immune scores (Yoshihara et al., 2013). The ESTIMATE algorithm has been applied to several cancer types and it has been identified that high immune or stromal scores were associated with favorable prognoses in osteosarcoma (Hong et al., 2020) and cervical squamous cell carcinoma (Pan et al., 2019), and unfavorable prognosis in gastric cancer (Wang et al., 2019), bladder cancer (Zhang et al., 2020), and acute myeloid leukemia (Ni et al., 2019). However, the ESTIMATE algorithms have not been previously used to explore the association between immune and stomal cells and the prognosis of SARC in adults.

This study aims to apply the ESTIMATE algorithm to the SARC RNA sequencing (RNA-seq) data from TCGA database. This will enable the construction of a TME related gene signature to predict the overall survival of patients with SARC.

MATERIALS AND METHODS

Database and ESTIMATE Algorithm Application

The RNA-seq read counts and clinical data of patients with SARC were taken from TCGA project. We downloaded the relative data from the Xena database (Goldman et al., 2019). The patients with both read count data and survival information were included in the following analyses. Raw counts data were normalized by the TMM method from the "edgeR" R package and then transformed with the voom method from the "limma" R package. The ESTIMATE algorithm was applied to the selected patients with SARC to calculate the immune and stromal scores via the "estimate" R package.

The Kaplan–Meier (KM) method was used to draw the survival curve. A log-rank test was applied to the KM plot. The best cutoff value was calculated to grade the SARC groups based on the level of immune or stromal scores. The stratified high and low groups were then used for the following analyses.

Tumor Immune Estimation Resource Analysis

To explore the association between immune scores or stromal scores and the immune cells, the SARC fragments per kilobase of transcript per million mapped reads data from the Xena database were transformed into transcripts per million and subjected to tumor immune estimation resource (TIMER) analysis (Li et al., 2020). Six tumor-infiltrating cell populations were analyzed: B cells, CD4+ T cells, CD8+ T cells, neutrophils, macrophages, and dendritic cells. KM analysis, with the establishment of optimal cutoff value, was performed to access the association between immune cell type and the prognosis of patients with SARC.

Identification of Differentially Expressed Genes Between High and Low Immune or Stromal Score Groups

The "limma" R package was used to find the differentially expressed genes (DEGs) between high and low immune or stromal score groups. The DEGs were defined as the genes with a fold change > 4 and adjusted p-value < 0.05 based on the results of the "limma" analysis. The results of the DEG analysis were visualized using volcano plots and heatmaps. The intersecting parts of the DEGs analyses of the immune and stromal scores groups were calculated and grouped by Venn diagram. The intersecting genes would then be used for functional analysis.

Functional Analysis of the Intersecting DEGs of Immune or Stromal Score Groups

Functional analyses were performed for intersecting DEGs of immune score or stromal score groups. Kyoto Encyclopedia of Genes and Genomes (KEGG) analysis and gene ontology (GO)

analysis, which consists of biological processes (BP), cellular components (CC), and molecular functions (MF), were used. The p-value < 0.05 and q-value < 0.05 were set as the cutoff value.

Survival Analysis of Intersecting DEGs and Clinical Predictive Model Construction

Univariate Cox analysis was applied for the high or low expression groups (Stratified by median value) of each DEG. DEGs with a p-value < 0.05 were considered to be a survival related DEG. The least absolute shrinkage and selection operator (lasso) analysis was performed to select the hub survival related genes. The selected survival related genes from lasso analysis were then used to calculate the risk score, which was calculated as ($\beta i \times \mathrm{Exp}i$) ($i$ = the number of hub survival related genes). The optimal cutoff value of the risk score was calculated, following which a KM plot was drawn. The area under the receiver operating characteristic curve (AUC) was calculated for the 1-year, 3-year, and 5-year survival prediction of patients with SARC.

A multivariate Cox model-based nomogram was constructed for the 1-year, 3-year, and 5-year predictions of the overall survival of patients with SARC. The internal validation was determined by discrimination and calibration with 1,000 bootstraps. The C-index was calculated and the calibration curve was plotted.

Drug Identification Analysis

Connectivity Map (CMap) analysis uses a reference database containing drug-specific gene expression profiles and compares it with a disease-specific gene signatures. This enables accurate drug identification for certain disease phenotypes (Lamb, 2007; Musa et al., 2018). The CMap dataset consists of cellular signatures that catalog transcriptional responses of human cells to chemical and genetic perturbation, which are then widely used as reference profiles for connectivity mapping analysis (Subramanian et al., 2017). In this study, we used the R package "Dr. Insight" to perform CMap analysis. It provides a connectivity mapping method to connect drugs (compounds) in the CMap dataset with query data (disease phenotype, such as immune and stromal scores). The results of the t-test statistic scores from the "limma" analysis were used as input data for this evaluation. We identified the drugs that targeted patients with SARC with lower immune or stromal scores that had worse survival. The drugs with a false discovery rate (FDR) < 0.1 were considered as key targets for the therapy of patients with SARC with lower immune or stromal scores.

Statistical Analysis

All the statistical analyses were performed using R-4.0.2. The "survminer" package was used for the KM analysis. The "immunedeconv" package was used for TIMER analysis. The "VennDiagram" package was used to draw the Venn diagram. The "pheatmap" package was used to plot the heatmap. The "clusterProfiler" package was used for the functional analyses. The "glmnet" package was used to perform the lasso analysis. The "ROCR" package was used for the AUC analysis. The "rms" package was used for the nomogram construction and validation. The "ggplot2" package was used to draw KM plots, box plots, volcano plots and histogram. For comparisons between two groups, Wilcoxon analysis was performed, while for comparisons among three or more groups, Kruskal–Wallis analysis was applied.

RESULTS

Data Selection and ESTIMATE Algorithm Results

As shown in **Figure 1**, we selected 255 patients with SARC with read counts data and clinical information. The detailed clinical information of the included patients is shown in **Table 1**. There were 139 (54.51%) patients 60 years or older and 116 (45.49%) patients under 60 years old, 139 (54.51%) were female and 116 (45.49%) were male, and 18 (7.06%) were African American patients and 223 were (87.45%) Caucasian American patients. The primary disease diagnosis for the patients were 56 dedifferentiated liposarcomas (21.96%), 25 fibromyxosarcomas (9.80%), 100 leiomyosarcomas (39.22%), 12 malignant fibrous histiocytomas (4.71%), and 33 undifferentiated SARCs (12.94%). The SARC disease type were 40 fibromatous neoplasms (15.69%), 58 lipomatous neoplasms (22.75%), 103 myomatous neoplasms (40.39%), 35 soft tissue tumors and SARC (13.73%), and 10 synovial-like neoplasms (3.92%). The primary site distribution was in connective, subcutaneous and other soft tissues in 114 (44.71%) patients, the retroperitoneum and peritoneum in 98 (38.43%) patients, and the uterus in 27 (10.59%) patients.

After using the ESTIMATE algorithm, the immune scores ranged from −2088.757 to 3342.350, while the stromal scores ranged from −1238.948 to 2525.174. The detailed immune scores and stromal scores are listed in **Supplementary Table 1**. We found that both the immune and stromal scores were significantly associated with age, gender, primary diagnosis, disease type, and primary site (**Figure 2** and **Supplementary Figure 1**, $p < 0.05$). In detail, the immune and the stromal scores were lower in younger patients with SARC than in old patients (**Figure 2A** and **Supplementary Figure 1A**), lower in females than males (**Figure 2B** and **Supplementary Figure 1B**), lower in leiomyosarcoma and undifferentiated SARCs than other primary diagnosed SARCs (**Figure 2C** and **Supplementary Figure 1C**), lower in myomatous neoplasms and synovial-like neoplasms than other disease types of SARC (**Figure 2D** and **Supplementary Figure 1D**), and lower in the uterus than other primary sites of SARC (**Figure 2E** and **Supplementary Figure 1E**). Besides this, we observed that there were no associations between immune scores or stromal scores and the SARC characteristics that comprised race, tumor total necrosis percent, tumor depth, person neoplasm cancer status, mitotic count, metastatic diagnosis, local disease recurrence, and leiomyosarcoma histologic subtype and margin status (**Supplementary Figures 2**, **3**).

We next evaluated the association between immune and stromal scores and the prognosis of patients with SARC, the

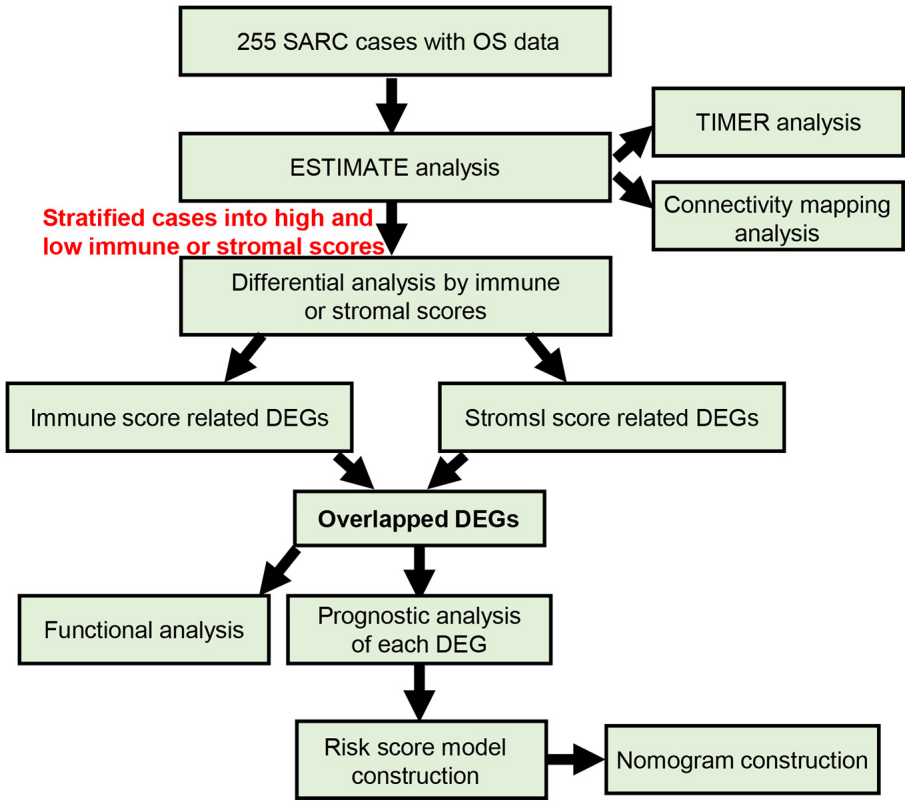

FIGURE 1 | The flow chart of current study.

optimal cutoff values were evaluated for KM analysis. We found that lower immune or stromal scores were associated with poorer overall survival of patients with SARC (**Figure 3**).

Association Between Infiltration Level of Immune Cells and the SARCs Immune or Stromal Scores

We next compared the infiltration level of immune cells between the higher or lower immune or stromal scores groups. We found CD4+ T cells, CD8+ T cells, neutrophils, macrophages, and dendritic cells were higher in the high immune or stromal score groups, while B cell infiltration was only higher in the immune score group (**Figure 4**). Moreover, we explored the association between the infiltration level of immune cells and the overall survival of patients with SARC (**Figure 5**). We found that CD4+ and CD8+ T cells were higher in patients with better overall survival (**Figures 5B,C**).

Comparison of Gene Expression Profile by Immune and Stromal Scores

We next separated the patients with SARC into two groups according to their immune score level or stromal score level. The high and low immune or stromal score groups were then used for DEG analysis. Heatmaps showed distinct gene expression profiles of high and low immune or stromal score groups (**Supplementary Figure 4**). The volcano plots showed that there were 834 upregulated genes and 173 downregulated genes in the immune score groups (**Figure 6A** and **Supplementary Table 2**), and there were 541 upregulated genes and 183 downregulated genes in stromal score groups (**Figure 6A** and **Supplementary Table 3**). The Venn diagram shows that there were 393 upregulated genes and 108 downregulated genes in the intersecting part between the groups (**Figure 6B**). These DEGs common to both groups were then used for the functional analysis.

Functional Analysis of Intersecting DEGs

As shown in **Figure 6C**, functional enrichment GO and KEGG analyses were applied for the intersected DEGs. The top five GO (biological process, cellular component, and molecular function) and KEGG terms were included. The detailed GO and KEGG analysis results are listed in **Supplementary Tables 4–7**.

The GO analysis showed the intersected DEGs were related to immunoglobulin related terms; such as immunoglobulin complex, immunoglobulin receptor binding, and immunoglobulin immune responses. In addition, the intersected DEGs were associated with KEGG terms like cytokine-cytokine receptor interaction, viral protein interaction with cytokine-cytokine receptor (**Figure 6C**). Furthermore, the B cell and T cell activation related terms were also enriched (**Supplementary Tables 4–7**).

TABLE 1 | The clinical characteristics of patients with SARC.

Characteristics	No. of patients	%
Age		
High	139	0.545
Low	116	0.455
Gender		
Female	139	0.545
Male	116	0.455
Race		
African American	18	0.071
Caucasian American	223	0.875
Other	14	0.055
Primary diagnosis		
Dedifferentiated liposarcoma	56	0.22
Fibromyxosarcoma	25	0.098
Leiomyosarcoma, NOS	100	0.392
Malignant fibrous histiocytoma	12	0.047
Undifferentiated sarcoma	33	0.129
Other	29	0.114
Disease type		
Fibromatous Neoplasms	40	0.157
Lipomatous Neoplasms	58	0.227
Myomatous Neoplasms	103	0.404
Soft Tissue Tumors and Sarcomas, NOS	35	0.137
Synovial-like Neoplasms	10	0.039
Nerve Sheath Tumors	9	0.035
Primary site		
Connective, subcutaneous and other soft tissues	114	0.447
Retroperitoneum and peritoneum	98	0.384
Uterus, NOS	27	0.106
Other	16	0.063
Stromal Score		
High	159	0.624
Low	96	0.376
Immune Score		
High	166	0.651
Low	89	0.349
Risk_Scores		
High	74	0.29
Low	181	0.71

Survival Analysis of Intersecting DEGs and Clinical Predictive Model Construction

To reveal the relationship of intersecting DEGs and the prognosis of SARC, we performed a univariate Cox analysis for each gene. There were 140 SARC survival related DEGs identified (**Supplementary Table 8**).

Among them, there were 138 survival favorable genes, of which 135 were upregulated in the higher immune or stromal score groups, and there were 2 survival unfavorable genes, which were both downregulated in the higher immune or stromal score groups. This was consistent with the results that patients with SARC with higher immune or stromal scores had better overall survival.

To obtain a more interpretable prognostic model, we performed a variable selection process by using the lasso-based Cox model. The genes of *MYOC*, *NNAT*, *MEDAG*, *TNFSF14*, *MYH11*, *NRXN1*, *P2RY13*, *CXCR3*, *IGLV3-25*, *IGHV1-46*, and *IGLV2-8* were selected as they had a non-zero value of coefficients (**Supplementary Table 9**). Among these genes, the increased expression of *NNAT* was associated with worse overall survival, and the elevated expression of *MYOC*, *MEDAG*, *TNFSF14*, *MYH11*, *NRXN1*, *P2RY13*, *CXCR3*, *IGLV3-25*, *IGHV1-46*, and *IGLV2-8* were associated with better overall survival (**Figure 7**). These lasso selected survival genes were then used to construct a risk score model. We found that the higher risk scores were strongly associated with worse overall survival of patients with SARC (**Figure 8A**). The AUC plots showed the risk score model was predictable (1-year, AUC = 0.75; 3-year, AUC = 0.692; 5-year, AUC = 0.695; **Figure 8B**). Furthermore, we built a Cox based nomogram for patients with SARC (**Figure 9A**). The calibration plots showed the risk model predicted the overall survival of patients with SARC well (**Figure 9B**). The C-index for the nomogram was 0.716.

Exploration of Potential Drug Targets

Utilizing CMap analysis, we identified the drugs that had potential therapeutic effects on patients with SARC that had low survival rates. The results showed that the histone deacetylases (HDAC) inhibitors trichostatin A and vorinostat were key drugs that might have therapeutic value (**Table 2**, p-value < 0.05, FDR < 0.1).

DISCUSSION

Using the ESTIMATE algorithm, we found that patients with SARC with higher immune or stromal scores had better overall survival. We also identified that higher immune or stromal scores represented higher infiltrating levels of CD4+ T cells, CD8+ T cells, neutrophils, macrophages, and dendritic cells. Furthermore, we observed that CD4+ T cells and CD8+ T cells were strongly associated with the survival of patients with SARC.

CD4+ and CD8+ T cell responses play a central role in the elimination of cancer cells (Ostroumov et al., 2018). A previous study found that a higher level of infiltration of CD8+ lymphocytes into synovial SARC was associated with a favorable overall patient survival (Oike et al., 2018). Moreover, patients with cutaneous angiosarcoma with higher levels of CD8+ lymphocytes in primary tumors survived longer when compared with patients with less of these cells. Furthermore, the CD8+ lymphocytes also correlated with a distinct metastasis-free period (Fujii et al., 2014). Another study revealed that the immune checkpoint therapy-mediated rejection of a nonimmunogenic SARC requires both CD4+ and CD8+ T cells (Alspach et al., 2019). Our findings confirmed the importance of CD4+ and CD8+ T cells in the progression of SARC.

The immune or stromal high and low groups' scores revealed 501 TME related DEGs. According to the enrichment analyses, these DEGs were associated with immunoglobulin related GO terms. Previously, the administration of immunoglobulin G has

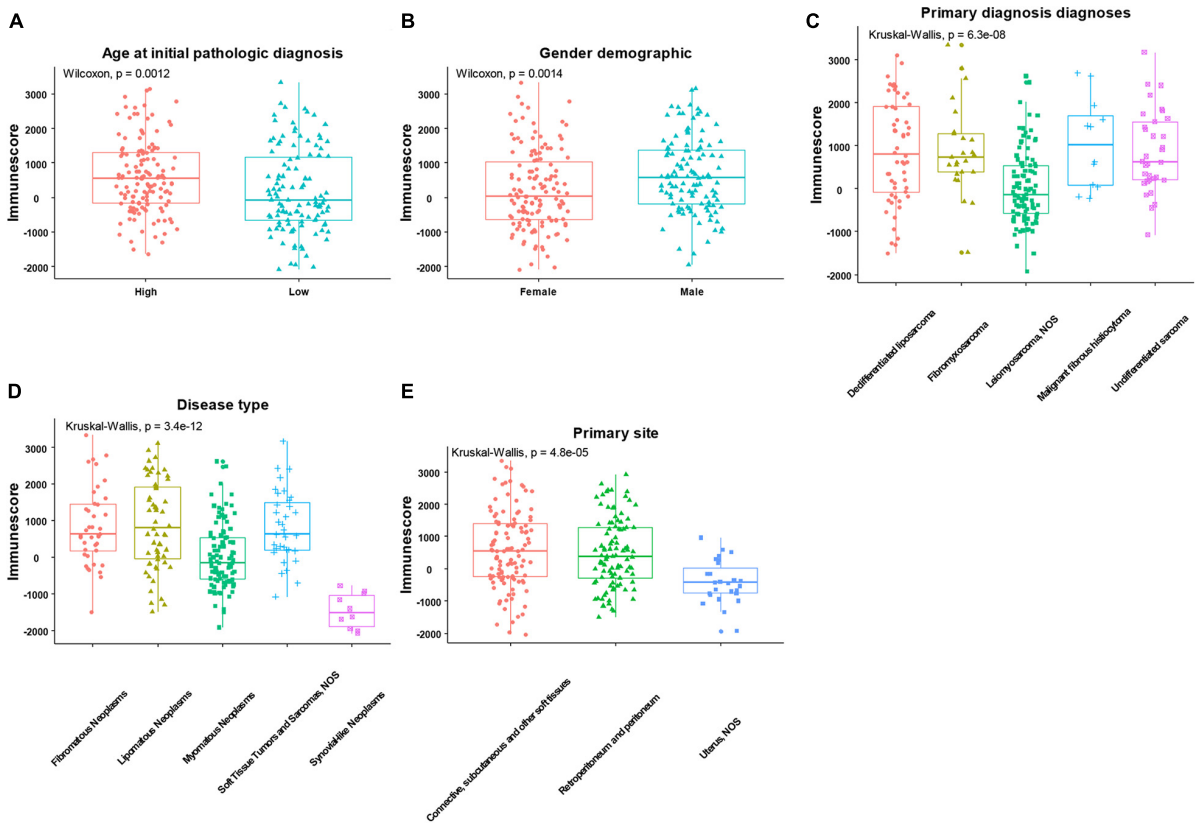

FIGURE 2 | The significant associations between immune score and the clinical factors of patients with SARC. The age **(A)**, gender **(B)**, primary diagnosis **(C)**, disease type **(D)**, and primary site **(E)** were significantly associated with the immune scores calculated by ESTIMATE algorithm.

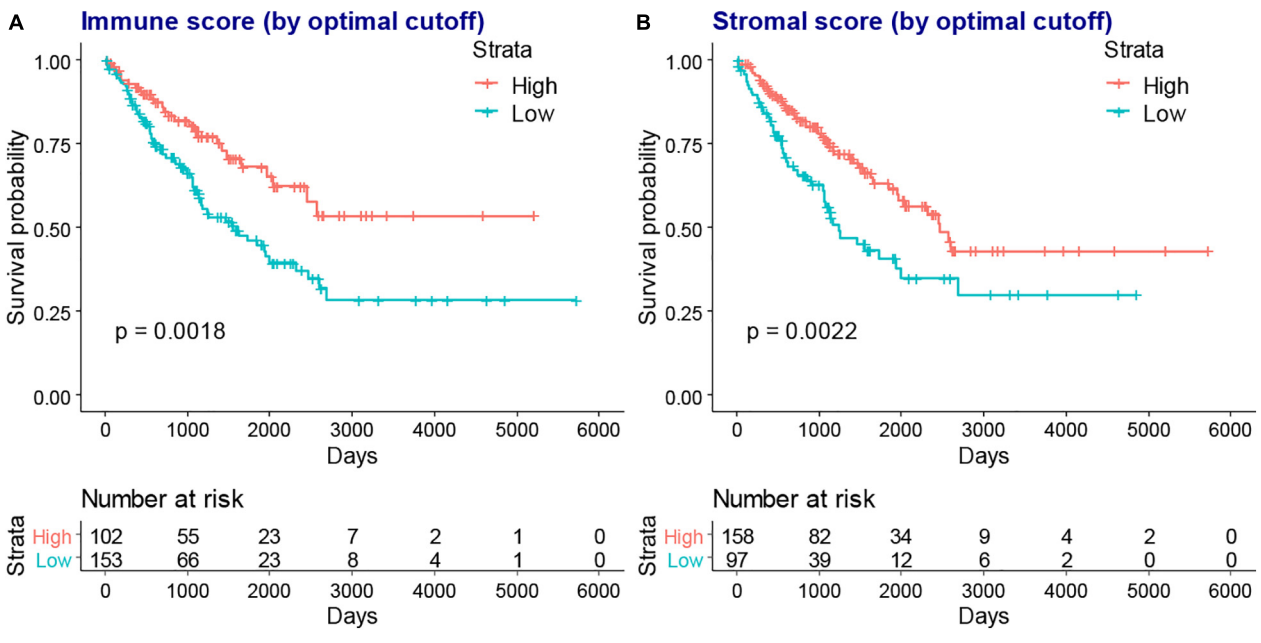

FIGURE 3 | The KM plot of immune scores or stromal scores and the overall survival of patients with SARC. The lower immune scores **(A)** and stromal scores **(B)** indicated worse overall survival in the KM plot model which stratified by optimal cutoff value.

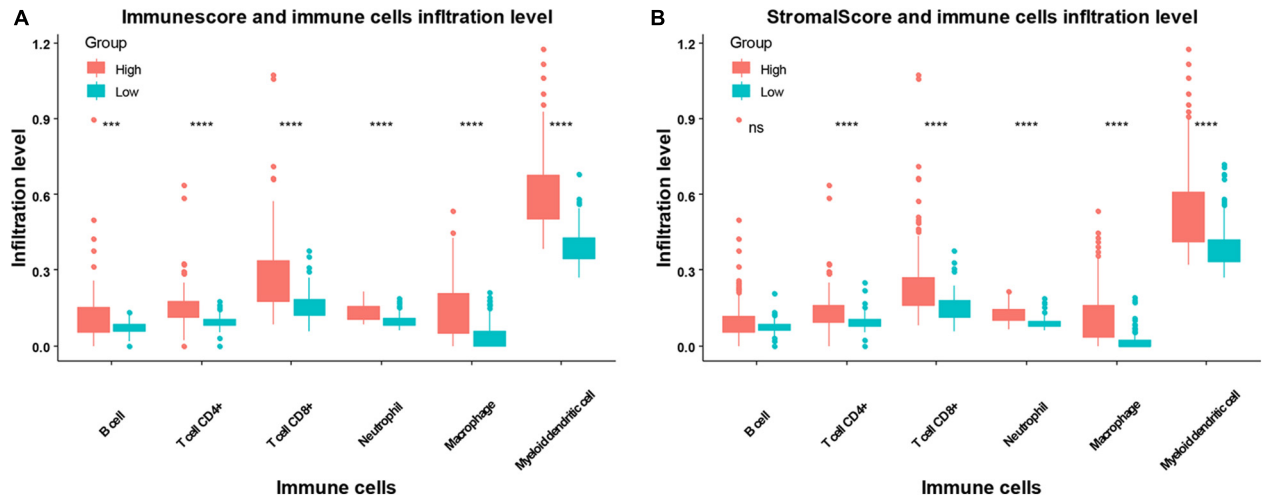

FIGURE 4 | The association between infiltration level of immune cells and the immune scores/stromal scores in patients with SARC. The infiltration levels of B cells, CD4+ T cells, CD8+ T cells, neutrophils, macrophages, and myeloid dendritic cell in patients with SARC according to **(A)** immune scores and **(B)** stromal scores.

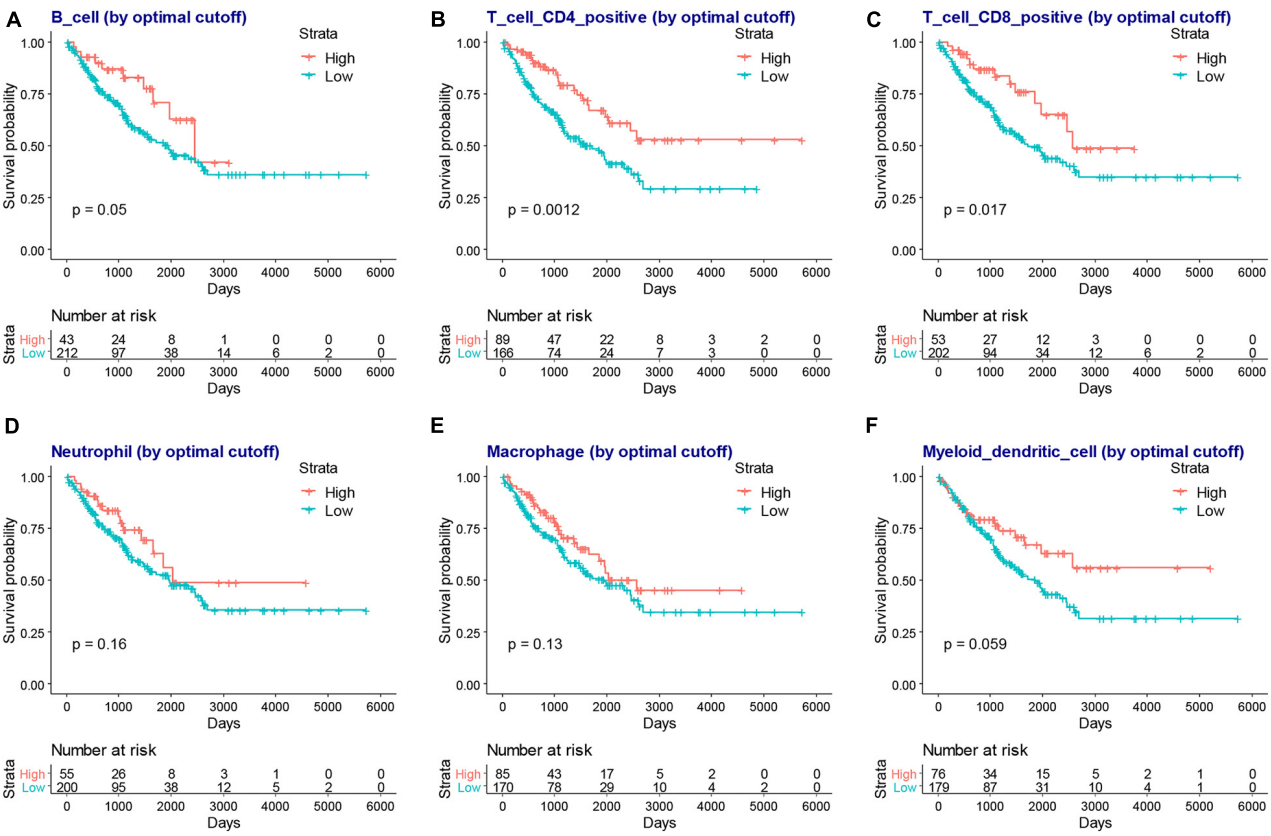

FIGURE 5 | The association between infiltration level of immune cells and the overall survival of patients with SARC. The KM plot of infiltration levels of B cells **(A)**, CD4+ T cells **(B)**, CD8+ T cells **(C)**, neutrophils **(D)**, macrophages **(E)**, and myeloid dendritic cells **(F)** and the overall survival of patients with SARC.

been shown to be able to inhibit cancer growth (Xu et al., 2019), furthermore, this specific immunoglobulin isotype (IgG) was also found to be associated with cancer prognosis (Hsu et al., 2019; Isaeva et al., 2019). In the lasso-based Cox model, the increased expression of immunoglobulin related genes *IGLV3-25*, *IGHV1-46*, and *IGLV2-8* were also identified to be hub genes associated with better survival, providing new insights into the relationship between immunoglobulins and SARC prognosis.

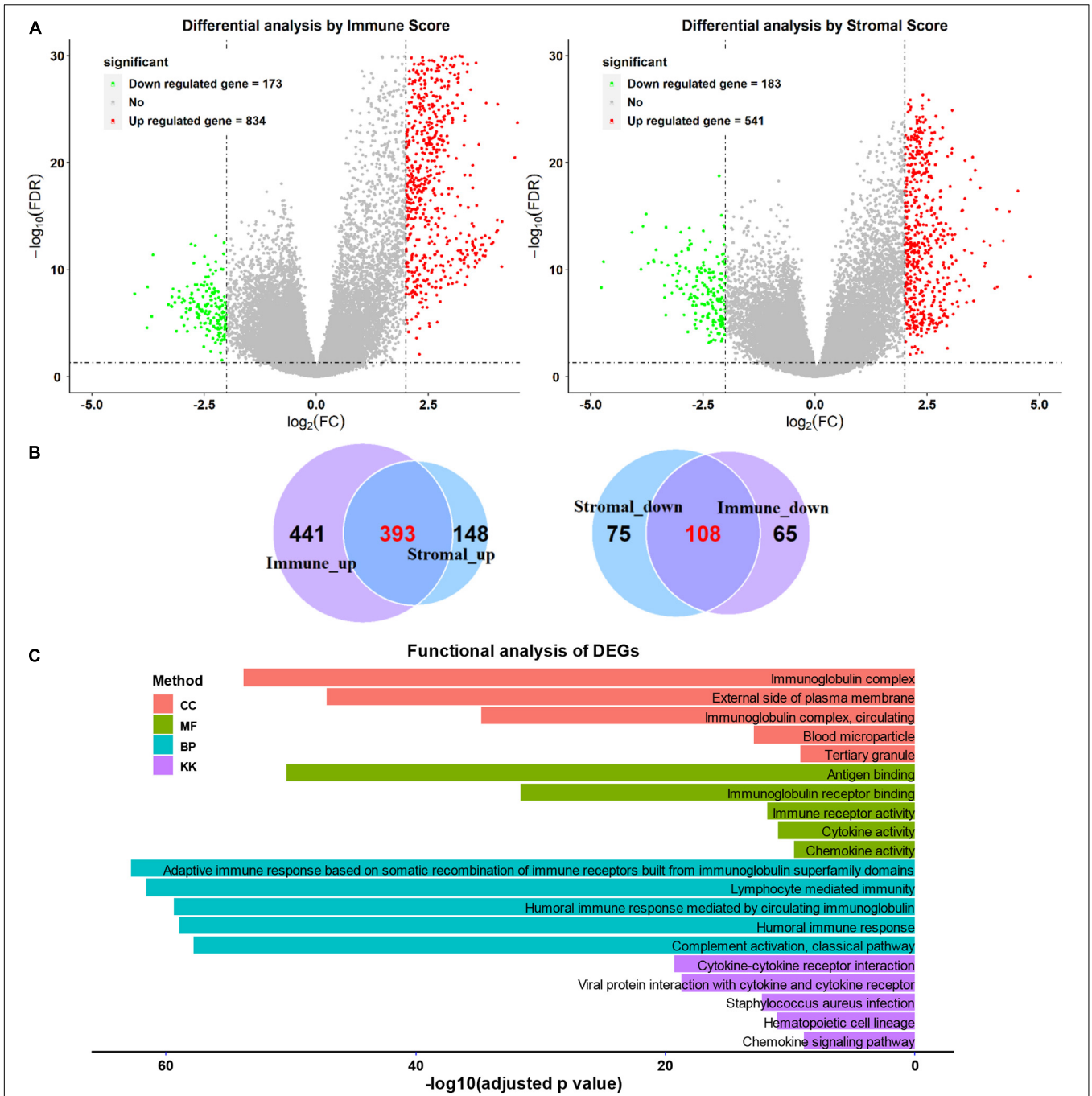

FIGURE 6 | Comparison of gene expression profiles with higher or lower immune scores or stromal scores in SARC. **(A)** The volcano plots were used to describe the differential expressed genes of immune scores and stromal scores. **(B)** The Venn plots were performed to reveal the intersections of up-regulated genes and down-regulated genes. **(C)** The top GO analyses terms and KEGG pathways terms enriched by the intersect DEGs.

Moreover, we also found that the high levels of expression of *NNAT* and the low levels of expression of *MYOC*, *MEDAG*, *TNFSF14*, *MYH11*, *NRXN1*, *P2RY13*, and *CXCR3* were associated with favorable overall survival of patients with SARC. Most of these genes were previously identified to be related to cancer prognosis, which is consistent with our findings. NNAT is a proteolipid involved in cation homeostasis. Its high expression was found to be associated with poor outcomes in a series of different cancers (Nass et al., 2017) MYOC is a skeletal muscle hypertrophy-promoting protein that was found to be downregulated in multiple cancer cachexia mouse models. The loss of MYOC in these models could induce phenotypes such as muscle fiber atrophy, sarcolemmal fragility, and impaired muscle regeneration (Judge et al., 2020). *MEDAG* is a gene

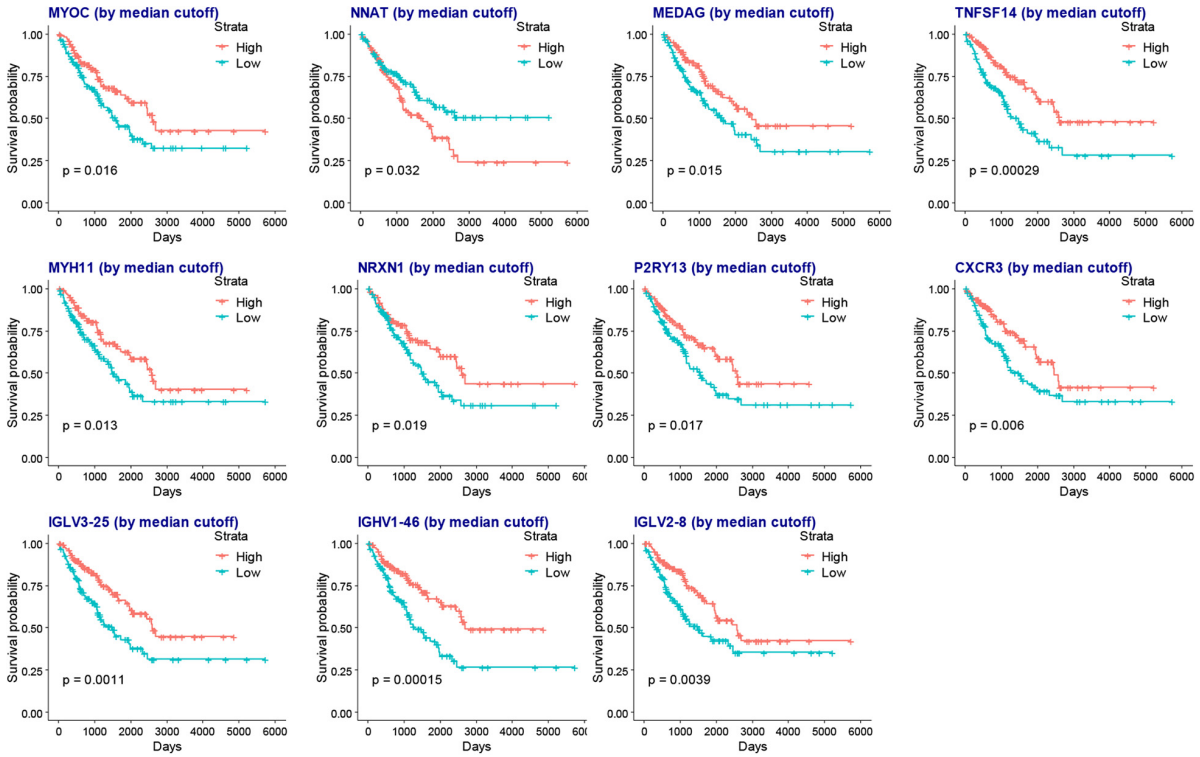

FIGURE 7 | The KM plots of lasso selected survival genes.

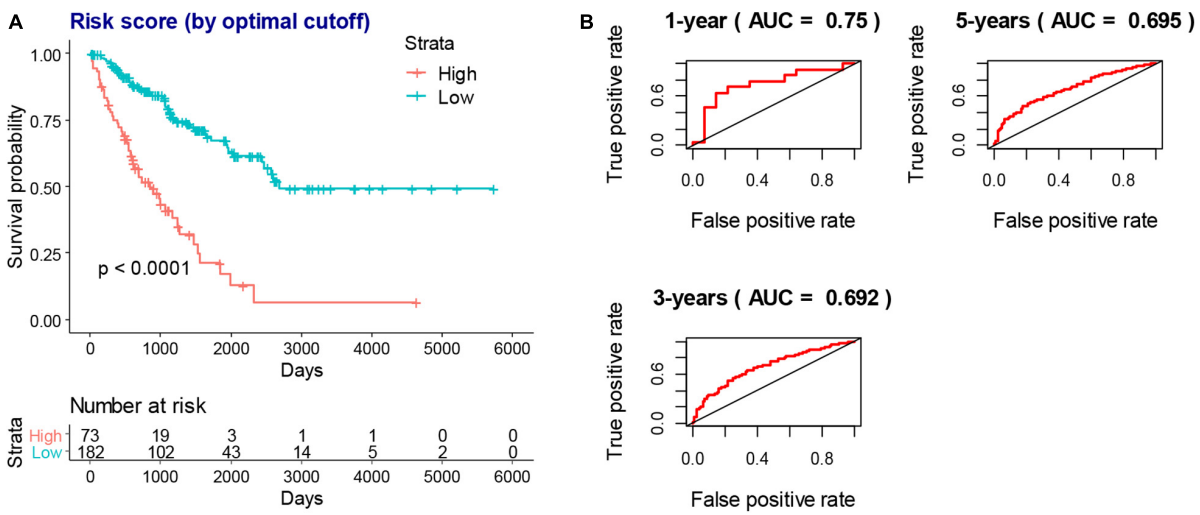

FIGURE 8 | The prognostic value of risk score model. **(A)** The higher risk scores indicated worse overall survival of SARC patients in KM models which stratified by best cutoff value. **(B)** The AUC plots of risk scores to predict the 1-year, 3-year, and 5-year overall survival of SARC patients.

involved in processes that promote adipocyte differentiation. Previously it was characterized to have a lower abundance in ovarian cancer ascites extracellular vesicles (Yamamoto et al., 2018) and ovarian cancer cells (Yeung et al., 2013). TNFSF14 is a protein primarily expressed in activated T cells, activated natural killer cells, and immature dendritic cells. It functions by stimulating effector cell functions and encouraging antitumor CD8+ T cells to enter tumors, aiding in the establishment of anti-tumoral memory (Skeate et al., 2020). *MYH11* encodes a protein that participates in muscle contraction through the hydrolysis of adenosine triphosphate; its expression levels are downregulated in several types of cancers (Alhopuro et al., 2008;

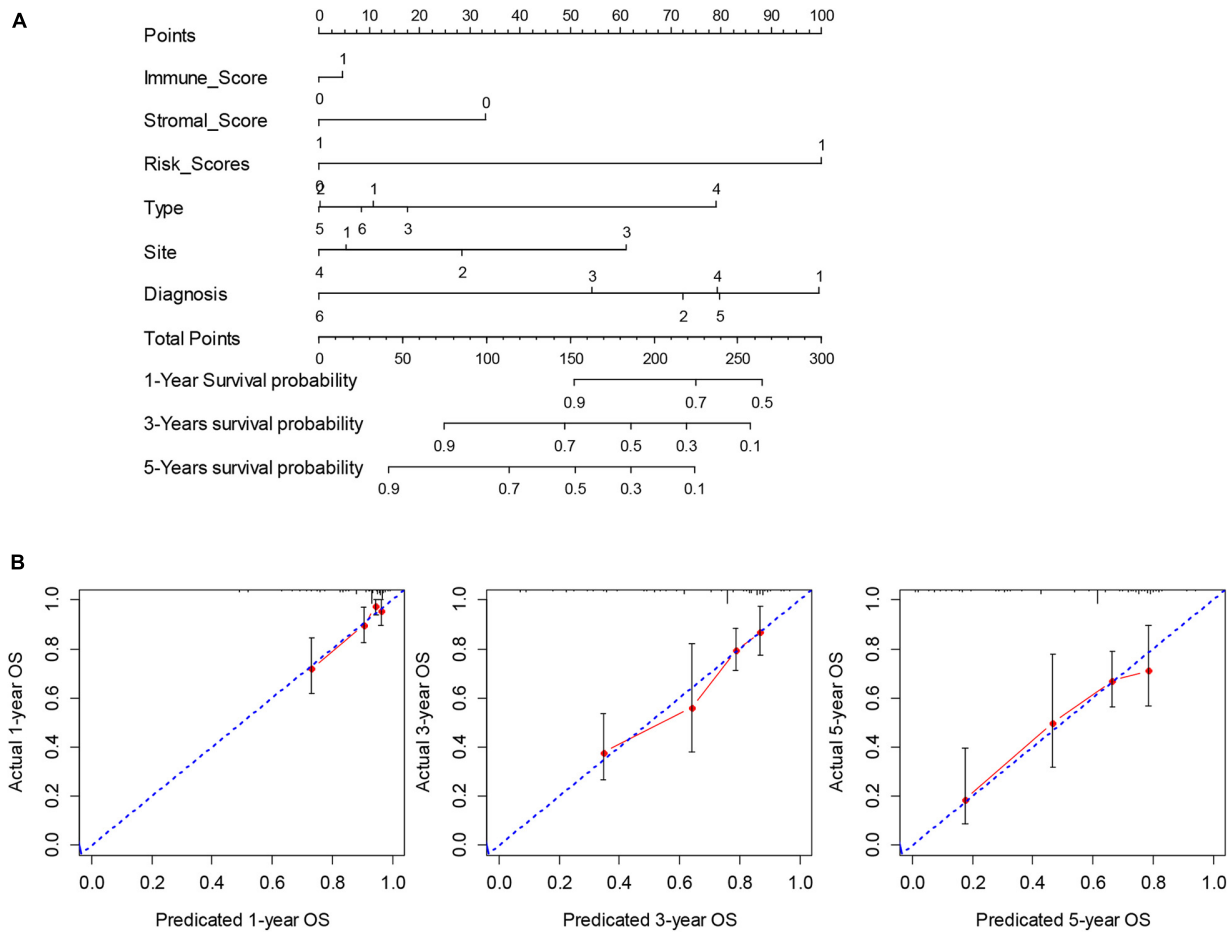

FIGURE 9 | The construction and validation of nomogram. **(A)** The multivariate Cox model based nomogram of SARC patients; Immune_Score: 0 = Low and 1 = High; Stromal_Score: 0 = Low and 1 = High; Risk_Score: 0 = Low and 1 = High; Type: 1 = Fibromatous Neoplasms, 2 = Lipomatous Neoplasms, 3 = Myomatous Neoplasms, 4 = Nerve Sheath Tumors, 5 = Soft Tissue Tumors and Sarcomas (Not Otherwise Specified) and 6 = Synovial-like Neoplasms; Diagnosis: 1 = Dedifferentiated liposarcoma, 2 = Fibromyxosarcoma, 3 = Leiomyosarcoma (Not Otherwise Specified), 4 = Malignant fibrous histiocytoma, 5 = Undifferentiated sarcoma and 6 = Others; Site: 1 = Connective, subcutaneous and other soft tissues, 2 = Retroperitoneum and peritoneum, 3 = Uterus (Not Otherwise Specified) and 4 = Others; **(B)** the calibration plots for the internal validation of current nomogram, the *x*-axis represents the nomogram predicted overall survival and the *y*-axis represents the actual overall survival of patients with SARC.

TABLE 2 | Key drugs that had potential therapeutic effects on SARC patients with lower immune or stromal scores.

Drug	*p* value	FDR
Immune score based		
trichostatin A_MCF7	2.67E-38	9.57E-35
trichostatin A_PC3	8.45E-28	1.51E-24
vorinostat_MCF7	1.38E-05	0.016
Stromal score based		
trichostatin A_MCF7	8.49E-39	3.04E-35
trichostatin A_PC3	2.80E-31	5.03E-28
vorinostat_MCF7	4.93E-05	0.059

Nie et al., 2020). *NRXN1* encodes a transmembrane protein that functions as a cell adhesion molecule in synaptic transmission (Reissner et al., 2008). Its high expression was observed to be associated with favorable overall survival of patients with oral cancers (Hirohata et al., 2018). *P2RY13* encodes a protein belongs to the family of G-protein coupled receptors, moreover, its high expression demonstrated significantly higher overall survival rates in patients with breast cancer (Xu et al., 2020) and lung adenocarcinoma (Fan et al., 2020).

After the survival analysis of TME related DEGs and the lasso based variable selection analysis, a risk score model was constructed with the key survival genes. The risk score model showed good predictions for the overall survival of patients with SARC. Furthermore, we combined the risk model with immune and stromal scores and the clinical variables to build a nomogram for the prognosis of patients with SARC. The nomogram was validated by discrimination and calibration procedures; it is the first nomogram built for the patients with SARC that includes immune related gene signatures.

We found that trichostatin A and vorinostat, which are pan-HDAC inhibitors of class I and II HDACs, had a potential therapeutic effect on the patients with lower immune or stromal scores and worse survival. HDACs play a critical role in the regulation of transcription by promoting the deacetylation of histone proteins (Kulka et al., 2020). The upregulation of specific HDACs have been found in different cancers, including SARC (Tang et al., 2017; Banik et al., 2019). HDAC inhibitors have been shown to have anti-inflammatory properties that can impact cancer therapy (Hull et al., 2016). HDAC inhibitors are closely associated with immunotherapy; they can enhance the expression of cancer antigens, decrease immunosuppressive cell populations like the myeloid-derived suppressor cell, regulate specific suppressive pathways, and induce specific chemokine expression on T cells (Banik et al., 2019). In SARCs, the HDAC inhibitors showed multiple tumor inhibitory effects that included upregulating tumor suppressor genes, downregulating oncogenes, promoting apoptosis (Su et al., 2010) and cell cycle arrest (Sakimura et al., 2005), decreasing invasion, metastasis and angiogenesis (Ailenberg and Silverman, 2003; Lee et al., 2015), inducing reactive oxygen species (ROS) production (Laporte et al., 2017), autophagy (Yamamoto et al., 2008), and cell differentiation (Di Pompo et al., 2015). Our study found that trichostatin A and vorinostat had the potential to reverse the lower immune status of the TME in SARCs and thereby improve the survival of patients; providing new insights into the relationship between HDAC inhibitors and SARC.

Our study had certain limitations. First, due to the lack of RNA seq or microarray SARC data, we only included TCGA data. However, we expect our results to be externally validated with future SARC genomic data. Secondly, the underlying mechanisms of SARC and the key survival genes and HDAC inhibitors should be further explored and characterized.

CONCLUSION

In summary, our study found that high immune and stromal cell infiltration levels were associated with better SARC prognosis. The risk gene signature related nomogram is a useful predictive tool for the overall survival of patients with SARC. Finally, we found that two HDAC inhibitors, trichostatin A and vorinostat, may have potential therapeutic value for patients with SARC and suggest this relationship be further investigated.

DATA AVAILABILITY STATEMENT

The original contributions presented in the study are included in the article/**Supplementary Material**, further inquiries can be directed to the corresponding author/s.

AUTHOR CONTRIBUTIONS

QW and DD designed the study. DD and LX analyzed the data and wrote the manuscript which was checked by QW. YS and JL collected the data. All authors contributed to the article and approved the submitted version.

FUNDING

This study was partially supported by the National Natural Science Foundation of China (Nos. 81572952 and 82073332).

SUPPLEMENTARY MATERIAL

The Supplementary Material for this article can be found online at: https://www.frontiersin.org/articles/10.3389/fgene.2021.620705/full#supplementary-material

Supplementary Figure 1 | The significant associations between stromal score and the clinical factors of patients with SARC. The age **(A)**, gender **(B)**, primary diagnosis **(C)**, disease type **(D)**, and primary site **(E)** were significantly associated with the stromal scores calculated by ESTIMATE algorithm.

Supplementary Figure 2 | The clinical factors of patients with SARC that were not associated with the immune scores. There were no association between the immune scores and the clinical factors of SARC, which comprised race, tumor total necrosis percent, tumor depth, person neoplasm cancer status, mitotic count, metastatic diagnosis, local disease recurrence, leiomyosarcoma histologic subtype, and margin status.

Supplementary Figure 3 | The clinical factors of SARC that were not associated with the stromal scores. There were no association between the stromal scores and the clinical factors of SARC, which comprised race, tumor total necrosis percent, tumor depth, person neoplasm cancer status, mitotic count, metastatic diagnosis, local disease recurrence, leiomyosarcoma histologic subtype, and margin status.

Supplementary Figure 4 | The heatmap of DEGs profiles between groups of high and low immune or stromal scores.

Supplementary Table 1 | The immune scores and stromal scores of 255 patients with SARC.

Supplementary Table 2 | The DEGs between high and low immune score groups.

Supplementary Table 3 | The DEGs between high and low stromal score groups.

Supplementary Table 4 | The functional analysis of overlapped DEGs with GO BP items.

Supplementary Table 5 | The functional analysis of overlapped DEGs with GO CC items.

Supplementary Table 6 | The functional analysis of overlapped DEGs with GO MF items.

Supplementary Table 7 | The functional analysis of overlapped DEGs with KEGG items.

Supplementary Table 8 | The significant survival related DEGs by univariate Cox analysis.

Supplementary Table 9 | The coefficients of each gene after the lasso analysis.

REFERENCES

Ailenberg, M., and Silverman, M. (2003). Differential effects of trichostatin A on gelatinase A expression in 3T3 fibroblasts and HT-1080 fibrosarcoma cells: implications for use of TSA in cancer therapy. *Biochem. Biophys. Res. Commun.* 302, 181–185. doi: 10.1016/s0006-291x(03)00150-5

Alhopuro, P., Phichith, D., Tuupanen, S., Sammalkorpi, H., Nybondas, M., Saharinen, J., et al. (2008). Unregulated smooth-muscle myosin in human intestinal Neoplasia. *Proc. Natl. Acad. Sci. U.S.A.* 105, 5513–5518.

Alspach, E., Lussier, D. M., Miceli, A. P., Kizhvatov, I., DuPage, M., Luoma, A. M., et al. (2019). MHC-II neoantigens shape tumour immunity and response to immunotherapy. *Nature* 574, 696–701. doi: 10.1038/s41586-019-1671-8

Banik, D., Moufarrij, S., and Villagra, A. (2019). Immunoepigenetics combination therapies: an overview of the role of HDACs in cancer immunotherapy. *Int. J. Mol. Sci.* 20:2241. doi: 10.3390/ijms20092241

Carter, S. L., Cibulskis, K., Helman, E., McKenna, A., Shen, H., Zack, T., et al. (2012). Absolute quantification of somatic DNA alterations in human cancer. *Nat. Biotechnol.* 30, 413–421. doi: 10.1038/nbt.2203

D'Angelo, S. P., Shoushtari, A. N., Keohan, M. L., Dickson, M. A., Gounder, M. M., Chi, P., et al. (2017). Combined KIT and CTLA-4 blockade in patients with refractory GIST and other advanced sarcomas: a phase Ib study of dasatinib plus Ipilimumab. *Clin. Cancer Res.* 23, 2972–2980. doi: 10.1158/1078-0432.ccr-16-2349

Di Pompo, G., Salerno, M., Rotili, D., Valente, S., Zwergel, C., Avnet, S., et al. (2015). Novel histone deacetylase inhibitors induce growth arrest, apoptosis, and differentiation in sarcoma cancer stem cells. *J. Med. Chem.* 58, 4073–4079. doi: 10.1021/acs.jmedchem.5b00126

Fan, T., Zhu, M., Wang, L., Liu, Y., Tian, H., Zheng, Y., et al. (2020). Immune profile of the tumor microenvironment and the identification of a four-gene signature for lung adenocarcinoma. *Aging (Albany NY)* 12. doi: 10.18632/aging.202269 [Epub ahead of print].

Fujii, H., Arakawa, A., Utsumi, D., Sumiyoshi, S., Yamamoto, Y., Kitoh, A., et al. (2014). CD8(+) tumor-infiltrating lymphocytes at primary sites as a possible prognostic factor of cutaneous angiosarcoma. *Int. J. Cancer* 134, 2393–2402. doi: 10.1002/ijc.28581

Garcia-Gomez, A., Rodriguez-Ubreva, J., and Ballestar, E. (2018). Epigenetic interplay between immune, stromal and cancer cells in the tumor microenvironment. *Clin. Immunol.* 196, 64–71. doi: 10.1016/j.clim.2018.02.013

Goldman, M., Craft, B., Hastie, M., Repeèka, K., Kamath, A., McDade, F., et al. (2019). The UCSC Xena platform for public and private cancer genomics data visualization and interpretation. *bioRxiv [Preprint]* doi: 10.1101/326470

Hanahan, D., and Coussens, L. M. (2012). Accessories to the crime: functions of cells recruited to the tumor microenvironment. *Cancer Cell* 21, 309–322. doi: 10.1016/j.ccr.2012.02.022

Hirohata, H., Yanagawa, T., Takaoka, S., Uchida, F., Shibuya, Y., et al. (2018). Synaptic-adhesion molecules neurexin 1 and neuroligin 1 as novel prognostic factors in oral squamous cell carcinoma. *J. Dents. Dent. Med.* 1:111.

Hong, W., Yuan, H., Gu, Y., Liu, M., Ji, Y., Huang, Z., et al. (2020). Immune-related prognosis biomarkers associated with osteosarcoma microenvironment. *Cancer Cell Int.* 20:83.

Hsu, H. M., Chu, C. M., Chang, Y. J., Yu, J. C., Chen, C. T., Jian, C. E., et al. (2019). Six novel immunoglobulin genes as biomarkers for better prognosis in triple-negative breast cancer by gene co-expression network analysis. *Sci. Rep.* 9:4484.

Hui, J. Y. (2016). Epidemiology and etiology of sarcomas. *Surg. Clin. North Am.* 96, 901–914. doi: 10.1016/j.suc.2016.05.005

Hull, E. E., Montgomery, M. R., and Leyva, K. J. H. D. A. C. (2016). Inhibitors as epigenetic regulators of the immune system: impacts on cancer therapy and inflammatory diseases. *Biomed. Res. Int.* 2016: 8797206.

Isaeva, O. I., Sharonov, G. V., Serebrovskaya, E. O., Turchaninova, M. A., Zaretsky, A. R., Shugay, M., et al. (2019). Intratumoral immunoglobulin isotypes predict survival in lung adenocarcinoma subtypes. *J. Immunother. Cancer* 7:279.

Judge, S. M., Deyhle, M. R., Neyroud, D., Nosacka, R. L., D'Lugos, A. C., Cameron, M. E., et al. (2020). MEF2c-dependent downregulation of myocilin mediates cancer-induced muscle wasting and associates with cachexia in patients with cancer. *Cancer Res.* 80, 1861–1874. doi: 10.1158/0008-5472.can-19-1558

Kulka, L. A. M., Fangmann, P. V., Panfilova, D., and Olzscha, H. (2020). Impact of HDAC inhibitors on protein quality control systems: consequences for precision medicine in malignant disease. *Front. Cell Dev. Biol.* 8:425. doi: 10.3389/fcell.2020.00425

Lamb, J. (2007). The Connectivity Map: a new tool for biomedical research. *Nat. Rev. Cancer* 7, 54–60. doi: 10.1038/nrc2044

Laporte, A. N., Barrott, J. J., Yao, R. J., Poulin, N. M., Brodin, B. A., Jones, K. B., et al. (2017). HDAC and proteasome inhibitors synergize to activate pro-apoptotic factors in synovial sarcoma. *PLoS One* 12:e0169407. doi: 10.1371/journal.pone.0169407

Lee, D. H., Zhang, Y., Kassam, A. B., Park, M. J., Gardner, P., Prevedello, D., et al. (2015). Combined PDGFR and HDAC inhibition overcomes PTEN disruption in chordoma. *PLoS One* 10:e0134426. doi: 10.1371/journal.pone.0134426

Li, T., Fu, J., Zeng, Z., Cohen, D., Li, J., Chen, Q., et al. (2020). TIMER2.0 for analysis of tumor-infiltrating immune cells. *Nucleic Acids Res.* 48, W509–W514.

Maki, R. G., Jungbluth, A. A., Gnjatic, S., Schwartz, G. K., D'Adamo, D. R., Keohan, M. L., et al. (2013). A pilot study of anti-CTLA4 antibody ipilimumab in patients with synovial sarcoma. *Sarcoma* 2013:168145.

Musa, A., Ghoraie, L. S., Zhang, S. D., Glazko, G., Yli-Harja, O., Dehmer, M., et al. (2018). A review of connectivity map and computational approaches in pharmacogenomics. *Brief. Bioinform.* 19, 506–523.

Nass, N., Walter, S., Jechorek, D., Weissenborn, C., Ignatov, A., Haybaeck, J., et al. (2017). High neuronatin (NNAT) expression is associated with poor outcome in breast cancer. *Virchows Arch.* 471, 23–30. doi: 10.1007/s00428-017-2154-7

Ni, J., Wu, Y., Qi, F., Li, X., Yu, S., Liu, S., et al. (2019). Screening the cancer genome atlas database for genes of prognostic value in acute myeloid leukemia. *Front. Oncol.* 9:1509. doi: 10.3389/fonc.2019.01509

Nie, M. J., Pan, X. T., Tao, H. Y., Xu, M. J., Liu, S. L., Sun, W., et al. (2020). Clinical and prognostic significance of MYH11 in lung cancer. *Oncol. Lett.* 19, 3899–3906.

Oike, N., Kawashima, H., Ogose, A., Hotta, T., Hatano, H., Ariizumi, T., et al. (2018). Prognostic impact of the tumor immune microenvironment in synovial sarcoma. *Cancer Sci.* 109, 3043–3054. doi: 10.1111/cas.13769

Ostroumov, D., Fekete-Drimusz, N., Saborowski, M., Kuhnel, F., and Woller, N. (2018). CD4 and CD8 T lymphocyte interplay in controlling tumor growth. *Cell Mol. Life Sci.* 75, 689–713. doi: 10.1007/s00018-017-2686-7

Pan, X. B., Lu, Y., Huang, J. L., Long, Y., and Yao, D. S. (2019). Prognostic genes in the tumor microenvironment in cervical squamous cell carcinoma. *Aging (Albany NY)* 11, 10154–10166. doi: 10.18632/aging.102429

Raj, S., Miller, L. D., and Triozzi, P. L. (2018). Addressing the adult soft tissue sarcoma microenvironment with intratumoral immunotherapy. *Sarcoma* 2018:9305294.

Reissner, C., Klose, M., Fairless, R., and Missler, M. (2008). Mutational analysis of the neurexin/neuroligin complex reveals essential and regulatory components. *Proc. Natl. Acad. Sci. U.S.A.* 105, 15124–15129. doi: 10.1073/pnas.0801639105

Sakimura, R., Tanaka, K., Nakatani, F., Matsunobu, T., Li, X., Hanada, M., et al. (2005). Antitumor effects of histone deacetylase inhibitor on Ewing's family tumors. *Int. J. Cancer* 116, 784–792. doi: 10.1002/ijc.21069

Skeate, J. G., Otsmaa, M. E., Prins, R., Fernandez, D. J., Da Silva, D. M., and Kast, W. M. (2020). TNFSF14: LIGHTing the way for effective cancer immunotherapy. *Front. Immunol.* 11:922. doi: 10.3389/fimmu.2020.00922

Su, L., Cheng, H., Sampaio, A. V., Nielsen, T. O., and Underhill, T. M. (2010). EGR1 reactivation by histone deacetylase inhibitors promotes synovial sarcoma cell death through the PTEN tumor suppressor. *Oncogene* 29, 4352–4361. doi: 10.1038/onc.2010.204

Subramanian, A., Narayan, R., Corsello, S. M., Peck, D. D., Natoli, T. E., Lu, X., et al. (2017). A next generation connectivity map: L1000 platform and the first 1,000,000 profiles. *Cell* 171, 1437–1452.e17.

Tang, F., Choy, E., Tu, C., Hornicek, F., and Duan, Z. (2017). Therapeutic applications of histone deacetylase inhibitors in sarcoma. *Cancer Treat. Rev.* 59, 33–45. doi: 10.1016/j.ctrv.2017.06.006

Tawbi, H. A., Burgess, M., Bolejack, V., Van Tine, B. A., Schuetze, S. M., Hu, J., et al. (2017). Pembrolizumab in advanced soft-tissue sarcoma and bone sarcoma

(SARC028): a multicentre, two-cohort, single-arm, open-label, phase 2 trial. *Lancet Oncol.* 18, 1493–1501. doi: 10.1016/s1470-2045(17)30624-1

Toulmonde, M., Penel, N., Adam, J., Chevreau, C., Blay, J. Y., Le Cesne, A., et al. (2018). Use of PD-1 targeting, macrophage infiltration, and IDO pathway activation in sarcomas: a phase 2 clinical trial. *JAMA Oncol.* 4, 93–97. doi: 10.1001/jamaoncol.2017.1617

Wang, H., Wu, X., and Chen, Y. (2019). Stromal-immune score-based gene signature: a prognosis stratification tool in gastric cancer. *Front. Oncol.* 9:1212. doi: 10.3389/fonc.2019.01212

Xu, M., Li, Y., Li, W., Zhao, Q., Zhang, Q., Le, K., et al. (2020). Immune and stroma related genes in breast cancer: a comprehensive analysis of tumor microenvironment based on the cancer genome atlas (TCGA) Database. *Front. Med. (Lausanne)* 7:64. doi: 10.3389/fmed.2020.00064

Xu, Q., Zhang, Z., Chen, Z., Zhang, B., Zhao, C., Zhang, Y., et al. (2019). Nonspecific immunoglobulin G is effective in preventing and treating cancer in mice. *Cancer Manag. Res.* 11, 2073–2085. doi: 10.2147/cmar.s188172

Yamamoto, C. M., Oakes, M. L., Murakami, T., Muto, M. G., Berkowitz, R. S., and Ng, S. W. (2018). Comparison of benign peritoneal fluid- and ovarian cancer ascites-derived extracellular vesicle RNA biomarkers. *J. Ovarian. Res.* 11:20.

Yamamoto, S., Tanaka, K., Sakimura, R., Okada, T., Nakamura, T., Li, Y., et al. (2008). Suberoylanilide hydroxamic acid (SAHA) induces apoptosis or autophagy-associated cell death in chondrosarcoma cell lines. *Anticancer Res.* 28, 1585–1591.

Yeung, T. L., Leung, C. S., Wong, K. K., Samimi, G., Thompson, M. S., Liu, J., et al. (2013). TGF-beta modulates ovarian cancer invasion by upregulating CAF-derived versican in the tumor microenvironment. *Cancer Res.* 73, 5016–5028. doi: 10.1158/0008-5472.can-13-0023

Yoshihara, K., Shahmoradgoli, M., Martinez, E., Vegesna, R., Kim, H., Torres-Garcia, W., et al. (2013). Inferring tumour purity and stromal and immune cell admixture from expression data. *Nat. Commun.* 4: 2612.

Zhang, Z., Chen, D., Li, Z., Liu, Z., Yan, L., and Xu, Z. (2020). Bioinformatics analysis to screen the key prognostic genes in tumor microenvironment of bladder cancer. *Biomed. Res. Int.* 2020:6034670.

Conflict of Interest: The authors declare that the research was conducted in the absence of any commercial or financial relationships that could be construed as a potential conflict of interest.

frontiers in Oncology

ORIGINAL RESEARCH
published: 09 February 2021
doi: 10.3389/fonc.2020.588360

Long Non-Coding RNA ELFN1-AS1 Promoted Colon Cancer Cell Growth and Migration *via* the miR-191-5p/ Special AT-Rich Sequence-Binding Protein 1 Axis

Yongjun Du[1†], *Yanmei Hou*[1†], *Yongbo Shi*[2†], *Juan Liu*[3] *and Tingxin Li*[4*]

[1] Department of Proctology, Hospital of Chengdu University of Traditional Chinese Medicine, Chengdu, China, [2] Department of Proctology, Zigong City Hospital of Traditional Chinese Medicine, Zigong City, China, [3] Huai'an Second People's Hospital and The Affiliated Huai'an Hospital of Xuzhou Medical University, Huai'an, China, [4] Health Management Center, Sichuan Provincial People's Hospital, University of Electronic Science and Technology of China, Chengdu, China

Long non-coding RNAs (lncRNAs) are reported to participate in tumor development. It has been manifested in previous researches that lncRNA *ELFN1-AS1* is involved in early-stage colon adenocarcinoma with potential diagnostic value. However, no studies have revealed the specific mechanism of *ELFN1-AS1* in colon cancer, and there are no other studies on whether *ELFN1-AS1* is associated with tumorigenesis. In our study, *ELFN1-AS1* with high expression in colon cancer was selected by TCGA analysis, and the survival analysis was carried out to verify it. Subsequently, qRT-PCR was adopted for validating the results in tissues and cell lines. Cell counting kit-8 (CCK8), 5-ethynyl-2'-deoxyuridine (EdU), cell colon, cell apoptosis, cell cycle, cell migration, and invasion assays were utilized to assess the role of *ELFN1-AS1* in colon cancer. Results uncovered that *ELFN1-AS1* expression was prominently raised in colon cancer cells and tissues. *ELFN1-AS1* decrement restrained cells to grow through interfering with distribution of cell cycle and promoting apoptosis. Meanwhile, *ELFN1-AS1* decrement weakened the capacity of cells to migrate and invade. What's more, *ELFN1-AS1* was uncovered to act as a competing endogenous RNA (ceRNA) to decrease miR-191-5p expression, thus raising *special AT-rich sequence-binding protein 1* (*SATB1*), a downstream target of ceRNA. To sum up, *ELFN1-AS1* drives colon cancer cells to proliferate and invade through adjusting the miR-191-5p/*SATB1* axis. The above results disclose that lncRNA *ELFN1-AS1* is possibly a novel treatment target for colon cancer cases.

Keywords: long non-coding RNA ELFN1-AS1, special AT-rich sequence-binding protein 1, colon cancer, ceRNA, miR-191-5p

OPEN ACCESS

Edited by:
Xiaochen Wang,
University of Texas Southwestern Medical Center, United States

Reviewed by:
Jing Zhao,
Brigham and Women's Hospital and Harvard Medical School, United States
Dongming Chen,
Nanjing Medical University, China

***Correspondence:**
Tingxin Li
litingxin@med.uestc.edu.cn

[†]These authors have contributed equally to this work

Specialty section:
This article was submitted to Cancer Genetics, a section of the journal Frontiers in Oncology

Received: *28 July 2020*
Accepted: *09 November 2020*
Published: *09 February 2021*

Citation:
Du Y, Hou Y, Shi Y, Liu J and Li T (2021) Long Non-Coding RNA ELFN1-AS1 Promoted Colon Cancer Cell Growth and Migration via the miR-191-5p/ Special AT-Rich Sequence-Binding Protein 1 Axis. Front. Oncol. 10:588360. doi: 10.3389/fonc.2020.588360

INTRODUCTION

The American Cancer Society statistics manifest that colon cancer has a incidence rate of 10.2% and a death rate of 9.2% in human, ascending from the fourth place to the second (1, 2). Colon cancer cases at the early stage are generally treated by tumor resection, and the combined therapy with chemotherapeutic drugs is usually applied in colon cancer cases at different stages, especially at the late stage (3). These drugs include cytotoxic drugs (oxaliplatin, 5-fluorouracil, capecitabine and irinotecan) and biological agents (panitumumab, bevacizumab and cetuximab) (4, 5). In the beginning, the combined chemotherapy is useful in most colon cancer cases, but owing to drug resistance, the disease recurs in approximately 50% of the cases, with over 10% reduction in the five-year survival rate of late-stage cases (6, 7). Besides, liver metastasis arises at the time of first diagnosis in about 25% of colon cancer cases, and occurs within three years after first surgery in about 50% of them (8). Thus, investigation of the molecular mechanism of metastasis meets the clinical needs.

Long non-coding RNAs (lncRNAs) exert vital impacts in diversely adjusting gene expression, including chromatin modification as well as transcriptional and posttranscriptional processing (9). Aberrant modulation of lncRNAs usually induces tumor to form, grow and metastasize (10). For example, lncRNA *DLEU2* adjusts non-small cell lung cancer cells to proliferate and invade by controlling the miR-30c-5p/SOX9 axis (11). In addition, the elevated lncRNA *PANDAR* indicates poor prognosis and boosts cervical cancer cells to proliferate (12). LncRNA *ELFN1-AS1* promotes esophageal cancer progression by up-regulating GFPT1 *via* sponging miR-183-3p (13). Meanwhile, *ELFN1-AS1* accelerates cell proliferation, invasion and migration *via* regulating miR-497-3p/CLDN4 axis in ovarian cancer (14). What more, previous study has revealed that *ELFN1-AS1* is involved in early-stage colon adenocarcinoma with potential diagnostic value (15). However, no studies have revealed the specific mechanism by which *ELFN1-AS1* plays a role in colon cancer, and researches on whether *ELFN1-AS1* is linked to tumorigenesis are deficient.

MicroRNAs (miRNAs) are small ncRNAs that bind to the three prime untranslated region (3'-UTR) of downstream mRNAs and give rise to mRNA degradation or translation inhibition (16). The aberrant modulation of miRNAs commonly boosts cancers to form and develop (17). For example, the elevated miRNA-146a represses biological behaviors of ESCC by IRS2 suppression (18). Besides, miR-146b-5p promotes papillary thyroid carcinoma cells to migrate and invade (19). It has been identified that miR-191-5p restrains tumor in renal cell carcinoma (20) and colon adenocarcinoma (21), but whether miR-191-5p is co-regulated with *ELFN1-AS1* to regulate colon cancer is unknown.

In this research, lncRNA *ELFN1-AS1* expression level was identified to rise in colon cancer cells and tissues. The rising *ELFN1-AS1* facilitated colon cancer cells to grow, migrate and invade. What's more, *ELFN1-AS1* sponged miR-191-5p and played a biological role.

MATERIALS AND METHODS

Collection of Colon Cancer Samples and Culture of Colon Cancer Cells

Twenty pairs of colon cancer samples were collected from Huai'an Second People's Hospital and The Affiliated Huai'an Hospital of Xuzhou Medical University. All patients gave the written informed consent, and all assay regimens gained the approval of the Clinical Research Ethics Committees of Huai'an Second People's Hospital and The Affiliated Huai'an Hospital of Xuzhou Medical University.

The normal colonic epithelial cell line NCM460 and colon cancer cell lines (SW620, HT-29, HCT 116, LoVo, and SW480) were purchased from Cell Bank of Typical Culture Preservation Commission, Chinese academy of Sciences. Then they were cultured in a humid environment with 5% CO_2 at 37°C in RPMI-1640 containing 10% fetal bovine serum.

Real-Time PCR Assay, Transfection of Cells as Well as Production and Transduction of Lentiviruses

TRIzol reagent (Invitrogen) was utilized for total RNA extraction from colon cancer cells as per the guideline of the manufacturer. After that, the extracted RNA was subjected to reverse transcription into cDNA using the Reverse Transcription Kit from Takara. **Table 1** displays the applied primers.

MiR-191-5p, anti-miR-191-5p, miR-NC, and anti-miR-NC that were applied for cell transfection were synthesized by Ruibo (Guangzhou, China), and the plasmid pcDNA-3.1-special AT-rich sequence-binding protein 1 (SATB1) was provided by Santa Cruz. As per the guideline of the manufacturer, transfection with oligonucleotides was executed with the use of lipofectamine 2000 reagent from Invitrogen.

The aforementioned shRNAs sequences aiming for *ELFN1-AS1* underwent cloning into the pLKO.1 vector from Addgene as

TABLE 1 | Primers used in the study.

	Forward	Reverse
ELFN1-AS1	5′- AAAAGTTGACGCCGCATTCT -3′	5′- GAGAATGGATTGTGGGTGCC-3′
miR-191-5p	5′-ACACTCCAGCTGGGCGACGAAAACCCUAA- 3′	5′- CTCAACTGGTGTCGTGGAGTCGGCAATTCAGTTGAGTTCCGTTG -3′
U6	5′-CTCGCTTCGGCAGCACA-3′	5′-AACGCTTCACGAATTTGCGT-3′
SATB1	5′- GATCATTTGAACGAGGCAACTCA-3′	5′- TGGACCCTTCGGATCACTCA-3′
GAPDH	5′- TCGGAGTCAACGGATTTGGTCGT-3′	5′- TGCCATGGGTGGAATCATATTGGA-3

per the guideline of the manufacturer. Lentiviruses aiming for *ELFN1-AS1* (sh-*ELFN1-AS1*) and the empty lentiviral vector (sh-NC) were employed to co-infect cells together with 8μg/mL Polybrene for subsequent assays.

Cell Counting Kit-8 Assay and 5-ethynyl-2′-deoxyuridine Assay

In a 96-well plate, the cells treated in advance were inoculated and then incubated with CCK8 reagent provided by DingGuo Bio for 2 h at 37°C. Finally, a microplate reader provided by BioTek was employed to detect the absorbance (450 nm).

Next, EdU assay was executed with the use of Cell-Light EdU Cell Proliferation/DNA Kit acquired from Guangzhou RiboBio Co., Ltd. (China). In detail, the cells were immobilized with 4% paraformaldehyde and dyed with Apollo Dye Solution subsequent to EdU incubation for 2 h, followed by mounting with Hoechst 33342. Ultimately, photographing and quantification were carried out for EdU-positive cells.

Transwell Assay, Cell Cycle, and Apoptosis Assay

Cells were inoculated into the Transwell chambers undergoing 30 min of Matrigel coating at 37°C on the upper side, while 500 μl of complete medium into the bottom side. After 48 h, the cells on the bottom side were rinsed with PBS, immobilized in 4% paraformaldehyde and dyed with crystal violet solution. Ultimately, photos were taken under a microscope. Analysis for cells in each group was conducted thrice.

Next, the cells were trypsinized for separation, rinsed twice with forecooling PBS, and immobilized in 70% ethanol at -20°C nightlong. Following suspension in 100 μg/ml of RNaseA and 50 μg/ml of propidium iodide (PI) both provided by KeyGen BioTECH, the immobilized cells were suspended and incubated at room temperature for 40 min. Eventually, the cells were filtered, and flow cytometry was executed to detect the cell cycle.

For apoptosis assay, the cells were washed with PBS and then stained using the Annexin V-FITC Apoptosis Detection Kit (Affymetrix eBioscience) according to the instructions. Ultimately, the cells were analyzed with a FACS flow cytometer (BD Biosciences).

Western Blot Detection

RIPA lysis buffer provided by Thermo Scientific was utilized for protein separation from cells, and the protein concentration was measured using BCA Protein assay kit from Beyotime. Later, electrophoresis was carried out for proteins separation, and the separated proteins were transferred onto a PVDF membrane and blocked by skim milk (5%). Afterwards, SATB1 (Lot No. ab92307) and GAPDH (Lot No. ab9484) primary antibodies from Abcam were applied for membrane incubation nightlong at 4°C, and secondary antibodies conjugated with horseradish peroxidase were utilized for sealing the membrane at room temperature for 1 h. Ultimately, BioSpectrum 600 Imaging System from UVP (CA, USA) was adopted to obtain images. The selected concentration in this research was 1: 500.

RNA-Binding Protein Immunoprecipitation Experiment

In RIP experiment, the EZ-Magna RIP Kit used in the RIP assay was commercially acquired from Millipore (Billerica, MA, USA). After miR-191-5p or miR-NC transfection into cells, Ago2-RIP assays were executed. In the first place, the cells underwent lysis by RIP lysis buffer with RNase and proteinase inhibitors provided by Millipore. Secondly, the RIP lysates were subjected to RIP buffer, which contained magnetic beads conjugated with human anti-Ago2 antibody or nonspecific mouse IgG antibody (Millipore). Next, the immunoprecipitates were digested using proteinase K, and the gathering of *ELFN1-AS1* was examined using RT-PCR and gel staining. Ultimately, the RNA concentration was detected *via* a NanoDrop spectrophotometer, and q-RT-PCR analysis was conducted for the purified RNA.

Dual Luciferase Reporter Assay

Following amplification of the 3'-UTRs of SATB1 and *ELFN1-AS1*, they were independently cloned into the firefly luciferase gene downstream in the pGL3 vector from Promega, which was named as wild-type (WT) 3'-UTR. According to the detection using QuickChange site-directed mutagenesis kit from Stratagene (Cedar Creek, USA), there were mutant miR-191-5p binding sites in SATB1 3'-UTR, which was called MUT 3'-UTR. Colon cancer cells were transfected together with WT-3'-UTR or MUT-3'-UTR and miR-NC or miR-191-5p. Subsequent to 48 h of transfection, dual luciferase reporter assay system provided by Promega was employed for the luciferase assay. Analysis in each group was executed thrice.

Subcellular Distribution

The Cytoplasmic and Nuclear RNA Purification Kit (Norgen Biotek Corp.) was used to examine RNA degradation in the cytoplasm or nucleus. SW620 and HT-29 cells were lysed on ice for 5 min and then centrifuged at 12,000xg for 3 min. The supernatant was collected to examine RNAs originating in the cytoplasm, and the nuclear pellet was employed to extract RNAs from the nuclei. Total RNA in each fraction was quantified using RT-qRCR with U6 and GAPDH as internal references for the nucleus and cytoplasm, respectively.

Immunofluorescence Staining

After immobilization and sealing, tissues were incubated in antibody of SATB1 (Invitrogen, Carlsbad, California, USA) at 4°C for 24 h. After being washed, cells were incubated in FITC-labeled IgG (H+L) (Beyotime, Nantong, China) for 60 min. Later, DAPI was used for nucleus staining. The protocol was described in detail in the previous study (22).

Tumor Formation in the Body

BALB/c-nu/nu mice at the age of five weeks received subcutaneous seeding of 2×10^6 SW620 cells (sh-*ELFN1-AS1* or sh-NC) in the flank. Tumor volumes were determined every 7 days and calculated as (length x width^2)/2. Twenty-eight days after subcutaneous injection, tumors were obtained and weighed following the execution of the mice. As per the US National Institute of Health Guidelines for Use of Experimental Animals,

the mice were maintained and received experiments in SPF Animal Laboratory at Xuzhou Medical University that were approved by the Ethnic Committee for Experimental Animals in Huai'an Second People's Hospital and The Affiliated Huai'an Hospital of Xuzhou Medical University.

Statistical Analysis

GraphPad Prism 6.0 software (GraphPad Software, Inc.) was used for statistical analyses. Experimental results are expressed as the mean ± standard deviation (SD). The statistically significant differences between tumor tissues and adjacent normal tissues were determined using paired Student's t-test. The statistically significant differences between other two groups were determined using Mann-Whitney U-test or unpaired Student's t-test, where appropriate. The comparisons among different groups (multigroup comparisons) were analyzed by one-way ANOVA followed by the *post hoc* Bonferroni test. Log-rank test and Kaplan-Meier method were used to assess survival rates. P <0.05 suggested a statistically significant difference.

RESULTS

LncRNA ELFN1-AS1 Expression Level was Raised in Colon Cancer Cells and Tissues

Based on TCGA database analysis, *ELFN1-AS1* with a high expression in colon cancer was selected as a research object (**Figure 1A**). RT-PCR was executed to inquire *ELFN1-AS1* expression level in the pairs of primary colon cancer tissues and non-tumor tissues. Results unraveled that colon cancer tissues expressed *ELFN1-AS1* at a markedly higher level than non-tumor colon tissues (**Figure 1B**). Similarly, colon cancer cells also expressed *ELFN1-AS1* at a notably higher level than NCM460 (**Figure 1C**). What's more, TCGA database analysis disclosed that raised *ELFN1-AS1* expression was related to short overall survival of colon cancer patients (**Figure 1D**).

Long Non-Coding RNA ELFN1-AS1 Decrement Restrained Colon Cancer *In Vitro*

SW620 and HT-29 cells with the highest *ELFN1-AS1* expression level were established firstly, and their *ELFN1-AS1* was pulled down (**Figure 2A**). As the transfection efficiency of sh-*ELFN1-AS1*-1 is best, sh-*ELFN1-AS1*-1 was selected as sh-*ELFN1-AS1* for further studies. CCK-8 assay, EdU, cell colony-forming experiment disclosed that *ELFN1-AS1* decrement prominently curbed cells to proliferate (**Figures 2B–D**). Moreover, flow cytometry uncovered that the cell frequency in sh-*ELFN1-AS1* group was higher at G1 phase and lower at the S phase (**Figure 2E**). Later, whether lncRNA *ELFN1-AS1* exerted impacts on apoptosis was figured out using apoptosis analysis. Results corroborated that *ELFN1-AS1* decrement triggered colon cancer cell apoptosis (**Figure 3A**). Ultimately, Transwell assay

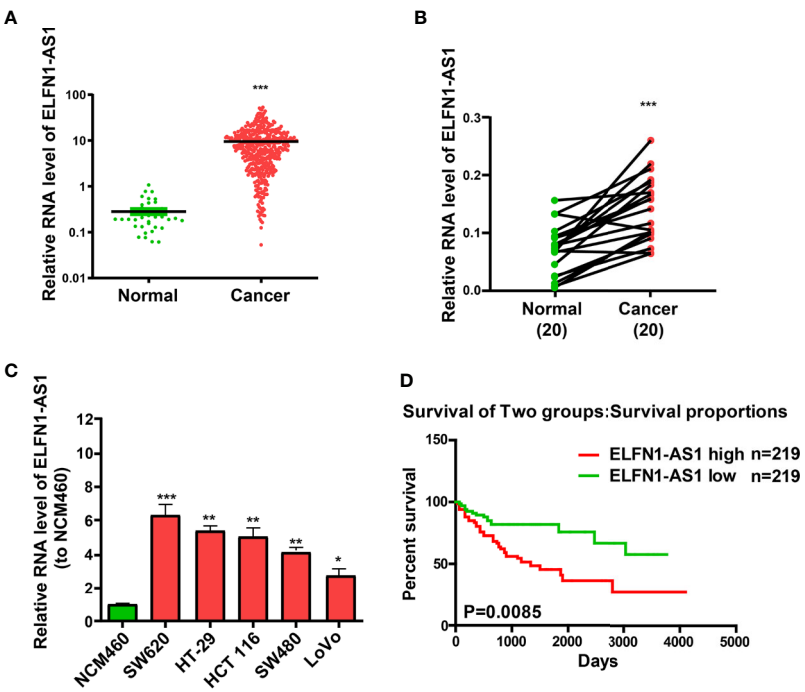

FIGURE 1 | LncRNA *ELFN1-AS1* expression level is raised in colon cancer tissues and cell lines. **(A)** TCGA data analysis is carried out to select *ELFN1-AS1* with high expression in colon cancer. **(B)** *ELFN1-AS1* expression prominently rises in the primary colon cancer tissues. **(C)** *ELFN1-AS1* expression is higher in colon cancer cells than in normal colonic epithelial cell line. **(D)** TCGA data analysis results showed that high *ELFN1-AS1* expression level is related to a shorter overall survival. Data are shown as the means ± SEM of three experiments. *P < 0.05, **P < 0.01, ***P < 0.001.

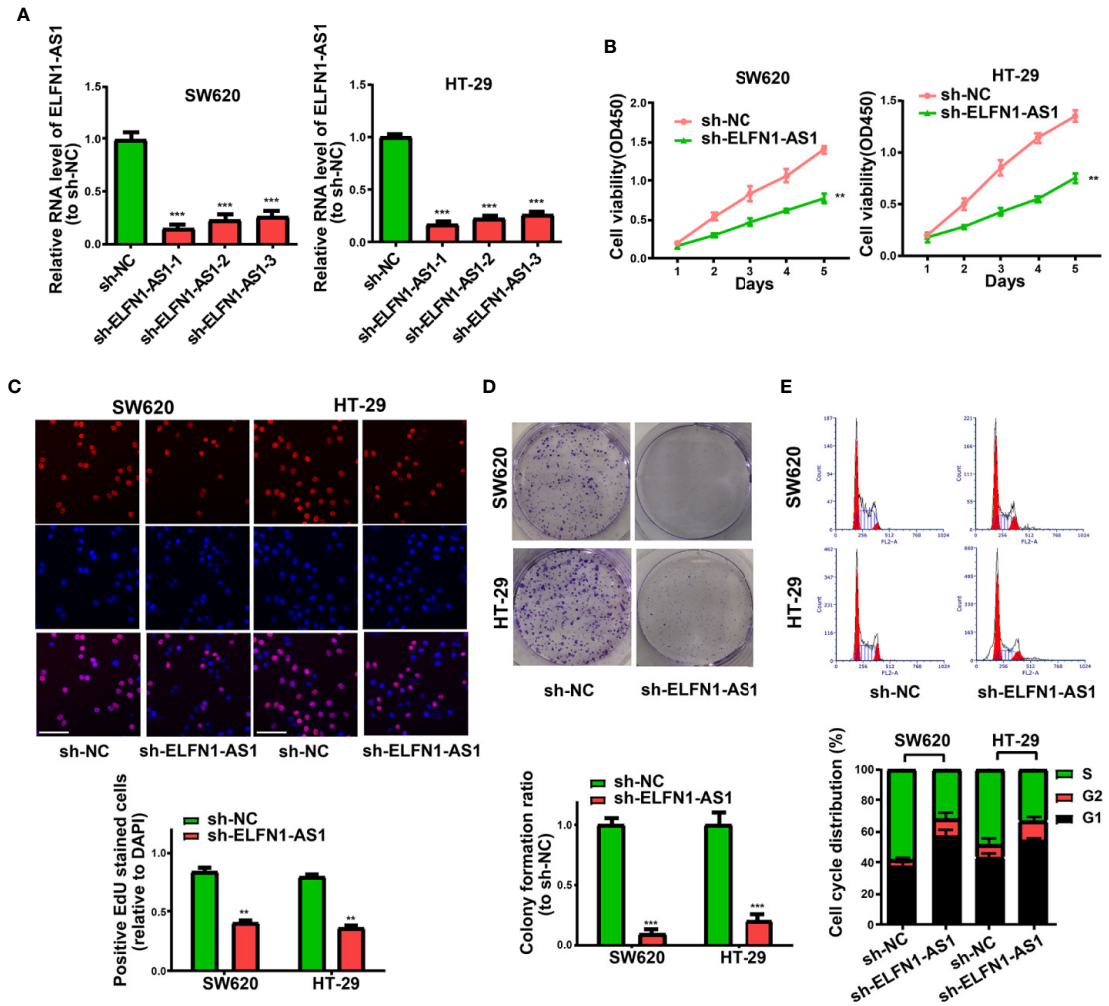

FIGURE 2 | LncRNA *ELFN1-AS1* decrement restrains colon cancer cell proliferation and cell cycle. **(A)** *ELFN1-AS1* expression in SW620 and HT-29 cells treated with sh-NC or *ELFN1-AS1* shRNAs. **(B)** CCK-8 assay, **(C)** EdU (bar = 100μm), and **(D)** cell colony-forming experiment were performed to test cell proliferation of SW620 and HT-29 cells. **(E)** sh-*ELFN1-AS1* cells show a remarkably lower frequency at S phase. Data are shown as the means ± SEM of three experiments. $^{**}P < 0.01$, $^{***}P < 0.001$.

was executed to determine lncRNA *ELFN1-AS1*'s impacts on colon cancer cell migration and invasion. It was disclosed that *ELFN1-AS1* repression alleviated colon cancer cell migration and invasion (**Figures 3B, C**).

Mutual Inhibition Between Long Non-Coding RNA ELFN1-AS1 and miR-191-5p Expression

lncRNA subcellular distribution determines the biological role (23). Colon cancer cells were separated into the cytoplasm and nuclear fractions to verify the *ELFN1-AS1* cellular location, with GAPDH and U6 as controls, respectively. RT-qPCR results revealed that *ELFN1-AS1* was mainly distributed in the cytoplasmic fraction of colon cancer cells (**Figure 4A**). MiRNAs with complementary base matching *ELFN1-AS1* was looked up using RegRNA 2.0 (http://regrna2.mbc.nctu.edu.tw/), among which emphasis was put on miR-191-5p, a recognized tumor-suppressing factor that restraining cancer cells to proliferate and invade (20, 21). Results manifested that relative to non-tumor colon tissues, miR-191-5p expression was decreased in colon cancer tissues (**Figure 4B**), and sh-*ELFN1-AS1* could significantly increase miR-191-5p levels in SW620 and HT-29 cells (**Figure 4C**). Besides, the biding sites between miR-191-5p and *ELFN1-AS1* were displayed in **Figure 4D**. Later, the speculated miR-191-5p binding site of *ELFN1-AS1* (*ELFN1-AS1*-WT) and a mutant miR-191-5p binding site of *ELFN1-AS1* (*ELFN1-AS1*-MUT) underwent cloning into reporter plasmids. Co-transfection with miR-191-5p and *ELFN1-AS1*-WT strongly weakened the luciferase activity, whereas co-transfection with miR-191-5p and *ELFN1-AS1*-MUT had no influence on the luciferase activity (**Figure 4D**). Then, whether miR-191-5p could negatively regulate *ELFN1-AS1* expression was tested. As

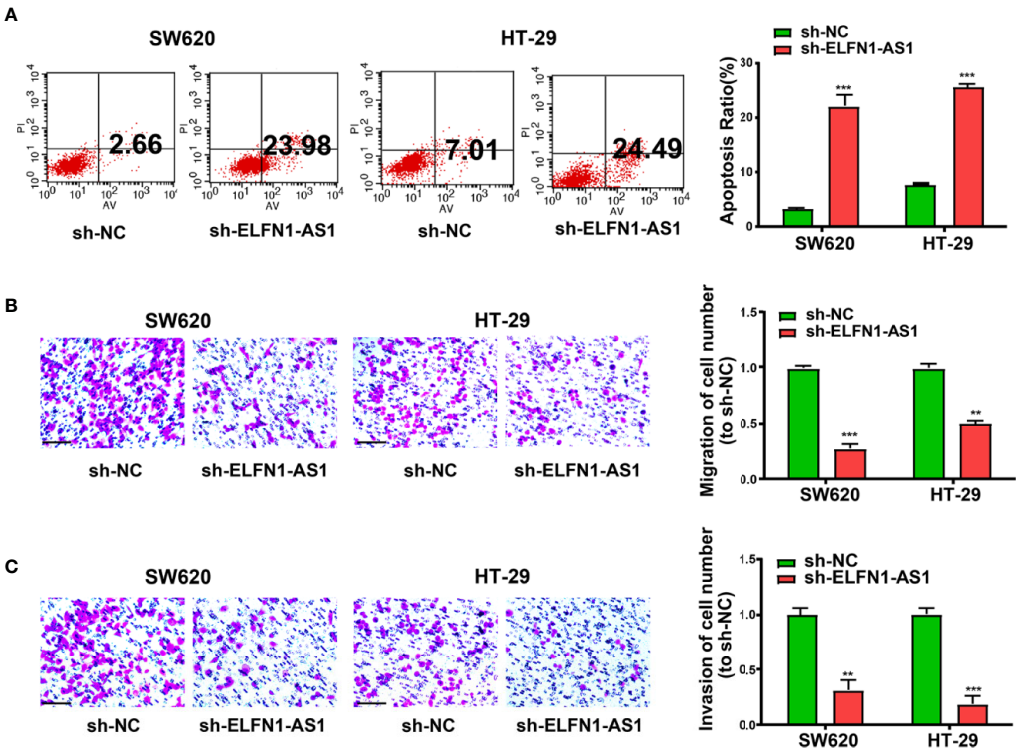

FIGURE 3 | LncRNA *ELFN1-AS1* down-regulation promotes colon cancer cell apoptosis, but inhibits cell migration and invasion. **(A)** *ELFN1-AS1* decrement aggravates colon cancer cell apoptosis. **(B)** *ELFN1-AS1* decrement weakens the ability of colon cancer cells to migrate (bar = 100 μm). **(C)** *ELFN1-AS1* decrement weakens the ability of colon cancer cells to invade (bar = 100 μm). Data are shown as the means ± SEM of three experiments. $^{**}P < 0.01$, $^{***}P < 0.001$.

displayed in **Figure 4E**, cells receiving miR-191-5p treatment expressed *ELFN1-AS1* at a reduced level, but those receiving anti-miR-191-5p treatment expressed *ELFN1-AS1* at a raised level. Finally, RIP assays verified the gathering of miR-191-5p and *ELFN1-AS1* in Ago2 immunoprecipitates rather than control IgG immunoprecipitates (**Figure 4F**). Collectively, the above data imply that miR-191-5p is able to bind to *ELFN1-AS1* in a direct way and to inversely regulate *ELFN1-AS1* expression.

Special AT-Rich Sequence-Binding Protein 1 Was the Direct Target of miR-191-5p

MiRNAs function primarily by modulating the downstream targets of them (24, 25). Then, the target genes of miR-191-5p were looked up using Targetscan 7.2 (http://www.targetscan.org/vert_72/, top ten genes) and miRDB (http://mirdb.org/, score ≥ 85). As shown in the **Figure 5A**, four target genes were found. Then, we detected the expression of these four genes (NEURL4, TAF5, TMOD2, and SATB1). We found that only the expression of SATB1 was downregulated after miR-191-5p mimics transfection in SW620 cells (**Figure 5B**). Thus, SATB1 was selected from the speculated target genes of miR-191-5p for later research. It was manifested by luciferase assay that the luciferase activities in SW620 and HT-29 cells receiving co-transfection with miR-191-5p and WT-SATB1-3'-UTR were weakened relative to other groups (**Figure 5C**). SATB1 expression level in colon cancer tissues was also detected. Western blot assay validated that SATB1 expression was elevated in colon cancer tissues relative to non-tumor colon tissues (**Figure 5D**). Immunofluorescence staining showed the same results (**Figure 5E**). Besides, miR-191-5p restrained SATB1 protein to be expressed in SW620 and HT-29 cells (**Figure 5F**). In sh-*ELFN1-AS1* cells, the level of SATB1 was discovered to be lower than that in sh-NC cells. Nevertheless, anti-miR-191-5p treatment restored SATB1 in sh-*ELFN1-AS1* cells (**Figure 5G**). In all, the above data suggest that the SATB1 is a downstream target gene of miR-191-5p and modulated by *ELFN1-AS1*.

Long Non-Coding RNA ELFN1-AS1 Decrement Impeded Tumor to Grow in the Body

Whether *ELFN1-AS1* decrement impeded tumor to grow in the body was explored. It was disclosed that the growth of SW620 cells was slower in the case of lncRNA *ELFN1-AS1* repression (**Figure 6A**). The average weight and volume of xenograft tumors in sh-*ELFN1-AS1* group were less than those in sh-NC group (**Figures 6B, C**). Later, lncRNA *ELFN1-AS1* expression in the resected tumor tissues was examined. Results unraveled that sh-*ELFN1-AS1* group had decreased *ELFN1-AS1* expression

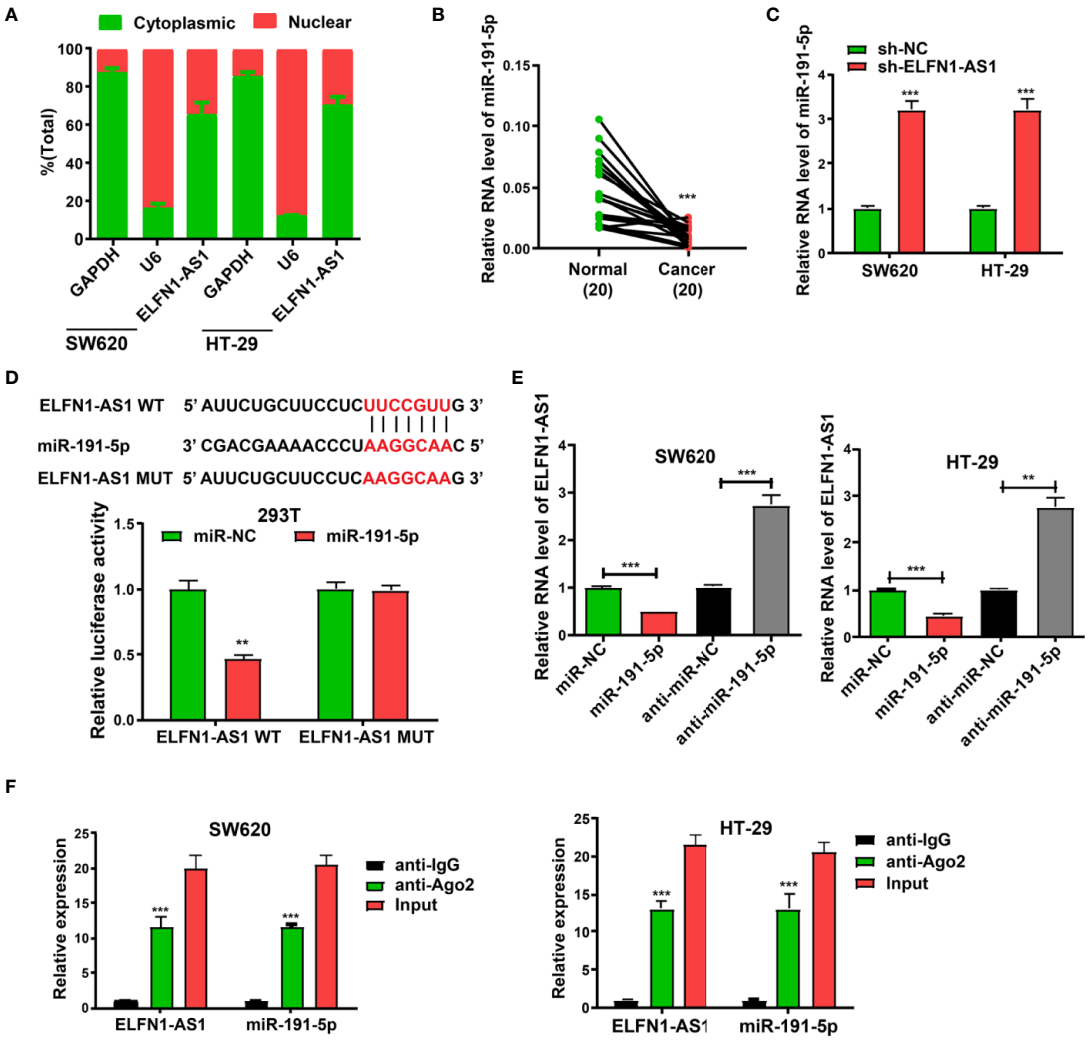

FIGURE 4 | Mutual repression between lncRNA *ELFN1-AS1* and miR-191-5p. **(A)** Cytoplasmic and nuclear levels of *ELFN1-AS1* in colon cancer cells assessed by RT-qPCR. **(B)** qRT-PCR assay reveals the miR-191-5p level in colon cancer tissues. **(C)** sh-*ELFN1-AS1* cells express miR-191-5p at a higher level than sh-NC cells. **(D)** The binding sites between miR-191-5p on *ELFN1-AS1*. And dual luciferase reporter assay was performed to verify binding relationship of miR-191-5p and *ELFN1-AS1*. **(E)** miR-191-5p inversely modulates *ELFN1-AS1* expression. **(F)** *ELFN1-AS1* and miR-191-5p gather in Ago2 immunoprecipitates compared with control IgG immunoprecipitates. Data are shown as the means ± SEM of three experiments. $^{**}P < 0.01$, $^{***}P < 0.001$.

relative to sh-NC group (**Figure 6D**). Lastly, staining was executed for tumor sections to detect SATB1 expression, and it was disclosed that SATB1 expression was expressed at a lower level in sh-*ELFN1-AS1* group (**Figure 6E**). To sum up, it can be inferred that *ELFN1-AS1* boosts the tumor to grow in the body.

Long Non-Coding RNA ELFN1-AS1 Regulated Colon Cancer Cell Proliferation, Invasion, Apoptosis, and Cycle Through miR-191-5p/SATB1 Axis

To verify the function of *ELFN1-AS1*/miR-191-5p/SATB1 in colon cancer, rescue experiments were carried out for SW620 and HT-29 cells. SW620 (sh-*ELFN1-AS1*) and HT-29 (sh-*ELFN1-AS1*) cells stably transfected with sh-*ELFN1-AS1* were cultured and divided into 3 groups and transfected with NC, anti-miR-191-5p, and pcDNA-SATB1, respectively. The results of CCK-8 and EdU experiments showed that the proliferation abilities of anti-miR-191-5p group and pcDNA-SATB1 group were significantly increased (**Figures 7A, B**). In addition, anti-miR-191-5p and pcDNA-SATB1 also enhanced the invasive abilities of SW620 (sh-*ELFN1-AS1*) and HT-29 (sh-*ELFN1-AS1*) cells (**Figure 7C**), but inhibited G1 arrest (**Figure 7D**) and apoptosis (**Figure 7E**) of colon cancer cells.

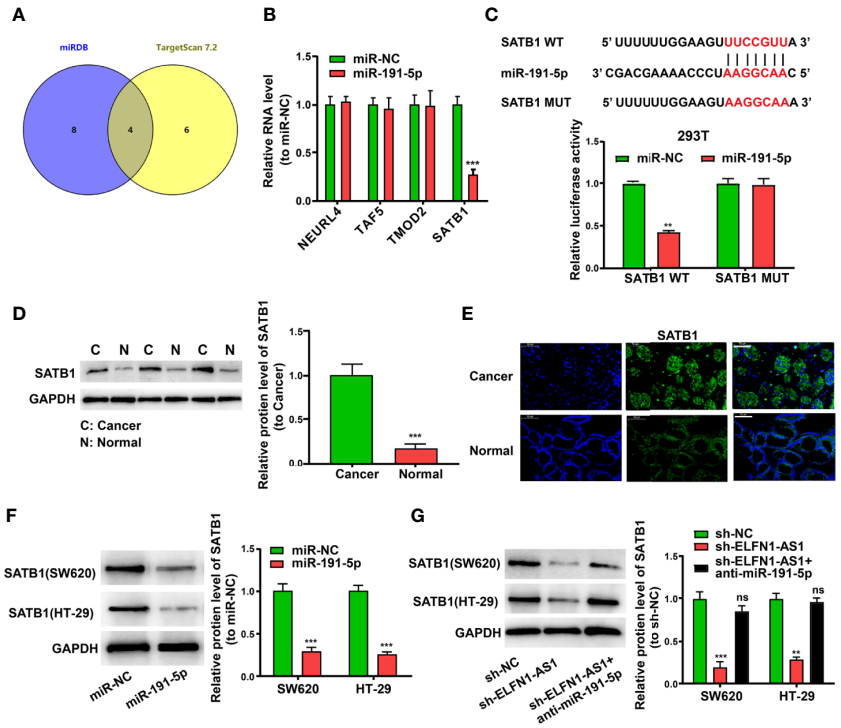

FIGURE 5 | miR-191-5p/SATB1 axis mediates *ELFN1-AS1*'s impacts on cell growth and invasion. **(A)** Bioinformatics analysis with miRDB and TargetScan 7.2. **(B)** The expression of the predictive target genes after miR-191-5p mimics transfection in SW620 cells. **(C)** The binding sites between miR-191-5p and SATB1. Dual luciferase assay uncovers that co-transfection with miR-191-5p and SATB1-WT evidently weakens the luciferase activity. **(D)** SATB1 protein expression rises in colon cancer tissues relative to normal tissues. C, cancer tissues; N, normal tissues. **(E)** Western blot assay discloses that colon cancer tissues express SATB1 at an elevated level than normal tissues. **(F)** miR-191-5p represses SATB1 protein expression in colon cancer cells. **(G)** Anti-miR-191-5p treatment gives rise to the restoration of SATB1 in sh-*ELFN1-AS1* cells. Data are shown as the means ± SEM of three experiments. $^{**}P < 0.01$. $^{***}P < 0.001$, ns, no significance.

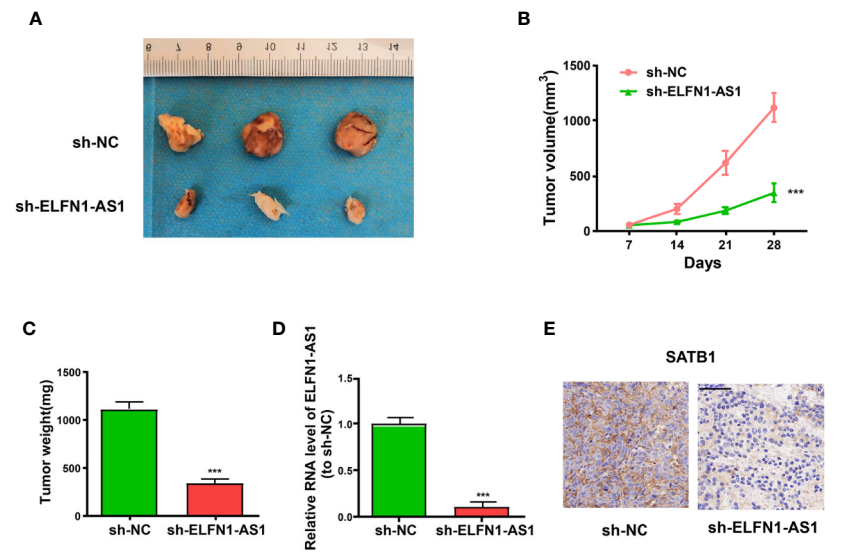

FIGURE 6 | *ELFN1-AS1* inhibition curbs the tumor to grow in the body. **(A)** Xenograft tumors. **(B)** The growth of xenograft tumors from sh-*ELFN1-AS1* cells is slower than that of xenograft tumors from sh-NC cells. **(C)** The mean weight of xenograft tumors. **(D)** *ELFN1-AS1* expression in xenograft tumors is determined. **(E)** *ELFN1-AS1* decrement pronouncedly reduces SATB1 in tumors compared with negative control group. $^{***}P < 0.001$.

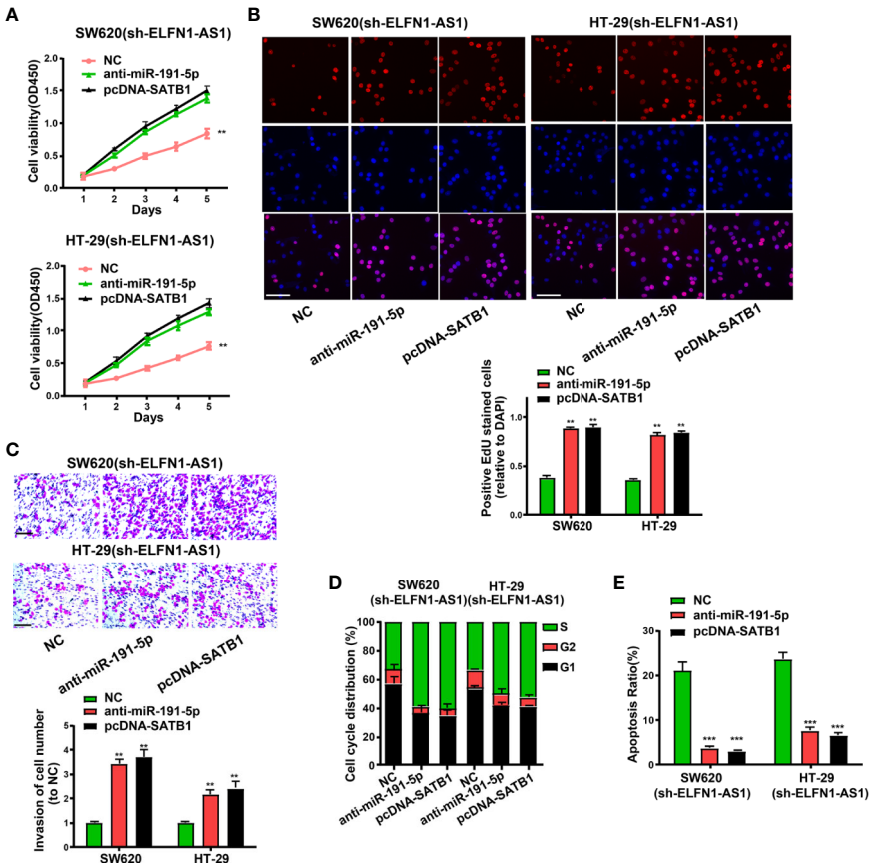

FIGURE 7 | lncRNA *ELFN1-AS1* modulates colon cancer cell proliferation, invasion, cell cycle, and cell apoptosis through miR-191-5p/SATB1 axis. **(A)** CCK-8 assay and **(B)** EdU assay reveal that anti-miR-191-5p and pcDNA-SATB1 promote cell proliferation in SW620 (sh-*ELFN1-AS1*) and HT-29 (sh-*ELFN1-AS1*) cells (bar = 100 μm). **(C)** Cell invasion assay in SW620 (sh-*ELFN1-AS1*) and HT-29 (sh-*ELFN1-AS1*) cells (bar = 100 μm). **(D)** Cell cycle assay in SW620 and HT-29 cells stably transfected with sh-*ELFN1-AS1*. **(E)** Cell apoptosis assay in SW620 and HT-29 cells stably transfected with sh-*ELFN1-AS1*. Data are show as the means ± SEM of three experiments. $^{**}P < 0.01$, $^{***}P < 0.001$.

DISCUSSION

Colon cancer ranks third among the most common cancers globally, and it is the second most frequently seen cause of death correlated with cancer (26). At present, prior to the development of new and effective treatment methods for colon cancer, there is a need to figure out the possible mechanisms by which colon cancer develops and progresses. Recently, lncRNAs have been indicated to exert pivotal effects in the development of different tumors, including colon cancer (27). TCGA data were used to analyze lncRNAs associated with colon cancer, high-expression *ELFN1-AS1* was selected as a research object and validated in population tissues and cells.

Functional assays unraveled that repression of *ELFN1-AS1* restrained SW620 and HT-29 cells to proliferate, migrate, and invade. Besides, *ELFN1-AS1* was disclosed to boost the G1-S phase transition of cell cycle and likely to protect SW620 and HT-29 cells from apoptosis. The abovementioned findings imply that *ELFN1-AS1* is an oncogene and it facilitates the formation of colon cancer.

SATB1 is a nuclear matrix-correlated protein involved in chromatin organization with a higher order and in modulating the expression of tissue-specific genes (28). It has been manifested that SATB1 is related to the development of different cancers, including oral squamous cell carcinoma (29), colorectal cancer (30), bladder cancer (31), and prostate cancer (32). Nonetheless, it has been reported that SATB1 decrement restrains breast cancer cells to proliferate, grow and invade by modulating gene expression (33). In this research, stably reducing *ELFN1-AS1* expression pronouncedly attenuated the abilities of colon cancer cells to proliferate and invade, which could be reversed by SATB1 overexpression.

This research has several deficiencies. First, a larger sample size is required to further explore the clinical value of *ELFN1-AS1*. Second, more target genes or miRNAs should be applied to interact with *ELFN1-AS1*. Third, more different mouse models need be used to further verified our conclusion.

In conclusion, *ELFN1-AS1* is prominently raised in colon cancer tissues and cell lines. Furthermore *ELFN1-AS1* could promote proliferation and migration of colon cancer cells through miR-191-5p/STAB1 axis.

DATA AVAILABILITY STATEMENT

The raw data supporting the conclusions of this article will be made available by the authors, without undue reservation.

ETHICS STATEMENT

The studies involving human participants were reviewed and approved by The Affiliated Huai'an Hospital of Xuzhou Medical University. The patients/participants provided their written informed consent to participate in this study. The animal study was reviewed and approved by The Affiliated Huai'an Hospital of Xuzhou Medical University.

AUTHOR CONTRIBUTIONS

YD and TL performed the experiments and prepared the manuscript. YH and YS collected and analyzed the data. YH supported the administration and technique, and provided the materials. JL and TL designed and supervised the study, and revised the manuscript. All authors contributed to the article and approved the submitted version.

FUNDING

NThis study was supported by The National Key R&D Program of China (No.2017YFC0113901 granted to Liu Yuping).

REFERENCES

1. Bray F, Ferlay J, Soerjomataram I, Siegel RL, Torre LA, Jemal A. Global cancer statistics 2018: GLOBOCAN estimates of incidence and mortality worldwide for 36 cancers in 185 countries. *CA Cancer J Clin* (2018) 68(6):394–424. doi: 10.3322/caac.21492
2. Wen J, Min X, Shen M, Hua Q, Han Y, Zhao L, et al. ACLY facilitates colon cancer cell metastasis by CTNNB1. *J Exp Clin Cancer Res* (2019) 38(1):401. doi: 10.1186/s13046-019-1391-9
3. Tamas K, Walenkamp AM, de Vries EG, van Vugt MA, Beets-Tan RG, van Etten B, et al. Rectal and colon cancer: Not just a different anatomic site. *Cancer Treat Rev* (2015) 41(8):671–9. doi: 10.1016/j.ctrv.2015.06.007
4. Banerjee A, Pathak S, Subramanium VD, Dharanivasan D, Murugesan R, Verma RS. Strategies for targeted drug delivery in treatment of colon cancer: current trends and future perspectives. *Drug Discovery Today* (2017) 22 (8):1224–32. doi: 10.1016/j.drudis.2017.05.006
5. Cartwright TH. Treatment decisions after diagnosis of metastatic colorectal cancer. *Clin Colorectal Cancer* (2012) 11(3):155–66. doi: 10.1016/j.clcc.2011.11.001
6. Meyers BM, Cosby R, Quereshy F, Jonker D. Adjuvant Chemotherapy for Stage II and III Colon Cancer Following Complete Resection: A Cancer Care Ontario Systematic Review. *Clin Oncol (R Coll Radiol)* (2017) 29(7):459–65. doi: 10.1016/j.clon.2017.03.001
7. Siegel RL, Miller KD, Fedewa SA, Ahnen DJ, Meester RGS, Barzi A, et al. Colorectal cancer statistics, 2017. *CA Cancer J Clin* (2017) 67(3):177–93. doi: 10.3322/caac.21395
8. Rosen AW, Degett TH, Gogenur I. [Individualized treatment of colon cancer]. *Ugeskr Laeger* (2016) 178(31).
9. Sun Q, Hao Q, Prasanth KV. Nuclear Long Noncoding RNAs: Key Regulators of Gene Expression. *Trends Genet* (2018) 34(2):142–57. doi: 10.1016/j.tig.2017.11.005
10. Sun W, Yang Y, Xu C, Guo J. Regulatory mechanisms of long noncoding RNAs on gene expression in cancers. *Cancer Genet* (2017) 216-217:105–10. doi: 10.1016/j.cancergen.2017.06.003
11. Zhou Y, Shi H, Du Y, Zhao G, Wang X, Li Q, et al. lncRNA DLEU2 modulates cell proliferation and invasion of non-small cell lung cancer by regulating miR-30c-5p/SOX9 axis. *Aging (Albany NY)* (2019) 11(18):7386–401. doi: 10.18632/aging.102226
12. Huang HW, Xie H, Ma X, Zhao F, Gao Y. Upregulation of LncRNA PANDAR predicts poor prognosis and promotes cell proliferation in cervical cancer. *Eur Rev Med Pharmacol Sci* (2017) 21(20):4529–35.
13. Zhang C, Lian H, Xie L, Yin N, Cui Y. LncRNA ELFN1-AS1 promotes esophageal cancer progression by up-regulating GFPT1 via sponging miR-183-3p. *Biol Chem* (2020) 401(9):1053–61. doi: 10.1515/hsz-2019-0430
14. Jie Y, Ye L, Chen H, Yu X, Cai L, He W, et al. ELFN1-AS1 accelerates cell proliferation, invasion and migration via regulating miR-497-3p/CLDN4 axis in ovarian cancer. *Bioengineered* (2020) 11(1):872–82. doi: 10.1080/21655979.2020.1797281
15. Liu JX, Li W, Li JT, Liu F, Zhou L. Screening key long non-coding RNAs in early-stage colon adenocarcinoma by RNA-sequencing. *Epigenomics* (2018) 10(9):1215–28. doi: 10.2217/epi-2017-0155
16. Tutar Y. miRNA and cancer; computational and experimental approaches. *Curr Pharm Biotechnol* (2014) 15(5):429. doi: 10.2174/1389201015051 40828161335
17. Zagryazhskaya A, Zhivotovsky B. miRNAs in lung cancer: a link to aging. *Ageing Res Rev* (2014) 17:54–67. doi: 10.1016/j.arr.2014.02.009
18. Liu H, Ren G, Zhu L, Liu X, He X. The upregulation of miRNA-146a inhibited biological behaviors of ESCC through inhibition of IRS2. *Tumour Biol* (2016) 37(4):4641–7. doi: 10.1007/s13277-015-4274-5
19. Lima CR, Geraldo MV, Fuziwara CS, Kimura ET, Santos MF. MiRNA-146b-5p upregulates migration and invasion of different Papillary Thyroid Carcinoma cells. *BMC Cancer* (2016) 16:108. doi: 10.1186/s12885-016-2146-z
20. Chen P, Pan X, Zhao L, Jin L, Lin C, Quan J, et al. MicroRNA-191-5p exerts a tumor suppressive role in renal cell carcinoma. *Exp Ther Med* (2018) 15 (2):1686–93. doi: 10.3892/etm.2017.5581
21. Chen XY, Zhang J, Hou LD, Zhang R, Chen W, Fan HN, et al. Upregulation of PD-L1 predicts poor prognosis and is associated with miR-191-5p dysregulation in colon adenocarcinoma. *Int J Immunopathol Pharmacol* (2018) 32:2058738418790318. doi: 10.1177/2058738418790318
22. Min X, Wen J, Zhao L, Wang K, Li Q, Huang G, et al. Role of hepatoma-derived growth factor in promoting de novo lipogenesis and tumorigenesis in hepatocellular carcinoma. *Mol Oncol* (2018) 12(9):1480–97. doi: 10.1002/1878-0261.12357
23. Miao H, Wang L, Zhan H, Dai J, Chang Y, Wu F, et al. A long noncoding RNA distributed in both nucleus and cytoplasm operates in the PYCARD-regulated apoptosis by coordinating the epigenetic and translational regulation. *PloS Genet* (2019) 15(5):e1008144. doi: 10.1371/journal.pgen.1008144
24. Bhaskaran M, Mohan M. MicroRNAs: history, biogenesis, and their evolving role in animal development and disease. *Vet Pathol* (2014) 51(4):759–74. doi: 10.1177/0300985813502820
25. Roberts JT, Borchert GM. Computational Prediction of MicroRNA Target Genes, Target Prediction Databases, and Web Resources. *Methods Mol Biol* (2017) 1617:109–22. doi: 10.1007/978-1-4939-7046-9_8
26. Cheng Y, Zhu Y, Xu J, Yang M, Chen P, Xu W, et al. PKN2 in colon cancer cells inhibits M2 phenotype polarization of tumor-associated macrophages via regulating DUSP6-Erk1/2 pathway. *Mol Cancer* (2018) 17(1):13. doi: 10.1186/s12943-017-0747-z
27. Wu Q, Meng WY, Jie Y, Zhao H. LncRNA MALAT1 induces colon cancer development by regulating miR-129-5p/HMGB1 axis. *J Cell Physiol* (2018) 233(9):6750–7. doi: 10.1002/jcp.26383
28. Nakayama Y, Mian IS, Kohwi-Shigematsu T, Ogawa T. A nuclear targeting determinant for SATB1, a genome organizer in the T cell lineage. *Cell Cycle* (2005) 4(8):1099–106. doi: 10.4161/cc.4.8.1862
29. Li YC, Bu LL, Mao L, Ma SR, Liu JF, Yu GT, et al. SATB1 promotes tumor metastasis and invasiveness in oral squamous cell carcinoma. *Oral Dis* (2017) 23(2):247–54. doi: 10.1111/odi.12602

30. Brocato J, Costa M. SATB1 and 2 in colorectal cancer. *Carcinogenesis* (2015) 36(2):186–91. doi: 10.1093/carcin/bgu322
31. Choudhary D, Clement JM, Choudhary S, Voznesensky O, Pilbeam CC, Woolbright BL, et al. SATB1 and bladder cancer: Is there a functional link? *Urol Oncol* (2018) 36(3):93 e13–21. doi: 10.1016/j.urolonc.2017.10.004
32. Mao LJ, Yang CH, Fan L, Gao P, Yang DR, Xue BX, et al. SATB1 promotes prostate cancer metastasis by the regulation of epithelial-mesenchymal transition. *BioMed Pharmacother* (2016) 79:1–8. doi: 10.1016/j.biopha.2016.01.038
33. Han HJ, Russo J, Kohwi Y, Kohwi-Shigematsu T. SATB1 reprogrammes gene expression to promote breast tumour growth and metastasis. *Nature* (2008) 452(7184):187–93. doi: 10.1038/nature06781

Conflict of Interest: The authors declare that the research was conducted in the absence of any commercial or financial relationships that could be construed as a potential conflict of interest.

frontiers in Genetics

ORIGINAL RESEARCH
published: 10 February 2021
doi: 10.3389/fgene.2021.625414

Identification of a 14-Gene Prognostic Signature for Diffuse Large B Cell Lymphoma (DLBCL)

*Pengcheng Feng[1], Hongxia Li[2], Jinhong Pei[1], Yan Huang[1] and Guixia Li[1]**

[1] Department of Basic Medicine, Changzhi Medical College, Changzhi, China, [2] Affiliated Hospital of Changzhi Institute of Traditional Chinese Medicine, Changzhi, China

Although immunotherapy is a potential strategy to resist cancers, due to the inadequate acknowledge, this treatment is not always effective for diffuse large B cell lymphoma (DLBCL) patients. Based on the current situation, it is critical to systematically investigate the immune pattern. According to the result of univariate and multivariate cox proportional hazards, LASSO regression and Kaplan-Meier survival analysis on immune-related genes (IRGs), a prognostic signature, containing 14 IRGs (AQP9, LMBR1L, FGF20, TANK, CRP, ORM1, JAK1, BACH2, MTCP1, IFITM1, TNFSF10, FGF12, RFX5, and LAP3), was built. This model was validated by external data, and performed well. DLBCL patients were divided into low- and high-risk groups, according to risk scores from risk formula. The results of CIBERSORT showed that different immune status and infiltration pattern were observed in these two groups. Gene set enrichment analysis (GSEA) indicated 12 signaling pathways were significantly enriched in the high-risk group, such as natural killer cell-mediated cytotoxicity, toll-like receptor signaling pathway, and so on. In summary, 14 clinically significant IRGs were screened to build a risk score formula. This formula was an accurate tool to provide a certain basis for the treatment of DLBCL patients.

Keywords: diffuse large B cell lymphoma, immune-related gene, immune prognostic model, risk score formula, immune infiltration

OPEN ACCESS

Edited by:
Xiaochen Wang,
University of Texas Southwestern Medical Center, United States

Reviewed by:
Jiheng Xu,
New York University, United States
Prashanth N. Suravajhala,
Birla Institute of Scientific Research, India

****Correspondence:***
Guixia Li
liguixia1990@163.com

Specialty section:
This article was submitted to Cancer Genetics, a section of the journal Frontiers in Genetics

Received: *02 November 2020*
Accepted: *21 January 2021*
Published: *10 February 2021*

Citation:
Feng P, Li H, Pei J, Huang Y and Li G (2021) Identification of a 14-Gene Prognostic Signature for Diffuse Large B Cell Lymphoma (DLBCL). Front. Genet. 12:625414. doi: 10.3389/fgene.2021.625414

INTRODUCTION

Diffuse large B cell lymphoma (DLBCL) is the most common subtype of non-hodgkin lymphoma (NHL), it can be divided into three molecular subtypes [germinal center B cell (GCB) subtype, activated B cell (ABC)-like subtype, and the unclassified subtypes.] according to the unique genetic signatures (Calado et al., 2010; Zhang et al., 2016). It has been thought as an aggressive disease caused by rapidly dividing malignant B cells. With further research of deeper genome sequencing and transcriptomic profiling, it has been proven that the complexity of DLBCL biology was seriously underestimated (Scott and Gascoyne, 2014; Opinto et al., 2020).

Abbreviations: DLBCL, diffuse large B cell lymphoma; NHL, non-hodgkin lymphoma; TCGA, the cancer genome atlas; GEO, gene expression omnibus; IRGs, immune-related genes; ImmPort, immunology database and analysis portal; OS, overall survival; LASSO, least absolute shrinkage and selection operator; K-M, Kaplan-meier; GSEA, gene set enrichment analysis; PD-L1, programmed cell death ligand 1; PD-1, programmed cell death protein 1; CTLA-4, cytotoxic T lymphocyte antigen-4; LAG-3, lymphocyte activation gene 3; TIM-3, T cell immunoglobulin-3.

The majority of DLBCL patients could be relieved after a standard regimen of rituximab in combination with chemotherapy, however, 40% of DLBCL patients had a poor prognosis without suitable curative therapies (Kim et al., 2012; Coiffier and Sarkozy, 2016; Carpìo et al., 2020; Zhou et al., 2020). Based on this situation, the researches of the treatment strategies on DLBCL remain important.

One of the features in the occurrence and development of carcinoma is the change of immune status. Tumor immune evading mechanisms were increasingly recognized crucial in the formation and development of multiple cancer (Motzer et al., 2014; Velcheti et al., 2014; Borghaei et al., 2015; Lin et al., 2016; Wallin et al., 2016). The fact decreased immunity stimulated the growth of cancer cells could be reversed, with the emergence of immunotherapy (Silver et al., 2015). Hence, cancer immunotherapy has become one of the major strategies to treat cancer and the researches about the relationship between immune cell and tumor have become a hot topic (Schumacher and Schreiber, 2015; Liu et al., 2017; Popovic et al., 2018; Sebastian et al., 2018). It is generally believed that a single immune marker is too farfetched to illustrate the complex immune environment. Therefore, it is necessary to find a multi-immune relevant-gene-based signature to help the physician predict patients' prognosis and characteristic of tumor microenvironment.

The therapy of immune checkpoint blockades had achieved unprecedented success in helping many cancer patients to extend overall survival (OS) (Gettinger et al., 2016; Reck et al., 2016; Rittmeyer et al., 2016). So, in the process of curing cancer, immunotherapy is always an important consideration. However, the benefited population was limited due to high heterogeneity in biological and clinical appearances (Georg et al., 2010; Dobashi and Akito, 2016; Gentzler et al., 2016). Several immune checkpoint inhibitors could enhance cytotoxicity by targeting programmed cell death protein 1 (PD-1) (CD279), programmed cell death ligand 1 (PD-L1) (CD274), cytotoxic T lymphocyte antigen-4 (CTLA-4), lymphocyte activation gene 3 (LAG-3) (CD223), and T cell immunoglobulin-3 (TIM-3) (HAVCR2). PD-1/PD-L1 could cause the host immune evasion and promotion of metastasis (Velcheti et al., 2014). CTLA-4 belonged to immunoglobulin-related receptors family and could respond to T-cell immune negative regulation (Rowshanravan et al., 2017; Hosseini et al., 2020). Blocking the expression of PD-1 and CTLA-4 improved the outcomes of patients in different cancers, but immune-related adverse events were observed. LAG-3, an immune inhibitory receptor, was regarded as the foremost target next to PD-1.

In this work, we combined clinical information with immune-related genes (IRGs) expression profiles from 216 DLBCL patients to evaluate the OS. The risk score formula was constructed to predict the individual survival time. Furthermore, the prognosis significance of multiple immune biomarkers was confirmed by the cancer genome atlas (TCGA)-DLBC and GSE32918. This result provided a model for immune-related work and was the critical step toward developing personalized strategies for DLBCL.

MATERIALS AND METHODS

Data Collection

The level-3 RNA-seq data and clinical data of DLBCL were downloaded from the TCGA and normalized by TCGAbiolinks R package. The raw datasets (GSE136971 and GSE32918) of DLBCL were downloaded from the gene expression omnibus (GEO) database. Limma package was used to screen the differential expression genes. Perl was used to transform ensemble IDs and probe names to symbols, separately. IRGs were obtained from the Immunology Database and Analysis Portal (ImmPort)[1]. Univariate cox proportional hazard regression was used to associate the IRGs with DLBCL patients' OS. Only IRGs with *P* value less than 0.05 were selected as putative genes for further analysis. Least absolute shrinkage and selection operator (LASSO) regression was performed to prevent the model overfitting, using ten-fold cross-validation to exam penalty parameter. Multivariate cox regression analysis was performed to assess the risk value of each IRGs signature, then a risk score was established as following:

Risk score = β gene1 × gene1 expression value + β gene 2 × gene 2 expression value + β gene 3 × gene 3 expression value + ·····+ β gene n × gene n expression value. n is the number of relative IRGs, β is the coefficient generated by the multivariate cox regression.

All data were downloaded from public databases and did not apply for approval of the local ethics committees. A methodological flowchart of this research was shown in **Supplementary Figure 1**.

IRGs Signature Construction and Confirmation

Low- and high-risk groups were generated based on the median risk scores of DLBCL patients. Kaplan-Meier (K-M) was performed to estimate survival distribution. "TimeROC" and "survival" packages were used to examine the suitability of survival prediction among risk models.

Tumor-Infiltrating Immune Cells

CIBERSORT from sangerbox[2] was used to explore the abundance of tumor-infiltrating immune cells. Ninety-eight IRGs were submitted to CIBERSORT, to predict the roles of immune infiltration in DLBCL. The correlations between IRGs and four immune checkpoints were analyzed using TCGA-DLBC tumor data by GEPIA[3]. The significant level was less than 0.05.

GSEA-Enrichment Analysis

To explore the potential biological function of IRGs, gene set enrichment analysis (GSEA) (v 4.1.0) was carried out, based on the gene expression data from low- and high-risk groups. C2.cp.KEGG.v7.2. symbols. gmt was selected as reference gene set database. Enrichment pathways were filtered under the condition of *P* value less than 0.05 and FDR *P* value less than 0.25.

[1]https://immport.niaid.nih.gov

[2]http://sangerbox.com/AllTools?tool_id=9703341

[3]http://gepia.cancer-pku.cn/

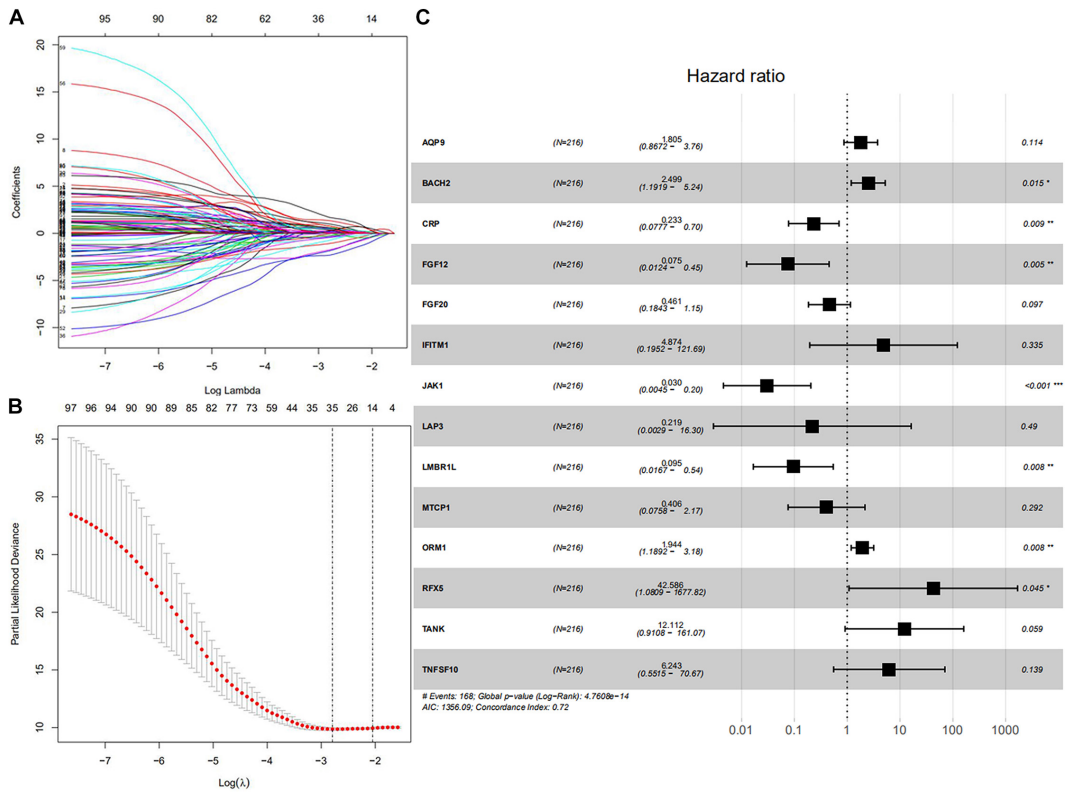

FIGURE 1 | Core IRGs OS relevant were Identified by Cox analysis. **(A)** LASSO coefficient profiles for 98 significant IRGs in univariate Cox. **(B)** Cross-validation for selecting the tuning parameters for the LASSO model. **(C)** Forest plots showed the relationships of 14 IRGs with OS in the training group. The unadjusted hazard ratios are presented with 95% CIs. $*P < 0.05$, $**P < 0.01$, and $***P < 0.001$.

CMap Analysis

Connectivity Map (CMap) (version 02)[4], was adopted to screen putative drugs targeting 14 IRGs. CMap is a website used to search connections among genes, diseases and drugs. All probe IDs, corresponding to 14 IRGs on HG-U133A, were obtained according to GPL96. The genes that hazard ratios were greater than 1 were marked "up" and less than were marked "down." The probe ID was input into files with "up" and "down" tags saved as ".grp" format. Small molecular drugs that were negatively correlated with the 14 IRGs signature might have the potential to treat DLBCL.

The Analysis of 14 IRGs Expression Level

The expression matrixes were searched in GEO database using lymph as a keyword to explore the expression level of 14 IRGs. The samples (GSM217767, GSM217768, GSM217769, GSM217770, GSM217771, GSM217772, GSM217773, GSM217774, and GSM217775) in GSE8762 were used as control. GSE64555 and GSE159472 were used as disease data sets. These three data were annotated with GPL570. In order to reduce the differences caused by different standardization methods in GEO data, two R packages, Affy and affPLM, were used to re-standardize the original data.

[4]https://portals.broadinstitute.org/cmap

RESULTS

The Preparation and Description of Clinical Data and Expression Data

Only individuals with complete clinical information could be used as experimental samples. In order to reduce errors as much as possible and make our model more reliable, the subjects which the survival time were less than 100 days and no survival information were abandoned. GSE136971, containing 216 samples, were used as a training group. No survival status information was recorded for GSM2329007 and GSM2329133. The survival time of GSM2329094, GSM2329071, GSM2329069, GSM2329022, and GSM2329976 was less than 100 days. These seven individual samples were deleted. GSE32918 (189 samples) and TCGA-DLBC (44 samples) were used as a validating group.

A Risk Formula Was Constructed Using Fourteen-Four IRGs

All symbol and synonyms of IRGs from ImmPort were downloaded, to avoid omissions. 7887 IRGs were obtained and summarized in **Supplementary Table 1**, 1328 IRGs were screened by merging the expression data of 7887 IRGs and GSE136971. Ninety-eight IRGs were related to OS and screened by univariate Cox proportional hazard regression.

TABLE 1 | The risk coefficient of 14 IRGs.

ID	exp(coef)	exp(-coef)	Low 95% CI	Low 95% CI	*P* value
AQP9	1.80452	0.55416	0.867163	3.7551	0.11439
BACH2	2.49894	0.40017	1.191857	5.2395	0.015325
CRP	0.2329	4.29369	0.077665	0.6984	0.009307
FGF12	0.07525	13.28981	0.012446	0.4549	0.004833
FGF20	0.46076	2.17031	0.18434	1.1517	0.097356
IFITM1	4.874	0.20517	0.195216	121.6904	0.334628
JAK1	0.03042	32.86862	0.004527	0.2045	0.000327
LAP3	0.2187	4.57247	0.002935	16.2981	0.489525
LMBR1L	0.09529	10.49381	0.016692	0.544	0.008172
MTCP1	0.40574	2.46462	0.075827	2.1711	0.29185
ORM1	1.94444	0.51429	1.189246	3.1792	0.008028
RFX5	42.58626	0.02348	1.080917	1677.8247	0.045341
TANK	12.11217	0.08256	0.910807	161.0709	0.058865
TNFSF10	6.24265	0.16019	0.551469	70.667	0.139076

The detailed results of univariate Cox proportional hazard regression were shown in **Supplementary Table 1**. Fourteen IRGs (AQP9, LMBR1L, FGF20, TANK, CRP, ORM1, JAK1, BACH1, MTCP1, IFITM1, TNFSF10, FGF12, RFX5, and LAP3) were identified by LASSO regression (**Figures 1A,B**). These IRGs were used to predict risk score by multivariate cox regression (**Figure 1C**). According to the risk coefficient of 14 IRGs from multivariate cox regression, a risk score formula was constructed as follows.

Risk score = (expression of AQP9 × 1.80452) + (expression of BACH2 × 2.49894) + (expression of CRP × 0.2329) + (expression of FGF12 × 0.07525) + (expression of FGF20 × 0.46076) + (expression of IFITM1 × 4.874) + (expression of JAK1 × 0.03042) + (expression of LAP3 × 0.2187) + (expression of LMBR1L × 0.09529) + (expression of MTCP1 × 0.40574) + (expression of ORM1 × 1.94444) + (expression of RFX5 × 42.58626) + (expression of TANK × 12.11217) + (expression of TNFSF10 × 6.24265). The result of multivariate Cox regression was shown in **Table 1**.

In this part, the relationship between gender and OS of DLBCL patients were explored, but there was no significant correlation between gender and survival.

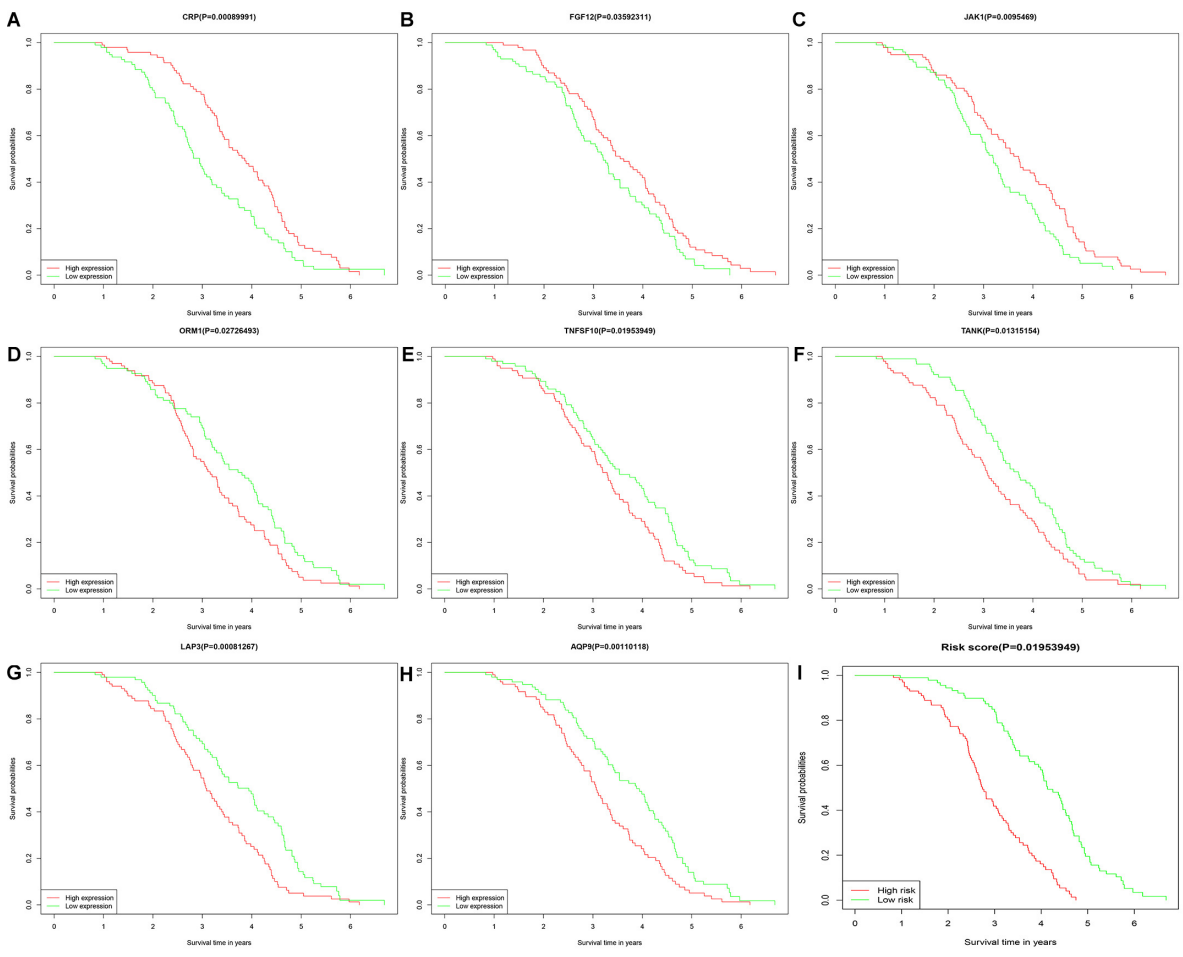

FIGURE 2 | Kaplan-Meier plotters showed about overall survival of 14 IRGs in DLBCL. The horizontal axis represented the survival time by month or year. The vertical axis represented survival probability. The high-risk group marked red and low-risk group marked green. There were six IRGs with no difference in OS between high and low risk groups. **(A–C)** CRP, FGF12, and JAK1. **(D–H)** ORM1, TNFSF10, TANK, LAP3, and AQP9. **(I)** The low-risk group and high-risk group.

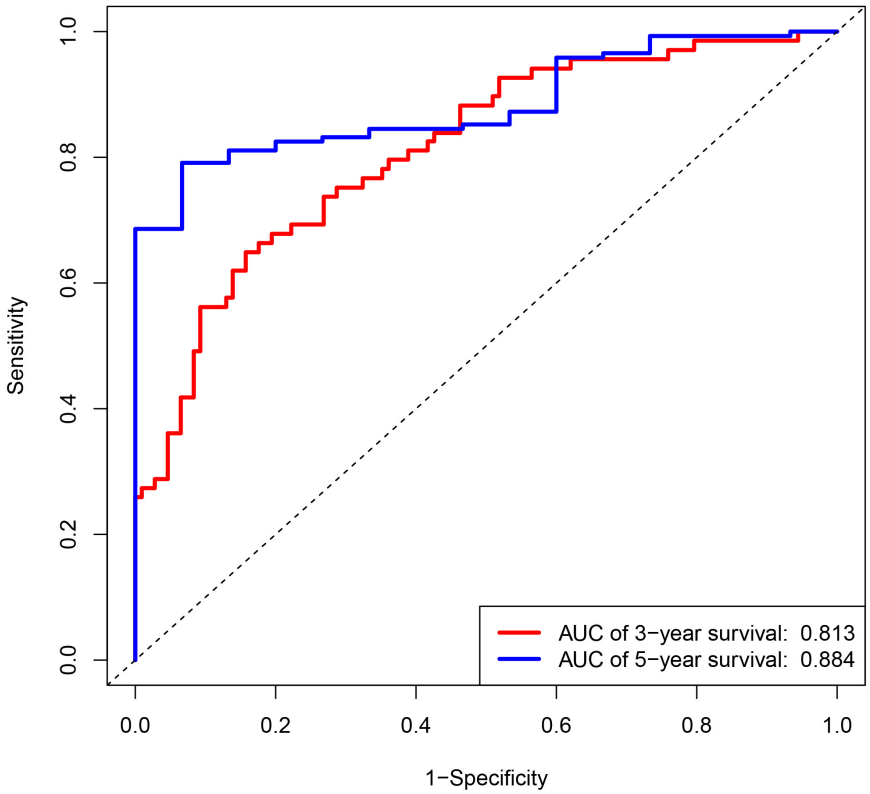

FIGURE 3 | Receiver operating characteristic (ROC) curves for 3- and 5-year survival probability according to 14 IRGs signature in the training group.

Using 14 IRGs Construct the Prognostic Risk Signature for DLBCL

Diffuse large B cell lymphoma patients were divided into low- and high-risk groups, according to the risk score calculated by formula, the median of the risk value was served as the cutoff value (cutoff = 1682). Survival curve and ROC curve were performed to test the suitability of the module. As shown in **Figures 2A–H**, the high expression of JAK1, CRP, and FGF12, may increase the risk of death, while, the high expression of AQP9, LAP3, ORM1, TANK, and TNFSF10, may increase the chance of survival. The K-M curve also indicated worse prognosis in the high-risk groups (**Figure 2I**). The areas under the curve (AUC) of 3- and 5-year ROC curve for the prognosis model were 0.813 and 0.884 (**Figure 3**).

Verification of the Prognostic Value of 14 IRGs Biomarkers

GSE32918 and TCGA-DLBC were used as validation cohorts in this work. Samples were divided into two groups according to the median risk score. Verification results were consistent with expectations, with the risk score increasing, the number of deaths increased. The AUC for 3- and 5-years survival in validation groups of GSE32918 were 0.779 and 0.709. The AUC for 3- and 5-years survival in validation groups of TCGA-DLBC were 0.824 and 0.813. The result of the K-M survival curve and ROC were shown in **Figure 4**.

Functional Annotation of the IRGs

Based on the GSE136971 expression data, we explored the difference between low- and high-risk groups using GSEA. Several significant enrichment signaling pathways were detected. Twelve significant pathways were differentially enriched in the low and high-risk groups, including chemokine signaling pathway, allograft rejection, viral myocarditis, leishmania infection, natural killer cell-mediated cytotoxicity, type I diabetes mellitus, graft versus host disease, amyotrophic lateral sclerosis (ALS), nod like receptor signaling pathway, apoptosis, Alzheimers' disease and toll-like receptor signaling pathway (**Figure 5** and **Table 2**).

Correlation Analysis Between IRGs and Immune Checkpoints

The four important immune checkpoints (LAG3, TIM3, CTLA-4, and PD-1/PD-L1) were widely used in cancer immunotherapy. To investigate the possible role of fourteen IRGs in ICB (immune checkpoint Blockade) therapy, the association of fourteen IRGs and four immune checkpoints were analyzed by Pearson's correlation analysis. Only the gene pairs which the *P*-value was less than 0.05 were shown in **Figure 6**. MTCP1 was negatively related to HAVCR2 (-0.42, $P = 0.0033$), TIM3 ($R = -0.31$, $P = 0.033$), and CTLA4 ($R = -0.3$, 0.038). The other 21 gene pairs were positive which *R* values were from 0.38 to 0.9, *P* values were less than 0.05.

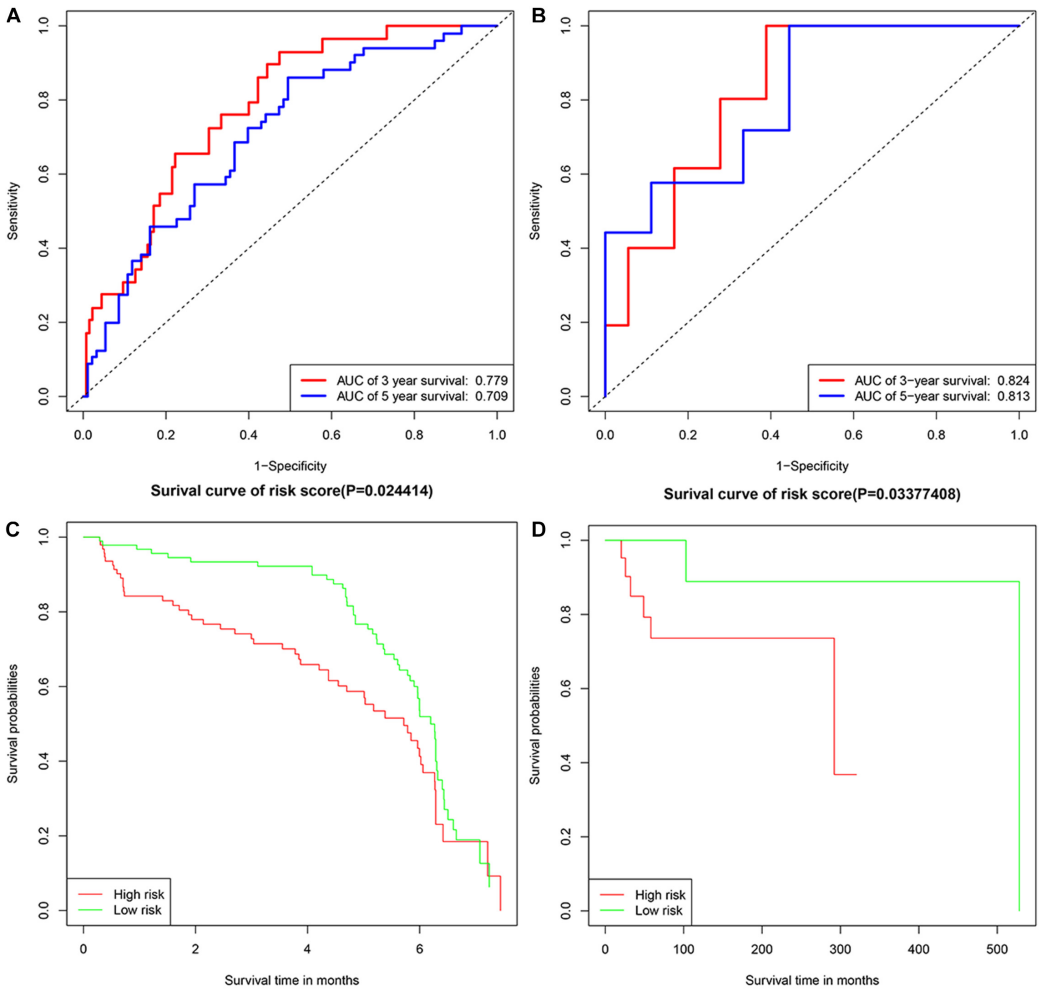

FIGURE 4 | The Kaplan-Meier plotters and ROC curves in validation groups. Panels **(A,B)** represented Kaplan-Meier plotters in TCGA-DLBC and GSE32918, separately. Panels **(C,D)** represented ROC curves in TCGA-DLBC and GSE32918, separately.

Immunocyte Infiltration in the Microenvironment

CIBERSORT was performed to understand the connection between IRGs and immune cell infiltration. The proportion of 22 immune cells was estimated according to the expression data of GSE136971. The immune score, stromal score and ESTIMATE score were calculated by ESTIMATE algorithm (**Figure 7**). Low-risk groups had higher level of immune infiltration. Furthermore, a significant difference was observed for the immune score (P = 1.9e-5) and ESTIMATE score (P = 4.4e-6). However, the difference of stromal score between low- and high-risk groups was not significant ($P \approx 0.056$). Six immune cells were observed between low- and high-risk groups (**Figure 8**). The higher expression level of CD8 T cells, CD4 memory T cells activated and M1 macrophages were shown in low-risk samples. Naïve B cells, regulatory T cells (Tregs) and monocytes were higher in high-risk individuals. In other 16 immune-related cells, expression differences were not statistically significant (**Supplementary Figure 2**).

Small Molecular Drugs Predicted by CMap

More than one probe in HG-U133A array was found to correspond to 14 IRGs, 15 probes were input "up" file and nine were input "down" file. Fourteen IRGs were uploaded to CMap to identify compounds that cured DLBCL, and ranked based on enrichment score (from −0.976 to 0.979) to screen the top 79 small molecular compounds ($P \leq 0.05$) (**Supplementary Table 2**). The drugs without P values were excluded. Therefore, these drugs might be the most promising novel candidates for DLBCL treatment.

Detect the Expression Level of 14 IRGs

The expression data of 14 IRGs were extracted from GSE8762, GSE64555, and GSE159472. The results of the differential expression of the 14 IRGs in the three data sets were same, except for JAk1. The differential expressions of JAK1 were significant higher expressed in disease samples both GSE136971 and GSE159472, however, in GSE64555, the expression of

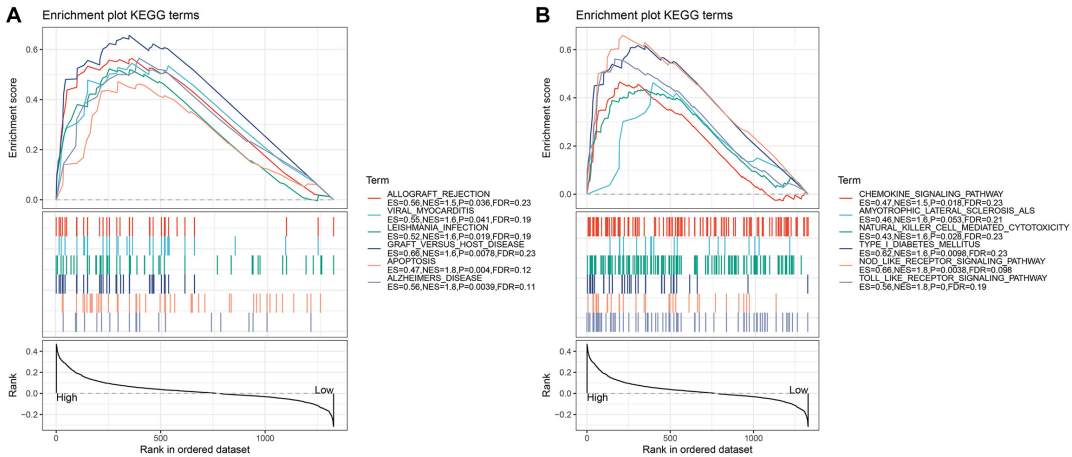

FIGURE 5 | (A,B) GSEA pathways enriched in the low- and high-risk groups according to the immune-related genes. There are too many results of GSEA enrichment, so it is divided into two graphs, panels **(A,B)**. Pathways enriched in the low-risk group. Vertical lines represented the positions of genes belonging to the set of special pathways. Negative enrichment score indicates a higher correlation with individuals in the low-risk group.

the normal samples was higher and in GSE159472 disease samples higher (**Figure 9**). It is possible that in the process of selecting test populations, differences in human bodies in different regions, or differences in some test populations, resulted in completely opposite results in the same disease sequencing process.

DISCUSSION

Although the combination treatment of Rituximab and standard CHOP chemotherapy had achieved unprecedented success in the prognosis and cure of DLBCL patients. However, the treatment of DLBCL is still tricky. Recently, immunotherapy is considered as a most potential treatment strategy and has shown strong strength in the treatment of cancers (Pitt et al., 2016; Llovet et al., 2018). As the present single biomarkers were not reliable enough to predict benefit from ICB therapy, the beneficiary group in DLBCL patients was few. It is essential to construct a multi-immune relevant-gene-based signature and analyze the correlation between the IRGs genes and immune checkpoints (Mushtaq et al., 2018).

Numerous previous studies had shown multi-immune related genes (IRGs) could be used as diagnostic tools and provided advice for the physician in multiple cancers (She et al., 2020; Zhang et al., 2020). However, the potential role of IRGs was not clear in DLBCL. Thus, a prognostic model was developed, which fourteen genes were included (AQP9, LMBR1L, FGF20, TANK, CRP, ORM1, JAK1, BACH1, MTCP1, IFITM1, TNFSF10, FGF12, RFX5, and LAP3), at the same time, its value of prognostic and prediction were analyzed.

The same gene may have different functions in different diseases. Poor prognostic factors had similar roles in different cancers, such as stimulating the proliferation and metastasis of tumor cell. High expression levels of AQP9 in renal cell carcinoma individual had the trend of bad prognosis (Yamada et al., 2019). However, high expression levels of AQP9 in gastric cancer and colorectal cancer patients were correlated with better OS (Huang et al., 2017; Thapa et al., 2018). The detailed information of the role of 13 IRGs play in different disease was shown in **Table 3**. All in all, our analysis results were in agreement with previous researches about these 14 genes. Therefore, all the present genes in this paper could be predicted as candidates for prognostic markers of DLBCL.

The impact of the sample size and external validation on the model were taken into account. GSE136971, containing 216 available individual samples, was used as a training group. Two external data were used to validate the validity of the model. DLBCL patients were divided into low- and high-risk score groups, risk score value was used as a parameter. The gene expression evaluating strategies of the different datasets might be different, especially, data was from different sources platforms. Different cutoff was used to eliminate the potential difference in training groups and validation groups. The high-risk groups tended to have worse OS; the prognostic value of this model

TABLE 2 | Detailed information of KEGG from GSEA.

KEGG NAMES	ES	NES	NOM p	FDR q
Toll like receptor signaling pathway	0.561	1.830	0.000	0.186
Alzheimers disease	0.565	1.811	0.004	0.114
apoptosis	0.472	1.763	0.004	0.123
Nod like receptor signaling pathway	0.659	1.757	0.004	0.098
Type I diabetes mellitus	0.617	1.637	0.010	0.233
Graft versus host disease	0.657	1.616	0.008	0.230
Natural killer cell mediated cytotoxicity	0.434	1.598	0.028	0.229
Amyotrophic lateral sclerosis (ALS)	0.463	1.594	0.053	0.207
Leishmania infection	0.522	1.589	0.019	0.190
Viral myocarditis	0.545	1.575	0.041	0.192
Allograft rejection	0.564	1.539	0.036	0.227
Chemokine signaling pathway	0.465	1.523	0.018	0.232

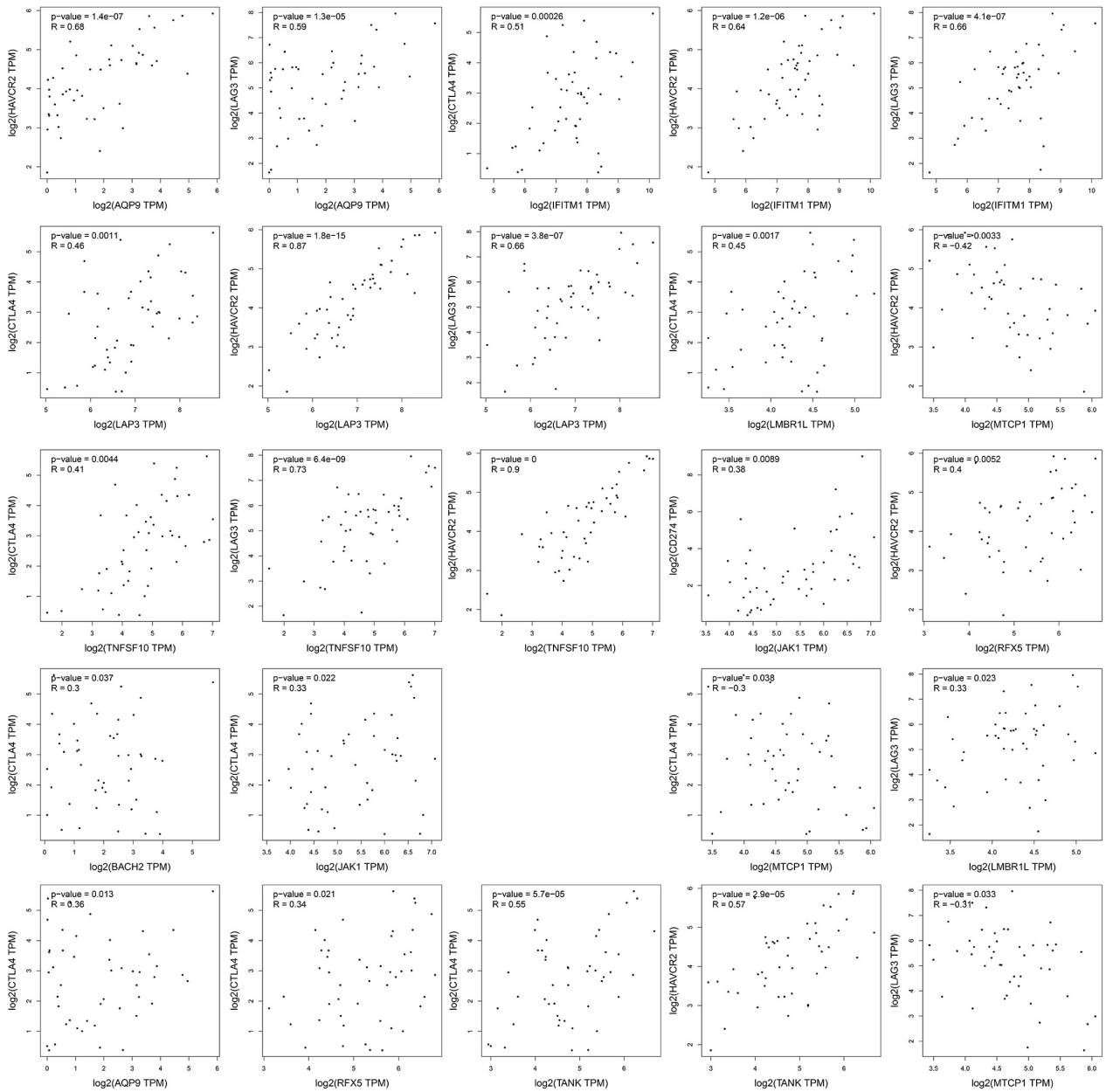

FIGURE 6 | The results of correlation analysis. The expression data of all gene had taken the logarithmic value of 2. The statistically insignificant experimental results were not shown.

remained robust in two validation groups. Moreover, the AUC values of the training groups and validation groups were larger than 0.7, so the model was reliable.

Gene set enrichment analysis was performed to have a deeper understand of the underlying molecular mechanisms of the occurrence and development of DLBCL. GSEA enrichment indicated that these pathways (chemokine signaling pathway, allograft rejection, viral myocarditis, leishmania infection, natural killer cell-mediated cytotoxicity, type I diabetes mellitus, graft versus host disease, nod like receptor signaling pathway, apoptosis, Alzheimer's disease and toll-like receptor signaling pathway.) were significantly related to the development of DLBCL. The abnormal expression of some chemotaxis, such as CCL3 and CCL4, were associated with bad prognosis in DLBCL (Takahashi et al., 2015). Viral myocarditis pathway involved autoimmune diseases (Zheng et al., 2016). The high expression of possible poor prognostic biomarker GJB2 caused bad prognostic through natural killer cell-mediated cytotoxicity pathway (Tang et al., 2020). Intrinsic anti-apoptosis was related to drug resistance and eventual fatal outcome in DLBCL patients to some extent (Muris et al., 2007; Cillessen et al., 2010; Liu et al., 2021).

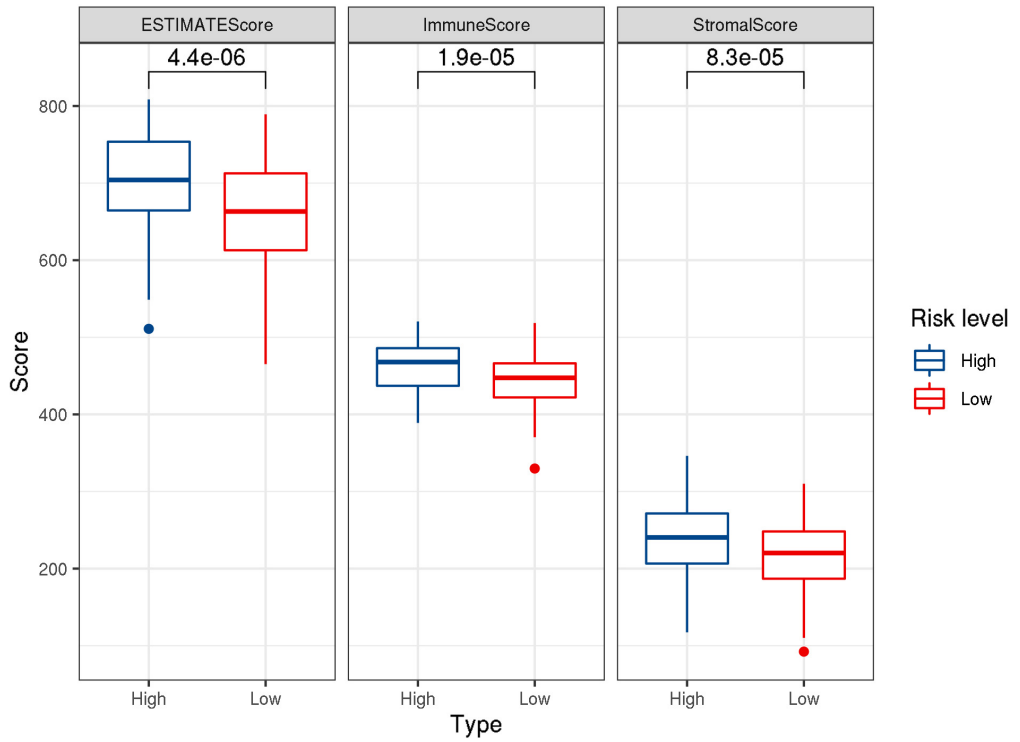

FIGURE 7 | Box-plots showed the difference in the scores of ESTIMATE, immune and stromal between the low- and high-risk groups.

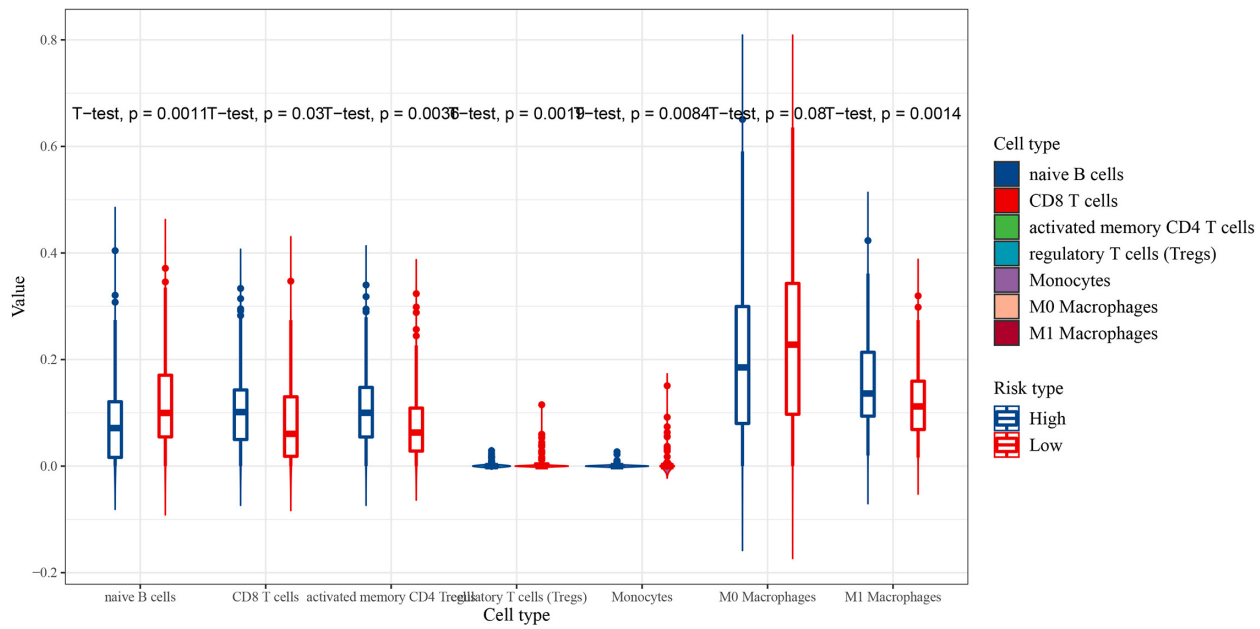

FIGURE 8 | The proportion of immune cell infiltration between the low-risk group (red) and high-risk group (blue) (significant differences between high and low risk groups).

Surprisingly, many studies had proved that there were gender differences in the occurrence and development of many diseases (Haitao et al., 2020; Strope et al., 2020). However, in this study, it was found that the OS rate and immune cell infiltration of DLBCL was not significantly related to gender. The differences in immune cells of gender in the same risk group were studied,

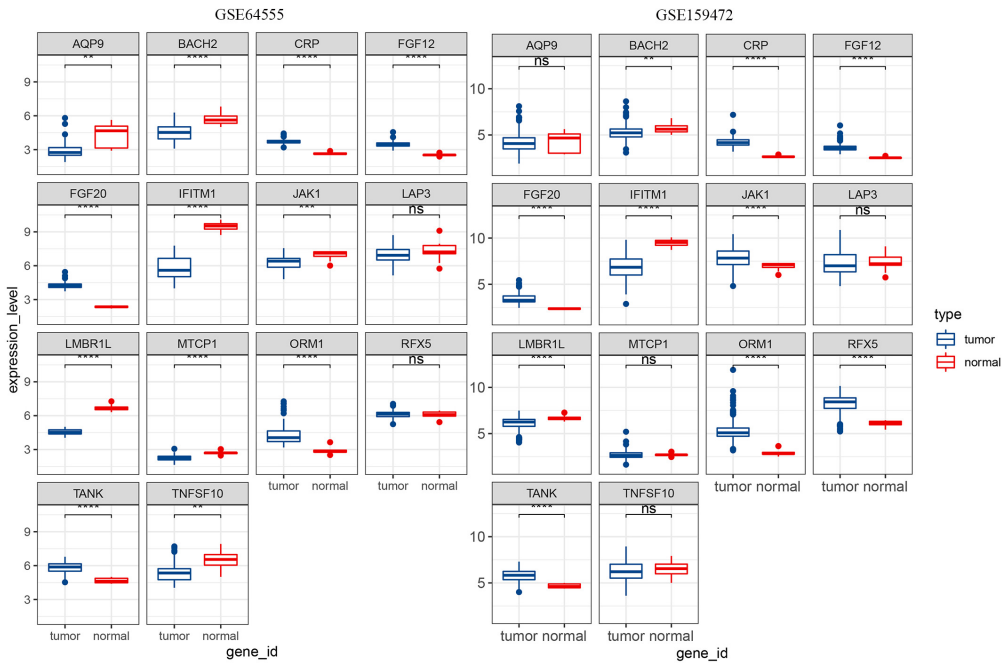

FIGURE 9 | The results of differential expression of 14 IRGs in two GEO data sets were shown.

TABLE 3 | The information of 13 IRGs related diseases and functions.

IRGs	Disease type	Functions
AQP9	Astrocytoma (Lv et al., 2018), hepatocellular carcinoma (Liao et al., 2020), breast cancer (Zhu et al., 2019), renal cell carcinoma (Yamada et al., 2019), melanoma (Gao et al., 2011) colorectal cancer and gastric cancer (Huang et al., 2017; Thapa et al., 2018)	Promote the invasion and motility inhibit cell apoptosis Overexpression of AQP9 were correlated to have better OS
LMBR1L	In mice (Choi et al., 2019)	Mutant LMBR1L impaired the development of lymphoid lineages
FGF20	Human hepatocellular carcinoma cells (Wang et al., 2017)	Stimulate the proliferation and migration of cancer cells
TANK		Antiviral innate immunity and negatively regulates NF-NF-κB signaling pathway (Kadkhodazadeh et al., 2012; Song et al., 2012).
CRP	BLBCL (Cao et al., 2012; Wang et al., 2016), breast cancer, non-metastatic clear cell renal cell carcinoma, non-small cell lung cancer and colorectal cancer risk (Nimptsch et al., 2015; Hu et al., 2016; Akamine et al., 2018; Preet et al., 2018a,b)	Inflammatory marker
ORM1	Rat model of septic stroke pathology	Neuroinflammation (Astrup et al., 2019; Higuchi et al., 2020; Mcguckin et al., 2020; Sharma et al., 2020)
JAK1		Immune deficiency in natural killer cells (Witalisz et al., 2019), the mutation of JAK1 was related to immune escape in many cancers (Xie et al., 2009; Albacker et al., 2017) apoptosis and growth in several cancers (Siavash et al., 2004) optimal fitness of activated B cell (Zhu et al., 2017)
BACH1	Lung cancer (Wiel et al., 2019), epithelial ovarian cancer, colon cancer, prostate cancer and colorectal cancer (Davudian et al., 2016; Shajari et al., 2017; Zhu et al., 2018; Han et al., 2019)	Stimulates glycolysis dependent lung cancer metastasis required for metastatic AsPC-1 cells (Sato et al., 2020) stimulate cancer cell metastasis
IFITM1	Lung cancer, colorectal cancer, inflammatory breast cancer, cervical squamous cell carcinoma and lung cancer (FangYu et al., 2015; Ogony et al., 2016; Jin et al., 2017; Zheng et al., 2017; Yan et al., 2019)	Silenced IFITM1 caused inhibited migration and invasion
TNFSF10	Amyloid-related disorders (Cantarella et al., 2015)	Stimulated proliferation and inflammation, and inhibited apoptosis (Huang et al., 2019) improvement and restrained immune/inflammatory response
FGF12	Esophageal squamous cell carcinoma (Bhushan et al., 2017a)	Silencing FGF12 inhibited apoptosis of radiation-induced cell and the cell migration and proliferation (Fumiaki et al., 2008; Bhushan et al., 2017b)
RFX5	Hepatocellular carcinoma	Promoted the progression of the cell cycle (Chen et al., 2020)
LAP3	Glioma cells (He et al., 2015), esophageal squamous cell (Zhang et al., 2014), ovarian carcinoma (Suganuma et al., 2005; Wang et al., 2015) breast cancer (Wang et al., 2020) and hepatocellular carcinoma (Tian et al., 2014)	Regulate cell proliferation, invasion and/or angiogenesis expressed in several malignant and affects tumor angiogenesis

but no significant differences were found. Male and female DLBCL patients may have the same immune pattern.

Our analysis result from ESTIMATE showed that high-risk group had higher immune cell infiltration scores. These research results were similar to the study of immune-related LncRNA in breast cancer (Shen et al., 2020). Naïve B cells and M0 macrophages cells had higher expression in low-risk score group, the expression of CD8 T cells, activated memory CD4 T cells and M1 macrophages cells were higher in the high-risk group. The infiltrating levels of CD8 T cells were associated with high-risk level and low OS (Jeong et al., 2017). The present and previous findings suggested that the infiltration of specific immune cells could cause bad prognosis.

It had some limitations in this work. First, the prognostic value of 14 IRGs was validated by two external data, but no *in vivo* or *in vitro* experimental study was carried out. Second, six IRGs (BACH2, FGF20, IFITM1, LMBR1L, MTCP1, and RFX5) part of risk model was all correlated to OS, but no difference was detected between low- and high-risk groups. The reason and rule of these IRGs were not explored.

In this work, we not only explored the role of the immune system in DLBCL development, but we provided an advanced treatment way.

CONCLUSION AND OUTLOOK

In this work, a risk score formula was established based on the 14 IRGs signature in DLBCL. According to these signatures, our study might present valuable clinical applications in personalized and precise treatment. The result of GSEA enrichment analysis indicated that the deterioration of DLBCL involved natural killer cell-mediated cytotoxicity and other 11 pathways. These 12 pathways were valuable to further analyze in cell and animal testing. Two strong correlation ($R > 0.8$) were found between TNSF10 and TIM-3 (HAVCR2), LAP3 and TIM-3. The expression level of TNSF10 and LAP3 could provide basis and guidance for immunotherapy. the infiltration and potential immune checkpoint blockade immunotherapy could be predicted. Furthermore, 79 small molecular were screened as potential drugs for DLBCL. Nevertheless, our conclusion should be tested by other public data and verified in future research.

DATA AVAILABILITY STATEMENT

The original contributions presented in the study are included in the article/**Supplementary Material**, further inquiries can be directed to the corresponding author/s.

ETHICS STATEMENT

Ethical review and approval was not required for the study on human participants in accordance with the local legislation and institutional requirements. Written informed consent for participation was not required for this study in accordance with the national legislation and the institutional requirements.

AUTHOR CONTRIBUTIONS

PF and GL were the major contributors in writing of this manuscript. GL was the responding author. YH, HL, and JP provided a few studies, ideas, and revised opinion. All authors have read and agreed to the published version of the manuscript.

ACKNOWLEDGMENTS

The authors would like to thank the Department of Basic Medicine at Changzhi Medical College.

SUPPLEMENTARY MATERIAL

The Supplementary Material for this article can be found online at: https://www.frontiersin.org/articles/10.3389/fgene.2021.625414/full#supplementary-material

Supplementary Figure 1 | A flowchart for methods was shown.

Supplementary Figure 2 | The proportion of immune cell infiltration between the low-risk group (red) and high-risk group (blue) (no significant differences between high and low risk groups).

REFERENCES

Akamine, T., Takada, K., Toyokawa, G., Kinoshita, F., Matsubara, T., et al. (2018). Association of preoperative serum CRP with PD-L1 expression in 508 patients with non-small cell lung cancer: A comprehensive analysis of systemic inflammatory markers. *Surgical Oncol. Oxford* 27, 88–94. doi: 10.1016/j.suronc.2018.01.002

Albacker, L. A., Wu, J., Smith, P., Warmuth, M., and Chmielecki, J. (2017). Loss of function JAK1 mutations occur at high frequency in cancers with microsatellite instability and are suggestive of immune evasion. *PLoS One* 12:e176181. doi: 10.1371/journal.pone.0176181

Astrup, L. B., Skovgaard, K., Rasmussen, R. S., Iburg, T. M., Agerholm, J. S., et al. (2019). Staphylococcus aureus infected embolic stroke upregulates Orm1 and Cxcl2 in a rat model of septic stroke pathology. *Neurol. Res.* 5, 399–412. doi: 10.1080/01616412.2019.1573455

Bhushan, A., Singh, A., Kapur, S., Borthakar, B. B., Sharma, J., et al. (2017a). Identification and validation of fibroblast growth factor 12 gene as a novel potential biomarker in esophageal cancer using cancer genomic datasets. *Omics J. Integrat. Biol.* 21, 616–631. doi: 10.1089/omi.2017.0116

Bhushan, A., Singh, A., Kapur, S., Borthakar, B. B., Sharma, J., et al. (2017b). Identification and validation of fibroblast growth factor 12 gene as a novel potential biomarker in esophageal cancer using cancer genomic datasets. *Omics J. Integrat. Biol.* 21, 616–631. doi: 10.1089/omi.2017.0116

Borghaei, H., Paz-Ares, L., Horn, L., Spigel, D. R., Steins, M., et al. (2015). Nivolumab versus Docetaxel in Advanced Nonsquamous Non-Small-Cell Lung Cancer. *N. Engl. J. Med.* 2, 123–135. doi: 10.1056/NEJMoa1507643

Calado, D. P., Zhang, B., Srinivasan, L., Sasaki, Y., Seagal, J., et al. (2010). Constitutive canonical NF-κB activation cooperates with disruption of BLIMP1 in the pathogenesis of activated b cell-like diffuse large cell lymphoma. *Cancer Cell* 18, 580–589. doi: 10.1016/j.ccr.2010.11.024

Cantarella, G., Di Benedetto, G., Puzzo, D., Privitera, L., Loreto, C., et al. (2015). Neutralization of TNFSF10 ameliorates functional outcome in a murine model of Alzheimer's disease. *Brain* 138, 203–216. doi: 10.1093/brain/awu318

Cao, Y., Shi, Y. X., Chen, J. O., Tan, Y. T., Cai, Y. C., et al. (2012). Serum C-reactive protein as an important prognostic variable in patients with diffuse large B cell lymphoma. *Tumour Biol.* 33, 1039–1044. doi: 10.1007/s13277-012-0337-z

Carpìo, C., Bouabdallah, R., Ysebaert, L., Sancho, J., Salles, G., et al. (2020). Avadomide monotherapy in relapsed/refractory DLBCL: Safety, efficacy, and a predictive gene classifier. *Blood* 135:2019002395. doi: 10.1182/blood.2019002395

Chen, D., Xie, X., Zhao, Y., Wang, X., Liao, W., et al. (2020). RFX5 promotes the progression of hepatocellular carcinoma through transcriptional activation of KDM4A. *Sci. Rep.* 10:14538. doi: 10.1038/s41598-020-71403-1

Choi, J. H., Zhong, X., McAlpine, W., Liao, T., Zhang, D., et al. (2019). LMBR1L regulates lymphopoiesis through Wnt/β-catenin signaling. *Science* 364:545. doi: 10.1126/science.aau0812

Cillessen, S. A. G. M., Meijer, C. J. L. M., Notoya, M., Ossenkoppele, G. J., and Oudejans, J. J. (2010). Molecular targeted therapies for diffuse large B-cell lymphoma based on apoptosis profiles. *J. Pathol.* 220, 509–520. doi: 10.1002/path.2670

Coiffier, B., and Sarkozy, C. (2016). Diffuse large B-cell lymphoma: R-CHOP failure-what to do? *Hematol. Am. Soc. Hematol. Educ. Program* 2016, 366–378. doi: 10.1182/asheducation-2016.1.366

Davudian, S., Shajari, N., Kazemi, T., Mansoori, B., Salehi, S., et al. (2016). BACH1 silencing by siRNA inhibits migration of HT-29 colon cancer cells through reduction of metastasis-related genes. *Biomed. Pharmacother.* 84, 191–198. doi: 10.1016/j.biopha.2016.09.021

Dobashi, and Akito. (2016). Molecular pathogenesis of diffuse large B-Cell lymphoma. *J. Clin. Exp. Hematopathol. Jceh* 56, 71–78. doi: 10.3960/jslrt.56.71

FangYu, DanXie, Ng, S. S., TungLum, C., Mu-YanCai, et al. (2015). IFITM1 promotes the metastasis of human colorectal cancer via CAV-1. *Cancer Lett.* 368, 135–143. doi: 10.1016/j.canlet.2015.07.034

Fumiaki, N., Kerstin, M., Akiko, H., Roland, R., Makoto, A., et al. (2008). Involvement of intracellular expression of FGF12 in radiation-induced apoptosis in mast cells. *J. Radiat. Res.* 49, 491–501. doi: 10.1269/jrr.08021

Gao, L., Gao, Y., Li, X., Howell, P., Kumar, R., et al. (2011). Aquaporins mediate the chemoresistance of human melanoma cells to arsenite. *Mole. Oncol.* 6, 81–87. doi: 10.1016/j.molonc.2011.11.001

Gentzler, R., Hall, R., Kunk, P. R., Gaughan, E., Dillon, P., et al. (2016). Beyond melanoma: Inhibiting the PD-1/PD-L1 pathway in solid tumors. *Immunotherapy* 8, 583–600. doi: 10.2217/imt-2015-0029

Georg Lenz Louis, M., and Staudt. (2010). Aggressive lymphomas. *N. Engl. J. Med.* 2010, 1417–1429. doi: 10.1056/NEJMra0807082

Gettinger, S., Rizvi, N. A., Chow, L. Q., Borghaei, H., Brahmer, J., et al. (2016). Nivolumab monotherapy for First-Line treatment of advanced Non-Small-Cell lung cancer. *J. Clin. Oncol.* 2016, 2980–2987. doi: 10.1200/JCO.2016.66.9929

Haitao, T., Vermunt, J. V., Abeykoon, J., Ghamrawi, R., Gunaratne, M., et al. (2020). COVID-19 and sex differences: Mechanisms and biomarkers. *Mayo Clin. Proc.* 95, 2189–2203. doi: 10.1016/j.mayocp.2020.07.024

Han, W., Zhang, Y., Niu, C., Guo, J., Li, J., et al. (2019). BTB and CNC homology 1 (Bach1) promotes human ovarian cancer cell metastasis by HMGA2-mediated epithelial-mesenchymal transition. *Cancer Lett.* 445, 45–56. doi: 10.1016/j.canlet.2019.01.003

He, X., Huang, Q., Qiu, X., Liu, X., Sun, G., et al. (2015). LAP3 promotes glioma progression by regulating proliferation, migration and invasion of glioma cells. *Int. J. Biol. Macromolecules* 72, 1081–1089. doi: 10.1016/j.ijbiomac.2014.10.021

Higuchi, H., Kamimura, D., Jiang, J. J., Atsumi, T., and Murakami, M. (2020). Orosomucoid 1 is involved in the development of chronic allograft rejection after kidney transplantation. *Int. Immunol.* 7, 493. doi: 10.1093/intimm/dxaa024

Hosseini, A., Gharibi, T., Marofi, F., Babaloo, Z., and Baradaran, B. (2020). CTLA-4: From mechanism to autoimmune therapy. *Int. Immunophar.* 80:106221. doi: 10.1016/j.intimp.2020.106221

Hu, H., Xia, W. K., Wu, X., Yu, T. H., Wu, Y., et al. (2016). Prognostic significance of lymphocyte-to-monocyte ratio and CRP in patients with nonmetastatic clear cell renal cell carcinoma: A retrospective multicenter analysis. *Oncotargets Ther.* 9, 2759–2767. doi: 10.2147/OTT.S101458

Huang, B., Yu, H., Li, Y., Zhang, W., and Liu, X. (2019). Upregulation of long noncoding TNFSF10 contributes to osteoarthritis progression through the miR-376-3p/FGFR1 axis. *J. Cell. Biochem.* 120, 19610–19620. doi: 10.1002/jcb.29267

Huang, D., Feng, X., Liu, Y., Deng, Y., Chen, H., et al. (2017). AQP9-induced cell cycle arrest is associated with RAS activation and improves chemotherapy treatment efficacy in colorectal cancer. *Cell Death Dis.* 8:e2894. doi: 10.1038/cddis.2017.282

Jeong, J., Oh, E. J., Yang, W. I., Kim, S. J., and Yoon, S. O. (2017). Implications of infiltrating immune cells within bone marrow of patients with diffuse large B-cell lymphoma. *Hum. Pathol.* 64, 222–231. doi: 10.1016/j.humpath.2017.04.012

Jin, B., Jin, H., and Wang, J. (2017). Silencing of Interferon-Induced transmembrane protein 1 (IFITM1) inhibits proliferation, migration, and invasion in lung cancer cells. *Oncol. Res.* doi: 10.3727/096504017X14844360974116 [Epub ahead of print].

Kadkhodazadeh, M., Amid, R., Ebadian, A. R., Shams, E., and Tamizi, M. (2012). TRAF family member-associated NF-KB activator (TANK) gene polymorphism in chronic periodontitis and peri-implantitis patients. *J. Long-Term Effects Med. Implants* 22, 127–136. doi: 10.1615/jlongtermeffmedimplants.v22.i2.30

Kim, Y. R., Min, Y. H., Hyunyoon, D., Shin, H., Mun, Y., et al. (2012). Prognostic factors in primary diffuse large B-cell lymphoma of adrenal gland treated with rituximab-CHOP chemotherapy from the Consortium for Improving Survival of Lymphoma (CISL). *J. Hematol. Oncol.* 5:49. doi: 10.1186/1756-8722-5-49

Liao, S., Chen, H., Liu, M., Gan, L., Li, C., et al. (2020). Aquaporin 9 inhibits growth and metastasis of hepatocellular carcinoma cells via Wnt/β-catenin pathway. *Aging* 12, 1527–1544. doi: 10.18632/aging.102698

Lin, Z., Chen, X., Li, Z., Luo, Y., Fang, Z., et al. (2016). PD-1 antibody monotherapy for malignant melanoma: A systematic review and Meta-Analysis. *PLoS One* 11:e160485. doi: 10.1371/journal.pone.0160485

Liu, K., Song, J., Yan, Y., Zou, K., Che, Y., et al. (2021). Melatonin increases the chemosensitivity of diffuse large B-cell lymphoma cells to epirubicin by inhibiting P-glycoprotein expression via the NF-κB pathway. *Transl. Oncol.* 14:100876. doi: 10.1016/j.tranon.2020.100876

Liu, X., Wu, S., Yang, Y., Zhao, M., Zhu, G., et al. (2017). The prognostic landscape of tumor-infiltrating immune cell and immunomodulators in lung cancer. *Biomed. Pharmacother.* 95, 55–61. doi: 10.1016/j.biopha.2017.08.003

Llovet, J. M., Robert, M., Daniela, S., and Finn, R. S. (2018). Molecular therapies and precision medicine for hepatocellular carcinoma. *Nat. Rev. Clin. Oncol.* 15, 599–616. doi: 10.1038/s41571-018-0073-4

Lv, Y., Huang, Q., Dai, W., Jie, Y., Yu, G., et al. (2018). AQP9 promotes astrocytoma cell invasion and motility via the AKT pathway. *Oncol. Lett.* 16, 6059–6064. doi: 10.3892/ol.2018.9361

Mcguckin, M. M., Giesy, S. L., Davis, A. N., Abyeta, M. A., and Boisclair, Y. R. (2020). The acute phase protein orosomucoid 1 is upregulated in early lactation but does not trigger appetite-suppressing STAT3 signaling via the leptin receptor. *J. Dairy Ence* 103, 4765–4776. doi: 10.3168/jds.2019-18094

Motzer, R. J., Rini, B. I., Mcdermott, D. F., Redman, B. G., Kuzel, T. M., et al. (2014). Nivolumab for metastatic renal cell carcinoma: Results of a randomized phase II trial. *J. Clin. Oncol.* 33, 1430–1437. doi: 10.1200/JCO.2014.59.0703

Muris, J. J. F., Ylstra, B., Cillessen, S. A. G. M., Ossenkoppele, G. J., Kluin-Nelemans, J. C., et al. (2007). Profiling of apoptosis genes allows for clinical stratification of primary nodal diffuse large B-cell lymphomas. *Br. J. Haemat.* 136, 38–47. doi: 10.1111/j.1365-2141.2006.06375.x

Mushtaq, M. U., Papadas, A., Pagenkopf, A., Flietner, E., Morrow, Z., et al. (2018). Tumor matrix remodeling and novel immunotherapies: The promise of matrix-derived immune biomarkers. *J. ImmunoTher. Cancer* 6:65. doi: 10.1186/s40425-018-0376-0

Nimptsch, K., Aleksandrova, K., Boeing, H., Janke, J., Lee, Y., et al. (2015). Association of CRP genetic variants with blood concentrations of C-reactive protein and colorectal cancer risk. *Int. J. Cancer* 136, 1181–1192. doi: 10.1002/ijc.29086

Ogony, J., Choi, H. J., Lui, A., Cristofanilli, M., and Lewis-Wambi, J. (2016). Interferon-induced transmembrane protein 1 (IFITM1) overexpression enhances the aggressive phenotype of SUM149 inflammatory breast cancer cells in a signal transducer and activator of transcription 2 (STAT2)-dependent manner. *Breast Cancer Res.* 18:25. doi: 10.1186/s13058-016-0683-7

Opinto, G., Vegliante, M. C., Negri, A., Skrypets, T., and Ciavarella, S. (2020). The tumor microenvironment of DLBCL in the computational era. *Front. Oncol.* 10:351. doi: 10.3389/fonc.2020.00351

Pitt, J. M., Vétizou, M., Daillère, R., Roberti, M. P., Yamazaki, T., et al. (2016). Resistance mechanisms to Immune-Checkpoint blockade in cancer: Tumor-Intrinsic and -Extrinsic factors. *Immunity* 44, 1255–1269. doi: 10.1016/j.immuni.2016.06.001

Popovic, A., Jaffee, E. M., and Zaidi, N. (2018). Emerging strategies for combination checkpoint modulators in cancer immunotherapy. *J. Clin. Investig.* 128, 3209–3218. doi: 10.1172/JCI120775

Preet, K. R., Rubal, Singh, B. R. P., Rajesh, V., Monisha, D., et al. (2018a). Association of elevated levels of C-reactive protein with breast cancer, breast cancer subtypes and poor outcome. *Curr. Problems Cancer* 2, 123–129. doi: 10.1016/j.currproblcancer.2018.05.003

Preet, K. R., Rubal, Singh, B. R. P., Rajesh, V., Monisha, D., et al. (2018b). Association of elevated levels of C-reactive protein with breast cancer, breast cancer subtypes and poor outcome. *Curr. Problems Cancer* 223:S1897824381. doi: 10.1016/j.currproblcancer.2018.05.003

Reck, M., Rodríguez-Abreu, D., Robinson, A. G., Hui, R., Cs Szi, T., et al. (2016). Pembrolizumab versus Chemotherapy for PD-L1-Positive Non-Small-Cell Lung Cancer. *N. Engl. J. Med.* 375:1823. doi: 10.1056/NEJMoa1606774

Rittmeyer, A., Barlesi, F., Waterkamp, D., Park, K., and Gandara, D. D. R. (2016). Atezolizumab versus docetaxel for patients with previously treated non-small-cell lung cancer (POPLAR): A multicentre, open-label, phase 2 randomised controlled trial. *Lancet* 2016, 1837–1846. doi: 10.1016/S0140-6736(16)00587-0

Rowshanravan, B., Halliday, N., and Sansom, D. M. (2017). CTLA-4: A moving target in immunotherapy. *Blood* 2017:741033. doi: 10.1182/blood-2017-06-741033

Sato, M., Matsumoto, M., Saiki, Y., Alam, M., and Igarashi, K. (2020). BACH1 promotes pancreatic cancer metastasis by repressing epithelial genes and enhancing Epithelial-Mesenchymal transition. *Cancer Res.* 80, 4018–4099. doi: 10.1158/0008-5472.CAN-18-4099

Schumacher, T. N., and Schreiber, R. D. (2015). Neoantigens in cancer immunotherapy. *Science* 348:69. doi: 10.1126/science.aaa4971

Scott, D. W., and Gascoyne, R. D. (2014). The tumour microenvironment in B cell lymphomas. *Nat. Rev. Cancer* 14, 517–534. doi: 10.1038/nrc3774

Sebastian, K., Stanislav, P., Felicitas, R., and Johannes, V. B. (2018). Rationale for combining bispecific t cell activating antibodies with checkpoint blockade for cancer therapy. *Front. Oncol.* 8:285. doi: 10.3389/fonc.2018.00285

Shajari, N., Davudian, S., Kazemi, T., Mansoori, B., Salehi, S., et al. (2017). Silencing of BACH1 inhibits invasion and migration of prostate cancer cells by altering metastasis-related gene expression. *Artif Cells Nanomed. Biotechnol.* 46, 1–10. doi: 10.1080/21691401.2017.1374284

Sharma, T., Datta, K. K., Kumar, M., Dey, G., and Bhagat, H. (2020). Intracranial aneurysm biomarker candidates identified by a Proteome-Wide study. *Omics J. Integrat. Biol.* 24:0057. doi: 10.1089/omi.2020.0057

She, Y., Kong, X., Ge, Y., Yin, P., Liu, Z., et al. (2020). Immune-related gene signature for predicting the prognosis of head and neck squamous cell carcinoma. *Cancer Cell Int.* 20, 1104–1107. doi: 10.1186/s12935-020-1104-7

Shen, Y., Peng, X., and Shen, C. (2020). Identification and validation of immune-related lncRNA prognostic signature for breast cancer. *Genomics* 112, 2640–2646. doi: 10.1016/j.ygeno.2020.02.015

Siavash, H., Nikitakis, N. G., and Sauk, J. J. (2004). Abrogation of IL-6-mediated JAK/STAT signaling by the cyclopentenone prostaglandin 15-Deoxy-Δ12,14-Prostaglandin J2 in oral squamous carcinoma cells. *Cancer Res.* 64, 1074–1080. doi: 10.1038/sj.bjc.6602055

Silver, D. J., Sinyuk, M., Vogelbaum, M. A., Ahluwalia, M. S., and Lathia, J. D. (2015). The intersection of cancer, cancer stem cells, and the immune system: Therapeutic opportunities. *Neuro Oncol.* 2, 153–159. doi: 10.1093/neuonc/nov157

Song, Q. L., He, X. X., Yang, H., Li, J., Chen, M., et al. (2012). Association of a TANK gene polymorphism with outcomes of hepatitis B virus infection in a Chinese Han population. *Viral Immunol.* 1, 73–78. doi: 10.1089/vim.2011.0053

Strope, J. D., Chau, C. H., and Figg, W. D. (2020). Are sex discordant outcomes in COVID-19 related to sex hormones? *Sem. Oncol.* 2020:06.002. doi: 10.1053/j.seminoncol.2020.06.002

Suganuma, T., Ino, K., Shibata, K., Kajiyama, H., Nagasaka, T., et al. (2005). Functional expression of the angiotensin II type1 receptor in human ovarian carcinoma cells and its blockade therapy resulting in suppression of tumor invasion, angiogenesis, and peritoneal dissemination. *Clin. Cancer Res.* 11, 2686–2694. doi: 10.1158/1078-0432.CCR-04-1946

Takahashi, K., Sivina, M., Hoellenriegel, J., Oki, Y., Hagemeister, F. B., et al. (2015). CCL3 and CCL4 are biomarkers for B cell receptor pathway activation and prognostic serum markers in diffuse large B cell lymphoma. *Br. J. Haematol.* 171, 726–735. doi: 10.1111/bjh.13659

Tang, Y., Zhang, Y., and Wu, Z. (2020). High GJB2 mRNA expression and its prognostic significance in lung adenocarcinoma: A study based on the TCGA database. *Med.* 99:e19054. doi: 10.1097/MD.0000000000019054

Thapa, S., Chetry, M., Huang, K., Peng, Y., Wang, J., et al. (2018). Significance of aquaporins' expression in the prognosis of gastric cancer. *Bioence Rep.* 38, R20171687. doi: 10.1042/BSR20171687

Tian, S. Y., Chen, S. H., Shao, B. F., Cai, H. Y., and Xu, A. B. (2014). Expression of leucine aminopeptidase 3 (LAP3) correlates with prognosis and malignant development of human hepatocellular carcinoma (HCC). *Int. J. Clin. Exp. Pathol.* 7, 3752–3762. doi: 10.1016/B978-0-12-800092-2.00013-7

Velcheti, V., Schalper, K. A., Carvajal, D. E., Anagnostou, V. K., Syrigos, K. N., et al. (2014). Programmed death ligand-1 expression in non-small cell lung cancer. *Lab. Invest. J. Tech. Methods Pathol.* 94, 107–116. doi: 10.1038/labinvest.2013.130

Wallin, J. J., Bendell, J. C., Funke, R., Sznol, M., Korski, K., et al. (2016). Atezolizumab in combination with bevacizumab enhances antigen-specific T-cell migration in metastatic renal cell carcinoma. *Nat. Commun.* 7:12624. doi: 10.1038/ncomms12624

Wang, J., Zhou, M., Wang, X., Xu, J., Chen, B., et al. (2016). Pretreatment C-reactive protein was an independent prognostic factor for patients with diffuse large B-cell lymphoma treated with RCHOP. *Clin. Chim. Acta* 459, 150–154. doi: 10.1016/j.cca.2016.05.033

Wang, S., Lin, H., Zhao, T., Huang, S., Fernig, D., et al. (2017). Expression and purification of an FGF9 fusion protein in E. Coli, and the effects of the FGF9 subfamily on human hepatocellular carcinoma cell proliferation and migration. *Appl. Microb. Biotechnol.* 101, 7823–7835. doi: 10.1007/s00253-017-8468-1

Wang, X., Ji, S., Ma, Y., Xing, X., Zhou, Y., et al. (2020). Vimentin plays an important role in the promotion of breast cancer cell migration and invasion by leucine aminopeptidase 3. *Cytotechnology* 72, 639–647. doi: 10.1007/s10616-020-00402-x

Wang, X., Shi, L., Deng, Y., Qu, M., Mao, S., et al. (2015). Inhibition of leucine aminopeptidase 3 suppresses invasion of ovarian cancer cells through down-regulation of fascin and MMP-2/9. *Eur. J. Pharmacol.* 768, 116–122. doi: 10.1016/j.ejphar.2015.10.039

Wiel, C., Le Gal, K., Ibrahim, M. X., Jahangir, C. A., Kashif, M., et al. (2019). BACH1 stabilization by antioxidants stimulates lung cancer metastasis. *Cell* 178, 330–345. doi: 10.1016/j.cell.2019.06.005

Witalisz, A., Klein, K., Prinz, D., Leidenfrost, N., Schabbauer, G., et al. (2019). Loss of JAK1 drives innate immune deficiency. *Front. Immunol.* 9:3108. doi: 10.3389/fimmu.2018.03108

Xie, H., Bae, H., Noh, J., Eun, J., Kim, J., et al. (2009). Mutational analysis of JAK1 gene in human hepatocellular carcinoma. *Neoplasma* 56, 136–140. doi: 10.4149/neo_2009_02_136

Yamada, Y., Arai, T., Kato, M., Kojima, S., Sakamoto, S., et al. (2019). Role of pre-miR-532 (miR-532-5p and miR-532-3p) in regulation of gene expression and molecular pathogenesis in renal cell carcinoma. *Am. J. Clin. Exp. Urol.* 7, 11–30.

Yan, J., Jiang, Y., Lu, J., Wu, J., and Zhang, M. (2019). Inhibiting of proliferation, migration, and invasion in lung cancer induced by silencing Interferon-Induced transmembrane protein 1 (IFITM1). *BioMed. Res. Int.* 2019, 1–9. doi: 10.1155/2019/9085435

Zhang, J., Zhang, J., Yuan, C., Luo, Y., Li, Y., et al. (2020). Establishment of the prognostic index of lung squamous cell carcinoma based on immunogenomic landscape analysis. *Cancer Cell Int.* 20, 01429–y. doi: 10.1186/s12935-020-01429-y

Zhang, L., Chen, Z., Zuo, W., Zhu, X., Li, Y., et al. (2016). Omacetaxine mepesuccinate induces apoptosis and cell cycle arrest, promotes cell differentiation, and reduces telomerase activity in diffuse large Bcell lymphoma cells. *Mole. Med. Rep.* 13, 3092–3100. doi: 10.3892/mmr.2016.4899

Zhang, S., Yang, X., Shi, H., Li, M., Xue, Q., et al. (2014). Overexpression of leucine aminopeptidase 3 contributes to malignant development of human esophageal squamous cell carcinoma. *J. Mole. Histol.* 45, 283–292. doi: 10.1007/s10735-014-9566-3

Zheng, W. Y., Zheng, W. X., and Hua, L. (2016). Detecting shared pathways linked to rheumatoid arthritis with other autoimmune diseases in a in silico analysis. *Mole. Biol.* 50, 462–469. doi: 10.1134/S0026893316030146

Zheng, W., Zhao, Z., Yi, X., Zuo, Q., Li, H., et al. (2017). Down-regulation of IFITM1 and its growth inhibitory role in cervical squamous cell carcinoma. *Cancer Cell Int.* 17:88. doi: 10.1186/s12935-017-0456-0

Zhou, Y., Li, G., and Xu, G. (2020). Kaempferol protects cell damage in in vitro ischemia reperfusion model in rat neuronal PC12 cells. *BioMed. Res. Int.* 2020, 2461079. doi: 10.1155/2020/2461079

Zhu, F., Hwang, B., Miyamoto, S., and Rui, L. (2017). Nuclear import of JAK1 is mediated by a classical NLS and is required for survival of diffuse large b-cell lymphoma. *Mole. Cancer Res.* 15, 348–357. doi: 10.1158/1541-7786.MCR-16-0344

Zhu, G. D., Liu, F., Ouyang, S., Zhou, R., Jiang, F. N., et al. (2018). BACH1 promotes the progression of human colorectal cancer through BACH1/CXCR4 pathway. *Biochem. Biophys. Res. Commun.* 499, 120–127. doi: 10.1016/j.bbrc.2018.02.178

Zhu, L., Ma, N., Wang, B., Wang, L., Zhou, C., et al. (2019). Significant prognostic values of aquaporin mRNA expression in breast cancer. *Cancer Manag. Res.* 11, 1503–1515. doi: 10.2147/CMAR.S193396

Conflict of Interest: The authors declare that the research was conducted in the absence of any commercial or financial relationships that could be construed as a potential conflict of interest.

frontiers in Genetics

ORIGINAL RESEARCH
published: 16 February 2021
doi: 10.3389/fgene.2021.623424

Correlations Between Tumor Mutation Burden and Immunocyte Infiltration and Their Prognostic Value in Colon Cancer

Zhangjian Zhou[1†], Xin Xie[2†], Xuan Wang[2], Xin Zhang[2], Wenxin Li[2], Tuanhe Sun[2], Yifan Cai[1], Jianhua Wu[1], Chengxue Dang[2] and Hao Zhang[2*]*

[1] Department of Oncology, The Second Affiliated Hospital of Xi'an Jiaotong University, Xi'an, China, [2] Department of Surgical Oncology, The First Affiliated Hospital of Xi'an Jiaotong University, Xi'an, China

Background: Colon cancer has a huge incidence and mortality worldwide every year. Immunotherapy could be a new therapeutic option for patients with advanced colon cancer. Tumor mutation burden (TMB) and immune infiltration are considered critical in immunotherapy but their characteristics in colon cancer are still controversial.

Methods: The somatic mutation, transcriptome, and clinical data of patients with colon cancer were obtained from the TCGA database. Patients were divided into low or high TMB groups using the median TMB value. Somatic mutation landscape, differentially expressed genes, and immune-related hub genes, Gene Ontology and KEGG, gene set enrichment, and immune infiltration analyses were investigated between the two TMB groups. Univariate and multivariate Cox analyses were utilized to construct a prognostic gene signature. The differences in immune infiltration, and the expression of HLA-related genes and checkpoint genes were investigated between the two immunity groups based on single sample gene set enrichment analysis. Finally, a nomogram of the prognostic prediction model integrating TMB, immune infiltration, and clinical parameters was established. Calibration plots and receiver operating characteristic curves (ROC) were drawn, and the C-index was calculated to assess the predictive ability.

Results: Missense mutations and single nucleotide polymorphisms were the major variant characteristics in colon cancer. The TMB level showed significant differences in N stage, M stage, pathological stage, and immune infiltration. $CD8^+$ T cells, activated memory $CD4^+$ T cells, activated NK cells, and M1 macrophages infiltrated more in the high-TMB group. The antigen processing and presentation signaling pathway was enriched in the high-TMB group. Two immune related genes (CHGB and SCT) were identified to be correlated with colon cancer survival (HR = 1.39, $P = 0.01$; HR = 1.26, $P = 0.02$, respectively). Notably, the expression of SCT was identified as a risk factor in the immune risk model, in which high risk patients showed poorer survival ($P = 0.04$). High immunity status exhibited significant correlations with immune response pathways, HLA-related genes, and immune checkpoint genes. Finally, including nine factors, our

OPEN ACCESS

Edited by:
Xiao-Jie Lu,
Nanjing Medical University, China

Reviewed by:
Valentina Silvestri,
Sapienza University of Rome, Italy
Weifeng Ding,
Nantong University, China

***Correspondence:**
Chengxue Dang
dangchengxue@mail.xjtu.edu.cn
Hao Zhang
hao.zhang@mail.xjtu.edu.cn

† These authors have contributed equally to this work

Specialty section:
This article was submitted to Cancer Genetics, a section of the journal Frontiers in Genetics

Received: *30 October 2020*
Accepted: *21 January 2021*
Published: *16 February 2021*

Citation:
Zhou Z, Xie X, Wang X, Zhang X, Li W, Sun T, Cai Y, Wu J, Dang C and Zhang H (2021) Correlations Between Tumor Mutation Burden and Immunocyte Infiltration and Their Prognostic Value in Colon Cancer. Front. Genet. 12:623424. doi: 10.3389/fgene.2021.623424

nomogram prediction model showed better calibration (C-index = 0.764) and had an AUC of 0.737.

Conclusion: In this study, we investigated the patterns and prognostic roles of TMB and immune infiltration in colon cancer, which provided new insights into the tumor microenvironment and immunotherapies and the development of a novel nomogram prognostic prediction model for patients with colon cancer.

Keywords: colon cancer, tumor mutation burden (TMB), immunocytes infiltration, prognosis prediction, bioinformatics

INTRODUCTION

Colon cancer is the most common neoplasm in the digestive system, contributing to approximately 1.1 million new cases and 550,000 deaths in 2018, which makes it the third ranking cancer based on incidence and the second leading cancer based on mortality among all malignances (Bray et al., 2018). The epidemiological characteristics show a modernity manner with a higher incidence in developed countries, such as European countries and Australia/New Zealand, than in developing countries (Brody, 2015; Bray et al., 2018). However, in China, the incidence of colon cancer exhibits a mixture of profiles with huge differences between urban and rural areas (Chen et al., 2016). Due to different lifestyles and socioeconomic statuses, the incidence of colon cancer in urban areas is higher than that in rural areas, while the mortality remains similar (Pan et al., 2017). With improvements in early screening methods and therapeutic strategies, new cases and death rates have decreased in elderly people over the past 10 years. Notably, for people < 50 years old, the incidence has increased for unknown reasons, which indicates that more investigations and research in young adults are warranted (Siegel et al., 2017).

For advanced patients who lose curable surgery opportunities, systematic or multidisciplinary therapeutic strategies, including chemotherapy, targeted therapy, and immunotherapy could be considered to improve the prognosis (Dienstmann et al., 2015; Auclin et al., 2017; Wu, 2018). To avoid immunosurveillance, tumor cells always upregulate the expression of immune checkpoint-related genes, such as programmed cell death protein-1 (PD-1) and cytotoxic T lymphocyte antigen 4 (CTLA4), during tumor development, which will cause T cell anergy or apoptosis (Leach et al., 1996; Iwai et al., 2002; Chan et al., 2019). However, with the discovery of improved survival in metastatic melanoma by ipilimumab, a CTLA-4 antibody, immunotherapy provides a new strategy for advanced metastatic tumors (Hodi et al., 2010). Recently, overall survival was increased in different tumors by administering immune checkpoint blockade therapy (ICB), including urothelial cancer, renal cell carcinoma, non-small cell lung cancer (NSCLC), and hematologic malignancies (Ansell et al., 2015; Borghaei et al., 2015; Motzer et al., 2015; Rosenberg et al., 2016; Goodman A. et al., 2017). To predict the response to immunotherapy, tumor mutation burden (TMB) is used as an evaluating marker (Samstein et al., 2019). Tumors with high TMB levels lead to more mutation derived neoantigens, inducing higher immunogenicity across diverse tumors (Goodman A. M. et al., 2017).

In colorectal cancer (CRC), mutation profiles can be divided into two types, mismatch repair deficient or high levels of microsatellite instability (dMMR-MSI-H) and mismatch repair proficient or low levels of microsatellite instability (pMMR-MSI-L) (Ganesh et al., 2019). The dMMR-MSI-H CRCs exhibit high levels of TMB and activated $CD8^+$ cytotoxic T cell infiltration, which results in survival improvement with ICB treatments (Llosa et al., 2015; Ganesh et al., 2019). However, patients with pMMR-MSI-L CRC show no response to current ICBs. To date, the potential mechanisms of TMB and immunocyte infiltration in colon cancer development are still controversial. In this study, we analyzed somatic mutations and immunocytes in filtration patterns of colon cancer based on data from The Cancer Genome Atlas (TCGA) database and constructed a novel nomogram model to estimate the prognosis of colon cancer patients, which might be helpful to explore proper therapeutic strategies for patients with colon cancer.

MATERIALS AND METHODS

Databases

We downloaded all available data on somatic mutations, transcriptome profiles, microsatellite instability (MSI) status, and clinical information of colon cancer separately from the TCGA database[1]. In total, 399 samples with somatic mutation data were analyzed to show the mutation landscapes of colon cancer. The transcriptome profiles of 398 colon cancer samples and 39 normal samples were extracted to explore immune infiltration characteristics and related genes or pathways. In addition, the clinical information of 452 patients with colon cancer was obtained, including age, race, sex, therapies, pathological stage, AJCC-TNM stages, and survival status. Then, 343 matched samples from mutation data, transcriptome data, and clinical data with the same sample ID were enrolled to analyze the TMB level, differentially expressed genes or pathways, immune infiltration status, and potential clinical application in prognostic prediction or therapeutic management. The workflow of this study is shown in **Supplementary Figure 1**.

[1]https://portal.gdc.cancer.gov/

Tumor Mutation Burden Analysis

To explore the mutation landscapes of colon cancer, the somatic mutation data were processed and analyzed by R software (version 4.0.2) with the "maftools" package[2]. TMB was defined as the total number of somatic mutations including somatic mutations, insertion-deletion mutations, coding, and base replacement of per million bases. The colon cancer patients were separated into the low-TMB and high-TMB groups using the median value of TMB. To analyze the correlations between TMB and clinicopathological factors of patients with colon cancer, we merged the TMB data with corresponding clinical information. The Wilcoxon rank-sum test was utilized for comparisons between two groups of clinical variables.

Microsatellite Instability (MSI) Analysis

The MSI status (MSI-H, MSI-L, and MSS) of colon cancer samples was obtained by R software with the "TCGAbiolinks" package. The genomes of cancer samples were tested by five mononucleotide markers (BAT25, BAT26, NR21, NR24, and MONO27) (Bacher et al., 2004). Samples were identified as MSI-H when >40% of the mononucleotide markers were altered, MSI-L when <40% of the mononucleotide markers were altered, and MSS when no mononucleotide marker was altered.

Gene Expression and Functional Enrichment Analysis

Before analyzing the gene expression differences between the low- and high-TMB groups of colon cancer patients, we combined the TMB data with the corresponding transcriptome profiles. Background correction, normalization, and visualization of raw transcriptome data were performed by R software with the "limma" package. Differentially expressed genes (DEGs) were determined between the low- and high-TMB groups by cutoff values of $|\log_2(\text{Fold Change})| > 1$ and $P\text{-value} < 0.05$. The expression of the top 20 DEGs in various samples is shown in the heat map constructed by R software with the "pheatmap" package.

To explore the functions and signaling pathways of genes that were differentially expressed between the two TMB groups, we performed a Gene Ontology (GO) function analysis and Kyoto Encyclopedia of Genes and Genomes (KEGG) pathway enrichment analysis using R software with the "org.Hs.eg.db," "clusterProfiler," "enrichplot," and "ggplot2" packages.

Gene Set Enrichment Analysis (GSEA)

To further investigate the enrichment of gene functions and signaling pathways between the low- and high-TMB groups, GSEA was performed based on the JAVA8 platform. We selected the "c2.cp.kegg.v7.0.symbols.gmt" gene sets as reference sets, which were obtained from the MSigDB database[3]. The significant enrichment of GO functions and KEGG pathways was considered only with a normalized P-value < 0.05 and a FDR q value < 0.25.

Immune Infiltration Analysis Between Low- and High-TMB Groups

To analyze the immune infiltration of each colon cancer sample, the relative fractions of immunocytes were calculated using the CIBERSORT algorithm (Newman et al., 2015). Quantification of each immunocyte subtype among colon cancer samples was based on the gene expression signatures of 22 different subtypes of immunocytes, LM22, which included gene sets from B cells (memory and naive B cells, and plasma cells), T cells (naive $CD4^+$ T cells, activated and resting memory $CD4^+$ T cells, $CD8^+$ T cells, regulatory T cells, follicle-assisted T cells and γδT cells), NK cells (resting and activated NK cells) and myeloid cells (resting and activated dendritic cells, monocytes, M0-2 macrophages, resting and activated mast cells, neutrophils, and eosinophils). The transcriptome data of colon cancer samples were submitted to the CIBERSORT web portal[4], with the algorithm using the default signature matrix at 1,000 permutations. The distributions of immunocytes in the low- and high-TMB groups were determined by R software with the "pheatmap" package. The Wilcoxon rank-sum test was exploited to compare the differential fractions of immune infiltration between these two groups, which were exhibited with P-values by R software with the "vioplot" package.

Immunity Profile Analysis of Colon Cancer by Single Sample Gene Set Enrichment Analysis (ssGSEA)

In this study, we also investigated the immunity profiles of every colon cancer sample based on transcriptome data, which included the type of immunocytes and immune related pathways, fractions of infiltrated immunocytes, expression of human leukocyte antigen (HLA) genes, and immune checkpoint genes. Gene expression landscapes of immunocytes and immune related pathways from both innate and specific immunity were analyzed and enriched by ssGSEA with the "GSVA" R package (Barbie et al., 2009). Based on immune enrichment scores calculated by the "Consensus Cluster Plus" package in ssGSEA, colon cancer samples were divided into the low- and high- immunity groups. Then, the tumor purity, ESTIMATE scores, immune scores, and stromal scores were analyzed and compared by the "estimate" package and the Mann–Whitney U test between low and high immunity groups.

Immune Related Hub Gene Analysis and Validation by the TIMER Database

To further investigate immune related hub genes in colon cancer, the expression level of immune related hub genes among 32 different tumors and correlations with immunocyte infiltration were analyzed and validated by the TIMER database[5]. The "Diff Exp" module was used to estimate the hub gene

[2]https://github.com/PoisonAlien/maftools

[3]http://software.broadinstitute.org/gsea/msigdb/

[4]http://cibersort.stanford.edu/

[5]https://cistrome.shinyapps.io/timer

expression between tumors and matched normal tissues of different types of cancer. In addition, the "Gene" module was applied to calculate the correlation between hub gene expression and immunocyte infiltration levels, including B cells, $CD4^+$ T cells, $CD8^+$ T cells, neutrophils, macrophages, and dendritic cells.

Construction of a Prognostic Risk Model by Immune-Related Genes

To identify immune related genes that were differentially expressed between different TMB groups, we obtained 1,811 immune-related genes from the Immunology Database and Analysis Portal (Immport). After overlapping with the DEGs from our TCGA cohort by R software with the "VennDiagram" package, univariate and multivariate Cox regression analyses were conducted to obtain the coefficient (β) of immune related hub genes. The risk score was calculated as follows: risk score = $\beta_1 \times$ expression of gene 1 + $\beta_2 \times$ expression of gene 2 + ... + $\beta_n \times$ expression of gene n. Then, patients with colon cancer were divided into low- and high-risk groups by the median risk score as the cutoff value. Kaplan–Meier analysis was conducted to compare the survival difference between the low- and high-risk groups.

Construction and Evaluation of the Nomogram Model for Patients With Colon Cancer

In our study, the survival probability of colon cancer patients from the TCGA database was estimated by the nomogram model integrating the TMB, immune infiltration and immune-related gene signatures with clinicopathologic features, which was also performed with the "rms" package in R software. For nomogram establishment, each level of factors (like male and female) is assigned a score, which reflects their influence degree on the outcome variable (death) in the nomogram model. Their influence on the survival of patients was quantified as the size of the regression coefficient in the multivariate Cox regression analysis. Then each score of each factor is added to get the total score. Finally, through the function transformation between the total score and the probability of the outcome event, the predicted survival probability of each patient is calculated. Calibration plots, ROC curves, and the C-index were generated to assess the performance of the nomogram model. The survival probability prediction and actual survival rate are displayed on the *y*-axis and *x*-axis separately in the calibration graphs, in which the 45-degree dotted line indicates an ideal prediction. The bootstrapping method was used as an internal validation to decrease the bias of the C-index's predictive ability.

Statistical Analysis

All statistical analyses as well as the visualizations were performed by R software (version 4.0.2) with related R packages. Correlations between the TMB, immune infiltrations, and MSI status were estimated using the Chi-square test and Fisher's exact test. Other detailed statistical methods are mentioned in the above sections. A P-value < 0.05 was considered statistically significant.

RESULTS

Tumor Mutation Profiles and MSI Status in Colon Cancer

We analyzed somatic mutation data of 399 colon cancer samples from the TCGA database. The "maftolls" R package was used to visualize the mutation annotation format of colon cancer. In general, missense mutations were the most frequent type among nine different types of mutations (**Figure 1A**). For different mutation variant types, single nucleotide polymorphisms (SNPs) showed a higher frequency than deletion (DEL) and insertion (INS) mutations, and C > T was the major type of single nucleotide variant classification (SNV, **Figures 1B,C**). In each sample, the number and classification of variants were analyzed and are shown in a boxplot (**Figures 1D,E**). Furthermore, we analyzed specific mutated genes among colon cancer samples and found the top 10 mutated genes, including TTN (49%), APC (75%), MUC16 (27%), SYNE1 (29%), TP53 (55%), KRAS (43%), FAT4 (23%), RYR2 (21%), PIK3CA (28%), and ZFHX4 (21%), which might play important roles in colon cancer biological processes (**Figure 1F**).

In addition, mutation details of each colon cancer sample are shown in a waterfall plot (**Figure 2A**), in which we could analyze different mutation types for each individual gene involved in colon cancer progression. Among these highly altered genes, the associations between each pair of genes are exhibited in **Figure 2B**, which shows that co-occurrence existed between PCLO and OBSCN, as well as ZFHX4 and FAT4. However, the associations between MUC16 and APC or TP53 were mutually exclusive (**Figure 2B**).

Furthermore, we obtained the MSI data of 459 patients with colon cancer from the TCGA database. Based on the category method of MSI, a total of 373 samples were classified as MSI-H and 86 samples were classified as MSI-L/MSS. Samples with matched TMB and MSI profiles were analyzed to estimate the correlation between TMB and MSI of colon cancer. As shown in **Table 1**, those patients with high TMB were more likely to be MSI-H ($P < 0.001$).

The Correlation Between TMB and Colon Cancer Clinicopathological Parameters

Due to the consideration of the TMB as a marker for tumor mutational status, we analyzed the TMB levels combined with different clinicopathological factors. After matching with mutation data, clinical data, and transcriptome data, a cohort consisting of 343 colon cancer samples was used in this study to investigate the differences between various TMB levels (**Table 2**). Colon cancer patients with higher clinical stages (Stage III-IV), advanced N stage (N1-2), and M1 stage showed significantly lower TMB levels. However, elderly patients aged > 65 years exhibited higher TMB levels. Unfortunately, we could not find any correlation between sex or T stage and TMB (**Figure 3**).

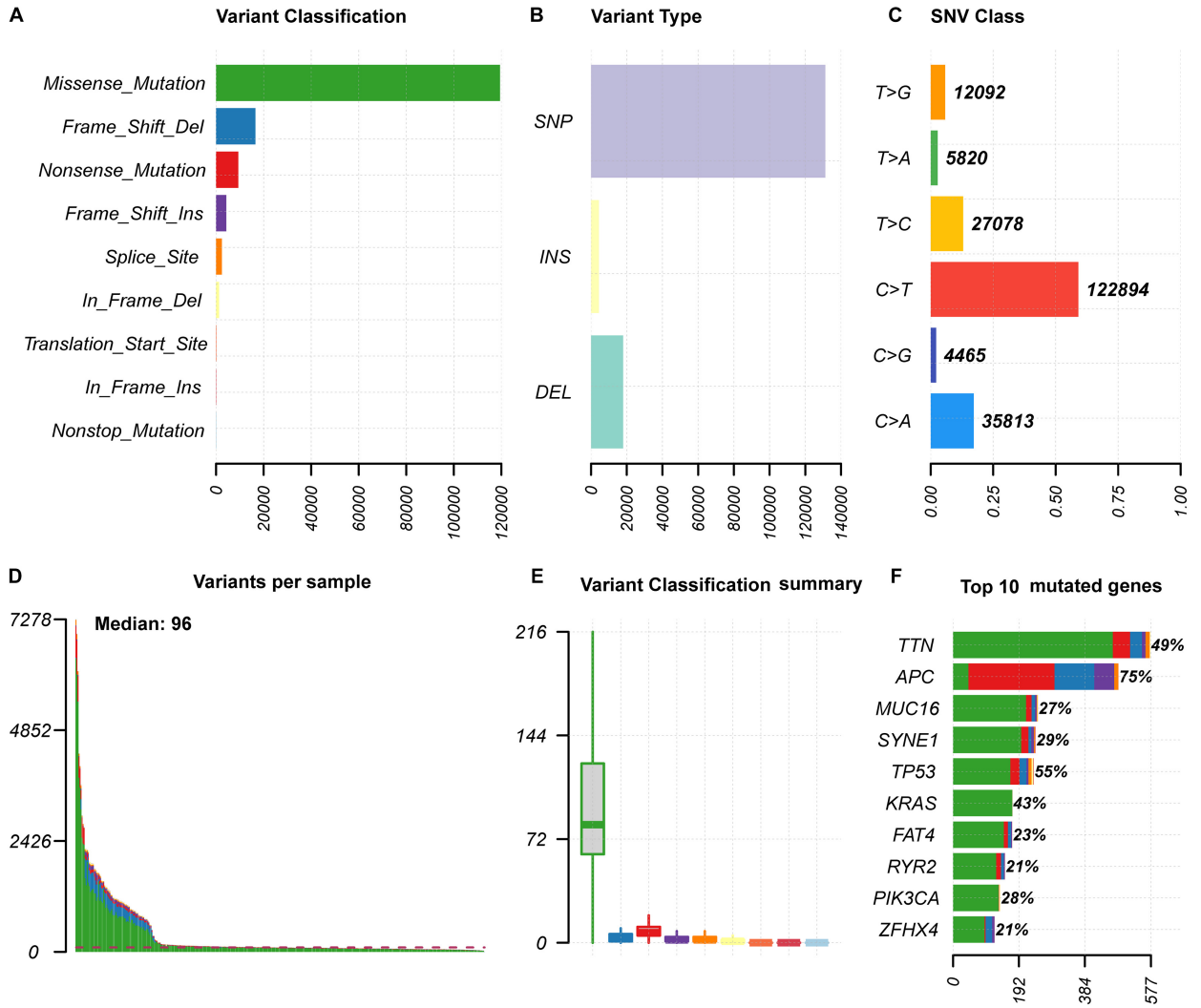

FIGURE 1 | The summary information of somatic mutation in colon cancer samples from the TCGA database. **(A)** Frequency of different mutation classification. **(B)** Frequency of mutational variant types. **(C)** Frequency of SNV class. **(D,E)** TMB level of each colon cancer samples. **(F)** Top 10 mutated genes in colon cancer samples. SNP, single nucleotide polymorphism; INS, insertion; DEL, deletion; SNV, single nucleotide variants.

Different Gene Expression Profiles and Immunocyte Characteristics Between the Low- and High-TMB Groups

To investigate the potential roles of TMB in the colon cancer process, we divided colon cancer patients into low- and high-TMB groups based on the medium value of TMB and analyzed DEGs in these two groups. With the cutoff value of $|\log_2(FC)| > 1$ and $P < 0.05$, the top 40 DEGs are shown in the heatmap (**Figures 4A,B**). Furthermore, KEGG pathway and GO enrichment analyses were also performed to explore potential signaling pathways and gene functions involved in tumor somatic mutations or immune responses (**Tables 3**, **4**, respectively). Notably, the antigen processing and presentation pathway was enriched in the high-TMB group, suggesting a potential correlation between the TMB level and the immune response process.

High TMB levels cause more neoantigens during the tumor process, leading to immune infiltration in the tumor microenvironment, which supports tumor initiation and development. In this study, the immunocyte characteristics were also investigated in different TMB groups. The relative percentages of 22 immunocyte subtypes of each colon cancer patient are exhibited by different colors in the box plot (**Figure 4C**). Furthermore, based on the Wilcoxon rank-sum test, $CD8^+$ T cells, activated $CD4^+$ memory T cells, follicular helper T cells, activated NK cells, and M1 macrophages showed higher fractions in the high-TMB group. In contrast, regulatory T cells (Tregs) and M0 macrophages accounted for a lower fraction in the high-TMB group (**Figure 4D**), which indicated that a high TMB promoted immunocyte infiltration in patients with colon cancer.

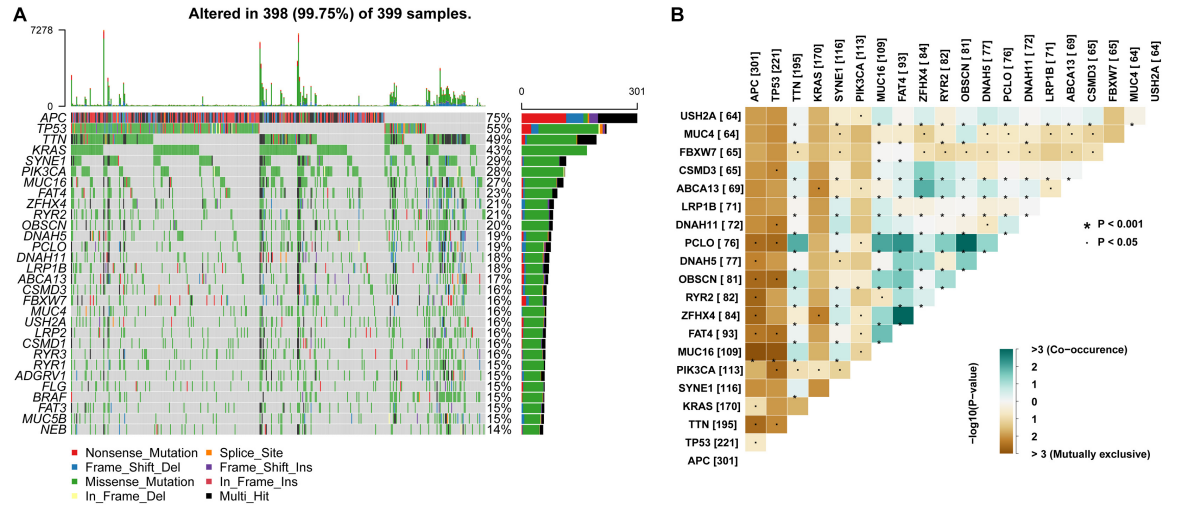

FIGURE 2 | Landscape and potential associations between mutation genes. **(A)** Waterfall plot showing mutation profiles of each gene in each colon cancer sample. The left panel shows the genes ordered by mutation frequency, which is listed in the right panel. **(B)** The co-occurrence or exclusive associations between top 20 mutation genes.

The Immune Infiltration Profiles in Colon Cancer

To further explore immune infiltration profiles in patients with colon cancer, 29 immunocyte subtypes and immune-related pathways were analyzed by ssGSEA for each colon cancer sample (**Figure 5A**). With the division of low- and high-immunity groups from the TCGA data, using an unsupervised consensus clustering analysis, several parameters were applied to estimate the immune infiltration profiles, including tumor purity, ESTIMATE score, Immune score, and Stromal score. As shown in **Figure 5B**, the immune score, stromal score, and corresponding ESTIMATE score were higher in the high immunity group while the tumor purity was lower when compared with those in the low immunity group. The fractions of infiltrating immunocytes were significantly different between these two groups; memory B cells, naive $CD4^+$ T cells, M0 macrophages, and activated mast cells were higher in the low-immunity group, whereas $CD8^+$ T cells, activated memory $CD4^+$ T cells, M1 and M2 macrophages, resting dendritic cells, and resting mast cells were increased in the high-immunity group, which suggests that more immune filtrations exist in the high-immunity group or in samples with low tumor purity (**Figure 5C**). In addition, the low immunity group exhibited significantly lower HLA related gene set expressions (**Figure 5D**).

To explore the biological behaviors among these immune subtypes, we performed GO and KEGG enrichment analyses. As shown in **Figure 5E**, the GO enrichment analysis revealed that a high immunity was related to the functions of the immunoglobulin complex, circulating immunoglobulin complex, immunoglobulin receptor binding, major histocompatibility complex class II (MHC-II) protein complex, and the regulation of neutrophil activation. The KEGG enrichment analysis showed that a high immunity was associated with allograft rejection, antigen processing and presentation, graft-versus-host disease, intestinal immune network for IgA production, and type I diabetes mellitus (**Figure 5F**). In addition, we also estimated the correlation between immune infiltration and MSI in colon cancer. As shown in **Table 1**, patients with high immune infiltration were more likely to be MSI-H ($P < 0.001$).

As critical targets for immunotherapy, 16 immune checkpoint genes were assessed in the low- and high-immunity groups. The results indicated significantly increased expression levels among these checkpoint genes in the high-immunity group, including BTLA, CTLA4, IDO1, LAG3, and PDCD1 (**Figure 6**), which suggested that colon cancer patients in the high-immunity group could exhibit a better response to immune checkpoint inhibitors, such as CTLA4 and PD1 inhibiting reagents.

Identification of Immune Related Genes and Their Prognostic Value in Patients With Colon Cancer

Since immunocyte infiltration was promoted by high TMB levels in colon cancer based on previous data, we further explored the correlation between immune related genes and patient prognosis. Data from IMMPORT and TCGA were analyzed, and

TABLE 1 | Correlations between tumor mutation burden, immune infiltrations, and microsatellite instability status in colon cancer.

	MSI-H (%)	MSI-L/MSS (%)	χ^2	*P*-value
TMB-H (%)	72 (18.2)	126 (31.8)		
TMB-L (%)	11 (2.8)	187 (47.2)	56.72	<0.001
Immunity-H (%)	59 (16.6)	197 (55.4)		
Immunity-L (%)	3 (0.8)	97 (27.2)	20.09	<0.001

MSI-H, microsatellite instability-high; MSI-L/MSS, microsatellite instability-low/stable; TMB-H, tumor mutation burden-high; TMB-L, tumor mutation burden-low; Immunity-H, immunity-high; Immunity-L, immunity-low.

TABLE 2 | Clinicopathological characteristics of colon cancer patients from TCGA database.

Characteristics		Patients Number (%)
Age	≦65	141 (41.11)
	>65	202 (58.89)
Sex	Male	177 (51.60)
	Female	166 (48.40)
T stage	T_1	9 (2.62)
	T_2	64 (18.66)
	T_3	229 (66.77)
	T_4	41 (11.95)
N stage	N_0	205 (59.77)
	N_1	81 (23.61)
	N_2	57 (16.62)
M stage	M_x	47 (13.70)
	M_0	246 (71.72)
	M_1	50 (14.58)
Status	Alive	275 (80.17)
	Dead	68 (19.83)

24 immune related genes with $|\log_2 FC| > 1$ were filtered as candidate risk genes to assess their correlation with prognosis (**Figure 7A**). In the univariate Cox analysis, two genes (CHGB and SCT) were shown to be correlated with the survival of patients with colon cancer (**Table 5**), while only SCT was found to be an independent prognostic factor based on the multivariate analysis ($P < 0.001$) (**Figure 7B**). In addition, we further investigated the expression level of SCT in 34 different tumors from the TIMER database and found that SCT expression was lower in colon cancer than in normal tissues (**Supplementary Figure 2A**). Furthermore, SCT expression showed significantly negative correlations with immunocyte infiltration, including B cell, $CD8^+$ T cell, and neutrophil cell infiltration. Positive correlations also existed between SCT expression and $CD4^+$ T cell and macrophages. However, there were no significant differences between tumor purity or dendritic cell infiltration with SCT expression (**Supplementary Figure 2B**). The colon cancer patients were then divided into low- and high-risk groups based on the median risk score (**Figure 7C**). Compared with patients in the low-risk group, those in the high-risk group indicated poorer survival probability based on our risk model ($P = 0.04$, **Figures 7D,E**), which suggested potential functions of the risk immune related genes in colon cancer prognosis.

The Nomogram Model to Predict the Prognosis of Patients With Colon Cancer

For colon cancer patient management and therapeutic strategies, prognosis is a critical factor. In this study, combined with TMB profiles, immunocyte infiltration status and clinicopathological data, we constructed a nomogram model to predict the prognosis of colon cancer patients, which contained nine factors: age, sex, race, radiation therapy or pharmaceutical status, pathological stage, immunity status, immunity risk scores, and TMB. Each

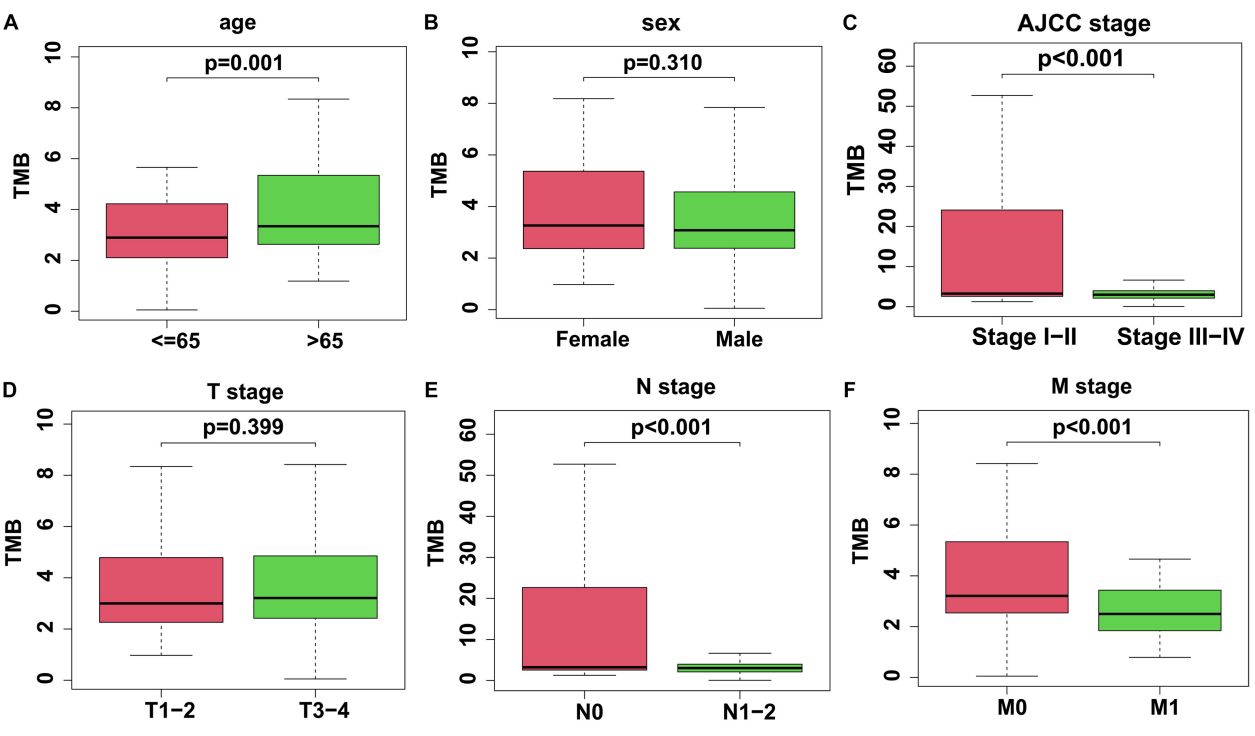

FIGURE 3 | The association between TMB and clinicopathological factors. **(A)** Elderly colon cancer patients > 65 years old exhibited a higher TMB level. **(B)** There was no significant difference of TMB level in different genders. **(C)** Colon cancer patients with Stage III-IV exhibited a lower TMB level. **(D)** No significant difference of TMB levels in different T stages. **(E,F)** TMB level was lower in colon cancer patients with N1-2 stage or M1 stage. TMB, tumor mutation burden.

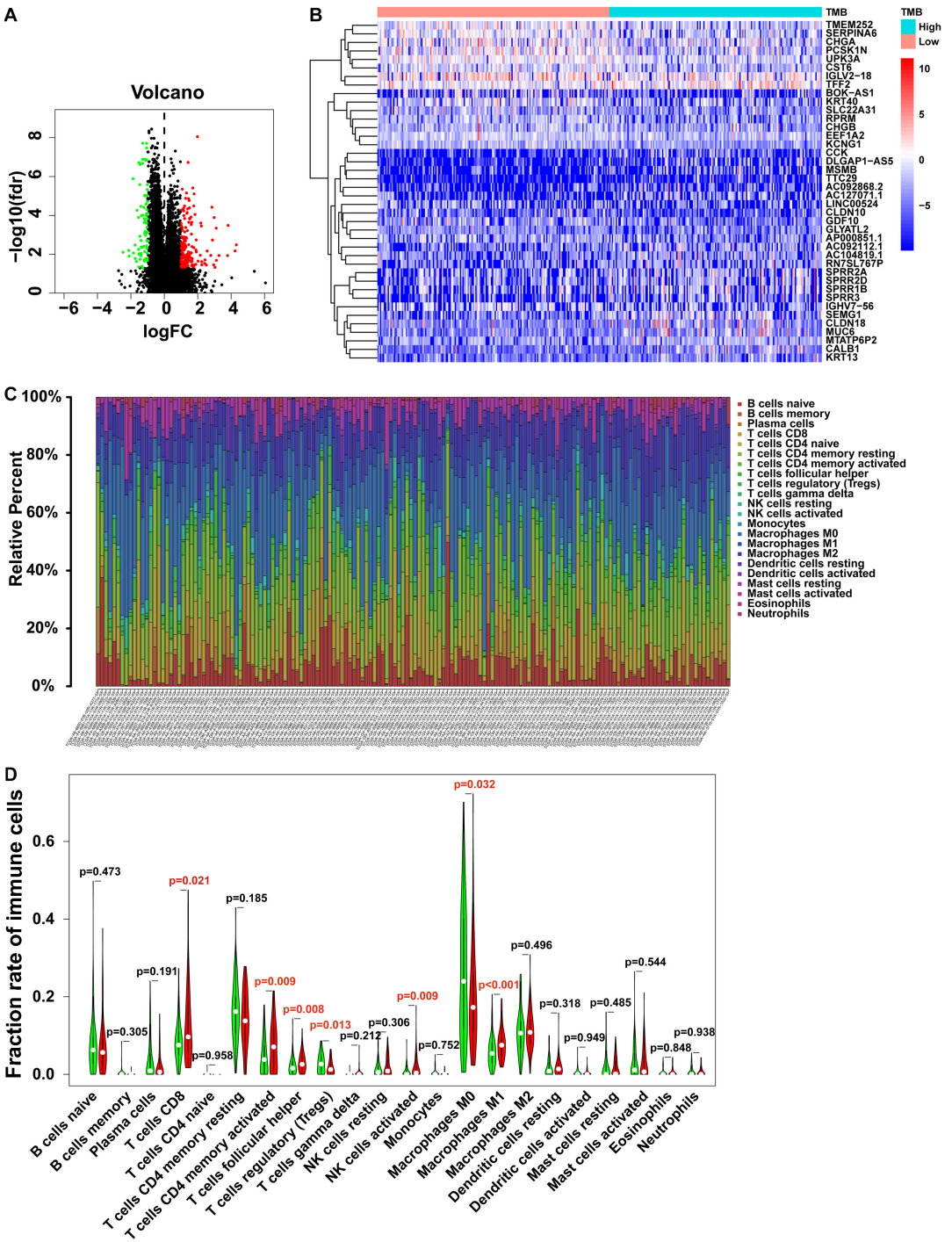

FIGURE 4 | Gene expression profiles and immunocytes fraction between low- and high-TMB groups. **(A)** Volcano plot shows the DEGs in colon cancer. Red represents the high TMB group, and green represents the low TMB group. **(B)** Top 40 DEGs from low- and high-TMB groups are shown in the heatmap. **(C)** The fraction of 22 immunocyte subtypes of each colon cancer sample is represented by different colors listed on the right panel of the bar plot. **(D)** The violin plot shows the differences of infiltrated immunocyte subtypes between low- (green) and high-TMB (red) groups. The statistical significance is represented in red with *P*-value < 0.05. DEGs, differentially expressed genes.

factor in the nomogram model was ascribed a weighted point that would be used to predict the survival of patients with colon cancer. In our nomogram model, being aged > 65 years was assigned 22 points, female was assigned 7 points, being Asian and African American were assigned 53 and 8 points respectively, having received radiation therapy was assigned 1

TABLE 3 | GESA for KEGG pathways between low- and high-TMB groups.

Group	Name	ES	NES	Nom *P*-value	FDR *q*-value
High TMB	KEGG ANTIGEN_PROCESSING_AND_PRESENTATION	0.684	1.948	0.004	0.125
Low TMB	KEGG_TIGHT_JUNCTION	–0.415	–1.654	0.014	0.221
	KEGG_PENTOSE_AND_GLUCURONATE_INTERCONVERSIONS	–0.570	–1.638	0.037	0.225
	KEGG_OTHER_GLYCAN_DEGRADATION	–0.655	–1.658	0.040	0.233
	KEGG_GLYCEROPHOSPHOLIPID_METABOLISM	–0.433	–1.664	0.006	0.245
	KEGG_BLADDER_CANCER	–0.440	–1.513	0.034	0.247

ES, enrichment score; NES, normalized enrichment score; NOM P-value, normalized P-value; FDR q-value, false discovery rate q-value.

TABLE 4 | GESA for GO analysis between low- and high-TMB groups.

Group	Name	ES	NES	Nom *P*-value	FDR *q*-value
GO_CC TMB High	GO_POSTSYNAPTIC_CYTOSOL	0.587	1.629	0.033	0.245
GO_CC TMB Low	GO_LATERAL_PLASMA_MEMBRANE	–0.604	–2.093	0	0.069
	GO_APICOLATERAL_PLASMA_MEMBRANE	–0.728	–2.040	0	0.081
	GO_VACUOLAR_PROTON_TRANSPORTING_V_TYPE_ATPASE_COMPLEX	–0.701	–1.944	0.006	0.189
	GO_MULTIVESICULAR_BODY	–0.554	–1.817	0.004	0.231
	GO_DENDRITIC_SPINE_MEMBRANE	–0.702	–1.706	0.006	0.245
GO_BP TMB High	GO_MITOTIC_SISTER_CHROMATID_SEGREGATION	0.654	2.125	0.002	0.062
	GO_NEGATIVE_REGULATION_OF_METAPHASE_ANAPHASE_TRANSITION_OF_CELL_CYCLE	0.751	2.166	0	0.066
	GO_RESPONSE_TO_UV_C	0.751	2.135	0	0.070
	GO_NEGATIVE_REGULATION_OF_CHROMOSOME_SEGREGATION	0.727	2.192	0	0.084
	GO_REGULATION_OF_CHROMOSOME_SEGREGATION	0.636	2.045	0.006	0.100
GO_BP TMB Low	GO_REGULATION_OF_CYTOPLASMIC_TRANSPORT	–0.626	–1.911	0.008	0.240
	GO_ENERGY_RESERVE_METABOLIC_PROCESS	–0.494	–1.917	0	0.243
	GO_NEGATIVE_REGULATION_OF_EMBRYONIC_DEVELOPMENT	–0.730	–2.099	0	0.245
	GO_RENAL_SODIUM_EXCRETION	–0.685	–1.912	0.002	0.245
	GO_REGULATION_OF_WNT_SIGNALING_PATHWAY_PLANAR_CELL_POLARITY_PATHWAY	–0.731	–1.919	0.008	0.248
GO MF TMB High	GO_TRANSMEMBRANE_RECEPTOR_PROTEIN_SERINE_THREONINE_KINASE_BINDING	–0.817	–2.199	0	0.020
	GO_RECEPTOR_SERINE_THREONINE_KINASE_BINDING	–0.689	–2.062	0	0.064
	GO_ACTIVIN_BINDING	–0.765	–1.950	0	0.104
	GO_LYSOPHOSPHOLIPASE_ACTIVITY	–0.676	–1.958	0	0.111
	GO_VITAMIN_TRANSMEMBRANE_TRANSPORTER_ACTIVITY	–0.640	–1.971	0	0.119

ES, enrichment score; NES, normalized enrichment score; NOM P-value, normalized P-value; FDR q-value, false discovery rate q-value.

point, not having any pharmaceutical treatment was assigned 29 points, pathological stage 4 was assigned 100 points, being from a low-immunity group was assigned 8 points, being in a high-risk group was assigned 12 points, and having a high TMB level was assigned 33 points. The total points were used to predict the 3- or 5-year survival of colon cancer patients, and higher total points indicated a worse prognosis (**Figure 8A**). The performance of the nomogram model was then assessed by Harrell's C-index, calibration plot and ROC curve analyses. Our nomogram model exhibited proper prediction accuracy and application potential for 5-year survival probability prediction with a close correspondence between the predicted curve and the actual survival plot, and a good C-index (0.764) and AUC (0.737) (**Figures 8B,C**). Notably, we further performed the Kaplan-Meier survival analyses and log-rank tests to estimate the survival differences between different pathological stages (Stage 1–4), immunity status (low or high immunity), TMB levels (low or high TMB), and immune gene signature based-risk groups (low or high risk). As shown in **Figure 8D**, the survival prognosis of colon cancer patients with higher pathological stages were worse than those with lower ones ($P < 0.001$). Patients with high immunity or low TMB were found to have better prognoses ($P = 0.013$ and 0.032, respectively) (**Figures 8E,F**). In the immune gene signature based-risk model, patients with high-risk scores had poorer prognoses ($P < 0.001$) (**Figure 8G**).

DISCUSSION

As the most frequent malignancy in the digestive system, colon cancer exhibits a high incidence and mortality, but unfortunately, has a poor prognosis and unsatisfactory therapeutic outcomes. With the improvements in imaging techniques to detect metastatic lesions, adjuvant multidisciplinary therapies for resectable stage III patients and neoadjuvant therapeutic strategies for local advanced colon cancer patients, the 5-year survival rates of all stages have increased from 51% (mid-1970s) to 66% (2006–2012) (Siegel et al., 2017;

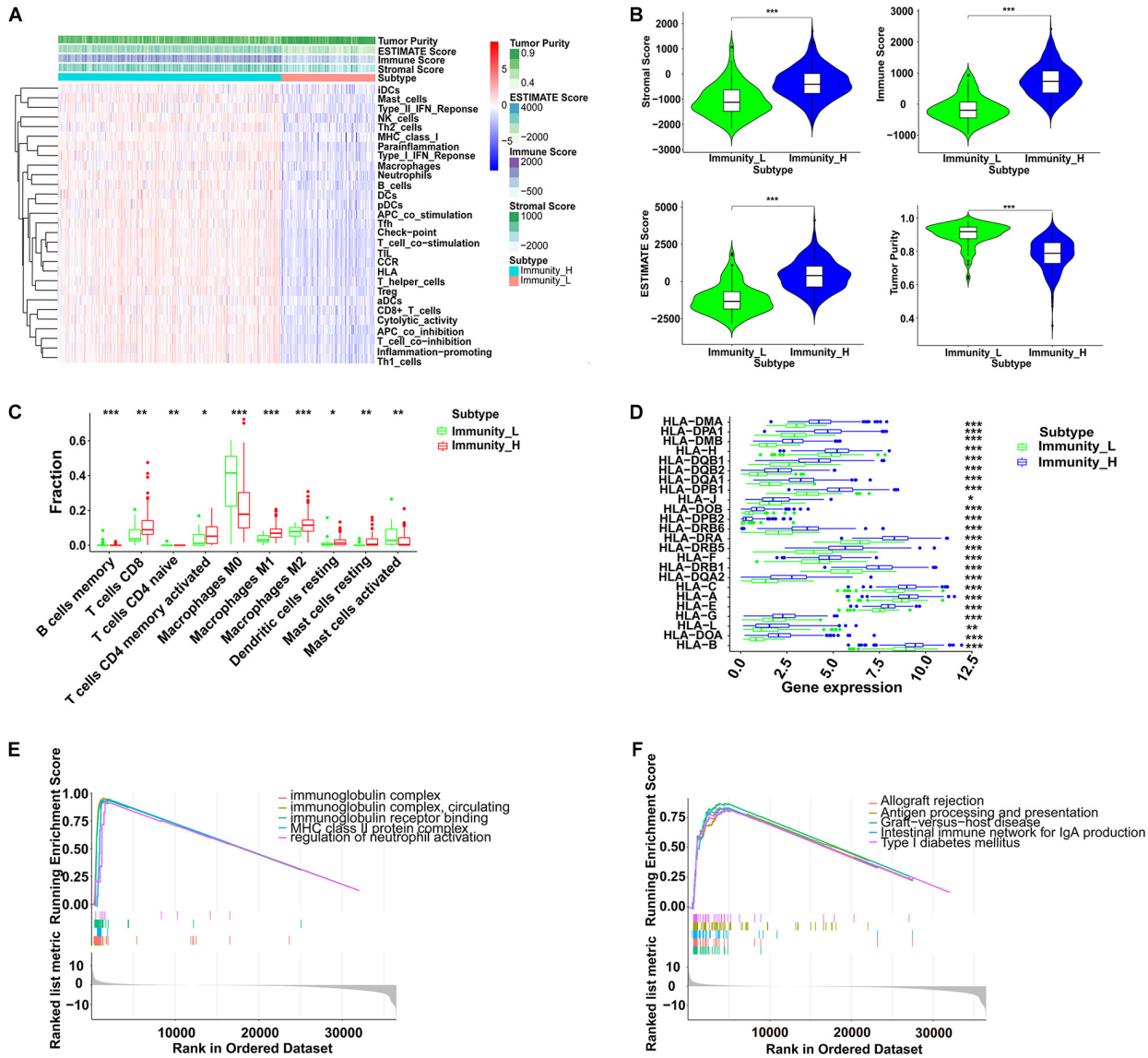

FIGURE 5 | Immunity profiles analysis in colon cancer. **(A)** By ssGSEA, immune related gene sets were enriched in different immunity groups. The tumor purity, ESTIMATE score, immune score, and stromal score were calculated and are shown in the heatmap. **(B)** The violin plots indicates that the high immunity group showed a significantly higher stromal score, immune score, and ESTIMATE score, but lower tumor purity (***$P < 0.001$). **(C)** The fractions of 10 infiltrated immunocyte subtypes in different immunity groups (*$P < 0.05$, **$P < 0.01$, ***$P < 0.001$). **(D)** The RNA expression levels of HLA related genes in different immunity groups (*$P < 0.05$, **$P < 0.01$, ***$P < 0.001$). **(E)** GSEA of GO in different immunity groups. **(F)** GESA of KEGG in different immunity groups. ssGSEA, single sample gene set enrichment analysis; HLA, human leukocyte antigen; GO, gene ontology; KEGG, Kyoto Encyclopedia of Genes and Genomes.

Howlader et al., 2020). In addition, for patients with distant metastasis, the 2-year survival rate increased from 21% (1989–1992) to 35% (2009–2012) (Surveillance, Epidemiology, and End Results [SEER], 2016). Thus, the exploration and development of proper therapies for advanced metastatic colon cancer patients are quite urgent and necessary. Since the discovery and successful application of immune checkpoint inhibitors or ICBs, such as ipilimumab and pembrolizumab, in metastatic melanoma and NSCLC, immunotherapy has become a potential choice for advanced cancer patients with distant metastasis (Garon et al., 2015; Robert et al., 2015). In 2017, immune checkpoint therapy was approved by the U.S. Food and Drug Administration for patients with dMMR-MSI-H CRCs (Ganesh et al., 2019). However, dMMR-MSI-H only accounts for approximately 15% of CRC patients. The detailed immune response mechanisms and effectiveness of ICBs are still controversial. In this study, we analyzed somatic mutation, MSI, immunocyte infiltration, transcriptome, and clinicopathological data from the public TCGA database and investigated the correlations between TMB, immune-related genes, immunocyte infiltration, and colon cancer progression.

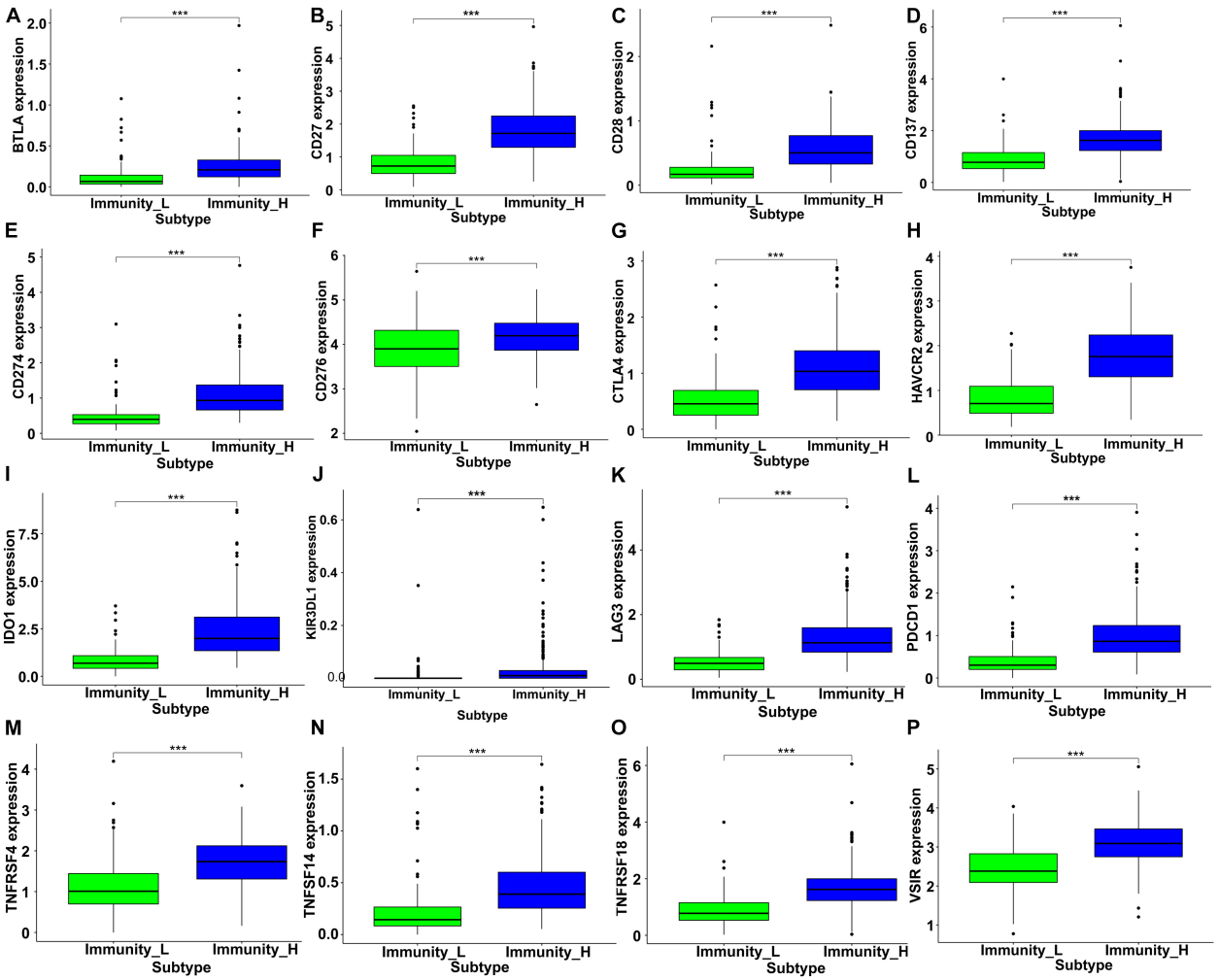

FIGURE 6 | The expression levels of immune checkpoint related genes in different immunity groups of colon cancer. The gene expression of **(A)** BTLA, **(B)** CD27, **(C)** CD28, **(D)** CD137, **(E)** CD274, **(F)** CD276, **(G)** CTLA4, **(H)** HAVCR2, **(I)** IDO1, **(J)** KIR3DL1, **(K)** LAG3, **(L)** PDCD1, **(M)** TNFRSF4, **(N)** TNFSF14, **(O)** TNFRSF18, and **(P)** VSIR were significantly higher in the high immunity group (***$P < 0.001$).

Somatic mutations always occur during cancer progression and are accompanied by mutated gene transcription, translation, and neoantigen peptide synthesis. Part of the neoantigens will then be processed and presented on the cell surface with MHC, which will be recognized and targeted by the immunocytes (Rizvi et al., 2015; Riaz et al., 2016; Chan et al., 2019). To quantify the somatic mutations, TMB was defined as the number of synonymous and non-synonymous mutations per million bases, including silent mutations, missense mutations, insertions or deletions, and copy number gains and losses. In tumors, TMB was found to be positively correlated with tumor neoantigen burden (Chan et al., 2019). Presenting variability among different types of tumors, TMB was found to be high in melanoma, NSCLCs, and squamous carcinomas, while in leukemias and some pediatric tumors, TMB was low (Alexandrov et al., 2013; Chalmers et al., 2017). In our study, we analyzed the mutation landscape in colon cancer samples from the TCGA database and found that missense mutations were the most frequent variant class, and that C > T was the major variant type for single nucleotides (**Figures 1A,C**). Additionally, we found the top mutated genes and their interactions, including APC, TP53, TTN, and KRAS, suggesting their critical roles in colon cancer carcinogenesis (**Figures 1F**, **2**) (Kwong and Dove, 2009; Wolff et al., 2018; Nakayama and Oshima, 2019). Furthermore, the TMB level was correlated with clinicopathological parameters in the matched colon cancer patient cohort, including AJCC stage, N stage, and M stage, indicating that the TMB level could be a risk factor in colon cancer development (**Table 2** and **Figure 3**).

Several detection methods were applied in clinical trials to evaluate the level of TMB from samples of patients with a malignancy. Including whole genome sequencing and whole exome sequencing (WES), the next-generation sequencing technique is used to detect genomic alterations (Büttner et al., 2019). As the WES covered the coding region of genes in the genome, it was used in many clinical trials to evaluate the TMB

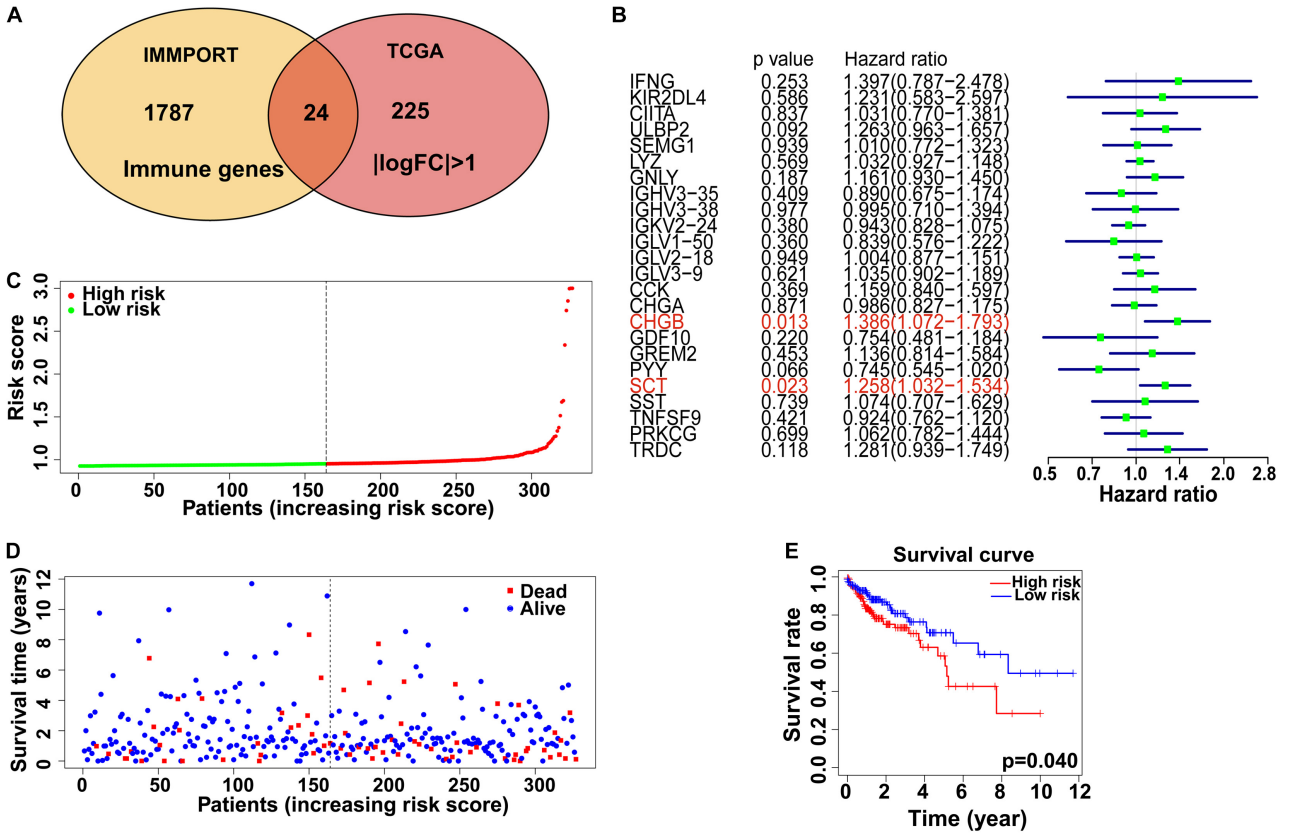

FIGURE 7 | Immune-related genes and relations with colon cancer prognosis. **(A)** Venn plot shows core immune genes between the Immport and TCGA database. **(B)** Hazard ratio was analyzed among 24 identified immune-related genes by univariate Cox regression analysis. Two hub genes (CHGB and SCT) indicated significant difference in survival of colon cancer patients. **(C)** Immune risk score calculated for each colon cancer patients. Patients were divided into high risk and low risk group by median risk score. **(D)** The survival time of different colon cancer patients. **(E)** Low immune risk group showed better 5-year survival than High risk group.

status in different types of cancer and is currently considered as a reference standard (Hugo et al., 2016; Carbone et al., 2017; Büttner et al., 2019). In CRC, the WES was applied to assess the TMB to investigate the response to pembrolizumab, one of the ICBs used in immunotherapy (Le et al., 2015). Furthermore, targeted gene panels focusing on cancer-related genes were also developed as an alternative technique to the WES in recent years, such as FoundationOne, FoundationOne CDx, and MSK-IMPACT (Powles et al., 2018; Büttner et al., 2019; Chang et al., 2019). However, the gene panel data of CRC is limited, more clinical trials are needed in future investigations.

Microsatellites, which are prone to being DNA replication error sites, refer to short, tandemly repeated sequences of mononucleotide, dinucleotide, or nucleotide repeats located in the genome (Yamamoto and Imai, 2015; Baretti and Le, 2018). As additional bases insertion or existing bases deletion from microsatellites, DNA mismatch errors occur during DNA replication, which can be supervised and corrected by the MMR system (Arana and Kunkel, 2010). For patients with MMR deficiency (dMMR), accumulated mismatch mutation and frameshift mutation will lead to the MSI phenotype, neoantigens production, and is related to carcinogenesis of several cancers, such as CRC, gastric cancer, pancreatic cancer, and endometrial cancer (Palomaki et al., 2009; Seo et al., 2009; Ghidini et al., 2020; Lin et al., 2020). In CRC, dMMR or high levels of MSI (MSI-H) were correlated with high TMB and immunocyte infiltration, which made dMMR-MSI-H CRC responsible for ICBs (Alexander et al., 2001; Llosa et al., 2015; Ganesh et al., 2019). Consistent with previous studies, our study indicated the positive correlation between TMB and MSI levels based on the analyses of transcriptome data from patients with colon cancer (**Table 1**).

Due to the high frequency of neoantigens in the high-TMB group, immune responses such as immunocyte infiltration would be more active. We investigated the percentage of 22 different subtypes of infiltrated immunocytes in each colon

TABLE 5 | Univariate Cox regression analysis.

Gene	HR	Lower 95% CI	Upper 95% CI	Cox *P*-value
CHGB	1.386	1.072	1.793	0.013
SCT	1.258	1.032	1.534	0.023

HR, hazard ratio; CI, confidence interval.

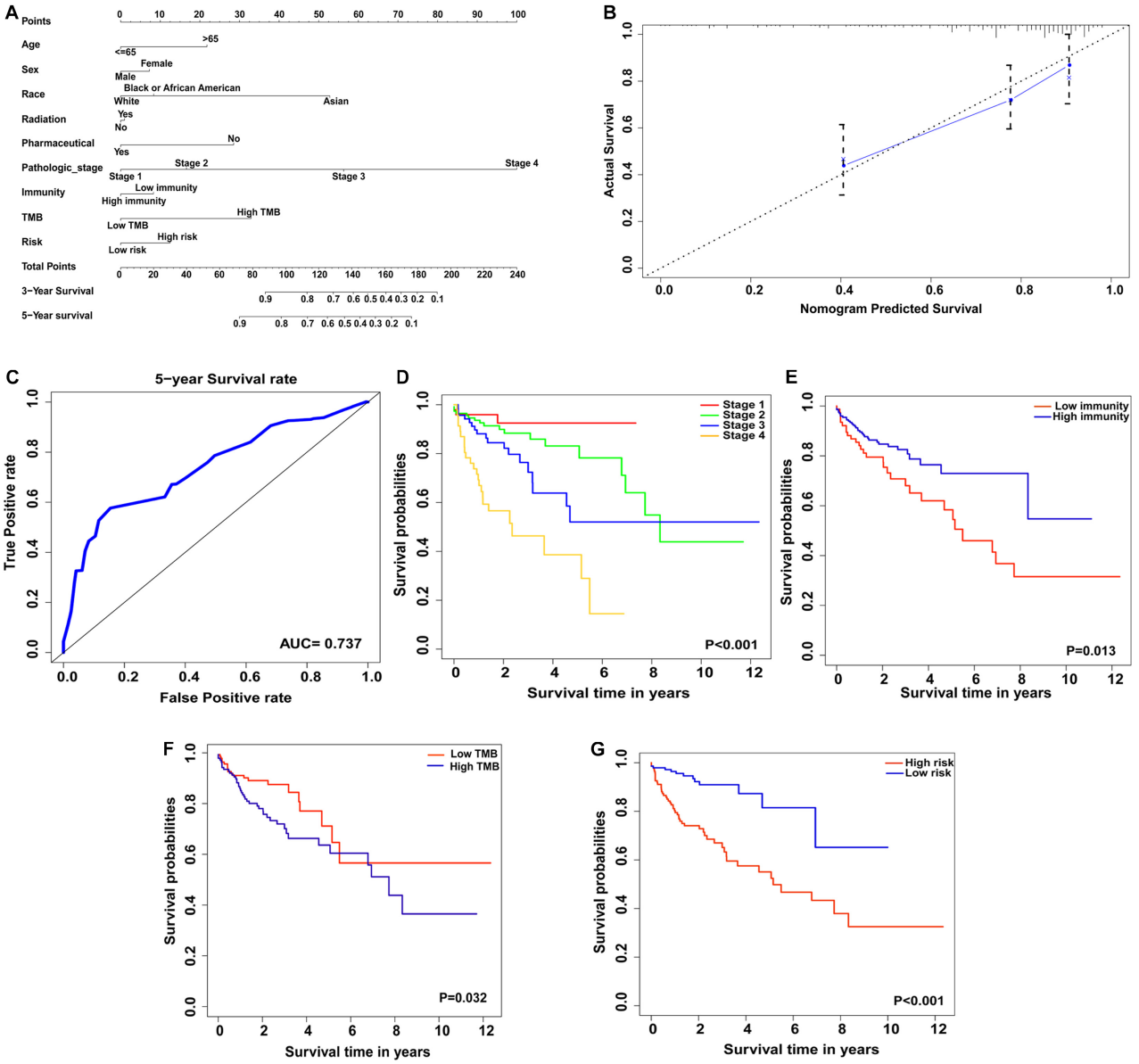

FIGURE 8 | Construction of nomogram model for prognosis prediction of colon cancer patients. **(A)** Nomogram model to predict the prognosis of colon cancer based on nine clinicopathological factors. **(B)** Calibration plot of the nomogram model. The dotted line represents the ideal prediction ability. **(C)** ROC curve of 5-year survival of colon cancer based on nomogram model prediction. **(D–G)** The clinical stages, immunity level, TMB level and immunity risk were significantly correlated with 5-year survival in nomogram model.

cancer patient and found that $CD8^+$ T cells, activated $CD4^+$ memory T cells, activated NK cells, and M1 macrophages were increased in the high-TMB group, indicating that the immunocyte-killing activity was increased in high-TMB colon cancer patients (**Figures 4C,D**), which is consistent with recent studies in gastrointestinal system malignancies (Zappasodi et al., 2018; Eso and Seno, 2020). Clinically, the cancer-related immune status is difficult to estimate due to limited information about cancer specific antigens. Recent studies suggest that similar T cell receptor (TCR) sequences could be clustered to identify cancer antigen-specific TCRs and evaluate immune status based on cancer genomics sequencing, which indicates new strategies for precise immunotherapy assessment (Zhang et al., 2020).

To further reveal the immune infiltration profiles, we investigated immunocytes and immune related genes and pathways by ssGSEA from transcriptome data and found different immune infiltration profiles among the low- and high-immunity groups divided by CIBERSORT (**Figures 5A–D**). In addition, immunoglobulin complex related functions and MHC-II complexes were enriched in the GO analysis. Allograft rejection, antigen processing, and presentation were the top ranked KEGG enriched pathways, indicating their

contributions to colon cancer immunity (**Figures 5E,F**). Notably, the expression of immune checkpoint genes, such as CTLA4 and PDCD1 (PD-1), was increased in the high-immunity groups, suggesting the potential therapeutic targets for ICBs application (**Figure 6**).

Immune-related genes were analyzed by combining the TCGA and IMMPORT databases. Two hub genes were revealed to be critical in the immunocyte infiltration mechanism in colon cancer by a univariable Cox regression model (**Figures 7A,B**). CHGB (chromogranin-B, CgB), which colocalizes with CHGA, is expressed in secretory granules of neuroendocrine cells and the function of CHGB is still limited. Paul et al. suggested that CHGB could be a prognostic marker in neuroendocrine tumors (Wanigasekara et al., 2015). Secreted by endocrine S cells in the proximal small intestinal mucosa, SCT (secretin) encoding preproprotein is involved in the regulation of duodenal pH, food intake, and water homeostasis (Afroze et al., 2013). Onori et al. (2010) found that SCT could inhibit the growth of cholangiocarcinoma *via* the cAMP-dependent signaling pathway, indicating its regulatory roles in gastrointestinal cancers. In this study, we further analyzed hub genes by a multivariable Cox regression model. We found that the expression level of SCT was significantly lower in colon cancer samples than in normal samples, and its correlation with immunocyte infiltration, suggested that SCT could be a critical gene in colon cancer development and tumor related immunocyte infiltration (**Supplementary Figure 2**). In general, these hub genes play roles in immunoglobin variation, immunocyte receptor constant, antigen recognition, and macrophage differentiation. However, the mechanistic details of these hub genes require further exploration.

Recent studies revealed that the responses and outcomes of ICBs were related to immunocyte infiltration in several types of cancers, including gastric cancer, breast cancer, CRC, and esophageal cancer (Simpson et al., 2010; Hu et al., 2017; Wei et al., 2018; Huang and Fu, 2019). In CRC, dMMR-MSI-H was considered to be a biomarker for the response to ICBs. However, limited by the low percentage of dMMR-MSI-H patients (∼15%), more precise prediction biomarkers are needed. In our study, we developed a novel nomogram prediction model based on data from the TCGA database. Nine clinicopathological factors were enrolled in our nomogram model: age, sex, race, radiotherapy and pharmacotherapy status, pathological stage, immunity status, TMB, and immunity risk (**Figure 8A**). Estimated by each factor in the nomogram model, the survival of patients with colon cancer was predicted by the nomogram total points, in which higher points meant a worse prognosis. Consistent with previous studies of tumor immunity, high immunity status in our nomogram model showed survival improvement in patients with colon cancer (**Figure 8E**) (Galon et al., 2006; Di Caro et al., 2014; Topalian et al., 2016). Notably, in our nomogram model, colon cancer patients with low TMB exhibited higher overall survival than high TMB patients, whereas high TMB predicted improved survival in patients with melanoma (**Figure 8F**) (Lauss et al., 2017). Due to the heterogeneous profiles of colon cancer, the correlation between TMB and patient survival, and the mechanisms of immunocyte infiltration in different immunotherapy protocols require further exploration.

CONCLUSION

In this study, we investigated the patterns of TMB and immunocyte infiltration in patients with colon cancer based on the TCGA database, which may provide valuable clues of immunotherapy for colon cancer. In addition, we established a nomogram model integrating TMB and immune infiltration with remarkable performance in prognosis prediction, indicating its potential application in the management of colon cancer patients.

DATA AVAILABILITY STATEMENT

The datasets presented in this study can be found in online repositories. The names of the repository/repositories and accession number(s) can be found in the article/ **Supplementary Material**.

AUTHOR CONTRIBUTIONS

All authors participated in the design of this study, and read and approved the final version of the manuscript. ZZ, XX, and XW were in charge of data obtainment and analysis. XZ, WL, and TS obtained the data. YC and JW were in charge of statistical analysis. ZZ and XX drafted the manuscript. CD and HZ supervised this study and revised the manuscript.

FUNDING

This study was supported by a grant from the Clinical Medicine and Cancer Research Center of Shaanxi Province (Grant No. 2019LCZX-02).

ACKNOWLEDGMENTS

We thank all authors of the studies included in this study. We also thank The Cancer Genome Atlas (TCGA) database for providing the free data, and the free R software which was used for analysis (http://www.r-project.org).

SUPPLEMENTARY MATERIAL

The Supplementary Material for this article can be found online at: https://www.frontiersin.org/articles/10.3389/fgene.2021.623424/full#supplementary-material

Supplementary Figure 1 | The workflow of this study.

Supplementary Figure 2 | The expression of SCT and its correlation with immunocytes infiltration. **(A)** The expression level of SCT in 32 different type of tumors and matched normal samples. $^{*}P < 0.05$, $^{**}P < 0.01$, $^{***}P < 0.001$. **(B)** The correlation of SCT expression level and immunocytes infiltration status of colon cancer based on the TIMER database validation.

REFERENCES

Afroze, S., Meng, F., Jensen, K., McDaniel, K., Rahal, K., Onori, P., et al. (2013). The physiological roles of secretin and its receptor. *Ann. Transl. Med.* 1:8.

Alexander, J., Watanabe, T., Wu, T. T., Rashid, A., Li, S., and Hamilton, S. R. (2001). Histopathological identification of colon cancer with microsatellite instability. *Am. J. Pathol.* 158, 527–535. doi: 10.1016/s0002-9440(10)63994-6

Alexandrov, L. B., Nik-Zainal, S., Wedge, D. C., Aparicio, S. A., Behjati, S., Biankin, A. V., et al. (2013). Signatures of mutational processes in human cancer. *Nature* 500, 415–421. doi: 10.1038/nature12477

Ansell, S. M., Lesokhin, A. M., Borrello, I., Halwani, A., Scott, E. C., Gutierrez, M., et al. (2015). PD-1 blockade with nivolumab in relapsed or refractory Hodgkin's lymphoma. *N. Engl. J. Med.* 372, 311–319. doi: 10.1056/NEJMoa1411087

Arana, M. E., and Kunkel, T. A. (2010). Mutator phenotypes due to DNA replication infidelity. *Semin. Cancer Biol.* 20, 304–311. doi: 10.1016/j.semcancer.2010.10.003

Auclin, E., Zaanan, A., Vernerey, D., Douard, R., Gallois, C., Laurent-Puig, P., et al. (2017). Subgroups and prognostication in stage III colon cancer: future perspectives for adjuvant therapy. *Ann. Oncol.* 28, 958–968. doi: 10.1093/annonc/mdx030

Bacher, J. W., Flanagan, L. A., Smalley, R. L., Nassif, N. A., Burgart, L. J., Halberg, R. B., et al. (2004). Development of a fluorescent multiplex assay for detection of MSI-High tumors. *Dis. Markers* 20, 237–250. doi: 10.1155/2004/136734

Barbie, D. A., Tamayo, P., Boehm, J. S., Kim, S. Y., Moody, S. E., Dunn, I. F., et al. (2009). Systematic RNA interference reveals that oncogenic KRAS-driven cancers require TBK1. *Nature* 462, 108–112. doi: 10.1038/nature08460

Baretti, M., and Le, D. T. (2018). DNA mismatch repair in cancer. *Pharmacol. Ther.* 189, 45–62. doi: 10.1016/j.pharmthera.2018.04.004

Borghaei, H., Paz-Ares, L., Horn, L., Spigel, D. R., Steins, M., Ready, N. E., et al. (2015). Nivolumab versus docetaxel in advanced nonsquamous non-small-cell lung cancer. *N. Engl. J. Med.* 373, 1627–1639. doi: 10.1056/NEJMoa1507643

Bray, F., Ferlay, J., Soerjomataram, I., Siegel, R. L., Torre, L. A., and Jemal, A. (2018). Global cancer statistics 2018: GLOBOCAN estimates of incidence and mortality worldwide for 36 cancers in 185 countries. *CA Cancer J. Clin.* 68, 394–424. doi: 10.3322/caac.21492

Brody, H. (2015). Colorectal cancer. *Nature* 521:S1. doi: 10.1038/521S1a

Büttner, R., Longshore, J. W., López-Ríos, F., Merkelbach-Bruse, S., Normanno, N., Rouleau, E., et al. (2019). Implementing TMB measurement in clinical practice: considerations on assay requirements. *ESMO Open* 4:e000442. doi: 10.1136/esmoopen-2018-000442

Carbone, D. P., Reck, M., Paz-Ares, L., Creelan, B., Horn, L., Steins, M., et al. (2017). First-line nivolumab in stage IV or recurrent non-small-cell lung cancer. *N. Engl. J. Med.* 376, 2415–2426. doi: 10.1056/NEJMoa1613493

Chalmers, Z. R., Connelly, C. F., Fabrizio, D., Gay, L., Ali, S. M., Ennis, R., et al. (2017). Analysis of 100,000 human cancer genomes reveals the landscape of tumor mutational burden. *Genome Med.* 9:34. doi: 10.1186/s13073-017-0424-2

Chan, T. A., Yarchoan, M., Jaffee, E., Swanton, C., Quezada, S. A., Stenzinger, A., et al. (2019). Development of tumor mutation burden as an immunotherapy biomarker: utility for the oncology clinic. *Ann. Oncol.* 30, 44–56. doi: 10.1093/annonc/mdy495

Chang, H., Sasson, A., Srinivasan, S., Golhar, R., Greenawalt, D. M., Geese, W. J., et al. (2019). Bioinformatic methods and bridging of assay results for reliable tumor mutational burden assessment in non-small-cell lung cancer. *Mol. Diagn. Ther.* 23, 507–520. doi: 10.1007/s40291-019-00408-y

Chen, W., Zheng, R., Baade, P. D., Zhang, S., Zeng, H., Bray, F., et al. (2016). Cancer statistics in China, 2015. *CA Cancer J. Clin.* 66, 115–132. doi: 10.3322/caac.21338

Di Caro, G., Bergomas, F., Grizzi, F., Doni, A., Bianchi, P., Malesci, A., et al. (2014). Occurrence of tertiary lymphoid tissue is associated with T-cell infiltration and predicts better prognosis in early-stage colorectal cancers. *Clin. Cancer Res.* 20, 2147–2158. doi: 10.1158/1078-0432.ccr-13-2590

Dienstmann, R., Salazar, R., and Tabernero, J. (2015). Personalizing colon cancer adjuvant therapy: selecting optimal treatments for individual patients. *J. Clin. Oncol.* 33, 1787–1796. doi: 10.1200/jco.2014.60.0213

Eso, Y., and Seno, H. (2020). Current status of treatment with immune checkpoint inhibitors for gastrointestinal, hepatobiliary, and pancreatic cancers. *Therap Adv. Gastroenterol.* 13:1756284820948773. doi: 10.1177/1756284820948773

Galon, J., Costes, A., Sanchez-Cabo, F., Kirilovsky, A., Mlecnik, B., Lagorce-Pagès, C., et al. (2006). Type, density, and location of immune cells within human colorectal tumors predict clinical outcome. *Science* 313, 1960–1964. doi: 10.1126/science.1129139

Ganesh, K., Stadler, Z. K., Cercek, A., Mendelsohn, R. B., and Shia, J. (2019). Immunotherapy in colorectal cancer: rationale, challenges and potential. *Nat. Rev. Gastroenterol. Hepatol.* 16, 361–375. doi: 10.1038/s41575-019-0126-x

Garon, E. B., Rizvi, N. A., Hui, R., Leighl, N., Balmanoukian, A. S., Eder, J. P., et al. (2015). Pembrolizumab for the treatment of non-small-cell lung cancer. *N. Engl. J. Med.* 372, 2018–2028. doi: 10.1056/NEJMoa1501824

Ghidini, M., Lampis, A., Mirchev, M. B., Okuducu, A. F., Ratti, M., Valeri, N., et al. (2020). Immune-based therapies and the role of microsatellite instability in pancreatic cancer. *Genes* 12:33. doi: 10.3390/genes12010033

Goodman, A., Patel, S. P., and Kurzrock, R. (2017). PD-1-PD-L1 immune-checkpoint blockade in B-cell lymphomas. *Nat. Rev. Clin. Oncol.* 14, 203–220. doi: 10.1038/nrclinonc.2016.168

Goodman, A. M., Kato, S., Bazhenova, L., Patel, S. P., Frampton, G. M., Miller, V., et al. (2017). Tumor mutational burden as an independent predictor of response to immunotherapy in diverse cancers. *Mol. Cancer Ther.* 16, 2598–2608. doi: 10.1158/1535-7163.mct-17-0386

Hodi, F. S., O'Day, S. J., McDermott, D. F., Weber, R. W., Sosman, J. A., Haanen, J. B., et al. (2010). Improved survival with ipilimumab in patients with metastatic melanoma. *N. Engl. J. Med.* 363, 711–723. doi: 10.1056/NEJMoa1003466

Howlader, N. N. A., Krapcho, M., Miller, D., Brest, A., Yu, M., Ruhl, J., et al. (eds) (2020). *SEER Cancer Statistics Review, 1975-2017*. Bethesda, MD: National Cancer Institute.

Hu, Z. I., Ho, A. Y., and McArthur, H. L. (2017). Combined radiation therapy and immune checkpoint blockade therapy for breast cancer. *Int. J. Radiat. Oncol. Biol. Phys.* 99, 153–164. doi: 10.1016/j.ijrobp.2017.05.029

Huang, T. X., and Fu, L. (2019). The immune landscape of esophageal cancer. *Cancer Commun.* 39:79. doi: 10.1186/s40880-019-0427-z

Hugo, W., Zaretsky, J. M., Sun, L., Song, C., Moreno, B. H., Hu-Lieskovan, S., et al. (2016). Genomic and transcriptomic features of response to anti-PD-1 therapy in metastatic melanoma. *Cell* 165, 35–44. doi: 10.1016/j.cell.2016.02.065

Iwai, Y., Ishida, M., Tanaka, Y., Okazaki, T., Honjo, T., and Minato, N. (2002). Involvement of PD-L1 on tumor cells in the escape from host immune system and tumor immunotherapy by PD-L1 blockade. *Proc. Natl. Acad. Sci. U.S.A.* 99, 12293–12297. doi: 10.1073/pnas.192461099

Kwong, L. N., and Dove, W. F. (2009). APC and its modifiers in colon cancer. *Adv. Exp. Med. Biol.* 656, 85–106. doi: 10.1007/978-1-4419-1145-2_8

Lauss, M., Donia, M., Harbst, K., Andersen, R., Mitra, S., Rosengren, F., et al. (2017). Mutational and putative neoantigen load predict clinical benefit of adoptive T cell therapy in melanoma. *Nat. Commun.* 8:1738. doi: 10.1038/s41467-017-01460-0

Le, D. T., Uram, J. N., Wang, H., Bartlett, B. R., Kemberling, H., Eyring, A. D., et al. (2015). PD-1 blockade in tumors with mismatch-repair deficiency. *N. Engl. J. Med.* 372, 2509–2520. doi: 10.1056/NEJMoa1500596

Leach, D. R., Krummel, M. F., and Allison, J. P. (1996). Enhancement of antitumor immunity by CTLA-4 blockade. *Science* 271, 1734–1736. doi: 10.1126/science.271.5256.1734

Lin, A., Zhang, J., and Luo, P. (2020). Crosstalk between the MSI status and tumor microenvironment in colorectal cancer. *Front. Immunol.* 11:2039. doi: 10.3389/fimmu.2020.02039

Llosa, N. J., Cruise, M., Tam, A., Wicks, E. C., Hechenbleikner, E. M., Taube, J. M., et al. (2015). The vigorous immune microenvironment of microsatellite instable colon cancer is balanced by multiple counter-inhibitory checkpoints. *Cancer Discov.* 5, 43–51. doi: 10.1158/2159-8290.cd-14-0863

Motzer, R. J., Escudier, B., McDermott, D. F., George, S., Hammers, H. J., Srinivas, S., et al. (2015). Nivolumab versus everolimus in advanced renal-cell carcinoma. *N. Engl. J. Med.* 373, 1803–1813. doi: 10.1056/NEJMoa1510665

Nakayama, M., and Oshima, M. (2019). Mutant p53 in colon cancer. *J. Mol. Cell. Biol.* 11, 267–276. doi: 10.1093/jmcb/mjy075

Newman, A. M., Liu, C. L., Green, M. R., Gentles, A. J., Feng, W., Xu, Y., et al. (2015). Robust enumeration of cell subsets from tissue expression profiles. *Nat. Methods* 12, 453–457. doi: 10.1038/nmeth.3337

Onori, P., Wise, C., Gaudio, E., Franchitto, A., Francis, H., Carpino, G., et al. (2010). Secretin inhibits cholangiocarcinoma growth via dysregulation of the cAMP-dependent signaling mechanisms of secretin receptor. *Int. J. Cancer* 127, 43–54. doi: 10.1002/ijc.25028

Palomaki, G. E., McClain, M. R., Melillo, S., Hampel, H. L., and Thibodeau, S. N. (2009). EGAPP supplementary evidence review: DNA testing strategies aimed at reducing morbidity and mortality from Lynch syndrome. *Genet. Med.* 11, 42–65. doi: 10.1097/GIM.0b013e31818fa2db

Pan, R., Zhu, M., Yu, C., Lv, J., Guo, Y., Bian, Z., et al. (2017). Cancer incidence and mortality: a cohort study in China, 2008-2013. *Int. J. Cancer* 141, 1315–1323. doi: 10.1002/ijc.30825

Powles, T., Loriot, Y., Ravaud, A., Vogelzang, N. J., Duran, I., Retz, M., et al. (2018). Atezolizumab (atezo) vs. chemotherapy (chemo) in platinum-treated locally advanced or metastatic urothelial carcinoma (mUC): immune biomarkers, tumor mutational burden (TMB), and clinical outcomes from the phase III IMvigor211 study. *J. Clin. Oncol.* 36, 409–409. doi: 10.1200/JCO.2018.36.6_suppl.409

Riaz, N., Morris, L., Havel, J. J., Makarov, V., Desrichard, A., and Chan, T. A. (2016). The role of neoantigens in response to immune checkpoint blockade. *Int. Immunol.* 28, 411–419. doi: 10.1093/intimm/dxw019

Rizvi, N. A., Hellmann, M. D., Snyder, A., Kvistborg, P., Makarov, V., Havel, J. J., et al. (2015). Cancer immunology. Mutational landscape determines sensitivity to PD-1 blockade in non-small cell lung cancer. *Science* 348, 124–128. doi: 10.1126/science.aaa1348

Robert, C., Schachter, J., Long, G. V., Arance, A., Grob, J. J., Mortier, L., et al. (2015). Pembrolizumab versus ipilimumab in advanced melanoma. *N. Engl. J. Med.* 372, 2521–2532. doi: 10.1056/NEJMoa1503093

Rosenberg, J. E., Hoffman-Censits, J., Powles, T., van der Heijden, M. S., Balar, A. V., Necchi, A., et al. (2016). Atezolizumab in patients with locally advanced and metastatic urothelial carcinoma who have progressed following treatment with platinum-based chemotherapy: a single-arm, multicentre, phase 2 trial. *Lancet* 387, 1909–1920. doi: 10.1016/s0140-6736(16)00561-4

Samstein, R. M., Lee, C. H., and Shoushtari, A. N. (2019). Tumor mutational load predicts survival after immunotherapy across multiple cancer types. *Nat. Genet.* 51, 202–206. doi: 10.1038/s41588-018-0312-8

Seo, H. M., Chang, Y. S., Joo, S. H., Kim, Y. W., Park, Y. K., Hong, S. W., et al. (2009). Clinicopathologic characteristics and outcomes of gastric cancers with the MSI-H phenotype. *J. Surg. Oncol.* 99, 143–147. doi: 10.1002/jso.21220

Siegel, R. L., Miller, K. D., Fedewa, S. A., Ahnen, D. J., Meester, R. G. S., Barzi, A., et al. (2017). Colorectal cancer statistics, 2017. *CA Cancer J. Clin.* 67, 177–193. doi: 10.3322/caac.21395

Simpson, J. A., Al-Attar, A., Watson, N. F., Scholefield, J. H., Ilyas, M., and Durrant, L. G. (2010). Intratumoral T cell infiltration, MHC class I and STAT1 as biomarkers of good prognosis in colorectal cancer. *Gut* 59, 926–933. doi: 10.1136/gut.2009.194472

Surveillance, Epidemiology, and End Results [SEER] (2016). *SEER*Stat Database: Incidence-SEER 18 Regs Research Data Hurricane Katrina Impacted Louisiana Cases, Nov. 2015 Sub (1973-2013 varying)-Linked To County Attributes-Total US, 1969-2014 Counties*. Bethesda, MD: National Cancer Institute, Department of Cancer Control and Population Sciences, Surveillance Research Program, Surveillance Systems Branch.

Topalian, S. L., Taube, J. M., Anders, R. A., and Pardoll, D. M. (2016). Mechanism-driven biomarkers to guide immune checkpoint blockade in cancer therapy. *Nat. Rev. Cancer* 16, 275–287. doi: 10.1038/nrc.2016.36

Wanigasekara, N. E. W., Bech, P., and Murphy, K. (2015). Chromogranin B: a possible prognostic biomarker for neuroendocrine tumours? *Endocr. Abstr.* 38:160. doi: 10.1530/endoabs.38.P160

Wei, M., Shen, D., Mulmi Shrestha, S., Liu, J., Zhang, J., and Yin, Y. (2018). The Progress of T cell immunity related to prognosis in gastric cancer. *Biomed. Res. Int.* 2018:3201940. doi: 10.1155/2018/3201940

Wolff, R. K., Hoffman, M. D., Wolff, E. C., Herrick, J. S., Sakoda, L. C., Samowitz, W. S., et al. (2018). Mutation analysis of adenomas and carcinomas of the colon: early and late drivers. *Genes Chromosomes Cancer* 57, 366–376. doi: 10.1002/gcc.22539

Wu, C. (2018). Systemic therapy for colon cancer. *Surg. Oncol. Clin. N. Am.* 27, 235–242. doi: 10.1016/j.soc.2017.11.001

Yamamoto, H., and Imai, K. (2015). Microsatellite instability: an update. *Arch. Toxicol.* 89, 899–921. doi: 10.1007/s00204-015-1474-0

Zappasodi, R., Merghoub, T., and Wolchok, J. D. (2018). Emerging concepts for immune checkpoint blockade-based combination therapies. *Cancer Cell* 33, 581–598. doi: 10.1016/j.ccell.2018.03.005

Zhang, H., Liu, L., Zhang, J., Chen, J., Ye, J., Shukla, S., et al. (2020). Investigation of antigen-specific t-cell receptor clusters in human cancers. *Clin. Cancer Res.* 26, 1359–1371. doi: 10.1158/1078-0432.ccr-19-3249

Conflict of Interest: The authors declare that the research was conducted in the absence of any commercial or financial relationships that could be construed as a potential conflict of interest.

frontiers in Oncology

ORIGINAL RESEARCH
published: 19 February 2021
doi: 10.3389/fonc.2020.617105

Downregulation of the lncRNA ASB16-AS1 Decreases LARP1 Expression and Promotes Clear Cell Renal Cell Carcinoma Progression *via* miR-185-5p/miR-214-3p

Mingzi Li[1†], Bingde Yin[2†], Mulin Chen[1†], Jingtao Peng[3], Xinyu Mu[1], Zhen Deng[1], Jiantao Xiao[4], Weiguo Li[1*] and Jie Fan[1*]*

[1] Department of Urology, Shanghai General Hospital, School of Medicine, Shanghai Jiaotong University, Shanghai, China, [2] Department of Urology, Minhang Hospital, Fudan University, Shanghai, China, [3] Department of Urology, Union Hospital, Tongji Medical College, Huazhong University of Science and Technology, Wuhan, China, [4] Department of Urology, Zhongnan Hospital of Wuhan University, Wuhan, China

Clear cell renal cell carcinoma (ccRCC) comprises approximately 75% of renal cell carcinomas, which is one of the most common and lethal urologic cancers, with poor quality of life for patients and is a huge economic burden to health care systems. It is imperative we find novel prognostic and therapeutic targets for ccRCC clinical intervention. In this study, we found that the expression of the long noncoding RNA (lncRNA) ASB16-AS1 was downregulated in ccRCC tissues compared with non-diseased tissues and was also associated with advanced tumor stage and larger tumors. By constructing cell and mouse models, it was found that downregulated lncRNA ASB16-AS1 enhanced cell proliferation, migration, invasion, and promoted tumor growth and metastasis. Furthermore, by performing bioinformatics analysis, biotinylated RNA pull-downs, AGO2-RIP, and luciferase reporter assays, our findings showed that downregulated ASB16-AS1 decreased La-related protein 1 (LARP1) expression by inhibiting miR-185-5p and miR-214-3p. Furthermore, it was found that overexpression of LARP1 reversed the promotive effects of downregulated ASB16-AS1 on ccRCC cellular progression. Our results revealed that downregulated ASB16-AS1 promotes ccRCC progression *via* a miR-185-5p-miR-214-3p-LARP1 pathway. We suggest that this pathway could be used to monitor prognosis and presents therapeutic targets for ccRCC clinical management.

Keywords: long non-coding RNA, lncRNA ASB16-AS1, miR-185-5p, miR-214-3p, LARP1, clear cell renal cell carcinoma

OPEN ACCESS

Edited by:
Xiao-Jie Lu,
Nanjing Medical University, China

Reviewed by:
Yan Ji,
University of Texas MD Anderson Cancer Center, United States
Weifeng Ding,
Nantong University, China
Yuyao Zhang,
Mass General Research Institute, United States

****Correspondence:***
Jie Fan
jief67@sina.com
Weiguo Li
joelwg@sina.com
Jiantao Xiao
urologist_xjt@163.com

[†]These authors share first authorship

Specialty section:
This article was submitted to Cancer Genetics, a section of the journal Frontiers in Oncology

Received: *14 October 2020*
Accepted: *29 December 2020*
Published: *19 February 2021*

Citation:
Li M, Yin B, Chen M, Peng J, Mu X, Deng Z, Xiao J, Li W and Fan J (2021) Downregulation of the lncRNA ASB16-AS1 Decreases LARP1 Expression and Promotes Clear Cell Renal Cell Carcinoma Progression via miR-185-5p/miR-214-3p. Front. Oncol. 10:617105. doi: 10.3389/fonc.2020.617105

INTRODUCTION

Renal cell carcinoma (RCC) is one of the most common types of urologic cancers accounting for more than 90% of renal malignancies (1, 2). Clear cell renal cell carcinoma (ccRCC) comprises approximately 75% of RCCs and is the most lethal pathological subtype of RCC (3). More than 30% of ccRCC patients are diagnosed with metastasized disease and have a 13-month median survival time (4). There are many risk factors such as dietary habits, occupational exposure, and physical inactivity that can lead to ccRCC tumorigeneses. The inefficiency of treatment and limitations in diagnosing ccRCC contribute to the poor quality of life for patients and the huge economic burden this disease has on health care systems (5, 6). Therefore, it is imperative we find novel diagnostic and therapeutic targets for clinical management and intervention.

Long noncoding RNAs (lncRNAs) are one type of noncoding RNA consisting of more than 200 nucleotides (7). The underlying molecular mechanisms of lncRNA have been revealed in the past decades. For example, LncRNAs can act as a molecular sponge for microRNAs (miRs) (8) or interact with proteins, modulating their functions (9). LncRNAs are involved in many biological functions, especially tumorigenesis (10–12). Recently, the roles of lncRNAs in ccRCC tumorigenesis have been partly demonstrated; He et al. found that MEG3 regulates ccRCC progression *via* sponging miR-7 (13); Yang FQ et al. investigated the role of HOXA11-AS in ccRCC progression *via* promoting ccRCC growth and invasion ability (14); Qi Y et al. demonstrated that PENG suppresses ccRCC proliferation *via* sponging miR-15b (15); and the tumor-suppressing role of HOTAIRM1 in ccRCC has recently been demonstrated (16). These studies suggest that lncRNAs play essential roles in ccRCC development.

ASB16-AS1 is localized to 17q21, and is approximately 2275 bp. Previous studies have reported that lncRNA ASB16-AS1 functions as a microRNA sponge and regulates cell proliferation, migration, invasion, and apoptosis in several cancers including hepatocellular carcinoma, glioma, non-small lung cancer, and cervical cancer (17–20), indicating that ASB16-AS1 play its crucial role in tumorigenesis. However, whether ASB16-AS1 exerts its function in ccRCC progression is poorly understood.

We hypothesized that ASB16-AS1 is involved in ccRCC progression and regulates ccRCC cell functions. Firstly, we tested ASB16-AS1 expression in ccRCC tissues. We then constructed *in vitro* and *in vivo* models to demonstrate the biological functions of ASB16-AS1 in ccRCC. Furthermore, we conducted bioinformatic analysis, AGO2-RIP, biotinylated RNA pull-downs, and luciferase reporter assays to elucidate the underlying molecular mechanisms of ASB16-AS1. Collectively, our data suggest that ASB16-AS1 could be used to monitor prognosis and presents therapeutic targets, altogether providing new insights regarding ccRCC basic research.

Abbreviations: AGO2, argonaute RISC catalytic component 2; ASB16-AS1, ASB16 antisense RNA 1; ccRCC, clear cell renal cell carcinoma; EdU, 5-ethynyl-2′-deoxyuridine; EMT, epithelial-mesenchymal transition; IHC, immunohistochemistry; LARP1, La-related protein 1; LncRNA, long noncoding RNA; MiR, microRNA; NOD/SCID, nonobese severe diabetic/severe combined immunodeficiency mice; RCC, Renal cell carcinoma; RIP, RNA binding protein immunoprecipitation; shRNA, short hairpin RNA.

MATERIALS AND METHODS

Clinical Samples

ccRCC tumors and adjacent non-diseased tissues were collected from 42 patients with ccRCC who received operative treatment at the Department of Urology, Shanghai General Hospital between August 2012 to December 2013. The specimens were collected from a tumor and a region at least 5 cm away from the tumor in each patient. The histological diagnosis was confirmed by two pathologists using hematoxylin and eosin stained sections. Following the American Joint Committee on Cancer (AJCC) guidelines, the pathological stage of each tumor was also determined by two pathologists. All patients provided informed consent.

Cell Culture and Transfection

The ccRCC cell lines A498, 786-O, 769-P, CAKI-1, OS-RC-2, ACHN, and the human kidney proximal tubular epithelial cell line, HK-2 and 293T, were purchased from The American Type Culture Collection (ATCC, USA). DMEM (Gibco, USA) with 10% FBS (Gibco, USA) and 1% penicillin/streptomycin (Gibco, USA) was used to culture cells at 37°C in a humidified atmosphere. The plasmids and short hairpin RNAs (shRNAs) used in this study were synthesized by and purchased from GenePharma (Shanghai, China). All transfections were conducted using lipofectamine 3000 or RNA iMax (Invitrogen, US) following the manufacturer's instructions.

Quantitative Real-Time PCR

Total RNA isolations were conducted using TRIzol Reagent (Invitrogen, US), and total cDNA was synthesized using the Superscript RT Kit (TOYOBO, Japan). Real-time PCR was performed using the SYBR Green PCR Master Mix Kit (TOYOBO, Japan). Endogenous glyceraldehyde 3-phosphate dehydrogenase (GAPDH) was used for normalization. The primers used in this study are as follows: LncRNA ASB16-AS1 forward: CGGCCCTGAGGCAAACATAC, reverse: TGAAACA CTGCGCCAACTTC; miR-185-5p forward: CCATGTGCCT GTGTCATGC, reverse: ATCTGCTGATCCCCGCCA; miR-214-3p forward: ACACTCCAGCTGGGACAGCAGGCA CAGACA, reverse: TGGTGTCGTGGAGTCG; LARP1 forward: GCAACCTAAAGACACTAC reverse: CCTCTTCT TCACTTCAATC; GAPDH forward: GCCTGCTTCACC ACCTTCT, reverse: GAACGGGAAGCTCACTGG. The 2 $^{-\Delta\Delta}$Ct method was used to calculate relative expression levels.

WESTERN BLOT

Proteins from cells and tissues were extracted using Radioimmunoprecipitation (RIPA) lysis buffer (Beyotime, China). Protein concentration was determined using the

bicinchoninic acid (BCA) kit (Beyotime, China). Next, protein samples were subjected to 10% SDS-PAGE and transferred to PVDF membranes. The membranes were blocked using 5% nonfat milk and washed three times in TBS with 0.1% Tween-20. The membranes were incubated with primary antibodies overnight at 4°C, followed by incubation with secondary antibodies for 1 h at room temperature. The primary antibodies used were; anti-LARP1 (1:1000, 13187S, CST), anti-E-cadherin (1:1,000, 14472S, CST), anti-Vimentin (1:1,000, 5741S, CST), and anti-GAPDH (1:5,000, ab8245, Abcam). The ECL Chemiluminescence System (Santa Cruz Biotechnology, US) was used to visualize antibody binding.

5-Ethynyl-2′-Deoxyuridine (EdU) Incorporation

Cell proliferation was determined using the Cell-Light EdU DNA Cell proliferation kit (RiboBio, China) following the manufacturer's instructions. Two days after transfection, 50 mM EdU was applied to cells an incubated for 2 h. DAPI was used to stain nucleic acids and Apollo Dye Solution used to stain cells. The cell proliferation rate was calculated using Image J software (NIH, USA).

Cell Invasion and Migration Assays

Cell invasion and migration assays were performed in 24-well transwell plates filled with a polycarbonate membrane (pore size, 8 μm) (Corning, US), and Matrigel basement membrane matrix (1 μg/μl) (BD Biosciences, US) was used to fill the membranes. Briefly, 100 μl of serum-free media suspension was used to fill the upper chamber and 600 μl DMEM with 10% FBS was used to fill the lower chamber. After 24 h, the membranes of chambers were treated with crystal violet staining and observed under the microscope. Six fields of view were randomly chosen and cell numbers were recorded. Experiments were repeated three times.

RNA Fluorescent *In Situ* Hybridization (FISH)

The FISH kit (Ribibio, China) was used to detect the location of ASB16-AS1 in the ccRCC cell line 786-O following the manufacturer's protocol. Briefly, 786-O cells were incubated with pre-hybridization solutions for 30 min. Probes were treated with 20 μM hybridization solution and allowed to hybridize for 12 h. Next, saline sodium citrate was used to wash slides three times before treating with DAPI for 20 min. Results were visualized using a confocal microscope.

Luciferase Reporter Assay

PmirGLO vectors (Promega, USA) harboring miR-185-5p and miR-214-3p sequences with wild-type or mutant binding sites for ASB16-AS1/LARP1 were used. The miR-185-5p mimic, miR-214-3p mimic, and the luciferase vectors were co-transfected into 786-O and 293T cells. The Dual-Luciferase Reporter Assay System (Promega, US) was used to detect luciferase activity.

RNA Immunoprecipitation

Anti-AGO2 (#03-110, Millipore, Germany) was used to perform RNA immunoprecipitation (RIP) by using the Magna RIP RNA-binding protein immunoprecipitation kit (Millipore, Germany). To analyze the RNA bound complexes qRT-PCR assay was performed. Anti-IgG was used as an isotype control.

RNA Pull-Down

Biotinylated ASB16-AS1, miR-185-5p, miR-214-3p, and control probes were synthesized and purchased from GenePharma (Shanghai, China). Co-immunoprecipitation buffer (Beyotime, China) was used to lyse cells which were then subjected to high amplitude. Cell lysates were incubated with ASB16-AS1, miR-185-5p, and miR-214-3p probe-streptavidin beads (Life, USA) overnight. TRIzol Reagent (Invitrogen, US) was used for RNA isolation and RNA bound complexes were analyzed by qRT-PC.

In Vivo Mouse Xenografts

The Committee for Animal Care and Use of Shanghai general Hospital approved our animal experiments. Six-week old nonobese severe diabetic/severe combined immunodeficiency (NOD/SCID) mice were randomly divided into two groups (n=5 each). The ccRCC 786-O cells pre-transfected with Sh-NC or Sh-ASB16-AS1 were then subcutaneously inoculated into the NOD/SCID mice (1×10^7 cells per tumor). From day 25 post inoculation, tumor volumes were measured every five days until day 45.

Immunohistochemistry

After surgery, all specimens were collected and fixed in formalin immediately. Then, specimens were all subjected to the process of dehydration, paraffinization, and embedded in paraffin blocks. Subsequently, specimens were cut into sections at 4 μm and dried in air 12 h. Tissue sections were undergoing the process of dehydration, paraffinization once again, and subjected to antigen retrieval with sodium citrate buffer upon heat stimulation. Endogenous peroxidase activity was blocked by 3% hydrogen peroxide for 5 min. Next, tissue sections were incubated with primary antibody (LARP1; Abcam; 1:200; ab245635), and biotinylated goat anti-mouse IgG. Results were visualized using the VECTASTAIN ABC kit (Vector Laboratories) according to manufacturer's protocol.

Statistical Analysis

All experiments were carried out at least three times unless otherwise stated. Statistical analysis was performed using SPSS 19.0 (IBM, USA). The differences between two groups were tested using a Student's t-test; whereas, a one-way ANOVA was used to analyze the difference between three or more group. Data are presented as mean ± SD, and $P < 0.05$ was considered as statistically significant.

RESULTS

The Expression of ASB16-AS1 in ccRCC Tissues

In order to investigate whether ASB16-AS1 plays a role in ccRCC progression, we tested ASB16-AS1 expression in 42 pairs of ccRCC tumor tissues and adjacent non-diseased tissues. We found that ASB16-AS1 expression in tumors was significantly

lower than in adjacent non-diseased tissues (**Figure 1A**). Moreover, ASB16-AS1 was abundantly expressed in later stage and larger tumors (**Figures 1B, C**), suggesting that ASB16-AS1 might be involved in ccRCC initiation and progression. Next, we measured ASB16-AS1 expression in different ccRCC cell lines and the human proximal tubular epithelial cell line HK-2. The results showed that ASB16-AS1 was abundantly expressed in 786-O cells and lowly expressed in 769-P cells (**Figure 1D**). Fluorescent *in situ* hybridization (FISH) shows that ASB16-AS1 is mainly located in the cytoplasm of 786-O cells (**Figure 1E**).

ASB16-AS1 Downregulation Promotes ccRCC Proliferation, Migration, and Invasion

Next, we determined the biological function of ASB16-AS1 in ccRCC progression. Cell models were generated by transfecting sh-NC or sh-ASB16-AS1 into 786-O cells, and OE-NC or OE-ASB16-AS1 into 769-P cells, respectively. Transfection efficiency is shown in **Figure 2A**. Cell proliferation was determined by EdU assays. As shown in **Figures 2B, C**, downregulation of ASB16-AS1 promoted cell proliferation in 786-O cells, and upregulation of ASB16-AS1 inhibited cell proliferation in 769-P cells. Cell migration and invasion was detected by performing Transwell assays. It was found that downregulation of ASB16-AS1 promoted migration (**Figures 2D, E**) and invasion (**Figures 2F, G**) in 786-O cells, and upregulation of ASB16-AS1 inhibited migration (**Figures 2D, E**) and invasion (**Figures 2F, G**) in 769-P cells. Next, epithelial-mesenchymal transition (EMT) was investigated by measuring E-cadherin and Vimentin protein expression in treated cells. As shown in **Figures 2H, I**, ASB16-AS1 overexpression promoted an EMT phenotype in 769-P cells, and ASB16-AS1 downregulation inhibited an EMT phenotype in 786-O cells. These results indicate that ASB16-AS1 is involved in ccRCC progression.

ASB16-AS1 Downregulation Promotes ccRCC Cell Growth and Metastasis *In Vivo*

In vivo experiments were applied to further assess the biological functions of ASB16-AS1 in ccRCC progression. Nonobese severe diabetic/severe combined immunodeficiency (NOD/SCID) mice (6 weeks old) were subcutaneously inoculated with 786-O cells (1×10^7 per tumor) which were pre-transfected with sh-NC or sh-ASB16-AS1. The representative images of excised tumors are shown in **Figure 3A**. From day 25 post inoculation, tumor volumes were recorded every 5 days until day 45 (**Figure 3B**),

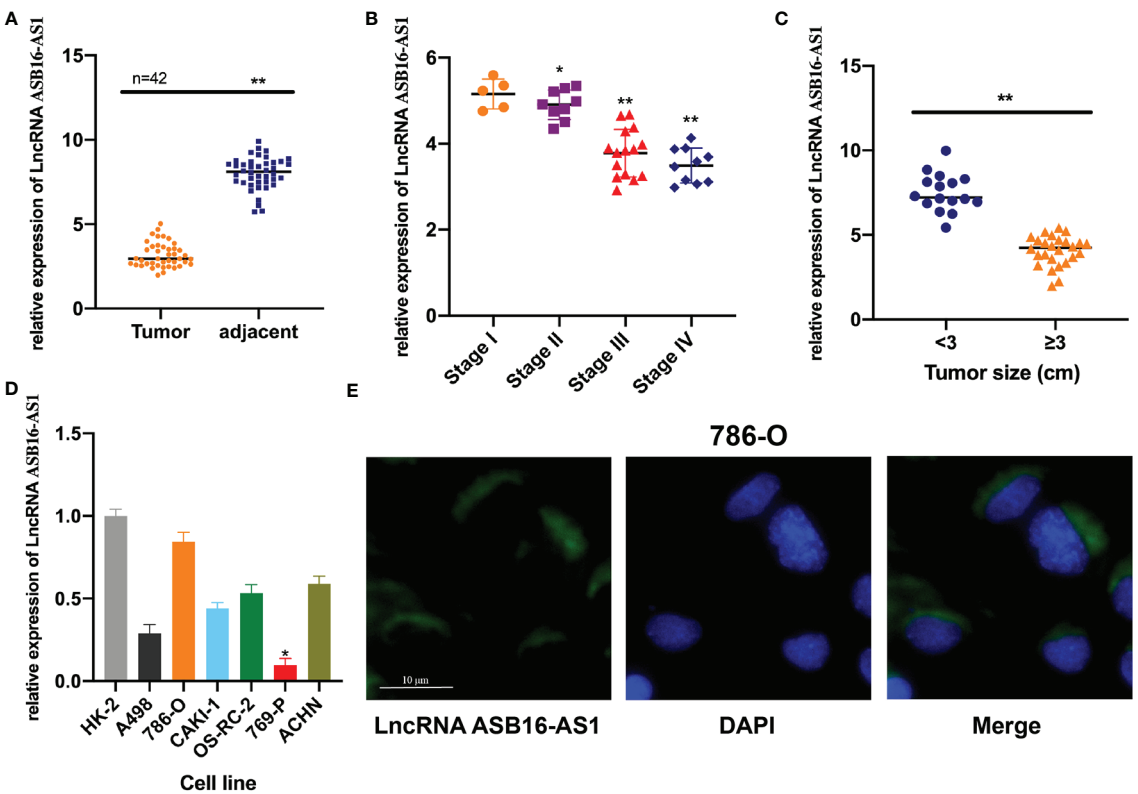

FIGURE 1 | The expression of ASB16-AS1 in renal cell carcinoma (RCC) tissues. **(A)** qRT-PCR analysis showing decreased ASB16-AS1 expression in 42 RCC tumor tissues compared with paired adjacent non-diseased tissues. **(B)** ASB16-AS1 expression is significantly decreased in RCC tumors of higher stages (N=5–15). **(C)** ASB16-AS1expression is significantly decreased in larger tumors (N=16 smaller tumors and 26 larger tumors). **(D)** The expression of ASB16-AS1 varies across different RCC cell lines and the human kidney proximal tubular epithelial cell line, HK-2. **(E)** Fluorescent *in situ* hybridization showing the cytoplasmic location of ASB16-AS1 in 786-O cells. Scale bar – 10 μm. All experiments were repeated at least three times. *$P < 0.05$, **$P < 0.01$.

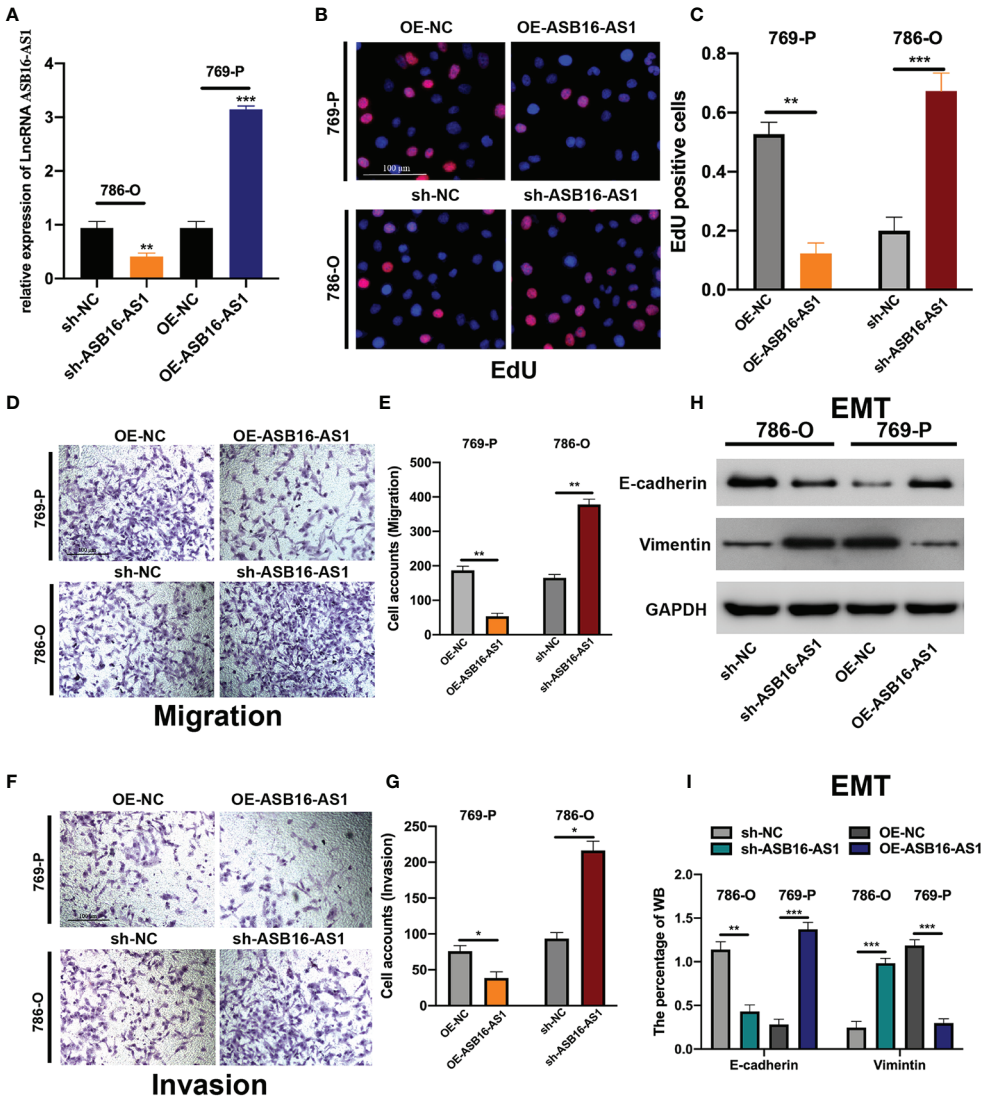

FIGURE 2 | ASB16-AS1 downregulation promotes renal cell carcinoma (RCC) proliferation, migration, and invasion. **(A)** The transfection efficiency of ASB16-AS1 siRNA/NC and OE/NC in 786-O and 769-P cells. **(B)** Representative images of EdU positive cells showing proliferation of shRNA treated 786-O and 769P cells, which are quantified in **(C)**. **(D)** Representative images of the transwell migration assays used to detect the migration of shRNA treated 786-O and 769P cells, which are quantified in **(E)**. **(F)** Transwell invasion assays were applied to detect the invasion of shRNA treated 786-O and 769P cells, which are quantified in (G). **(H)** Western blots of epithelial-mesenchymal-transition associated genes in shRNA treated 786-O and 769P cells, which are quantified in **(I)**. All experiments were repeated at least three times, scale bars -100 μm. $^{*}P < 0.05$, $^{**}P < 0.01$, $^{***}P < 0.001$.

comparative statistics of final tumor weights are shown in **Figure 3C**. it was suggested that downregulation of ASB16-AS1 significantly inhibits tumor growth compared with control levels of ASB16-AS1. Lung tissues from xenografted mice using hematoxylin and eosin staining showed that downregulation of ASB16-AS1 enhanced tumor metastasis (**Figure 3D**).

ASB16-AS1 Sponges miR-185-5p and miR-214-3p

Since lncRNA ASB16-AS1 is involved in ccRCC progression both *in vitro* and *in vivo* we sought to further understand the role of ASB16-AS1; therefore, we investigated its underlying molecular mechanisms. AGO2-RIP experiments were performed to assess the miRNA binding ability of ASB16-AS1. As shown in **Figures 4A, B**, compared with the anti-IgG group, ASB16-AS1 was significantly enriched in anti-AGO2 complexes in 786-O and 769-P cells. Next, we conducted bioinformatics analysis using the Miranda program (http://www.microrna.org/microrna/home.do). The expression of selected miRNAs was measured in 786-O cells and normalized to a control probe. We found that miR-185-5p and miR-214-3p were abundantly expressed (**Figure 4C**). Next, RNA pull-down assays using

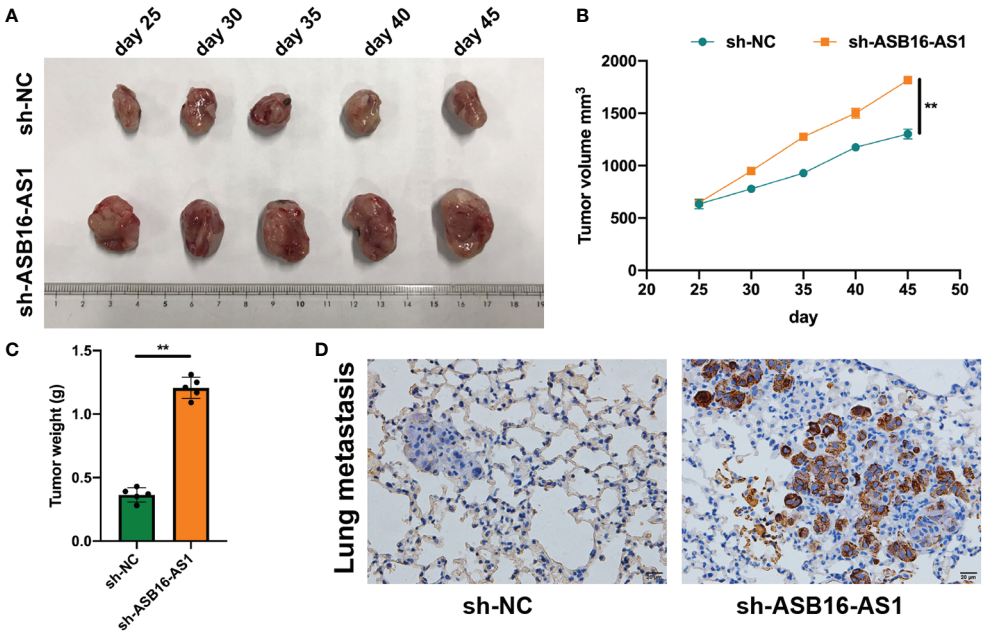

FIGURE 3 | ASB16-AS1 downregulation promotes renal cell carcinoma (RCC) cell growth and metastasis *in vivo*. Nonobese severe diabetic/severe combined immunodeficiency mice (6 weeks old) were subcutaneously inoculated with 786-O cells (1×10^7 per tumor) pre-transfected with Sh-NC or Sh-ASB16-AS1 (N=5 per condition). **(A)** Representative images of inoculated tumors which are quantified by volume in **(B)** which shows tumor volume increasing over time in the Sh-ASB16-AS1 pre-treated cell condition. **(C)** Final tumor weights show that Sh-ASB16-AS1 pre-treated cells produces heavier tumors (N=5 per condition). **(D)** Representative histological images of lung metastasis. Data are presented as mean ± S.D, scale bars – 20 μm. $^{**}P < 0.01$.

bio-miR-185-5p and bio-214-3p probes were performed. ASB16-AS1 was highly enriched in bio-miR-185-5p and bio-214-3p RNA complexes compared with bio-NC (**Figure 4D**). Subsequently, we constructed wild type (WT) and mutant (Mut) ASB16-AS1 binding sites for miR-185-5p and miR-214-3p, respectively (**Figure 4E**). Luciferase activity assays were conducted as shown in **Figures 4F, G**; the luciferase activity of the ASB16-AS1 WT sequence significantly reduced when co-transfected with miR-185-5p or miR-214-3p mimic in 293T and 786-O cells. The expression of miR-185-5p and miR-214-3p in Sh-ASB16-AS1 transfected 786-O cells was significantly greater than in the control group (**Figure 4H**). These data suggest that ASB16-AS1 interacted with miR-185-5p and miR-214-3p.

MiR-185-5p and miR-214-3p Inhibitors Rescue the Effects of Downregulated ASB16-AS1 on ccRCC Progression

To further demonstrate the association between ASB16-AS1 and miR-185-5p/miR-214-3p, and their biological functions in ccRCC, we generated cell models by transfecting 786-O cells with Sh-NC, Sh-ASB16-AS1, Sh-ASB16-AS1+NC-inhibitor, Sh-ASB16-AS1+miR-185-5p-inhibitor, and Sh-ASB16-AS1+miR-214-4p inhibitor. Transfection efficiencies are shown in **Figure 5A**. To assess the biological functions of treated 786-O cells, EdU, and Transwell assays were conducted. The promotive effects of downregulated ASB16-AS1 on cell proliferation (**Figure 5B**), cell invasion (**Figure 5C**), and cell migration (**Figure 5D**) were rescued by the miR-185-5p and miR-214-3p inhibitors. Furthermore, miR-185-5p and miR-214-3p inhibition effectively alleviated the enhancement of downregulated ASB16-AS1 on the EMT phenotype (**Figure 5E**). These data indicate that ASB16-AS1 regulates ccRCC progression *via* miR-185-5p and miR-214-3p.

LARP1 Is a Downstream Target for miR-185-5p/miR-214-3p

The downstream targets of miR-185-5p and miR-214-3p were predicted using the ENCORI database (http://starbase.sysu.edu.cn/index.php). Eleven putative targets of miR-185-5p and miR-214-3p were selected (**Figure 6A**), and measured in NC-mimic/miR-185-5p-mimic, NC-mimic/miR-214-3p-mimic, and OE-NC/OE-ASB16-AS1 transfected 786-O cells, respectively. It was found that miR-185-5p and miR-214-3p significantly suppressed La-related protein 1 (LARP1) expression (**Figures 6B, C**), results of the expression of HDGF and PIM1 NC-mimic/miR-214-3p-mimic transfected 786-O cells were in accordance with previous studies (21, 22). However, LARP1 was effectively upregulated upon ASB16-AS1 overexpression (**Figure 6D**). Therefore, we speculated that LARP1 might interact with miR-185-5p and miR-214-3p. Biotinylated RNA pull-downs using bio-miR-185-5p or bio-miR-214-3p were performed. As shown in **Figure 6E**, LARP1 was significantly enriched in bio-miR-185-5p and bio-214-3p RNA complexes compared with bio-NC. Next, The LARP1 WT and MuT

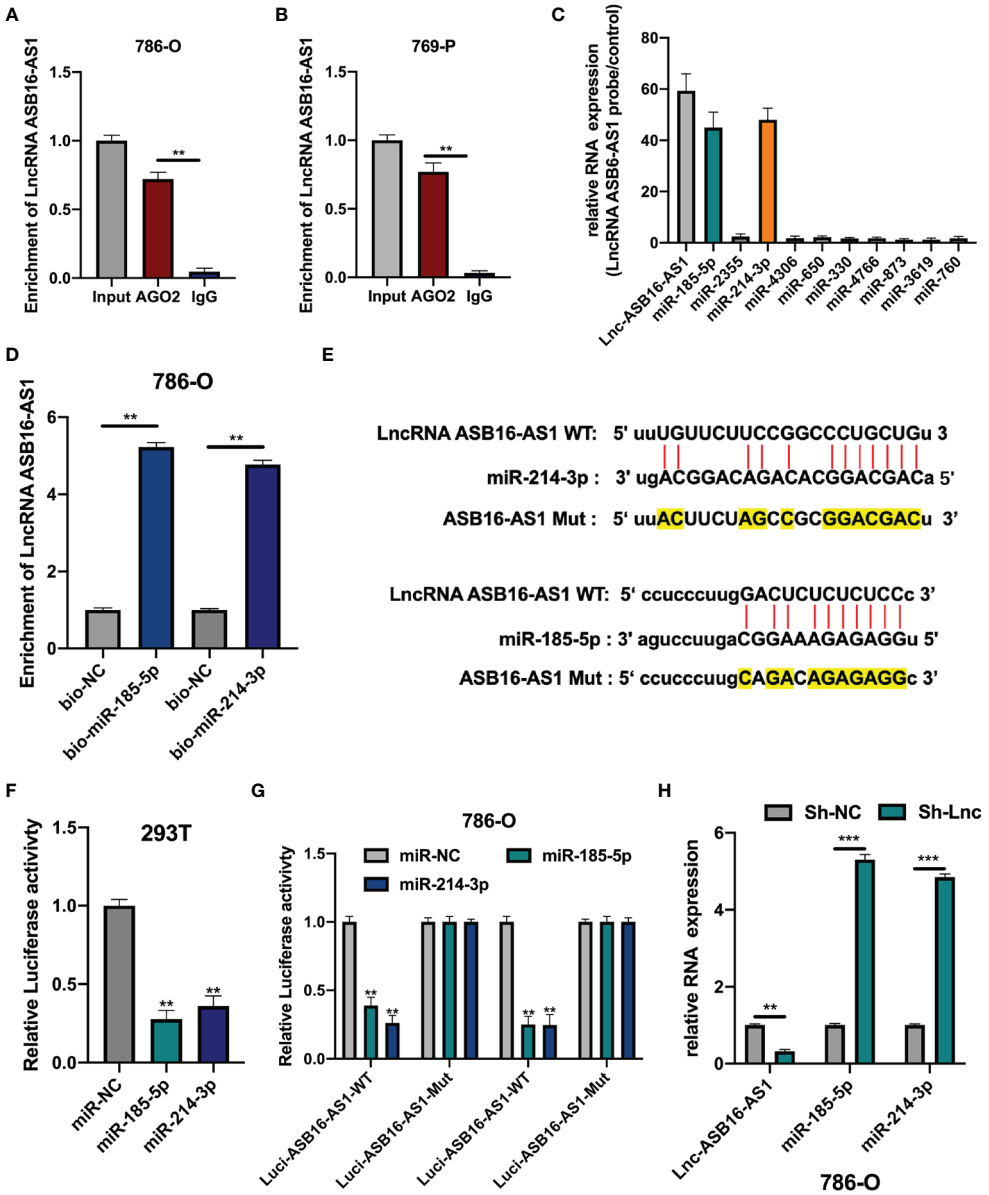

FIGURE 4 | ASB16-AS1 sponges miR-185-5p and miR-214-3p. **(A, B)** AGO2-RIP experiments were conducted to detect the potential miRNA binding ability of ASB16-AS1 by detecting the binding of ASB16-AS1 to the AGO2 protein in 786-O and 769-P cells, respectively. **(C)** The expression of potential miRNA targets in ASB16-AS1 probe RNA bound complexes (according to the number of supported AGO CLIP-seq experiments), measured by qRT-PCR and normalized to the control probe in 786-O cells. **(D)** Biotinylated RNA pull-downs were conducted to measure the enrichment of ASB16-AS1 in biotinylated miR-185-5p and miR-214-3p conditions. **(E)** Wild-type (WT) and mutated (MUT) sequences of the putative ASB16-AS1 miR binding sites aligned with miR-185-5p and miR-214-3p. Mutated bases are highlighted in yellow. **(F, G)** Luciferase reporter activity of Luc-ASB16-AS1-WT or MUT in 293T **(F)** and 786-O cells **(G)** after transfection with miR-185-5p and miR-214-3p. **(H)** relative RNA expression in Sh-NC and Sh-ASB16-AS1 transfected 786-O cells, measured by qRT-PCR. All experiments were repeated at least three times. $^{**}P < 0.01$, $^{***}P < 0.001$.

sequences targeted to miR-185-5p and miR-214-3p binding sites were constructed (**Figure 6F**). The LARP1 WT sequence effectively reduced luciferase activity when co-transfected with a miR-185-5p or miR-214-3p mimic in 293T cells (**Figures 6G, H**), demonstrating that LARP1 interacts with both miR-185-5p and miR-214-3p.

Downregulated ASB16-AS1 Promotes ccRCC Progression *Via* the miR-185-5p/miR-214-3p-LARP1 Pathway

Next, we assessed the role of LARP1 upon ASB16-AS1 downregulation. Firstly, EdU and Transwell assays were

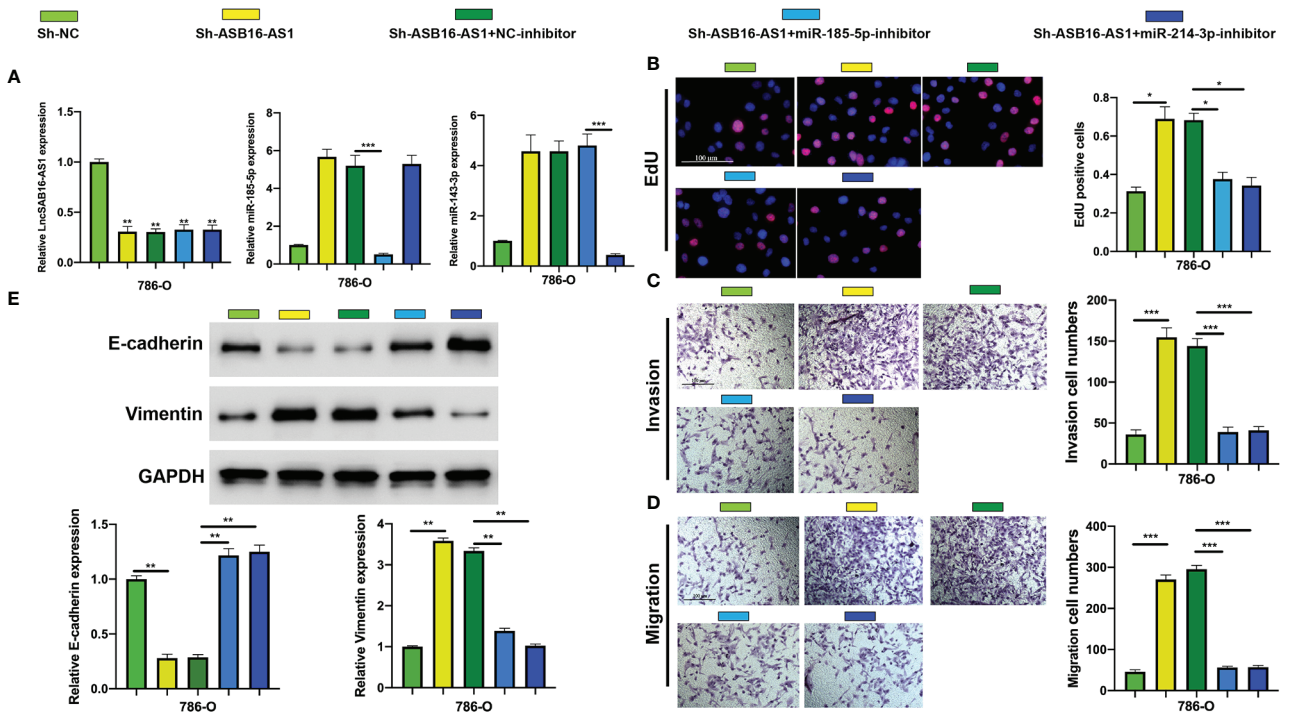

FIGURE 5 | MiR-185-5p and miR-214-3p inhibition rescues the promotive effects of downregulated ASB16-AS1 on HCC progression. **(A)** Cell models were generated by transfecting Sh-NC, Sh-ASB16-AS1, Sh-ASB16-AS1+NC-inhibitor, Sh-ASB16-AS1+miR-185-5p-inhibitor, and Sh-ASB16-AS1+miR-214-3p-inhibitor in 786-O cells, respectively. The expression of ASB16-AS1, miR-185-5p, and miR-214-3p in shRNAs and inhibitor conditions were measured by qRT-PCR. **(B)** Determination of cell proliferation ability by performing EdU assays. **(C)** Determination of cell invasion ability by using Transwell invasion assays. **(D)** Determination of cell migration ability by using Transwell migration assays. **(E)** Expression of the epithelial-mesenchymal-transition associated proteins E-cadherin and Vimentin were detected by western blot assays, which are quantified in the bottom left graphs. All experiments were repeated at least three times. Scale bars -100 μm, $^{*}P < 0.05$, $^{**}P < 0.01$, $^{***}P < 0.001$.

performed. As shown in **Figures 7A–F**, the promotive effects of downregulated ASB16-AS1 on cell proliferation (**Figures 7A, B**), cell invasion (**Figures 7C, D**), and cell migration (**Figures 7E, F**) were rescued by LARP1 overexpression. Moreover, LARP1 overexpression effectively alleviated the enhancement of downregulated ASB16-AS1 on the EMT phenotype both in 786-O cells and xenograft tumor tissues (**Figures 7G, H**). The expression of LARP1 significantly decreased in ccRCC tumor tissues compared with its adjacent normal tissues (**Figures 7I–K**). Spearman statics results suggested that the expression of ASB16-AS1 was strongly correlated with LARP1 expression in ccRCC tumor tissues. Our findings suggested that downregulated ASB16-AS1 play its promotive effect on ccRCC progression through miR-185-5p/miR-214-3p-LARP1 pathway.

DISCUSSION

Despite the improvement of RCC clinical management in the past decades, RCC still is the sixth most frequently diagnosed cancer in men and tenth in women, which has been a great threaten to people health (23). As one most lethal pathological subtype of RCC, the diagnosis and intervention of ccRCC present great challenge to urologist. While, its underlying mechanisms still remain unclear. The clinical intervention of ccRCC demands novel targets more than ever.

In the current study, our results demonstrate the role of ASB16-AS1 in ccRCC progression. By performing *in vitro* and *in vivo* experiments, we found that ASB16-AS1 expression was downregulated in ccRCC tissues, which was also associated with a later tumor stage and larger tumors. Subsequently, our findings demonstrated the biological functions of ASB16-AS1 in ccRCC progression. Downregulation of ASB16-AS1 promoted cell proliferation, migration, and invasion, regulated EMT associated genes in ccRCC cells and promoted tumor growth and metastasis in a xenograft mouse model. Furthermore, it was found that ASB16-AS interacts with miR-185-5p and miR-214-3p. It has been reported that miR-185-5p is involved in cancer development and regulates tumorigeneses *via* its involvement in cell proliferation, migration, invasion, and apoptosis (24–26). Additionally, miR-214-3p is involved in osteosarcoma, breast cancer, endometrial cancer, and lung cancer (27–30). These studies suggest that miR-185-5p and miR-214-3p play important roles in tumorigeneses and tumor development. However, neither have been studied in ccRCC.

Here, our findings suggested that ASB16-AS1 acted as a molecular sponge for miR-185-5p and miR-214-3p. Furthermore, the promotive effects of ASB16-AS1 on cell

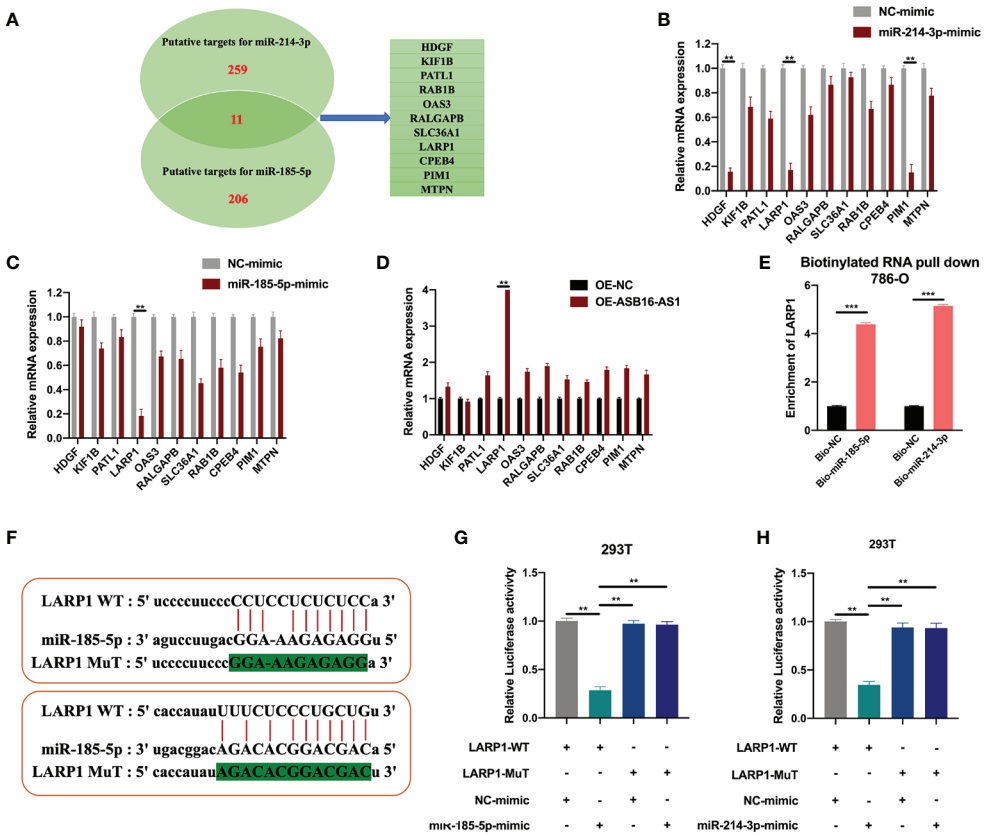

FIGURE 6 | LARP1 is a downstream target for miR-185-5p/miR-214-3p. **(A)** The downstream targets of miR-185-5p and miR-214-3p were predicted using the ENCORI database (http://starbase.sysu.edu.cn/index.php), with CLIP Data; high stringency (>=3) and Predicted program (microT, miRanda, miRmap, and PITA). Eleven potential mRNA targets were chosen. 786-O cells were transfected with NC-mimic/miR-185-5p mimic, NC-mimic/miR-214-3p, and OE-NC/OE-ASB16-AS1, respectively. **(B–D)** Relative mRNA expression of potential target mRNAs, measured by qRT-PCR. **(E)** Biotinylated RNA pull-down assays were performed and qRT-PCR experiments were conducted to determine the enrichment of LARP1 in Bio-NC/Bio-miR-185-5p, Bio-NC/Bio-miR-214-3p treated 786-O cells. **(F)** Wild-type (WT) and mutated (MUT) sequences of the putative LARP1 miR binding sites aligned with miR-185-5p, and miR-214-3p. **(G, H)** Luciferase reporter activity of Luc-LARP1-WT or MUT in 293T **(G)** and 786-O cells **(H)** after transfection with miR-185-5p and miR-214-3p mimics and NC-mimic. All experiments were repeated at least three times. $^{**}P < 0.01$, $^{***}P < 0.001$.

proliferation, migration, invasion, and EMT associated gene expression were rescued by miR-185-5p and miR-214-3p inhibition. While, the relationship between miR-185-5p and miR-214-3p, and their contribution in ccRCC cellular progression upon ASB16-AS1 downregulation still need further exploration. Moreover, the downstream transcriptional targets of ASB16-AS1 were not the final answer for its role in ccRCC biological progression. Therefore, bioinformatic tools, biotinylated RNA pull-down and luciferase reporter assays were used to identify its post-transcriptional target. Our findings found that LARP1 was targeted by miR-185-5p and miR-214-3p in 786-O and 293T cells.

LARP1, as one RNA binding protein, has been in-depth studied recently due to its capability to interact with mammalian target of rapamycin complex 1 (mTORC1) and act as a key repressor of ribosomal protein mRNA translation (31–34). The biological role of LARP1 was investigated in non-small cell lung cancer, ovarian cancer, and hepatocellular carcinoma (35–37). While, the molecular mechanisms of LARP1 in ccRCC progression still uncovered. Since the crucial role of LARP1 in ribosome production, which is an essential unit for cellular progression in all living organisms (38). We presumed that the biological effects of ASB16-AS1/miR-185-5p/miR-214-3p in ccRCC progression were functioned through regulating LARP1. Our results showed that overexpression of LARP1 reversed the promotive effects of downregulated ASB16-AS1 on ccRCC cellular progression and EMT phenotype. Furthermore, the expression ASB16-AS1 and LARP1 in ccRCC tumor tissues were suggested strongly correlated. Although, the role of ASB16-AS1/miR-185-5p/miR-214-3p/LARP1 pathway in ccRCC progression has been partially demonstrated. While, in the contrast with previous findings, our results implicated that LARP1 exerts its tumor suppressive effect in ccRCC cellular progression, which might owe to the timepoint-dependent feature of LARP1 knockdown (39). Furthermore, since the role of mTOR-LARP1 axis in cancer cellular progression is

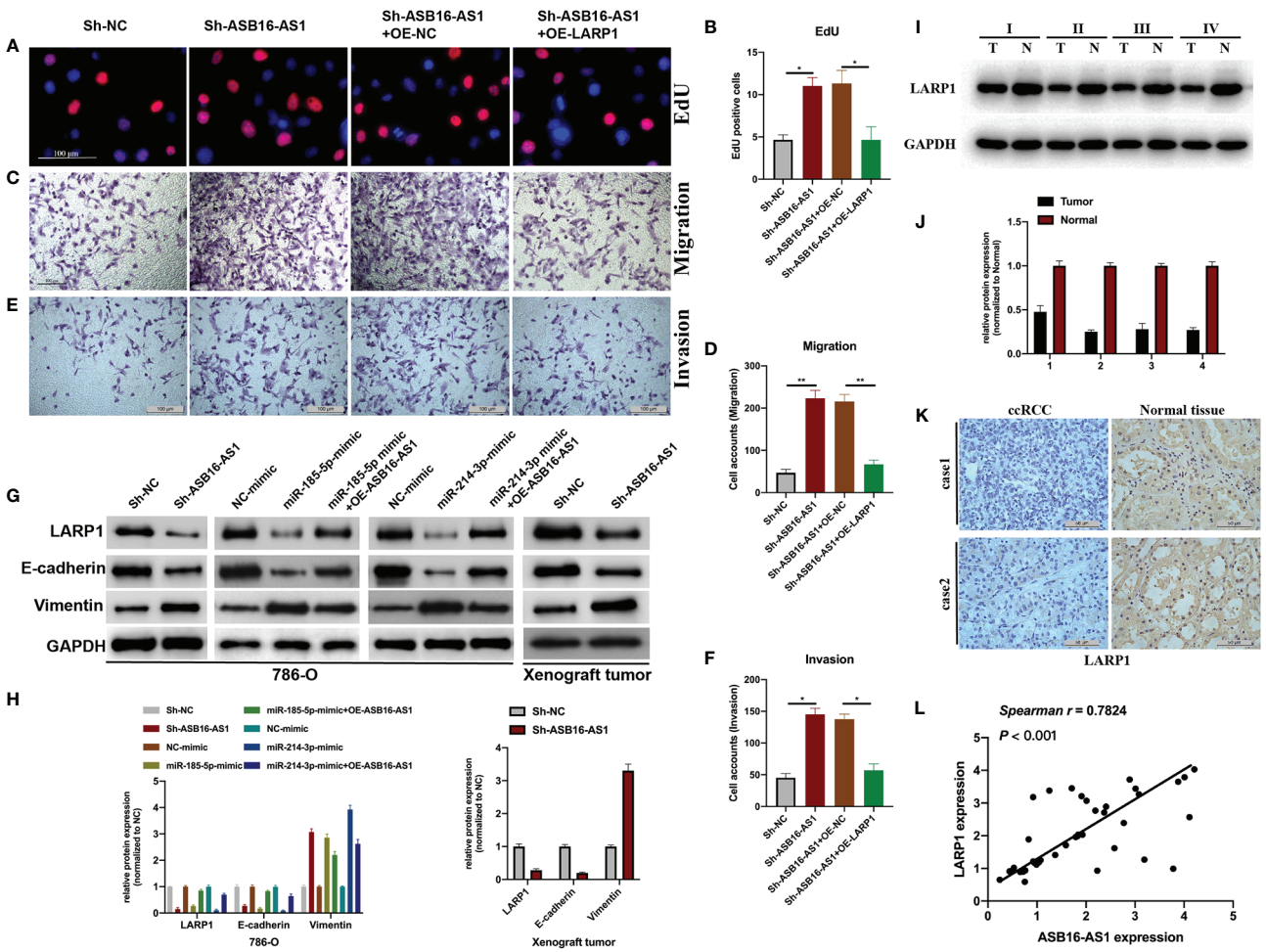

FIGURE 7 | Downregulated ASB16-AS1 promotes ccRCC progression *via* the miR-185-5p/miR-214-3p-LARP1 pathway. 786-O cells were stably transfected with Sh-NC, Sh-ASB16-AS1, Sh-ASB16-AS1+OE-NC, and Sh-ASB16-AS1+OE-LARP1. **(A, B)** Determination of cell proliferation using EdU assays (Scale bars -100 μm). **(C, D)** Determination of cell invasion ability using Transwell migration assays (Scale bars -100 μm). **(E, F)** Determination of cell migration ability using Transwell invasion assays (Scale bars -100 μm). **(G, H)** Expression of the epithelial-mesenchymal-transition associated proteins E-cadherin and Vimentin were detected by western blot assays. **(I, J)** Expression of LARP1 in four ccRCC tumor tissues and its adjacent normal tissues, which were randomly selected, were detected using western-blot. **(K)** Expression of LARP1 in two ccRCC tumor tissues and its adjacent normal tissues, which were randomly selected, were assessed using IHC assay (Scale bars -50 μm). **(L)** The expression correlation between ASB16-AS1 and LARP1 were analyzed using spearman statics. *$P < 0.05$, **$P < 0.01$.

universally agreed, we assumed that LARP1 might exert its function in ccRCC through this axis, which requires in-depth investigation in our future study.

CONCLUSION

In the current study, we demonstrate the interaction of miR-185-5p and miR-214-3p with LARP1 and show the role of the ASB16-AS1-miR-185-5p/miR-214-3p-LARP1 pathway in ccRCC progression. Collectively, our data determined the role of ASB16-AS1, miR-185-5p, and miR-214-3p in ccRCC progression. Moreover, we identified a mechanism of upstream regulation of LARP1 in ccRCC. We therefore provide new insights into ccRCC basic research, and present potential prognostic and therapeutic targets for ccRCC clinical management.

DATA AVAILABILITY STATEMENT

The data used to support the findings of this study are available from the corresponding author upon request.

ETHICS STATEMENT

The animal study was reviewed and approved by Shanghai General Hospital, School of Medicine, Shanghai Jiaotong University.

Written informed consent was obtained from the individual(s) for the publication of any potentially identifiable images or data included in this article.

AUTHOR CONTRIBUTIONS

JF, WL, and JX designed the research. ML, BY, and MC performed the research and wrote the manuscript. JP, ZD, and XM helped in the analysis of the data. All authors contributed to the article and approved the submitted version.

FUNDING

This work was supported by the Youth Program of National Natural Science Foundation of China (81803013 to JP),

REFERENCES

1. Ljungberg B, Campbell SC, Choi HY, Jacqmin D, Lee JE, Weikert S, et al. The epidemiology of renal cell carcinoma. *Eur Urol* (2011) 60(4):615–21. doi: 10.1016/j.eururo.2011.06.049
2. Kovacs G, Akhtar M, Beckwith BJ, Bugert P, Cooper CS, Delahunt B, et al. The Heidelberg classification of renal cell tumours. *J Pathol* (1997) 183(2):131–3. doi: 10.1002/(SICI)1096-9896(199710)183:2<131::AID-PATH931>3.0.CO;2-G
3. Ljungberg B, Campbell SC, Choi HY, Jacqmin D, Lee JE, Weikert S, et al. Corrigendum to "The Epidemiology of Renal Cell Carcinoma" [Eur Urol 2011;60:615-21]. *Eur Urol* (2011) 60(6):1317. doi: 10.1016/j.eururo.2011.09.001
4. Eggener SE, Yossepowitch O, Pettus JA, Snyder ME, Motzer RJ, Russo P. Renal cell carcinoma recurrence after nephrectomy for localized disease: predicting survival from time of recurrence. *J Clin Oncol* (2006) 24(19):3101–6. doi: 10.1200/JCO.2005.04.8280
5. Motzer RJ, Russo P. Systemic therapy for renal cell carcinoma. *J Urol* (2000) 163(2):408–17. doi: 10.1097/00005392-200002000-00004
6. Chow WH, Devesa SS. Contemporary epidemiology of renal cell cancer. *Cancer J* (2008) 14(5):288–301. doi: 10.1097/PPO.0b013e3181867628
7. Cabianca DS, Casa V, Bodega B, Xynos A, Ginelli E, Tanaka Y, et al. A long ncRNA links copy number variation to a polycomb/trithorax epigenetic switch in FSHD muscular dystrophy. *Cell* (2012) 149(4):819–31. doi: 10.1016/j.cell.2012.03.035
8. Wang KC, Chang HY. Molecular mechanisms of long noncoding RNAs. *Mol Cell* (2011) 43(6):904–14. doi: 10.1016/j.molcel.2011.08.018
9. Wang P, Xue Y, Han Y, Lin L, Wu C, Xu S, et al. The STAT3-binding long noncoding RNA lnc-DC controls human dendritic cell differentiation. *Science* (2014) 344(6181):310–3. doi: 10.1126/science.1251456
10. Bhan A, Soleimani M, Mandal SS, Long Noncoding RNA. and Cancer: A New Paradigm. *Cancer Res* (2017) 77(15):3965–81. doi: 10.1158/0008-5472.CAN-16-2634
11. Chan JJ, Tay Y. Noncoding RNA:RNA Regulatory Networks in Cancer. *Int J Mol Sci* (2018) 19:1310. doi: 10.3390/ijms19051310
12. Gutschner T, Diederichs S. The hallmarks of cancer: a long non-coding RNA point of view. *RNA Biol* (2012) 9(6):703–19. doi: 10.4161/rna.20481
13. He H, Dai J, Zhuo R, Zhao J, Wang H, Sun F, et al. Study on the mechanism behind lncRNA MEG3 affecting clear cell renal cell carcinoma by regulating miR-7/RASL11B signaling. *J Cell Physiol* (2018) 233(12):9503–15. doi: 10.1002/jcp.26849
14. Yang FQ, Zhang JQ, Jin JJ, Yang CY, Zhang WJ, Zhang HM, et al. HOXA11-AS promotes the growth and invasion of renal cancer by sponging miR-146b-5p to upregulate MMP16 expression. *J Cell Physiol* (2018) 233(12):9611–9. doi: 10.1002/jcp.26864
15. Qi Y, Ma Y, Peng Z, Wang L, Li L, Tang Y, et al. Long noncoding RNA PENG upregulates PDZK1 expression by sponging miR-15b to suppress clear cell renal cell carcinoma cell proliferation. *Oncogene* (2020) 39(22):4404–20. doi: 10.1038/s41388-020-1297-1
16. Hamilton MJ, Young M, Jang K, Sauer S, Neang VE, King AT, et al. HOTAIRM1 lncRNA is downregulated in clear cell renal cell carcinoma and inhibits the hypoxia pathway. *Cancer Lett* (2020) 472:50–8. doi: 10.1016/j.canlet.2019.12.022
17. Yao X, You G, Zhou C, Zhang D. LncRNA ASB16-AS1 Promotes Growth And Invasion Of Hepatocellular Carcinoma Through Regulating miR-1827/FZD4 Axis And Activating Wnt/beta-Catenin Pathway. *Cancer Manag Res* (2019) 11:9371–8. doi: 10.2147/CMAR.S220434
18. Zhang D, Zhou H, Liu J, Mao J. Long Noncoding RNA ASB16-AS1 Promotes Proliferation, Migration, and Invasion in Glioma Cells. *BioMed Res Int* (2019) 2019:5437531. doi: 10.1155/2019/5437531
19. Tan LJ, Liu JT, Yang M, Ju T, Zhang YS. LncRNA ASB16-AS1 promotes proliferation and inhibits apoptosis of non small cell lung cancer cells by activating the Wnt/beta catenin signaling pathway. *Eur Rev Med Pharmacol Sci* (2020) 24(4):1870–6. doi: 10.26355/eurrev_202002_20365
20. Liu W, Zhuang R, Feng S, Bai X, Jia Z, Kapora E, et al. Long non-coding RNA ASB16-AS1 enhances cell proliferation, migration and invasion via functioning as a ceRNA through miR-1305/Wnt/beta-catenin axis in cervical cancer. *BioMed Pharmacother* (2020) 125:109965. doi: 10.1016/j.biopha.2020.109965
21. Liu Y, Wang J, Dong L, Xia L, Zhu H, Li Z, et al. Long Noncoding RNA HCP5 Regulates Pancreatic Cancer Gemcitabine (GEM) Resistance By Sponging Hsa-miR-214-3p To Target HDGF. *Onco Targets Ther* (2019) 12:8207–16. doi: 10.2147/OTT.S222703
22. Wang X, Li H, Shi J. LncRNA HOXA11-AS Promotes Proliferation and Cisplatin Resistance of Oral Squamous Cell Carcinoma by Suppression of miR-214-3p Expression. *BioMed Res Int* (2019) 2019:8645153. doi: 10.1155/2019/8645153
23. Siegel RL, Miller KD, Jemal A. Cancer statistics, 2018. *CA Cancer J Clin* (2018) 68(1):7–30. doi: 10.3322/caac.21442
24. Fan HX, Feng YJ, Zhao XP, He YZ, Tang H. MiR-185-5p suppresses HBV gene expression by targeting ELK1 in hepatoma carcinoma cells. *Life Sci* (2018) 213:9–17. doi: 10.1016/j.lfs.2018.10.016
25. Shen F, Chang H, Gao G, Zhang B, Li X, Jin B. Long noncoding RNA FOXD2-AS1 promotes glioma malignancy and tumorigenesis via targeting miR-185-5p/CCND2 axis. *J Cell Biochem* (2019) 120(6):9324–36. doi: 10.1002/jcb.28208
26. Niu Y, Tang G. miR-185-5p targets ROCK2 and inhibits cell migration and invasion of hepatocellular carcinoma. *Oncol Lett* (2019) 17(6):5087–93. doi: 10.3892/ol.2019.10144
27. Han LC, Wang H, Niu FL, Yan JY, Cai HF. Effect miR-214-3p on proliferation and apoptosis of breast cancer cells by targeting survivin protein. *Eur Rev Med Pharmacol Sci* (2019) 23(17):7469–74. doi: 10.26355/eurrev_201909_18856
28. Cai H, Miao M, Wang Z. miR-214-3p promotes the proliferation, migration and invasion of osteosarcoma cells by targeting CADM1. *Oncol Lett* (2018) 16(2):2620–8. doi: 10.3892/ol.2018.8927
29. Fang YY, Tan MR, Zhou J, Liang L, Liu XY, Zhao K, et al. miR-214-3p inhibits epithelial-to-mesenchymal transition and metastasis of endometrial cancer cells by targeting TWIST1. *Onco Targets Ther* (2019) 12:9449–58. doi: 10.2147/OTT.181037
30. Yang Y, Li Z, Yuan H, Ji W, Wang K, Lu T, et al. Reciprocal regulatory mechanism between miR-214-3p and FGFR1 in FGFR1-amplified lung cancer. *Oncogenesis* (2019) 8(9):50. doi: 10.1038/s41389-019-0151-1
31. Fonseca BD, Zakaria C, Jia JJ, Graber TE, Svitkin Y, Tahmasebi S, et al. La-related Protein 1 (LARP1) Represses Terminal Oligopyrimidine (TOP) mRNA Translation Downstream of mTOR Complex 1 (mTORC1). *J Biol Chem* (2015) 290(26):15996–6020. doi: 10.1074/jbc.M114.621730
32. Hsu PP, Kang SA, Rameseder J, Zhang Y, Ottina KA, Lim D, et al. The mTOR-regulated phosphoproteome reveals a mechanism of mTORC1-mediated inhibition of growth factor signaling. *Science* (2011) 332(6035):1317–22. doi: 10.1126/science.1199498

33. Hong S, Freeberg MA, Han T, Kamath A, Yao Y, Fukuda T, et al. LARP1 functions as a molecular switch for mTORC1-mediated translation of an essential class of mRNAs. *Elife* (2017) 6:e25237. doi: 10.7554/eLife.25237
34. Philippe L, Vasseur JJ, Debart F, Thoreen CC. La-related protein 1 (LARP1) repression of TOP mRNA translation is mediated through its cap-binding domain and controlled by an adjacent regulatory region. *Nucleic Acids Res* (2018) 46(3):1457–69. doi: 10.1093/nar/gkx1237
35. Xu Z, Xu J, Lu H, Lin B, Cai S, Guo J, et al. LARP1 is regulated by the XIST/miR-374a axis and functions as an oncogene in non-small cell lung carcinoma. *Oncol Rep* (2017) 38(6):3659–67. doi: 10.3892/or.2017.6040
36. Hopkins TG, Mura M, Al-Ashtal HA, Lahr RM, Abd-Latip N, Sweeney K, et al. The RNA-binding protein LARP1 is a post-transcriptional regulator of survival and tumorigenesis in ovarian cancer. *Nucleic Acids Res* (2016) 44 (3):1227–46. doi: 10.1093/nar/gkv1515
37. Xie C, Huang L, Xie S, Xie D, Zhang G, Wang P, et al. LARP1 predict the prognosis for early-stage and AFP-normal hepatocellular carcinoma. *J Transl Med* (2013) 11:272. doi: 10.1186/1479-5876-11-272
38. Warner JR. The economics of ribosome biosynthesis in yeast. *Trends Biochem Sci* (1999) 24(11):437–40. doi: 10.1016/s0968-0004(99)01460-7
39. Berman AJ, Thoreen CC, Dedeic Z, Chettle J, Roux PP, Blagden SP. Controversies around the function of LARP1. *RNA Biol* (2020) 11:1733787. doi: 10.1080/15476286.2020.1733787

Conflict of Interest: The authors declare that the research was conducted in the absence of any commercial or financial relationships that could be construed as a potential conflict of interest.

frontiers in Oncology

ORIGINAL RESEARCH
published: 17 March 2021
doi: 10.3389/fonc.2021.605884

Exosomal LncRNA LBX1-AS1 Derived From RBPJ Overexpressed-Macrophages Inhibits Oral Squamous Cell Carcinoma Progress *via* miR-182-5p/FOXO3

Yilong Ai[†], *Haigang Wei*[†], *Siyuan Wu*[†], *Zhe Tang*, *Xia Li*[*] *and Chen Zou*[*]

Foshan Stomatological Hospital, School of Stomatology and Medicine, Foshan University, Foshan, China

Objectives: Macrophage-derived exosomes (Mφ-Exos) are involved in tumor onset, progression, and metastasis, but their regulation in oral squamous cell carcinoma (OSCC) is not fully understood. *RBPJ* is implicated in macrophage activation and plasticity. In this study, we assessed the role of Mφ-Exos with *RBPJ* overexpression (*RBPJ-OE* Mφ-Exos) in OSCC.

Materials and Methods: The long non-coding RNA (lncRNA) profiles in *RBPJ-OE* Mφ-Exos and THP-1-like macrophages (WT Mφ)-Exos were evaluated using lncRNA microarray. Then the functions of Mφ-Exo-lncRNA in OSCC cells were assessed *via* CCK-8, EdU, and Transwell invasion assays. Besides, luciferase reporter assay, RNA immunoprecipitation, and Pearson's correlation analysis were adopted to confirm interactions. Ultimately, a nude mouse model of xenografts was used to further analyze the function of Mφ-Exo-lncRNAs *in vivo*.

Results: It was uncovered that lncRNA *LBX1-AS1* was upregulated in *RBPJ-OE* Mφ-Exos relative to that in WT Mφ-Exos. *RBPJ-OE* Mφ-Exos and *LBX1-AS1* overexpression inhibited OSCC cells to proliferate and invade. Meanwhile, *LBX1-AS1* knockdown boosted the tumor to grow *in vivo*. The effects of *RBPJ-OE* Mφ-Exos on OSCC cells can be reversed by the *LBX1-AS1* knockdown. Additionally, mechanistic investigations revealed that *LBX1-AS1* acted as a competing endogenous RNA of miR-182-5p to regulate the expression of *FOXO3*.

Conclusion: Exo-*LBX1-AS1* secreted from *RBPJ-OE* Mφ inhibits tumor progression through the *LBX1-AS1*/miR-182-5p/*FOXO3* pathway, and *LBX1-AS1* is probably a diagnostic biomarker and potential target for OSCC therapy.

Keywords: OSCC, macrophage, exosomal lncRNA, RBPJ, FOXO3

OPEN ACCESS

Edited by:
Xiao-Jie Lu,
Nanjing Medical University, China

Reviewed by:
Arsheed A. Ganaie,
University of Minnesota Twin Cities, United States
Jeongsik Yong,
University of Minnesota Twin Cities, United States
Jinzhi Duan,
Brigham and Women's Hospital and Harvard Medical School, United States
Guoping Li,
Massachusetts General Hospital and Harvard Medical School, United States

***Correspondence:**
Chen Zou
chilli_62@163.com
Xia Li
fddentistlx@126.com

[†]*These authors have contributed equally to this work*

Specialty section:
This article was submitted to Cancer Genetics, a section of the journal Frontiers in Oncology

Received: *13 September 2020*
Accepted: *14 January 2021*
Published: *17 March 2021*

Citation:
Ai Y, Wei H, Wu S, Tang Z, Li X and Zou C (2021) Exosomal LncRNA LBX1-AS1 Derived From RBPJ Overexpressed-Macrophages Inhibits Oral Squamous Cell Carcinoma Progress via *miR-182-5p/FOXO3. Front. Oncol. 11:605884. doi: 10.3389/fonc.2021.605884*

INTRODUCTION

Oral squamous cell carcinoma (OSCC) is one of the most aggressive head and neck cancers and has a poor survival rate (1). Although multiple therapeutic strategies can be administered clinically to treat OSCC, the overall 5-year survival rate after diagnosis remains less than 50%, mainly owing to cancer metastasis to lymph nodes and distant sites (2, 3). Therefore, a better understanding of the molecular mechanisms underlying OSCC metastasis is essential to develop novel therapies against OSCC.

Increasing evidence unveils that exosomes (Exos) mediate the interactions between macrophages and cancer cells (4–6). M2 macrophage-derived exosomes facilitate hepatocarcinoma metastasis by transferring α β integrin to tumor cells (7), and M2 bone marrow-derived macrophage-derived exosomes shuffle microRNA-21 to accelerate immune escape of glioma by modulating PEG3 (8). Besides, downregulated lncRNA SBF2-AS1 in M2 macrophage-derived exosomes elevates miR-122-5p to restrict XIAP, thereby limiting pancreatic cancer development (9).

Long non-coding RNAs (lncRNAs) are a class of transcripts longer than 200 nucleotides with no protein-coding capacity and are poorly conserved (10). LncRNAs have also been found in Exos (11), and they are thought to modulate the expression of genes and miRNAs (12). Exosome-Transmitted lncRNAs can regulate growth of cancers (13, 14). Recent studies have unveiled the involvement of lncRNAs in OSCC progression by competitive sponging miRNAs (15, 16). For instance, lncRNA RC3H2 facilitates cell proliferation by targeting microRNA-101-3p/EZH2 axis in OSCC (17). However, whether Mφ-Exo-lncRNAs can regulate the progression of OSCC is unclear.

The Notch pathway is involved in several cancers progression (18, 19), and it is also believed to be responsible for the activation and differentiation of macrophages (20, 21). The recombination signal binding protein for immunoglobulin kappa J region (*RBPJ*) is often used as a marker for the activation of Notch signaling (22). Upon ligand binding, the Notch intracellular domain translocates into the nucleus and forms a complex with the transcription factor RBPJ to activate expression of Notch target genes (22). Loss of the Notch effector *RBPJ* promotes tumorigenesis (23). Moreover, Notch-*RBPJ* signal transduction regulates the transcription factor IRF8 to facilitate inflammatory macrophage polarization (24).

In the current research, we probed the impacts of Mφ-Exos overexpressing *RBPJ* (*RBPJ-OE* Mφ-Exos) on OSCC cell proliferation and invasion and compared them with Exos from THP-1-like macrophages (WT Mφ-Exos) (25). To further understand the regulatory mechanism of *RBPJ-OE* Mφ-Exos in OSCC, we also determined the differentially regulated lncRNAs when *RBPJ* was upregulated in Mφ-Exos. In addition, we identified the miRNA binding partners of the lncRNA upregulated in *RBPJ-OE* Mφ-Exos and their targets. The aim of this study was to further understand the mechanisms of macrophage-derived exosomes-lncRNA, and to identify diagnostic biomarkers and potential therapeutic targets.

MATERIALS AND METHODS

Cell Culture and Clinical Specimens

Human monocytic cell line THP-1 and OSCC cell lines (SCC-4 and CAL-27) were purchased from the Institute of Biochemistry and Cell Biology of the Chinese Academy of Sciences (Shanghai, China). THP-1 cells were cultured in RPMI-1640 medium provided by Gibco (Shanghai, China), and OSCC cells were cultured in Dulbecco's Modified Eagle medium (DMEM, Gibco, China) with 10% heat-inactivated fetal bovine serum (FBS) from Thermo Fisher Scientific (Shanghai, China), 100 U/ml penicillin, and 100 μg/ml streptomycin from HyClone Laboratories (Beijing, China) at 37°C in a moist incubator with 5% CO_2 and used in the exponential growth phase.

Forty paired OSCC tissues and para-tumor tissues were obtained from patients receiving surgery at Foshan Stomatological Hospital between 2016 and 2019. They were diagnosed by histopathology and received no treatment prior to the operation. Besides, all participants signed informed consent in written form before the research. This research gained the approval of the Ethics Committees of Foshan Stomatological Hospital, School of Stomatology and Medicine, Foshan University (FSU2016033), and was conducted *as per* the Helsinki Declaration.

Isolation of Exos Derived From THP-1 Mφ Cells With or Without the Overexpression of *RBPJ*

To obtain WT Mφ and *RBPJ-OE* Mφ, THP-1 cells underwent transfection with the pCMV6 empty vector or pCMV6 overexpressing *RBPJ* (OriGene, Rockville, MD, USA) and seeded at 1×10^6 cells/well in a six-well culture plate. Gradient centrifugation was utilized for Exo isolation from the cell culture medium. Specifically, the medium underwent 30-min centrifugation at 3,000 × g for removal of cells and cellular debris. Subsequent to collection of the supernatant, the medium underwent 30-min centrifugation again at 10,000 × g to discard larger microvesicles. Finally, 70-min Exo isolation from the supernatant was implemented at 110,000 × g and 4°C, and the Exos were reserved in phosphate buffered saline (PBS) at −80°C.

Transmission Electron Microscopy Assay

Exos for transmission electron microscopy (TEM) were prepared as mentioned above. Briefly, Exos were first fixed in 2.5% glutaraldehyde (pH 7.2) at 4°C, then washed in PBS, embedded in 10% gelatin, and fixed in 1% osmium tetroxide for 60 min at indoor temperature. Next, the embedded Exos were cut into 1 mm-thick blocks and dehydrated with gradient alcohol. The alcohol was then replaced with gradient mixture of Quetol-812 epoxy resin and propylene oxide. Afterwards, samples were embedded in Quetol-812 epoxy resin, polymerized at a temperature gradient, and cut into ultrathin sections using a Leica UC6 ultramicrotome. Finally, subsequent to dying by uranyl acetate and lead citrate, a transmission electron microscope was utilized for section observation.

Microarray Analysis

The isolation and quantification of the total RNAs were independently implemented using Trizol reagent provided by Life Technologies (Shanghai, China) and NanoDrop ND-1000. The enriched lncRNAs were then amplified and labeled fluorescently using the Quick Amp Labeling Kit (Agilent Technologies) *as per* the guideline of the manufacturer. In the meantime, we hybridize the labeled cRNAs onto an Arraystar Human lncRNA Array (8× 60K, version 2.0). Subsequent to rinsing and scanning of slides using an Agilent Scanner G2505B, the obtained images were assessed *via* Agilent Feature Extraction software (version 10.7.3.1). Quantile normalization and subsequent data processing were performed using GeneSpring GX software, version 11.5.1 (Agilent Technologies). Volcano plot filtering was used to identify the lncRNAs with statistically significant differences.

RNA Extraction and Quantitative Real-Time PCR (qRT-PCR)

The reverse transcription of mRNAs and lncRNAs into cDNAs was implemented using a reverse transcription kit from Takara (Beijing, China). Next, cDNAs were subjected to RT-PCR on a Quantstudio^{TM} DX system (Applied Biosystems, Singapore) under the following conditions: denaturation at 95°C for 30 s and (denaturation at 95°C for 5 s, at 60°C for 10 s, and at 72°C for 30 s) ×40 cycles. Afterwards, we utilized $2^{-\Delta CT}$ or $2^{-\Delta\Delta CT}$ to quantify mRNAs and lncRNAs by normalizing to GAPDH (26) and to determine the relative expression subsequent to the normalization of miRNA expression to small nuclear U6. Each experiment was separately performed in triplicate. All PCR primers were listed in **Table 1**.

Cell Transfection

LBX1-AS1 overexpression plasmid (p-lncRNA) and its negative control pcDNA3.1, small interfering RNAs (siRNAs) targeting *LBX1-AS1* and non-specific negative control oligos (si-NC), miR-182-5p mimics, inhibitor, and the negative control (NC), and the shRNAs were synthetized by GeneChem (Shanghai, China). Detailed sequences were depicted in **Table 1**. SCC-4 and CAL-27 cell lines underwent inoculation in six-well plates at 24 h prior to transfection with pcDNA3.1, p-lncRNA, si-NC, si-lncRNA, and miR-182-5p mimics or inhibitor under 50–60% cell confluence using Lipofectamine 3000 (Invitrogen) as per the guideline of the manufacturer. Later, the effects of knockdown or overexpression were examined by qRT-PCR using the RNAs that were extracted after 48-h transfection. For Exo treatment, OSCC cells were cultured in medium containing 5 μg/ml Exos from WT Mφ, *RBPJ-OE* Mφ or si-lncRNA and *RBPJ-OE* Mφ.

TABLE 1 | Sequences of primers for qRT-PCR and siRNA related sequence.

Name		Sequence
LBX1-AS1	Forward	5'- CAGGCGTTCCTTTCTTTCTG-3'
	Reverse	5'- AGGACAGACGCTTGAGGAAA-3'
FOXO3	Forward	5'- CGGACAAACGGCTCACTCT-3'
	Reverse	5'- GGACCCGCATGAATCGACTAT-3'
GAPDH	Forward	5'-GGCTGTTGTCATACTTCTCATGG-3'
	Reverse	5'-GGATCTCGCTCCTGGAAGATG-3'
U6	Forward	5'-CTCGCTTCGGCAGCACA-3'
	Reverse	5'-AACGCTTCACGAATTTGCGT-3'
miR-182-5p	Forward	5'- ACACTCCAGCTGGGTTTGGCAATG GTAGAACT-3'
	Reverse	5'- CTCAACTGGTGTCGTGGAGTCGGCAA TTCAGTTGAGAGTGTGAG-3'
LBX1-AS1 siRNA	Sense	5'- GGGGCGAGGAGGCGAGGGCUU-3'
	Antisense	5'- GCCCUCGCCUCCUCGCCCCUU-3'
miR-182-5p mimics	Sense	5'- UUUGGCAAUGGUAGAACUCACACU -3'
	Antisense	5'- UGUGAGUUCUACCAUUGCCAAAUU-3'
miR-182-5p inhibitor	Sense	5'- AGUGUGAGUUCUACCAUUGCCAAA-3'

Cell Proliferation Assays

Approximately 1.0×10^4 transfected SCC-4 and CAL-27 cells were cultured in 96-well plates, and then underwent 1-h incubation with CCK-8 reagent (Beyotime, Shanghai, China). The absorbance at 450 nm was recorded using an Infinite M200 multimode microplate reader (Tecan, Shanghai, China).

After approximately 48-h transfection, the 5-ethynyl-2'-deoxyuridine (EdU) assay kit provided by Ribo (Guangzhou, China) was utilized to examine the proliferation of SCC-4 and CAL-27 cells. Specifically, cells were grown in culture medium containing EdU (Invitrogen) solution (1:1,000). At the proliferative stage, the cells were labeled with EdU for 2 h, followed by rinsing with PBS (0.5 g/ml) thrice. Subsequently, the cells were stained by 4′,6-diamidino-2-phenylindole (DAPI) from Invitrogen for 10 min at indoor temperature in the dark and underwent PBS rinsing more than twice. Ultimately, assessment of the stained cells was implemented *via* the FACSCalibur DxP flow cytometer (BD Biosciences, Shanghai, China).

Cell Invasion Assays

Cell invasion was assessed in the Matrigel assay using the 24-well invasion chamber system equipped with polycarbonic membranes (diameter 6.5 mm, pore size 8 μm) from BD Biosciences (Santa Clara, CA, USA). Subsequent to incubation and dying, a microscope was adopted to quantify cells co-cultured with Exos and migrating through the membranes in four fields that were randomly chosen. Each assay was repeated at least three times with triplicate samples each time.

Luciferase Reporter Assay

Sequences of WT or MUT *LBX1-AS1* or the full length of the 3′-UTR of *FOXO3* with WT or MUT putative binding sites were interposed into the pmir-GLO vector from Promega Corp. (Beijing, China). 293T cells seeded into 24-well plates underwent co-transfection with 50 nM miR-182-5p mimics or a NC and 80 ng WT or MUT plasmids using Lipofectamine 2000 (Invitrogen)and the 80 ng of plasmids were later added with 5 ng of pRL-SV40. Lastly, luciferase intensity was determined using the Dual-Luciferase Reporter Assay Kit from Promega (Beijing, China) and a microplate reader.

RNA Binding Protein Immunoprecipitation (RIP) Assay

We carried out the RIP assay using a Magna RIP Kit from Millipore (Hongkong, China) *as per* the guideline of the manufacturer. Specifically, cells (1×10^7) were lysed with the

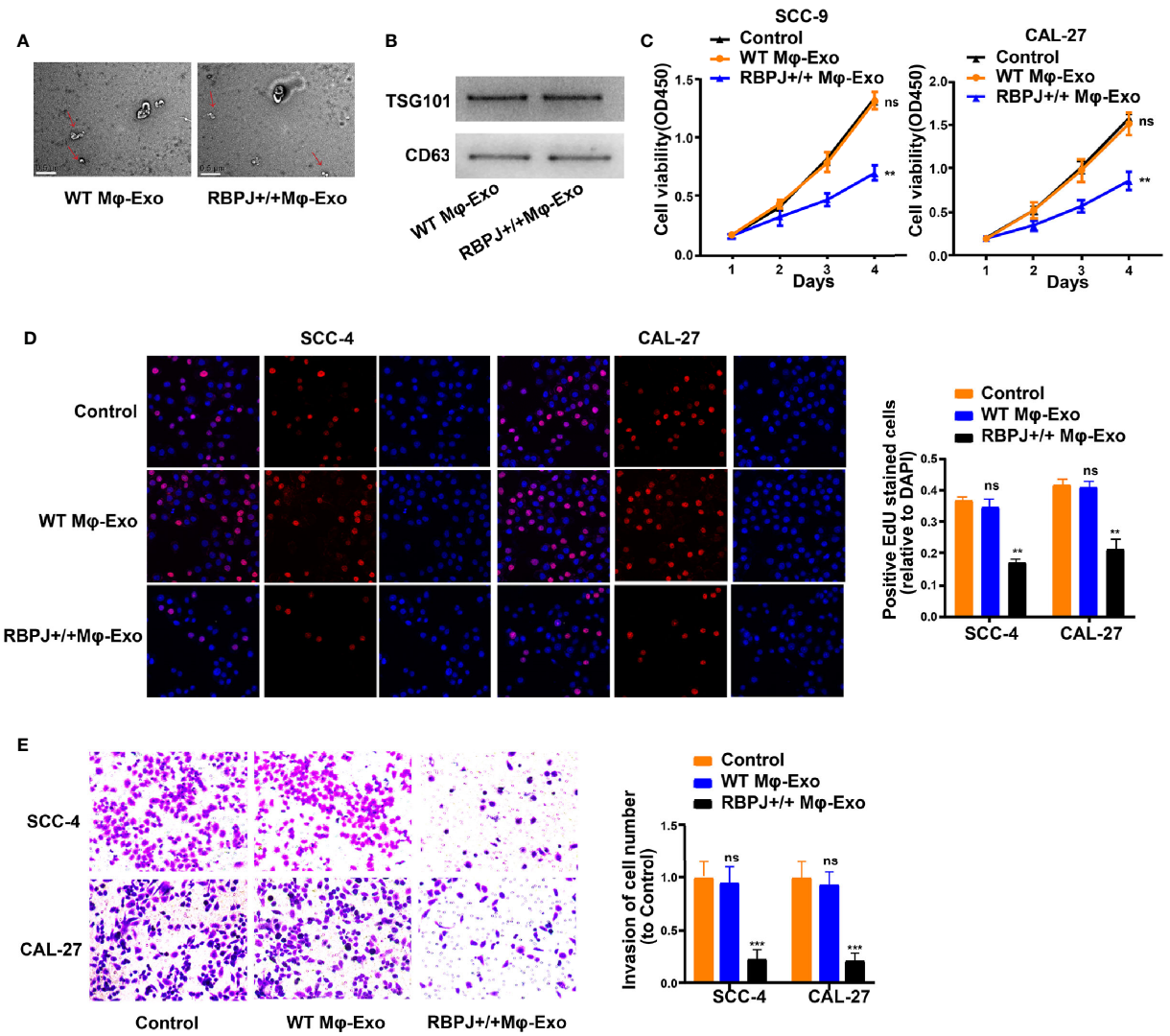

FIGURE 1 | Exosomes derived from macrophages overexpressing RBPJ inhibit proliferation and invasion of OSCC cells. **(A)** Exosomes isolated from WT THP-1 derived macrophages (WT Mφ-Exos) and RBPJ-overexpressed macrophages (RBPJ-OE Mφ-Exos) imaged by transmission electron microscopy (TEM). Scale bar = 0.5 μm. **(B)** Levels of exosome markers CD63 and TSG101 in WT or RBPJ-OE Mφ-Exos were determined by Western blotting. **(C, D)** Cell proliferation in OSCC cell lines SCC-4 and CAL-27 treated with WT Mφ-Exos, RBPJ-OE Mφ-Exos, or negative control was assessed by CCK-8 **(C)** and EdU assay **(D)**. **(E)** Transwell invasion assay is performed to indicate cell invasion. All experiments were performed three times. **P < 0.01 and ***P < 0.001 for statistical difference, ns: no significance.

lysis buffer provided in the kit and the lysate was separately put into two tubes [one with anti-Argonaute2 (AGO2) antibody and the other with a non-specific anti-IgG antibody (Millipore)]. The cell lysates were incubated nightlong at 4°C, and then incubated with magnetic beads for a further hour. Proteinase K was then added for sample incubation at 55°C for another hour. In the end, RNA extraction reagent (Solarbio, Beijing, China) was used to obtain the RNAs, and specific genes were detected and measured using qRT-PCR.

Western Blot Analysis

Cell lysis was performed in RIPA buffer (Beyotime, Nantong, China) containing protease and phosphatase inhibitors (Beyotime). A BCA Protein Assay kit (Beyotime) was utilized to identify protein concentration, and the samples (40 μg proteins per lane) underwent SDS-PAGE with 10% gel for separation. Next, proteins were electrotransferred onto a PVDF membrane (Beyotime) that was sealed by 5% BSA (Beyotime) for 1 h at indoor temperature. Later, we incubated the membrane with primary antibodies against TSG101 (1:1,000, ab125011, Abcam, Shanghai, China), CD63 (1:1,000, ab217345, Abcam, Shanghai, China), *FOXO3* (1:1,000, ab23683, Abcam, Shanghai, China), and GAPDH (1:1,000, ab8245, Abcam, Shanghai, China) at 4°C nightlong, and subsequently with secondary antibodies coupled to HRP (Beyotime, Nantong, China) at indoor temperature for 1 h. Immobilon ECL substrate (Millipore) was

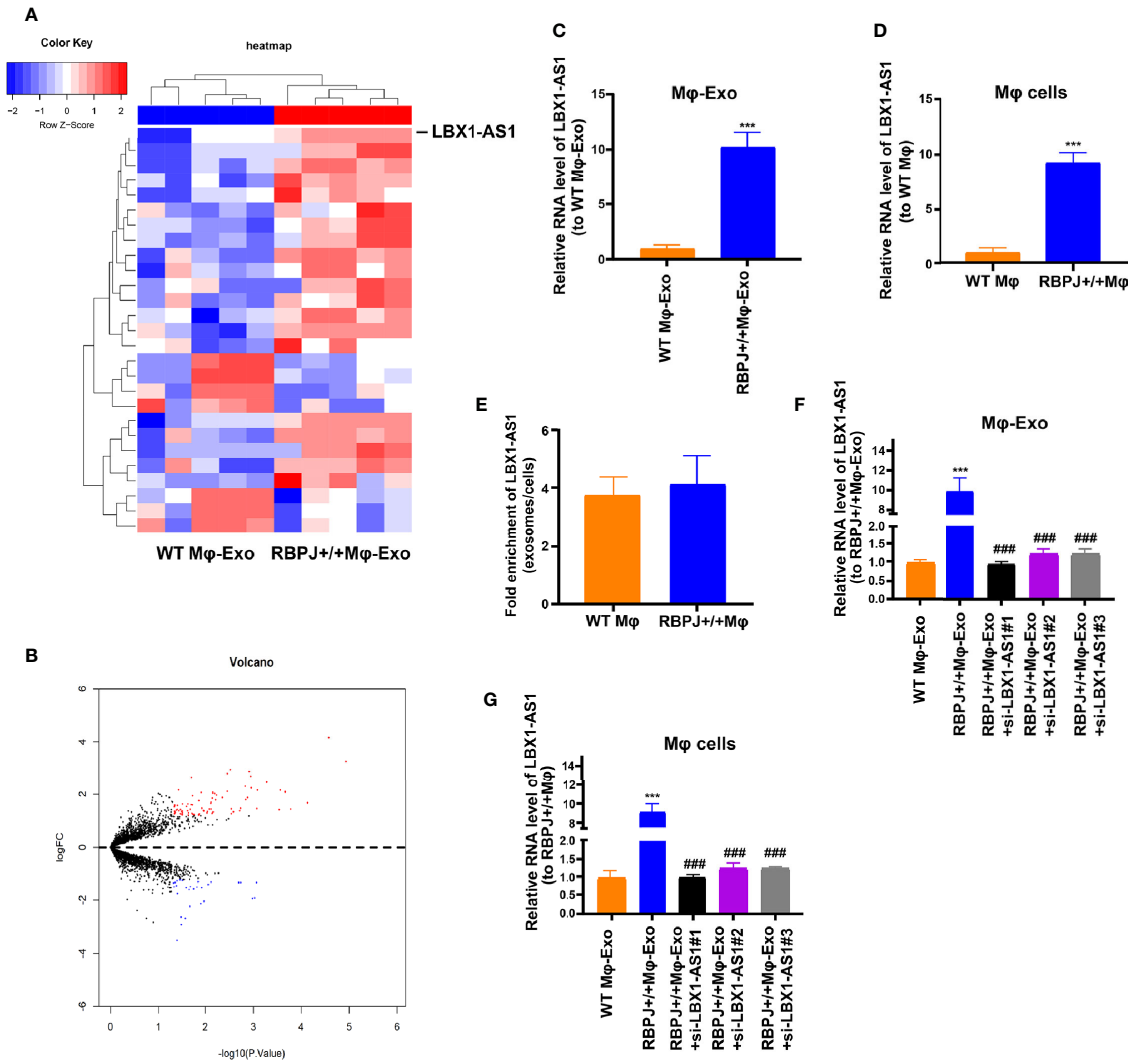

FIGURE 2 | LBX1-AS1 expression profiles in exosomes derived from RBPJ-overexpressed macrophages. **(A)** Cluster heatmap showing 27 aberrantly expressed LBX1-AS1s, including 24 upregulated and 3 downregulated LBX1-AS1s in exosomes derived from RBPJ-overexpressed macrophages compared to the controls. The red color represents high expression, whereas the blue color represents low expression. **(B)** Volcano map. **(C, D)** The relative expression of LBX1-AS1 in Mφ-Exos **(C)** and Mφ cells **(D)** was validated by qRT-PCR. **(E)** The fold change of LBX1-AS1 expression between the exosomes and their corresponding producer cells. **(F, G)** The qRT-PCR assay indicated the difference in the LBX1-AS1 expression in RBPJ-overexpressed Mφ cells transfected with or without LBX1-AS1 siRNA **(F)**, as well as in exosomes from those cells **(G)**. ***P < 0.001 *vs* WT Mφ-Exos, ###P < 0.001 *vs* RBPJ-OE Mφ-Exos.

used to generate signals, which were detected using the Optimax X-ray Film Processor provided by Protec (Shanghai, China).

Xenograft Nude Mouse Model

Six-week-old adult male BALB/C nude mice (n = 3/group) were commercially provided by Shanghai SLAC Laboratory Animal Co., Ltd. (Shanghai, China) and reserved in a SPF environment with a LD (12:12) cycle. All animal studies obtained the approval of the Institutional Animal Care and Use Committee of Foshan Stomatological Hospital, School of Stomatology and Medicine, Foshan University, and implemented in line with institutional and national guidelines. SCC-4 cells undergoing stable sh-NC or sh-lncRNA transfection, or WT Mφ-Exo, *RBPJ-OE* Mφ-Exo or *RBPJ-OE* Mφ-Exo-sh-lncRNA (5 μg/ml) pretreatment were hypodermically injected into the nude mice (1×10^6 cells per mouse) on the right upper back. Later, we utilized a caliper to determine the growth of tumor every 7 days for 35 days, and calculate its volume based on the formula: volume = (length × width^2)/2. Five weeks later, we intraperitoneally injected overdose pentobarbital (>120 mg/kg body weight) to kill all the mice so that they were unable to spontaneously breath. Afterwards, the xenograft tumor tissues were sampled for subsequent analyses.

Statistical Analysis

GraphPad Prism 6.0 software provided by GraphPad Inc. (San Diego, CA, USA) was utilized to statistically evaluate data. Experimental results were presented as mean ± standard

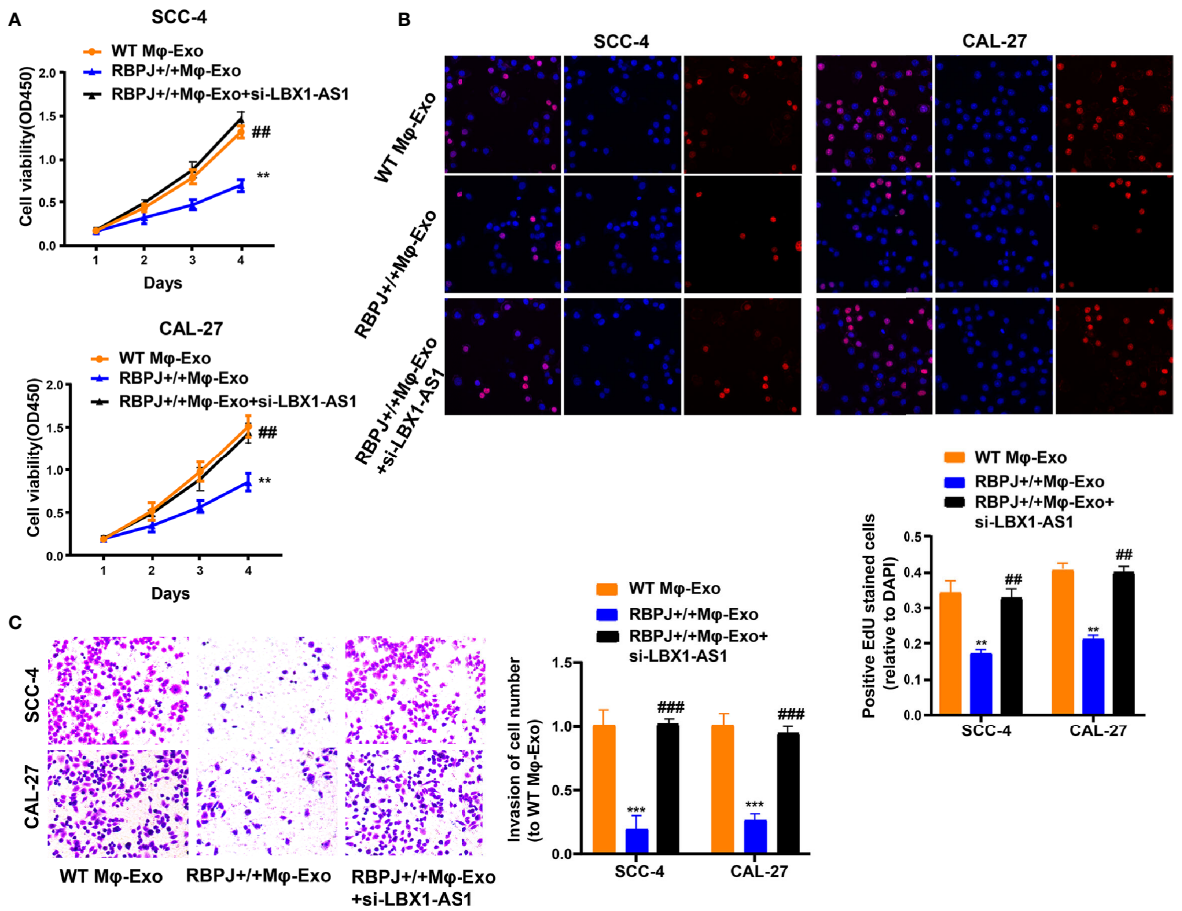

FIGURE 3 | Mφ-Exo-LBX1-AS1 inhibits proliferation and invasion of OSCC cells. To remove LBX1-AS1 from exosomes, siRNA of LBX1-AS1 was transfected into THP-1 cells and Mφ-Exos were collected at 48 h post-transfection (RBPJ-OE Mφ-Exo-si-LBX1-AS1). OSCC cell lines SCC-4 and CAL-27 were cocultured with WT Mφ-Exos, RBPJ-OE Mφ-Exos, or RBPJ-OE Mφ-Exo-si-LBX1-AS1. **(A, B)** Cell proliferation in OSCC cell lines SCC-4 and CAL-27 was assessed by CCK-8 assay **(A)** and EdU assay **(B)**. **(C)** Cell invasion in OSCC cell lines SCC-4 and CAL-27 was assessed by Transwell assay. All experiments were performed three times. **, $^{\#\#}$P < 0.01 and ***, $^{\#\#\#}$P < 0.001 as indicated. **/*** vs. WT Mφ-Exos, ##/### vs. RBPJ$^{+/+}$ Mφ-Exos.

deviation (SD). The statistically significant differences between tumor tissues and para-tumor tissues were determined using paired Student's t-test. Besides, the statistically significant differences between other two groups were detected using Mann-Whitney U-test or unpaired Student's t-test in light of conditions. Furthermore, the comparisons among different groups (multigroup comparisons) were implemented by one-way ANOVA and the *post hoc* Bonferroni test. Lastly, Pearson's correlation coefficient was determined to test associations among *LBX1-AS1*, miR-182-5p, and *FOXO3*. $P < 0.05$ signified statistically significant differences.

RESULTS

Mφ-Exos Overexpressing *RBPJ* Inhibit Proliferation and Invasion of OSCC Cells

WT Mφ-Exos and *RBPJ-OE* Mφ-Exos were isolated by ultracentrifugation and characterized by TEM (**Figure 1A**). To further confirm the identity of the Exos, the expression levels of CD63 and TSG101 (Exo markers) were evaluated. Western blot assessment showed that the isolated Exos were enriched with CD63 and TSG101 (**Figure 1B**). These data indicate the successful isolation of Exos from WT Mφ-Exos and *RBPJ-OE* Mφ-Exos.

To further investigate the effects of these two groups of Exos on the proliferation of OSCC cells, we cocultured SCC-4 or CAL-27 cells with Exos for 4 days and measured cell proliferation through CCK-8 and EdU experiments. As demonstrated in **Figures 1C–D**, the presence of *RBPJ-OE* Mφ-Exos significantly curbed SCC-4 and CAL-27 cells to proliferate when compared with WT Mφ-Exos or negative control groups. In addition, Transwell invasion assays indicated that *RBPJ-OE* Mφ-Exos were able to inhibit invasion of SCC-4 and CAL-27 cells (**Figure 1E**). Overall, these results confirm that the overexpression of *RBPJ* in Exos can suppress OSCC cells to proliferate and invade.

Expression Profiles of lncRNAs in *RBPJ-OE* Mφ-Exos

We wonder whether *RBPJ-OE* Mφ-Exos could influence the expression of *RBPJ* in OSCC cells. We performed qRT-PCR to detect the expression of *RBPJ* in the WT Mφ, *RBPJ*-OE Mφ, WT

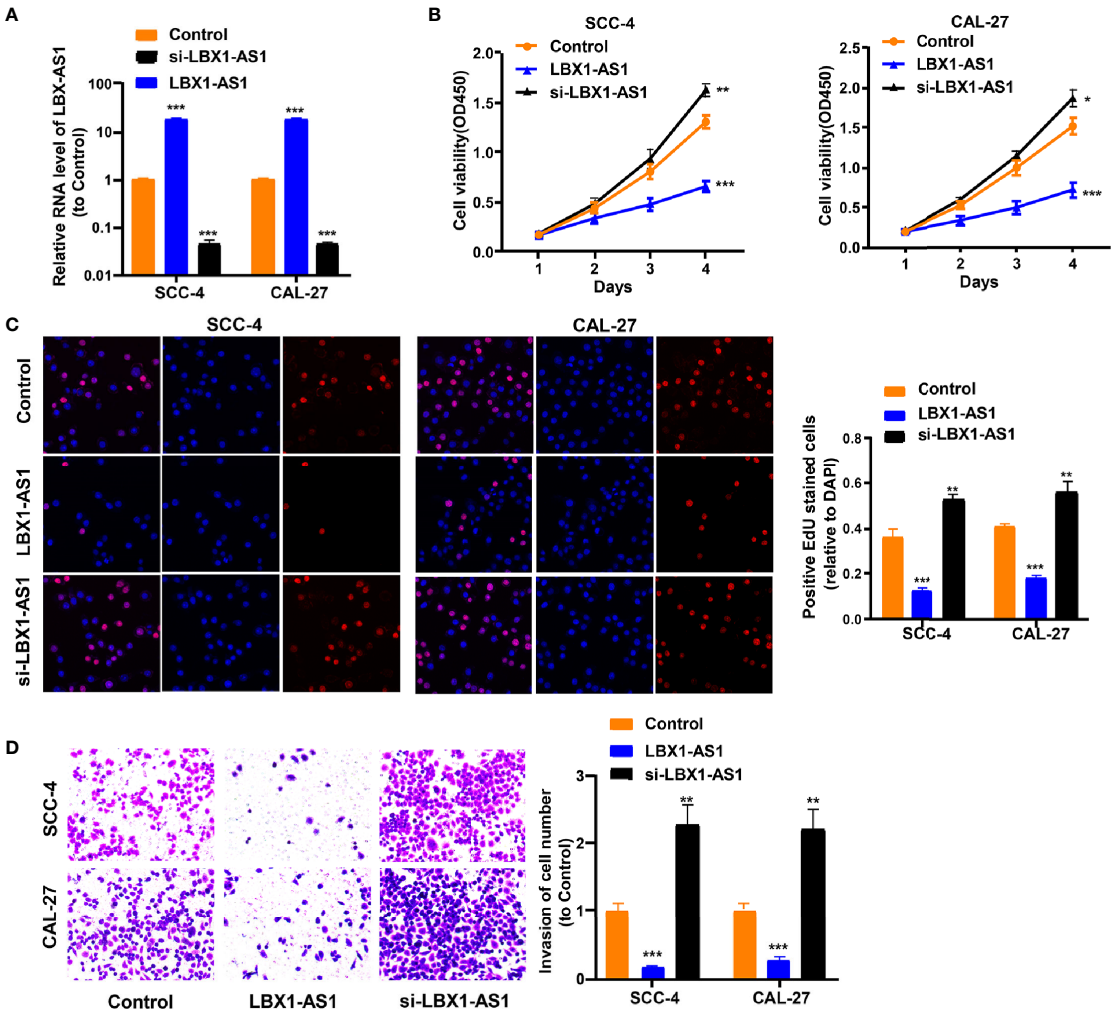

FIGURE 4 | LBX1-AS1 inhibits proliferation and invasion of OSCC cells. **(A, B)** SCC-4 and CAL-27 cells were transfected with LBX1-AS1 overexpression plasmids, siRNA and controls. **(B, C)** Cell proliferation in OSCC cell lines SCC-4 and CAL-27 was assessed by CCK-8 assay **(B)** and EdU assay **(C)**. **(D)** Cell invasion of OSCC cell lines SCC-4 and CAL-27 was assessed by Transwell invasion assay. All experiments were performed three times. *P < 0.05, **P < 0.01, and ***P < 0.001 for statistical differences.

Mφ-Exos, *RBPJ*-OE Mφ-Exos, WT Mφ-Exos treated SCC-4/CAL-27 cells, and *RBPJ*-OE Mφ-Exos treated SCC-4/CAL-27 cells. Our results showed that *RBPJ* mRNA is highly expressed in *RBPJ*-OE Mφ (**Supplementary Figure 1A**). Nevertheless, there is no significant difference of *RBPJ* level between WT Mφ-Exos treated SCC-4/CAL-27 cells and *RBPJ*-OE Mφ-Exos treated SCC-4/CAL-27 cells (**Supplementary Figure 1B**). As the PCR amplification cycles of *RBPJ* in WT Mφ-Exos and *RBPJ*-OE Mφ-Exos are higher than 40, we can't detect the expression level of it in the exosomes. This result means that *RBPJ* could not be enriched in macrophage exosomes. We wonder whether there are different expressions of lncRNAs between WT Mφ-Exos and *RBPJ-OE* Mφ-Exos. The lncRNA profiles in *RBPJ-OE* Mφ-Exos and WT Mφ-Exos were evaluated using a lncRNA microarray technique. Twenty-seven lncRNAs were differentially expressed (P < 0.05 and log2FC > 2.0 or < −2.0) in *RBPJ-OE* Mφ-Exos and the controls (**Figures 2A, B**). We have uploaded the data of this lncRNA profiles on ArrayExpress with the accession E-MTAB-9989. Among them, 24 lncRNAs dramatically rose up and 3 lncRNAs evidently declined. *LBX1-AS1* with the most obvious rising trend was selected and validated by qRT-PCR in *RBPJ-OE* Mφ-Exos and WT Mφ-Exos (**Figure 2C**). In the meantime, it was unveiled that *LBX1-AS1* was expressed in the *RBPJ-OE* Mφ at a notably higher level relative to that in the WT Mφ cells (**Figure 2D**). Compared with those in the producer cells, the levels of *LBX1-AS1* are enriched by approximately 4 folds in the *RBPJ-OE* Mφ-Exos (**Figure 2E**).

Mφ-Exo-*LBX1-AS1* Inhibits OSCC Cells to Proliferate and Invade

Since the *LBX1-AS1* level was the highest in *RBPJ-OE* Mφ-Exos, to remove its expression from Exos, the siRNA of *LBX1-AS1* was transfected into Mφ cells for 48 h, after which Exos were collected

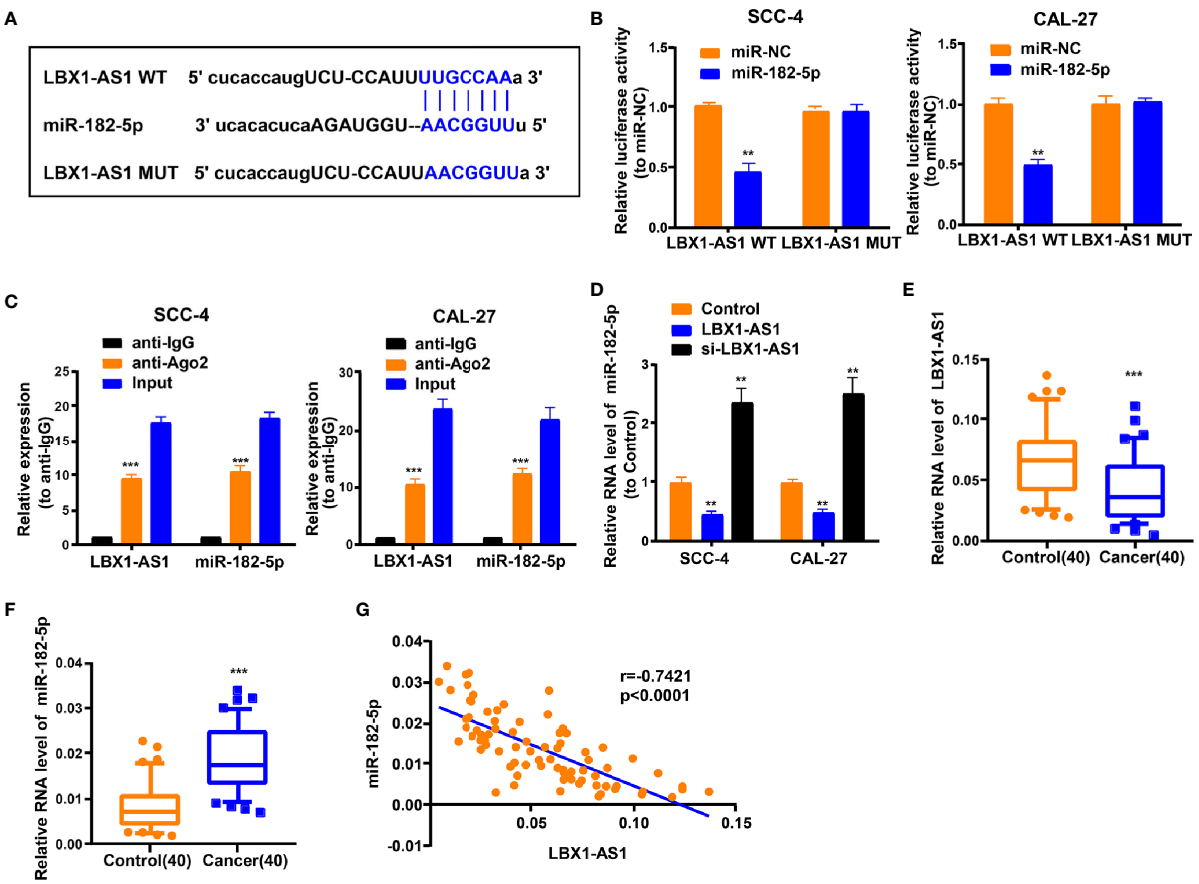

FIGURE 5 | LBX1-AS1 interacts with miR-182-5p. **(A)** Putative complementary sites within miR-182-5p and LBX1-AS1 were predicted by bioinformatics analysis. **(B)** Dual-luciferase reporter assays demonstrate that miR-182-5p is a direct target of LBX1-AS1 in OSCC cells. **(C)** The Ago2 RIP showed that Ago2 significantly enriched LBX1-AS1 and miR-182-5p. **(D)** The level of miR-182-5p was determined by qRT-PCR in SCC-4 and CAL-27 cells after transfection. **(E)** The expression level of LBX1-AS1 in 40 OSCC tissues and matched para-carcinoma normal tissues was determined by qRT-PCR. **(F)** The expression level of miR-182-5p in the above tissues was determined by qRT-PCR. **(G)** The expression levels of miR-182-5p are negatively correlated with LBX1-AS1 in OSCC tissues. **P < 0.01 and ***P < 0.001 for statistical differences.

(**Figures 2F–G**). Next, OSCC cell proliferation and invasion were investigated by coculturing cells with Mφ-Exos. The inhibitory effects of *RBPJ-OE* Mφ-Exos on the proliferation and invasion of OSCC cells (SCC-4 and CAL-27) were eliminated when *LBX1-AS1* was knocked down in Exos (**Figures 3A–C**). This would be expected if there was an association between *RBPJ* and *LBX1-AS1*.

To continuously figure out the biological role of *LBX1-AS1* in OSCC cells, SCC-4 and CAL-27 cells underwent transfection with a *LBX1-AS1* overexpression vector or siRNA#1 (**Figure 4A**). The results unveiled that *LBX1-AS1* overexpression significantly inhibited OSCC cells to proliferate and invade and *LBX1-AS1* downregulation significantly promoted it (**Figures 4B–D**). As with the overexpression of *RBPJ*, the overexpression of *LBX1-AS1* inhibited proliferation and invasion of OSCC cells.

LBX1-AS1 Interacts With miR-182-5p

For discovering more about the specific regulation of *LBX1-AS1*, we performed bioinformatics prediction (starBase). Bioinformatics analysis predicted that *LBX1-AS1* and miR-182-5p possessed complementary binding sites (**Figure 5A**). Then we carried out a dual-luciferase experiment in 293T cells to confirm this interaction by mutating the predicted binding site in *LBX1-AS1*. It was unveiled that the luciferase activity was reduced only in presence of WT *LBX1-AS1* and miR-182-5p mimics in OSCC cells (**Figure 5B**), which was further validated using an Ago2 RIP assay. MiRNA is a component of the RNA-induced silencing complex (RISC) containing Ago2. Ago2 is required for miRNA-mediated gene silencing. In this study, we analyzed if LBX1-AS1 and miR-182-5p constitute the same RISC and performed RIP assay in OSCC cells. It is shown that LBX1-AS1 and miR-182-5p were enriched in the immunoprecipitation from anti-Ago2 group than IgG control (**Figure 5C**). Moreover, the level of miR-182-5p was prominently lower in cells overexpressing *LBX1-AS1* and higher in cells with *LBX1-AS1* silenced (**Figure 5D**), indicating that miR-182-5p expression was strongly influenced by the level of *LBX1-AS1*. Besides, levels of *LBX1-AS1* and miR-182-5p were also analyzed in OSCC and matched para-carcinoma tissues, and the results further substantiated that OSCC tissues exhibited a lower *LBX1-AS1* level (**Figure 5E**) and a higher miR-182-5p level (**Figure 5F**). Besides, Pearson's analysis

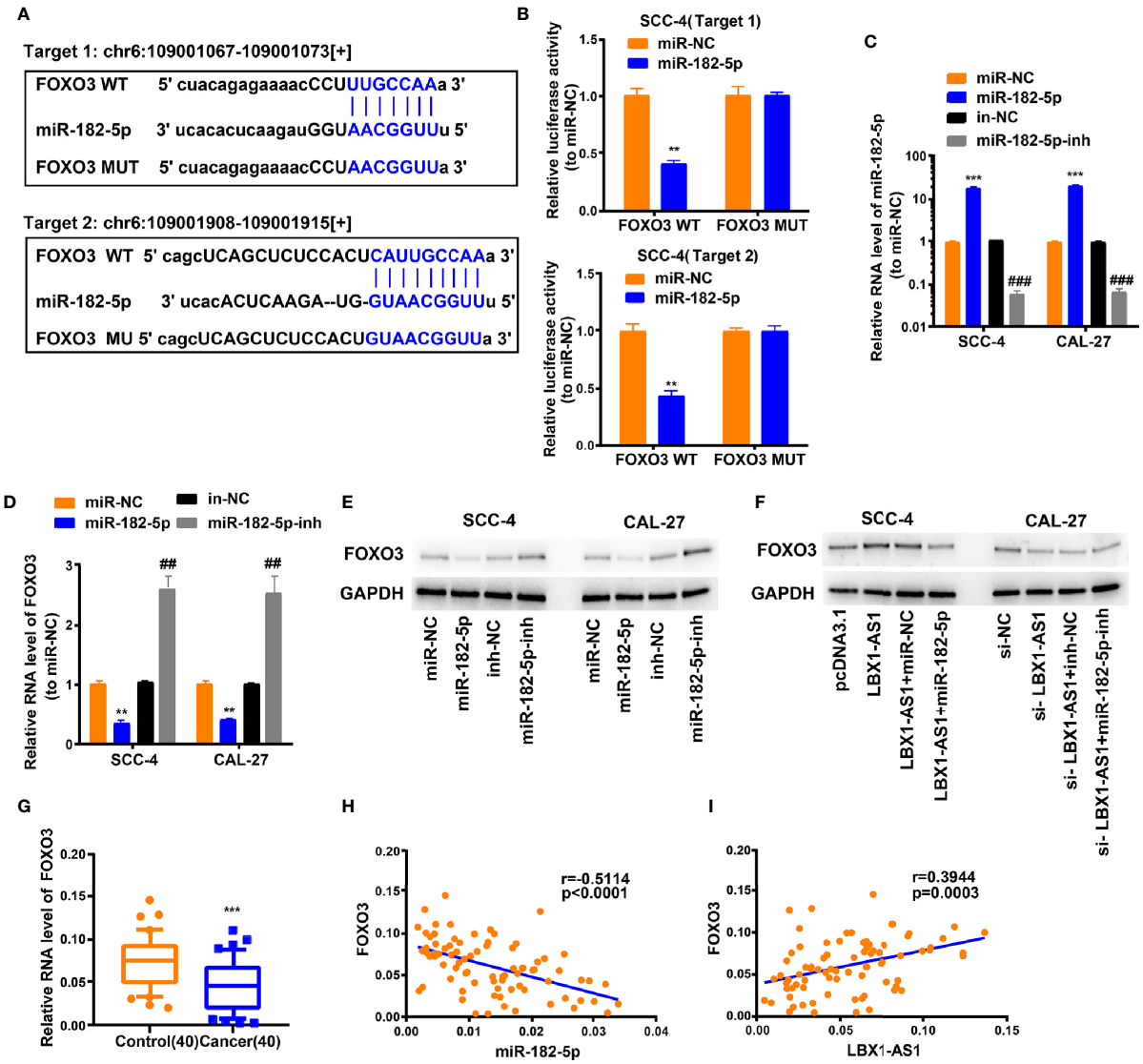

FIGURE 6 | LBX1-AS1/miR-182-5p axis is critical for FOXO3 expression. **(A)** Bioinformatics analysis revealed the predicted binding sites between FOXO3 and miR-182-5p. **(B)** Luciferase reporter assay demonstrated miR-182-5p mimics significantly decreased the luciferase activity of FOXO3-WT in SCC-4 cells. **(C)** The transfection efficiency of miR-182-5p mimics and inhibitor in SCC-4 and CAL-27 cells. **(D, E)** The mRNA **(D)** and protein **(E)** level of FOXO3 was detected through qRT-PCR and western blotting after transfection with miR-182-5p mimics and inhibitor in SCC-4 and CAL-27 cells. **(F)** LBX1-AS1 overexpression upregulated FOXO3 and siRNA downregulated FOXO3, this effect can be reversed by co-transfection with miR-182-5p mimics or miR-182-5p inhibitors (miR-182-5p-inh) in SCC-4 or CAL-27 cells respectively. **(G)** The expression levels of FOXO3 in 40 OSCC tissues and matched para-carcinoma normal tissues was determined by qRT-PCR. **(H)** Expression levels of FOXO3 negatively correlated with miR-182-5p in OSCC tissues. **(I)** Expression levels of FOXO3 positively correlated with LBX1-AS1 in OSCC tissues. **, $^{\#\#}P < 0.01$ and ***, $^{\#\#\#}P < 0.001$ as indicated. * vs. miR-NC; Control, # vs. in-NC.

confirmed a negative interrelation between *LBX1-AS1* and miR-182-5p (**Figure 5G**). This indicates that *LBX1-AS1* may compete to interact with miR-182-5p and prevent it from regulating other pathways.

LBX1-AS1 Represses OSCC Cells to Proliferate and Invade *via* the miR-182-5p/*FOXO3* Pathway

We next probed the potential binding sites of miR-182-5p. Target prediction and assessment were implemented using starBase (http://starbase.sysu.edu.cn) and miRDB (http://mirdb.org), which identified that miR-182-5p probably interacts with *FOXO3*, a tumor suppressor gene implicated in several cancers (27–29). Recent study also pointed out that miR-182-5p promotes hepatocellular carcinoma progression by repressing FOXO3a (30). Later, we mutated two potential miR-182-5p target sites in *FOXO3* (**Figure 6A**) and performed a luciferase reporter experiment, which ascertained that miR-182-5p overexpression in SCC-4 cells dramatically weakened the luciferase activity of *FOXO3* at both target sites (**Figure 6B**). Thereafter, we

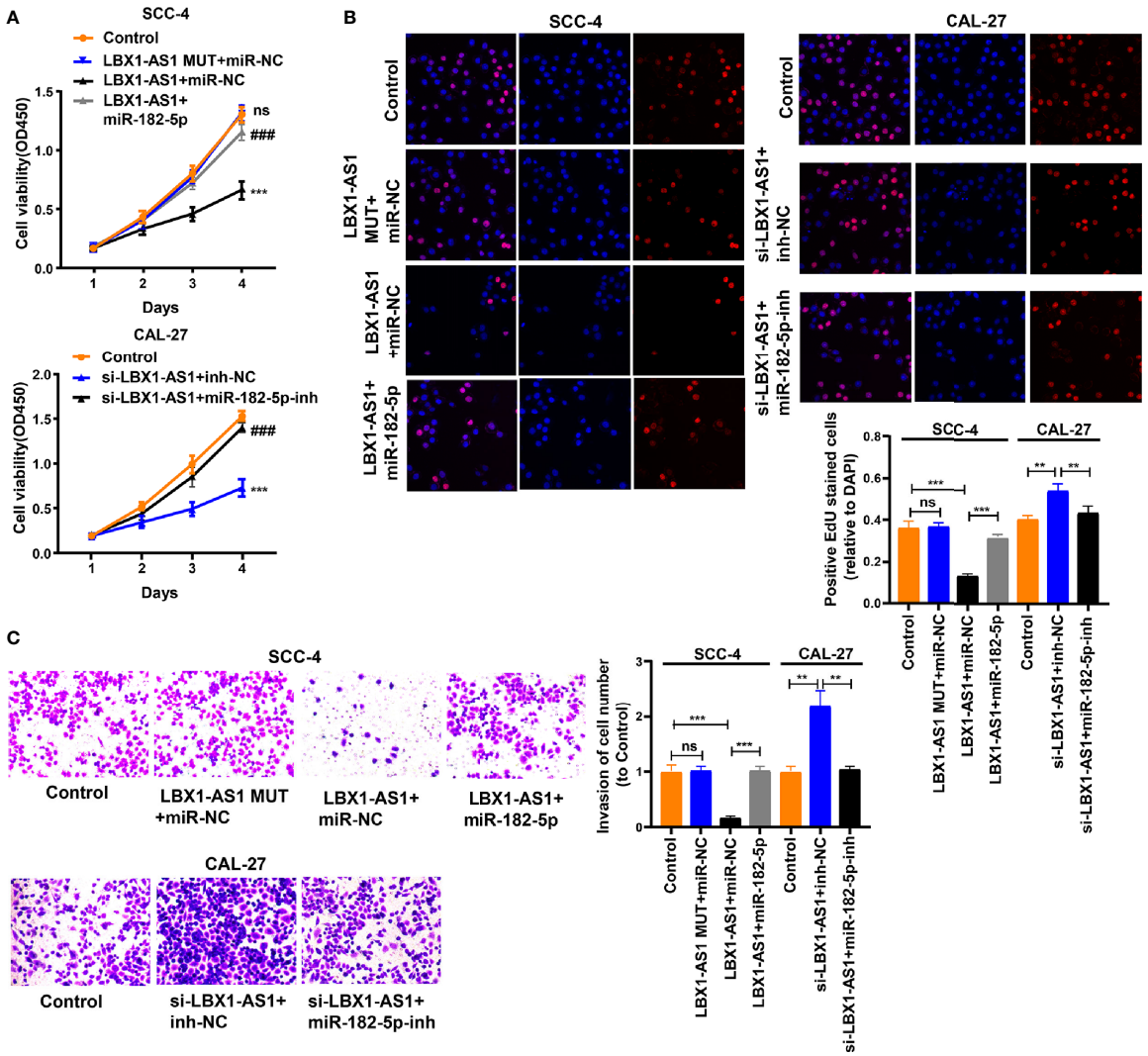

FIGURE 7 | LBX1-AS1 inhibits proliferation and invasion of OSCC cells by interacting with miR-182-5p and upregulating FOXO3 expression. **(A, B)** Cell proliferation in OSCC cell lines SCC-4 and CAL-27 was assessed using CCK-8 assay **(A)** and EdU assay **(B)**. **(C)** Cell invasion of OSCC cell lines SCC-4 and CAL-27 was assessed by Transwell invasion assay. All experiments were performed three times. **P < 0.01 and ***, ###P < 0.001 as indicated, ns, no significance. **/*** and ns *vs.* Control, ### *vs.* p-LBX1-AS1+miR-182-5p NC.

examined the transfection efficiency of miR-182-5p mimics and inhibitor (**Figure 6C**). The mRNA and protein levels of *FOXO3* dropped down in SCC-4 and CAL-27 cells overexpressing miR-182-5p but rose up in OSCC cells undergoing miR-182-5p inhibitor transfection (**Figures 6D–E**). Overexpression of *LBX1-AS1* upregulated *FOXO3* whereas miR-182-5p mimics transfection reversed it in SCC-4 cells (**Figure 6F**). Besides, downregulation of *LBX1-AS1* inhibited *FOXO3* whereas miR-182-5p inhibitor transfection reversed it in CAL-27 cells (**Figure 6F**). Relative to the matched paracarcinoma tissues, *FOXO3* was expressed at a lower level in OSCC tissues (**Figure 6G**). In OSCC tissues, *FOXO3* was negatively correlated with miR-182-5p, but positively correlated with *LBX1-AS1* expression (**Figures 6H–I**). Further, *LBX1-AS1* overexpression inhibited cells to proliferate and invade whereas miR-182-5p mimics transfection reversed it in SCC-4 and CAL-27 cells (**Figures 7A–C**). Nevertheless, LBX1-AS1 mutant plasmid can't inhibit the cell proliferation and invasion of OSCC cells (**Figures 7A–C**). It can be assumed that *LBX1-AS1* inhibits proliferation and invasion in OSCC cells by interacting with miR-182-5p and upregulating *FOXO3* expression.

RBPJ-OE Mφ-Exos Inhibits Tumor Growth Through the *LBX1-AS1*/miR-182-5p/*FOXO3* Pathway *In Vivo*

For proving the effect of Mφ-Exo-*LBX1-AS1* on the modulation of OSCC growth *in vivo*, SCC-4 cells transfected with sh-lncRNA or

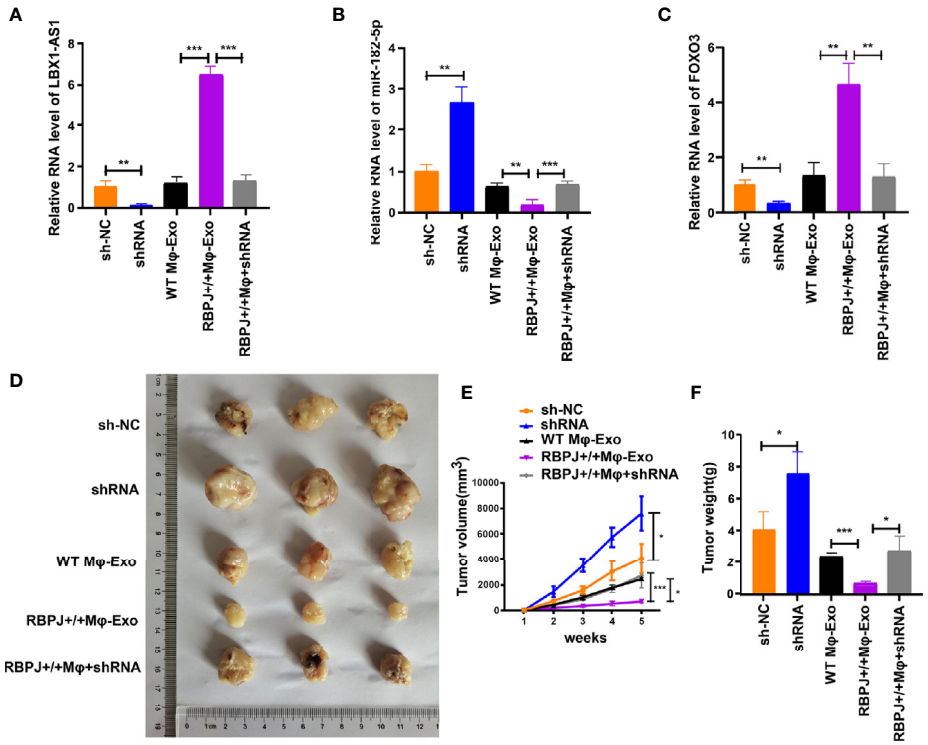

FIGURE 8 | RBPJ-OE Mφ-Exos inhibit tumor growth by LBX1-AS1/miR-182-5p/FOXO3 pathway in mouse xenograft tumor model. **(A)** The level of LBX1-AS1 was detected by qRT-PCR. **(B)** The level of miR-182-5p was detected by qRT-PCR. **(C)** The level of FOXO3 was detected by qRT-PCR. **(D)** Representative images of xenograft tumors (three mice per group) in nude mice. **(E)** Tumor volume is monitored every 7 days for 35 days. **(F)** The weights of xenograft tumors are summarized. *P < 0.05, **P < 0.01 and ***P < 0.001 for statistical differences.

sh-NC or cocultured with WT Mφ-Exos, *RBPJ-OE* Mφ-Exos, or *RBPJ-OE* Mφ-Exo-sh-lncRNA were subcutaneously injected into nude mice. The level of LBX1-AS1, miR-182-5p, and FOXO3 from the xenograft tumors were detected by qRT-PCR (**Figures 8A–C**). Tumors cultured with *RBPJ-OE* Mφ-Exos were significantly smaller, whereas those undergoing sh-lncRNA transfection were significantly larger. The greatest differences in the tumor volume and weight were observed in the tumors between *RBPJ-OE* Mφ-Exos group and sh-lncRNA group (**Figures 8D–F**). What's more, the inhibitory effects of *RBPJ-OE* Mφ-Exos on the tumor growth *in vivo* were eliminated when LBX1-AS1 was knocked down in Exos (**Figures 8D–F**). These results signify that *RBPJ-OE* Mφ-Exos might inhibit tumor growth through a *LBX1-AS1*/miR-182-5p/*FOXO3* pathway in xenograft tumor models.

DISCUSSION

Macrophages are abundant in the OSCC tumoral environment and associated with its progression (31, 32). Moreover, the macrophage environment is heterogenous with the progression of tumors dependent on alternatively polarized M2 macrophages and tumorigenic immune responses dependent on M1-polarized macrophages (33, 34). Therefore, improving the understanding of macrophage regulation in the tumoral environment is important in developing effective therapies for OSCC. Notch-*RBPJ* signaling is believed to regulate TLR-induced inflammatory macrophage polarization by the indirect regulation of M1-specific genes (24).

In this study, we examined whether overexpressing *RBPJ* in macrophages would influence OSCC cells. We found that *RBPJ-OE* Mφ-Exos could inhibit cell proliferation and invasion of OSCC cells. Furthermore, we probed their interrelations by investigating the differentially regulated lncRNAs in Mφ-Exos with upregulated *RBPJ*. Using the lncRNA microarray technique, we discovered that 27 Exo-lncRNAs were differentially regulated in WT Mφ-Exos with *RBPJ* overexpression, of which 24 were upregulated and 3 were downregulated. Later, we selected highest expressed lncRNA, *LBX1-AS1* for further analysis. Then we unveiled that the inhibitory effects of *RBPJ-OE* Mφ-Exos on the proliferation and invasion of OSCC cells (SCC-4 and CAL-27) were eliminated when *LBX1-AS1* was knocked down in Exos. Meanwhile, *LBX1-AS1* overexpression dramatically repressed OSCC cells to proliferate and invade. These associations required further investigation, so we searched for miRNAs that may interact with *LBX1-AS1*.

The public database (starBase) predicted that *LBX1-AS1* may interact with miR-182-5p, which was validated *via* dual luciferase

reporter and RIP assays. Our studies proved that LBX1-AS1 and miR-182-5p constitute the same RISC. Then, a negative correlation between miR-182-5p and *LBX1-AS1* in OSCC and matched para-carcinoma tissues was confirmed by Pearson's analysis. Thus, we deduced that *LBX1-AS1* may repress miR-182-5p to prevent it from interacting in other pathways. StarBase revealed that miR-182-5p interacted with *FOXO3*, a well-known tumor suppressor gene (27–29). Furthermore, FOXO3a reactivation mediates the synergistic cytotoxic effects of rapamycin and cisplatin in oral squamous cell carcinoma cells (35). In the current research, we found that *LBX1-AS1* overexpression upregulated *FOXO3* and inhibited cells to proliferate and invade whereas miR-182-5p mimics transfection reversed them in OSCC cells. What's more, *FOXO3* expression displayed a negative interrelation with miR-182-5p level and a positive correlation with *LBX1-AS1* level in OSCC tissues. *In vivo* assays further verified that *RBPJ-OE* Mφ-Exos might inhibit tumor growth through a *LBX1-AS1*/miR-182-5p/*FOXO3* pathway in xenograft tumor models.

This research has several deficiencies. First, the effect of the exosomes derived from LBX1-AS1-overexpressed macrophage cells on OSCC cells should be explored. Second, it is worth trying to inject RBPJ-overexpressed macrophage-derived exosomes daily into OSCC-injected mice to examine its therapeutic potential. Third, another macrophage activation method (non-transgenic) should be included in this study to further confirm the effects of activated macrophage-derived exosomes.

To conclude, *LBX1-AS1* suppress OSCC cells to proliferate and invade *via* the miR-182-5p/*FOXO3* pathway. Moreover, *RBPJ-OE* Mφ-Exos inhibits tumor growth by stimulating the *LBX1-AS1*/miR-182-5p/*FOXO3* pathway *in vitro* and *in vivo*. The above results indicate that *RBPJ-OE* Mφ-Exos probably play a potential regulation role in the OSCC progression and *LBX1-AS1* could be a biomarker for OSCC diagnosis and potential target for OSCC therapy.

DATA AVAILABILITY STATEMENT

The data presented in the study are deposited in the ArrayExpress repository, accession number (E-MTAB-9989).

ETHICS STATEMENT

The studies involving human participants were reviewed and approved by Foshan Stomatological Hospital, School of Stomatology and Medicine, Foshan University (FSU2016033). The patients/participants provided their written informed consent to participate in this study. The animal study was reviewed and approved by Foshan Stomatological Hospital, School of Stomatology and Medicine, Foshan University.

AUTHOR CONTRIBUTIONS

CZ and XL designed the study. YA, CZ, and ZT performed the experiments. HW and SW collected and analyzed the data. CZ was a major contributor in developing the first draft of this manuscript. CZ and XL revised this manuscript. All authors contributed to the article and approved the submitted version.

SUPPLEMENTARY MATERIAL

The Supplementary Material for this article can be found online at: https://www.frontiersin.org/articles/10.3389/fonc.2021.605884/full#supplementary-material

Supplementary Figure 1 | RBPJ-OE Mφ-Exos can't influence the expression of RBPJ in OSCC cells. **(A)** The relative expressions of RBPJ in WT Mφ and RBPJ-OE Mφ were detected by qRT-PCR. **(B)** The relative expressions of RBPJ in WT Mφ-Exos treated SCC-4/CAL-27 cells and RBPJ-OE Mφ-Exos treated SCC-4/CAL-27 cells were detected by qRT-PCR. ***P < 0.001, ns: no significance.

REFERENCES

1. Shaikh MH, Barrett JW, Khan MI, Kim HAJ, Zeng PYF, Mymryk JS, et al. Chromosome 3p loss in the progression and prognosis of head and neck cancer. *Oral Oncol* (2020) 109:104944. doi: 10.1016/j.oraloncology.2020.104944
2. Brocklehurst PR, Baker SR, Speight PM. Oral cancer screening: what have we learnt and what is there still to achieve? *Future Oncol* (2010) 6:299–304. doi: 10.2217/fon.09.163
3. Ong YLR, Tivey D, Huang L, Sambrook P, Maddern G. Factors affecting surgical mortality of oral squamous cell carcinoma resection. *Int J Oral Maxillofac Surg* (2020) 50:1–6. doi: 10.1016/j.ijom.2020.07.011
4. Xiao M, Zhang J, Chen W, Chen W. M1-like tumor-associated macrophages activated by exosome-transferred THBS1 promote malignant migration in oral squamous cell carcinoma. *J Exp Clin Cancer Res* (2018) 37:143. doi: 10.1186/s13046-018-0815-2
5. Linton SS, Abraham T, Liao J, Clawson GA, Butler PJ, Fox T, et al. Tumor-promoting effects of pancreatic cancer cell exosomes on THP-1-derived macrophages. *PloS One* (2018) 13:e0206759. doi: 10.1371/journal.pone.0206759
6. Zhu X, Shen H, Yin X, Yang M, Wei H, Chen Q, et al. Macrophages derived exosomes deliver miR-223 to epithelial ovarian cancer cells to elicit a chemoresistant phenotype. *J Exp Clin Cancer Res* (2019) 38:81. doi: 10.1186/s13046-019-1095-1
7. Wu J, Gao W, Tang Q, Yu Y, You W, Wu Z, et al. M2 macrophage-derived exosomes facilitate hepatocarcinoma metastasis by transferring alphaM beta2 integrin to tumor cells. *Hepatology* (2020). doi: 10.1002/hep.31432
8. Yang F, Wang T, Du P, Fan H, Dong X, Guo H. M2 bone marrow-derived macrophage-derived exosomes shuffle microRNA-21 to accelerate immune escape of glioma by modulating PEG3. *Cancer Cell Int* (2020) 20:93. doi: 10.1186/s12935-020-1163-9
9. Yin Z, Zhou Y, Ma T, Chen S, Shi N, Zou Y, et al. Down-regulated lncRNA SBF2-AS1 in M2 macrophage-derived exosomes elevates miR-122-5p to restrict XIAP, thereby limiting pancreatic cancer development. *J Cell Mol Med* (2020) 24:5028–38. doi: 10.1111/jcmm.15125
10. Wang Y, Wang Y, Luo W, Song X, Huang L, Xiao J, et al. Roles of long non-coding RNAs and emerging RNA-binding proteins in innate antiviral responses. *Theranostics* (2020) 10:9407–24. doi: 10.7150/thno.48520
11. Wang X, Pei X, Guo G, Qian X, Dou D, Zhang Z, et al. Exosome-mediated transfer of long noncoding RNA H19 induces doxorubicin resistance in breast cancer. *J Cell Physiol* (2020) 235:6896–904. doi: 10.1002/jcp.29585
12. Mao Q, Liang XL, Zhang CL, Pang YH, Lu YX. LncRNA KLF3-AS1 in human mesenchymal stem cell-derived exosomes ameliorates pyroptosis of

cardiomyocytes and myocardial infarction through miR-138-5p/Sirt1 axis. *Stem Cell Res Ther* (2019) 10:393. doi: 10.1186/s13287-019-1522-4
13. Zhang Y, Liu YT, Tang H, Xie WQ, Yao H, Gu WT, et al. Exosome-Transmitted lncRNA H19 Inhibits the Growth of Pituitary Adenoma. *J Clin Endocrinol Metab* (2019) 104:6345–56. doi: 10.1210/jc.2019-00536
14. Kang M, Ren M, Li Y, Fu Y, Deng M, Li C. Exosome-mediated transfer of lncRNA PART1 induces gefitinib resistance in esophageal squamous cell carcinoma via functioning as a competing endogenous RNA. *J Exp Clin Cancer Res* (2018) 37:171. doi: 10.1186/s13046-018-0845-9
15. Zhao C, Zou H, Wang J, Shen J, Liu H. A Three Long Noncoding RNA-Based Signature for Oral Squamous Cell Carcinoma Prognosis Prediction. *DNA Cell Biol* (2018) 37:888–95. doi: 10.1089/dna.2018.4317
16. Liu S, Liu LH, Hu WW, Wang M. Long noncoding RNA TUG1 regulates the development of oral squamous cell carcinoma through sponging miR-524-5p to mediate DLX1 expression as a competitive endogenous RNA. *J Cell Physiol* (2019) 234:20206–16. doi: 10.1002/jcp.28620
17. Qiao J, Liu M, Tian Q, Liu X. Microarray analysis of circRNAs expression profile in gliomas reveals that circ_0037655 could promote glioma progression by regulating miR-214/PI3K signaling. *Life Sci* (2020) 245:117363. doi: 10.1016/j.lfs.2020.117363
18. Kushwaha PP, Vardhan PS, Kapewangolo P, Shuaib M, Prajapati SK, Singh AK, et al. Bulbine frutescens phytochemical inhibits notch signaling pathway and induces apoptosis in triple negative and luminal breast cancer cells. *Life Sci* (2019) 234:116783. doi: 10.1016/j.lfs.2019.116783
19. Guo J, Li P, Liu X, Li Y. NOTCH signaling pathway and non-coding RNAs in cancer. *Pathol Res Pract* (2019) 215:152620. doi: 10.1016/j.prp.2019.152620
20. Nakano T, Katsuki S, Chen M, Decano JL, Halu A, Lee LH, et al. Uremic Toxin Indoxyl Sulfate Promotes Proinflammatory Macrophage Activation Via the Interplay of OATP2B1 and Dll4-Notch Signaling. *Circulation* (2019) 139:78–96. doi: 10.1161/CIRCULATIONAHA.118.034588
21. Lin Y, Zhao JL, Zheng QJ, Jiang X, Tian J, Liang SQ, et al. Notch Signaling Modulates Macrophage Polarization and Phagocytosis Through Direct Suppression of Signal Regulatory Protein alpha Expression. *Front Immunol* (2018) 9:1744. doi: 10.3389/fimmu.2018.01744
22. Xu T, Park SS, Giaimo BD, Hall D, Ferrante F, Ho DM, et al. RBPJ/CBF1 interacts with L3MBTL3/MBT1 to promote repression of Notch signaling via histone demethylase KDM1A/LSD1. *EMBO J* (2017) 36:3232–49. doi: 10.15252/embj.201796525
23. Kulic I, Robertson G, Chang L, Baker JH, Lockwood WW, Mok W, et al. Loss of the Notch effector RBPJ promotes tumorigenesis. *J Exp Med* (2015) 212:37–52. doi: 10.1084/jem.20121192
24. Xu H, Zhu J, Smith S, Foldi J, Zhao B, Chung AY, et al. Notch-RBP-J signaling regulates the transcription factor IRF8 to promote inflammatory macrophage polarization. *Nat Immunol* (2012) 13:642–50. doi: 10.1038/ni.2304
25. Auwerx J. The human leukemia cell line, THP-1: a multifacetted model for the study of monocyte-macrophage differentiation. *Experientia* (1991) 47:22–31. doi: 10.1007/BF02041244
26. Livak KJ, Schmittgen TD. Analysis of relative gene expression data using real-time quantitative PCR and the 2(-Delta Delta C(T)) Method. *Methods* (2001) 25:402–8. doi: 10.1006/meth.2001.1262
27. Liu C, Zhao Y, Wang J, Yang Y, Zhang Y, Qu X, et al. FoxO3 reverses 5-fluorouracil resistance in human colorectal cancer cells by inhibiting the Nrf2/TR1 signaling pathway. *Cancer Lett* (2020) 470:29–42. doi: 10.1016/j.canlet.2019.11.042
28. Salem M, Shan Y, Bernaudo S, Peng C. miR-590-3p Targets Cyclin G2 and FOXO3 to Promote Ovarian Cancer Cell Proliferation, Invasion, and Spheroid Formation. *Int J Mol Sci* (2019) 20. doi: 10.3390/ijms20081810
29. Park SH, Chung YM, Ma J, Yang Q, Berek JS, Hu MC. Pharmacological activation of FOXO3 suppresses triple-negative breast cancer in vitro and in vivo. *Oncotarget* (2016) 7:42110–25. doi: 10.18632/oncotarget.9881
30. Cao MQ, You AB, Zhu XD, Zhang W, Zhang YY, Zhang SZ, et al. miR-182-5p promotes hepatocellular carcinoma progression by repressing FOXO3a. *J Hematol Oncol* (2018) 11:12. doi: 10.1186/s13045-018-0599-z
31. Li X, Bu W, Meng L, Liu X, Wang S, Jiang L, et al. CXCL12/CXCR4 pathway orchestrates CSC-like properties by CAF recruited tumor associated macrophage in OSCC. *Exp Cell Res* (2019) 378:131–8. doi: 10.1016/j.yexcr.2019.03.013
32. Cai J, Qiao B, Gao N, Lin N, He W. Oral squamous cell carcinoma-derived exosomes promote M2 subtype macrophage polarization mediated by exosome-enclosed miR-29a-3p. *Am J Physiol Cell Physiol* (2019) 316:C731–40. doi: 10.1152/ajpcell.00366.2018
33. Bardi GT, Smith MA, Hood JL. Melanoma exosomes promote mixed M1 and M2 macrophage polarization. *Cytokine* (2018) 105:63–72. doi: 10.1016/j.cyto.2018.02.002
34. Orecchioni M, Ghosheh Y, Pramod AB, Ley K. Macrophage Polarization: Different Gene Signatures in M1(LPS+) vs. Classically and M2(LPS-) vs. Alternatively Activated Macrophages. *Front Immunol 10* (1084) 2019. doi: 10.3389/fimmu.2019.01084
35. Fang L, Wang H, Zhou L, Yu D. FOXO3a reactivation mediates the synergistic cytotoxic effects of rapamycin and cisplatin in oral squamous cell carcinoma cells. *Toxicol Appl Pharmacol* (2011) 251:8–15. doi: 10.1016/j.taap.2010.11.007

Conflict of Interest: The authors declare that the research was conducted in the absence of any commercial or financial relationships that could be construed as a potential conflict of interest.

frontiers in Oncology

ORIGINAL RESEARCH
published: 22 April 2021
doi: 10.3389/fonc.2021.626036

Long Noncoding RNA MLK7-AS1 Promotes Non-Small-Cell Lung Cancer Migration and Invasion *via* the miR-375-3p/YWHAZ Axis

Jingzhou Jia[1], *Jiwei Sun*[1], *Wenbo Wang*[1] *and Hongmei Yong*[2]*

[1] Department of Thoracic Surgery, Henan Provincial Chest Hospital, Zhengzhou, China, [2] Department of Oncology, The Affiliated Huai'an Hospital of Xuzhou Medical University and The Second People's Hospital of Huai'an, Huaian, China

Long noncoding RNAs act essential regulators in lung cancer tumorigenesis. Our research aimed to investigate the potential function and molecular mechanisms of MLK7-AS1 in NSCLC (non-small-cell lung cancer). QRT-PCR results indicated that the MLK7-AS1 expression level was upregulated in NSCLC cells and tissues. MLK7-AS1 strengthened cell migration and invasion in H1299 and A549 cells. Luciferase reporter assay found that MLK7-AS1 functioned as an endogenous sponge for miR-375-3p. Transwell assay results showed that miR-375-3p suppressed cell migration and invasion in H1299 and A549 cells. YWHAZ was confirmed as a target gene of miR-375-3p by Targetscan. YWHAZ overexpression promoted the invasion of H1299 and A549 cells. MLK7-AS1 upregulated YWHAZ expression and enhanced H1299 and A549 cell invasion by sponging miR-375-3p. MLK7-AS1 improved the metastasis ability of A549 *in vivo*. In conclusion, MLK7-AS1 was identified as a novel oncogenic RNA in NSCLC and can function as a potential therapeutic target for NSCLC treatment.

Keywords: non-small-cell lung cancer, noncoding RNA, MLK7-AS1, miR-375-3p, YWHAZ

OPEN ACCESS

Edited by:
Xiaochen Wang,
University of Texas Southwestern Medical Center, United States

Reviewed by:
Xianlin Xu,
Nanjing Medical University, China
Tuoye Xu,
Massachusetts General Hospital, United States

***Correspondence:**
Hongmei Yong
cjshazjj@163.com

Specialty section:
This article was submitted to Cancer Genetics, a section of the journal Frontiers in Oncology

Received: *04 November 2020*
Accepted: *05 March 2021*
Published: *22 April 2021*

Citation:
Jia J, Sun J, Wang W and Yong H (2021) Long Noncoding RNA MLK7-AS1 Promotes Non-Small-Cell Lung Cancer Migration and Invasion via the miR-375-3p/YWHAZ Axis. Front. Oncol. 11:626036. doi: 10.3389/fonc.2021.626036

INTRODUCTION

NSCLC is the main cause of thoracic neoplasms in the world (1, 2). Unfortunately, the rate of lung cancer diagnoses is increasing steadily in China (3). Considerable advances in operation and chemoradiotherapy have been achieved, but a high frequency of recurrence in patients with lung cancer remains a problem in lung cancer treatment (4). Understanding the mechanisms of NSCLC development is the cornerstone of solving clinical questions.

Long noncoding RNAs (lncRNAs) are noncoding RNA molecules longer than 200 nucleotides (5, 6). LINC01296 promotes proliferation in NSCLC viamiR-5095/Wnt axis (7). FLVCR1-AS1 downregulation suppresses cell invasion in NSCLC through Wnt/β-catenin signaling pathway (8). LINC00163 overexpression inhibits lung cancer progression by transcriptionally upregulating TCF21 expression (9). SLCO4A1-AS1 accelerates the colorectal cancer development through

Abbreviations: qPCR, Quantitative reverse transcription polymerase chain reaction; lncRNAs, long noncoding RNAs; ceRNA, competing endogenous RNA; NSCLC, non-small-cell lung cancer.

Wnt signaling pathway (10). lncRNA PVT1 facilitates the tumor progression in gallbladder cancer *via* the miR-143/HK2 axis (11). MLK7 antisense RNA 1 (MLK7-AS1) was previously identified as an oncogene in several tumors. For example, MLK7−AS1 can enhance ovarian cancer cells invasion by upregulating the expression of YAP1 (12). However, the role of MLK7−AS1 in NSCLC is largely unclarified.

MicroRNAs (miRNAs), small noncoding RNAs of 20–25 nucleotides in length, regulate the expression of downstream targets through post-transcriptional modulation (13, 14). Competing endogenous RNAs (ceRNA) is a vital mechanism regulating the progression of various cancers. In-depth studies have demonstrated that lncRNAs acted as a vital regulatory role in malignancies as competing endogenous RNAs. FLVCR1-AS1 enhances gastric cancer tumorigenesis by sponging miR-155 and targeting c-Myc (15). lncRNA SNHG16 accelerates the cancer cells migration and invasion abilities through sponging miR-520d-3p and targeting STAT3 in hemangioma (16). CeRNA network is the vital mechanism of tumor development (17). lncRNA ZEB1-AS1 promotes TGF-β1-induced invasion of bladder tumor cells *via* targeting the miR-200b/FSCN1 pathway (18). Thus, exploring the roles of lncRNAs in NSCLC can help scholars understand potential mechanisms from a new perspective.

In this study, we found MLK7−AS1 was upregulated in NSCLC, which indicated MLK7−AS1 was a favorable factor for NSCLC. To further demonstrate the role of MLK7−AS1 and the underlying mechanism in NSCLC, NSCLC cell lines and *in vivo* models was used, which would contribute to the understanding of the development and progression of NSCLC, thus could provide potential therapeutic target for NSCLC.

MATERIAL AND METHODS

Cell Culture

Three NSCLC lines (i.e., H1299, A549, and H1650) and the normal cell line BEAS-2B were cultured in an incubator (37°C, 5% CO_2) and in RPMI1640 (Gibco BRL, Gaithersburg, MD, USA) supplemented with 10% FBS (Gibco BRL, Gaithersburg, MD, USA).

Transwell Migration and Invasion Assay

Transwell migration and invasion assay was performed in accordance with previously described method (19). For the Transwell migration assays, the transfected H1299 and A549 ($N=5.5\times10^3$) cells were plated in top chambers with a noncoated membrane (Invitrogen, Carlsbad, CA). For the invasion assays, the transfected H1299 and A549 ($N=11\times10^3$) cells were plated in top chambers with a coated membrane. The number of invading cells was counted after fixed with 4% paraformaldehyde (Beyotime, Shanghai, China).

Cell Transfection and Lentivirus Production

The sequence of YWHAZ was cloned into the pcDNA3.1 vector and the empty vector acted as a negative control. The lentiviral vector for MLK7−AS1 was purchased from Kaiji Gene (Shanghai, China). mimic/inhibitor-miR-375-3p and mimic/inhibitor-NC were purchased from RiboBio (China, Guangzhou). Lipofectamine 2000 (Invitrogen, Carlsbad, CA) was utilized for transfection in accordance with the manufacturer's instructions.

Nuclear and Cytoplasmic RNA Isolation

Nuclear and cytoplasmic RNA was isolated in accordance with previously described methods (20, 21). The cytoplasm and nuclear RNAs of NSCLC cells were separated and extracted using a nuclear and cytoplasmic RNA purification kit (Invitrogen, Carlsbad, CA). qPCR assay was performed to detect the isolated RNA.

Quantitative Reverse Transcription PCR (qRT-PCR)

The RNA of NSCLC cells was isolated using TRIzol reagent (US, Life Technologies, USA). SYBR Green qRT-PCR on an ABI7300 real-time PCR machine was used to measure the expression levels of mRNAs. YWHAZ and GAPDH expression levels were examined using the following specific primers:

5′CCTGCATGAAGTCTGTAACTGAG3′,
5′GACCTACGGGCTCCTACAACA3′,
5′GGAGCGAGATCCCTCCAAAAT3′, and
5′GGCTGTTGTCATACTTCTCATGG3′.

Western Blot Analysis

The protein (15–20 mg) extracted from cells was used for Western blot analysis. The antibodies utilized in this study included anti-YWHAZ (1:1000; Cell Signaling Technology, USA) and GAPDH (1:1000; Cell Signaling Technology, USA). GAPDH (1:2000; Cell Signaling Technology, USA) was used as a loading control.

Luciferase Reporter Assay

Luciferase reporter assay was performed in accordance with previously described procedures (22). Wt-pmirGLO-, MLK7−AS1, wt-pmirGLO-YWHAZ, and their corresponding mutated vectors were constructed. Wt-pmirGLO or mut-pmirGLO was cotransfected into cells with miR-375-3p inhibitor or miR-375-3p mimic by using Lipofectamine 2000. Luciferase activity was detected 48h after transfection.

In Vivo Study

Six-week-old female nude mice were obtained from Medical Center of Yangzhou University. (Yangzhou, China). The A549 cell line stably overexpressing MLK7-AS1 was established. A lung metastasis mice model was also established with the intrasplenic injection of 5×10^6 stably overexpressing MLK7-AS1 or LV-NC cells. After 24 days, lung colonization capacity was evaluated. The number of lung metastatic foci was counted *via* H&E staining. This work was approved by the Medical Ethics Committee of Henan Provincial Chest Hospital.

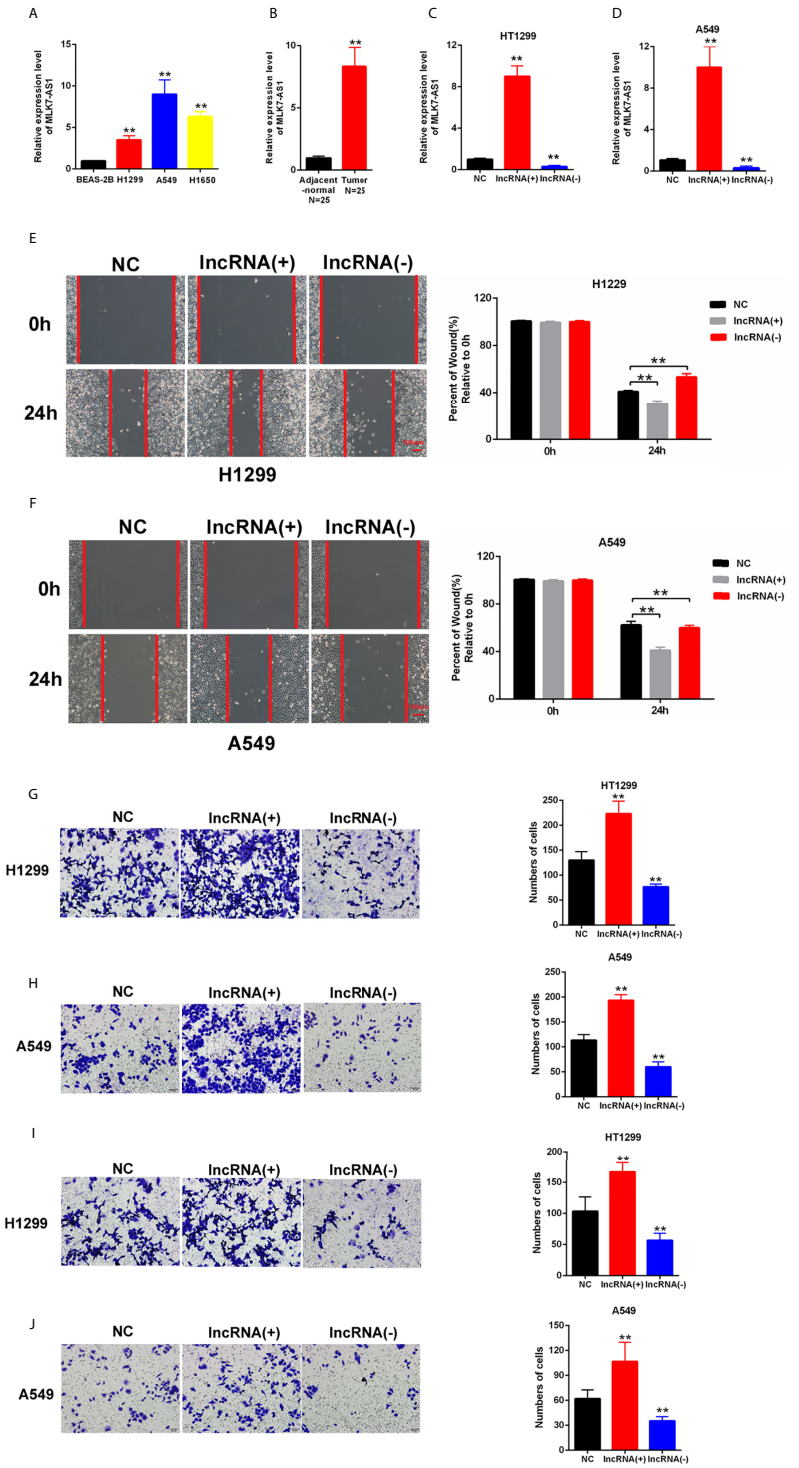

FIGURE 1 | Upregulated MLK7-AS1 enhanced the migration and invasion of NSCLC cells. **(A)** MLK7-AS1 expression level was upregulated in the NSCLC cell lines compared with that in the normal line. **(B)** MLK7-AS1 expression level was upregulated in NSCLC tissues compared with that in tumor-adjacent normal pairs (*N*=25). **(C, D)** LV-MLK7-AS1 and sh-MLK7-AS1 efficiency was measured through qRT-PCR. **(E, F)** Effect of MLK7-AS1 on migration detected through wound-healing assays. LV-MLK7-AS1 promoted cell migration, whereas sh-MLK7-AS1 inhibited cell migration in H1229 and A549. **(G, H)** Effect of MLK7-AS1 on migration detected through Transwell assays. LV-MLK7-AS1 strengthened cell migration, whereas sh-MLK7-AS1 suppressed cell migration in H1229 and A549. **(I, J)** Effect of MLK7-AS1 on invasion detected through Transwell assays. LV-MLK7-AS1 increased cell invasion, but sh-MLK7-AS1 decreased cell invasion in H1229 and A549. Data indicate the mean ± SD, n = 3. **P < 0.01 vs. control.

Statistical Analysis

GraphPad Prism 5.0 and SPSS 13.0 were used to analyze data. Statistical data were expressed as mean ± standard deviation. Differences were considered significant at P<0.05.

RESULTS

MLK7-AS1 Promoted the Migration and Invasion of NSCLC cells

MLK7-AS1 expression was detected by qPCR in NSCLC cell lines, namely, H1299, A549, H1650 compared with normal human bronchial epithelium BEAS-2B. As shown in **Figure 1A**. The expression level of MLK7-AS1 was upregulated NSCLC cell lines. Moreover, the expression level of MLK7-AS1 was upregulated in NSCLC tissues than in adjacent tissues (N=25) (**Figure 1B**). To explore the biological functions of MLK7-AS1, overexpression (LV-MLK7-AS1) and knockdown (sh-MLK7-AS1) assays were performed in H1299 and A549 cells. The efficiency of LV-MLK7-AS1 and sh-MLK7-AS1 was determined using qRT-PCR (**Figures 1C, D**). Wound-healing assays results indicated that MLK7-AS1 overexpression promoted the cells migration and silencing of MLK7-AS1 weakened the cells migration in H1299 and A549 (**Figures 1E, F**). Moreover, transwell assays indicated that the cell migration in H1299 and A549 was strengthened by MLK7-AS1 upregulation but was weakened by MLK7-AS1 downregulation (**Figures 1G, H**). The cell invasion in H1299 and A549 was promoted by MLK7-AS1 overexpression but was suppressed by MLK7-AS1 knockout

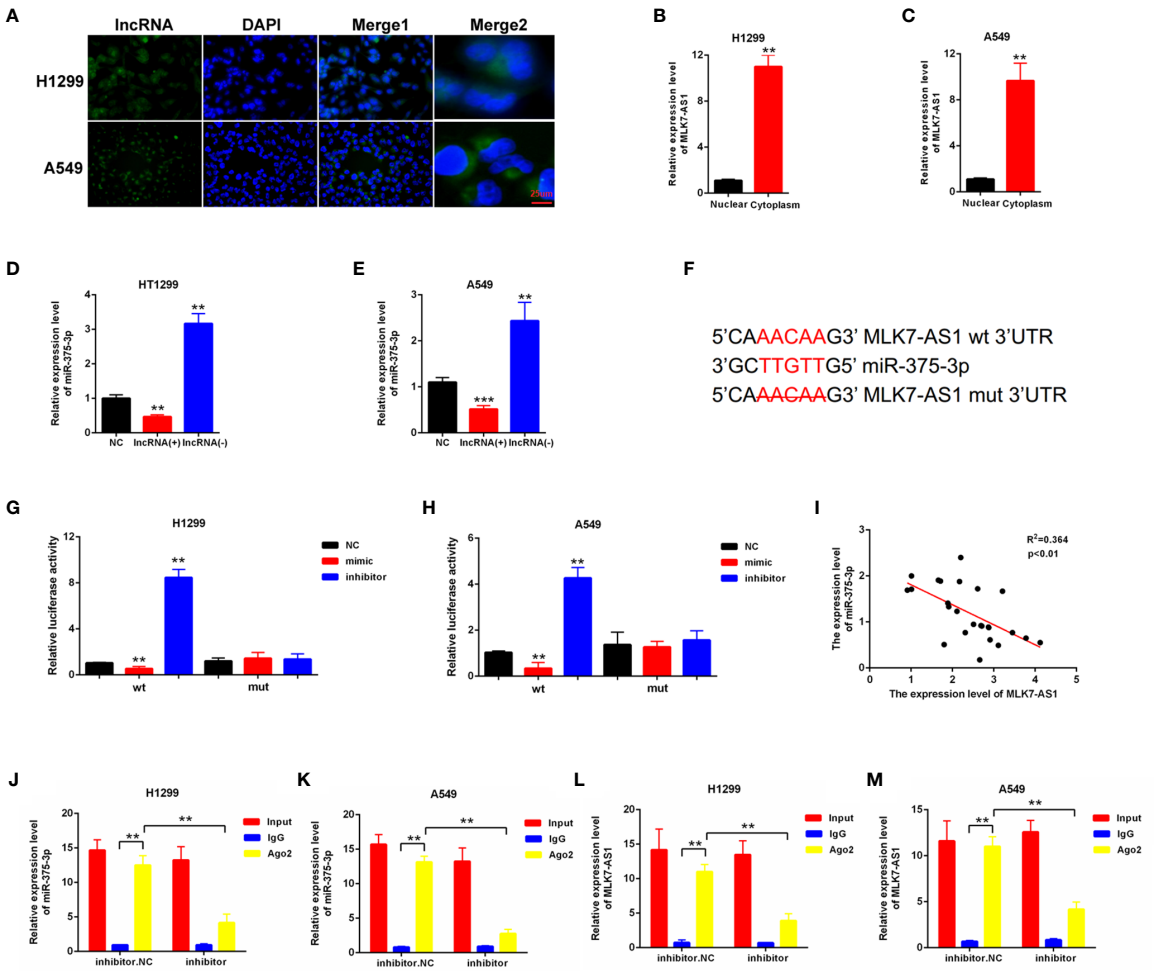

FIGURE 2 | miR-375-3p was predicted as a direct target of MLK7-AS1. **(A)** FISH assays were conducted to detect the location of MLK7-AS1 in H1299 and A549. MLK7-AS1 was mainly localized in the cytoplasm. **(B, C)** qRT-PCR was performed to determine the location of MLK7-AS1 in H1299 and A549. MLK7-AS1 expression level was higher in the cytoplasm than in nucleus. **(D, E)** qRT-PCR results showed that MLK7-AS1 upregulation decreased the miR-375-3p expression level, whereas MLK7-AS1 downregulation increased the miR-375-3p expression level. **(F)** Direct binding sites between MLK7-AS1 and miR-375-3p were presented. **(G, H)** Luciferase reporter assay was performed to confirm the direct binding relationship between MLK7-AS1 and miR-375-3p. **(I)** The regression analysis of correlation between the expression of MLK7-AS1 and miR-375-3p in lung cancer tissues (n=22). **(J–M)** After RIP assay in H1299 or A549, the levels of MLK7-AS1 and miR-375-3p were respectively quantified by RT-qPCR. Data indicate the mean ± SD, n = 3. **P < 0.01, ***P < 0.001 vs. control.

knockdown (**Figures 1I, J**). These results demonstrated that the MLK7-AS1 strengthened the NSCLC cells migration and invasion.

miR-375-3p Was Predicted as a Direct Target of MLK7-AS1

To explore whether competing endogenous RNA (ceRNA) was involved in the regulation of MLK7-AS1 in NSCLC, FISH assays were performed in H1299 and A549. MLK7-AS1 mainly localized in the cytoplasm (**Figure 2A**). QRT-PCR also indicated that MLK7-AS1 mainly expressed in the cytoplasm of H1299 and A549 cells (**Figures 2B, C**). The potential target miRNAs for MLK7-AS1 were predicted using lncBase (lncBase/Experimental/?r=lncBase) and StarBase v2.0 (http://starbase.sysu.edu.cn/). Among many candidates, miR-375-3p could act as a tumor suppressor in several tumors (23). Thus, miR-375-3p was identified as a prior candidate for MLK7-AS1. LV-MLK7-AS1 and sh-MLK7-AS1 were transfected in NSCLC cells to explore the relationship

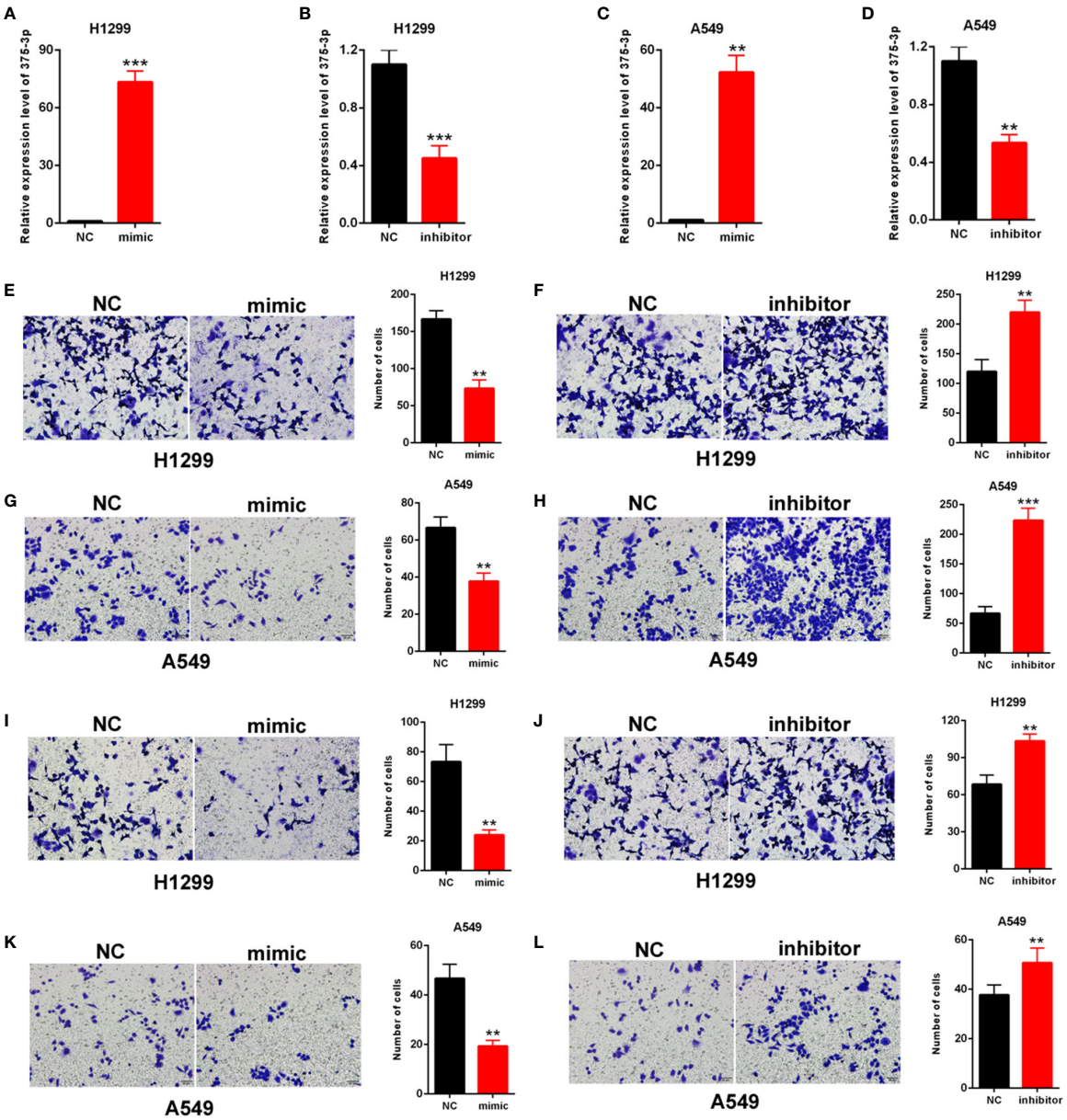

FIGURE 3 | Effects of miR-375-3p on the migration and invasion of NSCLC cells. **(A, B)** Efficiency of mimic/inhibitor-miR-375-3p was determined through qPCR in H1299. **(C, D)** Efficiency of mimic/inhibitor-miR-375-3p was determined through qRT-PCR in A549. **(E–H)** Effect of miR-375-3p on migration was detected through Transwell assays in H1299 and A549. Cell migration was promoted by miR-375-3p-mimic but was suppressed by miR-375-3p-inhibitor. **(I–L)** Effects of miR-375-3p on invasion detected through Transwell assays in H1299 and A549. Cell invasion was enhanced by miR-375-3p-mimic but was suppressed by miR-375-3p-inhibitor in H1299 and A549. Data indicate the mean ± SD, n = 3. **P < 0.01, ***P < 0.001 vs. control.

between MLK7-AS1 and miR-375-3p, which revealed that LV-MLK7-AS1 downregulated the miR-375-3p expression, whereas sh-MLK7-AS1 upregulated the miR-375-3p expression in H1299 and A549 cells (**Figures 2D, E**). StarBase v2.0 was used to predict the specific binding site between MLK7-AS1 and miR-375-3p, which result was shown in **Figure 2F**. Moreover, dual-luciferase reporter assays were performed in H1299 and A549. As shown in **Figures 2G, H**, luciferase activity could be inhibited by mimic-miR-375-3p but could be promoted by inhibitor-miR-375-3p in WT-MLK7-AS1 reporter. However, the mutant-type reporter gene (MT-MLK7-AS1 reporter) was not inhibited or increased in the luciferase activity by mimic-or inhibitor-miR-375-3p. In addition, we examined the expression levels of miR-375-3p in lung cancer tissues (n=22), and made the correlation analysis with the expression levels of MLK7-AS1 (**Figure 2I**). We found that the expression levels of miR-375-3p were negatively correlated with the expression levels of MLK7-AS1. A RIP assay was performed to examine whether MLK7-AS1 and miR-375-3p are in the same RISC complex. Then, RIP assays indicated that MLK7-AS1 and miR-375-3p were enriched in Ago2 compared with control IgG. Subsequently, miR-375-3p got a significant enrichment in the MLK7-AS1 pull down pellets compared with control IgG. Moreover, after transfection with inhibitor-miR-20a-5p, the expression levels of MLK7-AS1 and miR-375-3p enriched in Ago2 were downregulated (**Figures 2J–M**). Thus, miR-375-3p was a direct target of MLK7-AS1.

miR-375-3p Suppressed the Migration and Invasion of NSCLC Cells

H1299 and A549 were transfected with mimic/inhibitor of miR-375-3p to investigate the role of miR-375-3p in NSCLC cells. The efficiency of mimic-miR-375-3p and inhibitor-miR-375-3p was measured through qRT-PCR (**Figures 3A–D**). The cell migration was inhibited by mimic-miR-375-3p and was enhanced by inhibitor-miR-375-3p in H1299 and A549 (**Figures 3E–H**). The cell invasion was inhibited by mimic-miR-375-3p and was enhanced by inhibitor-miR-375-3p in H1299 and A549 (**Figures 3I–L**). Thus, miR-375-3p suppressed cell migration and invasion in H1299 and A549.

YWHAZ Was a Direct Target Gene of miR-375-3p

The potential target genes of miR-375-3p were predicted by StarBase v2.0. Among many candidates, YWHAZ was identified as an oncogene in several tumors (24, 25). Thus, YWHAZ was chosen as a prior candidate for miR-375-3p. As shown in **Figures 4A–H**, results indicated that the mRNA and protein expression level of YWHAZ was downregulated after transfection with mimic-miR-375-3p and was upregulated after transfection with inhibitor-miR-375-3p. The analysis through StarBase v2.0 revealed the direct binding sites between miR-375-3p and YWHAZ (**Figure 4I**). Moreover, dual-luciferase reporter experiments were performed in H1299 and A549. The luciferase activity was inhibited by mimic-miR-375-3p and was enhanced by

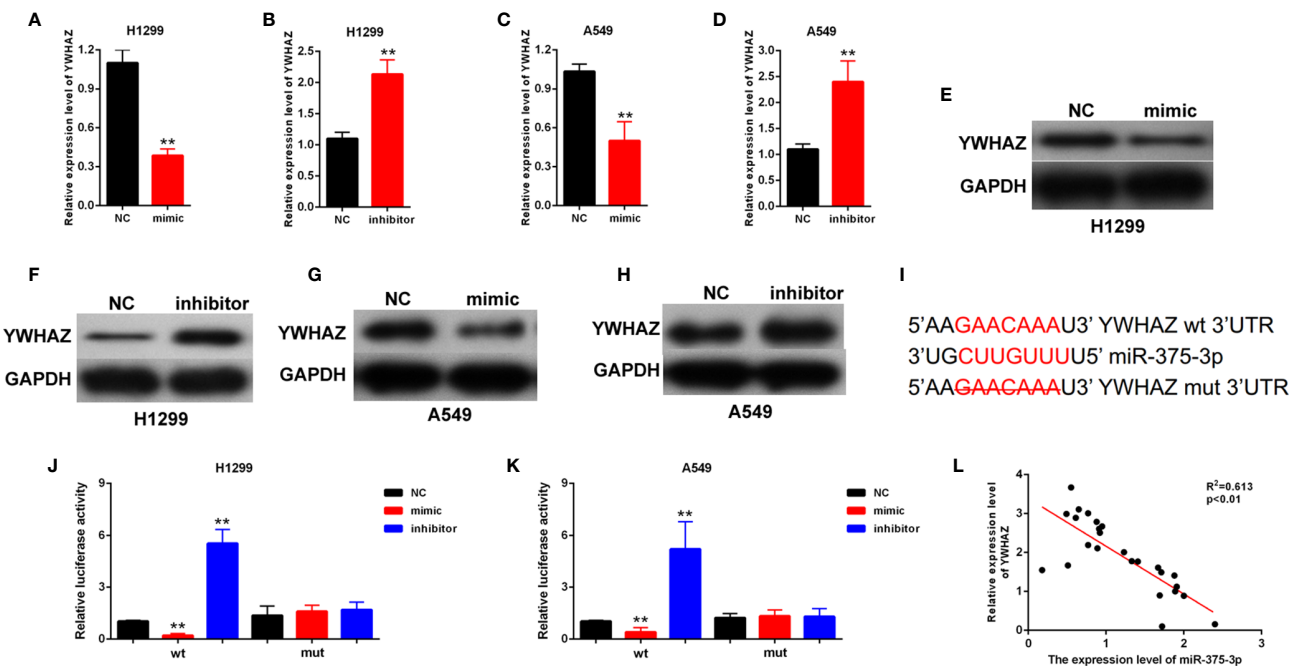

FIGURE 4 | YWHAZ was a direct target gene of miR-375-3p. **(A–D)** qRT-PCR results indicated that the expression level of YWHAZ was decreased by miR-375-3p-mimic but was increased by miR-375-3p-inhibitor. **(E–H)** Western blot results revealed that the expression level of YWHAZ was increased by miR-375-3p overexpression but was decreased by miR-375-3p. **(I)** Direct binding sites between miR-375-3p and YWHAZ were presented. **(J, K)** Luciferase reporter assays were performed in H1299 and A549. Direct binding relationship between miR-375-3p and YWHAZ was confirmed. **(L)** The regression analysis of correlation between the expression of miR-375-3p and YWHAZ in lung cancer tissues (n=22). Data indicate the mean ± SD, n = 3. **P < 0.01 vs. control.

inhibitor-miR-375-3p in WT-YWHAZ reporter. However, the mutant-type reporter gene (MT- YWHAZ reporter) was not inhibited or enhanced by mimic-miR-375-3p or inhibitor-miR-375-3p (**Figures 4J, K**). We found that the expression levels of YWHAZ were negatively correlated with the expression levels of miR-375-3p in lung cancer tissues (n=22, **Figure 4L**). As such, YWHAZ was a direct target gene of miR-375-3p.

MLK7-AS1 Upregulated the YWHAZ Expression Level and Promoted Invasion by Sponging miR-375-3p

YWHAZ was overexpressed in H1299 and A549 cells (**Figures 5A–D**). We found that the upregulation of YWHAZ promoted cell invasion in H1299 and A549 cells (**Figures 5E, F**). Restore experiments were performed in H1299 and A549, and the cells

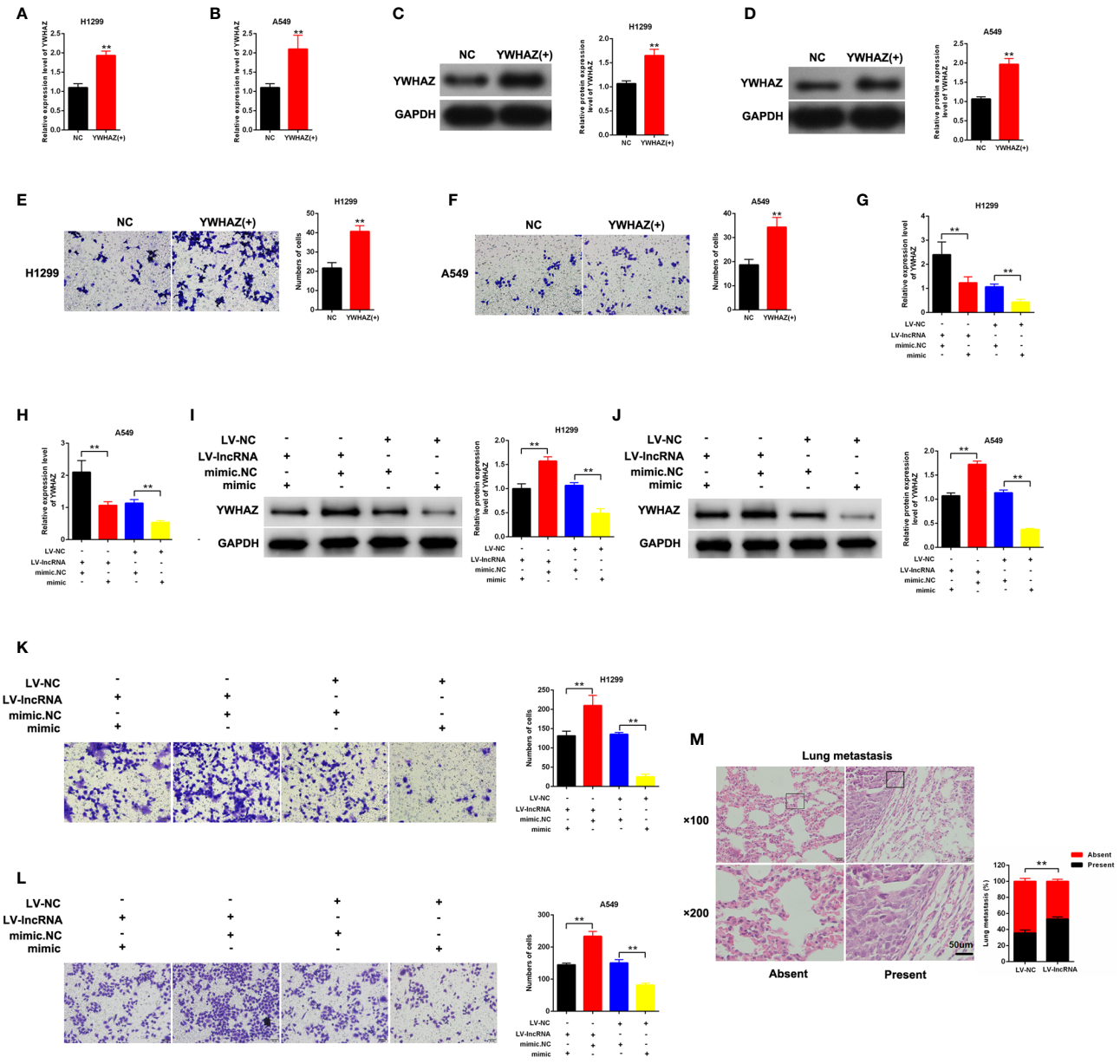

FIGURE 5 | MLK7-AS1 upregulated YWHAZ expression and promoted the invasion by acting as miR-375-3p sponge. **(A, B)** Efficiency of pcDNA3.1-YWHAZ was determined through qPCR in H1229 and A549 cells. **(C, D)** Western blot results showed that YWHAZ gene was successfully overexpressed after transfection with pcDNA3.1-YWHAZ. **(E, F)** Overexpression of YWHAZ enhanced cell invasion in H1229 and A549. **(G, H)** mRNA expression level of YWHAZ was detected through qPCR. H1299 and A549 cells were transfected with LV-MLK7-AS1 or mimic-miR-375-3p. **(I, J)** Protein expression level of YWHAZ was detected by western blot. H1299 and A549 cells were transfected with LV-MLK7-AS1 or mimic-miR-375-3p. **(K, L)** Invasion was detected through Transwell assays. Cells were transfected with LV-MLK7-AS1 or mimic-miR-375-3p. **(M)** Typical images for the lung metastasis of a mouse model. The percentage of mice with or without metastatic nodules in the lungs was counted. Data indicate the mean ± SD, n = 3., **P < 0.01 vs. control.

were cotransfected with mimic-miR-375-3p or LV-MLK7-AS1. miR-375-3p overexpression could restore the upregulation of YWHAZ in NSCLC cells after transfection with LV-MLK7-AS1 **(Figures 5G–J)**. mimic-miR-375-3p could restore the improvement of invasion ability in NSCLC cells after transfection with LV-MLK7-AS1 **(Figures 5K, L)**. Lastly, the stable MLK7-AS1-overexpression in A549 cell line was established. Lung metastasis models were established by inoculation of A549 cells. As shown in **Figure 5M**, MLK7-AS1 overexpression could enhance the metastasis ability of A549 cells. Thus, these results suggested that MLK7-AS1 upregulated the YWHAZ expression level and enhanced the invasion by acting as miR-375-3p sponge in NSCLC.

DISCUSSION

NSCLC is a highly aggressive tumor and has a poor five-year survival rate. Metastasis and recurrence are the important negative prognostic factors of NSCLC. Understanding the molecular mechanism of NSCLC development is helpful to address its poor survival rate. lncRNAs are important regulators of NSCLC progression. lncRNA NEF inhibits NSCLC proliferation by targeting glucose transport (26). LINC00702 inhibits tumor growth and invasion in NSCLC *via* the miR-510/PTEN axis (27). A novel lncRNA BC200 regulates the PI3K/AKT pathway and promoted the development of NSCLC (28).

In this study, MLK7-AS1 was identified as a vital regulator in NSCLC. Firstly, we found that MLK7-AS1 was upregulated in H1299, A549 and H1650 cell lines and NSCLC tissues, which suggested that MLK7-AS1 might participate in the progression of NSCLC. In order to study the role of MLK7-AS1 in NSCLC, overexpression and knockdown of MLK7-AS1 were performed. We found that LV-MLK7-AS1 strengthened the invasion of H1299 and A549, whereas, sh-MLK7-AS1 weakened the invasion of NSCLC cells. In-depth researches have proven that lncRNAs acted as an important regulatory role in malignancies as competing endogenous RNAs[14]. Then, miR-375-3p was identified as a direct target of MLK7-AS1. Previous studies suggested that miR-375-3p participates in tumor development. miR-375-3p may act as a tumor suppressor by targeting LAMC1 in HNSCC (29). However, the role of miR-375-3p in NSCLC is unknown.

Overexpression and knockdown assays were performed in NSCLC cells. Transwell assays indicated that the invasion of the NSCLC cells could be suppressed by mimic-miR-375-3p but could be enhanced by inhibitor-miR-375-3p. The binding between lncRNA and miRNA is according to bases of complementary matching principle (29). Then, dual-luciferase reporter assays were performed in H1299 and A549. miR-375-3p regulated the luciferase activity in WT-MLK7-AS1 reporter. But, the luciferace activity of the mutant-type reporter gene was not decreased or increased by miR-375-3p. Thus, miR-375-3p was a direct target of MLK7-AS1. By binding to the 3'UTR region of the coding gene, miRNAs downregulated the target genes expression (27). YWHAZ was predicted as a target gene for miR-375-3p. Results indicated that the mRNA and protein expression of YWHAZ were upregulated by mimic-miR-375-3p but was downregulated by inhibitor-miR-375-3p in H1299 and A549. Dual-luciferase reporter assays indicated that YWHAZ was a direct target gene for miR-375-3p. The role of YWHAZ in NSCLC was further investigated. YWHAZ enhances metastasis and is related to the poor survival in hepatocellular carcinoma (30). YWHAZ strengthens the gastric cancer cells growth ability by suppressing cell apoptosis and autophagy (24).

However, the role of YWHAZ in NSCLC is unclear. YWHAZ was overexpressed in NSCLS cells *via* pcDNA3.1-YWHAZ transfection. YWHAZ overexpression promoted the cell invasion in H1299 and A549. The effect of miR-375-3p in MLK7-AS1 function was investigated. The NSCLC cells were transfected with LV-MLK7-AS1 or mimic-miR-375-3p. Restore experiments confirmed that MLK7-AS1 promoted the cell invasion and upregulated the YWHAZ expression by sponging miR-375-3p. The effect of MLK7-AS1 was explored *in vivo*. A lung metastasis mouse model was established, and the MLK7-AS1 overexpression enhanced the metastasis ability of NSCLC cells *in vivo*.

CONCLUSION

In summary, our study reported that MLK7-AS1 was upregulated in NSCLC and can promote cell invasion *in vitro* and *in vivo* through upregulating miR-375-3p/YWHAZ axis. MLK7-AS1 might act as a potential diagnostic biomarker and therapeutic target for NSCLC.

DATA AVAILABILITY STATEMENT

The original contributions presented in the study are included in the article/supplementary material. Further inquiries can be directed to the corresponding author.

ETHICS STATEMENT

The animal study was reviewed and approved by Henan Provincial Chest Hospital.

AUTHOR CONTRIBUTIONS

WW and HY designed and revised the study. JJ performed the experiments and prepared the manuscript. JS and HY collected and analyzed the data. All authors contributed to the article and approved the submitted version.

REFERENCES

1. Altorki NK, Markowitz GJ, Gao D, Port JL, Saxena A, Stiles B, et al. The lung microenvironment: an important regulator of tumour growth and metastasis. *Nat Rev Cancer* (2019) 19:9–31. doi: 10.1038/s41568-018-0081-9
2. Lee WH, Loo CY, Ghadiri M, Leong CR, Young PM, Traini D. The potential to treat lung cancer via inhalation of repurposed drugs. *Adv Drug Delivery Rev* (2018) 133:107–30. doi: 10.1016/j.addr.2018.08.012
3. Chen W. Cancer statistics: updated cancer burden in China. *Chin J Cancer Res* (2015) 27:1. doi: 10.3978/j.issn.1000-9604.2015.02.07
4. Mahvi DA, Liu R, Grinstaff MW, Colson YL, Raut CP. Local Cancer Recurrence: The Realities, Challenges, and Opportunities for New Therapies. *CA Cancer J Clin* (2018) 68:488–505. doi: 10.3322/caac.21498
5. Chang ZW, Jia YX, Zhang WJ, Song LJ, Gao M, Li MJ, et al. LncRNA-TUSC7/miR-224 affected chemotherapy resistance of esophageal squamous cell carcinoma by competitively regulating DESC1. *J Exp Clin Cancer Res* (2018) 37:56. doi: 10.1186/s13046-018-0724-4
6. Sun J, Hu J, Wang G, Yang Z, Zhao C, Zhang X, et al. LncRNA TUG1 promoted KIAA1199 expression via miR-600 to accelerate cell metastasis and epithelial-mesenchymal transition in colorectal cancer. *J Exp Clin Cancer Res* (2018) 37:106. doi: 10.1186/s13046-018-0771-x
7. Hu X, Duan L, Liu H, Zhang L. Long noncoding RNA LINC01296 induces non-small cell lung cancer growth and progression through sponging miR-5095. *Am J Transl Res* (2019) 11:895–903.
8. Lin H, Shangguan Z, Zhu M, Bao L, Zhang Q, Pan S. lncRNA FLVCR1-AS1 silencing inhibits lung cancer cell proliferation, migration, and invasion by inhibiting the activity of the Wnt/beta-catenin signaling pathway. *J Cell Biochem* (2019) 120:10625–32. doi: 10.1002/jcb.28352
9. Guo X, Wei Y, Wang Z, Liu W, Yang Y, Yu X, et al. LncRNA LINC00163 upregulation suppresses lung cancer development though transcriptionally increasing TCF21 expression. *Am J Cancer Res* (2018) 8:2494–506.
10. Yu J, Han Z, Sun Z, Wang Y, Zheng M, Song C. LncRNA SLCO4A1-AS1 facilitates growth and metastasis of colorectal cancer through beta-catenin-dependent Wnt pathway. *J Exp Clin Cancer Res* (2018) 37:222. doi: 10.1186/s13046-018-0896-y
11. Chen J, Yu Y, Li H, Hu Q, Chen X, He Y, et al. Long non-coding RNA PVT1 promotes tumor progression by regulating the miR-143/HK2 axis in gallbladder cancer. *Mol Cancer* (2019) 18:33. doi: 10.1186/s12943-019-0947-9
12. Yan H, Li H, Li P, Li X, Lin J, Zhu L, et al. Long noncoding RNA MLK7-AS1 promotes ovarian cancer cells progression by modulating miR-375/YAP1 axis. *J Exp Clin Cancer Res* (2018) 37:237. doi: 10.1186/s13046-018-0910-4
13. Huang T, Yin L, Wu J, Gu JJ, Wu JZ, Chen D, et al. MicroRNA-19b-3p regulates nasopharyngeal carcinoma radiosensitivity by targeting TNFAIP3/NF-kappaB axis. *J Exp Clin Cancer Res* (2016) 35:188. doi: 10.1186/s13046-016-0465-1
14. Wang R, Sun Y, Yu W, Yan Y, Qiao M, Jiang R, et al. Downregulation of miRNA-214 in cancer-associated fibroblasts contributes to migration and invasion of gastric cancer cells through targeting FGF9 and inducing EMT. *J Exp Clin Cancer Res* (2019) 38:20. doi: 10.1186/s13046-018-0995-9
15. Liu Y, Guo G, Zhong Z, Sun L, Liao L, Wang X, et al. Long non-coding RNA FLVCR1-AS1 sponges miR-155 to promote the tumorigenesis of gastric cancer by targeting c-Myc. *Am J Transl Res* (2019) 11:793–805.
16. Zhao W, Fu H, Zhang S, Sun S, Liu Y. LncRNA SNHG16 drives proliferation, migration, and invasion of hemangioma endothelial cell through modulation of miR-520d-3p/STAT3 axis. *Cancer Med* (2018) 7:3311–20. doi: 10.1002/cam4.1562
17. Chen D, Sun Q, Cheng X, Zhang L, Song W, Zhou D, et al. Genome-wide analysis of long noncoding RNA (lncRNA) expression in colorectal cancer tissues from patients with liver metastasis. *Cancer Med* (2016) 5:1629–39. doi: 10.1002/cam4.738
18. Hua Z, Ma K, Liu S, Yue Y, Cao H, Li Z. LncRNA ZEB1-AS1 facilitates ox-LDL-induced damage of HCtAEC cells and the oxidative stress and inflammatory events of THP-1 cells via miR-942/HMGB1 signaling. *Life Sci* (2020) 247:117334. doi: 10.1016/j.lfs.2020.117334
19. Yang L, Gao Q, Wu X, Feng F, Xu K. Long noncoding RNA HEGBC promotes tumorigenesis and metastasis of gallbladder cancer via forming a positive feedback loop with IL-11/STAT3 signaling pathway. *J Exp Clin Cancer Res* (2018) 37:186. doi: 10.1186/s13046-018-0847-7
20. Liu D, Gao M, Wu K, Zhu D, Yang Y, Zhao S. LINC00152 facilitates tumorigenesis in esophageal squamous cell carcinoma via miR-153-3p/FYN axis. *BioMed Pharmacother* (2019) 112:108654. doi: 10.1016/j.biopha.2019.108654
21. Liu H, Deng H, Zhao Y, Li C, Liang Y. LncRNA XIST/miR-34a axis modulates the cell proliferation and tumor growth of thyroid cancer through MET-PI3K-AKT signaling. *J Exp Clin Cancer Res* (2018) 37:279. doi: 10.1186/s13046-018-0950-9
22. Geng W, Tang H, Luo S, Lv Y, Liang D, Kang X, et al. Exosomes from miRNA-126-modified ADSCs promotes functional recovery after stroke in rats by improving neurogenesis and suppressing microglia activation. *Am J Transl Res* (2019) 11:780–92.
23. Jamali L, Tofigh R, Tutunchi S, Panahi G, Borhani F, Akhavan S, et al. Circulating microRNAs as diagnostic and therapeutic biomarkers in gastric and esophageal cancers. *J Cell Physiol* (2018) 233:8538–50. doi: 10.1002/jcp.26850
24. Guo F, Jiao D, Sui GQ, Sun LN, Gao YJ, Fu QF, et al. Anticancer effect of YWHAZ silencing via inducing apoptosis and autophagy in gastric cancer cells. *Neoplasma* (2018) 65:693–700. doi: 10.4149/neo_2018_170922N603
25. Liu S, Jiang H, Wen H, Ding Q, Feng C. Knockdown of tyrosine 3-monooxygenase/tryptophan 5-monooxygenase activation protein zeta (YWHAZ) enhances tumorigenesis both in vivo and in vitro in bladder cancer. *Oncol Rep* (2018) 39:2127–35. doi: 10.3892/or.2018.6294
26. Chang L, Xu W, Zhang Y, Gong F. Long non-coding RNA-NEF targets glucose transportation to inhibit the proliferation of non-small-cell lung cancer cells. *Oncol Lett* (2019) 17:2795–801. doi: 10.3892/ol.2019.9919
27. Yu W, Li D, Ding X, Sun Y, Liu Y, Cong J, et al. LINC00702 suppresses proliferation and invasion in non-small cell lung cancer through regulating miR-510/PTEN axis. *Aging (Albany NY)* (2019) 11:1471–85. doi: 10.18632/aging.101846
28. Gao BB, Wang SX. LncRNA BC200 regulates the cell proliferation and cisplatin resistance in non-small cell lung cancer via PI3K/AKT pathway. *Eur Rev Med Pharmacol Sci* (2019) 23:1093–101. doi: 10.26355/eurrev_201902_16999
29. Cen WN, Pang JS, Huang JC, Hou JY, Bao WG, He RQ, et al. The expression and biological information analysis of miR-375-3p in head and neck squamous cell carcinoma based on 1825 samples from GEO, TCGA, and peer-reviewed publications. *Pathol Res Pract* (2018) 214:1835–47. doi: 10.1016/j.prp.2018.09.010
30. Chen M, Hu W, Xiong CL, Qu Z, Yin CQ, Wang YH, et al. miR-22 targets YWHAZ to inhibit metastasis of hepatocellular carcinoma and its down-regulation predicts a poor survival. *Oncotarget* (2016) 7:80751–64. doi: 10.18632/oncotarget.13037

Conflict of Interest: The authors declare that the research was conducted in the absence of any commercial or financial relationships that could be construed as a potential conflict of interest.

frontiers in Genetics

ORIGINAL RESEARCH
published: 28 April 2021
doi: 10.3389/fgene.2021.612011

TGFβ1: An Indicator for Tumor Immune Microenvironment of Colon Cancer From a Comprehensive Analysis of TCGA

*Jinyan Wang[1,2], Jinqiu Wang[3], Quan Gu[4], Yan Yang[1], Yajun Ma[1] and Quan'an Zhang[1]**

[1] Department of Oncology, Nanjing Jiangning Hospital, The Affiliated Jiangning Hospital of Nanjing Medical University, Nanjing, China, [2] Department of Oncology, The Affiliated Jiangning Hospital of Jiangsu Health Vocational College, Nanjing, China, [3] Department of Oncology, Dafeng People's Hospital, Yancheng, China, [4] Department of Oncology, The Affiliated Cancer Hospital of Nanjing Medical University, Nanjing, China

Background: Tumor microenvironment (TME) and tumor-infiltrating immune cells (TICs) greatly participate in the genesis and development of colon cancer (CC). However, there is little research exploring the dynamic modulation of TME.

Methods: We analyzed the proportion of immune/stromal component and TICs in the TME of 473 CC samples and 41 normal samples from The Cancer Genome Atlas (TCGA) database through ESTIMATE and CIBERSORT algorithms. Correlation analysis was conducted to evaluate the association between immune/stromal component in the TME and clinicopathological characteristics of CC patients. The difference analysis was performed to obtain the differentially expressed genes (DEGs). These DEGs were further analyzed by GO and KEGG enrichment analyses, PPI network, and COX regression analysis. Transforming growth factor β1 (TGFβ1) was finally overlapped from the above analysis. Paired analysis and GSEA were carried out to understand the role of TGFβ1 in colon cancer. The intersection between the difference analysis and correlation analysis was conducted to learn the association between TGFβ1 and TICs.

Results: Our results showed that the immune component in the TME was negatively related with the stages of CC. GO and KEGG enrichment analysis revealed that 1,110 DEGs obtained from the difference analysis were mainly enriched in immune-related activities. The intersection analysis between PPI network and COX regression analysis indicated that TGFβ1 was significantly associated with the communication of genes in the PPI network and the survival of CC patients. In addition, TGFβ1 was up-regulated in the tumor samples and significantly related with poor prognosis of CC patients. Further GSEA suggested that genes in the TGFβ1 up-regulated group were enriched in immune-related activities and the function of TGFβ1 might depend on the communications with TICs, including T cells CD4 naïve and T cells regulatory.

Conclusion: The expression of TGFβ1 might be an indicator for the tumor immune microenvironment of CC and serve as a prognostic factor. Drugs targeting TGFβ1 might be a potential immunotherapy for CC patients in the future.

Keywords: tumor-infiltrating immune cells, TGFβ1, colon cancer, indicator, tumor immune microenvironment

OPEN ACCESS

Edited by:
Xiaochen Wang,
University of Texas Southwestern Medical Center, United States

Reviewed by:
Olivia Fromigue,
Institut National de la Santé et de la Recherche Médicale (INSERM), France
Shengli Li,
Shanghai Jiao Tong University, China

***Correspondence:**
Quan'an Zhang
quananzhang_doctor@163.com

Specialty section:
This article was submitted to Cancer Genetics, a section of the journal Frontiers in Genetics

Received: *30 September 2020*
Accepted: *26 March 2021*
Published: *28 April 2021*

Citation:
Wang J, Wang J, Gu Q, Yang Y, Ma Y and Zhang Q (2021) TGFβ1: An Indicator for Tumor Immune Microenvironment of Colon Cancer From a Comprehensive Analysis of TCGA. Front. Genet. 12:612011. doi: 10.3389/fgene.2021.612011

BACKGROUND

Colon cancer (CC) is one of the most common causes of cancer-associated mortality in the United States (Goding Sauer et al., 2020). Although the overall incidence and mortality continue to decline, the incidence in young and middle-aged adults keeps rising (Siegel and Miller, 2020). Although considerable efforts have been made to improve the clinical outcomes of CC patients, CC is still a fatal disease (Zhang et al., 2019; Pan et al., 2020). Additionally, curative effect of multiple treatments, including chemotherapy, immunotherapy, and targeted therapy, are obviously reduced by drug resistance (Gao Q. et al., 2020). Hence, it is urgent to further explore the detailed molecular mechanism of CC and to identify the vital prognosis biomarkers of CC.

Recently, accumulating research has been focusing on understanding the role of the tumor microenvironment (TME) in the genesis and development of cancers. The TME is composed of multiple immune cells, stromal cells, extracellular matrix, and kinds of cytokines and chemokines (Xu et al., 2019). These components in the TME are in a dynamic process, greatly participate in tumor growth, invasion, metastasis, and drug resistance (Li and Wang, 2020; Mikami et al., 2020; Wang S. et al., 2020; Yang et al., 2020). The activation of tumor-infiltrating immune cells is an important parameter that acts as a prognostic biomarker and affects various tumor biological processes (Hu C. et al., 2020; Zhu et al., 2020). For instance, CD8-positive (CD8+) tumor-infiltrating lymphocytes (TILs) in the peri-tumoral microenvironment are significantly correlated with poor clinical outcome of salivary gland carcinoma patients (Kesar et al., 2020). Mechanically, interleukin-38 advances tumor growth by affecting $CD8^+$ TILs in the TME of lung cancer (Kinoshita et al., 2020). In addition, dual suppression of both PI3K-γ and colony stimulating factor-1/colony stimulating factor-1 receptor (CSF-1/CSF-1R) pathways in tumor associated macrophages (TAM) could remodel tumor immune microenvironment (TIME) and synergistically activate antitumor immune responses in pancreatic cancer (Li et al., 2020).

In the past 10 years, tumor-infiltrating immune cells (TICs) have emerged as potential therapeutic targets. The novel therapeutic strategy, known as immune checkpoint inhibition, focuses on inhibiting the molecular communication between tumor cells and immune cells. Cytotoxic T-lymphocyte-associated protein 4 (CTLA-4) and programmed cell death protein 1 (PD-1), commonly expressed on activated T-cells, have been recognized as the most reliable targets for the

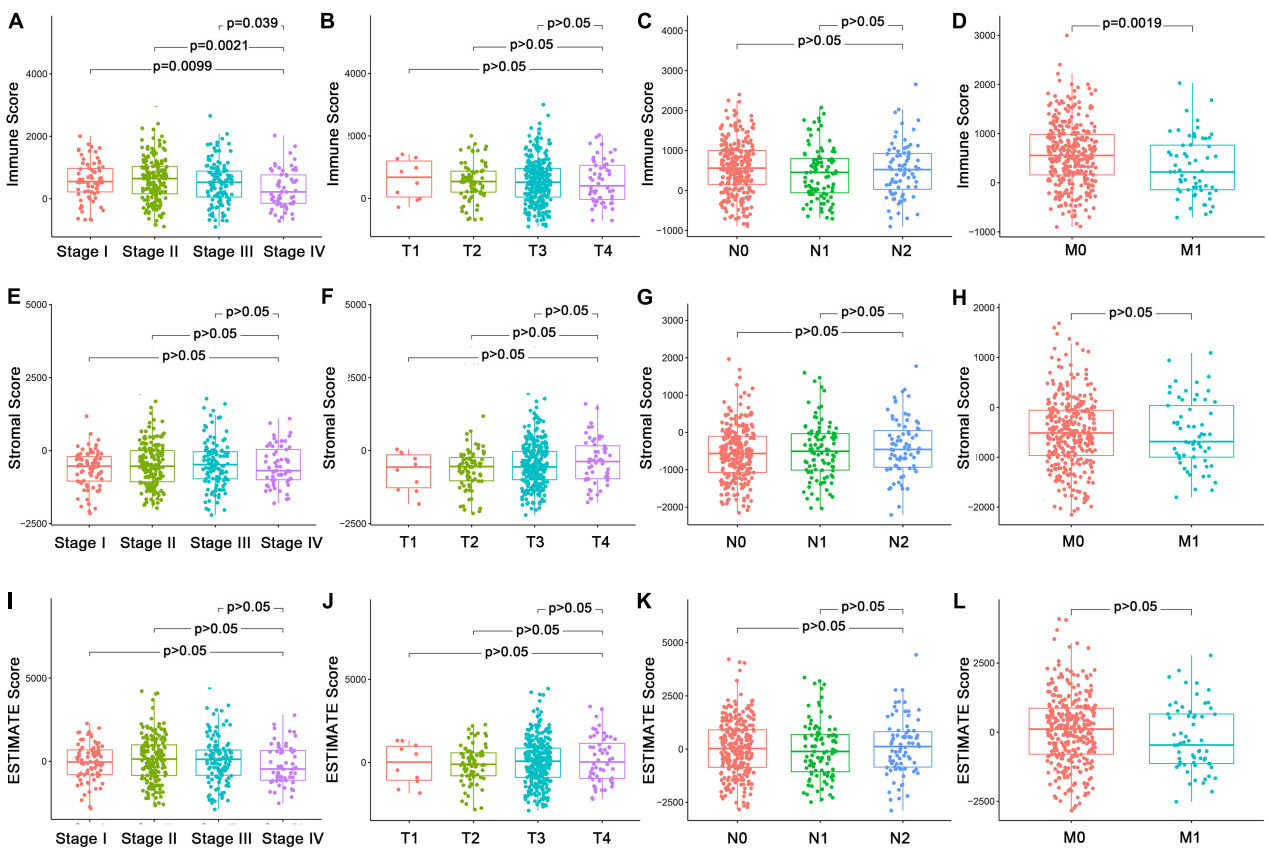

FIGURE 1 | Association of Immune Score, Stromal Score, and Estimate Score with the clinic–pathological features of CC Patients. **(A–D)** Association of Immune Score with stages and TNM classification by Kruskal–Wallis rank sum test. **(E–H)** Association of Stromal Score with stages and TNM classification Kruskal–Wallis rank sum test. **(I–L)** Association of Estimate Score with stages and TNM classification Kruskal–Wallis rank sum test.

immunological therapy of multiple cancers (Rotte, 2019; Liu and Zheng, 2020; Yu et al., 2020). According to the abundant clinical trials, PD-1 blocker alone, or combined with CTLA-4 have been proven to have good curative effect in various cancer types, including CC (Seidel et al., 2018; Guo et al., 2020). However, there is still a significant proportion of cancer patients who do not respond or initially respond and later develop tumor progression, indicating the existence of immune resistance (Gao A. et al., 2020). Fortunately, research has suggested that the TME and infiltrating immune cells are specific to different cancer types and might explain the immunotherapeutic responsiveness of cancers (Koirala et al., 2016; Jansen et al., 2019). As a result, further exploration of immune infiltration in CC TME is essential in clarifying the mechanisms underlying the progression of CC.

In this study, to investigate potential signatures for CC patients, we obtained a list of TME-related genes of prognostic value using immune/stromal scores after ESTIMATE algorithm-processing in multiple cohorts. Functional annotations and immune infiltration correlation were analyzed for significant hub genes. We hypothesized that TGFβ1 was correlated with poor prognosis, might act as an indicator for tumor immune microenvironment of CC, and potential immune therapies targeting TGFβ1 might provide new hope to colon patients.

MATERIALS AND METHODS

Data Collection Based on TCGA

We collected the transcriptome RNA-seq profiling, the clinical data of CC tissues, and normal colon tissues from the TCGA database[1]. Ultimately, 514 CC cases (473 tumor samples and 41 normal samples) and the corresponding clinical data were included. We also selected the gene chip of CC (GSE41258) from the GEO database[2]. GSE41258 contained 186 primary CC tissues and 54 corresponding normal colon tissues.

Calculation of Immune Score, Stromal Score, and ESTIMATE Score

R language version 3.6.3[3] was used to analyze the proportion of immune/stromal component in TME of each tumor sample through ESTIMATE algorithm. Immune Score, Stromal Score, and ESTIMATE Score reflected the corresponding ratio of immune component, stromal

[1]https://portal.gdc.cancer.gov/

[2]https://www.ncbi.nlm.nih.gov/

[3]https://www.r-project.org/

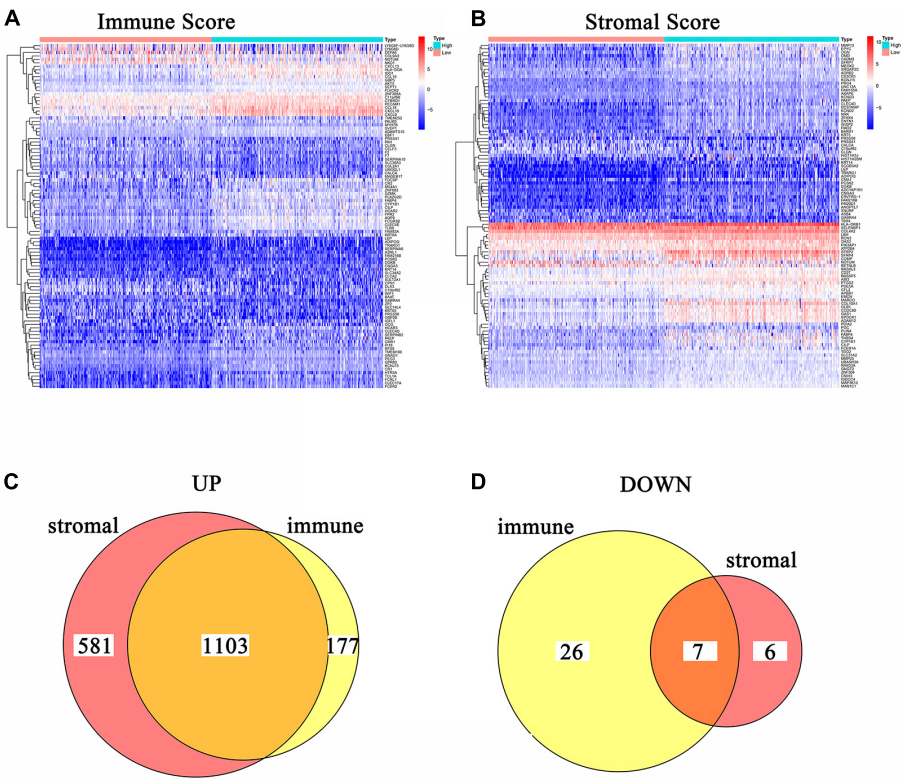

FIGURE 2 | Heatmaps and Venn plots of DEGs. **(A)** Heatmap for DEGs conducted by comparing high Immune Score tumor samples with low Immune Score tumor samples. Row name: the gene name. Column name: the ID of samples which are not shown in plot. DEGs were examined by Wilcoxon rank sum test with $q = 0.05$ and $\log2^{\text{fold-change}} > 1$ as the significance threshold. **(B)** Heatmap for DEGs conducted by comparing high Stromal Score tumor samples with low Stromal Score tumor samples. Row name: the gene name. Column name: the ID of samples which are not shown in plot. DEGs were examined by Wilcoxon rank sum test with $q = 0.05$ and $\log2^{\text{fold-change}} > 1$ as the significance threshold. **(C,D)** Venn plots of commonly overexpressed and downexpressed DEGs shared by Immune Score and Stromal Score.

component, and the sum of both in the TME. The higher score represented the larger ratio of immune/stromal component in the TME.

Survival Analysis

Survival and survminer packages in R were used for the survival analysis. Kaplan–Meier plot and log-rank tests were conducted to evaluate the relationship between survival rates and differentially expressed genes (DEGs). $P < 0.05$ was considered to be statistically significant.

Differential Analysis of Scores With Clinicopathological Characteristics

The differential analysis was performed by R language. Wilcoxon rank sum and Kruskal–Wallis rank sum test were based on the number of TNM stages for comparison.

Affirmation of DEGs Between High-Score and Low-Score Groups and Heatmaps

A total of 473 tumor samples were classified into the high-score group and the low-score group relying on the comparison

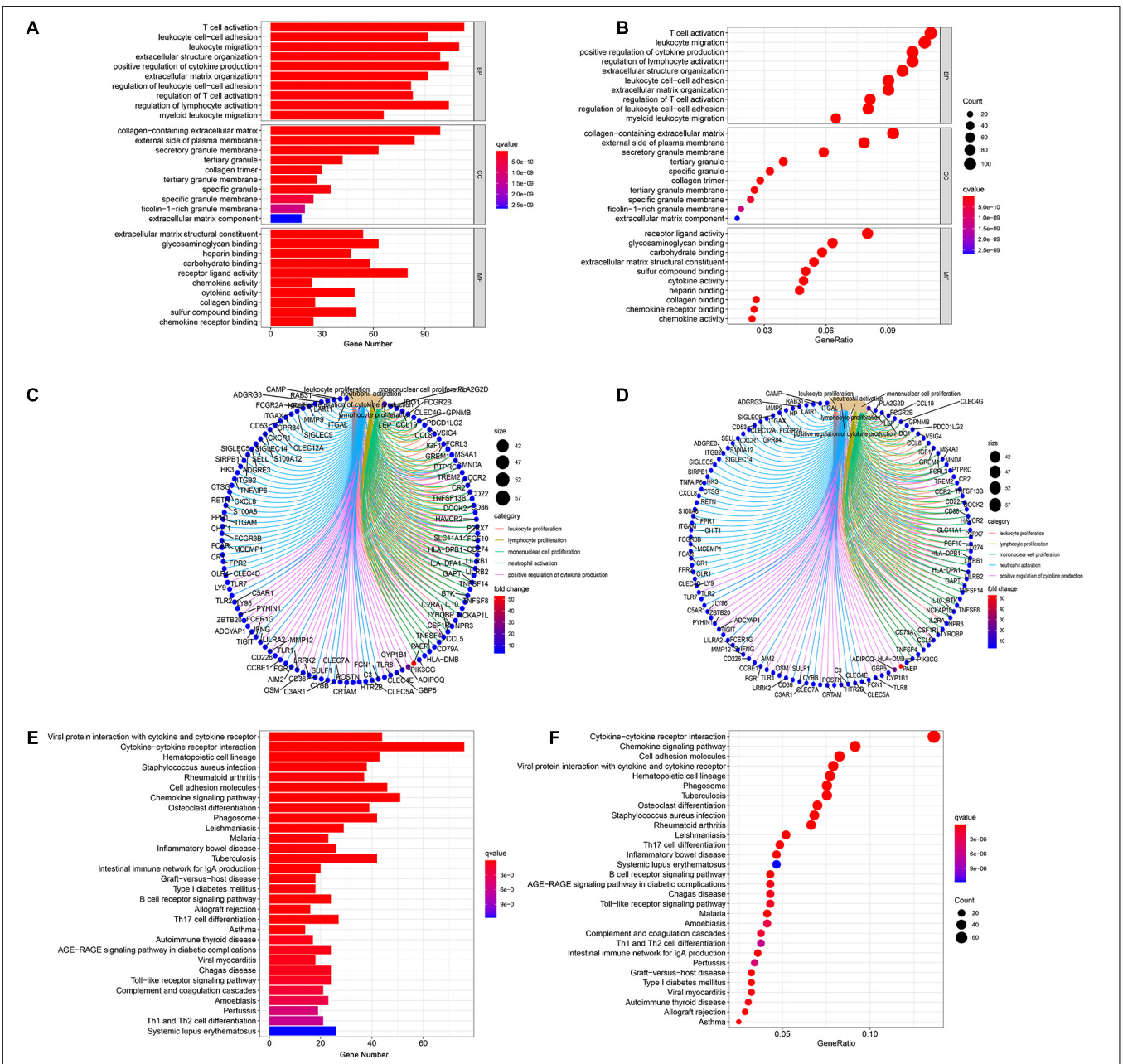

FIGURE 3 | Enrichment analysis GO and KEGG for 1,110 DEGs. **(A–C)** GO enrichment analysis for 1,110 DEGs, $p < 0.05$ was considered to be enriched significantly. **(D–F)** KEGG enrichment analysis for 1,110 DEGs, $p < 0.05$ was considered to be enriched significantly.

with the median score. Data analysis was performed by package limma in R. The fold change was calculated by log2 (high-score group/low-score group). A fold change (FC) > 1 and false discovery rate (FDR) < 0.05 were set up to screen DEGs. Heatmaps of DEGs were generated by pheatmap package in R.

Gene Ontology (GO) and Kyoto Encyclopedia of Genes and Genomes (KEGG) Enrichment Analyses

GO and KEGG enrichment analyses of 1,110 DEGs were carried out by clusterProfiler, enrichplot, and ggplot2 packages in R. $P < 0.05$ was considered to be statistically significant.

Protein–Protein Interaction (PPI) Network and Gene Set Enrichment Analysis

PPI network was constructed by the Search Tool for Retrieval of Interacting Genes/Proteins (STRING) database (version 11.0). Nodes with confidence of interactive relationship greater than 0.95 were applied. And the network was further reconstructed with Cytoscape of version 3.6.1. A functional profile of the gene set derived from the PPI was further retrieved by using Gene Set Enrichment Analysis (GSEA) 4.1.0. $P < 0.05$ was considered to be statistically significant.

COX Regression Analysis

Univariate COX regression was performed by package survival in R.

Tumor-Infiltrating Immune Cell Profile

TIC abundance profile in CC tumor samples was estimated by using CIBERSORT computational method. Finally, a total of 473 CC patients' tumor samples were included for further analysis with $p < 0.05$.

Correlation Analysis

Correlation analysis was carried out by using spearman's correlation analysis.

Analysis Process

We first downloaded the transcriptome RNA-seq profiling, the clinical data of CC tissues and normal colon tissues from the TCGA database, and gene chip of GSE41258 from GEO database. ESTIMATE algorithms were then used to analyze the proportion of immune/stromal component in the TME. Correlation analysis was carried out to evaluate the association between immune/stromal score and the clinic–pathological staging of CC Patients. The intersection analysis was used to obtain DEGs shared by immune score and stromal score. PPI

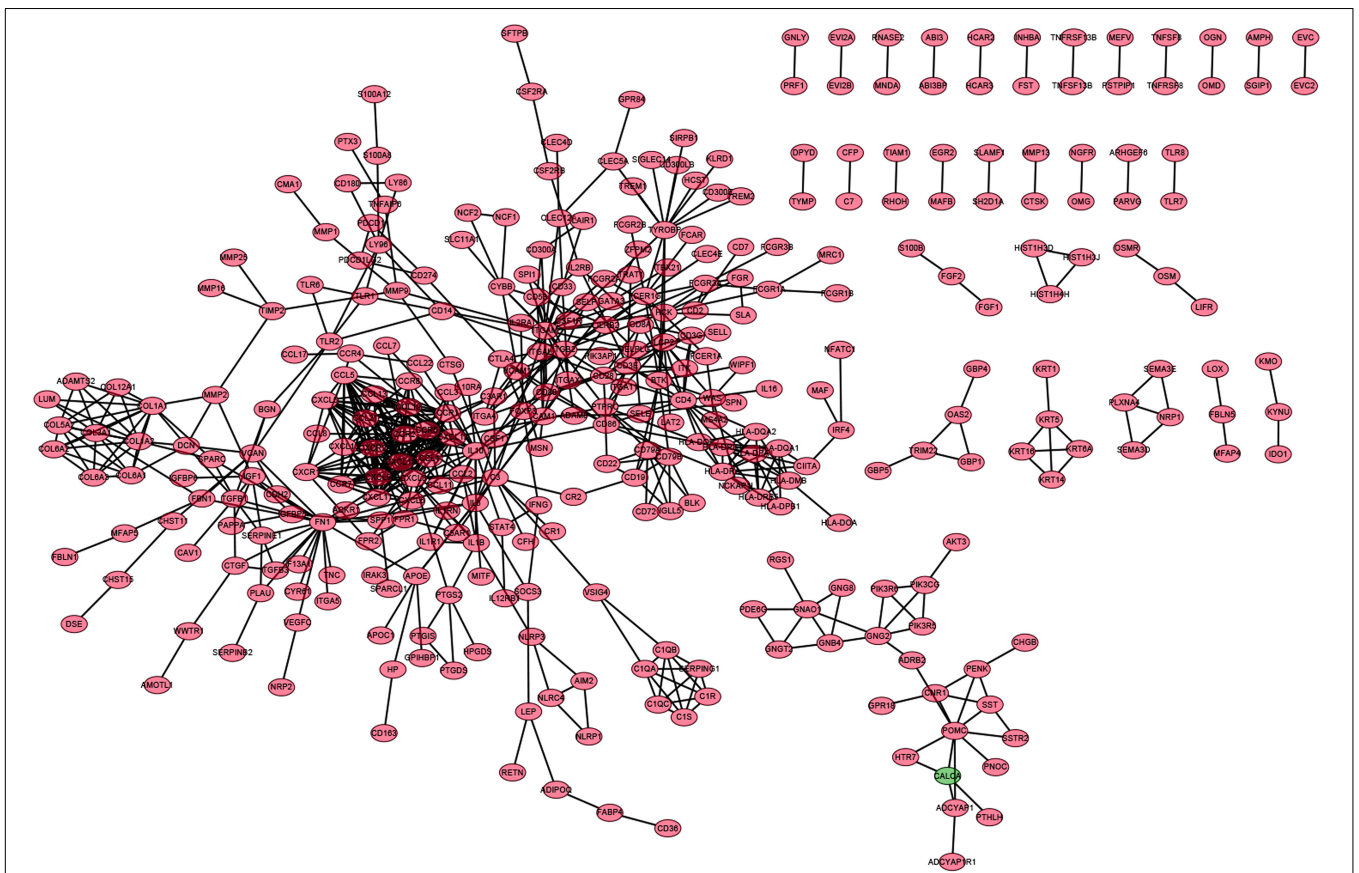

FIGURE 4 | PPI network of DEGs. PPI network was carried out with the nodes with interaction confidence value > 0.95.

network and univariate COX regression analysis were further conducted. The intersection analysis was carried out to find the DEGs which were both the top leading nodes in PPI network and the top factors of univariate COX regression. Finally, transforming growth factor β1 (TGFβ1) was obtained, and we focused on TGFβ1 and TGFβ signaling pathway component (smad and TGFβR) for the subsequent series of analysis, such as expression pattern analysis, survival analysis, clinic–pathological features correlation analysis, COX regression, GSEA, and correlation analysis with TICs.

RESULTS

Scores Were Associated With the Clinic–Pathological Features of CC Patients

In order to explore the underlying associations between the ratio of immune/stromal components and the clinic-pathological features (**Supplementary Table 1**), we analyzed the TNM stages of CC patients regarding Immune Score, Stromal Score, and ESTIMATE Score (**Figure 1**). Interestingly, There were significant differences in the Immune Score in stage I compared with stage II, III, and IV (**Figure 1A**, $p = 0.0099$, 0.0021, 0.039). In particular, Immune Score was negatively related with M classification of TNM stages (**Figure 1D**, $p = 0.0019$). However, Stromal Score and ESTIMATE Score had nothing to do with the TNM stages of CC patients (**Figures 1E–L**, $p > 0.05$). The above results indicated that the proportion of immune components might play an important role in the advance of CC, especially distant metastasis.

DEGs Shared by Immune Score and Stromal Score Were Significantly Associated With Immune-Related Activities

In order to acquire the detailed gene profile in TME, the difference analysis between high score and low score tumor samples were conducted. The results displayed that a total of 1,313 DEGs were acquired from the immune score group (high score tumor samples vs. low score tumor samples), among which 1,280 DEGs were up-regulated and 33 DEGs were down-regulated when compared to the median (**Figure 2A**). In addition, 1,697 DEGs were acquired from the stromal

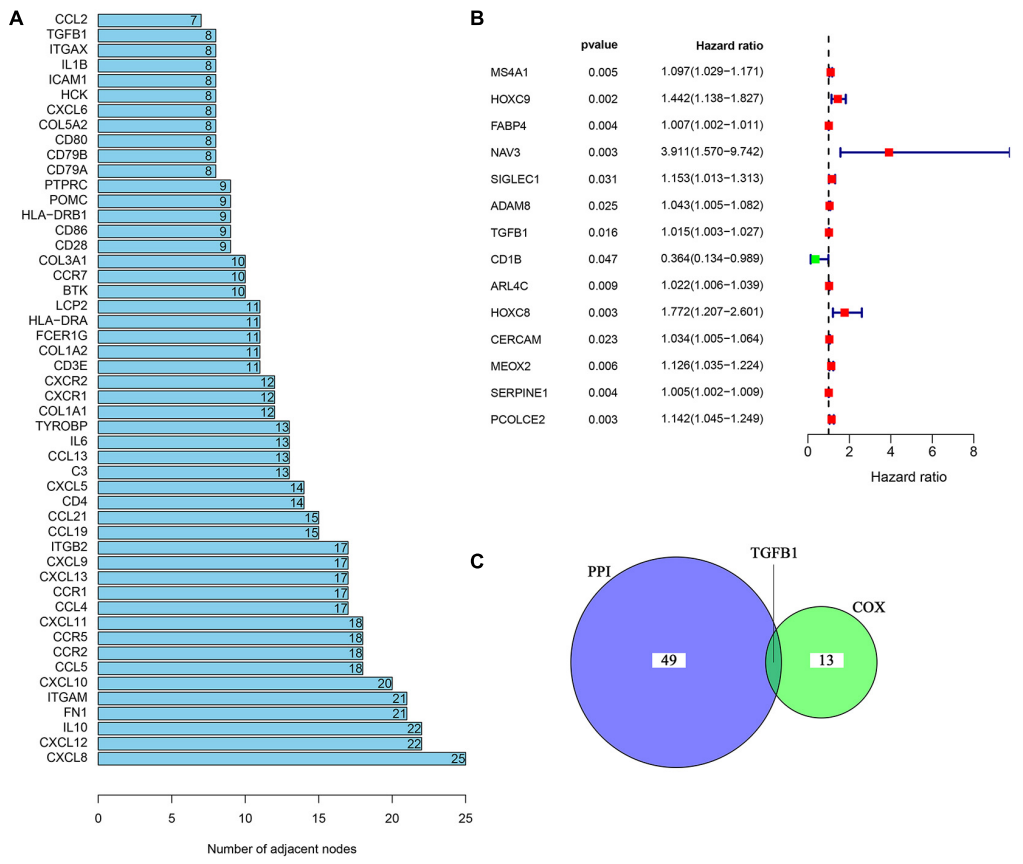

FIGURE 5 | Univariate COX regression analysis of DEGs. **(A)** The top 50 genes ranked by the number of nodes. **(B)** Univariate COX regression analysis of DEGs. $p < 0.05$ was considered as the significance threshold. **(C)** Venn plot displays the common genes shared by the top 50 genes in PPI and top significant genes in univariate COX regression analysis.

score group, including 1,684 up-regulated genes and 13 down-regulated genes (**Figure 2B**). Furthermore, the intersection analysis was carried out to obtain the up-regulated or down-regulated genes both in the immune score and stromal score. The Venn plot displayed that 1,103 genes were up-regulated and 7 genes were down-regulated in both the immune score and stromal score (**Figures 2C,D**). These DEGs, a total of 1,110 genes, might play a significant role in regulating the status of the TME. Therefore, GO enrichment analysis and KEGG enrichment analysis were used to evaluate the functions of these DEGs. GO enrichment analysis revealed that these DEGs were closely associated with immune-related GO terms, including T cell activation, leukocyte migration, positive regulation of cytokine production, and so on (**Figures 3A–C**). Besides, KEGG enrichment analysis indicated that 1,110 DEGs were significantly related with cytokine-cytokine receptor interaction, chemokine signaling pathway, positive regulation of cytokine production, mononuclear cell proliferation and so on (**Figures 3D–F**). From above, the functions of these DEGs seemed to be significantly associated with immune-related activities and might be a predominant characteristic of the TME in CC.

Intersection Analysis Between the PPI Network and Univariate COX Regression

In order to further explore the underlying mechanisms regarding these 1,110 DEGs, we first constructed the PPI network by using STRING database and Cytoscape software. The detailed interactions between 1,110 DEGs were displayed in **Figure 4**. The top 50 DEGs ranked by the number of nodes were shown in **Figure 5A**. Univariate COX regression analysis was conducted to find the most significant DEGs regarding the survival of CC patients (**Figure 5B**). Finally, the intersection analysis was carried out to find the DEGs which were both the top 50 leading nodes in the PPI network and the top 14 factors of the univariate COX regression. Transforming growth factor β1 (TGFβ1) was overlapping from the above analysis (**Figure 5C**).

TGFβ1 Was Associated With the Survival and Clinic–Pathological Staging of CC Patients

TGFβ1 was a pleiotropic cytokine and played a vital role in immune reconstruction (Chen et al., 2012; Kövy et al., 2020). Teixeira et al. (2011) discovered that TGFβ1 affected non-small cell lung cancer (NSCLC) susceptibility with impact in cellular microenvironment. In our study, the pairing analysis revealed that TGFβ1 was up-regulated in the tumor samples compared to that in the paired normal samples from the same patients (**Figure 6A**, p = 0.0025). We then divided CC samples into two groups, including TGFβ1 high-expression group and TGFβ1 low-expression group. The survival analysis revealed that CC patients with up-regulated TGFβ1 had shorter survival than that of down-regulated TGFβ1 (**Figure 6B**, p = 0.036). Specifically, the up-regulated TGFβ1 was related

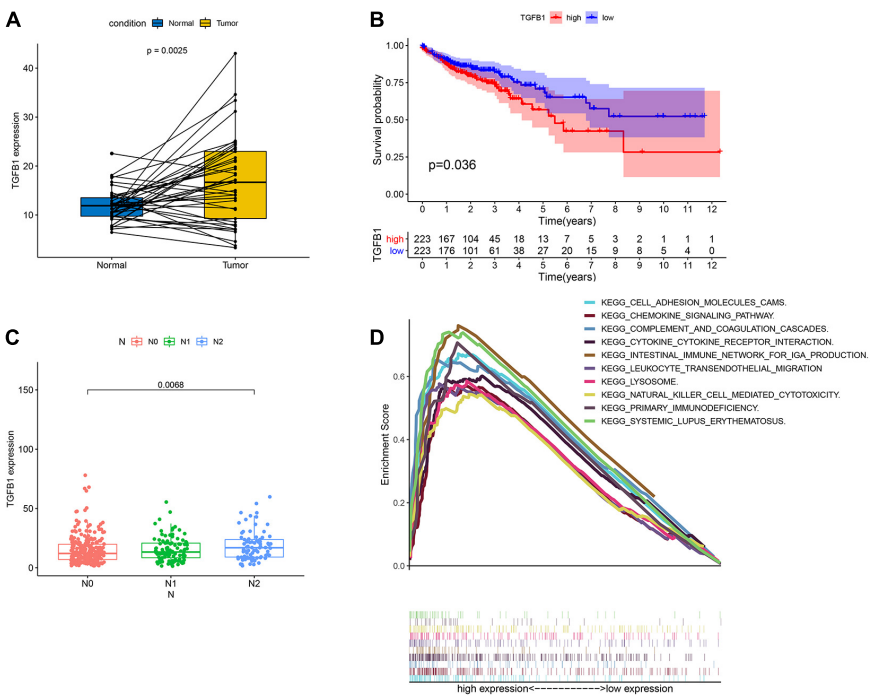

FIGURE 6 | The expression of TGFβ1 in CC patients and the association with survival, TNM classification and GSEA. **(A)** Paired differentiation analysis for expression of TGFβ1 in the colon cancer samples and the paired normal samples deriving from the same patient (p = 0.0025 by Wilcoxon rank sum test). **(B)** Survival analysis for colon cancer patients with high expression or low expression of TGFβ1. p = 0.036 by log-rank test. **(C)** Association of the expression of TGFβ1 with N stage by Kruskal–Wallis rank sum test; p = 0.0068. **(D)** GSEA for tumor samples with high expression or low expression of TGFβ1.

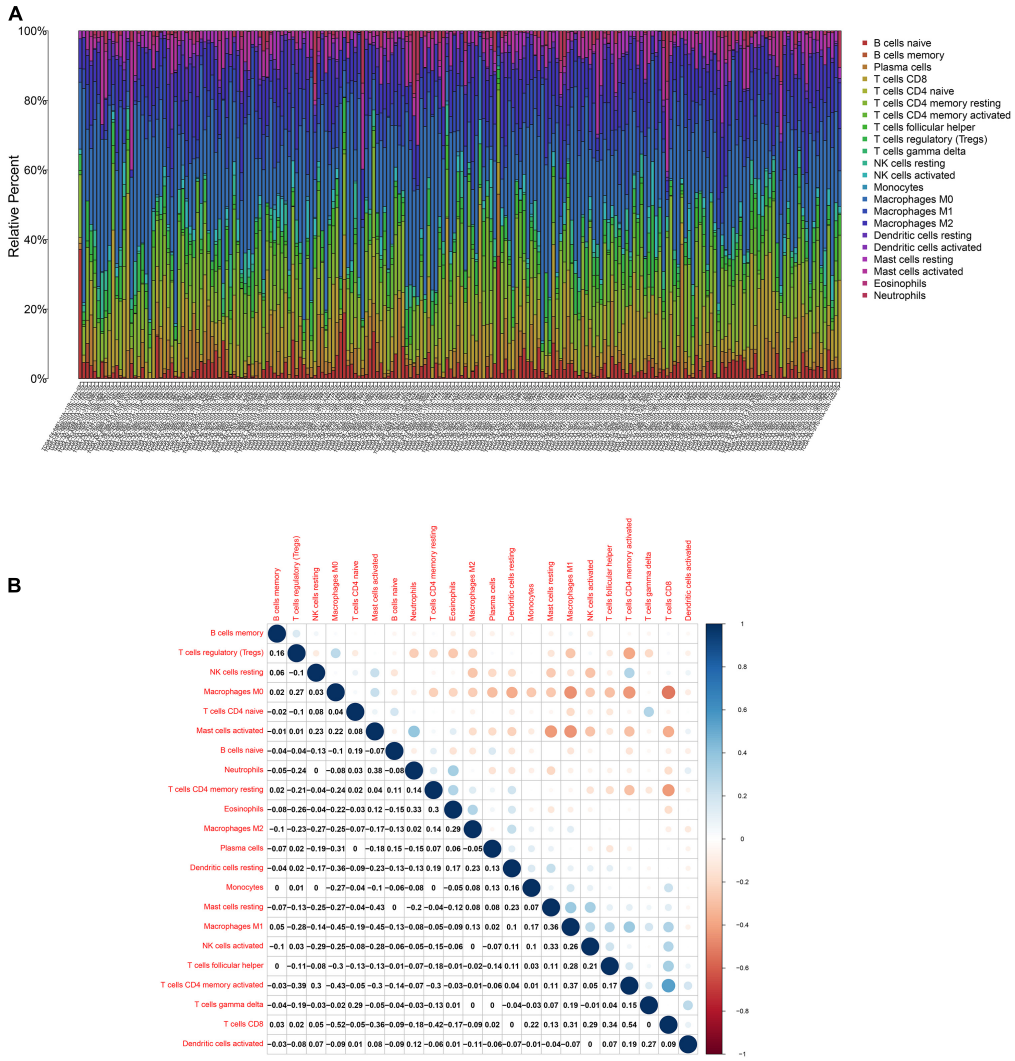

FIGURE 7 | TIC profile. **(A)** Barplot displays the ratio of 22 kinds of TICs in colon cancer samples. Column names: sample ID. **(B)** Heatmap displays the association between 22 kinds of TICs; each spot represents the *p*-value of correlation between two kinds of cells; Pearson coefficient was carried out for significance test.

to the lymph node stage of CC patients (**Figure 6C**). In conclusion, TGFβ1 was negatively associated with the prognosis of CC patients.

TGFβ1 Might Participate in the Modulation of the TME

Considering that the expression of TGFβ1 was negatively associated with the survival and lymph node stages of CC patients, GSEA was carried out in the up-regulated and the down-regulated groups compared with the median level of TGFβ1 expression, respectively. The genes in TGFβ1 up-regulated group were primarily enriched in immune-related activities, including cell adhesion molecules, chemokine signaling pathway, complement and coagulation, cytokine-cytokine receptor interaction and so on (**Figure 6D**). Nonetheless, few genes were enriched in the TGFβ1 down-regulated group. The above results indicated that TGFβ1 might participate in the modulation of TME.

TGFβ1 Signaling Pathway Was Associated With TICs in TIME

To further affirm the connection between TGFβ1 and the immune microenvironment, we applied CIBERSORT algorithm to examine the ratio of tumor-infiltrating immune cells in CC (**Figures 7A,B**). The difference test indicated that 5 kinds of TICs were significantly related with the expression of TGFβ1, such as T cells CD4 naïve, T cells CD4 memory activated, Tregs, NK cells resting, and eosinophils (**Figure 8A**). The correlation test revealed that neutrophils, Tregs, and T cells CD8 were positively related with the expression of TGFβ1, and T cells CD4 naïve was negatively related with the expression of TGFβ1 (**Figure 8B**). The intersection between the difference test and

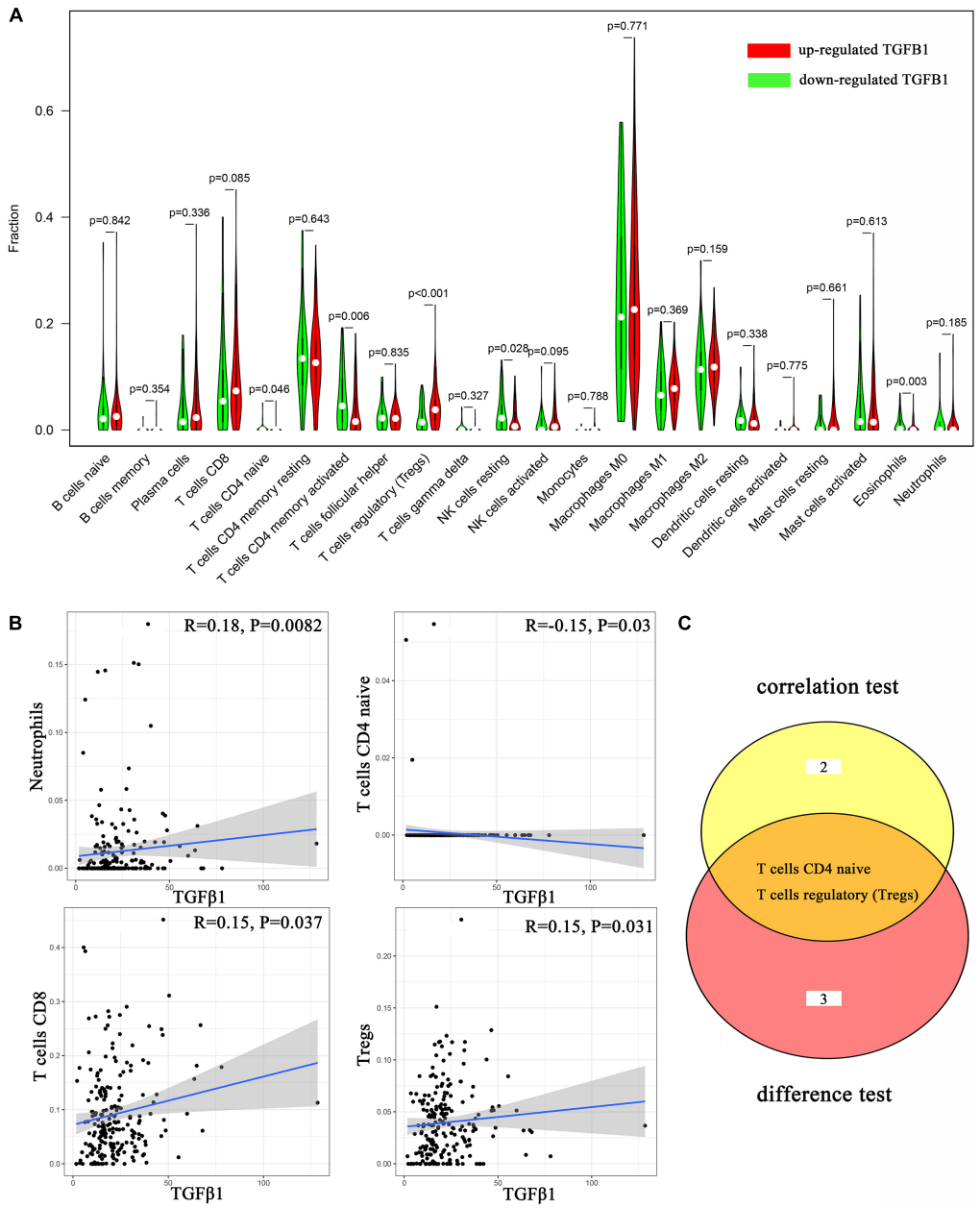

FIGURE 8 | Correlation analysis between TICs and TGFβ1. **(A)** Violin plot displays the differentiation of 22 kinds of TICs between colon cancer samples with high or low expression of TGFβ1; Wilcoxon rank sum was carried out for the significance test. **(B)** Scatter plot displays the association between 4 kinds of TICs and the expression of TGFβ1; Pearson coefficient was carried out for the correlation test; $p < 0.05$ was considered as the significance threshold and plotted. **(C)** Venn plot displays two kinds of TICs shared by difference and correlation tests showed in violin and scatter plots, respectively.

correlation test suggested that T cells CD4 naïve and Tregs were potentially associated with the expression of TGFβ1 (**Figure 8C** and **Supplementary Table 2**). In order to further confirm the correlation between TGFβ1 and TICs in TIME of CC, we conducted correlation analysis by using the data in GSE41258. The result indicated that several TICs, including B cells memory, T cells follicular helper, Tregs, NK cells resting, and dendritic cells resting, were significantly correlated with the expression level of TGFβ1 (**Figure 9**). From the above, we speculated that TGFβ1 might closely communicate with Tregs to greatly participate in the immune activities of the TIME in CC.

In addition, it was known that TGFβ1 participated in multiple biological processes through binding to TGFβR, including TGFβR1, TGFβR2, and TGFβR3 (Wang et al., 2019). We conducted correlation analysis between TGFβR and TICs in CC and found out that TGFβR took a great part in communicating

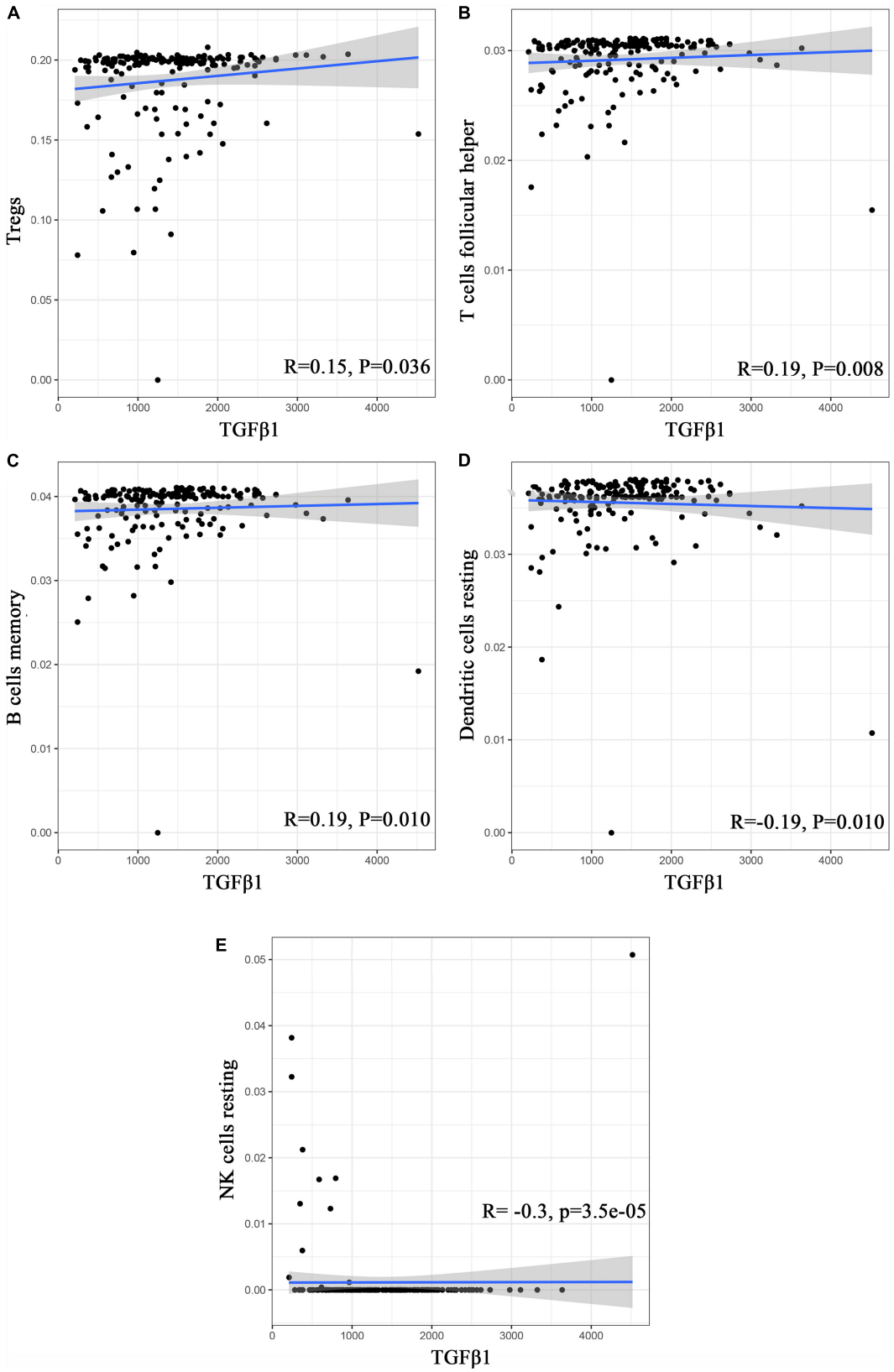

FIGURE 9 | Correlation analysis between TICs and TGFβ1 in the gene chip of GSE41258. **(A–E)** Scatter plot displays the association between 4 kinds of TICs and the expression of TGFβ1; Pearson coefficient was carried out for the correlation test; $p < 0.05$ was considered as the significance threshold and plotted.

TABLE 1 | Correlation analysis between TGFβR and TICs in TIME of CC.

TGFβ R	TICs	*P*–value
TGFβR1	B cells naive	0.040933844
	T cells CD8	8.39E-07
	T cells CD4 memory resting	0.000373437
	T cells regulatory (Tregs)	0.020476451
	NK cells activated	0.004390418
	Neutrophils	0.00519773
TGFβR2	B cells naive	0.045588132
	B cells memory	0.010537954
	Plasma cells	0.009197408
	T cells CD8	2.18E-07
	T cells CD4 memory resting	0.000106305
	T cells CD4 memory activated	0.002443409
	T cells follicular helper	0.002419206
	NK cells activated	2.85E-08
	Macrophages M0	0.013539433
	Macrophages M1	0.012813639
TGFβR3	B cells memory	0.00405551582282848

p > 0.05 was not displayed.

TABLE 2 | Correlation analysis between SMAD and TICs in TIME of CC.

SMAD	TICs	*P*-value
SMAD1	B cells naive	0.021093
	T cells CD4 memory resting	2.83E-06
	T cells regulatory (Tregs)	0.005022
	NK cells activated	0.010779
	Macrophages M1	0.021773
	Mast cells resting	0.018896
SMAD2	T cells CD4 memory resting	0.001936
	T cells follicular helper	0.020209
	T cells regulatory (Tregs)	4.25E-06
	Macrophages M0	0.000262
	Macrophages M1	0.04713
	Dendritic cells activated	0.004243
	Neutrophils	0.025751
SMAD3	T cells follicular helper	0.027115
	T cells gamma delta	0.032897
	Macrophages M2	0.041467
SMAD4	Plasma cells	0.012128
	T cells CD8	0.022337
	T cells CD4 memory activated	0.020959
	T cells follicular helper	0.003017
	T cells regulatory (Tregs)	7.93E-05
	Macrophages M0	0.000796
	Macrophages M1	0.002791
	Neutrophils	0.036174
SMAD5	B cells naive	0.000237
	T cells CD8	0.0007
	T cells CD4 memory resting	1.38E-09
	T cells regulatory (Tregs)	3.15E-06
	NK cells activated	0.029976
SMAD6	T cells CD8	0.047908
	T cells regulatory (Tregs)	2.54E-06
SMAD7	T cells CD8	0.021056
	T cells CD4 memory activated	8.65E-06
	T cells regulatory (Tregs)	6.54E-06
	NK cells activated	9.27E-05
	Macrophages M0	3.47E-06
	Macrophages M1	0.003951
SMAD9	B cells naive	0.000231
	T cells CD8	2.67E-07
	T cells CD4 naive	0.048259
	T cells CD4 memory resting	5.00E-08
	T cells CD4 memory activated	9.27E-05
	T cells follicular helper	0.003673
	NK cells activated	0.021077
	Macrophages M1	0.039982
	Macrophages M2	0.026902

p > 0.05 was not displayed.

with TICs in the TIME of CC (**Table 1**). In addition, smad proteins were critical downstream mediators of TGFβ signaling pathway and regulated the transcription of direct target genes of TGF-β (Luo, 2017). Corresponding correlation analysis was also conducted to evaluate the relationship between smad and TICs in the TIME of CC. The result showed that smad1-7, 9 were significantly associated with various TICs in the TIME of CC (**Table 2**). In conclusion, not only TGFβ1, but also TGFβ signaling pathway components were closely related with the TIME of CC, partly through communicating with multiple TICs. These results further indicated the potential role of TGFβ1 in the immune activity of the TME.

DISCUSSION

In recent years, great advances have been made in the exploration of the CC treatment. It gradually moves away from chemotherapy, which has been the standard treatment of CC for decades, toward immunotherapy that modulates immune responses against tumor cells (Franke et al., 2019; Chalabi et al., 2020). In the last few years, the TME was found to play a vital role in the initiation and progression of tumorigenesis (Corn et al., 2020; Uttam et al., 2020; Wang J. et al., 2020; Zhang Z. et al., 2020). Research has indicated that the TIME was closely related with the prognosis of cancers, including hepatocellular carcinoma (Hu Z.Q. et al., 2020), lung adenocarcinoma, lung squamous cell carcinoma (Zhang L. et al., 2020), and so on. Therefore, it is of great benefit to identify the vital potential biomarkers associated with the remodeling of the TME and prognosis, and develop more specific drugs against CC.

In this study, we attempted to comprehensively assess the TME of CC and identify TME-associated genes that related with the survival and clinic–pathological features of CC patients from the TCGA database. Firstly, we evaluated the proportion of the immune/stromal component in the TME and found out that the immune/stromal component was associated with the clinic–pathological staging of CC patients. Secondly, DEGs, shared by immune score and stromal score, were found out and further explored by the PPI network and univariate COX regression

analysis. Thirdly, TGFβ1 came to our eyes and we carried out survival analysis, clinic–pathological features correlation analysis, COX regression, GSEA, and TICs correlation analysis. Finally, based on the above research, we concluded that TGFβ1 and TGFβ signaling pathway components played a significant role in the TIME of CC potential through communicating with various TICs. TGFβ1 might be a potential biomarker for the status of the TIME in CC patients.

In Chen et al. (2017) carried out a meta-analysis and found out that up-regulated TGF-β had a favorable impact on overall survival (OS) and disease-free survival (DFS) in CC patients and might be used as a prognostic biomarker for CC patients undergoing surgery. Later, Zessner-Spitzenberg et al. (2019) also concluded that elevated levels of TGFβ served as a poor prognostic biomarker of CC. The TGFβ family included three isoforms, TGFβ1, TGFβ2, and TGFβ3, with TGFβ1 being the most prominent (Clark and Coker, 1998). TGFβ1 was a multi-functional cytokine and regulated a variety of biologic processes in the host, such as cell proliferation, apoptosis, differentiation, migration, invasion and angiogenesis (Massagué, 2000). In addition, it was aberrantly activated in the late-stages of tumorigenesis and the dysregulation of TGFβ1 signaling pathway contributed to various aspects of cancer progression (Zarzynska, 2014; Tang et al., 2018). Recently, studies indicated that TGFβ1 greatly participated in numerous immune regulatory functions, such as tumor immune suppression and escape (Hargadon, 2016). It was also significantly associated with the function of kinds of TICs, such as tumor-associated macrophages (Machado et al., 2014), dendritic cells (Laouar et al., 2008; Ramalingam et al., 2012), neutrophils (Fan et al., 2014), T cells (Chou et al., 2012), and natural killer cells (Viel et al., 2016), which might predict the prognosis in the treatment of CC (Galon et al., 2006). However, no further research was carried out to evaluate the relationship between TGFβ1 and TICs in regulating the TIME of CC. In our research, we found that TGFβ1 and TGFβ signaling pathway components might play a significant role in the TIME of CC partly through communicating with various TICs, and TGFβ1 might be a potential biomarker for the status of the TIME in CC patients. Further research might focus on the complicated communications between TGFβ1 and specific TICs in modulating the TIME of CC.

CONCLUSION

Our study implied that TGFβ1 greatly participated in the modulation of the colon cancer TIME through communicating with T cells CD4 naïve and Tregs. Furthermore, TGFβ1 might be a potential indicator of the status of the TIME in CC patients. Therefore, further investigations are needed to clarify the detailed mechanisms among TGFβ1, T cells CD4 naïve, and Tregs. Drugs targeting TGFβ1 might be a potential treatment for CC patients in the future.

DATA AVAILABILITY STATEMENT

The datasets presented in this study can be found in online repositories. The names of the repository/repositories and accession number(s) can be found in the article/ **Supplementary Material**.

AUTHOR CONTRIBUTIONS

JyW and QZ: conceptualization, writing—review, and editing. JqW: methodology and investigation. QG: software, resources, and data curation. QZ: validation. JyW: formal analysis. JyW, JqW, and QZ: writing—original draft preparation. YY: supervision. YM: project administration. JyW, YY, and QZ: funding acquisition. All authors have read and agreed to the published version of the manuscript.

FUNDING

This research was funded by the Natural Science Foundation of Jiangsu Province (grant no. BK20161110), Medical Research Grant of Jiangsu Commission of Health (grant no. M2020010), the Science Foundation of Jiangsu Health vocational college (grant no. JKC201948), the Science and Technology Development Fund of Nanjing Medical University (grant no. NMUB2019235), the Nanjing health science and Technology Development Fund (grant no. YKK18201), the Science and technology development fund of Nanjing Medical University (grant no. 2017NJMUZD091), and the Research and development fund of Kangda College of Nanjing Medical University (grant nos. KD2017KYJJYB017, KD2020KYJJZD006).

SUPPLEMENTARY MATERIAL

The Supplementary Material for this article can be found online at: https://www.frontiersin.org/articles/10.3389/fgene.2021.612011/full#supplementary-material

Supplementary Table 1 | The clinic–pathological features of CC Patients from TCGA database.

Supplementary Table 2 | The intersection between the difference test and correlation test.

REFERENCES

Chalabi, M., Fanchi, L. F., Dijkstra, K. K., Van den Berg, J. G., Aalbers, A. G., Sikorska, K., et al. (2020). Neoadjuvant immunotherapy leads to pathological responses in MMR-proficient and MMR-deficient early-stage colon cancers. *Nat. Med.* 26, 566–576. doi: 10.1038/s41591-020-0805-8

Chen, X. L., Chen, Z. Q., Zhu, S. L., Liu, T. W., Wen, Y., Su, Y. S., et al. (2017). Prognostic value of transforming growth factor-beta in patients with colorectal cancer who undergo surgery: a meta-analysis. *BMC Cancer* 17:240. doi: 10.1186/s12885-017-3215-7

Chen, Y., Dawes, P. T., Packham, J. C., and Mattey, D. L. (2012). Interaction between smoking and functional polymorphism in the TGFB1 gene is

associated with ischaemic heart disease and myocardial infarction in patients with rheumatoid arthritis: a cross-sectional study. *Arthritis Res. Ther.* 14:R81.

Chou, C. K., Schietinger, A., Liggitt, H. D., Tan, X., Funk, S., Freeman, G. J., et al. (2012). Cell-intrinsic abrogation of TGF-β signaling delays but does not prevent dysfunction of self/tumor-specific CD8 T cells in a murine model of autochthonous prostate cancer. *J. Immunol.* 189, 3936–3946. doi: 10.4049/jimmunol.1201415

Clark, D. A., and Coker, R. (1998). Transforming growth factor-beta (TGF-beta). *Int. J. Biochem. Cell Biol.* 30, 293–298.

Corn, K. C., Windham, M. A., and Rafat, M. (2020). Lipids in the tumor microenvironment: from cancer progression to treatment. *Prog. Lipid Res.* 80:101055. doi: 10.1016/j.plipres.2020.101055

Fan, Q. M., Jing, Y. Y., Yu, G. F., Kou, X. R., Ye, F., Gao, L., et al. (2014). Tumor-associated macrophages promote cancer stem cell-like properties via transforming growth factor-beta1-induced epithelial-mesenchymal transition in hepatocellular carcinoma. *Cancer Lett.* 352, 160–168. doi: 10.1016/j.canlet.2014.05.008

Franke, A. J., Skelton, W. P., Starr, J. S., Parekh, H., Lee, J. J., Overman, M. J., et al. (2019). Immunotherapy for colorectal cancer: a review of current and novel therapeutic approaches. *J Natl. Cancer Inst.* 111, 1131–1141. doi: 10.1093/jnci/djz093

Galon, J., Costes, A., Sanchez-Cabo, F., Kirilovsky, A., Mlecnik, B., Lagorce-Pagès, C., et al. (2006). Type, density, and location of immune cells within human colorectal tumors predict clinical outcome. *Science* 313, 1960–1964. doi: 10.1126/science.1129139

Gao, A., Chen, B., Gao, J., Zhou, F., Saeed, M., Hou, B., et al. (2020). Sheddable prodrug vesicles combating adaptive immune resistance for improved photodynamic immunotherapy of cancer. *Nano Lett.* 20, 353–362. doi: 10.1021/acs.nanolett.9b04012

Gao, Q., Li, X. X., Xu, Y. M., Zhang, J. Z., Rong, S. D., Qin, Y. Q., et al. (2020). IRE1α-targeting downregulates ABC transporters and overcomes drug resistance of colon cancer cells. *Cancer Lett.* 476, 67–74. doi: 10.1016/j.canlet.2020.02.007

Goding Sauer, A., Fedewa, S. A., Butterly, L. F., Anderson, J. C., Cercek, A., Smith, R. A., et al. (2020). Cancer statistics, 2020. *CA Cancer J. Clin.* 70, 7–30.

Guo, L., Wei, R., Lin, Y., and Kwok, H. F. (2020). Clinical and recent patents applications of PD-1/PD-L1 targeting immunotherapy in cancer treatment-current progress, strategy, and future perspective. *Front. Immunol.* 11:1508. doi: 10.3389/fimmu.2020.01508

Hargadon, K. M. (2016). Dysregulation of TGFβ1 activity in cancer and its influence on the quality of anti-tumor immunity. *J. Clin. Med.* 5:76. doi: 10.3390/jcm5090076

Hu, C., Wang, Y., Liu, C., Shen, R., Chen, B., Sun, K., et al. (2020). Systematic profiling of alternative splicing for sarcoma patients reveals novel prognostic biomarkers associated with tumor microenvironment and immune cells. *Med. Sci. Monit.* 26:e924126.

Hu, Z. Q., Xin, H. Y., Luo, C. B., Li, J., Zhou, Z. J., Zou, J. X., et al. (2020). Associations among the mutational landscape, immune microenvironment, and prognosis in Chinese patients with hepatocellular carcinoma. *Cancer Immunol. Immunother.* 70, 377–389. doi: 10.1007/s00262-020-02685-7

Jansen, C. S., Prokhnevska, N., and Kissick, H. T. (2019). The requirement for immune infiltration and organization in the tumor microenvironment for successful immunotherapy in prostate cancer. *Urol. Oncol.* 37, 543–555. doi: 10.1016/j.urolonc.2018.10.011

Kesar, N., Winkelmann, R., Oppermann, J., Ghanaati, S., Martin, D., Neumayer, T., et al. (2020). Prognostic impact of CD8-positive tumour-infiltrating lymphocytes and PD-L1 expression in salivary gland cancer. *Oral Oncol.* 111:104931. doi: 10.1016/j.oraloncology.2020.104931

Kinoshita, F., Tagawa, T., Akamine, T., Takada, K., Yamada, Y., Oku, Y., et al. (2020). Interleukin-38 promotes tumor growth through regulation of CD8(+) tumor-infiltrating lymphocytes in lung cancer tumor microenvironment. *Cancer Immunol Immunother.* 70, 123–135. doi: 10.1007/s00262-020-02659-9

Koirala, P., Roth, M. E., Gill, J., Piperdi, S., Chinai, J. M., Geller, D. S., et al. (2016). Immune infiltration and PD-L1 expression in the tumor microenvironment are prognostic in osteosarcoma. *Sci. Rep.* 6:30093.

Kövy, P., Meggyesi, N., Varga, L., Balassa, K., Bors, A., Gopcsa, L., et al. (2020). Investigation of TGFB1 -1347C>T variant as a biomarker after allogeneic hematopoietic stem cell transplantation. *Bone Marrow Transplant.* 55, 215–223. doi: 10.1038/s41409-019-0656-4

Laouar, Y., Town, T., Jeng, D., Tran, E., Wan, Y., Kuchroo, V. K., et al. (2008). TGF-beta signaling in dendritic cells is a prerequisite for the control of autoimmune encephalomyelitis. *Proc. Natl. Acad. Sci. U.S.A.* 105, 10865–10870. doi: 10.1073/pnas.0805058105

Li, M., Li, M., Yang, Y., Liu, Y., Xie, H., Yu, Q., et al. (2020). Remodeling tumor immune microenvironment via targeted blockade of PI3K-γ and CSF-1/CSF-1R pathways in tumor associated macrophages for pancreatic cancer therapy. *J. Control. Release* 321, 23–35. doi: 10.1016/j.jconrel.2020.02.011

Li, X., and Wang, J. (2020). Mechanical tumor microenvironment and transduction: cytoskeleton mediates cancer cell invasion and metastasis. *Int. J. Biol. Sci.* 16, 2014–2028. doi: 10.7150/ijbs.44943

Liu, Y., and Zheng, P. (2020). Preserving the CTLA-4 checkpoint for safer and more effective cancer immunotherapy. *Trends Pharmacol. Sci.* 41, 4–12. doi: 10.1016/j.tips.2019.11.003

Luo, K. (2017). Signaling cross talk between TGF-β/Smad and other signaling pathways. *Cold Spring Harb. Perspect. Biol.* 9:a022137. doi: 10.1101/cshperspect.a022137

Machado, C. M., Andrade, L. N., Teixeira, V. R., Costa, F. F., Melo, C. M., dos Santos, S. N., et al. (2014). Galectin-3 disruption impaired tumoral angiogenesis by reducing VEGF secretion from TGFβ1-induced macrophages. *Cancer Med.* 3, 201–214. doi: 10.1002/cam4.173

Massagué, J. (2000). How cells read TGF-beta signals. *Nat. Rev. Mol. Cell Biol.* 1, 169–178. doi: 10.1038/35043051

Mikami, S., Mizuno, R., and Kosaka, T. (2020). Significance of tumor microenvironment in acquiring resistance to vascular endothelial growth factor-tyrosine kinase inhibitor and recent advance of systemic treatment of clear cell renal cell carcinoma. *Pathol. Int.* 70, 712–723. doi: 10.1111/pin.12984

Pan, Z., Cai, J., Lin, J., Zhou, H., Peng, J., Liang, J., et al. (2020). A novel protein encoded by circFNDC3B inhibits tumor progression and EMT through regulating Snail in colon cancer. *Mol. Cancer* 19:71.

Ramalingam, R., Larmonier, C. B., Thurston, R. D., Midura-Kiela, M. T., Zheng, S. G., Ghishan, F. K., et al. (2012). Dendritic cell-specific disruption of TGF-β receptor II leads to altered regulatory T cell phenotype and spontaneous multiorgan autoimmunity. *J. Immunol.* 189, 3878–3893. doi: 10.4049/jimmunol.1201029

Rotte, A. (2019). Combination of CTLA-4 and PD-1 blockers for treatment of cancer. *J. Exp. Clin. Cancer Res.* 38:255.

Seidel, J. A., Otsuka, A., and Kabashima, K. (2018). Anti-PD-1 and Anti-CTLA-4 therapies in cancer: mechanisms of action, efficacy, and limitations. *Front. Oncol.* 8:86. doi: 10.3389/fonc.2018.00086

Siegel, R. L., and Miller, K. D. (2020). Colorectal cancer statistics, 2020. *CA Cancer J. Clin.* 70, 145–164.

Tang, J., Gifford, C. C., Samarakoon, R., and Higgins, P. J. (2018). Deregulation of negative controls on TGF-β1 signaling in tumor progression. *Cancers (Basel)* 10:159. doi: 10.3390/cancers10060159

Teixeira, A. L., Araújo, A., Coelho, A., Ribeiro, R., Gomes, M., Pereira, C., et al. (2011). Influence of TGFB1+869T>C functional polymorphism in non-small cell lung cancer (NSCLC) risk. *J. Cancer Res. Clin. Oncol.* 137, 435–439. doi: 10.1007/s00432-010-0896-6

Uttam, S., Stern, A. M., Sevinsky, C. J., Furman, S., Pullara, F., Spagnolo, D., et al. (2020). Spatial domain analysis predicts risk of colorectal cancer recurrence and infers associated tumor microenvironment networks. *Nat. Commun.* 11:3515.

Viel, S., Marçais, A., Guimaraes, F. S., Loftus, R., Rabilloud, J., Grau, M., et al. (2016). TGF-β inhibits the activation and functions of NK cells by repressing the mTOR pathway. *Sci. Signal.* 9:ra19. doi: 10.1126/scisignal.aad1884

Wang, J., Zhang, Q., Wang, D., Yang, S., Zhou, S., Xu, H., et al. (2020). Microenvironment-induced TIMP2 loss by cancer-secreted exosomal miR-4443 promotes liver metastasis of breast cancer. *J. Cell. Physiol.* 235, 5722–5735. doi: 10.1002/jcp.29507

Wang, S., Li, Y., Xing, C., Ding, C., Zhang, H., Chen, L., et al. (2020). Tumor microenvironment in chemoresistance, metastasis and immunotherapy of pancreatic cancer. *Am. J. Cancer Res.* 10, 1937–1953.

Wang, Y., Mack, J. A., and Maytin, E. V. (2019). CD44 inhibits α-SMA gene expression via a novel G-actin/MRTF-mediated pathway that intersects with TGFβR/p38MAPK signaling in murine skin fibroblasts. *J. Biol. Chem.* 294, 12779–12794. doi: 10.1074/jbc.ra119.007834

Xu, W. H., Xu, Y., Wang, J., Wan, F. N., Wang, H. K., Cao, D. L., et al. (2019). Prognostic value and immune infiltration of novel signatures in clear cell renal cell carcinoma microenvironment. *Aging (Albany NY)* 11, 6999–7020. doi: 10.18632/aging.102233

Yang, S. S., Ma, S., Dou, H., Liu, F., Zhang, S. Y., Jiang, C., et al. (2020). Breast cancer-derived exosomes regulate cell invasion and metastasis in breast cancer via miR-146a to activate cancer associated fibroblasts in tumor microenvironment. *Exp. Cell Res.* 391:111983. doi: 10.1016/j.yexcr.2020.111983

Yu, X., Gao, R., Li, Y., and Zeng, C. (2020). Regulation of PD-1 in T cells for cancer immunotherapy. *Eur. J. Pharmacol.* 881:173240. doi: 10.1016/j.ejphar.2020.173240

Zarzynska, J. M. (2014). Two faces of TGF-beta1 in breast cancer. *Mediators Inflamm.* 2014:141747.

Zessner-Spitzenberg, J., Thomas, A. L., Krett, N. L., and Jung, B. (2019). TGFβ and activin A in the tumor microenvironment in colorectal cancer. *Gene Rep.* 17:100501. doi: 10.1016/j.genrep.2019.100501

Zhang, L., Chen, J., Cheng, T., Yang, H., Li, H., and Pan, C. (2020). Identification of the key genes and characterizations of tumor immune microenvironment in lung adenocarcinoma (LUAD) and Lung Squamous Cell Carcinoma (LUSC). *J. Cancer* 11, 4965–4979. doi: 10.7150/jca.42531

Zhang, Y., Kang, M., Zhang, B., Meng, F., Song, J., Kaneko, H., et al. (2019). m(6)A modification-mediated CBX8 induction regulates stemness and chemosensitivity of colon cancer via upregulation of LGR5. *Mol. Cancer* 18:185.

Zhang, Z., Karthaus, W. R., Lee, Y. S., Gao, V. R., Wu, C., Russo, J. W., et al. (2020). Tumor microenvironment-derived NRG1 promotes antiandrogen resistance in prostate cancer. *Cancer Cell* 38, 279–96.e9.

Zhu, Y., Zhang, Z., Jiang, Z., Liu, Y., and Zhou, J. (2020). CD38 predicts favorable prognosis by enhancing immune infiltration and antitumor immunity in the epithelial ovarian cancer microenvironment. *Front Genet.* 11:369. doi: 10.3389/fgene.2020.00369

Conflict of Interest: The authors declare that the research was conducted in the absence of any commercial or financial relationships that could be construed as a potential conflict of interest.

frontiers in Oncology

ORIGINAL RESEARCH
published: 05 May 2021
doi: 10.3389/fonc.2021.603556

Pharmacological Inhibition and Genetic Knockdown of BCL9 Modulate the Cellular Landscape of Cancer-Associated Fibroblasts in the Tumor-Immune Microenvironment of Colorectal Cancer

Mengxuan Yang[1†], *Zhuang Wei*[2†], *Mei Feng*[3], *Yuanyuan Zhu*[3], *Yong Chen*[4*] *and Di Zhu*[1,5*]

[1] Central Hospital of Minhang District, Shanghai, China, [2] Key Laboratory of Systems Biology, Innovation Center for Cell Signaling Network, CAS Center for Excellence in Molecular Cell Science, Institute of Biochemistry and Cell Biology, Shanghai Institutes for Biological Sciences, Shanghai, China, [3] School of Pharmacy, Fudan University, Shanghai, China, [4] Department of General Surgery, Huai'an Second People's Hospital and the Affiliated Huai'an Hospital of Xuzhou Medical University, Huai'an, China, [5] New Drug Evaluation Center, Shandong Academy of Pharmaceutical Science, Jinan, China

OPEN ACCESS

Edited by:
Xiao-Jie Lu,
Nanjing Medical University, China

Reviewed by:
YFeng,
Zhejiang University, China
Shenglin Mei,
Harvard Medical School, United States

***Correspondence:**
Yong Chen
90chenyong@sina.com
Di Zhu
zhudi@vip.sina.com

[†]These authors have contributed equally to this work

Specialty section:
This article was submitted to Cancer Genetics, a section of the journal Frontiers in Oncology

Received: 07 September 2020
Accepted: 15 March 2021
Published: 05 May 2021

Citation:
Yang M, Wei Z, Feng M, Zhu Y, Chen Y and Zhu D (2021) Pharmacological Inhibition and Genetic Knockdown of BCL9 Modulate the Cellular Landscape of Cancer-Associated Fibroblasts in the Tumor-Immune Microenvironment of Colorectal Cancer. Front. Oncol. 11:603556. doi: 10.3389/fonc.2021.603556

Cancer-associated fibroblasts (CAFs) exert a key role in cancer progression and liver metastasis. They are activated in the tumor microenvironment (TME), but their prometastatic mechanisms are not defined. CAFs are abundant in colorectal cancer (CRC). However, it is not clear whether they are raised from local tissue-resident fibroblasts or pericryptal fibroblasts and distant fibroblast precursors, and whether they may stimulate metastasis-promoting communication. B-cell lymphoma 9/B-cell lymphoma 9-like (BCL9/BCL9L) is the key transcription cofactor of β-catenin. We studied the TME of CRC with single-cell sequencing and consequently found that *Bcl9* depletion caused a pro-tumor effect of CAFs, while inhibition of abnormal activation of Wnt/β-catenin signal through *Bcl9* depletion benefited T-cell–mediated antitumor immune responses. We also identified and evaluated four types of CAFs in CRC with liver metastasis. In summary, we demonstrate cell type landscape and transcription difference upon BCL9 suppression in CAFs, as well as how CAF affects cancer associated immune surveillance by inhibition of Wnt signaling. Targeting the Wnt signaling pathway *via* modulating CAF may be a potential therapeutic approach.

Keywords: colorectal cancer, cancer-associated fibroblasts, Wnt signaling, BCL9, tumor immune microenvironment

INTRODUCTION

Colorectal cancer (CRC) is a widespread malignancy and the third leading cause of cancer mortality worldwide (1). Most CRCs occur sporadically in patients without family history of intestinal diseases (2). An unhealthy diet rich in meat but poor in fruit and vegetables increases the rising incidence of CRC (3). Traditional treatment (i.e., surgery, radiotherapy, and chemotherapy

combined with targeted drugs) has improved the treatment of CRC. For example, combinations of targeted drugs containing epidermal growth factor receptor (EGFR) antibody and vascular endothelial growth factor (VEGF) antibody with chemotherapy such as FOLFIRI, XELOX/CAPOX, or FOLFOX have been shown to prolong survival in patients with CRC (4). However, treatment of patients with advanced recurrent or metastatic CRC is still inadequate. Therefore, it is necessary to determine molecules and signaling pathways that are critical for CRC and to find new therapeutic targets.

The Wnt signaling pathway, a tightly regulated, receptor-mediated transduction pathway, is important to the embryonic development and adult tissue homeostasis. Aberrantly activated in many tumors and others diseases, Wnt signaling plays a significant role in CRC given that 80% of patient samples in a large-scale study displayed APC and β-catenin mutations (5). Thus, Wnt pathway has emerged as a prospective anti-cancer target in CRC.

CAFs are the predominant cellular components of the stroma relative to primary and metastatic CRC (6, 7). Cancer cells can recruit CAFs to the TME by upregulating the expression of tissue inhibitors of metalloproteinases 1 (TIMP-1), which leads to increased CAF proliferation and migration by binding with CD63, its receptor on CAFs. The stroma of human CRCs expresses higher levels of TIMP-1 than its phenotypically normal counterpart (8).

CAFs can promote CRC cell proliferation, restrain tumor cell death, and elude tumor growth suppressors (9). CAFs of colorectum can discharge multiple growth factors, such as EGF, HGF, IGF1/2, PGE-2, PDGF, VEGF, and FGF-1 (10–12). For example, IGF1 can crosstalk with insulin-like growth factor 1 receptor (IGF-1R), thereby activating the mitogen-activated protein kinase (MAPK) and phosphoinositide 3-kinase (PI3K) signal pathways, and promoting cancer cell growth and survival (13). Moreover, HGF secreted by CAFs can phosphorylate the receptor tyrosine kinase c-Met and human epidermal growth factor receptor (EGFR2/EGFR3) in CRCs, and activate both MAPK and PI3K/AKT pathways (14). Consequently, these growth factors released by CAFs induce tumor cells proliferation and tumorigenicity in CRCs (15). Moreover, Hawinkels et al. demonstrated that the interaction between CRC cells and resident fibroblasts results in TGF-β1 signaling hyperactivation and differentiation of the resident fibroblasts into α-SMA$^+$ CAFs, which conversely leads to synthesis of TGF-β and proteinases in the TME, thus generating a cancer-promoting feedback cycle (10).

Tumor metastasis refers to a multistage process in which malignant cancer cells migrate to the surrounding tissues and continue their proliferation from the primary site through lymphatic channels, blood vessels, or body cavities. In this process, tumor cells detached from the primary site violate other tissues and eventually lead to metastatic tumors. Malignant tumor metastases are the main reason for the failure of tumor treatment. CAFs are abundant in CRC and play a critical role in cancer progression. They are enriched in the TME, but their prometastatic mechanisms in CRC with metastasis have not been defined (9, 10).

First, chemokines in the TME are conducive to tumor metastasis. In CRCs, PDGF-activated CAFs can facilitate tumor cells intravasation and distant metastases by secreting stanniocalcin1 (STC1) (16). Second, through increasing the production of extracellular matrix (ECM) and proteolytic enzymes, stromal TGFβ signaling promotes tumor metastasis (17, 18). It was shown that CAFs can lead to TGFβ signaling hyperactivation after incubation with supernatants from CRC cells (18). Moreover, CAFs are the main source of connective tissue constituents of the TME, including collagens and proteoglycans (19, 20). Third, the expression of tumor-promoting MMPs is higher in CAFs than in CRC cells (18, 20). Type IV collagen, a base for MMP-2 and MMP-9, is one of the key components of the basement membrane, which is essential for tumor invasion and metastasis (18, 21). Cancer cells may undergo epithelial mesenchymal transition (EMT), a transdifferentiation programme to get a highly invasive phenotype (22). Snail1 is an important transcriptional factor that exerts critical role in EMT. Snail1 expression is higher in colon CAFs than in normal fibroblasts, and it correlates with CRC cells migration and proliferation (23). Further studies revealed that a mechanically active heterotypic E-cadherin/N-cadherin adhesion between the CAFs and tumor cells can enable fibroblasts to drive cancer cell invasion (24).

Even though CAFs have been reported to be involved in tumorigenesis, angiogenesis, and metastasis, CAF-related anti-tumor immune response in CRC is still not clear. Apart from potent protumorigenic ability, some CAF subsets have tumor-inhibiting functions, which further supports the concept of CAF heterogeneity. Interestingly, there are at least two CAF subsets in the breast TME that can be distinguished by CD146 expression (25). Specifically, CD146$^+$ CAFs can lead to persistent estrogen-dependent proliferation and breast cancer cells sensitivity to tamoxifen, while CD146$^-$ CAFs can suppress estrogen receptor expression and response of cancer cells to estrogen, thereby resulting in tamoxifen resistance (25). Additionally, CAF peripheral cells in CRC show upregulation of podoplanin, a mucin-type transmembrane glycoprotein. Podoplanin is a significant indicator of favorable prognosis in patients with advanced CRC as shown in multivariate analysis of both disease-free survival and liver metastasis-free survival (26). Apart from this, upon co-culturing with CAFs treated with siRNA for podoplanin, CRC cells demonstrated decreased cell invasion, suggesting a protective role of CAFs against CRC cell invasion (26).

MATERIALS AND METHODS

Compounds and Short Hairpin RNA

hsBCL9$_{CT}$-24 was purchased from AnaSpec (Fremont, CA, USA) based on previous protocols (27). Analytical high-performance liquid chromatography (HPLC) and mass spectrometry (MS) were used to evaluate the synthesis and purification of peptides. hsBCL9$_{CT}$-24 was dissolved as a 10 mmol/L solution and was diluted prior to assay. pGIPZ- and/or pTRIPZ (inducible with

doxycycline)-based lentiviral shRNAs for mouse *Bcl9* shRNA#5 (V3LMM_429161), mouse *Bcl9l* shRNA#1 (V2LMM_69221), and non-targeting shRNA were obtained from Open Biosystems/GE Dharmacon. The non-targeting (NT) lentiviral shRNA expressing an shRNA sequence with no substantial homology to any mammalian transcript was used as a negative control.

Animal Tumor Specimens

For each tumor, at least four regions were sampled, including two regions in inner layers and two regions in outer layer. In total, six samples from six mice were collected. Detailed information is summarized in **Supplementary Table 1**. All the procedures were performed in accordance with the protocols approved by the School of Pharmacy in Fudan University's animal care committee (Approval number: 2020-04-YL-ZD-02) and with the guidelines of the Association for Assessment and Accreditation of Laboratory Animal Care International.

Specimen Processing

Fresh tumors from mice were collected in MACS Tissues storage solution (130-100-008, Miltenyi Biotec, Germany) in the operation room after surgical resection, and immediately transferred to Fudan laboratory for processing. Tissues were minced into pieces < 1 mm^3 on ice, shifted to a C tube (130-093-237, Miltenyi Biotec), and enzymatically digested by MACS Tumor Dissociation Kit (130-095-929, Mitenyi Biotec) in line with corresponding programs. The resulting suspension was filtered through a 40-μm cell strainer (Falcon) and washed by RPMI 1640 (C11875500BT, Gibco). Erythrocytes were removed by adding 2 ml Red Cell Lysis Buffer (555899, BD Biosciences). A Dead Cell Removal Kit (130-090-101, Miltenyi Biotec) was subsequently used to enrich live cells. After resuspension in RPMI 1640 (C11875500BT, Gibco), single-cell suspension was obtained. Trypan blue (15250061, Gibco) was next used to check whether cell viability was >90% to be qualified enough for library construction.

10× Library Preparation and Sequencing

Cell concentration was adjusted to 700–1200 cells/μl to run on a Chromium Single-Cell Platform (10× Genomics Chromium™). 10× library was generated in accordance with the manufacturer's protocol of 10× genomics Single Cell 3′ Reagent Kits v2. The clustering was carried on a cBot Cluster Generation System with TruSeq PE Cluster Kit v3. Qubit was used for library quantification. The final library was sequenced on an Illumina HiSeq3000 instrument using 150 bp paired-end reads.

Principal Component Analysis and t-SNE Analyses

The total number of unique molecular identifiers (UMIs) per cell was counted for the number of UMI sequences of high-quality single cells and genes in the sample. To normalize the number of UMIs in each cell to the median of the total UMI of all cells, we used the median normalization process. The similarity between cells was investigated by means of Principal component analysis (PCA) reduction dimension. The closer the expression trend of cellular genes, the closer the sample distance was. Using t-distributed stochastic neighbor embedding (t-SNE) to visualize the single cell clustering for the top 10 principal components of the PCA resulted in the largest variance explained. The protocol of the t-SNE presentation method was to recount the sample distance through the conditional probability of random neighbor fitting according to the Student's t distribution in the high dimensional space, so that the sample presented a clearly separated cluster in the low dimensional space.

Pathway and Functional Annotation Analysis

Through DAVID (https://david.ncifcrf.gov/), we conducted Kyoto Encyclopedia of Genes and Genomes (KEGG) pathway annotation and enrichment. KEGG is a database resource for investigation of the high-level functions and effects of the biological system (http://www.genome.jp/kegg/). Pathways with a Q value ≤0.05 were defined as significantly enriched. Analysis was performed base on The Gene Ontology database conducted the functional annotation, including biological process, cellular component, and molecular function classifications. To select only significant categories, we used a Fisher's exact test, and the GO terms with computed Q value ≤0.05 were considered as significant.

Gene Prognostic Performance in TCGA Samples

We downloaded the TCGA datasets, including COAD and READ, from cBioPortal (http://www.cbioportal.org/). Based on gene median expression level, the CRC samples were divided into the high- and low-expression groups. To compare the overall and disease-free survival among two groups, Kaplan-Meier curve was constructed. Log-rank P value and hazard ratios (HR) were calculated with SPSS 22.0. In TIMER analysis, correlation analysis of gene expression in tumor-infiltrating immune cells was performed.

Single Cell Data of Human Tumor Sample

Samples from patients with CRC were analyzed from the data base (SUB8333842). The study was approved by the Ethics Committee of Fudan University. Informed consent was obtained from every patient who agreed to provide specimens for scientific research.

Cell-Cell Interaction Analysis

Based on the above analysis of the expression abundance of ligand–receptor, we obtained the number of ligand–receptor interactions between two cell types, allowing a preliminary assessment of the communication relationship between the cells. To identify biological relevance, we used cellPhoneDB software to perform pairwise comparisons between all cell types in the dataset, and analyze the number of significantly enriched ligand–receptor interactions between two cell types. First, we randomly permuted the cluster labels of all cells (1,000 times by default) and determined the mean of the average ligand expression level in a cluster and the average receptor expression level in the interacting cluster. In this way we generated a null

distribution for each ligand–receptor pair in each pairwise comparison between two cell types. We obtained a *P* value for the likelihood of cell-type enrichment of each ligand–receptor pair. Wilcoxon rank sum test was used for statistical analyses.

GSVA Analysis

For CAFs and tumor cell population expression data, the average expression of each gene of the corresponding cell was calculated in each sample. GSVA analysis was performed on the sample expression data of the above four types of cells using the C2 KEGG pathway subclass data in the MsigDB database to obtain the GSVA score of each pathway in each sample. For the above four types of cell sample expression data, the C2 KEGG pathway subtype data were used in the MsigDB database to perform GSVA calculation Z-score analysis to obtain the GSVA Z-score of each pathway in each sample. The limma package in R was used to calculate the GSVA score data of the above four types of cells. Metastatic vs. nonmetastatic grouping was applied to calculate the difference, and obtain the *t* score and *P* value of each KEGG pathway. The pathways were filtered according to the marked P value and a bar chart was prepared based on *t* score. Corresponding Z-score was extracted for heatmaps based on selected channels.

Statistical Analysis

SPSS 22.0 was used in data analysis, and *t* test was used to determine the statistical significance. P values <0.05 were considered statistically significant.

RESULTS

Single-Cell RNA-seq of Mouse CT26 Tumor With Pharmacological Inhibition of BCL9

Cancer-associated fibroblasts (CAFs) are very critical in cancer progression when they are activated in the TME. To determine and specify whether they exhibit prometastatic mechanisms, we characterized the heterogeneity of mouse CT26 tumor in $hsBCL9_{CT}$-24 treatment. Based on our previous study (28), we conducted structure–activity relationship analyses in SAH-$BCL9_B$ to generate the newly generated peptide series, among which $hsBCL9_{CT}$-24 was found to potently disrupt Bcl9/β-catenin and demonstrate the most potent *in vitro* activity (29). Cancer-associated fibroblasts were investigated in these tumors. Six samples from six CT26 mice with a tumor were collected, and they were treated by $hsBCL9_{CT}$-24 or by vehicle as control. Tissues were minced rapidly and enzymatically digested with MACS Tumor Dissociation Kit according to corresponding procedure to a single-cell suspension, and run on a Chromium Single-Cell Platform (see methods). 10× library was generated according to the manufacturer's protocol. The clustering was implemented on a cBot Cluster Generation System with TruSeq PE Cluster Kit v3. Qubit was used for library quantification. The final library was sequenced on an Illumina HiSeq3000 instrument. Results of scRNA-seq with unique transcript counting through barcoding with UMIs (see Methods) were analyzed. Using t-SNE to group cells with similar expression profiles, graph-based clustering was run to build a sparse nearest-neighbor graph without prespecification of the number of clusters (**Supplementary Figure 1A** and **Figure 1A**). We identified five clusters (**Figure 1B**) based on the t-SNE dimensionality reduction and unsupervised cell clustering. The mean expression of every gene was calculated across all cells in the cluster, and the log2 fold change of differentially expressed genes was counted relative to the other clusters identified relevant genes that were enriched in different clusters. High expression of significant genes with the known markers of major cell types is shown in **Figure 1C**. The relevant genes were enriched by heatmaps of the clusters 0, 1, 2, 3, and 4. Five transcription factors showed the highest difference (log2 fold change) in expression regulation estimates between different clusters (**Figure 1D**). Each cluster was defined by expression of marker genes for the cell types (**Figures 1E–G**); *S100a9*, *Pdgfrb*, and *Ptx3*, were highly expressed in clusters 2, 0, and 4, respectively. Different clusters present difference of cell numbers and difference of genes in cluster 0, 1, 2, 3, and 4 (**Figures 1H, I**). Cluster 2 with high expression of *S1009a* was defined as CAF4. t-SNE of additional CAF marker genes, such as *S100a4*, *Pdgfa*, *Postn*, *Tnc*, was shown. (**Figures 1J–M**). *Bcl9* expression in different clusters in vehicle and $hsBCL9_{CT}$-24 group was also determined by t-SNE and UMAP (**Supplementary Figures 1C, E**).

Single-Cell RNA-seq of Mouse CT26 Tumor With Genetic Knockdown of *Bcl9*

The plasmid with knockdown (KD) shRNA-BCL9 was constructed and transfected into CT26 cells (**Supplementary Figure 1B**). The CT26 cells transfected with non-targeting (NT) shRNA were used as controls. CT26 expressing NT-shRNA and shRNA-BCL9 cells were implanted subcutaneously in Balb/c mice. Six tumor samples were operated (B18, NT-shRNA sample 18; B19, NT-shRNA sample 19; B22, NT-shRNA sample 22; B24, BCL9-shRNA sample 24; B25, BCL9-shRNA sample 25; and B29, BCL9-shRNA sample 29). Graph-based clustering was handled using t-SNE to gather cells with similar expression profiles and to construct a sparse nearest-neighbor graph without prespecification of the number of clusters (**Figure 2A** and **Supplementary Figure 1A**). We defined seven different cell clusters, named as C0–C6 according to their total cell numbers, presenting unique transcriptional profiles (**Figure 2B**).

We identified genes enriched in a different cluster through high expression of the known markers of major cell types shown in **Figure 2C**. We identified seven clusters (0, 1, 2, 3, 4, 5, and 6). The relevant genes were enriched by heatmap of the clusters 0, 1, 2, 3, 4, 5 and 6 (**Figure 2D**). Marker genes of the cell types defined above each cluster, *Rgs5, Dmkn*, and *Ass1*, were highly expressed in clusters 4, 0, and 2, respectively (**Figures 2E–G**). Different clusters presented different genes and different cell numbers (**Figures 2H, I**). Cluster 4 with high expression of *Rgs5* was defined as CAF4. t-SNE of additional CAF marker genes, such as *Fap*, *Tnc*, *Des*, *Pdgfra*, was shown. (**Figures 2J–M**).

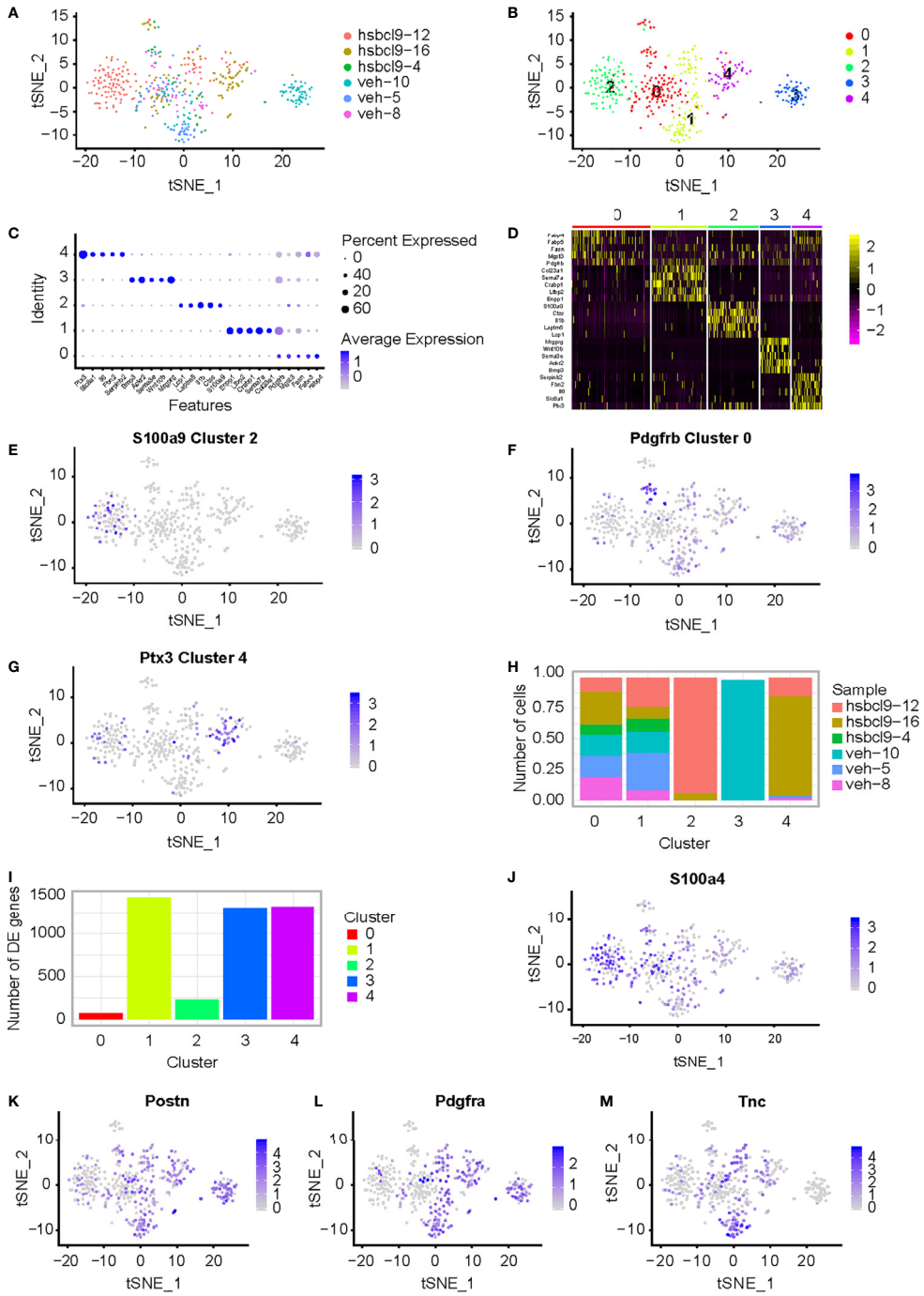

FIGURE 1 | CAF analysis in mouse CT26 tumor in hsBCL9$_{CT}$-24 treatment. **(A)** Single cell RNA-seq of mouse CT26 tumor; t-SNE of the six samples from CT26 tumor mice, which were treated by hsBCL9$_{CT}$-24 or by vehicle, were collected. **(B)** t-SNE plot expression of marker genes for the five different markers of tumor cell defined above each panel color-coded by their associated cluster. Five clusters high quality cells were collected for further analyses. **(C)** Bubble plots express different marker genes according to each cluster high specific expression gene separate different cells. **(D)** Five cluster cells were analyzed for different genes with heatmap. **(E–G)** Expression of marker genes for the cell types defined above each cluster; *S100a9*, *Pdgfrb*, and *Ptx3*, highly expressed in clusters 2, 0, and 4, respectively. **(H, I)** Different clusters present difference of cell numbers and genes among clusters 0, 1, 2, 3, and 4. **(J–M)** Expression of CAF marker genes for the cell types defined above each cluster; *S100a4*, *Postn*, *Pdgfra*, and *Tnc*, highly expressed in clusters 2, 0, and 4, respectively. Wilcoxon rank sum test was used for statistical analyses.

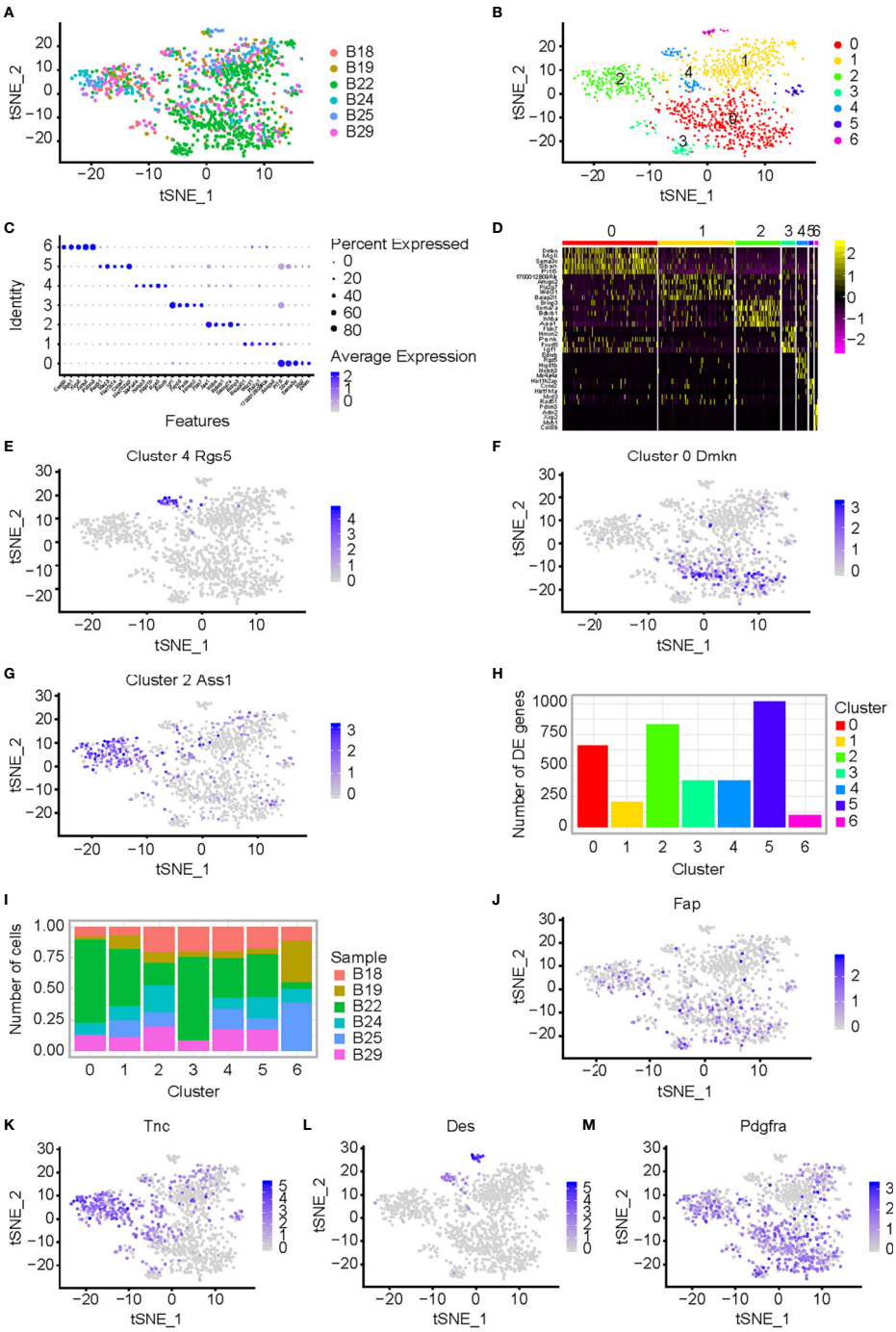

FIGURE 2 | CAF analysis in mouse CT26 tumor with BCL9 depletion. **(A)** Single cell RNA-seq of CT26 tumor cells; t-SNE of the six samples from CT26 tumor cells, which were treated by shRNA-BCL9 or NT-shRNA, were collected. The plasmid with shRNA-BCL9 was constructed and transfected into CT26 cells. The CT26 cells which transfected NT-shRNA were used as control. Six samples included: B18 (NT-shRNA sample 18), B19 (NT-shRNA sample 19), B22 (NT-shRNA sample 22), B24 (BCL9-shRNA sample 24), B25 (BCL9-shRNA sample 25), and B29 (BCL9-shRNA sample 29). **(B)** Seven distinct cell clusters, named as C0–C6 based upon their total cell numbers, expressed unique transcriptional profiles and marker gene. **(C)** Bubble plots show significant genes with high expression of the known markers of major cell types. **(D)** Heatmap shows significant difference in gene expression among seven clusters. **(E–G)** Expression of marker genes for the cell types defined above each cluster; *Rgs5*, *Dmkn*, and *Ass1*, highly expressed in clusters 4, 0, and 2, respectively. **(H, I)** Different clusters present difference in cell numbers and genes between clusters 0, 1, 2, 3, 4, 5, and 6. **(J–M)** Expression of CAF marker genes for the cell types defined above each cluster; *Fap*, *Tnc*, *Des*, and *Pdgfra*, highly expressed in clusters 2, 0, and 4, respectively. Wilcoxon rank sum test was used for statistical analyses.

Bcl9 expression in different clusters in NT-shRNA and Bcl9-shRNA group was also performed in t-SNE and UMAP (**Supplementary Figures 1D, F**).

Signaling Pathway and Transcription Factor Analysis

GSVA analysis was performed on the sample expression data of the above four types of cells (NT-shRNA and BCL9-shRNA) using the C2 KEGG pathway subclass data in the MsigDB database to obtain the GSVA score of each pathway in each sample. For the above four types of cell sample expression data, the C2 KEGG pathway subtype data were used in the MsigDB database to obtain the GSVA Z-score of each pathway in each sample. NT tumor vs knockdown group was applied to calculate the difference, and obtain the *t* score and P value of each KEGG pathway. The pathways were filtered based on the marked P value, and a bar chart was created based on *t* score. Corresponding Z-score was extracted for heatmap based on selected channels. Motif gene sets a direct comparison of tumor cells between NT group and *Bcl9* knockdown group revealed IK3, IRF pathway as the enriched signature in tumor cells (**Figure 3A**). Gene ontology relative regulation of vasculature development gene was the enriched signature in NT tumor cells (**Figure 3B**). Oncogenic signatures manifested PDG, MTOR, and PETEN pathway as the enriched signature in NT tumor cells (**Figure 3C**). We further explored immunologic signatures pathway and revealed that immunologic gene such as IL-2 and STAT1 was enriched in tumor cells (**Figure 3D**).

Single cell regulatory network inference and clustering (SCENIC) is a statistical method for simultaneous gene regulatory network reconstruction as well as cell-state identification from single cell RNA-seq data (http://scenic.aertslab.org). SCENIC can furnish unique insights into the mechanisms driving cellular heterogeneity. We applied SCENIC analysis to investigate the transcription factors underlying differences in CT26 tumor cell expression between NT and *Bcl9* KD tumor cells. We also identified Foxp4 as a candidate transcription factor underlying gene expression differences in NT and *Bcl9*-KD tumor cells (**Figures 4A, B**).

Cells Cross Talk Between CAFs and CT26 Tumor Cells

Tumorigenesis and tumor cells proliferation and metastasis always depend on tumor stromal cells. The TME has diverse functions, including matrix deposition and reforming tumor cells, and significantly influences therapeutic response and clinical outcome, through the circulatory and lymphatic systems interplay with surrounding cells to influence the development and progression of cancer (30). In addition, stromal cells such CAFs in the TME play indispensable roles in all stages of carcinogenesis by stimulating and facilitating uncontrolled cell proliferation. CAFs' extensive corresponding signaling interacts with tumor cells and cross talks with infiltrating leukocytes. In turn, tumor cells transform the TME to favor for tumor growth (31).

Analysis of the number and expression of ligand receptor pairs in CAF cells and CT 26 cells pairs was based on single cell gene expression matrix by CellPhoneDB software and construction of cell interaction network graph, so as to predict the potential communication between cells. The interaction was determined by calculating the average expression of receptors and ligands. After calculating the score for each ligand and receptor, we averaged the interaction score of the tumor model to determine the conservative interaction. According to the above results, CAFs were shown as a potential target for optimizing therapeutic strategies against cancer. We explored the cell interaction between NT and *Bcl9*-KD groups. The TGFβ-TGFβR and EGFR-NRG1 binding between receptor and ligand was obvious in CAF/CT26 subgroups, revealing a cross-talk between the CAFs and CT26 tumor cells through TGF pathway, which affects the expression of EGFR to transform the tumor cells (**Figures 5A, B**).

Heterogeneity of Human Cancer-Associated Fibroblasts

We used a database which included nine colon samples from colonic cancer patients, five of which were with metastasis and four without metastasis. We implemented principal component analysis on genes variably expressed across all 69,548 cells (n = 26,805 genes). We then sorted cells into types using graph-based clustering on the informative principal components (**Supplementary Figures 2A–C**). This technique identified cell clusters that, through marker genes, included cancer cells—markers *EpCAM, KRT8, KRT18*, and *KRT23*, fibroblasts—marker *COL1A1* (cancer cells, 4389 cells; fibroblasts, 2549 cells; **Supplementary Figures 2D, E**). We also compared difference of fibroblast enrichment between metastatic and nonmetastatic samples. We found that fibroblasts were increased in metastatic CRC compared with nonmetastatic CRC (**Supplementary Figure 2F**).

To compare with the findings obtained from mouse CAFs, we explored heterogeneity of human CAFs. In total, 2549 fibroblasts were detected among 9 samples. Next, we focused on CAFs in right-sided CRC-LM, and revealed seven subtypes in subclustering (**Supplementary Figure 2G**). A subset showing α-smooth muscle actin (α-SMA), fibroblast activation protein (FAP), periostin, neuron glial antigen-2 (NG2), tenascin-C, platelet-derived growth factor receptors α and β (PDGFR α and β), desmin, vimentin, and fibroblast specific protein-1 (FSP-1) was defined as CAFs. The cellular identity and origin of CAFs stem from various lineages, and the subpopulations we detected were highly consistent with the fibroblast identity. Analysis partitioned CAFs into four types (cluster 5, cluster 0, cluster 10, and cluster 14; **Supplementary Figure 2H**), where cluster 0 expressed *ESAM*, cluster 5 expressed *COL12A1*, cluster 14 expressed *POSTN*, and cluster 10 expressed *CFD* (**Supplementary Figure 2H**). We identified distinct populations of CAFs, including matrix CAFs (mCAFs) in cluster 5, vascular CAFs (vCAFs) in cluster 0, myofibroblastic CAFs (myCAFs) in cluster 14, and inflammatory CAFs (iCAF) in

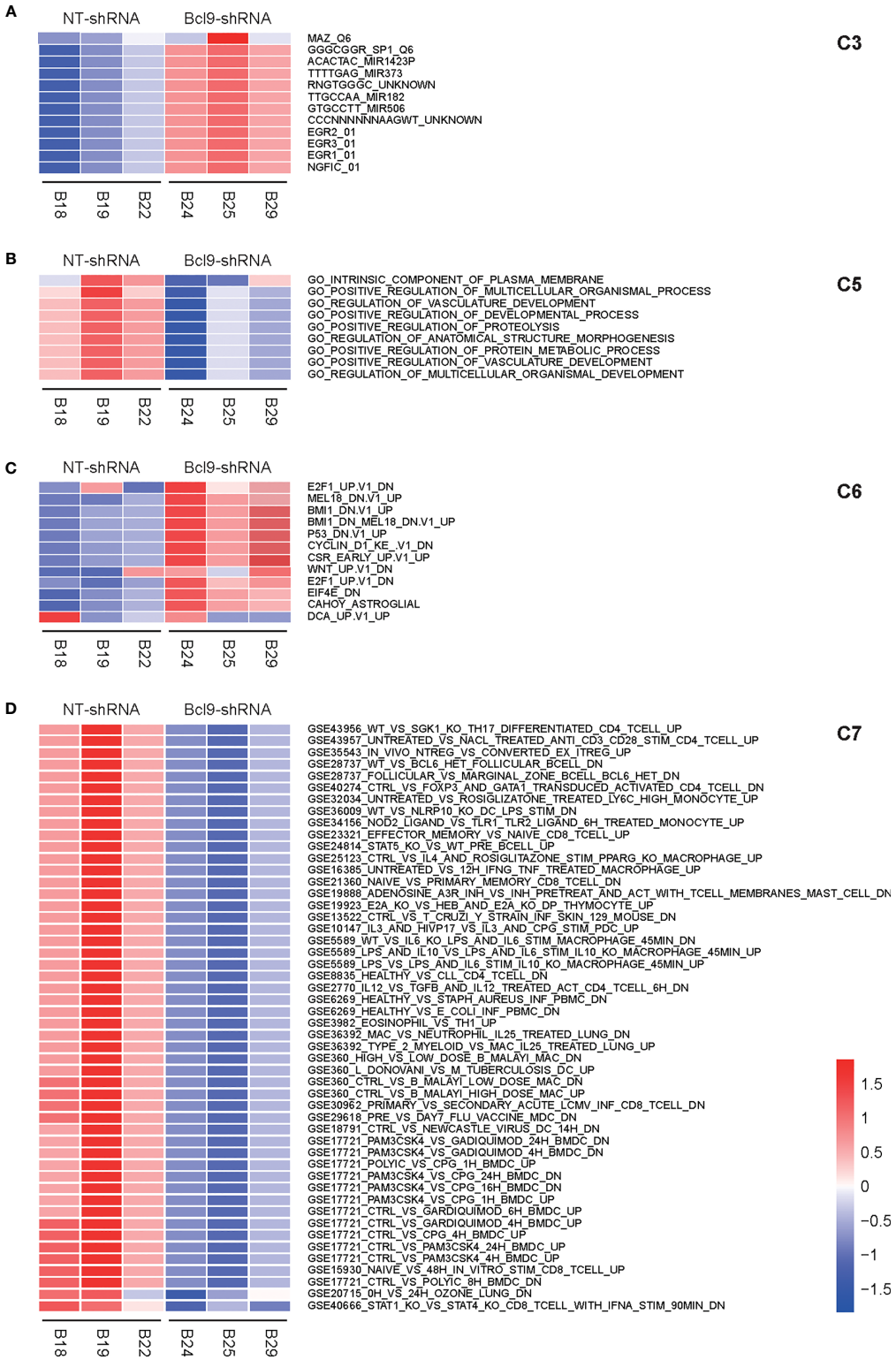

FIGURE 3 | GSVA analysis of CAF in mouse CT26 tumor. **(A)** Motif gene sets a direct comparison of tumor cells between NT group and Bcl9 knockdown group, revealing IK3 and IRF pathways as the enriched signatures in tumor cells. **(B)** Gene ontology relative regulation of vasculature development gene is the enriched signature in NT tumor cells. **(C)** Oncogenic signatures manifest PDG, MTOR, and PETEN pathways as the enriched signatures in NT tumor cells. **(D)** Immunologic signatures pathway, such as TGF, is the enriched signature in tumor cells.

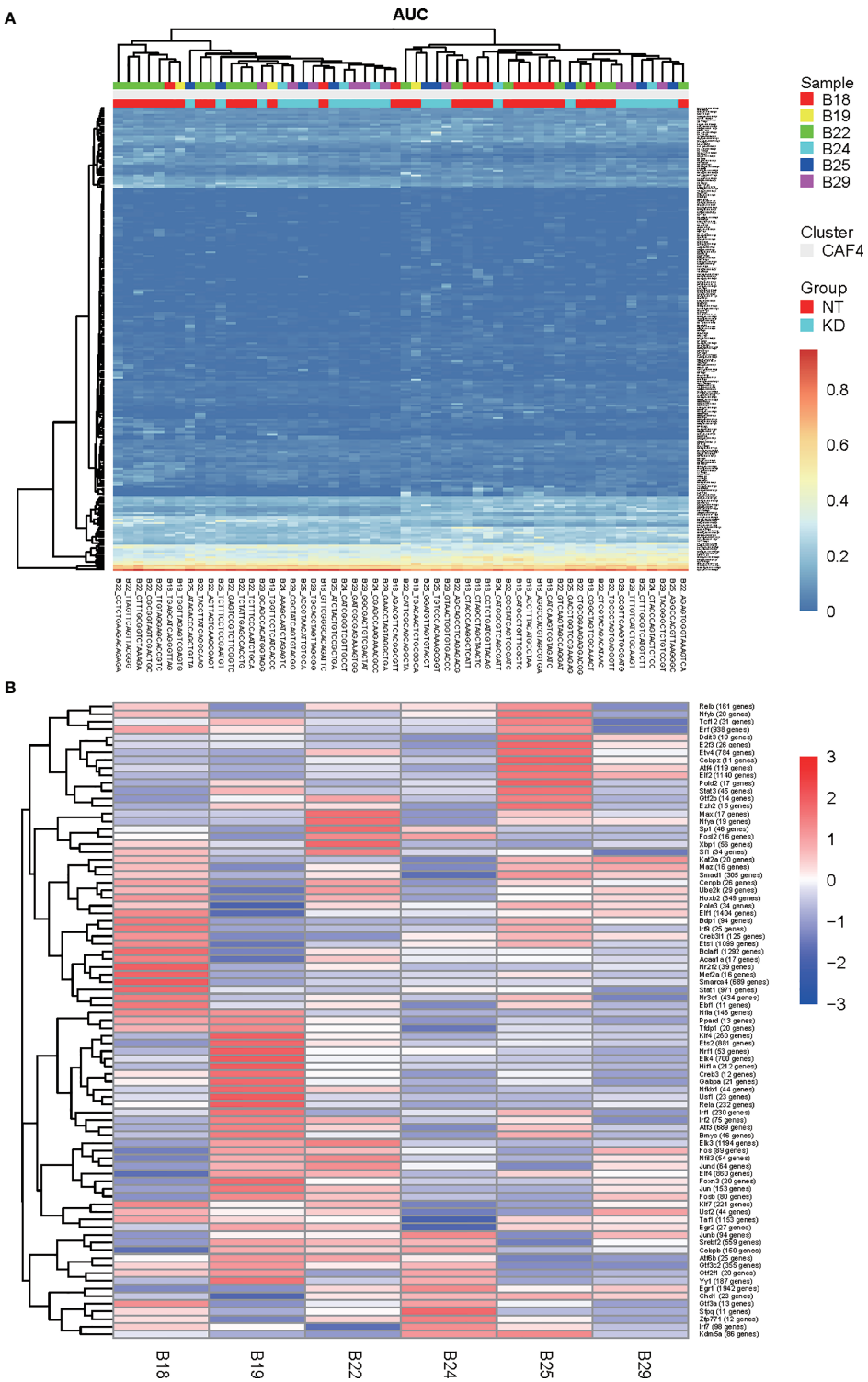

FIGURE 4 | SCENIC analysis of CAF in mouse CT26 tumor **(A, B)**. Single cell regulatory network inference and clustering (SCENIC) analysis. By using SCENIC to predict transcription factors and corresponding target genes, a transcription factor regulatory network module was constructed. By calculating the area under the curve (AUC), the higher the AUC value, the stronger the regulatory activity of transcription factors to activate target gene expression **(A)** SCENIC analysis to assess transcription factors which underlie differences in expression of CT26 tumor cell between NT and *Bcl9* KD tumor cells. **(B)** Average activity of regulons in different cell subpopulations.

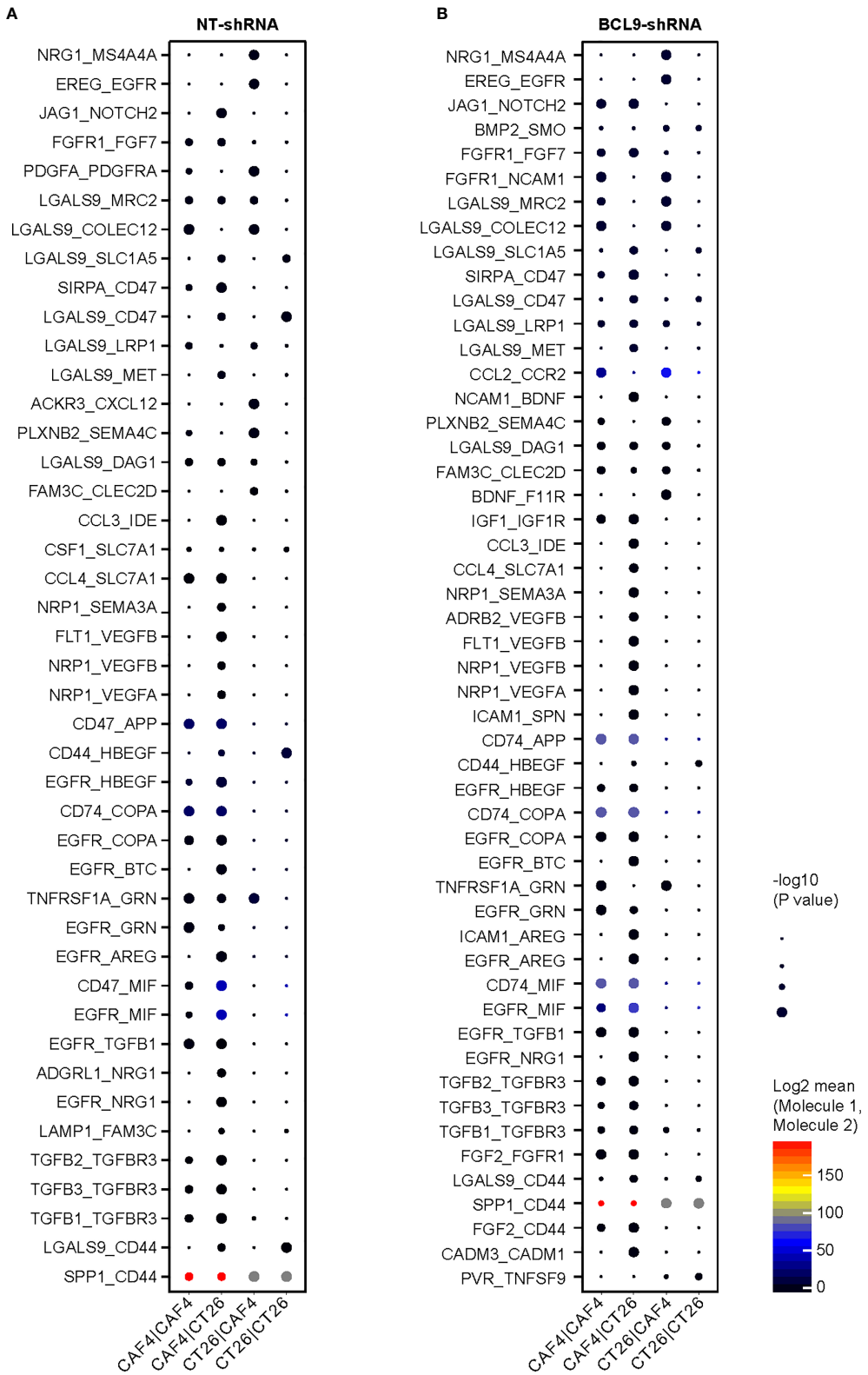

FIGURE 5 | Tumor CAF interaction in mouse CT26 tumor. Cell interaction in normal tumor (NT) and knockdown (KD) groups. **(A)** The binding between receptor and ligand is obvious in CAF/CT26 in NT subgroups. **(B)** The binding between receptor and ligand is obvious in CAF/CT26 in KD subgroups.

cluster 10 (**Supplementary Figure 2H**), which had high levels of cytokines and chemokines (32, 33).

Gene ontology annotation and enrichment were analyzed. In mCAFs, extracellular matrix organization, extracellular structure organization, and cell proliferation were significantly enriched (**Supplementary Figure 2I**). KEGG pathways analysis in CAF clusters was performed. For example, in CAF1, Wnt signaling and NF-κB signaling were enriched (**Supplementary Figure 2J**), indicating that CAFs are involved in complex structural and paracrine interactions in the TME, consistent with intratumoral CAF heterogeneity.

Cluster and Survival Analysis of Human Colon Cancer

To compare cell cluster and type profiles in tumor, we performed scRNA-seq in parallel in non-metastasis and metastasis CRC. We analyzed tumor samples from 13 colon cancer patients (SUB8333842). In the preliminary clustering (**Figure 6A**), we separated CAF cells and tumor cells. Extract the CAF cell population and perform re-clustering analysis (**Figure 6B**). As a result, the CAF cell subgroups can be divided into 3 clusters (**Figures 6B, C**). The expression patterns of these three clusters are comparable to those of mice. They mainly expressed collagen production, muscle-like and stromal cells related markers, such as MMP1, MYL9, COL1A1, etc (**Figures 6B, C**). In order to study which transcription factors are related to the formation of these subgroups, we conducted a Metascape analysis. As a result, shown in **Figure 6D**, the establishment of cluster0, cluster1, and cluster2 are mainly related to the transcriptional regulation of MZF1, SRF, and PSMB5, respectively.

In order to study the impact of the key marker genes of the CAF cell subpopulation on the prognosis of tumor patients, we used the first 50 key marker genes in the three clusters indicated in **Figures 6B, C** to perform GSVA analysis, and took the GSVA value as the basis for classification, The survminer method was used for optimal grouping, and the two groups with high and low GSVA values were separated, and survival analysis was performed on the two groups. Taking the HR obtained by the survival analysis into a volcano map (**Figures 7A, B**), it was found that the key marker genes of the CAF cell subpopulation had the greatest impact on the Kidney renal clear cell carcinoma (KIRC), and colon cancer Colon Adenocarcinoma (COAD) was also in the highly significant range (**Figures 7C, D**).

DISCUSSION

The treatment of advanced metastatic CRCs remains a challenge; thus, exploring new target molecules and therapeutic strategies is of paramount importance. The research progress of Wnt/β-catenin signaling pathway mechanisms has accelerated the discovery of new therapeutic methods targeting Wnt/β-catenin pathway in CRCs. Although most drugs are still in the very early stages of research, it is expected that they will help in curing the intractable CRCs in the near future.

CAFs are critical ingredients of the TME with diverse effects, such as changing matrix deposition and remolding, intensive mutual signal interactions with cancer cells and interplay with infiltrating T cells (33). CAFs play a key role in cancer progression and metastasis; however, their prometastatic mechanisms have not been investigated. CAFs are abundant in CRC (34), but it is still unclear where they are recruited from, whether they may enhance metastasis-promoting communication, and how they exchange information with cancer cells and cross talk with the TME. CRC is the most common cancer in the world, and faces an enormous therapeutic challenge. Surgery, radiotherapy, and chemotherapy combined with targeted drugs have advanced the treatment for early-stage CRC. However, the main cause of death and metastasis remains poorly understood (35). Recent reports have demonstrated that Wnt signaling pathway activation induces primary resistance to immunotherapy, and CAFs were suggested to interact with Wnt signaling pathway (36).

We explored the CAFs to clarify how they remodel the TME through inhibition of the Wnt signaling pathway by hsBCL9$_{CT}$-24 treatment or *Bcl9* knockdown. Pharmacological inhibition of Bcl9 in mice and genetic knockdown of *Bcl9* with shRNA in CT26 tumor cells was performed. We grouped the cells into types by using of graph-based clustering on the informative principal components. This technique identified cell clusters by marker genes, *S100a9*, *Pdgfrb*, and *Ptx3*, which were highly expressed in clusters of hsBCL9$_{CT}$-24–treated group. In CT26 tumor cells group where *Bcl9* was knocked down by shRNA, *Rgs5*, *Dmkn*, and *Ass1* were highly expressed. *S100a9* and *Rg55* are marker genes of CAFs. We found that *Bcl9* depletion can cause protumor effect in CAFs.

Tumor stromal cells are necessary in tumorigenesis and tumor cells proliferation. Development and metastasis in the TME influences therapeutic response and clinical outcome, as well as interplay with peripheral cells (37) through the circulatory and immunologic systems to affect the development and progression of cancer (30). Moreover, the stroma cells of the TME such as CAFs play key roles in carcinogenesis through stimulating and facilitating uncontrolled cell proliferation. We explored the cell interaction between NT and KD groups. The TGFβ-TGFβR and EGFR-NRG1 binding between receptor and ligand was obvious in CAF/CT26 subgroups, revealing that the CAFs and CT26 tumor cells cross talk through TGF pathway and affect the expression of EGFR to transform the tumor cells. Therefore, stromal cells such as CAFs are a promising target for optimizing therapeutic strategies against cancer. These results illustrate that inhibition of BCL9 can reduce CAF communication with tumor cells.

GSVA analysis manifested immunologic signatures pathway such as TGF as the enriched signature in tumor cells. We applied SCENIC analysis to unravel which transcription factors determine differences in CT26 tumor cell expression between NT and *Bcl9* KD tumor cells. We also identified Foxp4 as a candidate transcription factor underlying gene expression differences in NT and *Bcl9* KD tumor cells. KEGG pathways

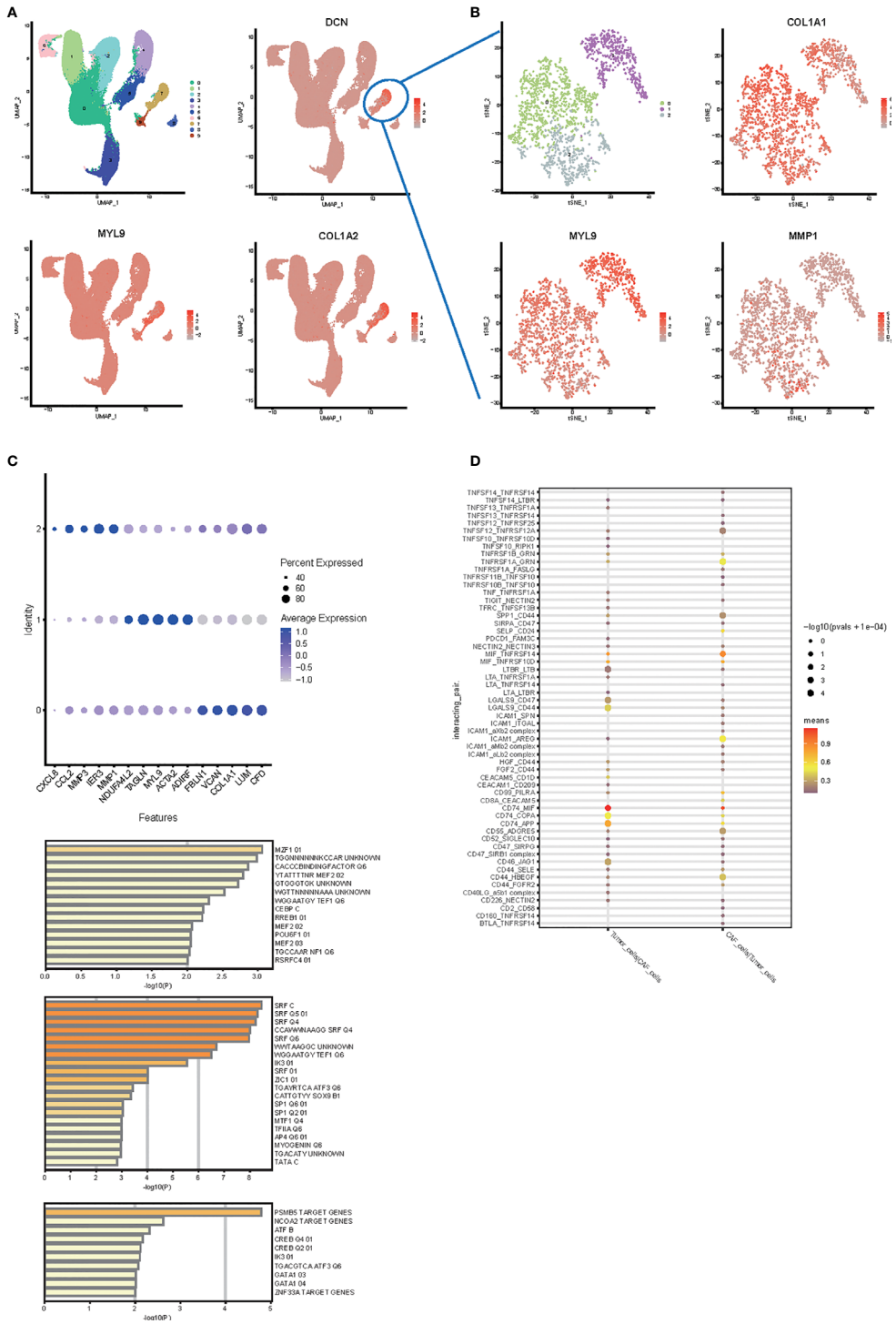

FIGURE 6 | Single cell RNA-seq analysis in human colon cancer samples. **(A)** UMAP plot and clustering analysis. The color map showed clusters, and the markers of CAF were plotted on the map (*DCN, MYL9, COL1A2*). Cluster 2 was identified as cancer cells and cluster 7 was identified as CAF. **(B)** t-SNE plot and clustering analysis for CAF subtype. The color map showed clusters, and the markers of each CAF subpopulation were plotted on the map (*MMP1, MYL9, COL1A1*). **(C)** Bubble plots express different marker genes according to each cluster high specific expression gene separate different cells of CAF. **(D)** Transcription factor analysis from metascape. The first 50 genes of each CAF subpopulation were used to analyze the transcription factors specifically regulated. **(E)** Cell interaction between CAF and tumor cell.

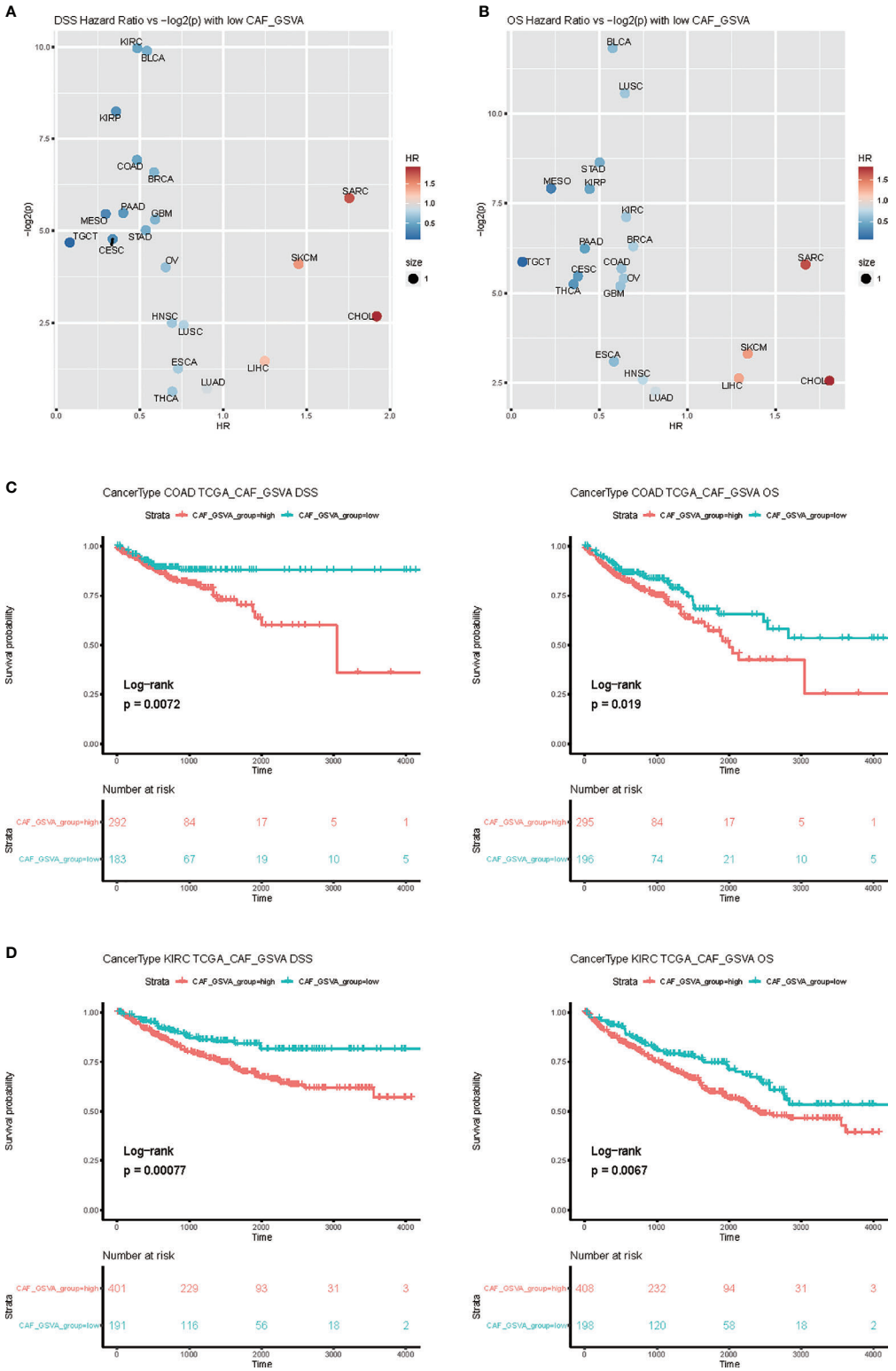

FIGURE 7 | Survival analysis of CAF related genes. **(A)** Select each 50 genes (**Supplementary Table 1**) related to the patient's CAF, and use GSVA to calculate the degree of enrichment in TCGA patients. Use this index to classify patients in different tumors and perform survival analysis. **(B)** The volcano graph of HR and p values, with Overall survival (OS) on the left and disease-specific survival (DSS) on the right. **(C, D)** Survival analysis of Kidney renal clear cell carcinoma (KIRC) and Colon Adenocarcinoma (COAD).

analysis in CAF clusters was performed. For example, in CAF1, Wnt signaling and NF-κB signaling were enriched.

IL-2 is a pleiotropic cytokine, and control the differentiation and homeostasis of both pro- and anti-inflammatory T cells is fundamental to determining the molecular details of immune regulation. The IL-2 receptor couples to JAK tyrosine kinases and activates the STAT5 transcription factors. Our data revealed that IL-2 and STAT1 was enriched in tumor cells (**Figure 3D**). TGF-β has been shown to play an essential role in establishing immunological tolerance TGF-β inhibits the proliferation of T cells as well as cytokine production *via* Foxp3-dependent and independent mechanisms. Our data shows that the TGFβ-TGFβR and EGFR-NRG1 interaction revealing a cross-talk between the CAFs and CT26 tumor cells, which changes the expression of EGFR consequentially transforming the tumor cells (**Figures 5A, B**). Bcl9 depletion could potentially benefit T-cell–mediated antitumor immune *via* modulating IL2 and TGFβ signaling.

In human colorectal tissue and tumor cells, a direct comparison of tumor cells between metastasis and non-metastasis tumors by GSVA analysis revealed that PTEN pathway, SMAD2 pathway, FGFR4 pathway, and JAK pathway were the enriched signatures in tumor cells. To assess which transcription factors underlie differences in tumor cell expression between metastasis and non-metastasis tumor cells SCENIC analysis was applied. We also identified STAT1 as a candidate transcription factor underlying gene expression differences in metastasis and non-metastasis tumor cells. STAT1 and FOS are associated with IFNγ signaling, which explains why the restraint of BCL9 can enhance the antitumor immune responses.

DATA AVAILABILITY STATEMENT

The data presented in the study are deposited in the FigShare repository, accession number/link: https://figshare.com/s/cd81407e68b809231131.

ETHICS STATEMENT

The animal study was reviewed and approved by School of Pharmacy, Fudan University.

AUTHOR CONTRIBUTIONS

MY prepared the figures and wrote the manuscript. ZW analyzed the data. MF prepared the samples. YZ analyzed the data and edited the manuscript. YC performed analysis and edited manuscript. DZ conceptualized and wrote the manuscript. All authors contributed to the article and approved the submitted version.

FUNDING

The current study was supported by the Science and Technology Commission of Shanghai (18ZR1403900 to DZ; and 18JC1413800 to DZ), the National Natural Science Foundation of China (81872895) (DZ), the project on joint translational research in Shanghai Institute of Materia Medica and Fudan University (FU-SIMM20181010) (DZ).

ACKNOWLEDGMENTS

We thank Shuru Shen for providing assistance in this study.

SUPPLEMENTARY MATERIAL

The Supplementary Material for this article can be found online at: https://www.frontiersin.org/articles/10.3389/fonc.2021.603556/full#supplementary-material

REFERENCES

1. Bray FI, Ferlay J, Soerjomataram I, Siegel RL, Torre LA, Jemal A. Global cancer statistics 2018: GLOBOCAN estimates of incidence and mortality worldwide for 36 cancers in 185 countries. *CA CANCER J CLIN* (2018) 68 (6):394–424. doi: 10.3322/caac.21492
2. Schatoff EM, Leach BI, Dow LE. Wnt Signaling and Colorectal Cancer. *Curr colorectal Cancer Rep* (2017) 13(2):101–10. doi: 10.1007/s11888-017-0354-9
3. Cross AJ, Ferrucci LM, Risch A, Graubard BI, Ward MH, Park Y, et al. A large prospective study of meat consumption and colorectal cancer risk: an investigation of potential mechanisms underlying this association. *Cancer Res* (2010) 70(6):2406–14. doi: 10.1158/0008-5472.CAN-09-3929
4. Watanabe T, Itabashi M, Shimada Y, Tanaka S, Ito Y, Ajioka Y, et al. Japanese Society for Cancer of the Colon and Rectum (JSCCR) Guidelines 2014 for treatment of colorectal cancer. *Int J Clin Oncol* (2012) 17(1):1–29. doi: 10.1007/s10147-015-0801-z
5. Morin PJ, Sparks A, Korinek V, Barker N, Clevers H, Vogelstein B, et al. Activation of beta -Catenin-Tcf Signaling in Colon Cancer by Mutations in beta -Catenin or APC. *Science* (1997) 275(5307):1787–90. doi: 10.1126/science.275.5307.1787
6. Herrera M, Islam ABMMK, Herrera A, Martin P, Garcia V, Silva J, et al. Functional heterogeneity of cancer-associated fibroblasts from human colon tumors shows specific prognostic gene expression signature. *Clin Cancer Res* (2013) 19(21):5914–26. doi: 10.1158/1078-0432.CCR-13-0694
7. Mueller L, Goumas F, Affeldt M, Sandtner S, Gehling UM, Brilloff S, et al. Stromal Fibroblasts in Colorectal Liver Metastases Originate From Resident Fibroblasts and Generate an Inflammatory Microenvironment. *Am J Pathol* (2007) 171(5):1608–18. doi: 10.2353/ajpath.2007.060661
8. Gong Y, Scott E, Lu R, Xu Y, Oh W, Yu QJPO. TIMP-1 promotes accumulation of cancer associated fibroblasts and cancer progression. (2013) 8(10):1–14. doi: 10.1371/journal.pone.0077366
9. Tommelein J, Verset L, Boterberg T, Demetter P, Bracke M, De Wever O. Cancer-associated fibroblasts connect metastasis-promoting communication in colorectal cancer. *Front Oncol* (2015) 5:63. doi: 10.3389/fonc.2015.00063
10. Nakagawa H, Liyanarachchi S, Davuluri RV, Auer H, Martin EW, de la Chapelle A, et al. Role of cancer-associated stromal fibroblasts in metastatic colon cancer to the liver and their expression profiles. *Oncogene* (2004) 23 (44):7366–77. doi: 10.1038/sj.onc.1208013
11. Peddareddigari VGR, Wang D, Dubois RNJCM. The Tumor Microenvironment in Colorectal Carcinogenesis. *Cancer Microenviron* (2010) 3(1):149–66. doi: 10.1007/s12307-010-0038-3

12. De Boeck A, Hendrix A, Maynard DM, Van Bockstal M, Daniels A, Pauwels P, et al. Differential secretome analysis of cancer-associated fibroblasts and bone marrow-derived precursors to identify microenvironmental regulators of colon cancer progression. *Proteomics* (2013) 13(2):379–88. doi: 10.1002/pmic.201200179
13. Valenciano A, Henriquezhernandez LA, Moreno M, Lloret M, Lara PCJTO. Role of IGF-1 Receptor in Radiation Response. *Transl Oncol* (2012) 5(1):1–9. doi: 10.1593/tlo.11265
14. De Wever O, Nguyen QD, Van Hoorde L, Bracke M, Bruyneel E, Gespach C, et al. Tenascin-C and SF/HGF produced by myofibroblasts in vitro provide convergent pro-invasive signals to human colon cancer cells through RhoA and Rac. *FASEB J Off Publ Fed Am Soc Exp Biol* (2004) 18(9):1016–8. doi: 10.1096/fj.03-1110fje
15. De Boeck A, Pauwels P, Hensen K, Rummens J, Westbroek W, Hendrix A, et al. Bone marrow-derived mesenchymal stem cells promote colorectal cancer progression through paracrine neuregulin 1/HER3 signalling. *Gut* (2013) 62(4):550–60. doi: 10.1136/gutjnl-2011-301393
16. Pena C, Cespedes MV, Lindh MB, Kiflemariam S, Mezheyeuski A, Edqvist P, et al. STC1 Expression By Cancer-Associated Fibroblasts Drives Metastasis of Colorectal Cancer. *Cancer Res* (2013) 74(4):1287–97. doi: 10.1158/0008-5472.CAN-12-1875
17. Calon A, Espinet E, Palomo-Ponce S, Tauriello DVF, Iglesias M, Céspedes MV, et al. Dependency of colorectal cancer on a TGF-β-driven program in stromal cells for metastasis initiation. *Cancer Cell* (2012) 22(5):571–84. doi: 10.1016/j.ccr.2012.08.013
18. Hawinkels LJAC, Paauwe M, Verspaget HW, Wiercinska E, van der Zon JM, van der Ploeg K, et al. Interaction with colon cancer cells hyperactivates TGF-β signaling in cancer-associated fibroblasts. *Oncogene* (2014) 33(1):97–107. doi: 10.1038/onc.2012.536
19. Rupp C, Scherzer M, Rudisch A, Unger C, Haslinger C, Schweifer N, et al. IGFBP7, a novel tumor stroma marker, with growth-promoting effects in colon cancer through a paracrine tumor–stroma interaction. *Oncogene* (2015) 34(7):815–25. doi: 10.1038/onc.2014.18
20. Torres S, Bartolome RA, Mendes M, Barderas R, Fernandezacenero MJ, Pelaezgarcia A, et al. Proteome Profiling of Cancer-Associated Fibroblasts Identifies Novel Proinflammatory Signatures and Prognostic Markers for Colorectal Cancer. *Clin Cancer Res* (2013) 19(21):6006–19. doi: 10.1158/1078-0432.CCR-13-1130
21. Martin MS, Pujuguet P, Martin FJPR. Practice. *Role Stromal Myofibroblasts Infiltrating Colon Cancer Tumor Invasion* (1996) 192(7):712–7. doi: 10.1016/S0344-0338(96)80093-8
22. Yang J, Weinberg RAJDC. Epithelial-Mesenchymal Transition: At the Crossroads of Development and Tumor Metastasis. *Dev Cell* (2008) 14 (6):818–29. doi: 10.1016/j.devcel.2008.05.009
23. Herrera A, Herrera M, Albacastellon L, Silva J, Garcia V, Loubatcasanovas J, et al. Protumorigenic effects of Snail-expression fibroblasts on colon cancer cells. *Int J Cancer* (2014) 134(12):2984–90. doi: 10.1002/ijc.28613
24. Labernadie A, Kato T, Brugues A, Serrapicamal X, Derzsi S, Arwert E, et al. A mechanically active heterotypic E-cadherin/N-cadherin adhesion enables fibroblasts to drive cancer cell invasion. *Nat Cell Biol* (2017) 19(3):224–37. doi: 10.1038/ncb3478
25. Brechbuhl HM, Finlay-Schultz J, Yamamoto TM, Gillen AE, Cittelly DM, Tan AC, et al. Fibroblast Subtypes Regulate Responsiveness of Luminal Breast Cancer to Estrogen. *Clin Cancer Res Off J Am Assoc Cancer Res* (2017) 23 (7):1710–21. doi: 10.1158/1078-0432.Ccr-15-2851
26. Yamanashi T, Nakanishi Y, Fujii G, Akishima-Fukasawa Y, Moriya Y, Kanai Y, et al. Podoplanin expression identified in stromal fibroblasts as a favorable prognostic marker in patients with colorectal carcinoma. *Oncology* (2009) 77 (1):53–62. doi: 10.1159/000226112
27. Takada K, Zhu D, Bird G, Sukhdeo K, Zhao J-J, Mani M, et al. Targeted Disruption of the BCL9/ -Catenin Complex Inhibits Oncogenic Wnt Signaling. *Sci Trans Med* (2012) 4:148ra17. doi: 10.1126/scitranslmed.3003808
28. Takada K, Zhu D, Bird GH, Sukhdeo K, Zhao JJ, Mani M, et al. Targeted disruption of the BCL9/β-catenin complex inhibits oncogenic Wnt signaling. *Sci Transl Med* (2012) 4(148):148ra17. doi: 10.1126/scitranslmed.3003808
29. Feng M, Jin JQ, Xia L, Xiao T, Mei S, Wang X, et al. Pharmacological inhibition of β-catenin/BCL9 interaction overcomes resistance to immune checkpoint blockades by modulating T<sub<reg</sub< cells. *Sci Adv* (2019) 5 (5):eaau5240. doi: 10.1126/sciadv.aau5240
30. Arneth B. Tumor Microenvironment. *Med (Kaunas Lithuania)* (2019) 56 (1):1–21. doi: 10.3390/medicina56010015
31. Zhu Y, Yu X, Thamphiwatana SD, Zheng Y, Pang Z. Nanomedicines modulating tumor immunosuppressive cells to enhance cancer immunotherapy. *Acta Pharm Sin B* (2020) 10(11):2054–74. doi: 10.1016/j.apsb.2020.08.010
32. Elyada E, Bolisetty M, Laise P, Flynn WF, Courtois ET, Burkhart RA, et al. Cross-species single-cell analysis of pancreatic ductal adenocarcinoma reveals antigen-presenting cancer-associated fibroblasts. *Cancer Discov* (2019) 9 (8):1102–23. doi: 10.1158/2159-8290.CD-19-0094
33. Bartoschek M, Oskolkov N, Bocci M, Lövrot J, Larsson C, Sommarin M, et al. Spatially and functionally distinct subclasses of breast cancer-associated fibroblasts revealed by single cell RNA sequencing. *Nat Commun* (2018) 9 (1):5150. doi: 10.1038/s41467-018-07582-3
34. Isella C, Terrasi A, Bellomo SE, Petti C, Galatola G, Muratore A, et al. Stromal contribution to the colorectal cancer transcriptome. *Nat Genet* (2015) 47 (4):312–9. doi: 10.1038/ng.3224
35. Tauriello DVF, Calon A, Lonardo E, Batlle EJMO. Determinants of metastatic competency in colorectal cancer. *Mol Oncol* (2017) 11(1):97–119. doi: 10.1002/1878-0261.12018
36. Kramer N, Schmollerl J, Unger C, Nivarthi H, Rudisch A, Unterleuthner D, et al. Autocrine WNT2 signaling in fibroblasts promotes colorectal cancer progression. *Oncogene* (2017) 36(39):5460–72. doi: 10.1038/onc.2017.144
37. Denton AE, Roberts EW, Fearon DT. Stromal Cells in the Tumor Microenvironment. *Adv Exp Med Biol* (2018) 1060:99–114. doi: 10.1007/978-3-319-78127-3_6

Conflict of Interest: The author declares that the research was conducted in the absence of any commercial or financial relationships that could be construed as a potential conflict of interest.

Advantages of publishing in Frontiers

OPEN ACCESS
Articles are free to read for greatest visibility and readership

FAST PUBLICATION
Around 90 days from submission to decision

HIGH QUALITY PEER-REVIEW
Rigorous, collaborative, and constructive peer-review

TRANSPARENT PEER-REVIEW
Editors and reviewers acknowledged by name on published articles

Frontiers
Avenue du Tribunal-Fédéral 34
1005 Lausanne | Switzerland

Visit us: www.frontiersin.org
Contact us: frontiersin.org/about/contact

REPRODUCIBILITY OF RESEARCH
Support open data and methods to enhance research reproducibility

DIGITAL PUBLISHING
Articles designed for optimal readership across devices

FOLLOW US
@frontiersin

IMPACT METRICS
Advanced article metrics track visibility across digital media

EXTENSIVE PROMOTION
Marketing and promotion of impactful research

LOOP RESEARCH NETWORK
Our network increases your article's readership